

VOLUME EDITOR: E. WEBER

**Supramolecular
Chemistry I**
*Directed Synthesis and
Molecular Recognition*

165 Topics in Current Chemistry



Springer

165 Topics in Current Chemistry

Supramolecular Chemistry I – Directed Synthesis and Molecular Recognition

Editor: E. Weber

With contributions by
J. Canceill, J.-C. Chambron, A. Collet,
Ch. Dietrich-Buchecker, H. D. Durst, J.-P. Dutasta,
F. H. Kohnke, B. Lozach, J.-P. Mathias, S. Misumi,
J.-P. Sauvage, J. F. Stoddart, D. A. Tomalia,
S. C. Zimmerman

With 168 Figures and 24 Tables



Springer-Verlag

Berlin Heidelberg New York
London Paris Tokyo
Hong Kong Barcelona
Budapest

This series presents critical reviews of the present position and future trends in modern chemical research. It is addressed to all research and industrial chemists who wish to keep abreast of advances in their subject.

As a rule, contributions are specially commissioned. The editors and publishers will, however, always be pleased to receive suggestions and supplementary information. Papers are accepted for "Topics in Current Chemistry" in English.

ISBN 3-540-56280-X Springer-Verlag Berlin Heidelberg New York
ISBN 0-387-56280-X Springer-Verlag New York Berlin Heidelberg

Library of Congress Catalog Card Number 74-644622

This work is subject to copyright. All rights are reserved, whether the whole or part of the material is concerned, specifically the rights of translation, reprinting, reuse of illustrations, recitations, broadcasting, reproduction on microfilm or in any other way, and storage in data banks. Duplication of this publication or parts thereof is permitted only under the provisions of the German Copyright Law, of September 9, 1965, in its current version, and permission for use must always be obtained from Springer-Verlag. Violations are liable for prosecution under the German Copyright Law.

© Springer-Verlag Berlin Heidelberg 1993
Printed in Germany

The use of general descriptive names, registered names, trademarks, etc. in this publication does not imply, even in the absence of a specific statement, that such names are exempt from the relevant protective laws and regulations and therefore for general use.

Typesetting: Th. Muntzer, Bad Langensalza; Printing: Heenemann, Berlin;
Binding: Lüderitz & Bauer, Berlin
51/3020-5 4 3 2 1 0 — Printed on acid-free paper

Guest Editor

Prof. Dr. *E. Weber*
Institut für Organische Chemie und Biochemie,
Universität Bonn,
Gerhard-Domagk-Str. 1,
W-5300 Bonn 1

Editorial Board

Prof. Dr. <i>Michael J. S. Dewar</i>	Department of Chemistry, The University of Texas Austin, TX 78712, USA
Prof. Dr. <i>Jack D. Dunitz</i>	Laboratorium für Organische Chemie der Eidgenössischen Hochschule Universitätsstraße 6/8, CH-8006 Zürich
Prof. Dr. <i>Klaus Hafner</i>	Institut für Organische Chemie der TH Petersenstraße 15, D-6100 Darmstadt
Prof. Dr. <i>Shô Itô</i>	Faculty of Pharmaceutical Sciences Tokushima Bunri University Tokushima 770/Japan
Prof. Dr. <i>Jean-Marie Lehn</i>	Institut de Chimie, Université de Strasbourg, 1, rue Blaise Pascal, B. P. Z 296/R8, F-67008 Strasbourg-Cedex
Prof. Dr. <i>Kenneth N. Raymond</i>	Department of Chemistry, University of California, Berkeley, California 94720, USA
Prof. Dr. <i>Charles W. Rees</i>	Hofmann Professor of Organic Chemistry, Department of Chemistry, Imperial College of Science and Technology, South Kensington, London SW7 2AY, England
Prof. Dr. <i>Joachim Thiem</i>	Institut für Organische Chemie, Universität Hamburg Martin-Luther-King-Platz 6, 2000 Hamburg 54, FRG
Prof. Dr. <i>Fritz Vögtle</i>	Institut für Organische Chemie und Biochemie der Universität, Gerhard-Domagk-Str. 1, 5300 Bonn 1, FRG

Preface

The need for the development of a highly integrated basic science as the foundation for molecular materials, for information storage, processing and transfer, for enzyme-like catalysis and reactivity, for molecular encapsulation and stabilisation is now fully recognized. This has resulted in increased communication between the various chemical disciplines which developed separately such as organic chemistry, inorganic chemistry, physical chemistry, analytical chemistry, and so on. Reunification of these sub-disciplines is taking place and the vehicle for reform is *Supramolecular Science*.

The term 'supramolecular' means "more complex than a molecule" or "composed of many molecules". In his Nobel Lecture [see (1988) *Angew. Chem.* 100: 91; (1988) *Angew. Chem., Int. Ed. Engl.* 27: 89], Jean-Marie Lehn gave the following definition: "Supramolecular Chemistry is the chemistry of the intermolecular bond, covering the structures and functions of the entities formed by association of two or more chemical species". Therefore the conceptual feature that distinguishes a supramolecular from a molecular species is not its size, but the possibility of splitting the species into molecular components that have an individual existence, at least in principle. Or, the other way round, supramolecular species are constructed by combining molecular building blocks in a similar way to molecules being obtained by the combination of atoms. In short, Supramolecular Chemistry is the chemistry beyond the molecule and deals mostly with noncovalent chemical bonds.

Only lately have covalently linked species also become included in supramolecular structures since they are formed of particular building blocks, e.g. the *Starburst/cascade dendrimers* (see Chapter 6 of this volume). Moreover, the *catenands* and *knots* (as shown in Chapter 5) are not subject either to covalent or typical noncovalent bonds, although the latter are important in the formation step, but rest upon a mechanical interlock or coiling.

On the other hand, host-guest systems being composed of preorganized macrocyclic, cage-type or rigid acyclic host molecules

and cationic or uncharged organic guest species are characteristic of noncovalent intermolecular forces. Examples are the complexes of rigid *molecular tweezers*, *cyclotrimeratrylenes* or *cryptophanes* and *chromoacerands* showing remarkable recognition properties for neutral molecules and cations, e.g. the chromoacerands are capable of signalling a specific cation or even one particular guest enantiomer by coloration. These structures and properties are the topics of Chapters 2, 3, and 4, respectively.

Understanding the synthesis of supramolecular structures is another important challenge. Fortunately, in this respect, enormous progress has been made during the last few years. "There are inherently simple ways of making apparently complex unnatural products from appropriate substrates without the need for reagent control or catalysis. It implies that the required stereoelectronic information is preprogrammed into the substrates of a chemical reaction; this allows the efficient and precise spontaneous self-assembly of these 'intelligent' substrates thus yielding large molecules with completely defined superstructures and/or organized molecular assemblies composed of unique molecular components" (cf. J. F. Stoddart (1991) In: H.-J. Schneider, H. Dürr (eds.) *Frontiers in supramolecular organic chemistry*, VCH-Verlagsgesellschaft, Weinheim). One way is Stoddart's concept of '*substrate-directed synthesis*', which is shown in Chapter 1 of the book. Another significant way is the so-called '*genealogical-directed synthesis*' involved in the construction of dendrons and dendrimers as described in Chapter 6.

Although the topics covered in the book are extremely useful from a fundamental and an applicative viewpoint, there are further important aspects in the wide scope of Supramolecular Chemistry, and the rapid pace of research in this field requires publication in more than one volume. This is the ambition of the editor who hopes that the present book will whet the appetite of the reader, while he is enjoying these six brilliantly written and informative articles.

I have pleasure in thanking all contributors for bringing this book to a successful completion.

Bonn, September 1992

Edwin Weber

Attention all "Topics in Current Chemistry" readers:

A file with the complete volume indexes Vols. 22 (1972) through 163 (1992) in delimited ASCII format is available for downloading at no charge from the Springer EARN mailbox. Delimited ASCII format can be imported into most databanks.

The file has been compressed using the popular shareware program "PKZIP" (Trademark of PKware Inc., PKZIP is available from most BBS and shareware distributors).

This file is distributed without any expressed or implied warranty.

To receive this file send an e-mail message to:

SVSERV@DHDSPRI6.BITNET.

The message must be: "GET /CHEMISTRY/TCC-CONT.ZIP".

SVSERV is an automatic data distribution system. It responds to your message. The following commands are available:

HELP	returns a detailed instruction set for the use of SVSERV,
DIR <i>(name)</i>	returns a list of files available in the directory "name",
INDEX <i>(name)</i>	same as "DIR",
CD <i><name></i>	changes to directory "name",
SEND <i><filename></i>	invokes a message with the file "filename",
GET <i><filename></i>	same as "SEND".

Table of Contents

Substrate-Directed Synthesis: The Rapid Assembly of Novel Macropolycyclic Structures via Stereoregular Diels-Alder Oligomerizations	
F. H. Kohnke, J. P. Mathias, J. F. Stoddart	1
Rigid Molecular Tweezers as Hosts for the Complexation of Neutral Guests	
S. C. Zimmerman	71
Cyclotrimeratrylenes and Cryptophanes: Their Synthesis and Applications to Host-Guest Chemistry and to the Design of New Materials	
A. Collet, J.-P. Dutasta, B. Lozach, J. Canceill	103
From Classical Chirality to Topologically Chiral Catenands and Knots	
J.-C. Chambron, Ch. Dietrich-Buchecker, J.-P. Sauvage . . .	131
Recognitory Coloration of Cations with Chromoacerands	
S. Misumi	163
Genealogically Directed Synthesis: Starburst/Cascade Dendrimers and Hyperbranched Structures	
D. A. Tomalia, H. D. Durst	193
Author Index Volumes 151–165	315

Substrate-Directed Synthesis: The Rapid Assembly of Novel Macropolycyclic Structures *via* Stereoregular Diels-Alder Oligomerizations**

Franz H. Kohnke¹, John P. Mathias², and J. Fraser Stoddart³

Department of Chemistry, The University, Sheffield S3 7HF, UK

Table of Contents

1 Introduction	3
1.1 Supramolecular Design Processes and Rapid Assembly	3
1.2 The Diels-Alder Approach	9
1.3 Belts and Cages in Supramolecular Chemistry	12
2 The Structure-Directed Synthesis of Kohnkene	17
2.1 Building Blocks and Autochthonous Reactivity	17
2.2 Completing a Molecular LEGO Set	25
2.3 Molecular Belts as Precursors to Novel Hydrocarbons	30
3 The Generality of the Substrate-Directed Approach	34
3.1 Strips, Coils, and Bigger Belts	34
3.2 Kinetic versus Thermodynamic Control within the Repetitive Diels-Alder Reaction Regime	46
3.2.1 Attempted Observation of Thermally-Promoted Reversibility in the Cycloadditions	46
3.2.2 Attempted Observation of High Pressure-Promoted Reversibility in the Cycloadditions	49

Present Addresses:

¹ Dipartimento di Chimica Organica e Biologica dell' Università di Messina, Salita Sperone 31, 98 166, Messina, Italy.

² Department of Chemistry, Harvard University, Cambridge, Massachusetts, 02138, USA.

³ School of Chemistry, University of Birmingham, Edgbaston, Birmingham, B15 2TT, UK.

** This work has been supported by the Science and Engineering Research Council, the Ministry of Defence in the United Kingdom, the Consiglio Nazionale delle Ricerche in Italy, and the National Economic Development Organization in Japan.

4 The Incorporation of [a,c]-Fusion into the Molecular LEGO Set – The Synthesis of Angular Belts and Cages	50
4.1 The Synthesis of an Angular Belt	50
4.2 Trinacrene – The Synthesis of a Molecular Cage	56
5 Conclusions and Future Prospects	59
7 References	61

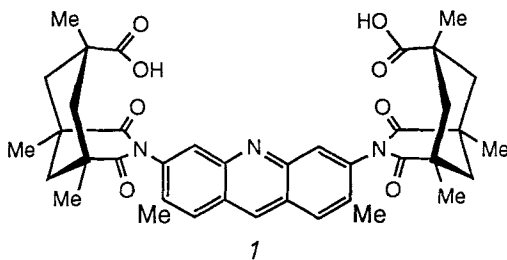
An increasing appreciation of molecular architecture and design will provide a greater impetus to tackle the exciting and elaborate structural targets that will confront chemistry in the twenty-first Century. It is, therefore, of the utmost importance that methods by which outwardly complex chemical systems can be assembled selectively, rapidly, and efficiently, are devised. Towards this goal, a trebly diastereoselective tandem Diels-Alder reaction sequence has been developed. Subsequently, we have demonstrated how this synthetic methodology can be utilized for the synthesis of novel macropolycyclic molecular structures. In each cycloaddition, the stereoelectronic characteristics, that are inherent in part of the rigid bicyclic frameworks of both bisdienophile and bisdiene building blocks, are used to dictate their respective modes of reaction. The outcome of this substrate-directed approach to organic synthesis allows the rapid and highly-controlled assembly of an increasing range of apparently complex molecular structures. The diastereoselectivities that are witnessed in each cycloaddition are rationalized as involving kinetically-controlled transition-state effects. The rationalization is based upon maximal vicinal staggering and the subsequent minimization of torsional strain within the rigid bicyclic framework in the transition state. In this survey, the application of the repetitive Diels-Alder approach for the synthesis of a wide range of macropolycyclic molecular structures is examined. The potential of these compounds as ideal precursors in the preparation of intriguing hydrocarbons is revealed. The pivotal role played by the sequential use of mild and forcing conditions – most notably the use of thermally- and high pressure-promoted Diels-Alder reactions – to produce oligomeric compounds in a predictable and stepwise manner is documented. Throughout these discussions, special attention has been given to the methods employed for the purification and characterization of this new class of unnatural products.

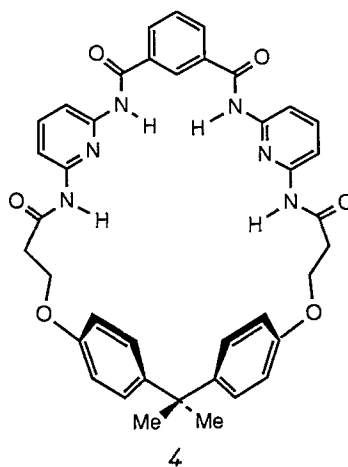
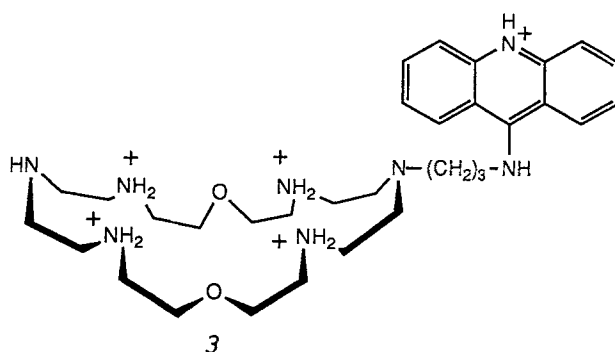
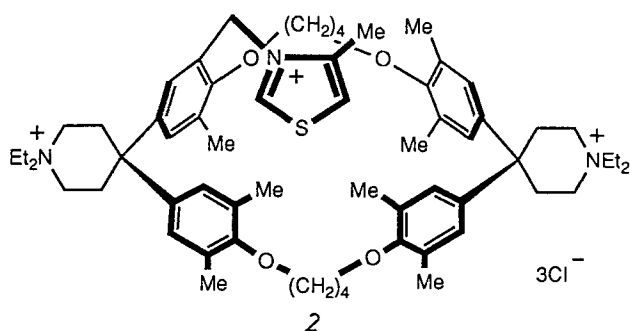
1 Introduction

1.1 Supramolecular Design Processes and Rapid Assembly

Through the many triumphs of natural product synthesis, chemists have acquired an unrivalled appreciation of chemical reactivity and synthetic methodology [1]. The disconnection approach [1, 2] shows how a structurally-complex target molecule may be broken down formally into suitable precursors which may then be assembled in a highly-designed synthetic program. However, even in the most elaborate examples [3], the synthesis of relatively small, unimolecular entities is still being considered. Furthermore, the approaches used in these syntheses often preclude any cooperativity from operating in the synthetic scheme. This must bring into question the usefulness of such procedures in the synthesis of the increasingly elaborate targets – both natural and unnatural – that are being identified in the burgeoning fields of biotechnology [4] and new materials [5]. In many of these cases, it is the overall molecular structure and ordering of functionality that is of paramount importance. Having extensively studied reactivity, the questions now being asked by chemical scientists are: (1) How much do we really know about molecular architecture, and (2) how do we obtain a compound with a desired structure in a rapid, yet controlled fashion? Increasingly, the new synthetic goals will reside in the void which lies between the unimolecular systems and the widely recognized information storage systems with high molecular weights, such as the nucleic acids, the proteins, and the glycoconjugates. A successful solution to these contemporary problems in synthesis will require unparalleled economy and efficiency in the synthetic methodologies which are developed.

The advent [6] and rapid development [7] of supramolecular chemistry has served increasingly to focus the minds of chemical scientists upon methods which might improve many aspects of molecular architecture, organization, and assembly. Above all, the desire to design and create microenvironments with specific features to aid (i) selective guest binding, (ii) transport of bound guests, and (iii) catalysis of reactions, has culminated in the delineation of those factors of critical importance in this area of molecular recognition. These factors include the steric and electronic complementarity [8] between host and guest, and the preorganization [9] of those features responsible for binding. The result has been the synthesis [10–13] of host molecules of many highly-diverse structural forms. The structures in 1–4 serve to illustrate this fact.





A premium is now being placed upon increasing the macroscopic expression of the recognition event, i.e. designing molecules with a function as well as with a form. An elegant demonstration of this approach is the supramolecular liquid crystal reported recently by Lehn [14]. As shown in Fig. 1, two complementary sub-units associate via hydrogen-bonding to form the rigid central element of the mesogenic supermolecule.

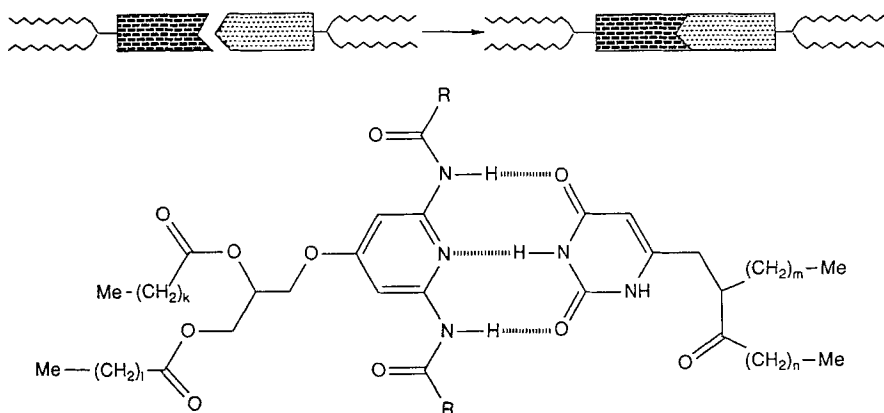


Fig. 1. A schematic representation of the formation of a mesogenic supermolecule. Lehn [14] has used hydrogen-bonding between the two complementary sub-units to form the rigid central core

Eschenmoser [15] has recently alluded to the concepts of structure-directed synthesis and autochthonous reactivity – the propensity of certain systems to undergo reactions as a consequence of their intrinsic molecular structural factors – within the context of certain biomolecules, particularly the organic cofactor, vitamin B₁₂. The formation of the AD ring junction in the corrin ligand had to be regarded as a major hurdle in any proposed chemical synthesis of cobyrinic acid (5) (Fig. 2), and hence of vitamin B₁₂. However, driven initially by the desire to identify a dark, and therefore potentially biomimetic, variant of the photochemical

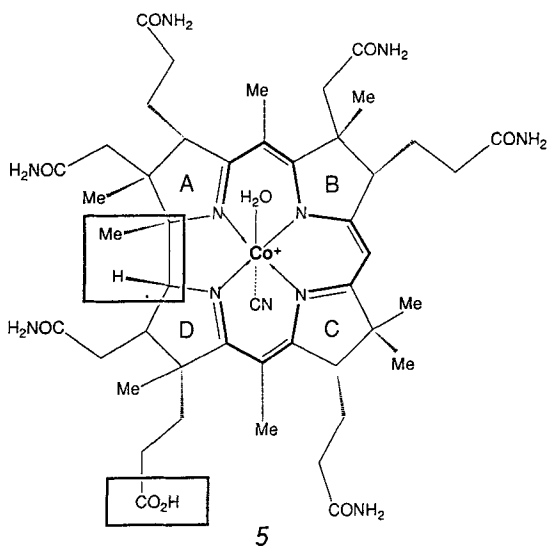


Fig. 2. The synthesis of cobyrinic acid (5) marked effectively the completion [15b, c, h, i, j] of the synthesis of vitamin B₁₂ by Woodward and Eschenmoser. Extensive studies subsequently by Eschenmoser [15a–e] have revealed that many of the structural features are attainable with surprising ease from structurally-appropriate precursors. Most notably, the four highlighted (bold) structural features represent thermodynamically-favored arrangements

AD ring closure, Eschenmoser, above all, has shown that the AD ring junction is a structural element which is formed extremely readily, and in a variety of ways, from structurally-appropriate precursors [15]. Furthermore, extensive investigations of other structural elements in **5**, such as (i) the dimensions of the macrocyclic ring and the characteristic arrangement of double bonds associated with the corrin chromophore, (ii) the constitutional arrangement of the side chains around the corrin ligand's periphery, and (iii) the specific attachment of the nucleotide loop to the propionic acid side chain situated on ring D, provoked Eschenmoser to make the comment [15a] that structural elements in **5** appeared to 'self-assemble with surprising ease under structurally appropriate preconditions; the amount of external instruction required for their formation turns out to be surprisingly small in view of the complexity and specificity of these structural elements'.

Thus, the elaborate outward complexity of a molecular structure, such as that exemplified by vitamin B₁₂, can, in principle, obscure what may be a straightforward, mechanistically comprehensible, synthetic protocol that leads to its formation.

Many other examples of outwardly complex molecular structures, whose salient architectural features appear to self-assemble from their constituent building blocks, have been documented [16]. The formation of the DNA double helix from its constituent chains is perhaps the quintessential example, whilst the perfect reconstitution of the intact tobacco mosaic virus from its constituent RNA and protein monomers also exhibits all the hallmarks of a cooperative self-assembly process [17]. The same is true of ribonuclease. Reconstitution of this enzyme in the presence of mercaptoethanol, to allow reversible exchange of the four disulfide bridges, proceeds smoothly to generate eventually only the active conformation from many possible isomeric states [18]. In each of these cases, the thermodynamic stability of the product is vital in directing its synthesis. These syntheses could therefore be termed product-directed.

Studies by Ringsdorf [19] on the ability of various amphiphilic molecules to form monolayers, multilayers, micelles, and liposomes, coupled with the potential uses of such systems in many different scientific areas, have caused him to comment [19] that 'self-organization and the construction of supramolecular systems is an interdisciplinary area which cannot be understood without the cooperation of different fields of science'. In short, cooperativity requires cooperation!

Coupling these ideas with the thesis that many of the molecular building blocks of proteins, nucleic acids, and polysaccharides are of prebiotic origin [20] has forced us to ask [21] whether such processes, starting from simple building blocks and proceeding to complex unnatural products, may represent a well-based approach towards the preparation of large, highly-ordered supramolecular arrays. One would therefore be assessing the extent to which simultaneous multiple-bond formation, and perhaps 'self-assembly' itself, may be applicable as a general synthetic paradigm (see Fig. 3).

Dramatic progress is being made in the area of product unnatural synthesis [22] with the recently reported polynuclear double-stranded helicates (see Scheme 1, Fig. 3) [23, 24], catenanes (see Scheme 1) [25–27], rotaxanes (see Scheme 2) [26, 27], as well as with the monolayers [28] developed by Whitesides [29] and others [30].

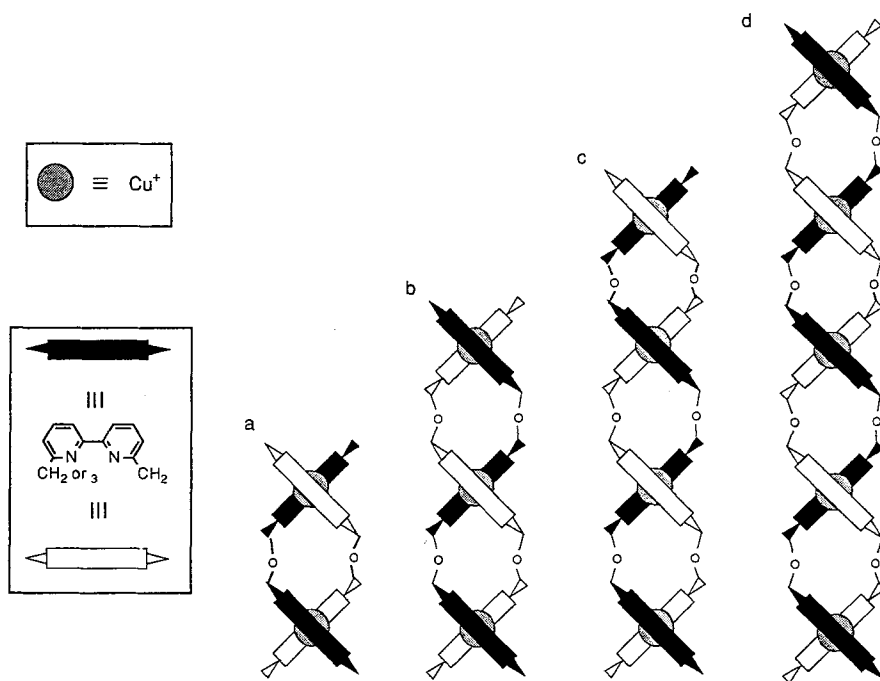
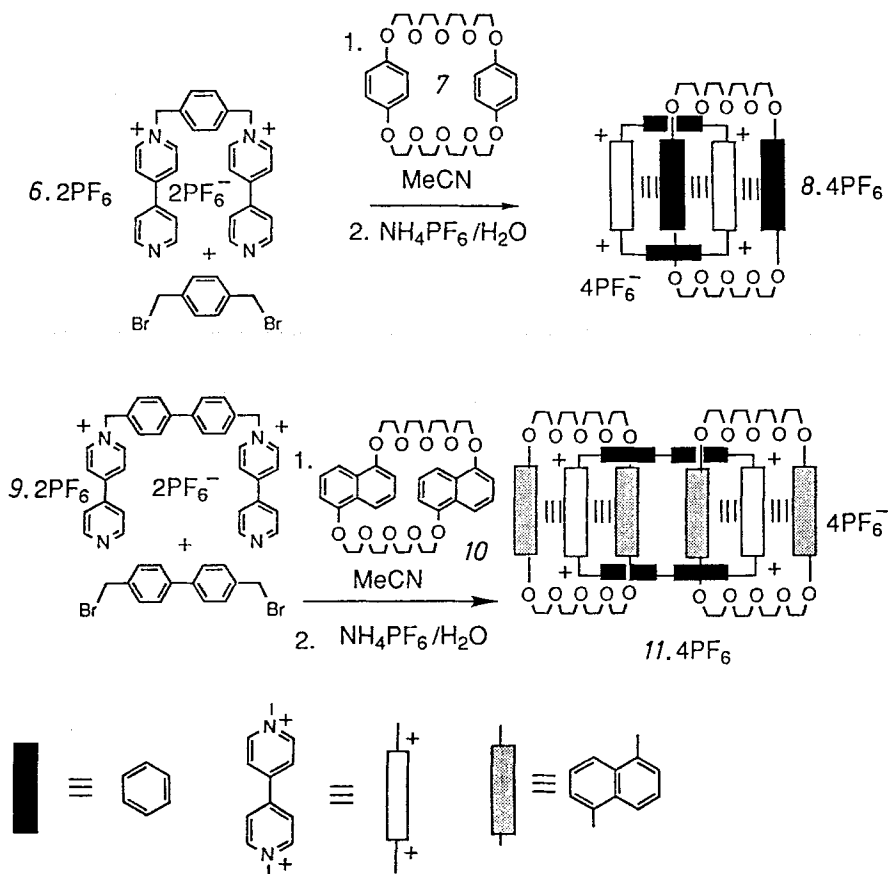


Fig. 3a–d. A diagrammatic representation of double-stranded helicases [23, 34] containing (a) two, (b) three, (c) four, and (d) five 2,2'-bipyridine subunits [23]. The Cu(I) ions function as a template around which the helicases can assemble. Furthermore, this assembly process exhibits (i) self-self recognition in the preferential pairing to the same ligand in the presence of others in the reaction mixture, and (ii) positive cooperativity in which the complexation of one metal ion facilitates the binding of the next

These systems illustrate clearly the potential power of the same gross structural properties and phenomena evident in natural systems, such as self-assembly [31], self-replication [32], cooperativity [33], and self-self recognition [34], utilizing both covalent and noncovalent bonding. Within a purely inorganic framework, the preferential formation of certain metal clusters and assemblies of C_n and Si_m , which form with particular ease when $n = 60$ and $m = 45$, represent further examples [35a–c]. Indeed, the recent isolation [35d] of the C_{60} compound, which has been dubbed buckminsterfullerene (Fig. 4), and homologs [35e–h] is now leading to a full investigation of their structural and physical properties.

The increased structural control evident in these recent studies is allowing access to novel compounds based on highly-organized three-dimensional molecular structures. At a fundamental level, these structures are beginning to address some of the potential features envisaged in the increasing application of molecules in both a mechanical [36] and electronic [37] context.



Scheme 1. Noncovalent bonding provides the ordering between the subunits prior to catenation as a result of covalent bond formation in the template-directed syntheses [26] of a [2] catenane $8.4 PF_6$ from $6.2 PF_6$ and **7**, and a [3] catenane $11.4 PF_6$ from $9.2 PF_6$ and **10**

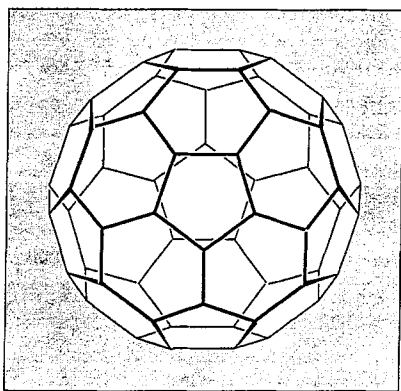
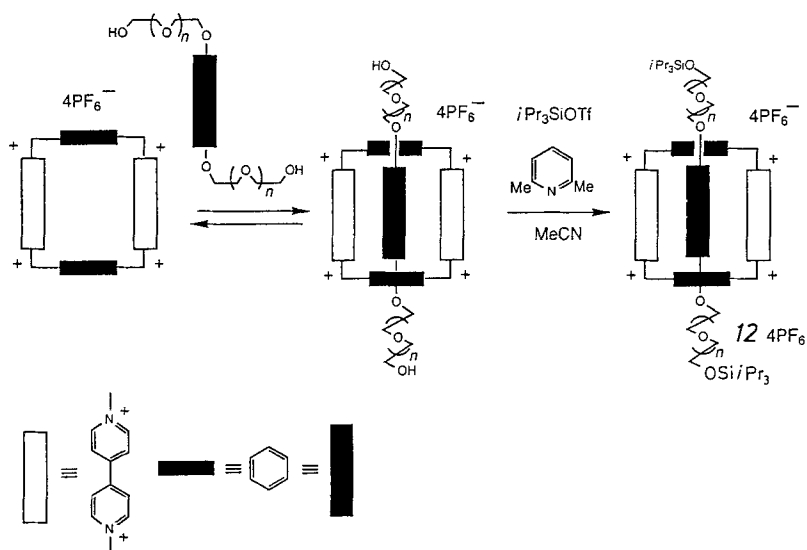


Fig. 4. Compounds like C_{60} – buckminsterfullerene alias footballene – have been the subject in recent years of much speculation [35a, b], since they constitute a third allotropic form of carbon. The recent isolation [35c, d] of C_{60} and C_{70} is now allowing their structural, physical, and chemical properties to be investigated [35e–h]



Scheme 2. Rotaxanes, such as **12**, are another group of compounds [26] that are accessible by the noncovalent bonding of the subunits prior to their further synthetic elaboration by covalent bond formation

1.2 The Diels-Alder Approach

A primary goal of one of our research programs in Sheffield was to examine the suitability of a repetitive Diels-Alder reaction sequence for the construction of rigid, highly-ordered macropolycyclic belt-type and cage-type compounds (Fig. 5) [38]. It was particularly important to be able to maintain complete control over the stereogenic centers created during reactions between bisdienes and bisdienophiles in such processes, without relying on catalysts or chiral auxiliaries. Instead, stereoelectronic information preprogrammed into the molecular frameworks of these building blocks was used to dictate their subsequent modes of reaction. In this

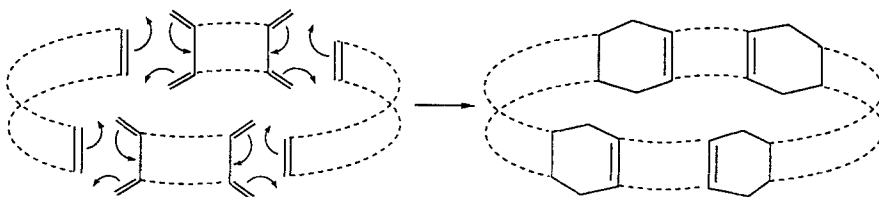


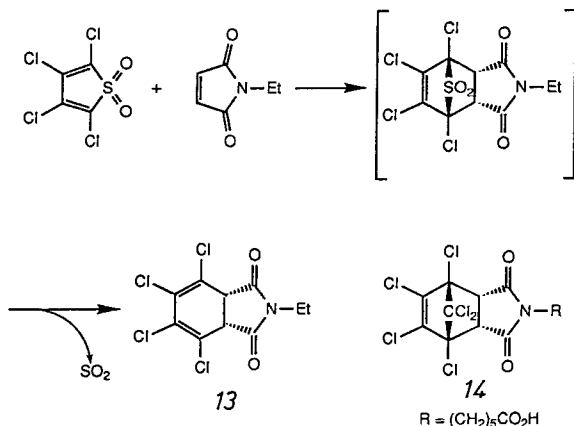
Fig. 5. Schematic representation illustrating the basic premise of the repetitive Diels-Alder oligomerization process [21]. The macropolycyclization occurs as a consequence of the reaction between bisdiene and bisdienophilic building blocks whose relative stereochemistries and stereoelectronic characteristics dictate the structural outcome of the reaction

respect, it constitutes a kinetically-controlled substrate-directed approach to synthesis.

The generality of this approach allows flexibility in design to be incorporated into the structural, electronic, and physical characteristics of the target molecules. Indeed, providing certain rules are maintained regarding the reactivities and stereoselectivities associated with the building blocks, a facile entry into a wide range of apparently complex molecular structures can be imagined [21].

The synthesis of macropolycyclic arrays — both linear and cyclic — and their derivatives is an area of growing current interest since it provides compounds of considerable academic and technological interest [39]. Although several different synthetic strategies can be envisaged for the production of polyacene and cyclacene derivatives, none have surpassed the utilization of pericyclic reactions, most notably the Diels-Alder cycloaddition, for the construction [40] of the laterally-fused six-membered ring backbone.

Diels-Alder chemistry has been a powerful tool in the armament of the synthetic organic chemist for more than half a century [41]. However, although the reaction was first reported over sixty years ago [42], activity in the field has never been greater than it is today. Successful application of the Woodward-Hoffmann Rules [43] and frontier molecular orbital theory [44] have rendered the outcome of the reaction predictable both mechanistically and in terms of the regiochemistry and stereochemistry observed. As a multiple bond-forming process, it offers a procedure by which up to four chiral centers may be created in a single synthetic step. Moreover, through the use of chiral dienes and dienophiles, along with Lewis Acid catalysts, impressive asymmetric induction [45] and catalysis [46] of the reaction have been achieved. The highly-ordered transition state attained during the reaction has made it a natural target for work in the field of catalytic antibodies.



Scheme 3. The highly-ordered transition state associated with the Diels-Alder reaction has made it a natural target for work in the field of catalytic antibodies [15]. Indeed, Hilvert [15a] has reported recently the first successfully antibody-catalyzed Diels-Alder reaction. Monoclonal antibodies elicited to the boxed hapten **14** provided both acceleration of and multiple turnover of the cycloaddition between tetrachlorothiophene dioxide and *N*-ethyl maleimide. The initial adduct decomposes by the chelotropic-extrusion of sulfur dioxide affording the dihydrophthalimide derivative **13**

The recent report of the first abzyme-catalyzed Diels-Alder reaction (Scheme 3) by Hilvert [47] represents an exciting breakthrough of great potential. Ultimately, one can envisage access to a wide range of tailored 'Diels-Alderases' [47].

The highly-ordered transition state is responsible for the negative volume of activation associated with the cycloaddition process and results in the significant acceleration of the reaction when it is performed under elevated pressures [48, 49]. The first successful demonstration of a pressure effect upon the rate of a chemical process was described one hundred years ago by Röntgen [50] in relation to the inhibition of the hydrochloric acid-catalyzed inversion of sucrose at pressures of up to 0.5 kbar. The very large effects of pressure upon the rates of Diels-Alder cycloadditions were evident from some of the earliest studies [51] of the reaction itself. Reaction rates can easily be tripled by application of 1 kbar of pressure, whereas a 60-fold acceleration can commonly be achieved by the application of 5 kbars of pressure. The attainment of the highly-organized, quasi-aromatic, transition state during the cycloaddition between the diene and dienophile is associated with a decrease in volume with respect to that of the reactants. This effect results in a negative volume of activation ΔV^\ddagger , for the process. The magnitude of ΔV^\ddagger is frequently in the range -30 – -40 $\text{cm}^3 \text{mol}^{-1}$; thus the reaction is favored by increasing pressure. Reactions governed by secondary-orbital interactions possess a further organizing factor associated with the transition state, which is absent in both reactants and products and that increase the extent of the acceleration. The synthetic outcome of this effect is most obvious in those cases

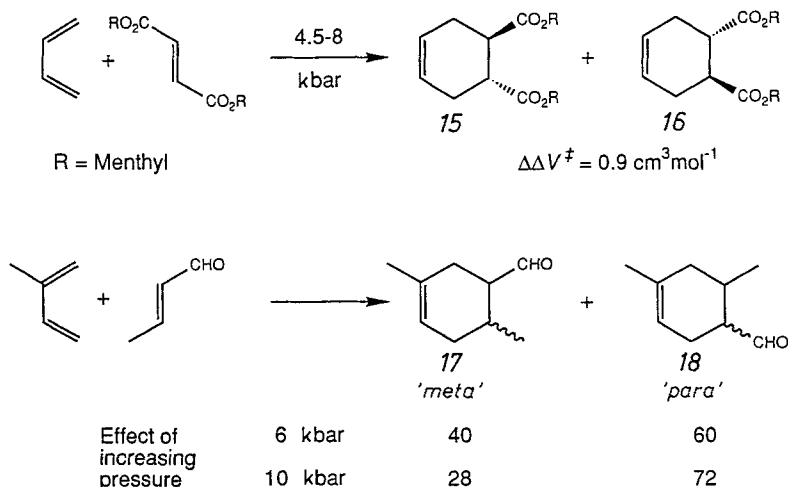


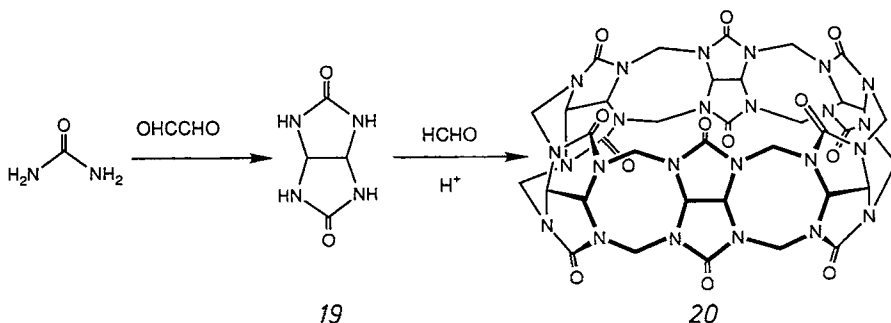
Fig. 6. Controlling stereochemistry and regiochemistry in Diels-Alder reactions by the application of very high pressure. The potential for using elevated pressures to obtain asymmetric induction is based upon exploiting the different volumes of activation between the competing diastereoisomeric transition states [48, 54]. In the first example, a $\Delta\Delta V^\ddagger$ of $0.9 \text{ cm}^3 \text{mol}^{-1}$ favors the formation of diastereoisomer **15** over diastereoisomer **16** as the pressure is increased. In the second example, the increased ratio of **18** relative to **17** illustrates the importance of pressure variations in the control of regiochemistry

in which *exo*- and *endo*-addition products can be formed. The favorable secondary orbital interactions involved in the *endo* transition state render the magnitude of $\Delta V_{endo}^{\ddagger}$ less than that of $\Delta V_{exo}^{\ddagger}$. Consequently, increasing pressure favors *endo*-addition over *exo*-addition.

The thermolability associated with many furan-based Diels-Alder adducts, such as the 7-oxabicycloheptanes, renders their synthesis under atmospheric conditions difficult without significant thermally-induced product degradation. However, under high pressure conditions, the syntheses are accelerated without danger of thermal degradation, consequently allowing access to a wide range of such compounds [52]. Moreover, the decomposition of an adduct will normally result in an increase in volume and so be effectively retarded at elevated pressures. It is only recently that high-pressure liquid-phase chemistry has gained general acceptance as a synthetic tool. Significant progress has occurred as a result of the pioneering studies of Dauben [53] and technological advances in the design and construction of the high pressure reaction systems. The possibilities for regio-chemical and stereochemical control, culminating in asymmetric induction by exploiting the different ΔV^{\ddagger} values for competing processes (Fig. 6) [54], are still in their infancy.

1.3 Belts and Cages in Supramolecular Chemistry

Compounds possessing belt-type and cage-type structures have played a central role in the development of supramolecular chemistry. The nonadecacyclic cage molecule cucurbituril (Scheme 4), reported originally in 1905 [55] and recently rediscovered and fully characterized by Mock [56], has provided a platform for an extensive and systematic study [57] of the highly-specific inclusion of alkylammonium cations and alkyldiammonium cations. The high specificity of this particular molecular recognition is a consequence of the juxtaposition of the ostensibly lipophilic interior of the cavity and the lipophobic portals, each associated with six carbonyl groups, coupled with the structural rigidity of the macropolycyclic

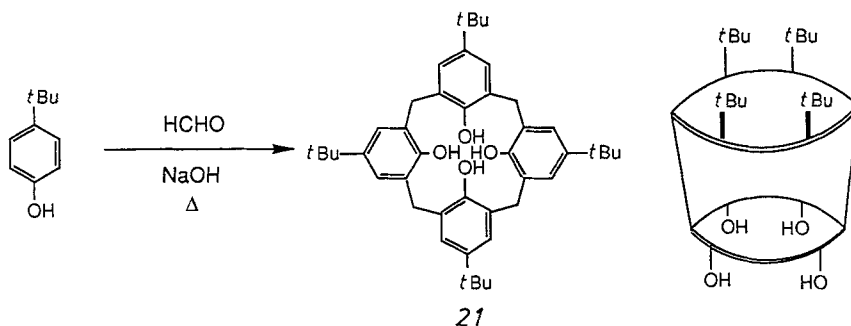


Scheme 4. The acid-catalyzed synthesis of cucurbituril **20** [55, 56] displays all of the hallmarks of a product-directed self-assembly. The product is obtained from urea, glyoxal, and formaldehyde through the intermediacy of the glycoluril **19**

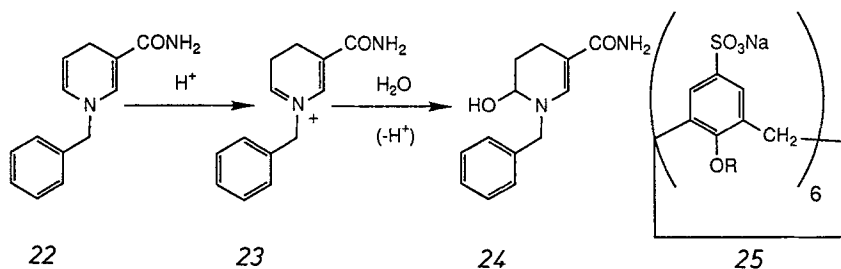
skeleton. This rigidity imposes a kinetic nature upon the ligation of the alkylammonium and alkyldiammonium guests. The rate of complex formation correlates closely with the molecular diameter of the cationic ligand, but not with the subsequent thermodynamic stability of the complex formed. This observation is in sharp contrast to the majority of complexation studies performed on more flexible hosts in which the complex formation is controlled thermodynamically. However, the kinetic ligation is reminiscent of the inherently dynamic nature of the biological recognition processes so many chemical scientists are attempting presently to model. The formation of cucurbituril occurs surprisingly easily from urea, glyoxal, and formaldehyde via a thermodynamically-controlled multi-equilibria set of reactions which display the characteristics of product-directed self-assembly.

A similar product-directed synthetic protocol can be applied to the production of the calixarene class of molecular receptors [58], so successfully pioneered by Gutsche [58, 59]. Although questions concerning the variability of the reaction outcome are still receiving attention, the general procedure, involving a base-induced reaction (Scheme 5) between formaldehyde and certain *para*-substituted phenols, allows ready access to a wide range of calixarenes. Extensive X-ray crystallographic studies have been performed upon calixarene inclusion complexes in the solid state [60]. These investigations have revealed the cone-shaped conformation to be one of several different conformations that can be adopted as a consequence of both the structural flexibility and the substitution pattern associated with the aromatic rings of the calixarene.

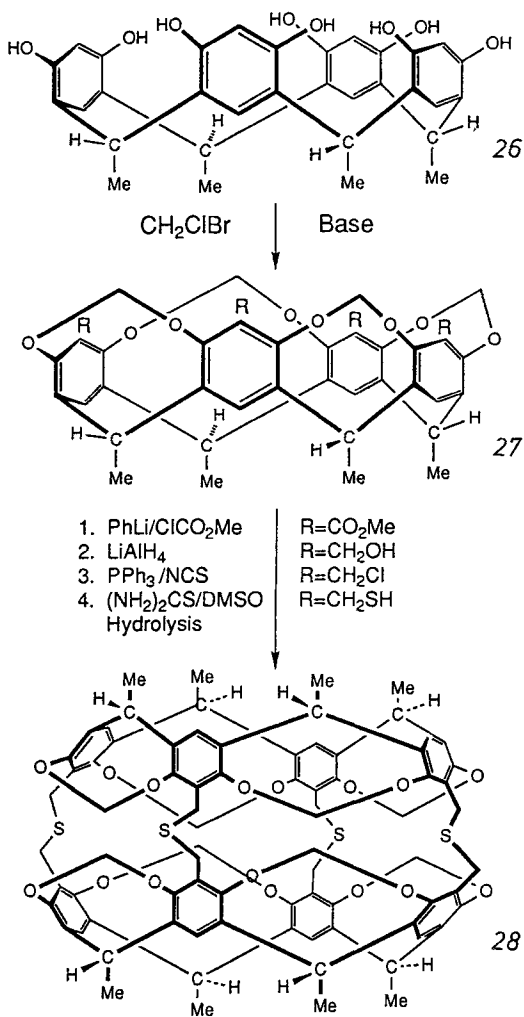
Although promiscuous in their choice of guest-compounds, the only well-defined catalytic system based upon the calixarenes, which has been documented, is the one described by Shinkai [61]. He has studied the acid-catalyzed addition of water (Scheme 6) to *N*-benzyl-1,4-dihydronicotinamide in the presence of a *para*-sulfonatocalix[6]arene and its methoxycarbonyl derivative. The polyanionic nature of the upper rim, containing the sulfonate groups, provides a site for the stabilization of the cationic intermediate. The lower rim, which carries the phenolic



Scheme 5. Base-induced condensation of certain phenols with formaldehyde leads to the production of the calixarene class of molecular receptors [58–60], e.g. **21**. The cone conformation shown in the box is only one of several possible conformations.



Scheme 6. In spite of being good host molecules, there is only one well-documented [61] catalytic system based upon the calixarenes. The acid-catalyzed addition of water to *N*-benzyl-1,4-dihydronicotinamide **22** to give **24** via **23** is accelerated by the calix[6]arene derivative **25**.

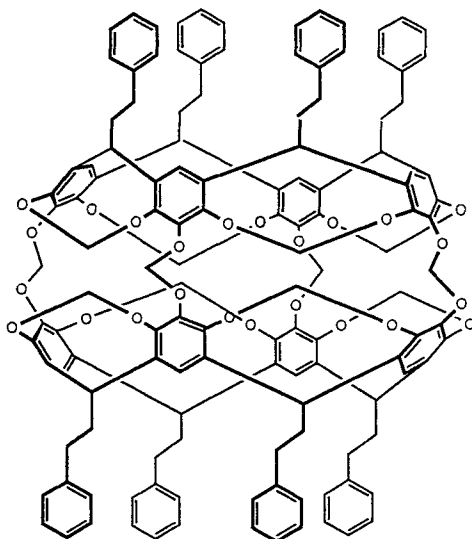


Scheme 7. The rigidification by Cram of the calix[4]resorcinarene **26** to give the cavitand **27** [65] provides the basis for the progression to the closed-shell carcerand structure **28** [66, 67].

or carboxyl groups, provides the necessary proton-donating site, to allow a comparable mode of action to that exemplified by the natural enzyme, glyceraldehyde-3-phosphate dehydrogenase [62]. Fluorescence measurements clearly confirm the presence of the substrate within the cavity.

Access to compounds of the calixresorcinarene class [63] can be achieved by an acid-catalyzed reaction between resorcinol and various aldehydes. The ease of synthesis of many calixarenes and calixresorcinarenes, along with the ready availability of the starting materials, renders them of great potential for studying both academically and industrially motivated problems. These span many areas [58] from adhesives to the selective metal ion response of calixarene monolayers [64].

The observation by Cram [65] that the rigidity of the calixresorcinarenes can be increased by bridging the remaining free hydroxyl groups on adjacent aromatic rings by methylene groups resulted in the cavitand class of macropolycycles (Scheme 7). The wide range of crystalline solvates formed with small molecules, such as MeCN, PhMe, CH_2Cl_2 , and CHCl_3 , reveals a high complementarity between host and guest. A further intuitive progression led Cram to consider covalently linking two cavitands. The outcome was the synthesis (Scheme 7) of the first closed molecular container compounds – the so-called carcerands [66]. Although the carcerands were initially difficult to handle and characterize, as a consequence of their extreme insolubility, the recent addition of solubilizing lipophilic arms to furnish compounds, such as **29**, has subsequently allowed NMR spectroscopic analyses to be performed on the carcerands and, more intriguingly, to probe the behaviour of the encapsulated solvent molecules [67]. The potential of the carcerands to act as slow-release drug-delivery systems and as targeted immunoprotein-associated chemotherapeutic agents, for example, will ensure much interest in these new compounds in the future.



29

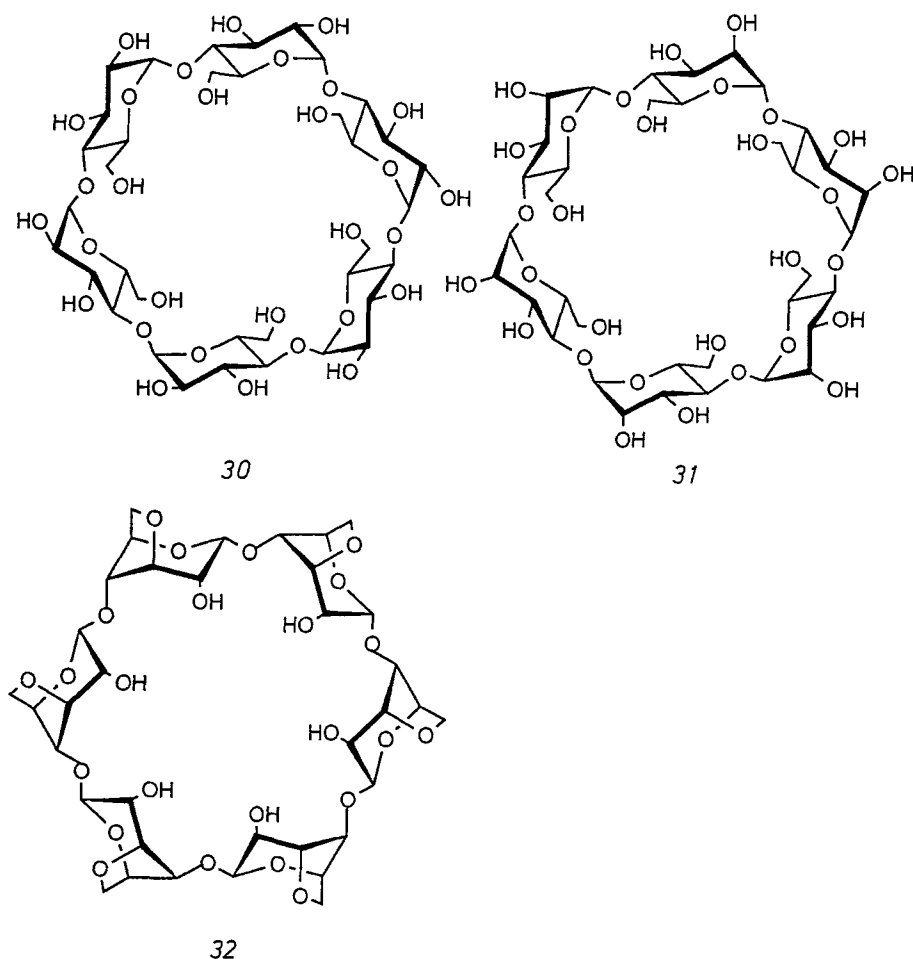


Fig. 7. The total synthesis of α -cyclodextrin **30** by Ogawa [73a] was followed by his total synthesis of a 'manno-isomer' **31** [73b] of α -cyclodextrin **30**. The potential for chemical variation of the cyclodextrin skeleton by total synthesis is considerable. The recent report of the peranhydro α -cyclodextrin **32** simultaneously by two groups [75] constitutes another important gross structural modification of the cyclodextrin skeleton

The distinguished history of the cyclodextrins, and the central role played by the pioneering studies of Cramer [68] on the molecular recognition characteristics of these compounds, in what is today widely-recognized as supramolecular chemistry, merits special mention. The recent thematic issue of Carbohydrate Research [69], which was devoted to cyclodextrins, illustrated their ever-widening application in many different fields of science and technology. Their macrocyclic constitutions are effectively rendered pseudomacropolycyclic by the cyclic network of hydrogen bonds between secondary hydroxyl groups on adjacent D-glucopyranose rings [70]. This rigidifying effect creates a toroidal cavity that can host many

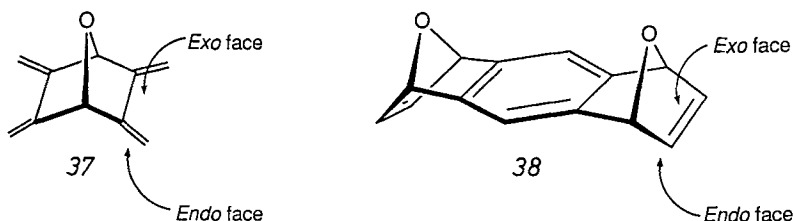
guests. Indeed, the cyclodextrins have formed the basis of some extremely elegant receptor [71] and catalytic systems [72]. Two recent synthetic advances (Fig. 7) may, however, serve to dispel the myth that cyclodextrins are locked in a structural straightjacket, amenable only to peripheral chemical modification. The chemical synthesis of a 'manno isomer' of α -cyclodextrin by Ogawa [73] followed hard on the heels of his first total synthesis [74] of α -cyclodextrin itself. Although the latter may be of purely academic interest, on account of the ready availability of the parent cyclodextrin from microbial sources, these modifications should open the door to a wide chemical variation of the basic cyclodextrin skeleton. The recent report [75] of the synthesis of a peranhydro α -cyclodextrin **32** provides yet another novel demonstration of the alteration of the gross structural properties of the cyclodextrin skeleton. The dehydration process forces each D-glucopyranose ring out of its original 4C_1 in **30** to a 1C_4 chair conformation in **32**, thereby altering the nature of the cavity from an essentially lipophilic environment to one flanked by glycosidic, glucopyranose, and free hydroxyl oxygen atoms. The subsequent effects of this structural modification upon the physical properties and binding characteristics of the peranhydro cyclodextrin merit further investigation.

2 The Substrate-Directed Synthesis of Kohnkene

2.1 Building Blocks and Autochthonous Reactivity

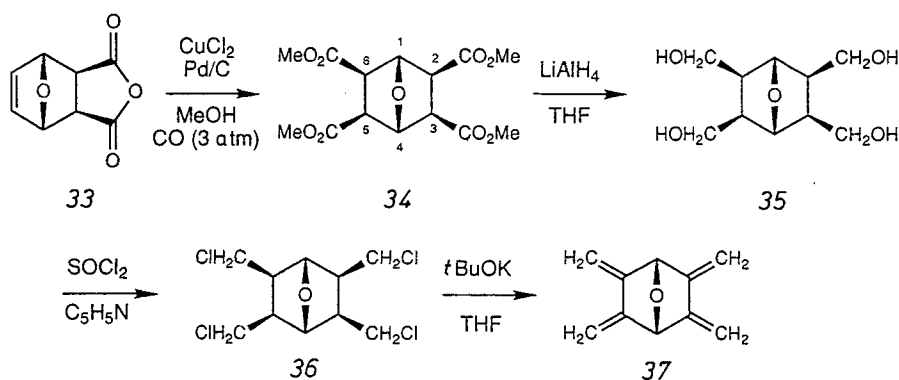
In any synthetic plan based upon a repetitive oligomerization or polymerization methodology, the failure to control strictly the mode of reaction will lead to exponentially increasing problems regarding product isolation and the consequent efficiency of the process. Especially in those cases where stereogenic centers are created, some stereochemical uncertainty associated with isomer production, and consequent heterogeneity at a configurational level, is often encountered. In modern synthetic chemistry, the production of mixtures of isomers is usually considered to be undesirable. In the case of the Diels-Alder reaction, this heterogeneity can be circumvented by using carefully chosen building blocks in which the stereoelectronic information, contained within the π -systems of both diene and dienophile, manifests itself in their highly stereoselective combination.

Observations from the recent literature on the facial-selectivities which operate during cycloadditions of π -systems incorporated into the bicyclic 7-oxabicyclo[2.2.1]heptane framework have suggested that the electronic influences inherent



within that particular rigid bicyclic system might provide an ideal means of controlling the Diels-Alder reactivity of (i) exocyclic *s-cis*-butadiene moieties, such as those present in the bisdiene **37**, and (ii) endocyclic dienophilic moieties, such as those present in the bisdienophile **38**.

As a result of its bicyclic nature, the chosen bisdiene **37**, 2,3,5,6-tetramethyldiene-7-oxabicyclo[2.2.1]heptane [76a], confers an inherently curved shape upon its subsequent Diels-Alder adducts which makes such species structurally capable of forming a macropolycyclic belt. The endoxide bridge in **37** also imparts increased solubility upon the subsequent Diels-Alder adducts, thus aiding their isolation and characterization. The solubility of these species renders them amenable to further synthetic manipulation by deoxygenation, giving rise ultimately, to a novel range of unsaturated hydrocarbons.



Scheme 8. The synthesis of bisdiene **37** [78, 112] follows the procedure described by Vogel [76]. Carbomethoxylation [77] of **33** affords the tetraester **34** with the all-*exo*-configuration [78]. The whole reaction sequence (**33** → **34** → **35** → **36** → **37**) can be performed on a large scale to provide access to significant quantities of the bisdiene **37**

Our synthesis (Scheme 8) of **37** followed that described by Vogel [76b] and is readily amenable to large scale preparation. The thermodynamic product **33** of the reaction between furan and maleic anhydride was subjected to Pd/CuCl₂ catalyzed carbomethoxylation [77], under 3 atmospheres of carbon monoxide, with simultaneous esterification of the anhydride ring. This procedure afforded the all-*exo* tetraester **34** with high diastereoselectivity. Although confirmed ultimately by X-ray crystallography [78], this stereochemical assignment was based initially upon the lack of any sizable coupling constant between the bridgehead hydrogen atoms (1,4-H) and the adjacent *endo*-methine hydrogen atoms (2,3,5,6-H) in the ¹H NMR spectrum of **34**. This observation contrasts with the 4–5 Hz *J* value which characterizes the ¹H NMR spectrum for the bridgehead and adjacent *exo*-methine hydrogen atoms observed (Figure 8) in similar systems [79]. This coupling constant criterion plays a vital confirmatory role in the stereochemical assignment of the ring junctions in many more complex compounds discussed later, for which solid state structures are not available.

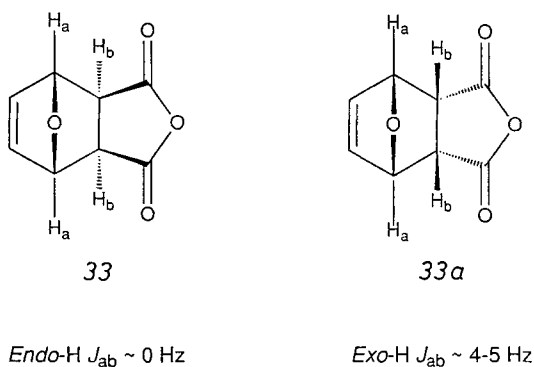


Fig. 8. The magnitude of vicinal ^1H coupling constants in **33** and **33a** allow the stereochemistry of the newly-created chiral centers during the oligomerizations to be assigned

Reduction (lithium aluminium hydride/tetrahydrofuran) of the tetraester **34** to the tetraol **35**, followed by chlorination (thionyl chloride), afforded **36** in good yield. This tetrachloride was then subjected to base-promoted β -elimination (potassium *tert*-butoxide) giving the desired bisdiene **37** in quantitative yield without purification. The sensitivity of **37** toward both thermal and photochemical degradation and its propensity to polymerize necessitated its immediate use following its preparation.

The effect upon the π -facial diastereoselectivity exhibited by exocyclic *s-cis*-butadiene moieties, such as those present in **37**, as a consequence of the electronic influences inherent in the rigid (7-oxa)bicyclo[2.2.1]heptane framework, has been the subject of much investigation and discussion [80–85] both experimentally and theoretically. Cycloadditions with common dienophiles, such as benzoquinone, methyl vinyl ketone, and methyl acrylate, have been observed to proceed predominantly at the *endo*-face of the diene moiety in the vast majority of reactions studied. The only notable exceptions to *endo*-face addition are reactions with extremely reactive dienophiles such as benzyne, dimethyl acetylenedicarboxylate, and tetracyanoethene [86]. The most compelling rationalization for the *endo*-face reactivity has been that proposed by Paquette and Gleiter [84]. It is based upon a consideration of the outcome of the mixing of the bicyclic σ -orbital framework with the diene π -orbitals. Calculations have revealed that, although there is negligible mixing between the bicyclic σ -framework and the diene HOMO (π_A), as a result of their highly disparate energies, the lower energy SHOMO (π_S) enters into a strong interaction with this framework. The consequent disrotatory tilt of the π -orbitals on the exocyclic methylene carbon atoms increases the frontier electron density on the *exo*-face of the system, whilst concomitantly decreasing that on the *endo*-face. Upon approach of a dienophile to the *exo*-face, a strong antibonding interaction develops between the HOMO of the dienophile and the diene π_S orbital. The extent of this interaction is such that the four center/four electron destabilization generated during *exo*-face attack has a calculated magnitude of 3–4 kcal mol $^{-1}$ at a distance of 2.18 Å [87]. Thus, the diastereoselectivity observed in the reactions of diene π -systems, such as those in the bisdiene **37**, can be interpreted reasonably as a kinetically-controlled interaction between the

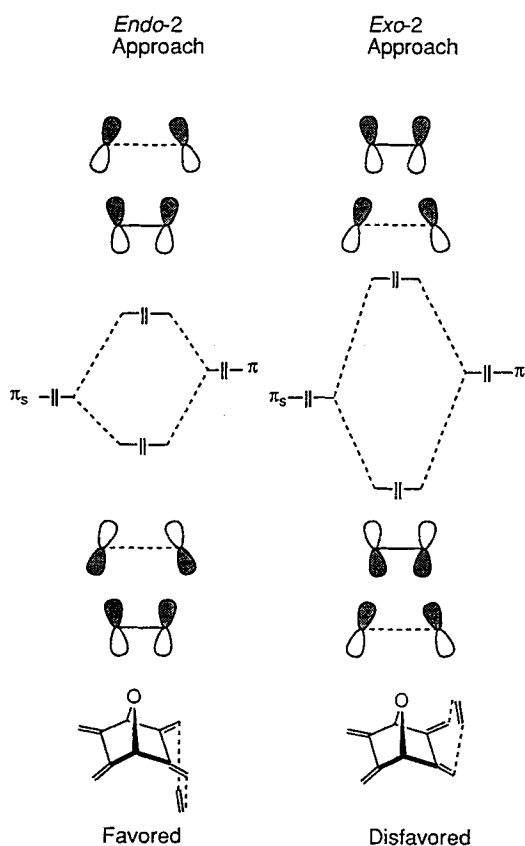
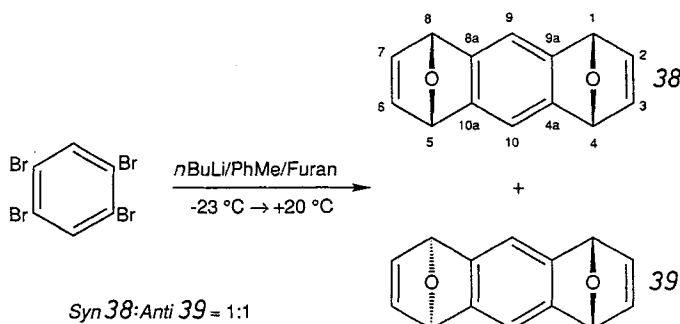


Fig. 9. A schematic representation of the interaction between the π_s orbital (SHOMO) of the *s-cis*-butadiene unit in **37** and the π -orbital (HOMO) of the dienophilic component of **38**, assuming the formation of *syn*-adducts [82, 84, 85]. The four center/four electron destabilization of *exo*-face approach (*exo*-2) is characterized by a larger net antibonding energy [87] than *endo*-face approach (*endo*-2) which is consequently favored. The orbitals show the effects of the disrotatory tilts which they are believed to experience. Note that in the terms *endo*-2 and *exo*-2, the 2 refers to the diene unit. Subsequently, the terms *endo*-1 and *exo*-1 are also employed where the 1 refers to the ene portions of the dienophilic unit



Scheme 9. The synthesis of the *syn*-bisdienophile **38** [90, 112] is initiated by the lithiation of 1,2,4,5-tetrabromobenzene with *n*-butyllithium. Trapping of the bisaryne equivalent thus generated in situ with 2 equivalents of furan affords the anthracene bisendoxide constitution as an equimolar mixture of the *syn*- and *anti*-isomers, **38** and **39**, respectively

occupied orbitals of the reactants. Therefore, it is clearly a direct consequence of the stereoelectronic information inherently present within the bicyclic frameworks.

For bisdienophiles, such as **38**, both the exceptional reactivity and *exo*-face diastereoselectivity exhibited by the endocyclic dienophile units within the 7-oxabicyclo[2.2.1]heptane framework, have been discussed at considerable length in the literature [88, 89]. The synthesis (Scheme 9) of **38**, which follows the method described by Hart [90], proceeds via the bisaryne equivalent generated by the low temperature ($-23\text{ }^{\circ}\text{C}$) lithiation of 1,2,4,5-tetrabromobenzene with *n*-butyllithium. Trapping of the bisaryne equivalent in situ with two equivalents of furan affords two diastereoisomeric bisadducts in an approximately 1:1 ratio. The desired *syn*-isomer **38** is chromatographically less mobile than **39** in which the two endoxide bridges assume the *anti*-configuration. Whilst both adducts, **38** and **39**, are indistinguishable by ^1H and ^{13}C NMR spectroscopies, X-ray structural analyses of single crystals of both adducts has allowed unambiguous assignments of their stereochemistries to be made (Figure 10) [91].

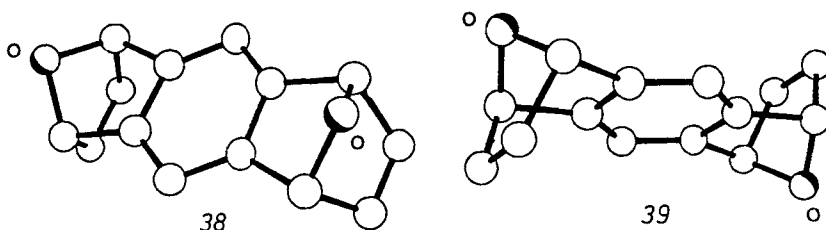


Fig. 10. The X-ray crystal structures of the *syn*- and *anti*-bisdienophiles, **38** and **39**, respectively, clearly show the relative configurations between the two endoxide bridges

The bicyclic nature and relative configurations of the two endoxide bridges in **38** imposes a curvature upon the molecule which is compatible with the subsequent macropolycyclization to give a belt-type structure. Furthermore, the endoxide bridges can be easily removed from subsequent cycloadducts by dehydration, making such compounds amenable to further synthetic modification.

In the context of the *exo*-face diastereoselectivity exhibited during cycloadditions by the dienophilic moieties in **38**, both molecular orbital calculations [89, 92, 93–95] and X-ray crystallographic analyses [96] have indicated a small, but significant, degree of pyramidalization of the alkene unit. The distortion is such that the olefinic hydrogen atoms are displaced into the *endo*-face [97]. Any other form of structural deformation is rendered virtually impossible by the bicyclic nature of the unit [98]. The origin of the pyramidalization has been attributed [99] to a staggering of the vicinal bonds associated with the olefinic and adjacent bridgehead positions. This deformation minimizes, as far as possible, the torsional strain interaction [89, 92, 92a, 93b, 95, 100, 101] between the olefinic hydrogen atom and the eclipsing hydrogen atom on the bridgehead position in the rigid bicyclic framework. An immediate consequence of this pyramidalization is to

effect a disrotatory tilt of the π_x orbitals of the double bond and so hence allow a mixing with the highest-occupied σ -orbitals of the bicyclic framework. The overall effect of the mixing is to create a node on the *endo*-face of the molecule which results in the frontier orbital electron density of the olefin being decreased on the *endo*-face and concomitantly increased on the *exo*-face [89, 101–103].

In addition, the further consequences of this π -allylic pyramidalization for the transition state of the cycloaddition process are even more profound [89, 92, 95, 100–102, 104]. As illustrated in the Newman projection in Fig. 11, the transition state for bond formation on the *exo*-face allows almost perfect staggering of the bonds under construction with those on the adjacent bridgehead position. In contrast, *endo*-face attack results in an almost completely eclipsed geometry. Calculations by Houk et al. [101] have allowed the difference in activation energy for the two competing processes to be estimated at up to 6 kcal mol^{-1} in favor of *exo*-face attack and the consequent minimization of torsional strain in the transition state. It is important to stress, however, that, although the ground-state pyramidalization is not directly responsible for the diastereoselectivity observed in the predominance of *exo*-face attack, which is clearly a transition-state phenomenon, both the pyramidalization and the diastereoselectivity have a common origin in the relief of torsional strain associated with the staggering of vicinal bonds.

It is with these factors in mind that Seebach's recent studies [105] on the stereoselective addition to pyramidalized dioxinone systems have caused him to

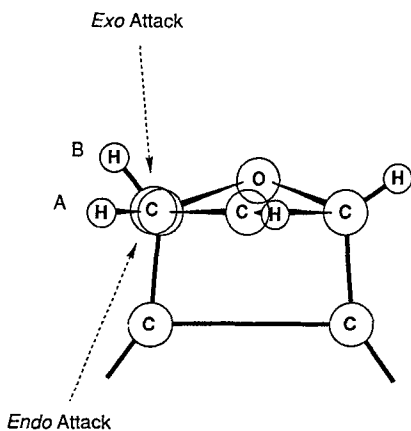


Fig. 11. A Newman projection along a selected carbon (olefinic)–carbon (bridgehead) bond in a structural fragment of the *syn*-bisdienophile **38**. This projection shows that the torsional interaction between the olefinic hydrogen atoms (*A*) and the vicinal bridgehead hydrogen atoms (*B*) are relieved by pyramidalization of (*A*) into the *endo*-face. More important in the context of the trebly-diastereoselective Diels-Alder reaction, is the staggering of the bonds under construction on the *exo*-face and the vicinal bonds on the bridgehead carbon atoms. Calculations by Houk et al. [88, 101, 102] have suggested that the difference in the activation energies for the two transition states, as a consequence of their staggered and eclipsed natures, could be as much as 6 kcal mol^{-1} .

comment that 'if a small degree of pyramidalization of a trigonal center next to a tetrahedral center is caused by the tendency to minimize torsional strain, approach of a reagent from the same direction into which pyramidalization has occurred will minimize torsion even more'. He goes on to suggest that pyramidalization may be used, albeit cautiously, as a design criterion for predicting the steric course of a reaction. The advent of crystallographic data-bases make this kind of structural information increasingly accessible to the synthetic organic chemist.

Clearly, in the case under consideration, attack of the bisdiene **37** (Scheme 8) toward the *endo*-face of the bisdienophile **38** (Scheme 9) would lead to a much greater eclipsing strain as the transition state was approached. The olefinic hydrogen atoms would initially be forced back into an eclipsing position with respect to the adjacent bridgehead hydrogen atoms, thus imparting a relatively high activation energy upon this process. By contrast, such an unfavorable situation is not encountered in the staggered geometry imposed by *exo*-face attack. This argument would suggest that the energy difference between the two competing transition states could be considerably larger than that associated with the initial ground state pyramidalization, i.e. the energy difference is magnified in the transition state of the reaction.

Bond-formation towards the *exo*-face of dienophilic units such as those in **38** may also receive a degree of stereoelectronic assistance [106–108] as a result of antiperiplanar $\sigma \rightarrow (\sigma)^*$ hyperconjugative donation from the strained σ_{1-9a} and σ_{4-4a} carbon–carbon single bonds (Scheme 9) to the σ -orbitals under construction on the *exo*-face (see Fig. 9). The corresponding situation for *endo*-face approach is less favorable, the endoxide (C–O) bonds are not able to assume such an antiperiplanar relationship.

Understanding and predicting stereoselectivities is a very delicate process. Because of the exponential relation which is involved, a product ratio greater than 99:1 results from a difference of 2.8 kcal mol^{−1} in the free energies of activation between the two diastereoisomeric transition states at 25 °C. However, a reduction of this free energy difference to 1.8 kcal mol^{−1} still gives rise to a product ratio of 96:4. Clearly, the origins of the subtle energy differences between diastereoisomeric transition states, which contain unusually long and weak bonds and abnormal bond angles are not easy to identify. Nevertheless, a combination of the various arguments for the respective diastereoselectivities exhibited by both the diene and dienophilic moieties in **37** and **38** allows a prediction [109] to be made regarding which of the four possible diastereoisomeric products (**40**, **40a–40c**), resulting from their cycloaddition, should predominate (Figure 12). However, a note of caution must be given at this juncture. Many of the calculations reported in the literature refer to molecules in a static stereochemical state. Clearly, during a chemical reaction, dynamic stereochemical effects must be taken into consideration.

In both **37** and **38** (Schemes 8 and 9), the higher frontier electron densities are associated with the *exo*-faces of the respective π -systems. Intuitively, one would expect [110] reaction to occur between a face of low electron density and one of high electron density [111], resulting in either an *exo*-1/*endo*-2 or an *endo*-1/*exo*-2 interaction. However, recalling the strong preference for approach to the *endo*-faces

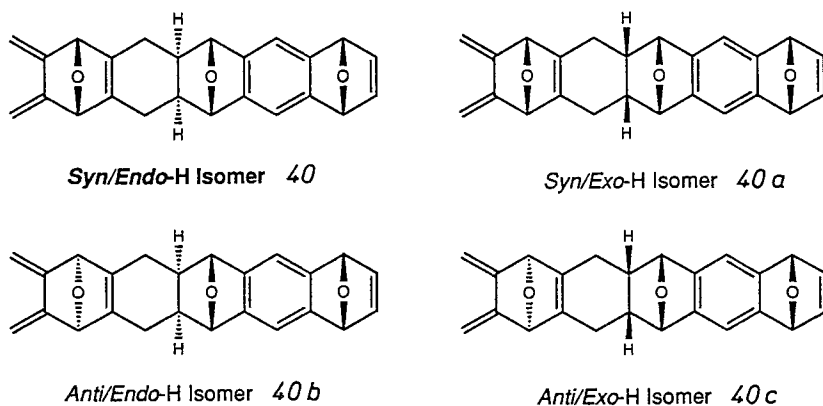


Fig. 12. The four diastereoisomeric 1:1 adducts which can be formed on reaction of the bisdiene **37** with the *syn*-bisdienophile **38**. The stereoelectronic control in operation during the reaction is such that only the *syn/endo*-H isomer **40** has been detected [21, 38, 110, 112]. The 'remote' stereochemical descriptors, *syn* and *anti*, refer to the relative configurations of the endoxide bridges across each newly-formed cyclohexene ring. The 'close' stereochemical descriptors, *exo*-H and *endo*-H, refer to the relative configuration adopted by the hydrogen atoms at the ring junctions associated with the newly created chiral centers

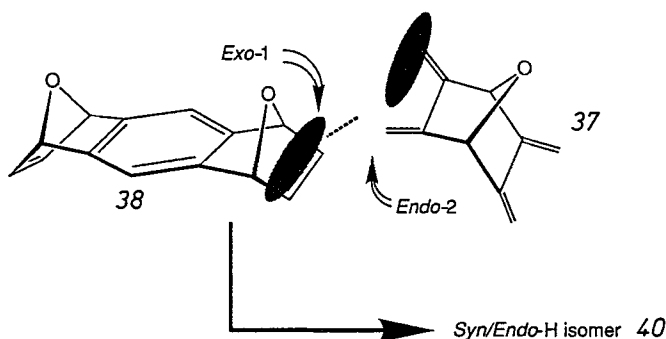


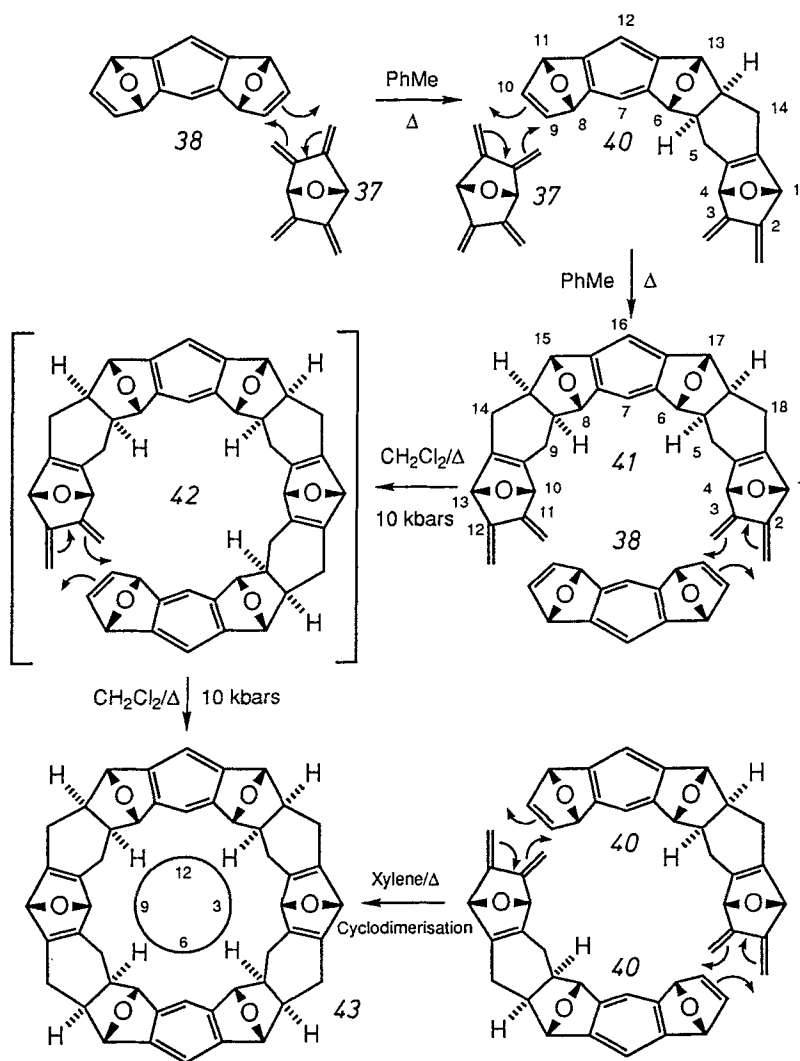
Fig. 13. By combining the factors that govern the reactivities and selectivities of the building blocks, **37** and **38**, a qualitative understanding [21, 110] of the origin of the treble diastereoselectivity exhibited in their mutual cycloaddition to give a 1:1 adduct can be achieved. Combining π -faces of high (dark) and low (light) electron density in a way that allows *exo*-face reaction (*exo*-1 approach) at the bisdienophile **38** and infers *endo*-face reaction (*endo*-2 approach) at the bisdiene **37**, does indeed afford the observed 1:1 adduct **40** with *syn/endo*-H stereochemistry across the newly-formed cyclohexene ring, providing that the two reactants approach each other in the more sterically-accessible manner which leaves the endoxide bridges *syn* with respect to each other across the newly-formed cyclohexene ring, via a *syn/exo*-1/*endo*-2 transition state

of **37**, as a consequence of the destabilization associated with *exo*-face attacks on **37**, and coupling this effect with the torsional factors favoring *exo*-face attacks on **38** would appear to favor strongly the *exo*-1/*endo*-2 interaction (Fig. 13). The stereochemical outcome of the reaction would appear to be dictated only by the stereoelectronic information inherent within the structural frameworks of the starting materials. Thus, the reaction is said to proceed in an autochthonous manner [15].

2.2 Completing a Molecular LEGO Set

The synthetic progression towards the macropolycyclic[12]cyclacene derivative **43**, dubbed kohnkene, is summarized in Scheme 10. Reaction of 2.0 molar equivalents of the bisdiene **37** with the bisdienophile **38** in toluene, heated under reflux for 12 hours, afforded only one 1:1 adduct **40** (24%) and only one 2:1 adduct **41**, in 61% yield [112]. In both cases, the stereochemistry observed across the newly-formed cyclohexene rings is *syn/endo*-H. Subsequently, the yield of the more synthetically-useful 2:1 adduct **41** was optimized to over 80% by utilization of a 2.5 molar excess of **37**. Just as only one of the four diastereoisomeric 1:1 adducts (**40**) is observed in a single reaction between **37** and **38**, the observed 2:1 adduct **41** represents only one of the ten possible diastereoisomeric products that can be obtained from the reaction of **38** with 2 molar equivalents of **37**. Since there are four ‘close’ (*exo*-1, *endo*-1, *exo*-2, and *endo*-2) and two ‘remote’ (*syn* and *anti*) configurational approaches the bisdiene **37** and the bisdienophile **38** could adopt (Figs. 12 and 13) relative to each other during cycloaddition, there are eight different transition states leading to four diastereoisomeric 1:1 adducts, i.e. there is a two-fold degeneracy between reaction pathways and reaction products. The fact that only one 1:1 adduct – the *syn/endo*-H isomer **40** – is formed (Fig. 12) via a *syn/exo*-1/*endo*-2 transition state (Fig. 13) implies that complete traible diastereoselectivity is being expressed during this Diels-Alder reaction. This remarkable stereochemical event is only surpassed by the fact that it is repeated giving only one 2:1 adduct **41** and ultimately again and again affording kohnkene **43** (Scheme 10). Thus, a stereoelectronically-controlled molecular LEGO set has been revealed.

The fact that the repetitive Diels-Alder reactions between **37** and **38** are stopped completely upon the production of the 2:1 adduct **41** under atmospheric pressure, illustrates a further facet of the reactivity of the bisdiene **37**. This compound is reported to undergo mono and bis addition [76, 80, 81, 113] in cycloadditions with moderately reactive dienophiles at very different rates. Indeed, mono-addition reportedly occurs approximately 100–300 times faster than bis-addition. This rate difference is believed to occur primarily as a result of the introduction, during mono-addition, of an endocyclic double bond on the opposite sides of the ring from the remaining exocyclic *s-cis*-butadiene unit. The outcome of this differential reactivity is that a discrete, stepwise, repetitive Diels-Alder protocol can be devised in which use is made of alternatively mild and forcing conditions to control the oligomerization process. In the case of bis-addition involving **41**, further cycloaddi-



Scheme 10. The molecular LEGO set employed in the synthesis of kohnkene **43** [21, 112]. Both the thermally-promoted and high pressure-promoted Diels-Alder reactions proceed with the same remarkable treble diastereoselectivities. The clock-face shown in the middle of structure **43** provides a convenient frame of reference for the discussion of structural features in the macropolycycle

tion of the remaining diene units requires high pressure for the reaction to proceed at an acceptable rate.

The melting points of the 1:1 adduct **40** and the 2:1 adduct **41** exceed 300 °C and their molecular ions appear at m/z 356 and 502, respectively in the electron impact mass spectrum (EIMS). Confirmation of the overall C_5 molecular symmetry possessed by structure **40** was provided by the observation of (i) 11 resonances,

with 2 overlapping at 143.1 ppm, in the broadband-decoupled ^{13}C NMR spectrum for the 12 types of heterotopic carbon atoms, and (ii) separate, well-resolved signals in the ^1H NMR spectrum for all 10 sets of heterotopic hydrogen atoms. The observation of a sharp singlet at δ 4.91 for the bridgehead hydrogen atoms 6,13-H allows the assignment of *endo*-H stereochemistry [114, 115] to the adjacent methine hydrogen atoms, 5a, 13a-H. However, it is not possible to distinguish unequivocally between the *syn/endo*-H and *anti/endo*-H diastereoisomers by NMR spectroscopic methods. The definitive characterization of the structure of the 1:1 adduct **40** was finally provided by an X-ray structural analysis (Fig. 14) of single crystals of the mono adduct **44** which is formed between **40** and anthracene in toluene when a solution of them is heated under reflux. Although the solid state structure reveals the presence of two crystallographically-independent molecules, associated with the conformations **44a** and **44b**, both possess the same relative *syn*-configurations with respect to the endoxide bridges. This is consistent with the original 1:1 adduct **40** having the *syn/endo*-H configuration. It is apparent

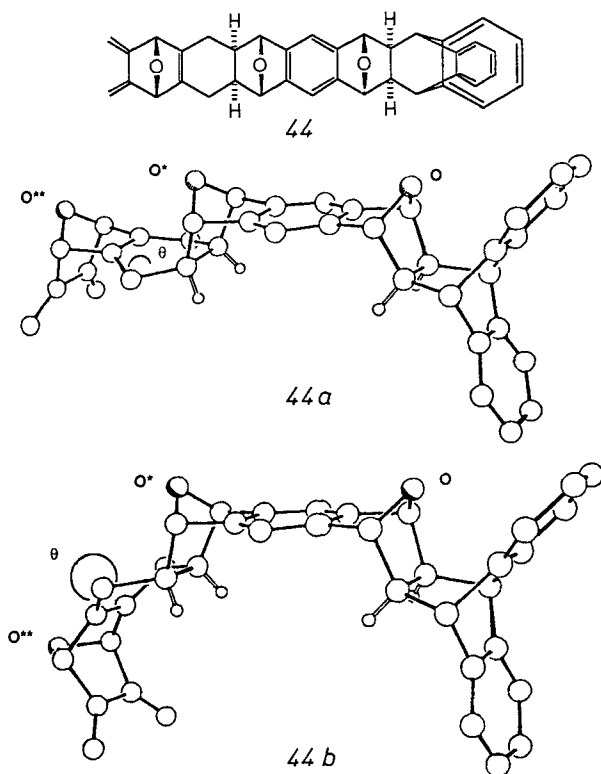


Fig. 14. X-Ray crystallographic analysis of **44** reveals the presence of two crystallographically-independent molecules of the same relative configurations [38, 112]. The major difference in the solid state structures of **44a** and **44b** is the conformation adopted by the cyclohexene rings wherein the hinge angles (θ) differ

from both conformations that the methine hydrogen atoms resulting from cycloaddition with anthracene also adopt the *endo*-H configuration. This observation confirms that the *exo*-face of the dienophilic unit in **40** is the preferred one for the approach of dienes. The significant solid state structural differences between **44a** and **44b** reside in the different boat conformations adopted by the cyclohexene rings. The boat conformation in **44a** has a hinge angle θ of 155° on the β -face, whereas in **44b** θ is 220° . The consequences for the overall curvature of the molecule is illustrated in Fig. 14. The contraction of the O*–O** distance in **44a** with respect to that in **44b** imparts a greater overall curvature upon conformation **44b**. The tilting of oxygen bridge O** towards the exocyclic *s-cis*-butadiene system has been attributed to the polarization of the π -electron density associated with the endocyclic double bond in the direction of the *exo*-face and the consequent repulsive interaction with the *syn*-related oxygen lone pair [80, 96a, b, 116, 117]. It has been proposed [80] that the extra strain necessary to restore the ethereal and etheno bridges to a more symmetrical position during cycloaddition to the diene unit could account for the reduced reactivity associated with the formation of bisadducts in such systems.

The fact that the 2:1 adduct **41** (Scheme 10) is formed directly from **40**, under atmospheric pressure, with the same *syn/endo*-H diastereoselectivity across the newly-formed cyclohexene rings imparting the C_{2v} molecular symmetry upon the structure, is supported by the observation of (i) only 9 resonances in the broadband-decoupled ^{13}C NMR spectrum for the 9 types of heterotopic carbon atoms, and (ii) separate resonances in the ^1H NMR spectrum for the 8 sets of heterotopic hydrogen atoms. The appearance of the signal for the hydrogen atoms associated with the bridgehead positions at C-6,8,15,17 as a sharp singlet is again consistent with exclusively *endo*-H stereochemistry at the adjacent methine centers. Although it has not been possible to perform X-ray crystallographic analysis to vindicate unambiguously the structure shown in **41**, it is compelling to note that the outcome of its subsequent reactions — most notably the final macropolycyclic ring-closure step — can only be interpreted in terms of the assigned (*syn/endo*-H/*syn/endo*-H) relative configuration to compound **41**.

Initially, the macropolycycle kohnkene **43** (Scheme 10) was prepared in 3.5% yield by thermal cyclodimerization of the 1:1 adduct **40** in refluxing xylene. However, the synthetic route of choice is the one which proceeds via the 2:1 adduct **41**. Ring-closure of **41** can be achieved by incorporating it with the *syn*-bisdienophile **38** in a high pressure-mediated intermolecular Diels-Alder reaction to give, presumably, the intermediate **42** which undergoes a final intramolecular Diels-Alder reaction affording **43**. The overall yield of this two-step reaction is 36%. The failure to isolate any products other than kohnkene **43** indicates that the high pressure-mediated cycloadditions between **41** and **38** both proceed with the same treble diastereoselectivities as those observed previously at atmospheric pressure for the reaction between **37** and **38**. The use of high pressure not only circumvents the problems of low reactivity associated with the second cycloaddition to the diene units in **41**, but it also takes advantage of the negative volumes of activation associated with the attainment of the highly-ordered transition states in the sequence of two Diels-Alder reactions (cf. Sect. 2.1). High

pressure accelerates these two cycloaddition processes selectively with respect to any competing reactions. Most importantly, the two cycloadditions are accelerated relative to any thermally-promoted degradations which are largely responsible for the very poor yield (3.5%) observed during the cyclodimerization of **40**.

The structural characterization of kohnkene **43** was aided by the high molecular symmetry (D_{2h}) of the molecule. The observation of (i) only 7 resonances in the broadband-decoupled ^{13}C NMR spectrum for the 7 types of heterotopic carbon atoms, (ii) separate resonances in the ^1H NMR spectrum for the 6 sets of heterotopic hydrogen atoms, and (iii) the lack of any signals for either the olefinic or *s-cis*-butadiene reactive termini were consistent with a closed macropolycyclic structure. The observation of a molecular ion at m/z 713 for $[\text{M} + \text{H}]^+$ in the positive-ion fast atom bombardment mass spectrum (FABMS) provided further evidence for the structure **43**. Final unambiguous identification of **43** was achieved by its X-ray crystallographic analysis (Fig. 15). After much effort, highly unstable single crystals were obtained by slow evaporation of a chloroform solution of **43**. Upon removal of the solvent, the crystals collapsed rapidly to give an amorphous powder. This problem was overcome by collecting data whilst the crystals were maintained in a sealed tube under an atmosphere of chloroform.

The macropolycycle **43** possesses a crystallographic center of symmetry. Consequently, the two aromatic residues are parallel with an interplanar separation between them of 7.9 Å. Examination of the unit cell provides an explanation for the high instability of the crystals. The macropolycyclic rings are arranged in parallel edge-to-face layers with 12 disordered chloroform molecules sandwiched

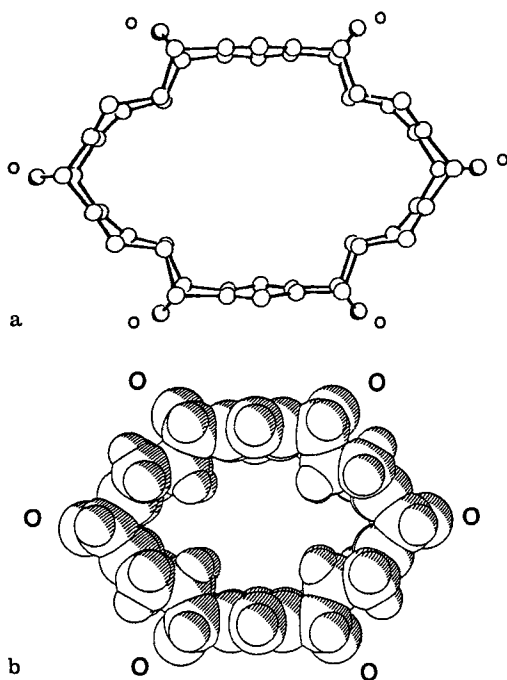


Fig. 15a, b. The structural characterization of kohnkene **43** was completed by a full X-ray crystallographic analysis of single crystals grown by slow evaporation of a chloroform solution of **43**. Both (a) ball-and-stick and (b) space-filling representations are shown. The six endoxide bridges can be seen clearly flanking the outer rim of the cavity, whereas the cavity itself is occupied partially by the 4 pairs of *endo*-methine hydrogen atoms

in between them. These molecules of solvation are lost spontaneously upon removal of the crystals from their mother liquors, with concomitant collapse of the crystals. The reduction of the hinge angle (θ) to 130° from that observed in the anthracene adduct **44b** (155° , Fig. 14) provides a quantitative measure of the increased strain imposed upon the system by the closure of the macropolycyclic ring. The interplanar separation of the aromatic residues is of the appropriate amount to accommodate an aromatic guest molecule. Indeed, preliminary piezoelectric studies have demonstrated [118] a selective response of **43** to nitrobenzene. Whether an interaction between the nitrobenzene and the aromatic residues in the cavity of **43** is occurring as a consequence of stabilizing edge-to-face interaction [119, 120] has not been established with any certainty.

2.3 Molecular Belts as Precursors to Novel Hydrocarbons

In addition to being an appealing and novel synthetic target in its own right, kohnkene **43** represents a key precursor to a wide range of exotic hydrocarbons (Fig. 16). In particular, access to the $[n]$ beltenes [121], the $[n]$ collarenes [122], and the $[n]$ cyclacenes [123–136], along with many other saturated hydrocarbons, can be envisaged.

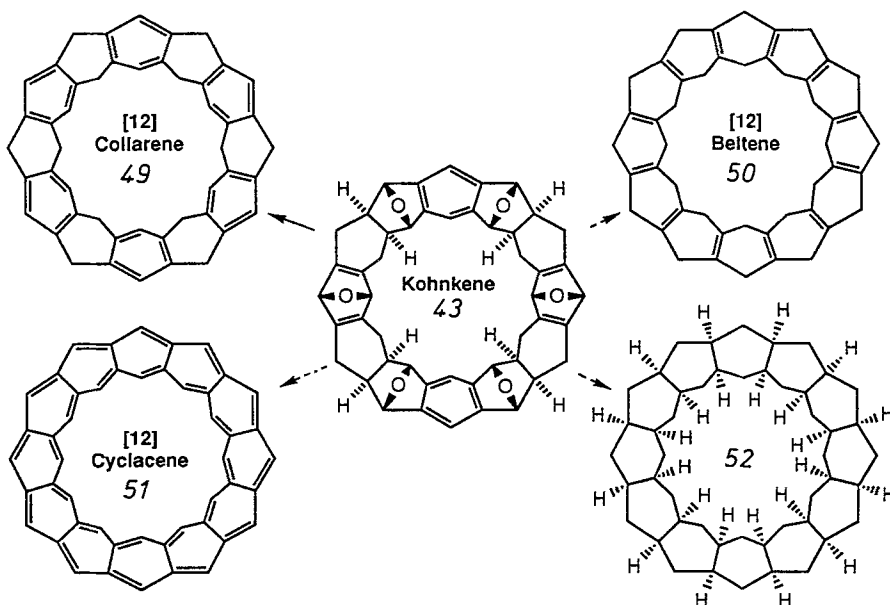
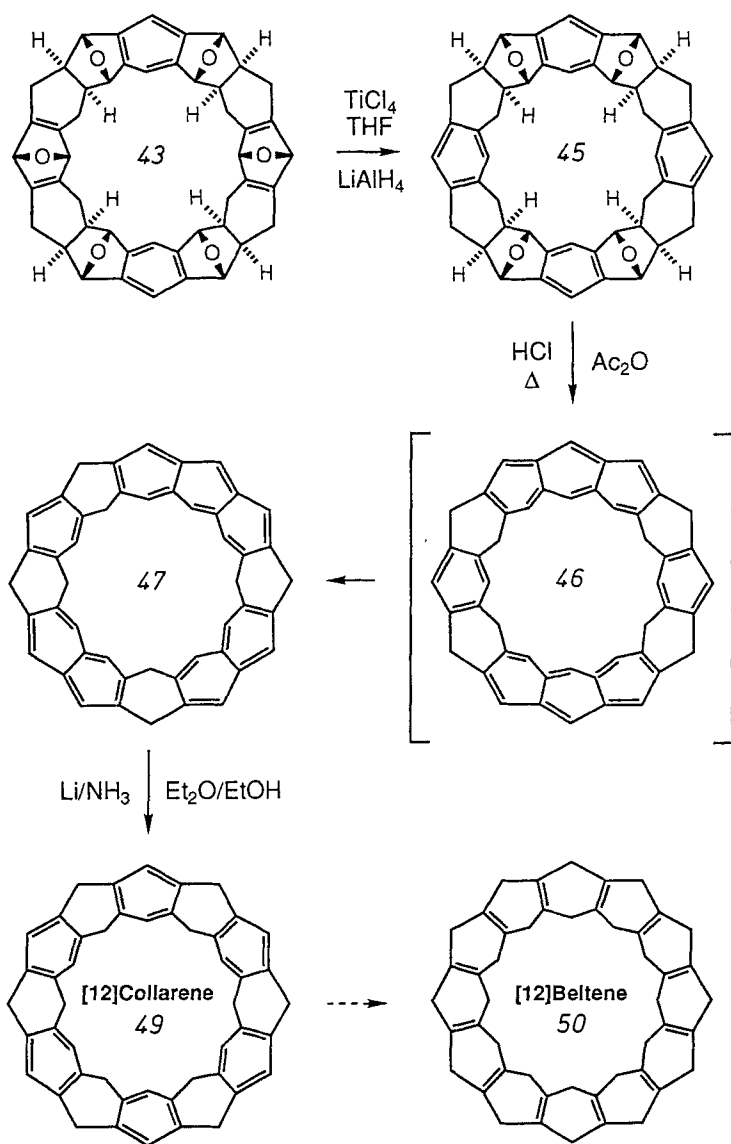


Fig. 16. Apart from being an appealing target in its own right, kohnkene **43** represents a potential precursor to a wide range of extremely novel cyclacene derivatives such as **49**, **50**, and **51**, and saturated hydrocarbons, such as **52**. To date, [12]collarene **49** marks the extent to which further synthetic elaboration [122] has progressed in our laboratories



Scheme 11. The synthetic route to [12]collarene **49** progresses via deoxygenation of kohnkene **43** to afford dideoxykohnkene **45**. Acid-catalyzed dehydration of **45** gives a mixture of isomeric hydrocarbons, including presumably **46**, from which **47** is isolated as the major product (56%) [21, 122]. A Birch reduction of **47** ceases upon the production of the highly-stable [12]collarene structure **49**

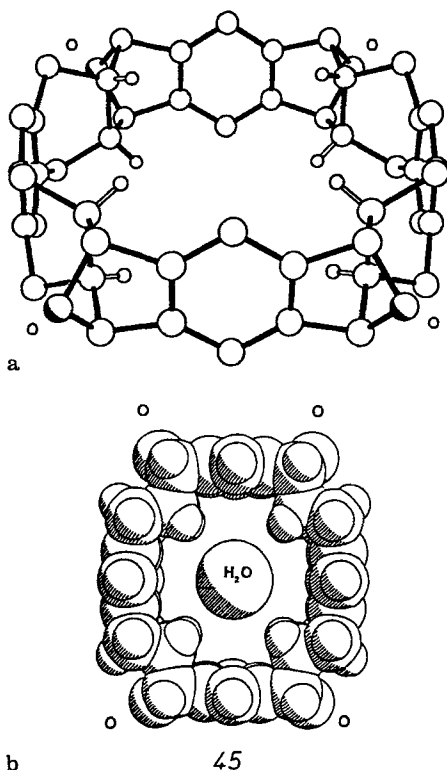


Fig. 17a, b. The X-ray crystal structure of dideoxykohnkene **45** [122]. Deoxygenation of kohnkene **43** results in the incorporation of two further aromatic rings into the macropolycycle. Both the ball-and-stick (**a**) and the space-filling (**b**) representations illustrate the increased rigidity of the cavity expressed in its 'Celtic cross-like' structure

Deoxygenation [127, 128] of the two 7-oxabicyclo[2.2.1] heptadiene moieties located at 3 and 9 o'clock within the macropolycyclic framework of **43** afforded (Scheme 11) dideoxykohnkene **45** in 43% yield. Positive-ion FABMS revealed a strong molecular ion at m/z 680 for **45** with very little fragmentation consistent with retention of the highly-stable closed macropolycyclic structure. The D_{2h} molecular symmetry of **45** is in complete agreement with the observation of (i) 7 resonances in the broadband-decoupled ^{13}C NMR spectrum for the 7 types of heterotopic carbon atoms, and (ii) separate signals in the ^1H NMR spectrum for the 6 sets of heterotopic hydrogen atoms. The greatly increased aromatic nature of the cavity in **45** is illustrated by the enhanced shieldings experienced by the four sets of *endo*-hydrogen atoms which are directed towards the center of the cavity. With respect to kohnkene, they exhibit an upfield shift of 0.73 ppm which lowers them on the δ scale from 1.85 in **43** to 1.12 in **45**. Confirmation of structure **45** (Fig. 17) was obtained by an X-ray structural analysis [122] of single crystals grown by vapor diffusion of chloroform into a methanolic solution of **45**. The major feature of the solid state structure is the rigid 'Celtic cross-like' nature of the hydrophobic cavity, with the interplanar separation of the parallelly-disposed aromatic residues increasing from 7.9 Å in **43** to 9.6 Å for those located at 6 and 12 o'clock respectively in **45**. The separation of the mean planes of the aromatic

rings located at 3 and 9 o'clock in **45** is 8.9 Å. The reduction in the hinge angle (θ) associated with the four cyclohexene boat conformations to 123° provides a further qualitative indication of the increase in macrocyclic strain as a consequence of the introduction of the two planar aromatic residues. Intriguingly, a highly disordered water molecule resides at the crystallographic center of the macropolycyclic ring, even although it would appear to be too remote to enter into any stabilizing interaction via hydrogen bonding or van der Waal's interactions with the inner surface of the cavity itself. The hydrogen atoms of the water molecule are directed principally towards the opposing pairs of *endo*-methine hydrogen atoms at 1.30 and 7.30 on the macropolycycle, whilst maintaining a distance of

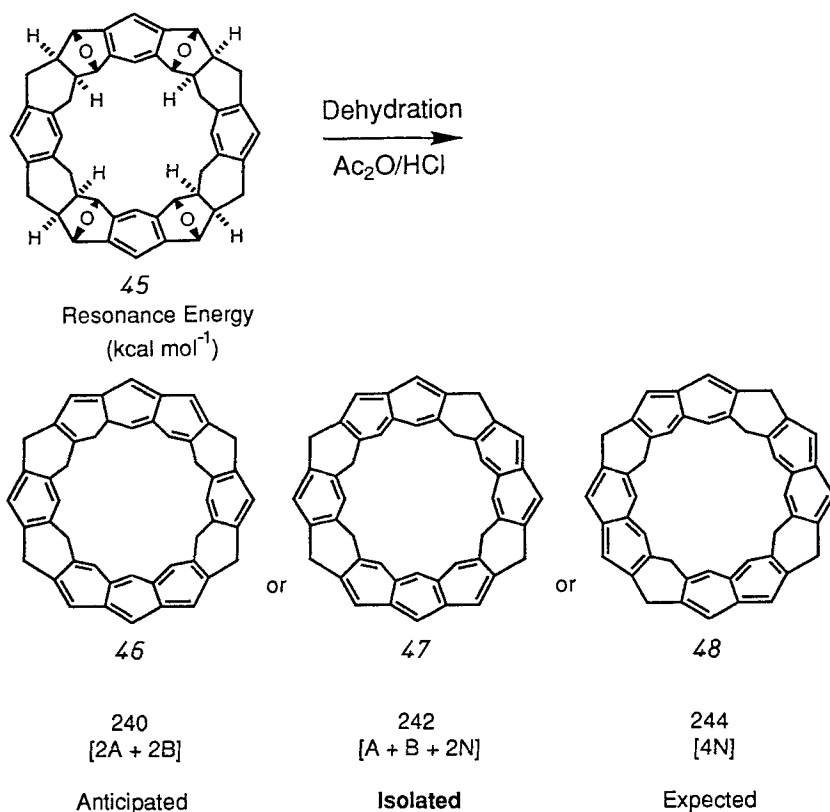


Fig. 18. The adduct isolated from the dehydration of dideoxykohnkene **45** is only one of many possible constitutionally-isomeric products. Symmetry considerations played an important part in the identification of **47** [122] as the major isolated product because it is the only constitutionally-asymmetric hydrocarbon. In calculating the resonance energies (RE's) displayed in the boxes, A, B, and N represent Anthracene, Benzene, and Naphthalene units, respectively, and are assumed, to a first approximation, to have RE's of 84, 36, and 61 kcal mol⁻¹, respectively

at least 2.7 Å from the cavity wall. The oxygen atom of the water molecule is 3.5 Å distant from any of the four sets of *endo* hydrogen atoms or indeed from any other potentially interactive sites in dideoxykohnkene **45**.

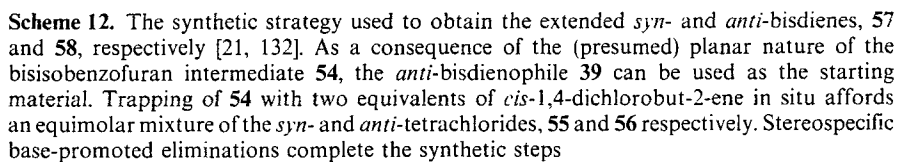
Dehydration [122] of **45** afforded a mixture of isomeric hydrocarbons from which **47** (Scheme 11) was isolated as the major product (56%) after silica gel chromatography using hot benzene as the eluant. The complete dehydration of **45** is supported by the observation of a strong molecular ion (EIMS) at m/z 608 for **47** with a similarly strong peak at m/z 304 for the doubly-charged ion. Although not the expected product, the asymmetric constitution characteristic of **47** is consistent with the presence of four anisochronous AB systems in the ^1H NMR spectrum associated with the four constitutionally-heterotopic 1,4-cyclohexadiene units uniquely present in **47** and absent in the other two constitutional isomers, **46** and **48**, shown in Fig. 18. The appearance of resonances at δ 6.91 and 7.77 for the hydrogen atoms associated with the single benzene ring and the central benzenoid ring of the single anthracene unit, respectively, are also consistent with structure **47** proposed for the hydrocarbon. The significant upfield shift of the signal resonating at δ 7.77 from its more usual chemical shift value (~ 8.2 ppm) associated with the hydrogen atoms on the central benzenoid ring of anthracene derivatives, may be a consequence of the lower aromatic character of this ring as a result of its presumably deformed shape.

In an attempt to prepare [12]beltene **50** (Scheme 11), a Birch reduction was performed on **47**. However, this reaction ceased upon production of the highly-symmetrical [12]collarene **49** for which desorption EIMS clearly revealed a molecular ion at m/z 612 for **49** with little fragmentation. This observation is consistent with the extremely high stability of the compound **49**. High-field ^1H NMR spectroscopy showed the presence of only one AB system associated with the homotopic 1,4-cyclohexadiene units [129]. The identification of only one long range allylic coupling constant is considered to be a manifestation of the rigid boat-like conformation adopted by the highly-strained 1,4-cyclohexadiene units.

3 The Generality of the Substrate-Directed Approach

3.1 Strips, Coils, and Bigger Belts

The success of a repetitive Diels-Alder approach for the rapid assembly of the [12]cyclacene derivative kohnkene **43** (Scheme 10) raises the obvious questions concerning the generality and adaptability of such a synthetic approach and therefore its potential to afford a range of new chemical compounds. It is reasonable to assume that introducing different structural elements or functionalities into the bisdiene and bisdienophile building blocks should allow the construction of compounds with different molecular architectures. Their use would also provide further understanding of the effects of structural modifications upon the reactive π -systems and consequently upon the diastereoselectivities that are expressed during cycloadditions.



The synthetic route (Scheme 12) to the extended bisdiene **57** followed that described recently by Hart [130]. Reaction of the *anti*-bisdienophile **39** with two equivalents of 1,2,3,4-tetraphenylcyclopentadienone afforded the pentacene derivative **53** in almost quantitative yield. Although the relative configuration of the endoxide bridges is undoubtedly that of the starting (*anti*) bisdienophile, the relative stereochemistries of the carbonyl bridges are most likely to be both *syn* and *anti* giving rise to a mixture of diastereoisomers. However, this stereochemical heterogeneity is of no lasting consequence in the production of the bisisobenzofuran [131] intermediate **54**. Thermolytic decomposition of **53** results in the chelotropic expulsion of carbon monoxide, followed by a facile retro-Diels-Alder reaction in which two equivalents of 1,2,3,4-tetraphenylbenzene are produced along with the diradical **54**. Trapping of **54** with the weak dienophile, *cis*-1,4-dichlorobut-2-ene, *in situ* resulted in the production (Scheme 12) of a diastereoisomeric mixture of the *syn*- and *anti*-tetrachlorides, **55** and **56**, respectively, in a combined isolated yield of 65% [132]. As a result of the (presumed) planar nature [133] of the bisisobenzofuran equivalent **54**, the original *anti*-endoxide stereochemistry is unlikely to be retained. Thus, the generation of an equimolar mixture of *syn*- and *anti*-isomers must reflect, either a simultaneous non-stereoselective reaction of both diene units, or, alternatively, a stepwise procedure in which the mode of the second cycloaddition is independent of the mode of the first. The different configurations of the two tetrachlorides **55** and **56** render them easily separable by silica gel chromatography. The less polar *anti*-isomer **56** is the chromato-

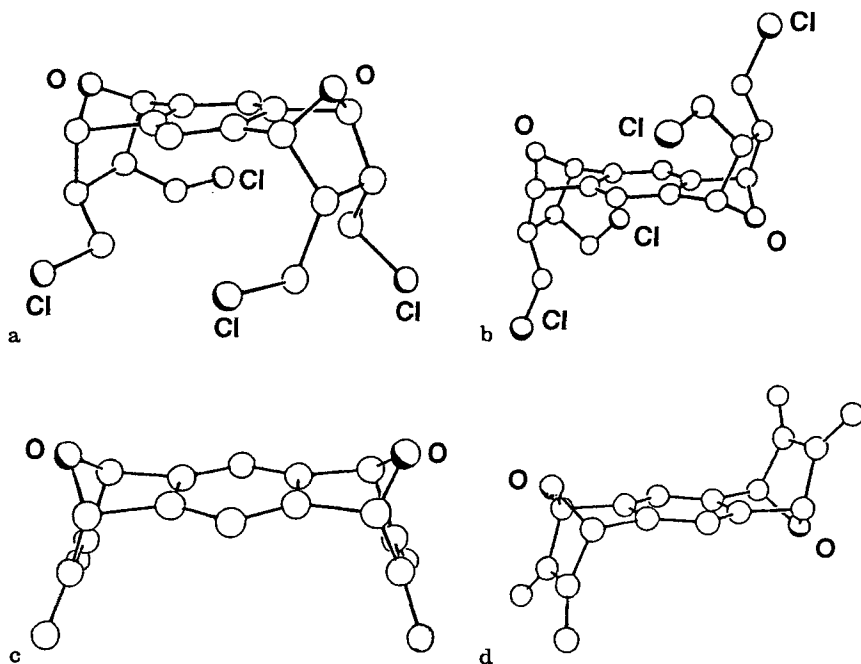
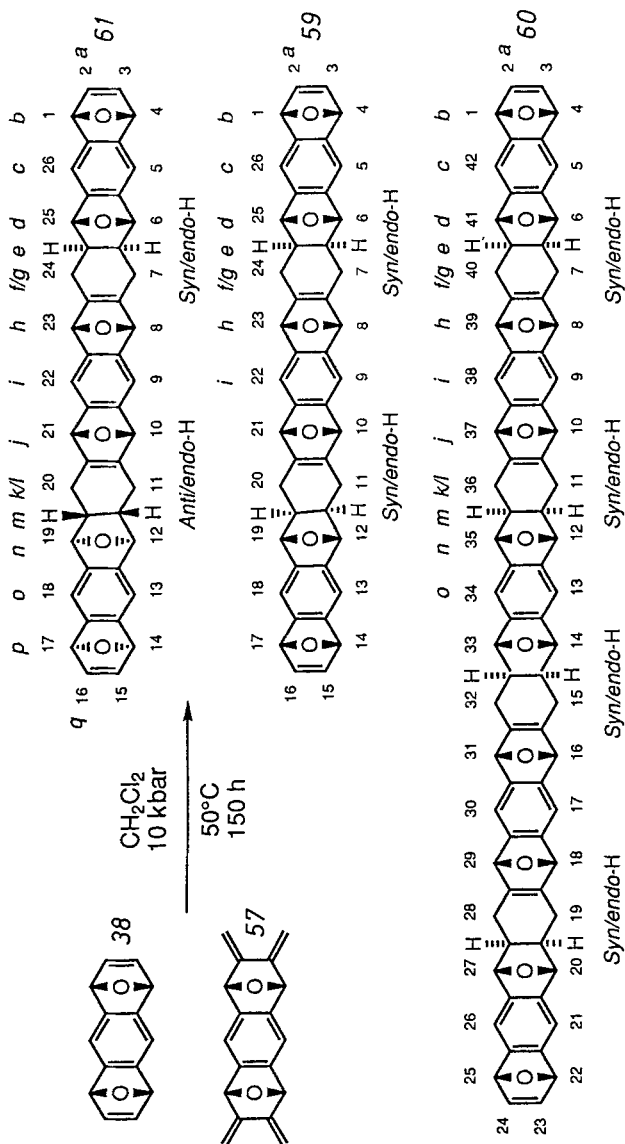


Fig. 19a–d. The X-ray crystal structures of the **a** *syn*- and **b** *anti*-tetrachlorides, **55** and **56**, respectively [79], and the extended **c** *syn*- and **d** *anti*-bisdienes, **57** and **58**, respectively [134, 135]

phically more mobile species when a chloroform-carbon tetrachloride mixture (1:1 v/v) is employed as the eluant. Single crystals of **55** and **56** were grown by vapor diffusion of hexane and pentane, respectively, into dichloromethane solutions. Both sets of crystals were suitable for X-ray crystallographic analysis [79]. The different relative configurations for the endoxide bridges assigned above were confirmed by the solid state structures (Fig. 19). Close inspection of these structures reveals that all the chloromethyl groups have the *endo*-configuration, indicating that, although the approach of the dienophile could occur from either above or below the plane of the diene systems in **54** (Scheme 12), the reaction is highly diastereoselective with respect to each furan ring and leads to the *endo*-configuration exclusively. As a consequence, a vicinal coupling constant of 4 Hz between the bridgehead hydrogen atoms (1,4,5,8-H) and the *exo*-methine hydrogen atoms (2,3,6,7-H) can be observed in the ^1H NMR spectrum of the tetrachloride adducts, **55** and **56**. The observation of a coupling constant of this magnitude between the bridgehead hydrogen atoms and the adjacent *exo*-methine hydrogen atoms provides a positive means by which the configuration (i.e. *exo* or *endo*) of the methine hydrogen atoms on the newly-created chiral centers can be deduced from ^1H NMR spectra.

Base-promoted stereospecific β -eliminations, using potassium *tert*-butoxide in tetrahydrofuran at 0 °C, have been performed on both **55** and **56** to afford (Scheme 12) the extended *syn*- and *anti*-bisdienes, **57** and **58**, respectively, in quantitative yield [132]. The presence of the central aromatic ring between the six-membered bicyclic rings carrying the two diene units acts, not only as a rigid spacer unit, but it also stabilizes the exocyclic *s-cis*-butadiene moieties, and so significantly reduces their Diels-Alder reactivity. Whilst this deactivation necessitates the use of high pressure when they are used as building blocks in synthesis, it does allow the full spectroscopic characterization of both **57** and **58** to be carried out with ease. The appealing aspect of this synthetic approach to the extended *syn*-bisdiene **57** is the utilization as the starting material of the *anti*-bisdienophile **39** (Scheme 12) which is obtained alongside the *syn*-bisdienophile **38** and consequently is available without any extra synthetic effort. The more synthetically-valuable *syn*-bisdienophile **38** can therefore be used exclusively as a building block for macropolycyclic compounds in later Diels-Alder oligomerizations. Single crystals of both **57** and **58**, suitable for X-ray structural analysis were obtained [134, 135] by vapor diffusion of pentane into dichloromethane solutions. Their solid state structures are shown in Fig. 19. The curved nature of the extended *syn*-bisdiene **57** is evident.

Since the sp^2 character of the orbitals in the aromatic ring diametrically-opposite the exocyclic *s-cis*-butadiene moieties in **57** and **58** (Scheme 12) reduces their Diels-Alder reactivity, ultra-high pressure is required to promote their reaction with dienophiles. Indeed, reaction of **57** with two equivalents of the *syn*-bisdienophile **38** under 10 kbar of pressure in dichloromethane at 45 °C for 150 h afforded (Scheme 13), after column chromatography on silica gel using chloroform containing 2% methanol as eluant, two major products [132]. The chromatographically more mobile and major product of the reaction, was characterized as the 2:1 adduct **59**. Its formation results from reaction of one equivalent of the extended *syn*-bisdiene **57** with two molar equivalents of the *syn*-bisdienophile **38**. The



Scheme 13. High pressure-promoted cycloaddition between the *syn*-bisdienophile **38** and the *syn*-bisdiene **57** has afforded [21, 132] three fully characterized products, **59**, **60**, and **61**. The 2:1 adduct **59**, with *syn/endo*-H stereochemistry across both of the newly-formed cyclohexene rings, is the major component of the reaction mixture. However, a minor 2:1 isomer **61**, which has *anti/endo*-H stereochemistry across one of the newly-formed cyclohexene rings, has also been characterized. The conformation adopted by the 3:2 adduct **60** is of considerable interest. ^1H NMR Spectroscopy suggests that the terminal dienophilic units may overlap to afford a 'Swiss-roll'-like conformation

observation of a molecular ion at m/z 682 for $[M]^+$ in the positive-ion FABMS is consistent with the proposed constitution of **59**. The C_{2v} molecular symmetry, as revealed in the structure of **59**, is supported fully by the observation of (i) 12 resonances in the ^{13}C NMR spectrum for the 12 types of heterotopic carbon atoms and (ii) separate resonances in the ^1H NMR spectrum for the 9 sets of heterotopic hydrogen atoms. Three different resonances are clearly visible in the ^1H NMR spectrum of **59** at δ 5.59, 5.32, and 4.90. These correspond to the hydrogen atoms associated with the bridgehead positions, 1,4,14,17-H, 8,10,21,23-H, and 6,12,19,25-H, respectively. The signal centered on δ 5.59 exhibits both a vicinal and allylic coupling to the proximal olefinic hydrogen atoms, 2,3,15,16-H, ($J_{1,2} \sim J_{1,3}$ 1.3 Hz) consistent with the presence of the two dienophilic systems in structure **59**, whilst the resonance associated with 6,12,19,25-H at δ 4.90 appears as a sharp singlet. The lack of any multiplicity in this signal suggests that the adjacent methine hydrogen atoms, 6a,12a,18a,24a-H, must have the *endo*-configuration. The fact that **59** reacts with the bisdiene **37** (Scheme 8) to afford the macropolycyclic derivative **63** (see later) supports the assignment of *syn/endo*-H stereochemistry across both of the newly-formed cyclohexene rings. Consequently, in the formation of **59**, the very high degree of treble diastereoselectivity expressed in the Diels-Alder reaction between the bisdiene **37** and the bisdienophile **38** has been retained in the reaction of the extended *syn*-bisdiene **57** with the *syn*-bisdienophile **38**. The stereochemistry is generated via exclusively *endo*-face approach to the diene units in **57** and *exo*-face approach to the dienophilic units in **38**. This, however, is not the whole story.

The detection and characterization (Scheme 13) of the minor isomer **61** of the 2:1 adduct **59** is of considerable interest [132]. The *anti/endo*-H configuration present across one of the newly-formed cyclohexene rings in **61** appears to be the result of mutual *exo*-face approach involving both the dienophile and diene units, i.e. the stereoelectronic control which has operated previously on the diene π -system has been relieved to a small extent. Whereas the molecular ion obtained for **61** by positive-ion FABMS is observed at m/z 682 for $[M]^+$, in common with that obtained for **59**, separate resonances are observed in the ^1H NMR spectrum for the 17 sets of heterotopic hydrogen atoms present in **61**, including those associated with the 6 discrete bridgehead hydrogen atom environments. The number of signals observed in the ^1H NMR spectrum is indicative of a low overall molecular symmetry (C_s) for **61**. Confirmation of the C_s molecular symmetry for this compound is provided by the observation in the ^{13}C NMR spectrum of 23 signals for the 23 heterotopic types of carbon atoms. Most important, the *endo*-H stereochemistry, as a result of the exclusively *exo*-face reaction of the dienophilic moiety in **38** with the diene **57**, has been preserved. Retention of the *endo*-H configuration is indicated by the appearance in the ^1H NMR spectrum of the signals for 6,25-H and 12,19-H, at δ 4.91 and 4.90, respectively, as sharp singlets, which show no coupling behavior to the adjacent *endo*-methine hydrogen atoms. The ^1H NMR chemical shift data, which is summarized in matrix-fashion in Table 1, is particularly useful in emphasizing some of the structural similarities, whilst highlighting the structural differences between these adducts and some of the cyclacene derivatives reported later in this review.

Table 1. A comparison of the ^1H NMR chemical shift data for structurally-related hydrogen atoms located on the Diels-Alder oligomerization adducts, provides a means by which their structural similarities and differences may be highlighted. The alphabetic descriptors correspond to those included in the Schemes outlining the syntheses of these compounds

$^1\text{H}^a$	q	p	o	n	m	m/l	j	i	h
59	—	—	—	—	—	—	—	7.08	5.32
60^b	—	—	7.08	4.92	1.60 to 1.69	2.35 to 2.55	5.35 or 5.32	(s, 2H) 7.05	(s, 4H) 5.32 or 5.35
61	6.95	5.58 or 5.56 (dd, 2H)	(s, 2H) 7.06 or 7.04 (dd, 2H)	(s, 4H) 4.91 or 4.90 (s, 2H)	(m, 4H) 1.82 to 1.92 (m, 2H)	(m, 8H) 2.30 to 2.60 (m, 4H)	(s, 4H) 5.32 or 5.31 (s, 2H)	(s, 4H) 7.07 (s, 2H)	(s, 4H) 5.31 or 5.32 (s, 2H)
63	—	—	—	—	—	—	—	7.12	5.31
65	—	—	—	—	—	—	—	(s, 2H) 7.11	(s, 4H) 5.30
67	—	—	—	—	—	—	—	(s, 2H) 7.11	(s, 4H) 5.30
								(s, 2H)	(s, 4H)

^a In many cases, it is not possible to differentiate with certainty assignments of hydrogen atoms to signals with very similar δ values

^b The δ values (recorded in boldface) for protons a, b, and c are all shifted to higher field relative to those for the 'same' hydrogen atoms in **59** and **61**

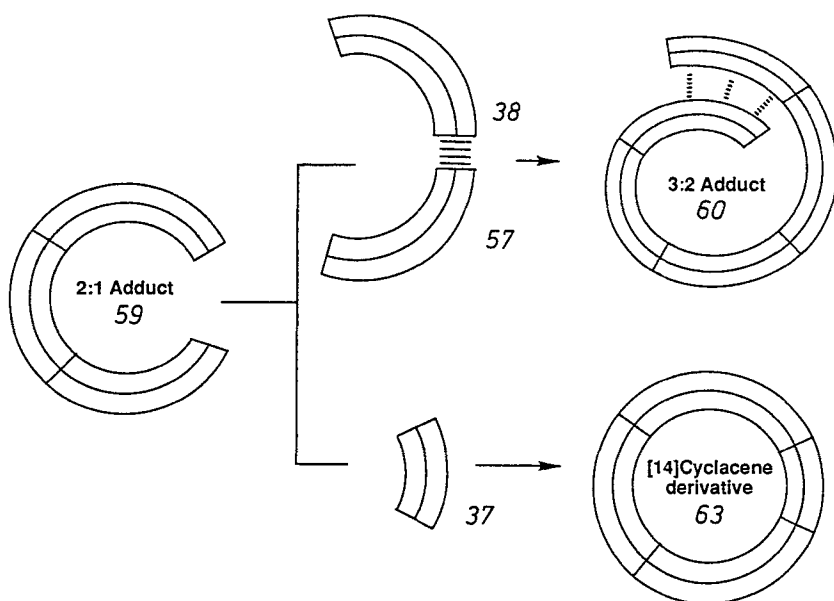
The isolation of **61**, as well as the expected *syn/endo*-H/*syn/endo*-H isomer **59** (Scheme 13), illustrates, for the first time, evidence for the existence of a second reaction pathway operating during these repetitive Diels-Alder reactions. HPLC analysis of the reaction mixture, isolated after a high pressure reaction between **38** and **57**, revealed the product ratio of **59**:**61** to be 18:1. The question of whether **61** owes its origin to the existence of a second, less favorable reaction pathway in a kinetically-controlled process, or is, in fact, the outcome of a degree of thermodynamic control, involving a retro Diels-Alder reaction, followed by recombination, will be discussed in Section 3.2.

The final compound to be eluted from the column was another solid material, which was characterized [132] as the bisdienophilic 3:2 adduct **60** (Scheme 13). In this case, 3 equivalents of the *syn*-bisdienophile **38** have reacted with 2 equivalents of the extended *syn*-bisdiene **57**. The observation of molecular ions at m/z 1155 for $[\text{M} + \text{H}]^+$ by positive-ion FABMS and at m/z 1153 for $[\text{M} - \text{H}]^-$ by negative-ion FABMS is consistent with the constitution shown by the molecular

f/g	e	d	c	b	a	w	x/y	z
2.35 to 2.55 (m, 8H)	1.78 to 1.82 (m, 4H)	4.90 (s, 4H)	7.05 (s, 4H)	5.59 (dd, 4H)	6.85 (dd, 4H)	—	—	—
2.35 to 2.55 (m, 8H)	1.60 to 1.69 (m, 4H)	4.85 (s, 4H)	6.98 (s, 4H)	5.42 (dd, 4H)	6.52 (dd, 4H)	—	—	—
2.30 to 2.60 (m, 4H)	1.82 or 1.92 (m, 2H)	4.90 or 4.91 (s, 2H)	7.04 or 7.06 (s, 2H)	5.56 or 5.58 (dd, 2H)	6.91 (dd, 2H)	—	—	—
2.35 to 2.55 (m, 8H)	1.80 to 1.94 (m, 4H)	4.92 (s, 4H)	6.95 (s, 4H)	4.87 (s, 4H)	—	1.58 to 1.74 (m, 4H)	2.35 to 2.55 (m, 8H)	5.04 (s, 2H)
2.20 to 2.70 (m, 8H)	1.80 to 1.90 (m, 4H)	4.92 (s, 4H)	—	4.82 (s, 4H)	—	1.55 to 1.65 (m, 4H)	2.20 to 2.70 (m, 8H)	3.10 (t, 2H)
2.30 to 2.67 (m, 8H)	1.80 to 1.87 (m, 4H)	4.92 (s, 4H)	6.94 (s, 4H)	4.86 (s, 4H)	—	1.62 (br s, 4H)	—	5.01 (s, 2H)

formula **60**. The observation of separate resonances for (i) the 20 types of heterotopic carbon atoms in the ^{13}C NMR and (ii) the 15 sets of heterotopic hydrogen atoms in the ^1H NMR spectrum, support the structural assignment of **60**. In particular, the observation in the ^1H NMR spectrum of 5 discrete signals at δ 5.42, 5.35, 5.32, 4.92, and 4.85 for the hydrogen atoms, 1,4,22,25-H, 8,18,29,39-H, 10,16,31,37-H, 12,14,33,35-H, and 6,20,27,41-H, respectively, provides further evidence for this structure. The coupling constants ($J_{1,2} \sim J_{1,3}$ 1.3 Hz) visible between the signals for the terminal bridgehead hydrogen atoms (1,4,22,25-H) and the adjacent olefinic hydrogen atoms 2,3,23,24-H, indicate the presence of the dienophilic units at the termini of **60**. The observation of sharp singlets showing no observable multiplicity at δ 4.92 and 4.85 for 12,14,33,35-H and 6,20,27,41-H, respectively, is also consistent with the *syn/endo*-H stereochemistry across each of the four newly-formed cyclohexene rings in **60**, and hence the operation of high, if not complete, treble diastereoselectivity during each cycloaddition in this Diels-Alder oligomerization process.

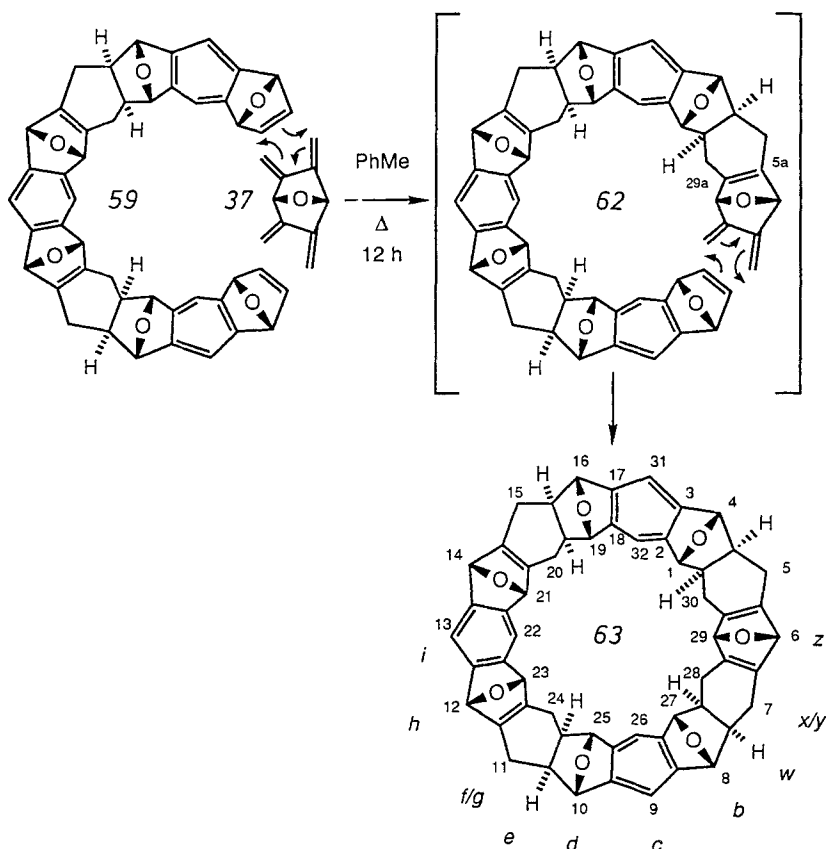
The gross conformation adopted by the 3 : 2 adduct **60** is of considerable interest. Since the compound possesses 19 laterally-fused six-membered rings, its inherent curvature, as evidenced by the inspection of molecular models, must result in mutual overlap of the dienophilic termini. Two gross conformations, that could conceivably be adopted, are (i) a helical spring-like one, in which the backbone of the molecule is distorted above and below the mean plane perpendicular to, and bisecting, the six-membered rings which are centrally-located, or, (ii) a coiled 'Swiss-roll' type of structure in which the two ends of the molecule overlap and occupy the same plane. The upfield shifts (Table 1) of 0.36, 0.17, and 0.07 ppm, respectively, associated with the hydrogen atoms, 2,3,23,24-H, 1,4,22,25-H, and 5,21,26,42-H, respectively, when compared to the signals for the equivalent hydrogen atoms in the ^1H NMR spectrum of the 2 : 1 adduct **59**, suggest a mutual overlapping of the termini of the molecule so that the hydrogen atoms identified enter (Scheme 14) into the shielding cone of the aromatic ring at the opposite end of the molecule. Attempts to verify the existence of this 'Swiss roll' conformation by X-ray crystallography have been unsuccessful, since vapor diffusion of pentane, hexane, and diisopropyl ether into dichloromethane solutions of **60**, as well as slow evaporation of a chloroform solution of **60**, failed to give single crystals suitable for X-ray structural analysis.



Scheme 14. A diagrammatic representation of the macropolycyclization of the 2 : 1 adduct **59** with the bisdiene **37** to afford the [14]cyclacene derivative **63** [21, 132]. The stereoelectronic match between the termini of the starting materials is such that the bisdiene 'snaps' into place, without the anticipated need for high pressure. Alternatively, reaction of **59** with the 1 : 1 adduct, formed between **38** and **57**, may be responsible for the production of the 3 : 2 adduct **60**. The cartoon drawn of **60** illustrates the overlap between opposite termini which is suggested by ^1H NMR spectroscopy

The failure to isolate a [16]cyclacene derivative from the reaction between the *syn*-bisdienophile **38** and the extended *syn*-bisdiene **57** (Scheme 13), as well as the evidence for some overlap between the reactive termini in the nonadecacyclic 3:2 adduct **60**, suggests that the optimum ring size for a closed macropolycycle made up of these building blocks may indeed be smaller than that provided by 16 laterally-fused sixmembered rings.

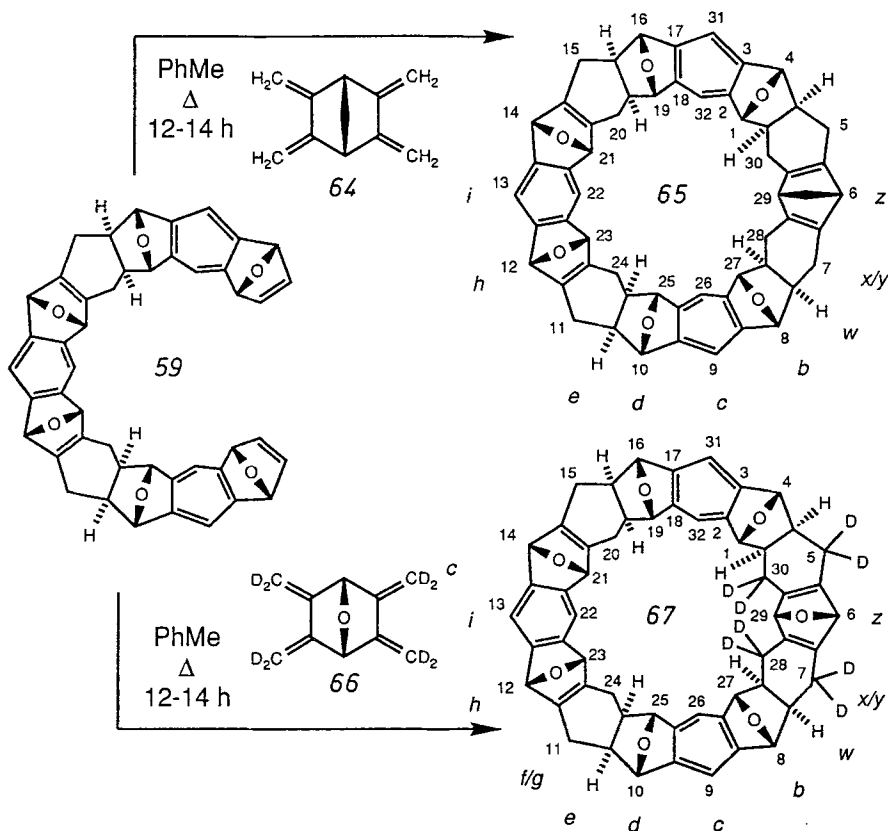
This led us to surmise that closure of the 2:1 adduct **59** with one equivalent of the bisdiene **37** to afford a [14]cyclacene derivative, such as **63** (Scheme 15), might be a favorable process. Indeed, on heating a small excess of the bisdiene **37** with the 2:1 adduct **59** under reflux in toluene for 14 h, such a macropolycyclic ring closure proceeds in an extremely efficient manner [132]. The facile nature of this macropolycyclization was unexpected. The initial intermolecular Diels-Alder reaction between **37** and **59** was expected to yield the acyclic adduct **62**. The



Scheme 15. High pressure is not always necessary: macropolycyclization of the 2:1 adduct **59** with the bisdiene **37** affords the [14]cyclacene derivative **63** in a remarkably facile reaction [21, 132]. Although it is presumably an intermediate, no trace of the acyclic adduct **62** has been detected in this process. The acceleration of the final intramolecular cycloaddition is rationalized as being a result of the extremely favorable stereoelectronic match between the remaining diene and dienophilic units in **62**

consequent introduction of sp^2 character into the bond diammetrically-opposed to the remaining exocyclic *s-cis*-butadiene unit (C5a–C29a) should deactivate this diene unit towards the final intramolecular Diels-Alder reaction. This effect has been illustrated in the requirement for high pressure to promote the cycloaddition between **38** and **41** to afford kohnkene **43** (Scheme 10). Thus, the need for a high pressure reaction to achieve macropolycyclization was anticipated. However, to date, no trace of the acyclic adduct **62** (Scheme 15) has ever been detected during the thermally-promoted macropolycyclization. The reaction proceeds directly to the macropolycycle **63**, without the need for high pressure, giving this [14]cyclacene derivative in 78% yield after column chromatography. This observation is in accord with the failure to isolate any intermediates immediately prior to macropolycyclization in the [12]cyclacene series. Isolation and purification of the [14]cyclacene derivative **63** is aided by its remarkable solubility in chlorinated solvents. The acceleration of the final intramolecular cycloaddition to give **63** can be ascribed to the favorable juxtaposition of the reactive termini immediately prior to ring closure. The terminal diene and dienophilic units in **62** must constitute an almost perfect stereoelectronic match with respect to each other. The outcome of this perfect fit is to allow the bisdiene **37** to be inserted easily into position. The observation of a molecular ion for **63** at m/z 829 for $[M + H]^+$ by positive-ion FABMS is consistent with the constitution shown in the structural formula **63**. Furthermore, the lack of any major fragmentation ions is in marked contrast with the pronounced fragmentation patterns observed for the acyclic adducts **59**, **60**, and **61**. This observation would suggest that a substantial degree of stabilization is associated with the attainment of a closed macropolycyclic belt-like structure. The inference of this statement is that retro-Diels-Alder processes, which would lead to cleavage of the macropolycycle and result in fragmentation patterns similar to those observed in the FABMS for the acyclic molecular strips, are not occurring. This lack of a pronounced fragmentation pattern is a common feature of the macropolycyclic compounds such as kohnkene **43** and its analogs. The observation of (i) 15 separate resonances in the broadband-decoupled ^{13}C NMR spectrum for the 15 types of heterotopic carbon atoms and (ii) 12 separate resonances in the ^1H NMR spectrum for the 12 sets of heterotopic hydrogen atoms is consistent with the overall C_{2v} molecular symmetry of the [14]cyclacene derivative **63**. The absence of any signals associated with the presence of diene or dienophilic termini provides particularly compelling evidence for the closed macropolycyclic structure **63**. The appearance as singlets in the ^1H NMR spectrum of all four signals associated with the bridgehead hydrogen atoms (i) 12,14,21,23-H, (ii) 6,29-H, (iii) 10,16,19,25-H, and (iv) 1,4,8,27-H, at δ 5.31, 5.04, 4.92, and 4.87, respectively, indicates both cycloadditions have proceeded to afford the expected *syn/endo*-H configurations across the two newly-formed cyclohexene rings. The facile production of **63** from **59** provides further convincing evidence that the structure of **59** has the *syn/endo*-H/*syn/endo*-H configuration resulting from two consecutive trebly diastereoselective Diels-Alder reactions.

Analogous macropolycyclizations starting from **59** have subsequently been performed with the methylene-bridged bisdiene **64** and the octadeuteriated



Scheme 16. Analogous macropolycyclizations to that reported for the synthesis of **63** have been performed upon **59** using the methylene-bridged bisdiene **64** and the octadeuterated bisdiene **66** to afford the [14]cyclacene derivatives, **65** and **67**, respectively. In both cases, the products are isolated in yields exceeding 80%, without the need for high pressure to promote the ring-closure reaction

oxygen-bridged bisdiene **66** to afford the [14]cyclacene derivatives **65** and **67** as solids, in 86% and 72% yields, respectively (Scheme 16). Purification of both adducts was achieved by column chromatography on silica gel using dichloromethane containing 2% 2-propanol as eluant. The synthetic sequence used for the preparation of **64** [136] is similar to that employed in the synthesis of the 7-oxa analogue **37** (Scheme 8). In the case of **64**, the Diels-Alder adduct of maleic anhydride and cyclopentadiene provided the starting material for the synthesis.

Both macropolycyclizations (**59** + **64** → **65**) and (**59** + **66** → **67**) proceed in an equally facile manner to that described for the synthesis of the original [14]cyclacene derivative **63**. Neither reaction of **64** or **66** with the 2:1 adduct **59** requires high pressure to effect the final ring closure. These facts reinforce the suggestion that the bicyclic bisdienes **64** and **66** with a bicyclo[2.2.1]heptane framework constitute a good stereoelectronic match for the reactive termini present in **59**. The resonances

observed in the ^1H NMR spectrum at δ 4.86 and 4.92 for the hydrogen atoms associated with the bridgehead positions, 1,4,8,27-H and 10,16,19,25-H, respectively, both appear as sharp singlets, confirming the *endo*-configuration for the adjacent methine hydrogen atoms and the overall *syn/endo*-H stereochemistry across the newly-formed cyclohexene rings in both **65** and **67**. The observation of molecular ions by positive-ion FABMS, for $[\text{M} + \text{H}]^+$ at m/z 827 and 837, for **65** ($\text{C}_{57}\text{H}_{46}\text{O}_6$, $M = 826$) and **67** ($\text{C}_{56}\text{H}_{36}\text{D}_8\text{O}_7$, $M = 836$), respectively, with little evidence of fragmentation ions, is consistent with the highly-stable macrocyclic belt-like structure for both of these compounds.

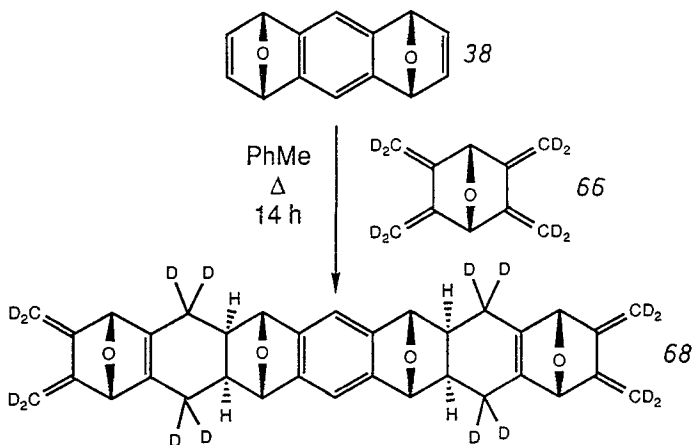
3.2 Kinetic Versus Thermodynamic Control Within the Repetitive Diels-Alder Reaction Regime

The isolation of the minor 2:1 adduct **61**, in addition to the major 2:1 adduct **59**, in the reaction between the *syn*-bisdienophile **38** and the extended *syn*-bisdiene **57** (Scheme 13), provides firm evidence for the existence of a second reaction pathway, in which *anti/endo*-H stereochemistry is being created across a small proportion of the newly-formed cyclohexene rings in the Diels-Alder reactions. This observation raises questions concerning the mechanistic factors responsible for the stereochemical outcome of these repetitive Diels-Alder reactions. Three different scenarios can be envisaged. If kinetic control is operating, then the observed diastereoselectivities will be a direct result of the difference in the free energies of the transition states leading to the diastereoisomeric products. In this case, the relative rates of different reactions will be a consequence of the stereoelectronic factors associated with the π -systems, some of which may favor and some of which may disfavor reaction. Alternatively, the sequence of Diels-Alder reactions may conceivably be operating under thermodynamic control. If this should be the case, then the observed product distribution will merely reflect the relative stabilities of the products. Thus, equilibration would be occurring throughout the process via rapid retro-Diels-Alder reactions, followed by recombination, until the most stable Diels-Alder adducts predominate. Finally, there is always the possibility, of course, that both kinetic and thermodynamic control would favor the same products. The reversibility of the Diels-Alder reaction is well-documented [41] and so it is vital to consider whether the sequence of repetitive Diels-Alder reactions is being controlled kinetically or thermodynamically — if indeed it is possible to draw this distinction.

3.2.1 Attempted Observation of Thermally-Promoted Reversibility in the Cycloadditions

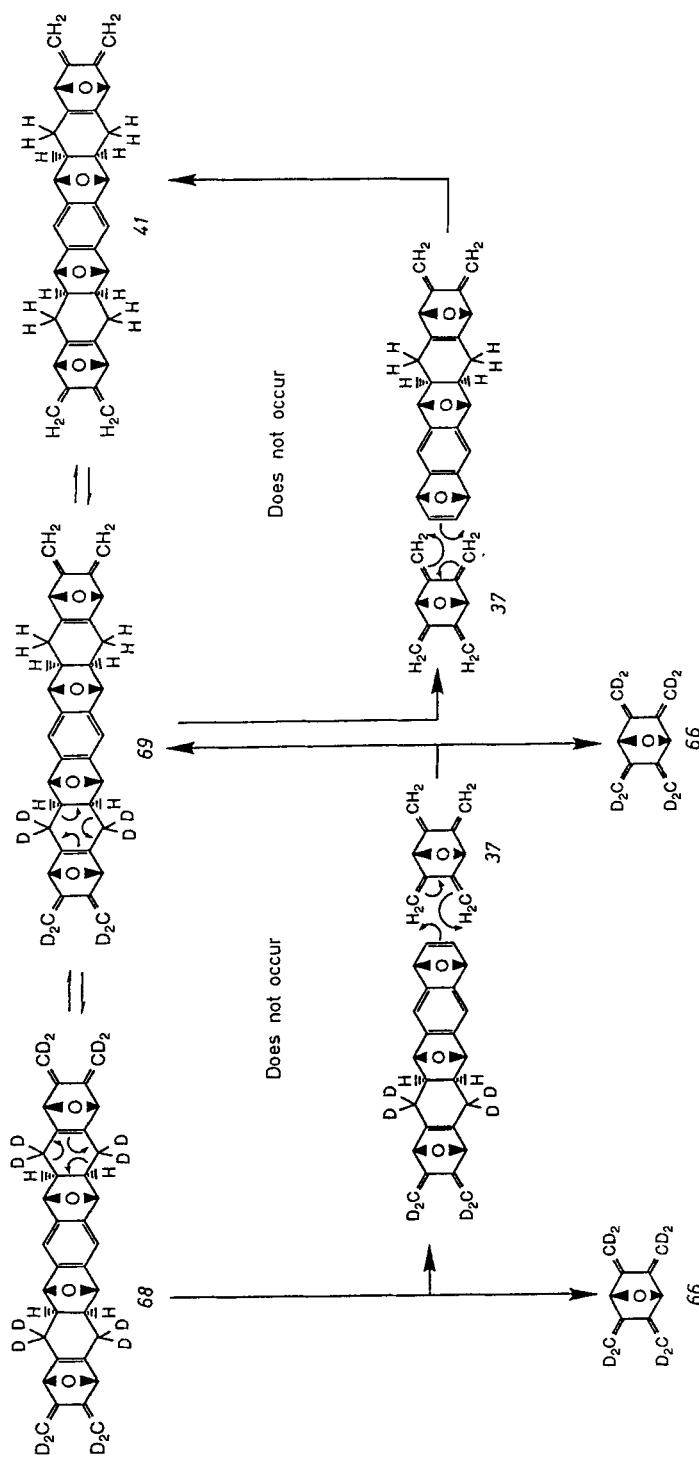
The hexadecadeuterio 2:1 adduct **69** was identified as a suitably labeled substrate for equilibration reactions with the bisdiene **37** (see Scheme 18). The degree of incorporation of **37** into **68**, as a consequence Diels-Alder reactions following retro-Diels-Alder reactions would be reflected by the replacement of the deuterium atoms in **68** as a result of an equilibration process which would lead eventually to the production of the unlabeled 2:1 adduct **41**. The synthesis of the labeled

2:1 adduct **68** from the *syn*-bisdienophile **38** and the octadeuterio bisdiene **66** (Scheme 17) was analogous to that employed in the synthesis of the unlabeled 2:1 adduct **41**. The observation of only four signals in the ^1H NMR spectrum of **68** is consistent both with its C_{2v} molecular symmetry and the degree of deuteration indicated in the structural formula for **68**. The lack of signals in the ^1H NMR spectrum of **68** associated with both the endocyclic and exocyclic methylene groups, along with the appearance of a singlet for the *endo*-methine hydrogen atoms (5a,8a,14a,17a-H), supports the structural assignment of **68**. Moreover, the vicinal coupling, normally evident between the *endo*-methine hydrogen atoms (5a,9a,13a,17a-H) and the methylene hydrogen atoms (5,9,14,18- H_2) is absent, thus confirming the presence of deuterium labels on positions C-5,9,14,18. These conclusions are supported fully by the ^1H NMR spectrum of **68**. The signals for the endocyclic dideuteriomethylene groups resonate at δ 2.25 and 2.55 and the exocyclic ones can be identified as signals resonating in the range δ 4.85–5.15.



Scheme 17. Reaction of a 2 molar equivalent of the octadeuterated bisdiene **66** with the *syn*-bisdienophile **38** affords the hexadecadeutero 2:1 adduct **68**

It is important that any attempted equilibrations are performed under identical conditions to those used for the preparation of the adducts under investigation. The only variation made to these attempted equilibration conditions from those used for the syntheses of **41** and **68** was the use of considerably greater excess of the unlabeled bisdiene **37** in order to drive the equilibrium towards the formation of **41**. The hexadecadeutero 2:1 adduct **68** was heated under reflux in toluene with 10 molar equivalents of the bisdiene **37** for ca. 48 hours (Scheme 18). By this time, indications of thermally-promoted degradation of the starting materials had become evident by TLC investigation. If thermodynamic equilibration had been occurring via retro-Diels-Alder reactions of **68**, followed by scrambling of the labeled and unlabeled bisdienes, **66** and **37**, respectively, prior to recombination

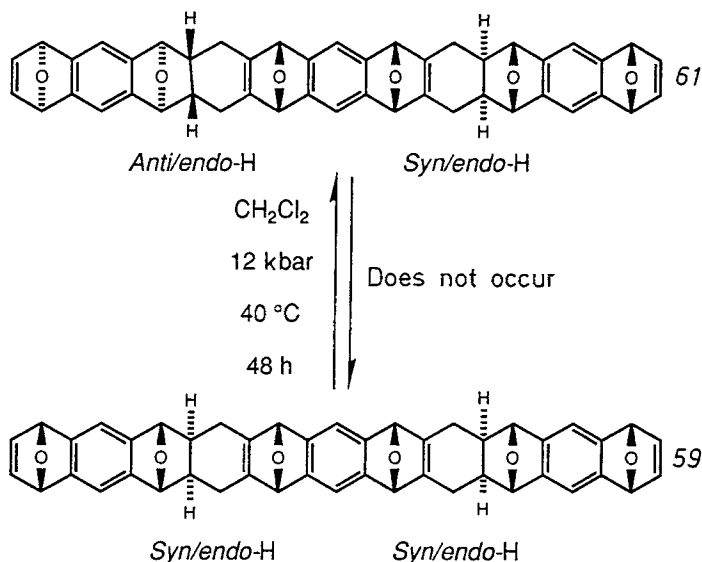


Scheme 18. If the repetitive Diels-Alder reaction adducts reported were being formed under thermodynamic control, heating the hexadecadeutero 2:1 adduct **68** under reflux in toluene in the presence of a 10 molar equivalent of the bisdiene **37** should give rise to a mixture of compounds comprised of **68**, **69**, and **41**. A retro Diels-Alder reaction of **68**, followed by scrambling of the labeled bisdiene **66** with the excess of the bisdiene **37** should favor preferential cycloaddition with **37** to afford **69**. The excess of **37** should ultimately drive the equilibration process toward the unlabeled 2:1 adduct **41**. No evidence for such an equilibration process has been found

by Diels-Alder reaction, then a 10 molar excess of **37** in the reaction mixture should favor its preferential incorporation into the fully-labeled 2:1 adduct **68**. This equilibration mechanism, if indeed it operates, would result in a distribution of products composed of the hexadecadeuterio 2:1 adduct **68**, the octadeuterio 2:1 adduct **69**, and the unlabeled 2:1 adduct **41**. A proposed mechanism which supports such a scrambling process is illustrated in Scheme 18. ^1H NMR Spectroscopy and positive-ion FABMS were employed as the analytical tools to assess the outcome of the attempted equilibration. The observation of molecular ions by positive-ion FABMS at m/z 541 for $[\text{M} + \text{Na}]^+$ and m/z 519 for $[\text{M} + \text{H}]^+$ arising from the fully-labeled 2:1 adduct **68**, and the absence of peaks corresponding to **41** (m/z 503 for $[\text{M} + \text{H}]^+$ and m/z 525 for $[\text{M} + \text{Na}]^+$) and **69** (m/z 511 for $[\text{M} + \text{H}]^+$ and m/z 533 for $[\text{M} + \text{Na}]^+$) indicated that no incorporation of **37** into the labeled 2:1 adduct **68** had occurred. The total lack of any compounds detected is consistent with the absence of any thermodynamic equilibration process operating in the course of these reactions. This result indicates that the repetitive sequence of Diels-Alder reactions is unidirectional. Thus the formation of the products is associated with kinetic, rather than thermodynamic control.

3.2.2 Attempted Observation of High Pressure-Promoted Reversibility in the Cycloadditions

Another appraisal of the mechanism which operates in these repetitive Diels-Alder reactions, was based directly on the isolation of a minor 2:1 adduct **61** alongside the major 2:1 adduct **59** from the reaction of the *syn*-bisdienophile **38** with the



Scheme 19. Pressurization of the minor 2:1 adduct **61** alone, fails to produce any of the major 2:1 adduct **59**. If the formation of these adducts was occurring under thermodynamic control, the minor 2:1 adduct **61** which is the least stable, should equilibrate to the major, and hence more stable, 2:1 adduct **59**

extended *syn*-bisdiene **57** (Scheme 13). If the 18:1 ratio for **59**:**61** obtained by HPLC analysis, reflects the different stabilities of the two adducts, as a consequence of a thermodynamic process, then pressurization of **61** alone, under identical conditions to those employed in its synthesis, should effect a re-equilibration and establish the previously observed (equilibrium?) ratio of 18:1 in favor of **59** over **61** (Scheme 19). However, HPLC analysis of the reaction mixture following such an attempted equilibration, showed no trace of the formation of the chromatographically less mobile major 2:1 isomer **59** alongside the minor 2:1 isomer **61**. Instead, the minor isomer **61** was completely unaffected by the high pressure reaction conditions that had led to its formation in the first place. This observation suggests strongly that there is no mechanism available to the stereoisomeric 2:1 adducts by which their equilibration can occur.

The clear failure to observe any evidence for the reversibility of the Diels-Alder reactions employed in the synthesis of cyclacene and polyacene derivatives leads inevitably to the proposal that only kinetic control is operating under the conditions employed in the syntheses. This conclusion gives authority to the arguments used – which are based upon transition state geometries – to explain the diastereoselectivities observed in each cycloaddition. Furthermore, these findings are in close agreement with the strong implication present in the literature [80, 82, 84, 85, 87, 89, 100] that in this kind of transition state molecular recognition is a kinetically-controlled phenomenon.

4 The Incorporation of [a,c]-Fusion into the Molecular LEGO Set – The Synthesis of Angular Belts and Cages

The compounds, which have been described in Sections 2 and 3 of this review, have been composed solely of [a,d]-fused six-membered rings. However, as the first part of a research program designed to increase the scope of the repetitive Diels-Alder synthetic methodology, the angular *syn*-bisdienophile **74** was identified as a suitable building block to be employed in repetitive Diels-Alder reactions.

4.1 The Synthesis of an Angular Belt

The constitution of the angular *syn*-bisdienophile **74** (see Scheme 20) maintains the bicyclic nature of the two dienophilic units. However, the [a,c]-fusion present in the phenanthrene constitution reduces the end-to-end symmetry of the π -systems, rendering the two olefinic carbon atoms in each dienophilic unit constitutionally-heterotopic. The effect of this reduction in the symmetry of the π -systems in **74** upon the diastereoselectivities exhibited in its cycloadditions was of considerable interest to us. Furthermore, the incorporation of two phenanthrene units into a macropolycyclic belt could ultimately lead to the preparation of an angular isomer **70** of [12]cyclacene **50** (Fig. 20). Compared with [12]cyclacene **50**, the angular isomer **70** has some appealing electronic features associated with it.

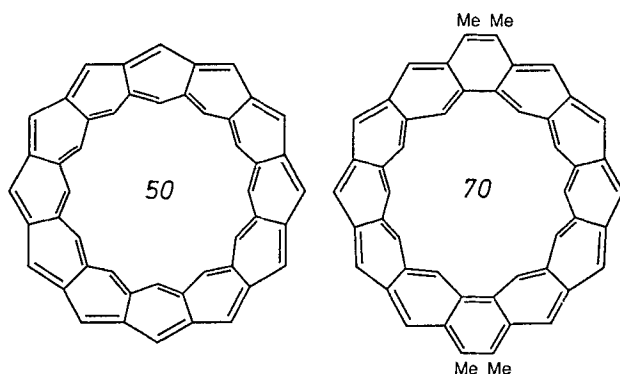
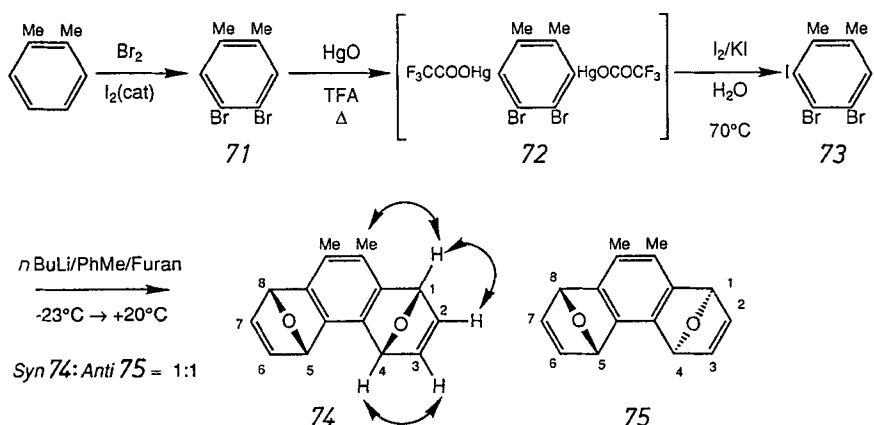


Fig. 20. In comparing the [12]cyclacene **50** with the angular derivative **70**, the introduction of [a,c]-fusion may lead to an increase in electronic stability. If each cyclacene is viewed as two independent annulenes, joined by a series of σ -bonds, then **70** represents a situation in which both annulenes — inner and outer rims with 22 and 26 π -electrons, respectively — correspond to Hückel-type $[4n + 2]$ systems

Firstly, the increased stabilities of polyacenes incorporating [a,c]-fusion into their six-membered ring constitution, with respect to those exhibited by purely [a,d]-fused polyacenes, has been well documented in the literature [137, 138]. The stability of linear acenes decreases rapidly as the skeleton grows. Indeed, hexacene marks the limit to which the isolation of these homologs has been achieved to date. Indeed, the very high reactivities of extended linear acenes are a reflection of the 'dilution' in their aromaticities and their consequent behaviour as polyenes. Secondly, **70** is a molecule in which the number of conjugated π -electrons along any pathway traced is such that the aromatic character is predicted on the basis of the Hückel rules [139]. The electronic situation in **70** can most simply be considered to be that consisting of two independent [N]annulenes, joined by a system of σ -bonds involving alternating carbon atoms. The inner rim corresponds to a [22]annulene, and the outer rim corresponds to a [26]annulene. In both cases, the number of conjugated π -electrons is such that a $[4n + 2]$ electronic configuration is produced with $n = 5$ and $n = 6$, respectively, for the π -systems comprising the inner and outer rims of the macropolycycle.

The angular bisdienophiles **74** and **75** (Scheme 20) can be disconnected to an angular bisaryne equivalent, which is available by a synthetic procedure similar to that employed for the synthesis of the laterally-fused bisdienophiles described in Sections 2 and 3. Hart has shown [140] that lithiation of 4,5-dibromo-3,6-diiodo-*o*-xylene **71** with 2 molar equivalents of *n*-butyllithium, followed by trapping of the bisaryne equivalent generated in situ with two equivalents of furan, affords compounds with the phenanthrene skeleton.

The syntheses of **74** and **75** is outlined in Scheme 20. Bromination of *o*-xylene, using a catalytic amount of iodine, afforded 4,5-dibromo-*o*-xylene **71** as a crystalline solid after recrystallization from methanol [141]. The appearance of only one singlet for the aromatic hydrogen atoms in the ^1H NMR spectrum of **71** confirms the regiochemical outcome of the bromination. Treatment of **71** with



Scheme 20. The synthesis of the angular bisdienophiles **74** and **75** proceeds via the angular bisaryne precursor **73**. The relative configurations of the endoxide bridges in **75** have been assigned by X-ray crystallographic analysis. The connectivities shown on structure **74** have been confirmed by NOE difference spectroscopy

mercuric oxide in trifluoroacetic acid heated under reflux for 2 hours generated a thick white precipitate of 4,5-dibromo-3,6-[bis(trifluoroacetato)mercuri]-*o*-xylene **72** [140]. This intermediate was subsequently iodinated in situ to produce 4,5-dibromo-3,6-diiodo-*o*-xylene **73** in 73% overall yield [141]. Lithiation of **73** with *n*-butyllithium, followed by trapping of the bisaryne equivalent, generated in situ, with two equivalents of furan, afforded an equimolar mixture of the angular *syn*- and *anti*-bisdienophiles, **74** and **75**, respectively. Fractional recrystallization of the crude reaction product from toluene gave a pure sample of the angular *anti*-bisdienophile **75**. The complete separation of **74** from **75** was achieved by column chromatography on silica gel, using chloroform containing 1% 2-propanol as the eluant. Single crystals, suitable for X-ray structural analysis, of the chromatographically more mobile adduct **75** were obtained by vapor diffusion of pentane into a chloroform-*d* solution of **75**. The solid state structure of **75** (Figure 21) confirmed that this isomer has the *anti*-configuration and hence it follows that its stereoisomer **74** must possess the *syn*-configuration.

The lower symmetries, C_s and C_2 , respectively, of the angular bisdienophiles **74** and **75** with respect to their laterally-fused analogs is evident from the increased number of signals observed in their ^1H and ^{13}C NMR spectra. The signals for

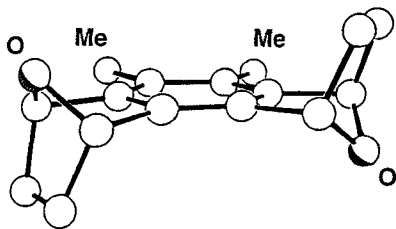


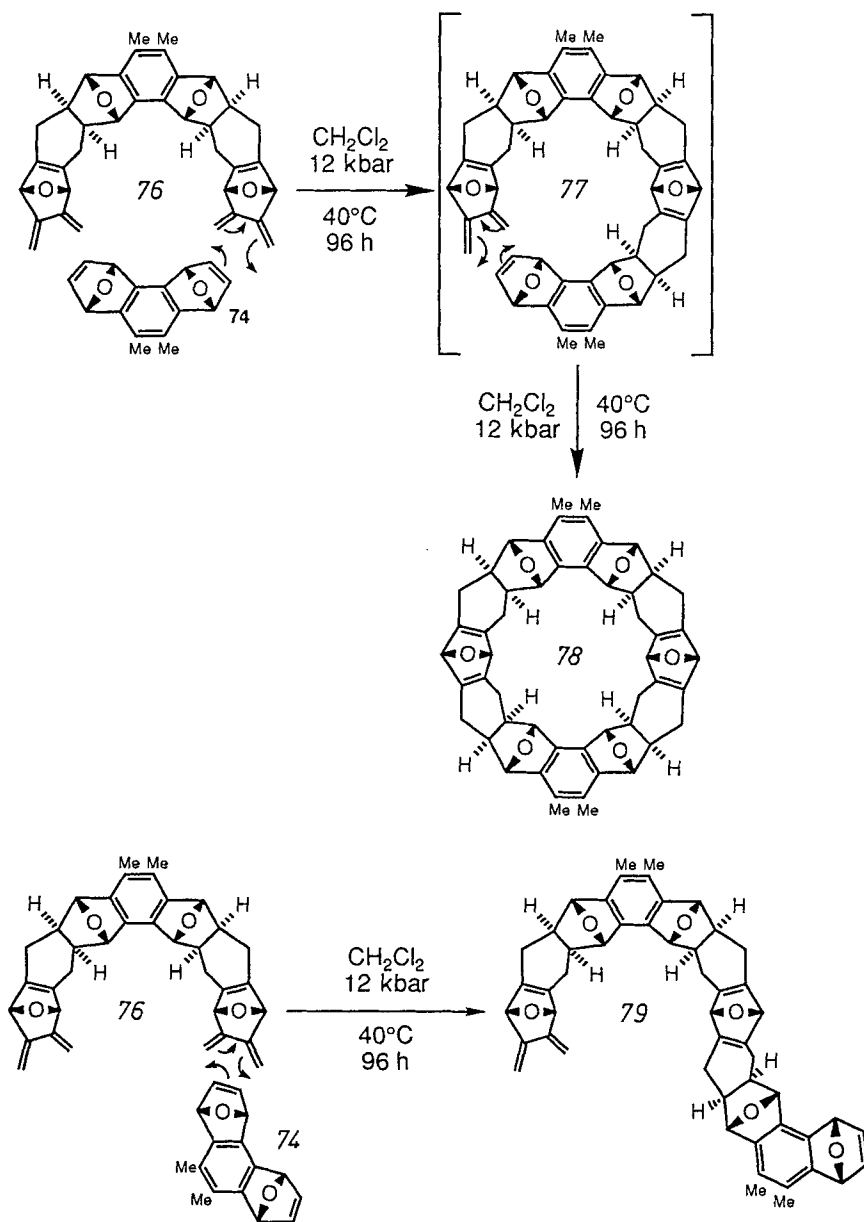
Fig. 21. The X-ray crystal structure of **75** shows that it has the *anti*-configuration

the olefinic hydrogen atoms (2,3,6,7-H) in the ^1H NMR spectrums of the spectroscopically identical adducts **74** and **75** show a vicinal and allylic coupling constant ($J_{1,2}$ 2 Hz, $J_{1,3}$ 1 Hz, respectively) to the bridgehead hydrogen atoms (1,4,5,8-H). A mutual coupling constant ($J_{2,3}$ 6 Hz) is also observed between the signals for the olefinic hydrogen atoms themselves. These coupling constants confirm that there is significant desymmetrization of the dienophilic π -systems in **74** and **75** with respect to their laterally-fused analogs. The signals in the ^1H NMR spectrum for the hydrogen atoms, 1,2,7,8-H, that are situated on the outer rim of the angular bisdienophiles occur at slightly different chemical shifts to those for the corresponding hydrogen atoms, (3,4,5,6-H) that are situated on the inner rim of the dienophiles.

Reaction of the angular *syn*-bisdienophile **74** with a 2.5 molar equivalent of the bisdiene **37** heated under reflux in toluene for 4 h in the absence of light afforded, after column chromatography on silica gel using chloroform containing 1.5% methanol as the eluant, a solid which was characterized as the 2:1 adduct **76**, in 91% yield (Scheme 21). The same treble diastereoselective adherence to *syn/endo*-H stereochemistry across the newly-formed cyclohexene rings, that has been observed overwhelmingly in the cycloadditions of [a,d]-fused bisdienophiles, was clearly maintained in the cycloadditions between the dienophilic units in the angular bisdienophile **74** and the bisdiene **37**. This conclusion, which is consistent with the observation in the ^1H NMR spectrum of **76** of the signals associated with the 6,7-H and 14,17-H hydrogen atoms as sharp singlets showing no observable coupling constant, confirms that the adjacent methine hydrogen atoms (5a,7a-H and 13a,17a-H, respectively) adopt the *endo*-configuration. In fact, the [a, c]-fused bisdienophile **74** appears not only to exercise the same high degree of treble diastereoselectivity in cycloadditions but to do so at an accelerated rate, compared to that exhibited by its [a, d]-fused analog **38** (Scheme 10). The initial configurational assignments in **76** were confirmed by the outcome of the macropolycyclization reaction carried out with a further equivalent of the angular *syn*-bisdienophile **74** under high pressure to afford the angular [12]cyclacene derivative **78** as one of the products of the reaction, together with the acyclic derivative **79** (Scheme 21).

The angular nature of the angular *syn*-bisdienophile **74** means that there are two possible modes for the initial intermolecular Diels-Alder reaction between **74** and **76**, that are constitutionally different (Scheme 22). One of these brings the two remaining reactive termini close together in the intermediate 2:2 adduct **77**. This mode can therefore be followed by intramolecular macropolycyclization to afford the angular belt **78**. The second constitutional mode exhibited in the initial intermolecular cycloaddition places the remaining reactive termini too far apart for any subsequent intramolecular cycloaddition to be possible. Consequently a novel acyclic adduct **79** is produced. Indeed, reaction of **76** with 1 molar equivalent of the angular *syn*-bisdienophile **74** under 12 kbar pressure in dichloromethane at 40 °C for 48 h afforded the two constitutionally-isomeric products **78** and **79** in the expected 1:1 ratio, after column chromatography on silica gel using dichloromethane containing 3% 2-propanol as the eluant (Scheme 21). The chromatographically less mobile product was characterized as the angular belt **78**. It revealed a strong molecular ion at m/z 767 for $[\text{M} - \text{H}]^-$ in the negative-ion

54

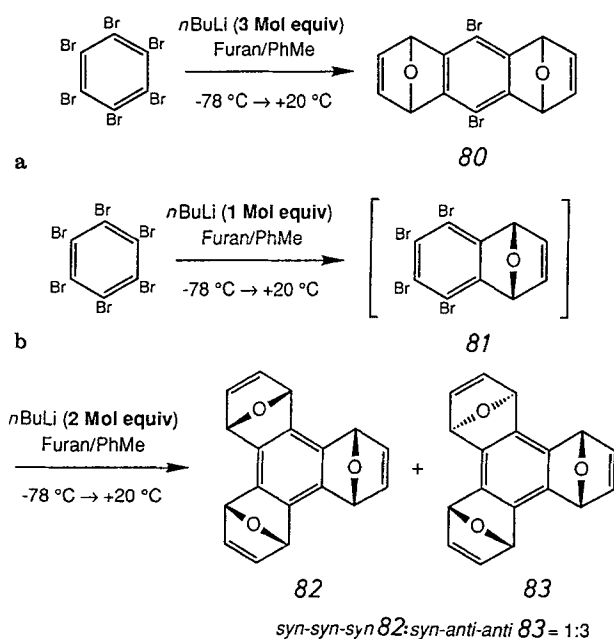


Scheme 22. The angular nature of the bisdienophile **74** means that there are two possible constitutionally-different modes for the initial intermolecular Diels-Alder reaction with **76**. The first one brings the reactive termini close enough together in **77** to undergo a final intramolecular macropolycyclization to afford **78**. The second one, however, places the remaining termini too distant to react in an intramolecular fashion, thus affording the novel acyclic adduct **79** which is terminated at one end by a diene unit and at the other end by a dienophilic unit

FABMS. The lack of a pronounced fragmentation pattern in the FABMS is consistent with the attainment of a highly-stable macropolycyclic structure. Uniquely, replacement of the 15-crown-5/18-crown-6 matrix employed in the FABMS experiment with the more conventional 3-nitrobenzylalcohol (NOBA) matrix resulted in a very strong pseudo molecular ion at m/z 921 for $[M - H + \text{NOBA}]^-$ in the negative-ion FABMS. This observation suggests that some kind of stabilizing interaction must be occurring between the macropolycyclic adduct **78** and the π -electron-deficient NOBA matrix. The higher C_{2v} symmetry of **78** with respect to that of the asymmetric acyclic adduct **79** is illustrated by (i) the observation in the broadband-decoupled ^{13}C NMR spectrum of separate signals for the 14 types of heterotopic carbon atoms and (ii) the observation in the ^1H NMR spectra of 10 signals for the 10 sets of heterotopic hydrogen atoms present in **78**. The ^1H NMR spectrum of **78** shows the presence of 3 bridgehead hydrogen atom environments, with signals at δ 4.91, 4.98, and 5.06, for 4,8,11,15-H, 1,18,22,23-H, and 6,13,20,25-H, respectively. The chromatographically more mobile adduct **79** revealed a very weak molecular ion in the positive-ion FABMS at m/z 769 for $[M + H]^+$. Both the ^1H and ^{13}C NMR spectra are consistent with the very low symmetry (C_1) of the acyclic adduct **79**. The appearance in the ^1H NMR spectrum of the signals for the bridgehead hydrogen atoms (1',4',7,8,15,18-H) as singlets confirms that the adjacent methine hydrogen atoms all adopt the *endo*-configurations, and, therefore *syn/endo*-H configurations have been generated across all of the three newly-formed cyclohexene rings in **79**. The presence of both diene and dienophilic units in **79** can be inferred from the appearance in the ^1H NMR spectrum of their respective signals. However, neither sets of signals exhibit the upfield shifts which are usually associated with the close juxtapositioning of the termini in these molecules. The lack of any such shifts suggests that the origin of these signals is to be found in the acyclic adduct **79** rather than in the acyclic adduct **77**, which has not been detected but which undoubtedly precedes the intramolecular cycloaddition to afford the angular belt **78**.

4.2 Trinacrene – The Synthesis of a Molecular Cage

The successful introduction of [a, c]-fused aromatic residues into macropolycyclic systems such as **78** (Scheme 22) suggests that the benzene ring may be used as a trivalent nucleus, with all three bicyclic rings in the [a, c]relationship, as shown in the trisdienophiles **82** and **83** shown in Scheme 23. However, treatment of hexabromobenzene with 3 equivalents of *n*-butyllithium does not generate the trisaryne equivalent [142] that is required for the synthesis of **82** and **83**. Instead, this direct approach afforded substantial amounts of the [a, d]-fused bisdienophile **80**. However, a two-step procedure, in which the monoadduct **81** is produced in situ, before further lithiation and trapping in situ, does afford the two configurationally-isomeric trisdienophiles **82** and **83** as outlined in Scheme 23. Although the two trisdienophiles are produced in the statistically-expected ratio of 1 : 3 in favor of the *syn-anti-anti* isomer **83**, the overall yields are 0.6% and 1.8%, for **82** and **83**, respectively. The relative configurations of the two trisdienophiles **82** and **83**



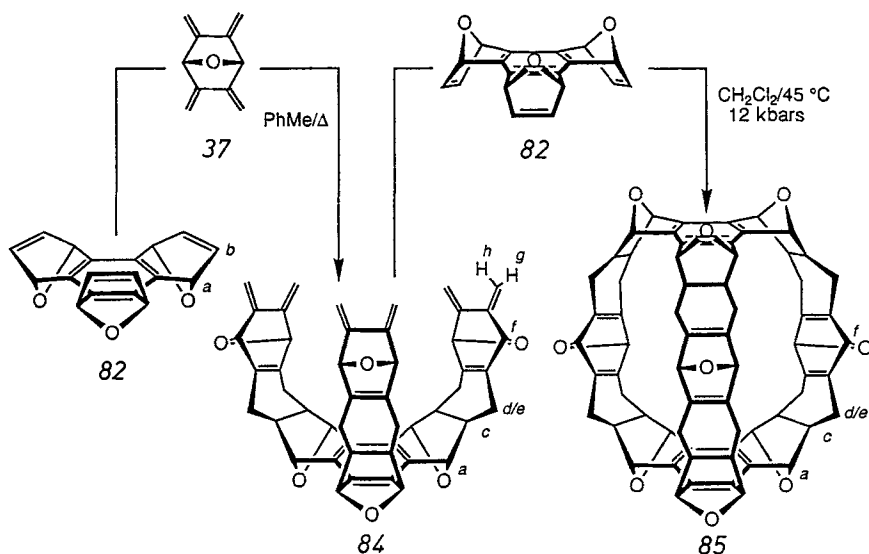
Scheme 23. The synthesis [142] of the trisdienophiles **82** and **83** cannot be achieved by the direct lithiation of hexabromobenzene as shown in (a). Instead, the stepwise procedure shown in (b) must be employed. However, the yields of **82** and **83** are still extremely poor, i.e. in the region of 0.6% and 1.8% respectively

can easily be deduced from their ^1H and ^{13}C NMR spectra by considering their very different molecular symmetries, namely C_{3v} and C_s , respectively.

Reaction (Scheme 24) of the all-*syn* trisdienophile **82** with 3.3 equivalents of the bisdiene **37**, in toluene heated under reflux for 14 h, afforded the 3:1 adduct **84** in 48% yield [142]. The C_{3v} molecular symmetry of **84** is confirmed by the observation of (i) 8 signals in the broadband-decoupled ^{13}C NMR spectrum for the 8 types of heterotopic carbon atoms and (ii) 7 signals in the ^1H NMR spectrum for the 7 sets of heterotopic hydrogen atoms. The *syn/endo*-H stereochemistry across each newly-formed cyclohexene ring in **84** is indicated by the appearance of the signal for the bridhead hydrogen atoms (6,7,14,15,22,23-H) as a singlet which shows no vicinal coupling constant to the adjacent methine hydrogen atoms. The closure of the molecular cage was achieved [142] by the high pressure-mediated reaction of **84** with 1 equivalent of the all-*syn* trisdienophile **82** to afford trinacene **85** after one trebly diastereoselective intermolecular cycloaddition followed by two intramolecular cycloadditions. The ^1H NMR spectrum of **85** exhibits only 5 signals for the 5 sets of heterotopic hydrogen atoms. This observation is consistent with the very high molecular symmetry (D_{3h}) of the molecular cage. The ^1H NMR chemical shifts that are recorded in matrix fashion in Table 2 highlight some of the similarities and differences in the structures and molecular symmetries of the compounds in the angular series and the trinacene cage series. Posi-

Table 2. A comparison of the ^1H NMR chemical shift data for structurally-related hydrogen atoms located on the angular adducts, **74**, **76**, and **78**, and the trinacrene triad **82**, **84**, and **85**, provides a means by which their structural and symmetry characteristics can be compared and contrasted. The compounds are ordered in such a way that allows direct comparison to be made between the most closely related molecules

^1H	a	a'	b	b'	c	c'
74	5.73 (dd, 2H)	5.78 (dd, 2H)	6.98 (ddd, 2H)	6.84 (ddd, 2H)	—	—
82	5.73 (dd, 6H)	—	6.78 (dd, 6H)	—	—	—
76	5.02	5.08	—	—	1.70 to 1.88	1.70 to 1.88
84	(s, 2H) 4.98	(s, 2H) —	—	—	1.68 to 1.81 (m, 6H)	(m, 8H) —
78	(s, 6H) 4.91	4.98	—	—	1.37 to 1.48 (m, 4H)	1.60 to 1.71 (m, 4H)
85	(s, 4H) 4.92	(s, 4H) —	—	—	1.58 to 1.62 (m, 12H)	—



Scheme 24. The molecular LEGO set used for the synthesis [142] of the molecular cage compound — trinacrene **85**

d/e	d'/e'	f	f'	g	g'	h	h'
—	—	—	—	—	—	—	—
—	—	—	—	—	—	—	—
2.30 to 2.70	2.30 to 2.70 (m, 8H)	4.99 5.00 (s, 2H)	5.00 or 4.99 (s, 2H)	510	510 (s, 4H)	5.01	5.01 (s, 4H)
2.28 to 2.73 (m, 12H)	—	5.02	—	5.10	—	4.99	—
2.30 to 2.80 (m, 16H)	2.30 to 2.80 (m, 16H)	(s, 6H) 5.06	5.06 (s, 4H)	(brs, 6H) —	—	(brs, 6H) —	—
2.35 to 2.88 (m, 24H)	—	5.10	—	—	—	—	—
		(s, 6H)					

tive-ion FABMS revealed a strong molecular ion at m/z 991 for $[M + H]^+$ arising from **85**.

The preparation of the esthetically-appealing trinacrene cage compound **85** marks a culmination in the first stage of our long-term research goal, which is directed toward the rapid, yet highly controlled, synthesis of outwardly complex molecular structures. Having demonstrated the initial success of the repetitive Diels-Alder oligomerization sequence, by the synthesis of kohnkene **43** (Scheme 10), we have successfully extended this methodology to allow the preparation of several different structural motifs, such as the [14]cyclacene derivatives **63** (Scheme 15), **65** (Scheme 16), and **67** (Scheme 16), the angular belt **78** (Scheme 21), and the cage **85** (Scheme 24). From this firm foundation, the synthesis of increasingly elaborate molecular structures can be envisaged. Now, having demonstrated a method by which to attain the form, attention will be paid, increasingly, to the function of these substrate-directed molecular structures.

5 Conclusions and Future Prospects

One of the primary aims of the research program described in this review has been the incorporation of bisdiene and bisdienophilic building blocks into the synthesis of novel macropolycyclic structures by a repetitive Diels-Alder oligo-

merization sequence. In addition to the structurally-appealing targets identified for total synthesis, it was envisaged that the syntheses themselves might be accomplished in such a way that would allow the structural factors, which may aid or hinder the trebly diastereoselective repetitive Diels-Alder oligomerization process, to be probed. Toward this end, a series of bisdiene and bisdienophilic building blocks have been synthesized, characterized, and incorporated into the synthesis of novel macropolycycles. This family of building blocks has served as the perfect vehicle for the establishment of a stepwise, highly-controlled synthetic methodology towards the production of several outwardly-complex molecular structures. Control of the outcome of these repetitive Diels-Alder reactions can be achieved with a high degree of oligoselectivity on top of their treble diastereoselectivity, by the alternate use of thermally-promoted and high pressure-promoted cycloadditions. In all but one of the examples studied, the cycloadditions between bisdiene and bisdienophilic building blocks have proceeded to generate exclusively the *syn/endo*-H stereochemistry across each newly-formed cyclohexene ring. The irreversible nature of the macropolycyclizations carried out with the undecacene derivative **59** and the bisdienes **37**, **64**, and **66** reinforces the notion that the reactivities of the substrates are dictated by the stereoelectronic requirements that are pre-programmed into their respective molecular structures (Scheme 16). The reactive termini of the building blocks represent ideal stereoelectronic matches for each other. Thus, the treble diastereoselectivities, that are exhibited in all the Diels-Alder combinations of bisdiene and bisdienophilic building blocks, can be said truly to be a result of autochthonous reactivity.

The synthesis of macropolycyclic structures, and their subsequent synthetic elaboration, is both synthetically challenging, and esthetically appealing. However, these studies have illustrated that access to other structural groups is possible by the repetitive Diels-Alder methodology. The acyclic 'Swiss-roll' compound **60** (Schemes 13 and 14), the angular belt **78** (Scheme 22), and trinacrene **85** (Scheme 84) all provide convincing evidence of this fact. Indeed, investigations currently being performed using *anti*-fused building blocks, such as the *anti*-bisdienophile **39** (Scheme 9) and the *anti*-bisdiene **58** (Scheme 12), are opening up the way to the synthesis of extended 'molecular wave' structures.

In response to a more fundamental question, a qualitative understanding of the origins of the treble diastereoselectivity exhibited in each cycloaddition has been developed. Arguments based on discussions in the literature have been combined with synthetic observations made in our own laboratories to assess the factors which control the reactivities and selectivities of exocyclic *s-cis*-butadiene units, and endocyclic bisdienophilic units incorporating the [2.2.1]bicycloheptane skeleton. The *syn/endo*-H stereochemistry generated across each newly-formed cyclohexene ring in the cycloadditions between bisdiene and bisdienophilic building blocks is, we believe, a consequence of transition state considerations, and therefore a result of kinetic control. In spite of the sometimes tacitly assumed reversibility of the Diels-Alder reaction, evidence is provided in this review that confirms here at least the unidirectional nature of the cycloadditions under discussion.

In summary, the success of the trebly diastereoselective repetitive Diels-Alder oligomerization process for the synthesis of outwardly complex molecular structu-

res is evident in the expression of the information which is stored as an intrinsic structural feature in the molecular frameworks of the building blocks. In this way, their subsequent mode of reaction is dictated in a substrate-directed, autochthonous manner.

Acknowledgments: Research is rarely, if ever, done in isolation. We acknowledge the input — both practical and intellectual — of many people to the particular research program we have just reviewed. We are most grateful to Dr. N. S. Isaacs (University of Reading) for performing many of the high pressure reactions, to Mr. P. R. Ashton and Dr. N. Spencer (University of Sheffield) for recording fast atom bombardment mass spectra and nuclear magnetic resonance spectra, respectively, and to Dr. D. J. Williams and Ms. A. M. Z. Slawin (Imperial College London) for carrying out the X-ray crystal structure determinations. Prof. W. D. Ollis brought a fresh and critical mind to bear on our presentation of the research results: we thank him for the many suggested improvements he recommended on reading the draft manuscript: they have resulted in a much improved version reaching the editor. The research was supported by the Science and Engineering Research Council and the Ministry of Defence in the United Kingdom, and by the University of Messina in Italy.

7 References

1. Corey EJ, Cheng X-M (1989) The logic of chemical synthesis. Wiley, New York
2. Warren SG (1982) Organic chemistry. The disconnection approach. Wiley, Chichester
3. (a) Corey EJ (1988) Chem Soc Rev 17: 111; (b) Kishi Y et al (1989) J Am Chem Soc 111: 7525; (c) Kishi Y et al (1989) J Am Chem Soc 111: 7530
4. (a) Davies JE, Gassen HG (1983) Angew Chem Int Ed Engl 22: 13; (b) Williams RJP (June 1990) Chimicaoggi 8: 41; (c) Schultz PG (1989) Angew Chem Int Ed Engl 28: 1283; (d) Dervan PB (1986) Science 232: 464; (e) Povsic TJ, Dervan PB (1989) J Am Chem Soc 111: 3059
5. (a) Peppas NA, Walker CM (June 1990) Chimicaoggi. 8: 17; (b) Mark H. (1990) Adv Mater 2: 7; (c) Praefcke K, Kohne B, Singer D (1990) Angew Chem Int Ed Engl 29: 177; (d) Tieke B (1990) Adv Mater 2: 222; (e) Grant P (1990) Adv Mater 2: 232
6. (a) Pedersen CJ (1967) J Am Chem Soc 89: 2045; (b) Pedersen CJ (1967) J Am Chem Soc 89: 7017; (c) Dietrich B, Lehn J-M, Sauvage J-P (1969) Tetrahedron Lett 2885; (d) Dietrich B, Lehn J-M, Sauvage J-P (1969) Tetrahedron Lett 2889; (e) Cram DJ (1974) Science 183: 803
7. (a) Breslow R (1982) Science 218: 532; (c) Stoddart JF (1983) Annu Rep Prog Chem B80: 353; (d) Colquhoun HM, Stoddart JF, Williams DJ (1986) Angew Chem Int Ed Engl 25: 487; (e) Stoddart JF (1989) Ann Rep Prog Chem B86: 353; (f) Lehn J-M (1985) Science 227: 849; (g) Lutter HD, Diederich F (1986) Angew Chem Int Ed Engl 25: 1125; (h) Lehn J-M (1988) Angew Chem Int Ed Engl 27: 89; (i) Cram DJ (1988) Angew Chem Int Ed Engl 27: 1009; (j) Pedersen CJ (1988) Angew Chem Int Ed Engl 27: 1021; (k) Seebach D (1988) Angew Chem Int Ed Engl 27: 1624; (l) Vögtle F (1989) Supramolekulare Chemie. BG Teubner, Stuttgart; (m) Seward EM, Hopkins RB, Sauerer W, Tam S-W, Diederich F (1990) J Am Chem Soc 112: 1783; (n) Shinkai S

- (1990) *Bioorg. Chem Front* 1: 161; (o) Tanaka Y, Kato Y, Aoyama Y (1990) *J Am Chem Soc* 112: 2807; (p) Venkata T, Rao S, Lawrence DS (1990) *J Am Chem Soc* 112: 614; (q) Cramer KD, Zimmerman SC (1990) *J Am Chem Soc* 112: 3680; (r) Ballester P, Mitra Tadayoni B, Branda N, Rebek Jr J (1990) *J Am Chem Soc* 112: 3685; (s) Breslow R, Berger D, Huang D-L (1990) *J Am Chem Soc* 112: 3686; (t) Whitlock BJ, Whitlock HW (1990) *J Am Chem Soc* 112: 3910; (u) Kim YH, Webster WO (1990) *J Am Chem Soc* 112: 4592; (v) Friedman AE, Chambron J-L, Sauvage J-P, Turro NJ, Barton JK (1990) *J Am Chem Soc* 112: 4960; (w) Hunter CA, Sanders JKM (1990) *J Am Chem Soc* 112: 5525; (x) Harmata M, Barnes CL (1990) *J Am Chem Soc* 112: 5655; (y) Anderson HL, Hunter CA, Nafees N, Sanders JKM (1990) *J Am Chem Soc* 112: 5780; (z) Bryant JA, Ho SP, Knobler CB, Cram DJ (1990) *J Am Chem Soc* 112: 5837
8. Diederich F (1988) *Angew Chem Int Ed Engl* 27: 362
9. Cram DJ (1986) *Angew Chem Int Ed Engl* 25: 1039
10. Hosseini MW, Blacker AJ, Lehn J-M (1990) *J Am Chem Soc* 112: 3896
11. Rebek Jr J (1987) *Science* 235: 1478
12. Chang S, Hamilton AD (1988) *J Am Chem Soc* 110: 1318
13. Jimenez L, Diederich F (1989) *Tetrahedron Lett* 30: 2759
14. (a) Brienne M-J, Gabard J, Lehn J-M, Stibor I (1989) *J Chem Soc Chem Commun* 1868; (b) Fourquay C, Lehn J-M, Levelut A-M (1990) *Adv Mater* 2: 254
15. (a) Eschenmoser A (1988) *Angew Chem Int Ed Engl* 27: 5; (b) Eschenmoser A (1976) *Chem Soc Rev* 5: 377; (c) Eschenmoser A, Winter CE (1977) *Science* 196: 1410; (d) Kräutler A, Platz A, Nordmann R, Hodgson KO, Dunitz JD, Eschenmoser A (1976) *Helv Chim Acta* 59: 924; (e) Pflatz A, Bühler N, Neier R, Hirai K, Eschenmoser A (1977) *Helv Chim Acta* 60: 2653; (f) Brown CE, Katz JJ, Shemin D (1972) *Proc Natl Acad Sci USA* 69: 2585; (g) Rasetti V, Pflatz A, Kratsky C, Eschenmoser A (1972) *Proc Natl Acad Sci USA* 69: 16. The conclusions appear to be that: (1) The macropolycyclic precursor of vitamin B₁₂, uroporphyrinogen III, is the thermodynamically-favored product from the self-condensation of porphobilinogen. (2) In the presence of a complexing metal, pyrocorphin is more stable than the tautomeric porphyrinogen. The pyrocorphin nucleus can also undergo regioselective C-protonation to generate the corrin chromophore. Thus, the arrangement of the double bonds in the ligand is a self-constituting structural element. (3) The smaller coordination hole of the corrin ligand is suited ideally to cobalt(II). The destabilising 'ruffling' of the corrin ligand is not necessary as it is in the case of the porphyrin. (4) The kinetic attachment of the nucleotide chain to the propionic acid residue on ring D reflects the thermodynamic stability of the pre-reaction complex over the 7 other possible isomers. Aspects of the synthesis of vitamin B₁₂ are recounted in (h) Woodward RB (1968) *Pure Appl Chem* 17: 760; (i) Woodward RB (1971) *Pure Appl Chem* 25: 283; (j) Woodward RB (1973) *Pure Appl Chem* 32: 145
16. Lindsey, JS (1991) *Nouv J Chem* 15: 153
17. (a) Fraenkel-Conrat H, Williams RC (1955) *Proc Natl Acad Sci USA* 41: 690; (b) Casper DLD (1980) *Biophys J* 32: 103; (c) Klug A (1983) *Angew Chem Int Ed Engl* 22: 565
18. Anfinsen CB (1973) *Science* 181: 223
19. Ringsdorf H, Schlarb B, Venzmer J (1988) *Angew Chem Int Ed Engl* 27: 113
20. (a) Miller SL, Orgel LE (1955) *J Am Chem Soc* 77: 351; (b) Ferris JP (1966) *J Am Chem Soc* 88: 1074; (c) Miller SL, Orgel FE (1974) *The origin of life on earth*. Prentice-Hall, New Jersey. For a contemporary view of the origin of life and the theory of surface metabolism, see Wächtershauser G (1988) *Microbiological Rev* 52: 452
21. (a) Kohnke FH, Mathias JP, Stoddart JF (1989) *Molecular recognition: chemical and biological problems*, Roberts, SM (Ed). The Royal Society of Chemistry, Cambridge, pp 223–269; (b) Kohnke FH, Mathias JP, Stoddart JF (1989) *Angew Chem Int Ed Engl* 28: 1103
22. See, for example (a) *Synthesis of non-natural products: challenge and reward* (1986) *Tetrahedron* 42: 1549–1915; (b) Stoddart JF (1988) *Nature* 334: 10; (c) Lehn J-M

- (1990) *Angew Chem Int Ed Engl* 29: 1304; (d) Seebach D (1990) *Angew Chem Int Ed Engl* 29: 1320
23. (a) Lehn J-M, Rigault A, Siegel JS, Harrowfield J, Chevier B, Moras D (1987) *Proc Natl Acad Sci USA* 84: 2565; (b) Lehn J-M, Rigault A (1988) *Angew Chem Int Ed Engl* 27: 1095
24. (a) Constable EC, Drew MGB, Ward MD (1987) *J Chem Soc Chem Commun* 1600; (b) Constable EC, Drew MGB, Ward MD (1988) *J Chem Soc, Chem Commun* 1450; (c) Barley M, Constable EC, Corr SA, McQueen RCS, Nutkins JC, Ward MD, Drew MGB (1988) *J Chem Soc, Dalton Trans* 2655; (d) Constable EC, Ward MD, Tocher DA (1990) *J Am Chem Soc* 112: 1256; (e) Constable EC, Elder SM, Healy J, Ward MD, Tocher DA (1990) *J Am Chem Soc* 112: 4590
25. (a) Frisch HL, Wasserman E (1961) *J Am Chem Soc* 83: 3789; (b) Harrison IT, Harrison S (1967) *J Am Chem Soc* 89: 5723; (c) Dietrich-Buchecker CO, Sauvage J-P (1987) *Chem Rev* 87: 795; (d) Dietrich-Buchecker CO, Sauvage J-P (1988) *Angew Chem Int Ed Engl* 28: 89; (e) Dietrich-Buchecker CO, Sauvage J-P, Kern J-M (1989) *J Am Chem Soc* 111: 7791; (f) Dietrich-Buchecker CO, Hemmert C, Sauvage J-P (1988) *New J Chem* 14: 603; (g) Dietrich-Buchecker CO, Guilhem J, Pascard C, Sauvage J-P (1990) *Angew Chem Int Ed Engl* 29: 1154; (h) Dietrich-Buchecker CO, Hemmert C, Khemiss A-K, Sauvage J-P (1990) *J Am Chem Soc* 112: 8002
26. (a) Ashton PR, Goodnow TT, Kaifer AE, Reddington MV, Slawin AMZ, Spencer N, Stoddart JF, Vicent C, Williams DJ (1989) *Angew Chem Int Ed Engl* 28: 1396; (b) Stoddart JF (1990) *Chirality in drug design and synthesis*, Brown C (ed). Academic Press, London, pp 53–81; (c) Stoddart JF (1991) *Frontiers in supramolecular organic chemistry and photochemistry*, Schneider, H-J, Dürr H (Eds). VCH, Weinheim, pp 000–000; (d) Stoddart JF (1991) *Host-guest molecular interactions: from chemistry to biology*, Ciba Foundation Symposium 158, Wiley, Chichester, pp 5–22; (e) Reddington MV, Slawin AMZ, Spencer N, Stoddart JF, Vicent C, Williams DJ (1991) *J Chem Soc, Chem Commun* 630; (f) Ashton PR, Brown CL, Chrystal EJT, Goodnow TT, Kaifer AE, Parry KP, Philp D, Slawin AMZ, Spencer N, Stoddart JF, Williams DJ (1991) *J Chem Soc, Chem Commun* 634; (g) Anneli PL, Spencer N, Stoddart JF (1991) *J Am Chem Soc* 113: 5131; (h) Anneli PL, Ashton PR, Spencer N, Slawin AMZ, Stoddart JF, Williams DJ (1991) *Angew Chem Int Ed Engl* 30: 1036; (i) Ashton PR, Brown CL, Chrystal EJT, Goodnow TT, Kaifer AE, Parry KP, Slawin AMZ, Spencer N, Stoddart JF, Williams DJ (1991) *Angew Chem Int Ed Engl* 30: 1039; (j) Ashton PR, Brown CL, Chrystal EJT, Parry KP, Pietraskiewicz M, Spencer N, Stoddart JF, Williams DJ (1991) *Angew Chem Int Ed Engl* 30: 1042; (k) Philp D, Stoddart JF (1991) *Syn Lett* 445; (l) Brown CL, Philp D, Stoddart JF (1991) *Syn Lett* 459; (m) Brown CL, Philp D, Stoddart JF (1991) *Syn Lett* 462; (n) Anneli PL, Ashton PR, Ballardini R, Balzani V, Delgado M, Gandolfi MT, Goodnow TT, Kaifer AE, Philp D, Pietraskiewicz M, Prodi L, Reddington MV, Slawin AMZ, Spencer N, Stoddart JF, Vicent C, Williams DJ (1992) *J Am Chem Soc* 114: 193
27. Schill G (1971) *Catenanes, rotaxanes, and knots*. Academic Press, New York
28. (a) Williams RJP (1988) *Nature* 332: 393; (b) Rubenstein I, Steinberg S, Tor Y, Shanzer A, Sagiv J (1988) *Nature* 332: 426; (c) Arnett EM, Harvey NG, Rose PL (1989) *Acc Chem Res* 22: 131; (d) Ebersole RC, Miller VA, Moran JR, Ward MD (1990) *J Am Chem Soc* 112: 3239; (e) Kuhn H (1989) *Thin Solid Films* 178: 1; (f) Arduengo III AJ, Moran JR, Rodriguez-Parada J, Ward MD (1990) *J Am Chem Soc* 112: 6153
29. (a) Whitesides GM, Ferguson GS (1988) *CHEMTRACTS* 1: 171; (b) Bain CD, Whitesides GM (1988) *J Am Chem Soc* 110: 5897; (c) Bain CD, Whitesides GM (1988) *J Am Chem Soc* 110: 6560; (d) Wilson MD, Whitesides GM (1988) *J Am Chem Soc* 110: 8718; (e) Bain CD, Biebuyck H, Whitesides GM (1989) *Langmuir* 5: 723; (f) Bain CD, Whitesides GM (1989) *Angew Chem Int Ed Engl* 28: 506; (g) Whitesides GM, Biebuyck H (1989) *Molecular recognition: chemical and biological problems*, Roberts, SM (Ed). The Royal Society of Chemistry, Cambridge pp 270–85; (h) Bain CD, Whitesides GM (1989) *J Phys Chem* 93: 1670; (i) Wilson MD, Ferguson GS, Whitesides GM (1990) *J Am Chem Soc* 112: 1244

30. (a) Nuzzo RG, Dubois LH, Allara DL (1990) *J Am Chem Soc* 112: 558; (b) Dubois LH, Zegarski BR, Nuzzo RG (1990) *J Am Chem Soc* 112: 570; (c) Chidsey CED, Bertozzi CR, Putvinski TM, Mujsie AM (1990) *J Am Chem Soc* 112: 4301
31. Bain CD, Troughton EB, Tao Y-T, Evall J, Whitesides GM, Nuzzo RG (1989) *J Am Chem Soc* 111: 321
32. (a) Rebek Jr J (1990) *Angew Chem Int Ed Engl* 29: 245; (b) Tjivika T, Ballester P, Rebek Jr J (1990) *J Am Chem Soc* 112: 1249
33. Strobel SA, Dervan PB (1989) *J Am Chem Soc* 111: 7286
34. Koert U, Harding MM, Lehn J-M (1990) *Nature* 349: 339
35. (a) Duncan MA, Rouvray DH (Dec 1989) *Sci Am* 261: 60; (b) Kroto HW (1988) *Science* 242: 1139; (c) Stoddart JF (1990) *Angew Chem Int Ed Engl* In press; (d) Krätschmer W, Lamb LD, Fostiropoulos K, Huffman DR (1990) *Nature* 347: 354; (e) Taylor R, Hare JP, Abdul-Sada AK, Kroto HW (1990) *J Chem Soc, Chem Commun* 1423; (f) Ajie H, Alvarez MM, Anz SJ, Beck RD, Diederich F, Fostiropoulos K, Huffman DR, Krätschmer W, Rubin Y, Sensharma D, Whetten R (1990) *J Phys Chem* 94: 8630; (g) Johnson RD, Meijer G, Bethune DS (1990) *J Am Chem Soc* 112: 8983; (h) Haufler RE, Conceicao J, Chibante LPF, Chai Y, Byrne NE, Flanagan S, Haley MM, O'Brien SC, Pan C, Ziao Z, Billups WE, Ciufolini MA, Hauge RH, Margrave JL, Wilson LJ, Curl RF, Smalley RE (1990) *J Phys Chem* 94: 8634
36. (a) Feynman RP (1960) *Sat Rev* 432: 45; (b) Mitchel P (1982) *Cell function and differentiation*, Part B. Akoyonoglou, A (Ed). AR Liss, New York pp 399–408; (c) Mitchel P (1984) *FEBS Lett* 176: 287
37. See, for example, (a) Carter F (1982) *Molecular electronic devices*. Marcel Dekker, New York; (b) Aviram A (1988) *J Am Chem Soc* 110: 5687; (c) Garnier F (1989) *Angew Chem Int Ed Engl* 28: 513; (d) Häarer D (1989) *Angew Chem Int Ed Engl* 28: 1544; (e) Reinhoudt DN, Südholt AC (1990) *Adv Mater* 2: 23; (f) Kuhn H (1989) *Molecular electronics*. Hong FT (Ed). Plenum, pp 3–24; (g) Tour JM, Wu R, Schumm JS (1990) *J Am Chem Soc* 112: 5662. For a thought-provoking look at artificial life and the processes that may find application in such systems, see Langton CG (Ed) (1989). *Artificial Life*, Addison-Wesley, USA
38. (a) Kohnke FH, Stoddart JF (1989) *Pure Appl Chem* 61: 1581; (b) Stoddart JF (1989) *J Incl Phenom* 7: 227
39. Kivelson S, Chapman OL (1983) *Phys Rev B* 28: 7236; (b) Vögtle F (1983) *Top Curr Chem* 115: 157; (c) Alder RW, Sessions RB (1985) *J Chem Soc, Perkin Trans* 1849; (d) Kenny PW, Miller LL (1988) *J Chem Soc, Chem Commun* 84
40. (a) Bailey WJ, Detter EJ, Economy J (1962) *J Org Chem* 27: 3479; (b) Angus Jr AO, Johnson RP (1983) *J Org Chem* 48: 273; (c) LeHollier CS, Gribble GW (1983) *J Org Chem* 48: 2304; (d) Miller LL, Thomas AD, Wilkins LL, Weil DA (1986) *J Chem Soc, Chem Commun* 661; (e) Thomas AD, Miller LL (1986) *J Org Chem* 51: 4160; (f) Christopf WC, Miller LL (1986) *J Org Chem* 51: 4169; (g) Chiba T, Kenny PW, Miller LL (1987) *J Org Chem* 53: 4327; (h) Christopf WC, Miller LL (1987) *Tetrahedron* 43: 681; (i) Block E, Putman D (1990) *J Am Chem Soc* 112: 4072; (j) Blatter K, Schlüter A-D, Wegner G (1989) *J Org Chem* 54: 2396; (k) Blatter K, Schlüter A-D (1989) *Chem Ber* 122: 1351; (l) Blatter K, Schlüter A-D (1989) *Macromolecules* 22: 3506; (m) Vogel T, Blatter K, Schlüter A-D (1989) *Makromol Chem Rapid Commun* 10: 427; (n) Wager M, Wohlfarth W, Müller K (1988) *Chimia* 42: 377
41. (a) Wasserman A (1965) *Diels-Alder reactions: organic background and photochemical aspects*. Elsevier, Amsterdam; (b) Sauer J, Sustmann R (1980) *Angew Chem Int Ed Engl* 19: 779; (c) Paquette LA (1984) *Asymmetric Synthesis*, Volume 3. Morrison JD (Series Ed). Academic Press, New York pp 455–501
42. Diels O, Alder K (1928) *Ann Chem* 460: 98
43. Woodward RB, Hoffmann R (1970) *The conservation of orbital symmetry*. Verlag-Chemie, Weinheim
44. Houk KN (1975) *Acc Chem Res* 8: 361
45. (a) Masamune S, Reed III LA, Davis, JT, Choy W (1983) *J Org Chem* 48: 4441; (b) Oppolzer W (1984) *Angew Chem Int Ed Engl* 23: 876; (c) Evans DA, Chapman KT,

- Bisaha J (1984) *J Am Chem Soc* 106: 4261; (d) Masamune S, Choy W, Peterson JS, Sita LR (1985) *Angew Chem Int Ed Engl* 24: 1; (e) Chapuis C, Jurczak J (1987) *Helv Chim Acta* 70: 436; (f) Takahashi I, Hashimoto S, Ikota N, Tomioka K, Koga K (1987) *Tetrahedron Lett* 28: 5687; (g) Evans DA, Chapman KT, Bisaha J (1988) *J Am Chem Soc* 110: 1235; (h) Furuta K, Miwa Y, Inagawa K, Yamamoto H (1988) *J Am Chem Soc* 110: 6254; (i) Corey EJ, Inwinkelried R, Pikul S, Xiang YB (1989) *J Am Chem Soc* 111: 5493; (j) Bonnesen PV, Pockett CL, Honeychuck RV, Hersh WH (1989) *J Am Chem Soc* 111: 6070; (k) Rebiere F, Riant O, Kagan HB (1990) *Tetrahedron Asymmetry* 1: 199
46. (a) Narasaka K, Inoue M, Okada N (1986) *Chem Lett* 1109; (b) Narasaka K, Inoue M, Yamada Y, Nakashima M (1989) *J Am Chem Soc* 111: 5340
 47. (a) Hilvert D, Hill KW, Nared KD, Auditor M-T M (1989) *J Am Chem Soc* 111: 9261; (b) Braisted AG, Schultz PG (1990) *J Am Chem Soc* 112: 7430
 48. (a) Isaacs NS (1981) *Liquid-phase high-pressure chemistry*. Wiley, Chichester; (b) LeNoble WJ (1988) *Organic high-pressure chemistry*. Elsevier, Amsterdam
 49. (a) Asano T, LeNoble WJ (1978) *Chem Rev* 78: 407; (b) Isaacs NS, George AV (1987) *Chem Brit* 23: 47
 50. Röntgen WC (1892) *Ann Phys* 45: 91
 51. (a) Fawcett EW, Gibson RO (1934) *J Chem Soc* 387; (b) Fawcett EW, Gibson RO (1934) *J Chem Soc* 396
 52. See particularly, Chapter 4 in Reference 48a
 53. (a) Dauben WG, Kozikowski AP (1974) *J Am Chem Soc* 96: 3664; (b) Dauben WG, Krabbenhoft HO (1976) *J Am Chem Soc* 98: 199; (c) Dauben WG, Kessel CR, Takemura KH (1980) *J Am Chem Soc* 102: 6893
 54. (a) El Yanov BS, Klabinovskii EI, Gonikberg MG, Porfenova GM, Godenova LF (1971) *Bull Acad Sci SSSR Ser Khim* 557; (b) Brun C, Jenner G, Deluzarch A, Libs S (1972) *Bull Soc Chim Fr* 2332; (c) Jurczak J (1979) *Bull Chem Soc Jpn* 52: 3438
 55. Behrend R, Meyer E, Rusche F (1905) *Justus Liebigs Ann Chem* 339: 1
 56. (a) Freeman WA, Mock WL, Shih N-Y (1981) *J Am Chem Soc* 103: 7367; (b) Mock WL, Irra TA, Wepseic JP, Manimaran TL (1983) *J Org Chem* 48: 3619
 57. (a) Mock WL, Shih N-Y (1983) *J Org Chem* 48: 3618; (b) Mock WL, Shih N-Y (1986) *J Org Chem* 51: 4440; (c) Mock WL, Shih N-Y (1988) *J Am Chem Soc* 110: 4706; (d) Mock WL, Shih N-Y (1989) *J Am Chem Soc* 111: 2697; (e) Mock WL, Pierpont J (1990) *J Chem Soc, Chem Commun* 1509
 58. Gutsche CD (1989) *Calixarenes — monographs in supramolecular chemistry*. Stoddart JF (Series Ed). The Royal Society of Chemistry, Cambridge
 59. (a) Andreotti CD, Calestani G, Ugozzoli F, Arduini A, Ghidini E, Pochini A, Ungaro R (1987) *J Incl Phenom* 5: 123; (b) Gutsche CD, Dhawan B, Levine JA, No KC, Bauer JL (1983) *Tetrahedron* 39: 409; (c) Gutsche CD (1988) *Pure Appl Chem* 60: 483; (d) Gutsche CD, Alain I, Iqbal M, Mangiafico T, Nam KC, Roges J, See KA (1989) *J Incl Phenom* 7: 61
 60. Gutsche CD, Iqbal M, Stewart D (1986) *J Org Chem* 51: 742
 61. (a) Shinkai S, Koreishi H, Mori S, Sune T, Manube O (1985) *Chem Lett* 1033; (b) Shinkai S, Mori S, Koreishi H, Tsubaki T, Manube O (1986) *J Am Chem Soc* 108: 2409
 62. Moras D, Olsen KW, Sabesan MN, Buehner M, Ford GC, Rossman MG (1975) *J Biol Chem* 250: 9137
 63. (a) Erdtman H, Högberg S, Abrahamsson S, Nilsson B (1968) *Tetrahedron Lett* 1679; (b) Högberg AGS (1980) *J Am Chem Soc* 102: 6064
 64. Ishikawa Y, Kunitake T, Matsuda T, Otsuka T, Shinkai S (1989) *J Chem Soc, Chem Commun* 736
 65. (a) Karbach S, Cram DJ (1982) *J Am Chem Soc* 104: 5826; (b) Cram DJ, Karbach S, Kim YH, Baczynskyj L, Kallemeyn GW (1985) *J Am Chem Soc* 107: 2575; (c) Cram DJ, Karbach S, Kim HE, Knobler CB, Maverick EF, Ericson JL, Helgeson RC (1988) *J Am Chem Soc* 110: 2229; (d) Cram DJ, Karbach S, Kim YH, Baczynskyj L, Marti L, Sampson RM, Kallemeyn GW (1988) *J Am Chem Soc* 110: 2554
 66. Sherman JC, Cram DJ (1989) *J Am Chem Soc* 111: 4527

67. (a) Tunsted T, Tucker J, Dalcanale E, Weiser J, Bryant JA, Sherman JC, Helgeson RC, Knobler CB, Cram DJ (1989) *J Org Chem* 54: 1305; (b) Bryant JA, Blanda MT, Vincenti M, Cram DJ (1990) *J Am Chem Soc* In press
68. (a) Cramer F (1951) *Chem Ber* 84: 851; (b) Cramer F (1951) *Chem Ber* 84: 855; (c) Cramer F (1956) *Recl Trav Chim Pays-Bas* 75: 891
69. For a collection of invited papers featuring cyclodextrin chemistry in 1989, (1989) *Carb Res* 192: 1–370
70. See, for example, St. Jacques M, Sundarajan KT, Taylor KJ, Marchessault RH (1976) *J Am Chem Soc* 98: 4386
71. (a) Stoddart JF, Zarzycki R (1988) *Recl Trav Chim Pays-Bas* 107: 515; (b) Alston DR, Ashton PR, Lilley TH, Stoddart JF, Zarzycki R, Slawin AMZ, Williams DJ (1989) *Carb Res* 192: 259
72. (a) Komiyama M (1989) *J Am Chem Soc* 111: 3046; (b) Breslow R, Kool E (1988) *Tetrahedron Lett* 29: 1635; (c) Bergmann N, Schmidtchen FF (1982) *Tetrahedron Lett* 29: 6235
73. (a) Mori M, Ito Y, Ogawa T (1989) *Tetrahedron Lett* 30: 1273; (b) Mori M, Ito Y, Ogawa T (1989) *Carb Res* 192: 131
74. Takahashi T, Ogawa T (1987) *Carb Res* 164: 277
75. (a) Ashton PR, Ellwood P, Staton I (1991) *Angew Chem Int Ed Engl* 30: 80; (b) Gadele A, Defaye J (1991) *Angew Chem Int Ed Engl* 30: 79
76. (a) Vogel P, Florey A (1974) *Helv Chim Acta* 57: 200; (b) Mahaim C, Carrupt P-A, Hagenbuch J-P, Florey A, Vogel P (1980) *Helv Chim Acta* 62: 1149
77. James DE, Stille JK (1976) *J Am Chem Soc* 98: 1810
78. Kohnke FH, Stoddart JF, Slawin AMZ, Williams DJ (1988) *Acta Crystallogr C* 44: 736
79. Kohnke FH, Mathias JP, Stoddart JF, Slawin AMZ, Williams DJ (1990) *Acta Crystallogr C* 46: 1043
80. Vogel P (1983) in: Watson WH (ed) *Stereochemistry and reactivity of systems containing π -electrons*. Verlag Chemie, Deerfield Beach, Florida, pp 147–201
81. (a) Tornare J-M, Vogel P (1984) *J Org Chem* 49: 2501; (b) Metrel J-L, Vogel P (1985) *Helv Chim Acta* 68: 334
82. Paquette LA (1983) in: Watson WH (ed) *Stereochemistry and reactivity of systems containing π -electrons*. Verlag Chemie, Deerfield Beach, Florida, pp 41–73
83. (a) Avenati M, Hagenbuch J-P, Mahaim C, Vogel P (1980) *Tetrahedron Lett* 3167; (b) Avenati M, Carrupt P-A, Quarroz D, Vogel P (1982) *Helv Chim Acta* 65: 188; (c) Mahaim C, Vogel P (1982) *Helv Chim Acta* 65: 866
84. (a) Paquette LA, Carr RVC, Bohm MC, Gleiter R (1980) *J Am Chem Soc* 102: 1186; (b) Bohm MC, Carr RVC, Gleiter R, Paquette LA (1980) *J Am Chem Soc* 102: 7218; (c) Paquette LA, Carr RVC, Arnold E, Clarby J (1980) *J Org Chem* 45: 4907; (d) Paquette LA, Charumilind P, Kravetz TM, Bohm MC, Gleiter R (1983) *J Am Chem Soc* 105: 3126; (e) Paquette LA, Schaefer AG, Blount JF (1983) *J Am Chem Soc* 105: 3642; (f) Paquette LA, Kravetz TM, Bohm MC, Gleiter R (1983) *J Org Chem* 48: 1250; (g) Paquette LA, Green KE, Hsu L-Y (1984) *J Org Chem* 49: 3650
85. (a) Paquette LA, Bellamy F, Bohm MC, Gleiter R (1980) *J Org Chem* 45: 4913; (b) Paquette LA, Carr RVC, Charumilind P, Blount JF (1980) *J Org Chem* 45: 4922
86. Highly reactive dienophiles such as benzyne, dimethyl acetylenedicarboxylate, and tetracyanoethene constitute the only consistent exceptions to endo-face attack. See, for example (a) Tornare J-M, Vogel P, Pinkerton AA, Schwarzenbach D (1985) *Helv Chim Acta* 68: 2195; (b) Metral J-L, Lauterwein J, Vogel P (1986) *Helv Chim Acta* 69: 1287; (c) Burnier G, Schwager L, Vogel P (1986) *Helv Chim Acta* 69: 1310
87. Gleiter R, Paquette LA (1983) *Acc Chem Res* 16: 328
88. Houk KN (1983) in: Watson WH (ed) *Stereochemistry and reactivity of systems containing π -electrons*. Verlag Chemie, Deerfield Beach, Florida, pp 1–40
89. (a) Alder K, Stein G (1931) *Justus Liebigs Ann Chem* 485: 211; (b) Alder K, Stein G (1935) *Justus Liebigs Ann Chem* 515: 185; (c) Schleyer PvR (1967) *J Am Chem Soc* 89: 701; (d) Brown HC, Hammer WJ, Kawakami JH, Rothberg I, Van der Judt DL (1967) 89: 6381; (e) Brown HC, Kawakami JH, Liu K-T (1973) *J Am*

- Chem Soc 95: 2209; (f) Huisgen R, Ooms PHJ, Mingen M, Allinger NL (1980) 102: 3951
90. (a) Hart H, Raja N, Meador MA, Ward DL (1983) J Org Chem 48: 4357 (b) Hart H, Lai C-Y, Nwokogu GC, Shamouilian S (1987) Tetrahedron 43: 5203
 91. Kohnke FH, Stoddart JF, Slawin AMZ, Williams DJ (1988) Acta Crystallogr C44: 738
 92. Rondan NG, Paddon-Row MN, Houk KN (1981) J Am Chem Soc 103: 2436
 93. (a) Wipff G, Morokuma K (1980) Tetrahedron Lett 21: 4445; (b) Burkert U (1981) Angew Chem Int Ed Engl 20: 572; (c) Spanget-Larsen J, Gleiter R (1980) Tetrahedron Lett 21: 2435
 94. Gleiter R, Bohm MC (1983) in: Watson WH (ed) Stereochemistry and reactivity of systems containing π -electrons. Verlag Chemie, Deerfield Beach, Florida, pp 105–146
 95. (a) Caramella P, Rondan NG, Paddon-Row MN, Houk KN (1981) J Am Chem Soc 103: 2438; (b) Houk KN, Rondan NG, Brown FK, Jorgensen WL, Madura JD, Spellmeyer DC (1983) J Am Chem Soc 105: 5980
 96. (a) Pinkerton AA, Schwarzenbach D, Stibbard JHA, Carrupt P-A, Vogel P (1981) J Am Chem Soc 103: 2095; (b) Hagenbuch J-P, Vogel P, Pinkerton AA, Schwarzenbach D (1981) Helv Chim Acta 64: 1818; (c) Watson WH, Galloy J, Bartlett PD, Roof AAM (1981) J Am Chem Soc 103: 2022; (d) Bartlett PD, Combs Jr GL, Thi Li A-X, Watson WH, Galloy J, Kimura M (1982) J Am Chem Soc 104: 3131
 97. Pinkerton AA, Carrupt P-A, Vogel P, Boschi T, Thuy NH, Roulet R (1978) Inorg Chem Acta 28: 123
 98. See, for example Greenberg A, Liebmann JF (1978) Strained organic molecules. Academic Press, New York
 99. Houk KN, Paddon-Row MN, Rondan NG (1983) J Mol Struct (THEOCHEM) 103: 197
 100. Houk KN, Paddon-Row MN, Rondan NG, Wu Y-D, Brown FK, Spellmeyer DC, Metz JT, Loncharich RJ (1986) Science (Washington DC) 231: 1109
 101. (a) Rondan NG, Paddon-Row MN, Caramella P, Mareda J, Mueller P, Houk KN (1982) J Am Chem Soc 104: 4974; (b) Paddon-Row MN, Rondan NG, Houk KN (1982) J Am Chem Soc 104: 7162; (c) Houk KN (1983) Pure Appl Chem 55: 277
 102. Mazzocchi PH, Stahly B, Dodd J, Domelsmith LN, Rozeboom MD, Caramella P, Houk KN (1980) J Am Chem Soc 102: 6482
 103. The non-equivalent extension of the π -orbitals has been proposed to govern the *exo*-face attack observed in these cases. See Burgess EM, Liotta CL (1981) J Org Chem 46: 1703
 104. Perturbations responsible for small ground state distortions can result in much larger energy differences between competing transition states for reactions. See, for example (a) Bürgi H-B, Dunitz JD (1983) Acc Chem Res 16: 153; (b) Bürgi H-B, Dunitz JD (1987) J Am Chem Soc 109: 2924; (c) Bürgi H-B, Deubler-Steudle KC (1988) J Am Chem Soc 110: 4953; (d) Bürgi H-B, Deubler-Steudle KC (1988) J Am Chem Soc 110: 7291; (e) Allen FH, Kirby AJ (1984) J Am Chem Soc 106: 6197; (f) Briggs AJ, Glenn R, Jones PG, Kirby AJ, Ramaswamy P (1984) J Am Chem Soc 106: 6200; (g) Jones PG, Kirby AJ (1984) J Am Chem Soc 106: 6207
 105. (a) Seebach D, Zimmermann J, Gysel U, Ziegler R, Ha T-K (1988) J Am Chem Soc 110: 4763; (b) Seebach D, Zimmermann J (1986) Helv Chim Acta 69: 1147
 106. Winter CE (1987) J Chem Ed 64: 587
 107. (a) Cieplak AS (1981) J Am Chem Soc 103: 4540; (b) Johnson CR, Tait BD, Cieplak AS (1987) J Am Chem Soc 109: 5875; (c) Cheung CK, Tseng LT, Lin M-H, Striivastava S, LeNoble WJ (1986) J Am Chem Soc 108: 1598; (d) Striivastava S, LeNoble WJ (1987) J Am Chem Soc 109: 5874
 108. For a review of stereoelectronically-assisted bond making and bond breaking in biological systems, see Gorenstein DG (1987) Chem Rev 87: 1047
 109. Predicting stereoselectivities is still a young science. Indeed, there are several different models for deducing the most favorable mode of attack to a trigonal center. See, for example, refs. 100 and 105–107, in addition to (a) Vogel E, Carvatti G, Franck D, Aristoff P, Moody Ch, Becher A, Felix D, Eschenmoser A (1987) Chem Lett 219; (b) Cherest M, Felkin H, Prudent N (1968) Tetrahedron Lett 2199; (c) Cherest M, Felkin H (1968) Tetrahedron Lett 2205

110. Ellwood P, Mathias JP, Stoddart JF, Kohnke FH (1988) *Bull Soc Chim Belges* 97: 669
111. See, for example, (a) Kahn SD, Pau CF, Overmann LE, Hehre WJ (1986) *J Am Chem Soc* 108: 7381; (b) Kahn SD, Hehre WJ (1987) *J Am Chem Soc* 109: 663
112. Kohnke FH, Slawin AMZ, Stoddart JF, Williams DJ (1987) *Angew Chem Int Ed Engl* 26: 892
113. (a) Carrupt P-A, Vogel P (1979) *Tetrahedron Lett* 4533; (b) Bessiere Y, Vogel P (1980) *Helv Chim Acta* 63: 232; (c) Pilet O, Vogel P (1981) *Helv Chim Acta* 64: 2563; (d) Pilet O, Birbaum J-L, Vogel P (1983) *Helv Chim Acta* 66: 19; (e) Tornare J-M, Vogel P (1985) *Helv Chim Acta* 68: 1069
114. Luo J, Hart H (1987) *J Org Chem* 52: 4833
115. (a) Wittig G, Reuther W (1972) *Ann Chem* 761: 20; (b) Takeshita H, Mori A, Sano S, Fujise Y (1975) 48: 1661
116. Irrngartinger H, Deuter J, Charumilind P, Paquette LA (1989) *J Am Chem Soc* 111: 9236
117. Carrupt P-A, Vogel P (1985) *J Mol Struct (THEOCHEM)* 124: 9
118. Elmosalamy MAF, Moody GJ, Thomas JDR, Kohnke FH, Stoddart (1989) *Anal Proc* 26: 12
119. Gould RO, Gray AM, Taylor P, Walkinshaw MD (1985) *J Am Chem Soc* 107: 5921; (b) Burley SK, Petsko GA (1985) *Science (Washington DC)* 229: 23; (c) Burley SK, Petsko GA (1986) *FEBS Lett* 203: 139; (d) Burley SK, Petsko GA (1988) *Adv Prot Chem* 39: 125; (e) Jorgensen WL, Severance M (1990) *J Am Chem Soc* 113: 4768
120. Nishio M, Hirota M (1989) *Tetrahedron* 45: 7201
121. Alder RW, Sessions RB (1985) *J Chem Soc Perkin Trans 2*: 1849
122. Ashton PR, Isaacs NS, Kohnke FH, Slawin AMZ, Spencer C, Stoddart JF, Williams DJ (1988) *Angew Chem Int Ed Engl* 27: 966
123. Milgrom L (1988) *New Scientist* 3 Dec 61
124. Stoddart JF (1988) *Chem Brit* 24: 1203
125. Balaban AT (1980) *Pure Appl Chem* 52: 1409
126. Vögtle F (1983) *Topp Curr Chem* 115: 157
127. (a) Hart H, Nwokogu GC (1981) *J Org Chem* 46: 1251; (b) Xing YD, Huang NZ (1982) *J Org Chem* 47: 140
128. (a) Wong HNC, Man Y-M, Mak TCW (1987) *Tetrahedron Lett* 28: 6359; (b) Wong HNC (1989) *Acc Chem Res* 22: 145; (c) Pons J-M, Santelli M (1988) *Tetrahedron* 44: 4295
129. Rabideau PW (ed) (1989) *Conformational analysis of cyclohexenes, and cyclohexadienes*. Verlag-Chemie, New York
130. (a) Luo J, Hart H (1988) *J Org Chem* 53: 1341; (b) Luo J, Hart H (1989) *J Org Chem* 54: 1762
131. For a discussion of isobenzofurans and their reactions, see, for example (a) Fieser LF, Haddadin MJ (1964) *J Am Chem Soc* 86: 2081; (b) Fieser LF, Haddadin MJ (1965) *Can J Chem* 43: 1599; (c) Friederichsen W (1980) *Adv Het Chem* 26: 135; (d) Rodrigo R (1988) *Tetrahedron* 44: 2093
132. Ashton PR, Isaacs NS, Kohnke FH, Mathias JP, Stoddart JF (1989) *Angew Chem Int Ed Engl* 28: 1258
133. Several classical valence isomers of the bisisobenzofuran 54 can be drawn, however, this classical biradical representation serves to illustrate both the bisdiene and radicalic behaviour demonstrated by this species.
134. Kohnke FH, Mathias JP, Stoddart JF, Slawin AMZ, Watts DJ, Williams DJ (1990) *Acta Crystallogr C* 46: 1046
135. Kohnke FH, Mathias JP, Stoddart JF, Slawin AMZ, Watts DJ, Williams DJ (1990) *Acta Crystallogr C* 46: 1049
136. Florey A, Vogel P (1975) *Helv Chim Acta* 58: 1488
137. Balaban AT (1988) *Rev Roum de Chem* 33: 699
138. Clar E (1942) *Chem Ber* 75: 1330

- 139. (a) Jackson LM, Sondheimer F, Amiel Y, Ben-Efraim DA, Gaoni Y, Wolosky R, Bothner-By AA (1962) *J Am Chem Soc* 82: 4307; (b) Clar E (1972) *The aromatic sextet*. Wiley, London
- 140. This reaction has previously been reported to yield only one, unidentified, isomer. See Hart H, Shamouilian S (1981) *J Org Chem* 46: 4874
- 141. Mathias JP, Slawin AMZ, Stoddart JF, Williams DJ Unpublished results
- 142. Ashton PR, Isaacs NS, Kohnke FH, D'Alcontres GS, Stoddart JF (1989) *Angew Chem Int Ed Engl* 28: 1261

Rigid Molecular Tweezers as Hosts for the Complexation of Neutral Guests

Steven C. Zimmerman

Department of Chemistry, University of Illinois, 1209 West California Street, Urbana,
Illinois 61801, USA

Table of Contents

1 Introduction	72
1.1 Definitions and Scope	73
2 Complexation of Neutral Guests by Non-Macrocyclic	
Hosts Using π-Stacking	73
2.1 Concept and Other Approaches	73
2.2 Design of Molecular Tweezers	76
2.3 Synthesis of Molecular Tweezers	77
2.4 Structure of Molecular Tweezers	78
2.5 Complexation by Molecular Tweezers	81
3 Complexation of Neutral Guests by Non-Macrocyclic	
Hosts Using π-Stacking and Hydrogen Bonding	84
3.1 Concept and Design	84
3.2 Synthesis and Structure of Molecular Tweezers and Refinement of Design	87
3.3 Complexation of Nucleotide Bases by Molecular Tweezers	92
3.3.1 Nature and Strength of Complex with 9-Propyladenine	92
3.3.2 Nucleoside Selectivity	95
3.3.3 Origin of Complexation Strength	95
4 Summary and Outlook	99
5 References	100

1 Introduction

The concept of non-covalent interactions between molecules is a very old one, dating to the Greek and Roman empires [1–3]. However, modern ideas about these interactions began to emerge only in the later half of the 19th century. At this time, Van der Waals explained the nonideal behavior of gases by assuming molecules to be hard spheres that could attract one another. In addition to this and other important developments, it was during this period that Emil Fischer made his famous analogy between the way a substrate and enzyme interact to the way that a key fits into a lock [4]. This prophetic statement is now illustrated in most basic biochemistry textbooks by a cartoon similar to that depicted in Fig. 1. The enzyme, which is large relative to the substrate, has clefts and depressions on its surface complementary to the shape of the substrate.

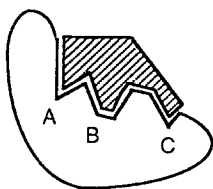


Fig. 1. Schematic representation of Fisher's Lock-Key Concept in an enzyme-substrate complex

Organic chemists' desire to understand and imitate the non-covalent interactions found in nature is comparatively new. Pioneering work focused on cyclodextrin inclusion complexes [5] and crown ether-metal ion interactions [6–8]. The naturally occurring cyclodextrins and the serendipitously discovered crown ethers [8] are both macrocyclic in structure. Many subsequent studies used macrocycles by design. Presumably, this structural choice was guided both by analogy to the earlier systems and an intuitive sense that macrocycles experience fewer conformational restrictions upon complexation than their acyclic counterparts. In fact, this intuition has found extensive experimental support, and is now embodied in Cram's *principle of preorganization* [9]. This principle states that complex stability will be maximized when the constituent parts are structurally organized for complexation and low solvation.

Macrocycles have the additional benefit that their finite cavity dimensions make them inherently selective in binding due to *size exclusion*. Preorganization and size selectivity does not come without limitations. The very large, rigid cavities required to bind large molecules are difficult to construct, although progress in this area has been reported recently [10, 11]. It is interesting that the binding sites of biomolecules (e.g. enzymes, antibodies) rarely have cavities that surround a substrate (antigen), but rather have clefts and depressions on their surface as discussed above and illustrated in Fig. 1.

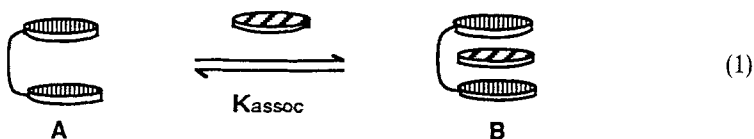
1.1 Definitions and Scope

Cram has defined *hosts* and *guests* as organic molecules or ions whose binding sites *converge* and *diverge*, respectively, in forming a complex [12]. This review describes recent efforts in Urbana to develop non-macrocyclic hosts for neutral guests. These hosts, which contain preorganized aromatic clefts, are called *molecular tweezers*, a term coined by Whitlock [13] to describe hosts that contain two aromatic chromophores covalently linked by a single spacer unit. A suitable spacer will allow the π -surfaces of the molecular tweezer to converge on the two divergent π -faces of an aromatic guest in a *sandwich complex* held together by two π -stacking interactions. More sophisticated molecular tweezers carry an additional functional group oriented toward the aromatic cleft so that π -stacking and hydrogen bonding can occur simultaneously. Both types of hosts can engage in *multi-site interactions* with appropriate guests. A central theme of this review is that properly constructed molecular tweezers can complex large guests with affinities that greatly exceed expectations based on the strength of the individual contacts. Understanding the origin of this *complex additivity in binding energies* is a special challenge. This review emphasizes work carried out in the author's laboratory. An excellent review of related systems has been published recently [14].

2 Complexation of Neutral Guests by Non-Macrocyclic Hosts Using π -Stacking

2.1 Concept and Other Approaches

The association of aromatic chromophores in solution is well documented, although the driving force for complexation is a matter of continuing debate. In organic solvents, a favorable interaction generally occurs only when one partner is a π -donor and the other a π -acceptor [15]. Exceptions include large aromatic systems, such as porphyrins, which readily self-associate in chloroform [16]. The electron donor-acceptor (EDA) complexes formed between π -donors and π -acceptors are believed to be held together by electrostatic, polarization, dispersion, and charge transfer forces. EDA forces are weak with association constants in common organic solvents generally ranging from 0.1 to 1000 M^{-1} , but usually less than 10 M^{-1} . The importance of the component forces to the stability of these complexes is not known although it is believed that the charge transfer interaction is not the dominant one [15].



One interest in molecular tweezers relates to their potential for increasing the stability of EDA complexes. As shown in Eq. (1), this potential derives from the ability of the molecular tweezer (A) to form a π -sandwich complex (B). Whether such a complex forms and the second chromophore contributes significantly to the stability of the complex will depend upon many factors, including the enthalpic strength of the second π -stacking interaction and the enthalpic and entropic loss necessary for adopting the required geometry.

The few systems reported to test this idea have met with mixed success. Foster investigated the complexation of 1,3,5-trinitrobenzene (TNB) by a series of bis-anilines (**1**) and found association constants to be exactly twice that for TNB-dialkylaniline complexes (Table 1) [17]. This finding was attributed to a purely statistical advantage for bis-aniline **1**. A bis-donor naphthalenophane **2** was shown to complex TNB in chloroform with an association constant of 274 M^{-1} [18]. While this is significantly stronger than the complex formed between 1,4-dimethoxynaphthalene and TNB ($K_{\text{assoc}} = 74 \text{ M}^{-1}$), a careful analysis of complexation shifts led to the conclusion that the TNB was externally bound [18]. The increase in association constant observed with **2** was proposed to arise from an increase in naphthalene π -base strength through an edge-face charge transfer as in **3**. Thus, neither of these systems appear to form a sandwich complex.

Stoddart has extensively investigated the interaction of dibenzocrown ethers with the dipyridinium dications, diquat and paraquat [19]. Dibenzocrown ether

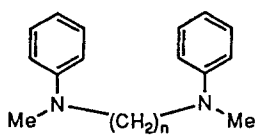
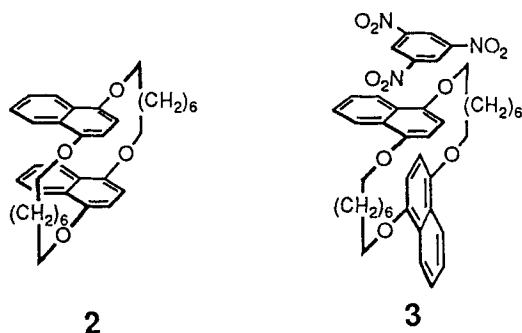
**1**

Table 1. Association constants for 1,3,5-trinitrobenzene complexes of bis-anilines **1** and related molecules in CHCl_3 at 35.5°C^a

Donor	$K_{\text{assoc}} (\text{Kg mol}^{-1})$
1a , $n = 2$	1.1 ± 0.1
1b , $n = 3$	1.1 ± 0.1
1c , $n = 4$	1.4 ± 0.1
1d , $n = 5$	1.4 ± 0.1
1e , $n = 6$	1.5 ± 0.1
<i>N</i> -ethyl- <i>N</i> -methylaniline	0.7 ± 0.1
<i>N</i> -methyl- <i>N</i> -propylaniline	0.7 ± 0.1

^a Taken from Ref. 17



4 and diquat form complexes in acetone, the association constants of which were sensitive to the length of the polyether chains as seen in Table 2 [20]. The data were interpreted in terms of a V-shaped conformation for dibenzo-27-crown-9, where both aromatic rings interact with diquat but not in a face-face arrangement. The chains in dibenzo-30-crown-10 are sufficiently long to allow a U-shaped conformation in which a perfect face-face π -sandwich complex can form. This proposal is supported by single crystal X-ray structure determination of complex **5** [21]. One interesting feature of the X-ray structure of **5** is the finding that the four aryl ether oxygens are each within van der Waals distance of the nitrogen atoms of diquat. This feature is common to several related structures and suggests a strong electrostatic component to the complexation [21].

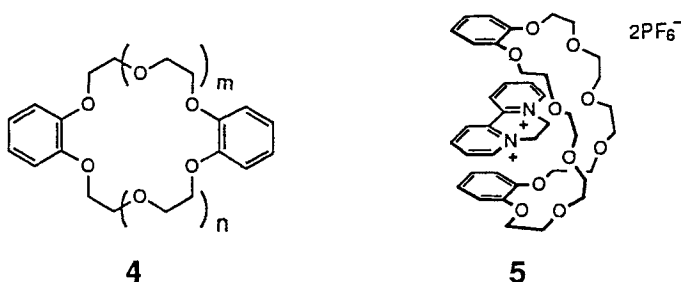


Table 2. Association constants (K_{assoc}) for 1 : 1 complexes between diquat and dibenzocrown ethers **4** in acetone at 25.5 °C^a

Receptor	m	n	K_{assoc} (M^{-1})
DB27C9	3	2	410
DB30C10	3	3	17500
DB33C11	4	3	10800
DB36C12	4	4	2000

^a Taken from Ref. 20

2.2 Design of Molecular Tweezers

In designing molecular tweezers, both complexing chromophores and an appropriate spacer unit must be chosen. The property of the chromophores that is most likely to affect the complexation strength is its π -donor or acceptor strength. The size and shape is also important as larger chromophores generally are more polarizable thereby enhancing dispersive and polarization interactions. Although the chromophores are important, the critical element of the molecular tweezers is the spacer unit. Features of concern in the design of the spacer are:

a) *Interchromophore separation and orientation.* A common feature of the X-ray analysis of donor-acceptor complexes is a face-face, but offset arrangement of the chromophores with inter-ring distances between 3.2 and 3.5 Å [22]. Thus, an optimum spacer might hold the chromophores in parallel planes with a 6.4–7.0 Å separation.

b) *Rigidity.* Chen and Whitlock showed that the rigid diyne spacer in molecular tweezer **6** prevented self-association of the caffeine rings thereby increasing its binding power over a flexible (saturated) analogue [13]. An even higher degree of preorganization will be obtained if the spacer can maintain a syn-orientation of the complexing chromophores. In the case of **6**, free rotations in the spacer unit allow many conformations to be populated.



c) *Ease and flexibility of synthesis.* Of course, the molecular tweezer should be easily synthesized. Ideally, the route will be sufficiently flexible to allow attachment of different chromophores near the end of the synthesis.

With these issues in mind, dibenz[*c,h*]acridine was chosen as a spacer. As a result of its U-shape, chromophores attached at C-2 and C-12 could be held in parallel planes (Fig. 2). The C-2 to C-12 distance is known to be 7.24 Å from the X-ray structure [23], however, the interchromophore distance in the molecular

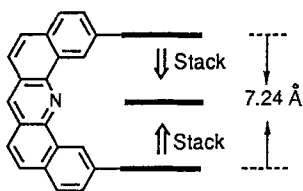


Fig. 2 Schematic representation of a molecular tweezer containing a dibenz[*c,h*]acridine spacer

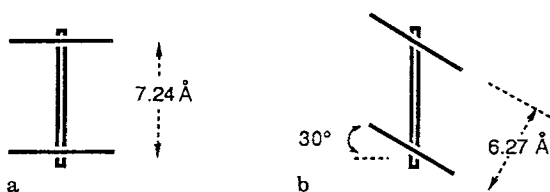
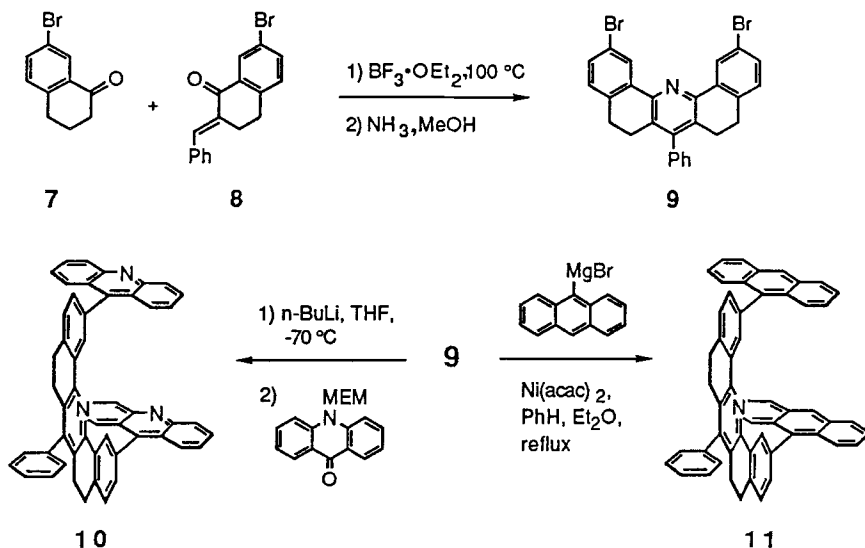


Fig. 3. Schematic representation of the relationship between spacer-chromophore dihedral angle and interchromophore separation

tweezers is not constrained to this value. Instead, it represents a maximum separation since rotations around the aryl-aryl bonds reduce the perpendicular interchromophore distance by an amount directly dependent on the dihedral angle (Fig. 3). Molecular mechanics calculations suggest that rotations of a 9-anthryl group $\pm 30^\circ$ from perpendicularity will cost ca. 2 kcal mol⁻¹ [24]. Such rotations lead to a 6.24 Å separation between anthracene rings. Thus, this molecular tweezer can readily adjust the size of its aromatic cleft and thereby close to the optimum separation for binding an aromatic guest.

2.3 Synthesis of Molecular Tweezers

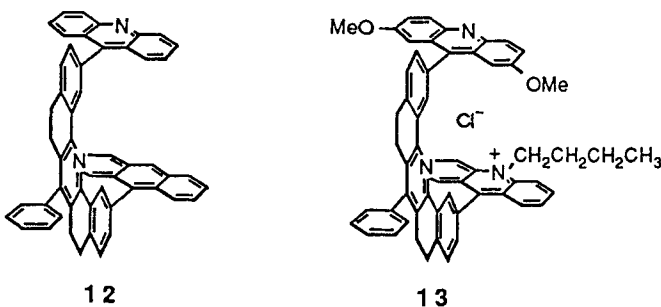
The synthesis of molecular tweezers **10** and **11** are outlined in Scheme 1. Their spacers differ in two ways from the hypothetical system of Fig. 2: They are not fully oxidized and they carry a phenyl substituent. The phenyl group is an artifact of the synthesis, but does provide the advantage of being easily functionalized



Scheme 1. Synthesis of symmetrical molecular tweezers **10** and **11**

and remote from the binding cleft. Thus, it is in a position where solubility properties can be altered and where immobilization might be realized. The tetrahydrodibenzacridine spacer in **10** and **11** has more flexibility than the fully aromatic spacer in Fig. 2, but this does not substantially alter the properties of these molecular tweezers [25, 26].

The synthesis [25, 26] began with 7-bromo-1-tetralone (**7**), available in multi-gram quantity in three steps from succinic anhydride and bromobenzene [27, 28] (Scheme 1). Treatment of **7** with an aromatic aldehyde and base produces the corresponding benzylidene (e.g., **8**) which couples with **7** in boron trifluoride etherate to form a pyrylium salt. This pyrylium salt is not isolated but treated with ammonia to afford functionalized spacer **9**. As seen in Scheme 1, the attachment of anthracene [29] or acridine chromophores occurs in a single step. Alternatively, stepwise attachment of the aromatic chromophores allows construction of molecular tweezers **12** and **13** carrying different chromophores. With respect to efficiency, tweezers **10** and **11** are synthesized in six steps from inexpensive starting materials with overall yields of 11% and 14%, respectively.



2.4 Structure of Molecular Tweezers

In order to determine whether the dibenzacridine spacer prevents association of the attached chromophores, Whitlock's "cyclization shift" analysis was performed [18, 30]. This analysis involves comparing the ^1H NMR chemical shifts of the acridine and anthracene rings in **10** and **11**, respectively, with analogous monochromophores such as 9-phenylacridine and 9-phenylanthracene. Large upfield shifts for **10** and **11** would indicate intramolecular stacking (i.e. collapse of binding cleft). In fact, all molecular tweezers synthesized to date exhibit only small cyclization shifts, indicating that the dibenz[c,h]acridine spacer effectively isolates the complexing chromophores and that the molecular tweezers possess open binding clefts [26].

Molecular tweezers such as **10** have two elements of conformational flexibility that together determine its structure. The most significant of these involves rotation around the spacer-chromophore bonds. As described above, all dihedral angles

within 30° of perpendicularity would be accessible. With respect to the barrier to rotation, the aryl-aryl rotation is “invisible” in **10** and **11**, but unsymmetrically substituted molecular tweezers **14–19** exhibit ^1H NMR spectra consistent with the presence of a 1:1 mixture of atropisomers [26]. Coalescence studies afforded the data in Table 3. Despite the fact that the fully oxidized molecular tweezers should have a reduced time-averaged distance between the acridine rings, their barrier to atropisomer interconversion is negligibly higher. This was unexpected because examination of CPK models suggested that large non-bonded interactions would be experienced as the chlorine and/or tert-butyl substituent in **18** and **19** passed through the cleft. Overall, the results indicate freely rotating chromophores regardless of substitution or whether the spacer is oxidized. Thus, an entropy price will be paid upon complexation due to loss of this free rotation.

The second conformational issue concerns the tetrahydrodibenzacridine spacer. By analogy with 9,10-dihydrophenanthrene, the spacer should be nonplanar with a

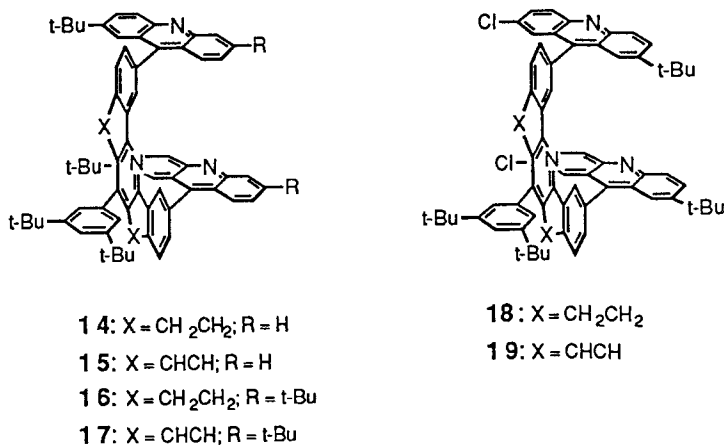


Table 3. Atropisomerism of molecular tweezers^a

Compd	Group Observed	T_c (K)	ΔG_c^\ddagger (kcal mol ⁻¹)
14	2- <i>t</i> -Bu	366	19
15	2- <i>t</i> -Bu	363	19
16	2- <i>t</i> -Bu	413	21
	6- <i>t</i> -Bu	393	21
17	2- <i>t</i> -Bu	404	22
	6- <i>t</i> -Bu	425	22
18	7- <i>t</i> -Bu	387	21
19	7- <i>t</i> -Bu	398	22

^a Taken from Ref. 26

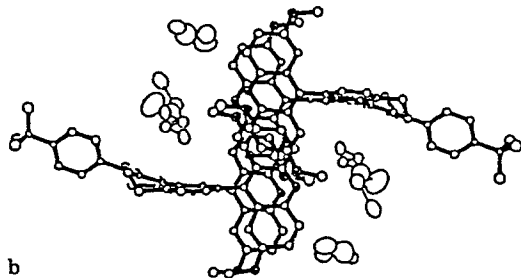
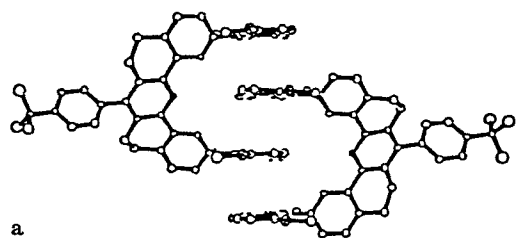


Fig. 4a, b. Views from the side (a) and top (b) of the crystal packing of molecular tweezer **21a**. Solvent molecules (dichloroethane) have been omitted in (a) for clarity

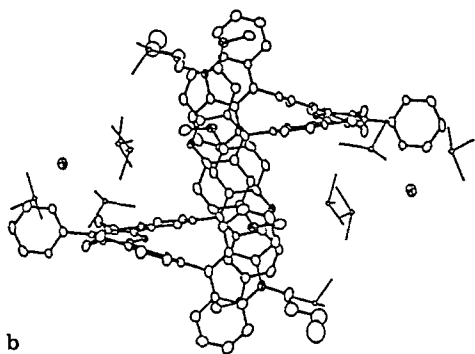
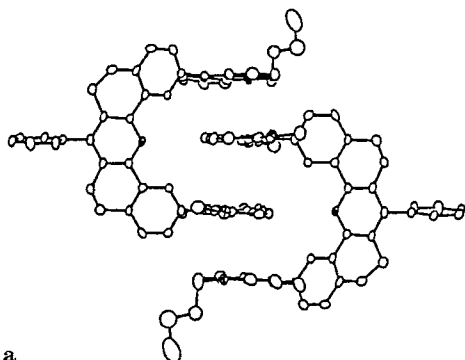


Fig. 5a, b. Views from the side (a) and top (b) of the crystal packing of molecular tweezer **13**. Solvent molecules (chloroform) and counterion have been omitted in (a) for clarity

dihedral angle of 15–20° between the terminal phenyl rings and the internal pyridine [31]. Because there are two reduced rings, the spacer can adopt a *meso*-form that is crescent shaped or a *d,l*-form that is helical. Again by analogy to 9,10-dihydrophenanthrene, the interconversion of these forms should have a low barrier ($< 10 \text{ kcal mol}^{-1}$) [31], and molecular mechanics calculations indicate that the *meso* and *d,l*-forms will be nearly isoenergetic [24]. Indeed, the two forms are seen in the X-ray analysis of molecular tweezers **13** and **21a**. Tweezer **21a** adopts the *meso* conformation and as a result the acridines are aligned vertically (Fig. 4). The acridines are also held in parallel planes separated by 6.8 Å, allowing each cleft to partially complex two neighbors, forming a continuous up-down-up stack. In contrast, the structure of **13** reveals a spacer in the *d,l*-conformation so that the acridine and acridinium rings are splayed apart slightly (Fig. 5). Interestingly, the “donor” chromophores alone form an infinite stack.

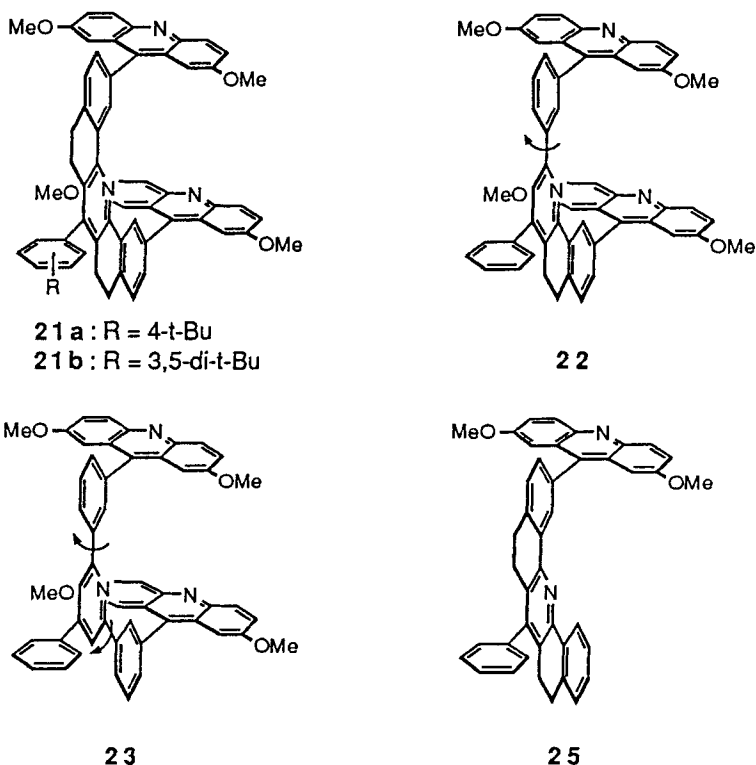
2.5 Complexation by Molecular Tweezers

Most molecular tweezers studied were highly soluble only in halogenated solvents, while a few were soluble in a range of solvents. Binding studies were carried out in chloroform since it solubilizes the hosts and guests of interest and is not a strongly competitive solvent in electron donor-acceptor studies [15]. Prior to carrying out complexation studies it is imperative to check for potential aggregation of host and guest under the conditions used. Only molecular tweezer **13**, containing both donor and acceptor chromophores, showed a tendency to aggregate in chloroform solution.

Molecular tweezers such as **10** showed no affinity ($K_{\text{assoc}} < 3 \text{ M}^{-1}$) for π -donor guests like naphthalene and anthracene. However, π -acceptors such as trinitrobenzene (TNB) and nitrated fluorenones were bound. The complexation experiments were performed by titrating a solution of the guest with the host and recording the upfield chemical shifts of the guest protons by ^1H NMR. Alternatively, the host could be titrated with guest and the increase in absorbance at the charge transfer band monitored.

From the complexation data in Table 4, several conclusions can be drawn. First, all the molecular tweezers form complexes with 2,4,5,7-tetranitrofluorenone (TENF) that are significantly more stable than those formed from analogous monochromophores. For example, the association constants for complexes **21b**·TENF and **11**·TENF are larger than the analogous singly stacked complexes **24**·TENF and **20**·TENF by 10^3 and 10^4 fold, respectively [32–34]. Results from several studies indicated that the increase in complex stability seen with the molecular tweezers results from the second complexing chromophore and the formation of a π -sandwich complex. Thus, evidence that the spacer plays only a minor role is the finding that **25** complexes TENF with a binding constant qualitatively similar to that measured for **24** (Table 4).

The second π -stacking interaction in the **11**·TENF complex increases its $-\Delta G^\circ$ by 5 kcal mol^{-1} over that of the **20**·TENF complex (Table 4). A simple approach for predicting how large an increase in stability should be expected for the second



π -stack might involve summing the energies of the individual interactions. Since a single stacking interaction is worth $-\Delta G^\circ = 0.7 \text{ kcal mol}^{-1}$, this analysis would predict that $-\Delta G^\circ$ for the 11·TENF complex should be twice that value, i.e. $-\Delta G^\circ = 1.4 \text{ kcal mol}^{-1}$. The observed $-\Delta G^\circ$ of $5.9 \text{ kcal mol}^{-1}$ is significantly higher, indicating that this simple analysis is not valid.

Indeed, this is a case of *complex additivity of binding energies*, a phenomenon commonly seen in biological systems [35, 36]. Jencks has attributed the complex additivity in many systems to changes in translational and rotational entropy [36]. For example, the two complexing chromophores of the molecular tweezers are covalently connected. This means that the enthalpy of the second π -stacking interaction comes without paying the translational and rotation entropy price a second time.

The close proximity of the binding contacts in the molecular tweezers means that an interplay between them may also contribute to the complex additivity of binding energies. One possibility, that is discussed below, is that the proximity of the complexing chromophores prevents solvation of the binding cleft. A second possibility is synergism between the π -stacking interactions. However, this seems unlikely given that in termolecular EDA complexes, the second stacking interaction is weaker than the first [37, 38].

Table 4. Complexation data obtained from the ^1H NMR or UV-visible titration of 2,4,5,7-tetranitrofluorenone (TENF) with various hosts in chloroform^a

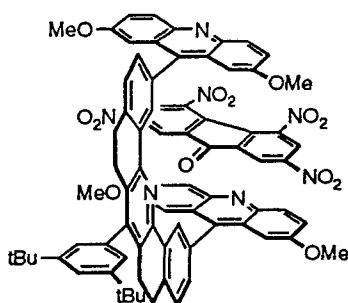
Entry	Compd	$\Delta\delta_{\text{max}}$, ppm		λ_{max} (CT, nm)	K_{assoc} (M^{-1})	$-\Delta G^\circ$ (kcal mol $^{-1}$)
		H-1(8)	H-3(6)			
1	9-phenyl anthracene (20)			650	3	0.7
2	11			656	20000	5.9
3	12			654	2800	4.7
4	10			509	900	4.0
5	21b	> 1.3	0.33		3400	4.7
6	22	> 1.3	0.32		700	3.8
7	23	> 1.3	0.32		170	2.9
8	9-phenyl-2,7-dimethoxy acridine (24)	—	0.51		5	0.9

^a Taken from Refs 25, 26, 32–34. For entries 1–4, ΔG° determined at 298 K. For entries 5–8, ΔG° determined at 288 K

How important is the enforced syn orientation of the complexing chromophores? This was determined by removing either one or both of the ethano bridges in the spacer of **21**, giving flexible molecular tweezers **22** and **23** [33]. As seen in Table 4 (entries 5–7), a loss of 0.9 kcal mol $^{-1}$ in complex stability (for TENF) is accrued with the introduction of each free rotation. This value is a reasonable one for the cost of freezing the rotation of a carbon-carbon bond [39]. An alternative explanation is that the ethano bridges provide the molecular tweezer access to an enthalpically unfavorable, but productive, binding conformation. This seems less likely given the energetics of the rotation in 2-phenylpyridine [40]. Thus, the higher degree of preorganization enjoyed by **21b** derives from the fact that its conformation is close to that required for binding. Highly preorganized systems are desolvated. The possibility that the enforced syn-orientation in **21b** results in a poorly solvated cleft cannot be ruled out, but if true it might have been expected that freezing out the second free rotation in **23** would have produced a much larger increase than did the first. Studies with different solvents are expected to shed additional light on this issue [41].

The complexation shifts ($\Delta\delta_{\text{max}}$, Table 4) for TENF indicate an offset, π -stacked complex in which the carbonyl is oriented toward the spacer as in **26**. While this might result from aligning the dipoles of TENF and the acridine rings, the same geometry is favored with the anthracene tweezers. It is most likely that the overall orientation is controlled by the nitro groups at the 4- and 5-position of the fluorenone ring which resist inclusion in the binding cleft because they are twisted from planarity by ca. 40° [42, 43].

Electron donor-acceptor interactions are important in the examples in Table 4. This means that the molecular tweezers affinity for a particular guest can be modulated. For example, the affinity that **10** has for TENF can be increased by substituting the acridines with methoxy groups (i.e. **21**). Does this increase in



26

complex stability reflect the increased π -donor potential of both chromophores or just one? Studies with **10**, **11**, and **12** help answer this question. As seen in Table 4 (entries 2–4), replacing one and then both acridines of **10** with the stronger π -donor anthracene chromophores results in incremental increases in binding affinity. Thus, molecular tweezers containing two good donor chromophores are superior to those with just one good donor, and these in turn are superior to molecular tweezers with two poor donors.

3 Complexation of Neutral Guests by Non-Macrocyclic Hosts Using π -Stacking and Hydrogen Bonding

3.1 Concept and Design

The molecular tweezers described above complex π -acceptor aromatic guests in chloroform using electron donor-acceptor interactions. Several strategies can be envisaged for increasing the versatility of these hosts. For example, water-soluble molecular tweezers might be expected to complex a wide range of aromatic guests, with the binding affinities dependent more on the extent of overlap between the host and the guest, than on their electronic complementarity. This expectation arises from the fact that the hydrophobic effect, not EDA interactions, becomes the major driving force for binding in aqueous solution [44]. Thus, work toward water-soluble molecular tweezers is in progress.

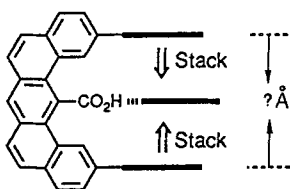


Fig. 6. Schematic representation of a molecular tweezer containing a dibenzanthracene spacer with a carboxylic acid converging on the binding cleft

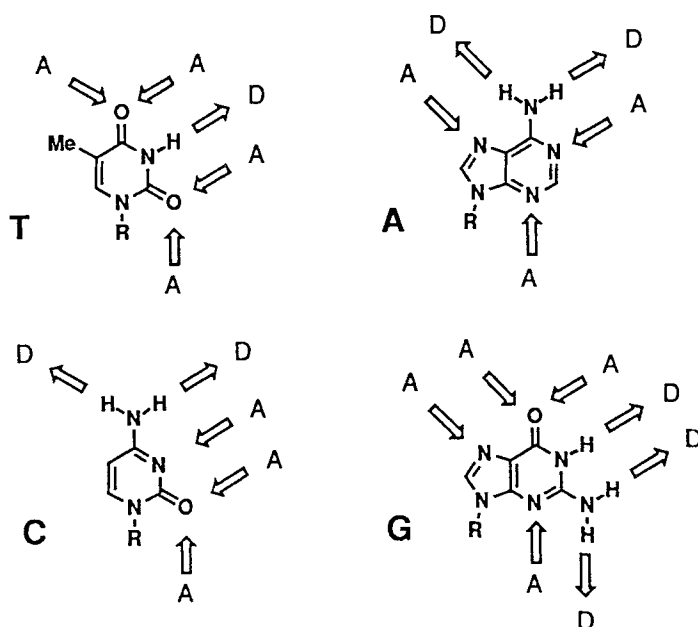


Fig. 7 Hydrogen bond donor (D) and acceptor (A) sites on the four common nucleotide bases

An alternative approach to increasing the versatility of the molecular tweezers, is to use additional binding forces that would operate in organic solvents. Indeed, at the outset of this work a major goal was to incorporate a functional group(s) in the molecular tweezer cleft that would be capable of hydrogen bonding to nucleotide bases. Such a molecular tweezer is shown schematically in Fig. 6. With an appropriate spatial relationship between the functional groups, a nucleotide base might be complexed by the π -stacking forces involved in many drug-DNA interactions [45] and by the hydrogen bonding contacts involved in protein-DNA recognition [46]. The existence of these latter interactions was postulated some years ago.

It was realized that the most selective interactions between the nucleotide bases and amino acid side chains would involve more than one hydrogen bond. Therefore, the residues of aspartate (Asp), glutamate (Glu), asparagine (Asn), glutamine (Gln), and arginine (Arg) are the most likely candidates [47]. However, most of the side-chains of these amino acids cannot distinguish between the four bases by themselves. This is because each of the common nucleotide bases have adjacent hydrogen bond donor and acceptor sites that are complementary to the side chains of Asp, Glu, Asn, and Gln (Fig. 7). The adjacent donor sites in guanosine are unique, and can be recognized by a carboxylate of either Asp or Glu. Likewise, only cytosine has adjacent acceptor sites and these can interact selectively with the guanidinium sidechain of Arg.

In double stranded DNA (RNA) the situation is different because several sites are occupied by the Watson-Crick hydrogen bonds [48] (Fig. 8). Thus, a carboxylic

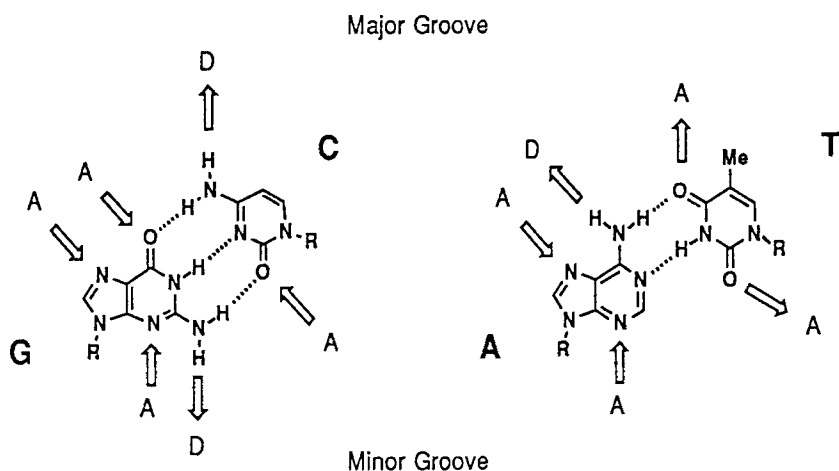


Fig. 8. Hydrogen bond donor (*D*) and acceptor (*A*) sites exposed in the grooves of double helical DNA

acid or amide can recognize an A-T base-pair in the major groove or a G-C base-pair in the minor groove, while Arg can recognize a G-C base-pair in the major groove. Several protein-DNA complexes have been examined crystallographically, but a clear recognition mechanism has not emerged [49–51]. As seen in Fig. 9, the idealized interactions are found, but so are more complex motifs. The strength of a few functional group-nucleotide base interactions have been determined in model studies. Most relevant to the current discussion is the work of Lancelot [52], who studied the association of butyric acid and several nucleotide bases in chloroform. For 9-ethyladenine, the association constant is 160 M^{-1} , a composite value that represents the three complexes shown in Fig. 10. The type 1 complex is favored over the type 7 by a ratio of 3 : 1, and both are stronger than the type 3 complex that contains only a single hydrogen bond. Since the four common nucleotide bases contain adjacent donor and acceptor sites, it isn't surprising that butyric acid is only weakly selective towards them (*vide supra*).

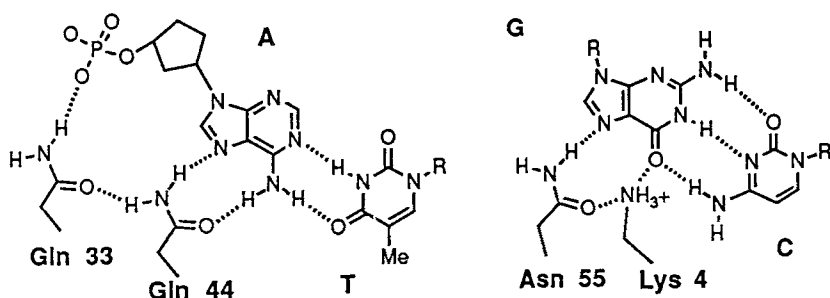


Fig. 9. Two hydrogen bonding motifs found in the lambda repressor-operator complex. Taken from Ref. 50

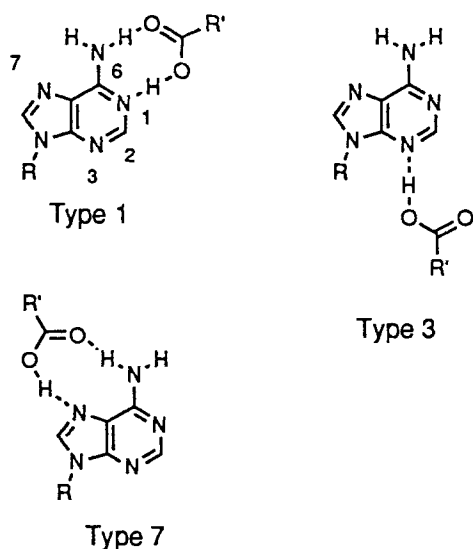
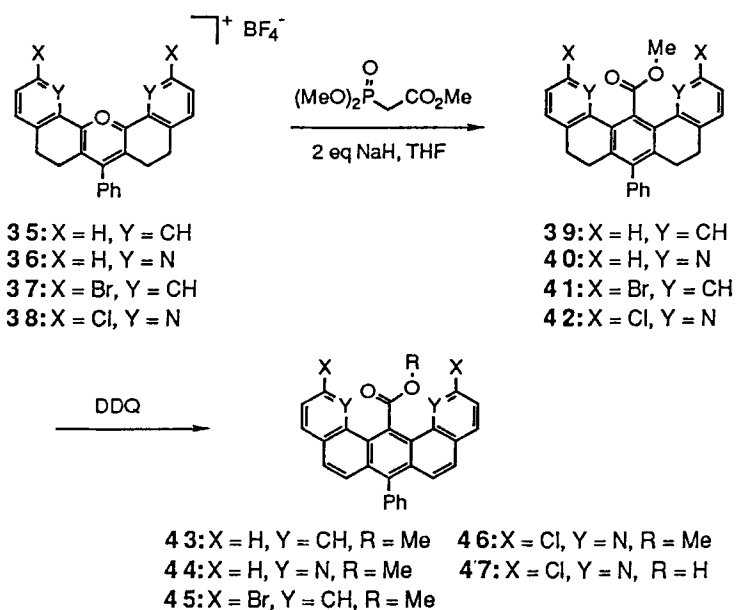


Fig. 10. Three complexes proposed to form between butyric acid and 9-ethyladenine. Taken from Ref. 52

The lack of selectivity and efficiency with which a single carboxylic acid binds nucleotide bases makes it an unlikely candidate for incorporation into a host for nucleotide guests. Nonetheless, it proved synthetically expedient to do so with molecular tweezers such as **11** and **21**. The issue addressed was whether the aromatic chromophores in the molecular tweezer represented in Fig. 6 could cooperate with the acid group to increase the binding efficiency and selectivity of the host.

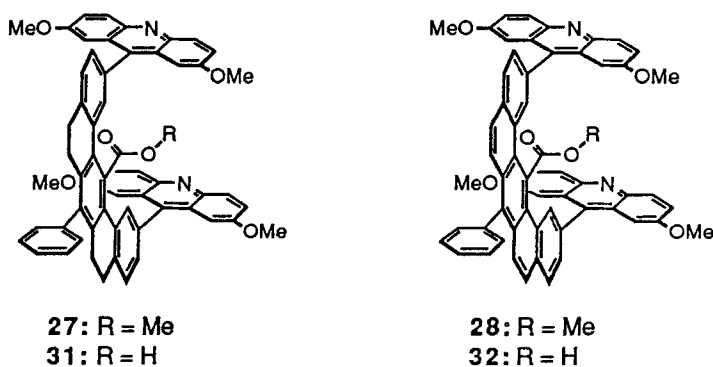
3.2 Synthesis and Structure of Molecular Tweezers and Refinement of Design

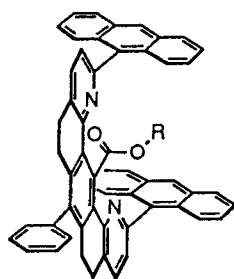
In a model study [53], synthetic routes were developed to the spacer units found in molecular tweezers **27–34**. The key step in these syntheses (Scheme 2) is the condensation of a pyrylium salt (**35**, **36**) with trimethylphosphonoacetate to produce spacers (**39**, **40**) with an ester group attached to the central bay region carbon [54, 55]. The structure of **43**, the first such spacer to be synthesized, was found to be poorly suited for incorporation into a molecular tweezer due to large distortions in the aromatic system [53]. These distortions are the result of strongly unfavorable peri interactions between C-1(13) and the ester group. They induce an end-to-end helical twist of ca. 40° in the aromatic system (Fig. 11) and cause the C-2 to C-12 distance to increase to 8.2 Å from the 7.24 Å distance found in the earlier dibenz[*c,h*]acridine spacer (*vide supra*). While the greater flexibility in spacer **39** would likely increase the severity of these problems, the incorporation of nitrogen atoms peri to the ester group as in **40** and **44** could alleviate this strain since a nitrogen lone-pair might be smaller and/or more compressible than a C-H



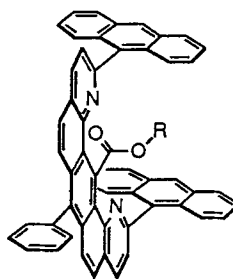
Scheme 2. Synthesis of spacer units containing an ester (carboxylic acid) in the central bay-region

bond. Indeed, **44** was synthesized (Scheme 2) and its X-ray structure indicated a π -system closer to planarity, with a C-2 to C-12 distance of 7.54 Å (Fig. 11). The structures of tweezers **27**–**30** were examined computationally with two assumptions [56]. First, anthracene rings replaced the dimethoxyacridine chromophores in **27** and **28** and were assumed to give similar results. Secondly, the low energy conformations of the methyl esters were assumed to closely resemble those of the corresponding carboxylic acids that would be used in binding experiments. As seen in Fig. 12, the binding cleft becomes progressively tighter along the series **27**→**28**→**29**→**30**. Each of these tweezers represents a discrete step toward an





29: R = Me
33: R = H



30: R = Me
34: R = H

optimized receptor and each is worthy of synthesis in order to examine the relationship between preorganization and complexation efficiency.

Toward this end, halo-spacers **41**, **42**, **45** and **46** were synthesized (Scheme 2), and the appropriate chromophores were attached [56, 57]. Tweezers **27** and **28** are synthesized in only 7 and 8 steps, respectively, from bromobenzene and succinic anhydride. The synthesis of **29** required 13 steps from cyclohexanone, pyrrolidine, and acrylonitrile. Although this synthesis is two steps longer than an alternative

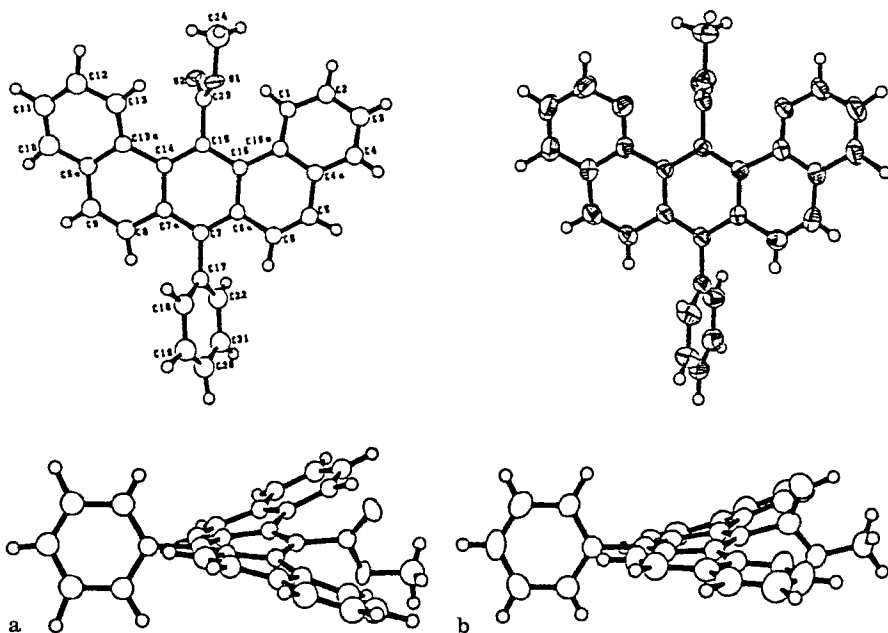


Fig. 11a, b. Two ORTEP views of ester **43** (a) and **44** (b). Thermal ellipsoids represent 35% probability contours. Taken from Ref. 53

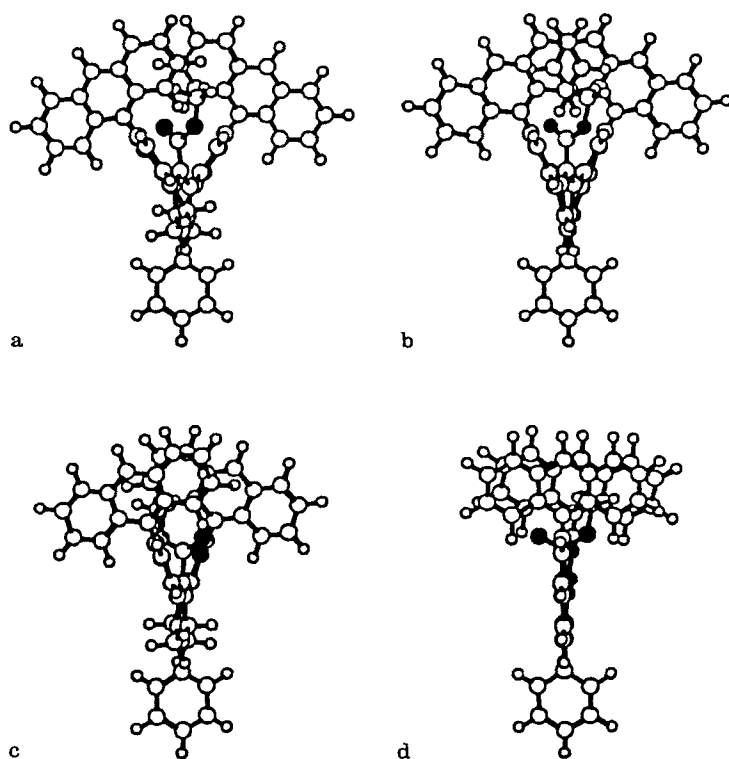
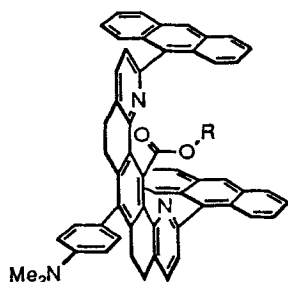


Fig. 12a–d. Top view of the calculated minimum energy conformations of molecular tweezers **27** (a), **28** (b), **29** (c), and **30** (d). See text and Ref. 56 for details

route to analogous tweezer **48** [57, 58], it is more efficient and general, and most importantly, allows access to the fully unsaturated tweezer **30** [56, 57].

The X-ray structure of **27** is very close to the calculated structure (Fig. 13). The large upfield chemical shifts observed in the ^1H NMR spectra of the methyl esters



48 : R = Me
49 : R = H

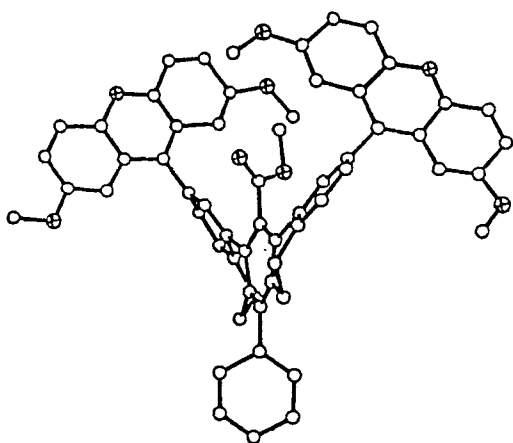


Fig. 13. Side (a) and Top (b) views of the X-ray structure of **27**. Top view is a more open projection than shown for analogous calculated structure in Fig. 12a

in **27–30** provide additional evidence that the calculated structures accurately reflect the degree of organization of the binding clefts (Table 5). Thus, the upfield chemical shifts of the methyl esters increase in the order **30** > **29** > **28** > **27**. The trend appears to reflect the spatial orientation of the chromophores rather than differences in their anisotropic shielding (i.e. anthracene vs acridine) since **27** has been synthesized with anthracene chromophores and the ^1H NMR chemical shift of its methyl ester resonance is unchanged.

Table 5. Upfield ^1H NMR chemical shift of methyl esters in molecular tweezers **27–30**

Molecular tweezer	Chemical shift of methyl ester (ppm)	Spacer	Chemical shift of methyl ester (ppm)	$\Delta\delta$ (ppm)
27	2.72	41	3.91	1.19
28	2.73	45	4.35	1.62
29	1.71	42	4.08	2.37
30	1.42	46	4.58	3.16

To complete the synthesis of the nucleotide hosts, the hindered tweezer esters needed to be converted to the corresponding carboxylic acids. One possible method presented itself with the surprising finding that treatment of **45** with lithium triethylborohydride produced the corresponding carboxylic acid! However, lithium triethylborohydride did not react at all with the more hindered ester in **27**. Neither could the esters in molecular tweezers **27–30** and **48** be converted to the corresponding carboxylic acids (**31–34**, **49**) hydrolytically. Therefore, the nucleophilic reagents, boron trichloride in methylene chloride or cyanide in hot DMSO, were employed with success [56].

3.3 Complexation of Nucleotide Bases by Molecular Tweezers

As discussed in Sect. 2.5, the ability of the host and guest to self-associate must be established prior to any complexation studies. Carboxylic acids **33**, **34**, **47**, and **49** showed no tendency to aggregate in chloroform [59]. In contrast, the ^1H NMR of carboxylic acid **31** contained several broad resonances that were consistent with a zwitterionic structure and/or an aggregate [56]. For this reason, complexation studies have not been carried out with the highly twisted molecular tweezers **31** or **32**. For the guests used in these studies, dimerization constants were known and indicated that self-association would be negligible under the concentrations used.

3.3.1 Nature and Strength of Complex with 9-Propyladenine

The interaction of 9-propyladenine (**50**) and **49** was studied in chloroform-*d* by ^1H NMR and in chloroform by UV-visible spectroscopy [58, 59]. A non-overlapping absorption ($\lambda_{\text{max}} = 386 \text{ nm}$) of the anthracene rings in **49** exhibited a metachromic shift upon addition of **50**, a result that is consistent with the formation of a complex containing π -stacking. Tweezer **49** and **50** altered each other's ^1H NMR spectrum in a manner consistent with π -stacking and hydrogen bonding. Thus, as seen in Fig. 14, complexation induced upfield shifts in the aromatic protons of both the host and guest, but a downfield shift in the N-6 protons of **50**. The upfield shifts are consistent with aromatic stacking, while downfield shifts are expected for protons involved in hydrogen bonds.

Binding constants were obtained by nonlinear least squares fitting of the titration data [58–60]. Tweezers **49**, **33**, and **34** bound **50** with association constants (K_{assoc}) of 25000, 14000, and 120000 M^{-1} , respectively (Table 6) [57–59]. The synthesis of **49** required the incorporation of a dimethylamino substituent and this represents

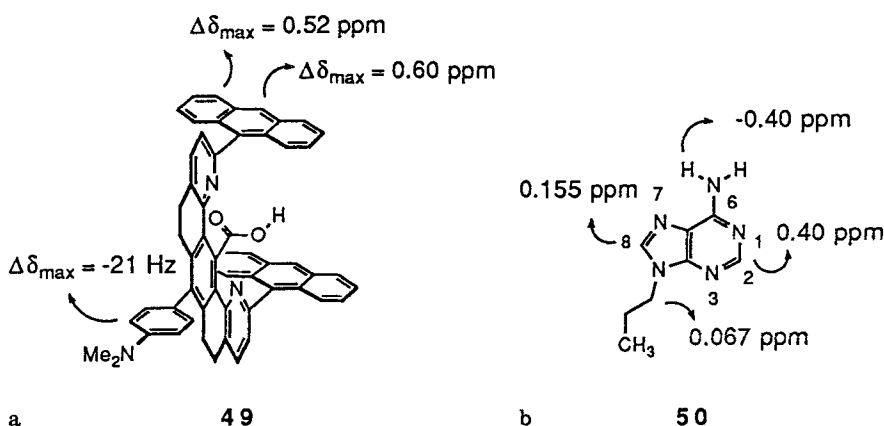
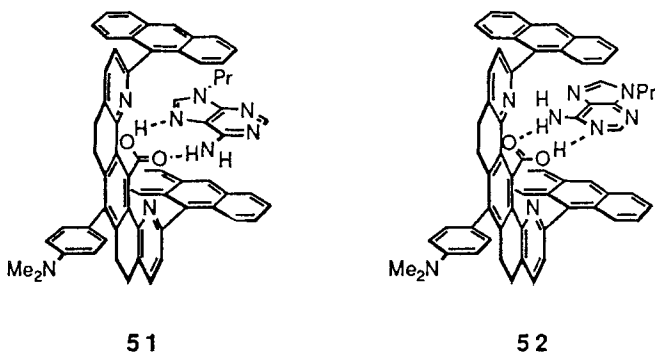


Fig. 14a, b. ^1H NMR complexation shifts in host **49** (a) and complexation shifts in 9-propyladenine (**50**) at ca. 40% saturation by host **49**. Data from Ref. [58, 59]

the only structural difference between **49** and **33**. The difference that these compounds show in their affinity for **50** is close to the limit of experimental error ($\Delta\Delta G^\circ = 0.5 \text{ kcal mol}^{-1}$) and probably more related to the conditions of the titrations than to the small difference in their structures. For example, the concentrations used in the UV-visible studies were significantly lower than those in the ^1H NMR studies.



The spectroscopic changes seen in the host-guest titrations and the high association constants suggest the formation of inclusion complexes such as **51** and **52**. Work with analogues gave supporting evidence, and further suggested **51** best represents the structure of the complex between **49** and **50**. Thus, ester **48** showed no affinity for **50** and dimethylation of N-6 of 9-ethyladenine (**53**) seriously compromises complex stability (entries 4 and 5, Table 6). These two results indicate the importance of the hydrogen bonding sites. Monomethylated derivative **54** and adenine analogue **55** indicate the preferred geometry of the adenine complex. The N-methyl group in **54** prefers to orient away from the imidazolyl ring, and thus

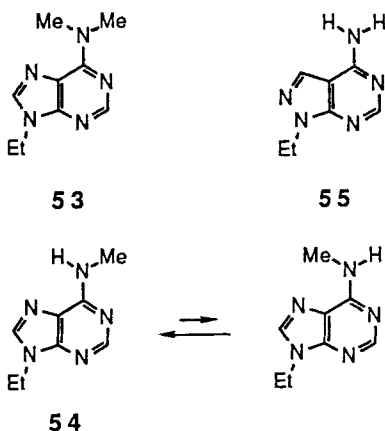
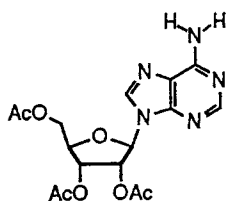
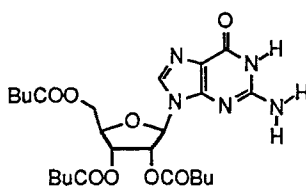
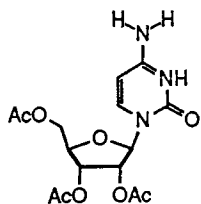
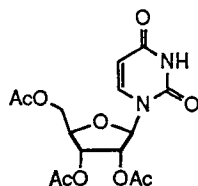


Table 6. Association constants (K_{assoc}) of 1:1 complexes between various hosts and nucleosides or their analogues in chloroform at 298 K^a

Entry	Method	Host	Guest	K_{assoc} (M^{-1})	$-\Delta G_{298^\circ}$
1	A	49	50	25000	6.0
2	B	33	50	14000	5.7
3	B	34	50	120000	6.9
4	A	48	50	< 5	< 1.0
5	A	49	53	380	3.5
6	A	49	54	30000	6.1
7	A	49	55	11000	5.5
8	A	49	adenosine 56	15000	5.7
9	A	49	guanosine 57	2800	4.7
10	A	49	cytidine 58	213	3.2
11	A	49	uridine 59	132	2.9

^a Taken from Ref. 57–59. Method A: ¹H NMR. Method B: UV-visible

blocks the formation of the type 1 complex shown in Fig. 10 [52, 61]. Yet this guest binds to tweezer **49** as tightly as does **50** (entry 6, Table 6). Pyrrolopyrimidine **55** was examined because it can form a type 1 complex, but the type 7 geometry is unavailable. While **55** still binds tightly to **49**, its complexation shifts are quite different from those seen in **50** and **54**. It can be concluded that the **49**·**50** complex more closely resembles **51**. A reasonable explanation for this preference is that the larger degree of host-guest π -overlap in the type 7 complex (**51**) overwhelms the small energetic preference that carboxylic acids show for the type 1 complex. Thus, in complex **52** the imidazolyl ring of the adenine nucleus projects out of the cleft into the solvent.

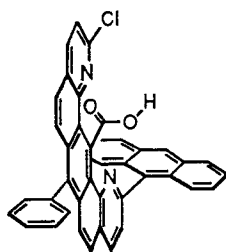
**56****57****58****59**

3.3.2 Nucleoside Selectivity

In comparison to butyric acid, the microenvironment of the carboxylic acid in **49** alters its complexation efficiency and the preferred geometry of its adenine complex. The nucleoside selectivity is also altered and improved to the extent that **49** can be considered a moderately selective host. As seen in Table 6 (entries 8–11), **49** selectively binds purines, with the association constants following the order A (**56**) > G (**57**) \gg (**58**) C \geq (**59**) U. The maximum selectivity is $\Delta\Delta G^\circ = 2.8 \text{ kcal mol}^{-1}$, while for butyric acid the selectivity was $\text{Me}_2\text{G} \geq \text{C} \geq \text{A} \geq \text{U}$ with only $1.3 \text{ kcal mol}^{-1}$ separating the strongest and weakest complexes [52].

3.3.3 Origin of Complexation Strength

What is the origin of the strong binding of 9-propyladenine? A simple component analysis underscores the importance of the individual binding contacts. As seen in Table 7, spacer acid **47** binds 9-propyladenine with an association constant of only 280 M^{-1} , while the single anthracene ring in **60** markedly increases its affinity for **50** ($K_{\text{assoc}} = 5200 \text{ M}^{-1}$), and in turn the second anthracene in molecular tweezer **34** brings the stability up even further ($K_{\text{assoc}} = 120000 \text{ M}^{-1}$). In free energy, each anthracene contributes ca. 2 kcal mol^{-1} , while hydrogen bonding alone is worth $2.7 \text{ kcal mol}^{-1}$. Enthalpies of complexation have been measured and suggest a larger overall contribution by the π -surfaces. However, the accuracy of the measurements is in doubt for two reasons. First, the enthalpies of binding were determined from a van't Hoff plot that spanned only 30 K due to difficulties in measuring the very high association constants exhibited by **34** at low temperatures. Secondly, Adrian and Wilcox have shown that enthalpies and entropies of binding in a related host-guest system will vary depending on the concentration of small amounts of water in the chloroform [62].



60

The component analysis described above shows that the aromatic cleft in **34** contributes $4.2 \text{ kcal mol}^{-1}$ toward the free energy of complexation of 9-propyladenine (**50**). An alternative approach to determining the contribution made by the aromatic cleft would be to measure the free energy obtained in a complex between **50** and a molecular tweezer containing an aromatic cleft, but no carboxylic acid group. This analysis, which has been carried out using molecular tweezer **11**,

Table 7. Association constants (K_{assoc}) of 1:1 complexes between various hosts and **50** in chloroform at 298 K and pKa values of hosts determined in 4:1 dioxane-water^a

En- try	Meth- od	Acid	pKa ^b	K_{assoc} ^c	$-\Delta H^\circ$ ^d	$-\Delta S_{298}^\circ$ ^e	$-\Delta G_{298}^\circ$ ^d
1	B	34	13.0 \pm 0.1	120000	13	20	6.9
2	B	60	11.4 \pm 0.1	5200	9	13	5.1
3	A	47	9.9 \pm 0.1	280	4	2	3.3
4	A	4-methoxybenzoic (61)	7.26 \pm 0.05	440			3.6
5	A	benzoic (62)	6.92 \pm 0.04	540			3.7
6	A	4-chlorobenzoic (63)	6.48 \pm 0.05	630			3.8
7	A	4-cyanobenzoic (64)	5.81 \pm 0.06	950			4.1
8	A	11		≤ 5			≤ 1

^a See Ref. 29 and 59. Method A: ¹H NMR. Method B: UV-visible. ^b Entries 1–3 spectrophotometrically, entries 4–7 potentiometrically. ^c M^{−1}. ^d kcal mol^{−1}. ^e cal deg^{−1} mol^{−1}

leads to the opposite conclusion: the aromatic cleft contributes nothing to the stability of the **34**·**50** complex (Fig. 15). The discrepancy between the analyses in Fig. 15 is another example of *complex additivity in binding energies*, the phenomenon discussed in Sect. 2.5 [35, 36].

The complex additivity in this system may also result from changes in translational and rotational entropy. For example, in the **11**·**50** complex (Fig. 15) a favorable π -stacking enthalpy as high as 9 kcal mol^{−1} could be offset by a large negative entropy of complexation (e.g. -28 cal deg^{−1} mol^{−1} or 8 kcal mol^{−1} at 298 K), leaving the very small $-\Delta G^\circ$ that is observed. In the **34**·**50** complex, the hydrogen bonding would help to pay this entropic cost so that the enthalpy of π -stacking is observed in the free energy of binding. Thus, the very high stability of the complex between molecular tweezer **34** and **50** may derive in large part from a favorable π -stacking interaction between host and guest. In this respect, the anthracene rings in **34** are well suited for the role given the very high polarizability of anthracene and other large aromatic systems [63, 64].

As discussed in Section 2.5, complex additivity in binding energies may be observed in the absence of entropic effects if the binding contacts involved are close to each other [35]. Proximity allows the groups to communicate either through space or through contacts to the guest. For example, in the **34**·**50** complex, the π -system and the hydrogen bonding may interact synergistically since partial proton transfer to 9-propyladenine (**50**) is likely to enhance the π -stacking interaction by strengthening the donor-acceptor interactions. Alternatively, the complex additivity in binding energies seen in Fig. 15 may result from a through space interaction between the carboxylic acid and the anthracene rings. Two possibilities for this through space interaction are: (1) the anthracene rings alter the pKa of the carboxylic acid group, increasing its affinity for adenine, and (2) the anthracene rings sterically desolvate the carboxylic acid.

The first possibility was examined by titrating carboxylic acids **47**, **56**, and **34** in 4:1 dioxane-water. As seen in Table 7 and Fig. 16, each anthracene ring raises

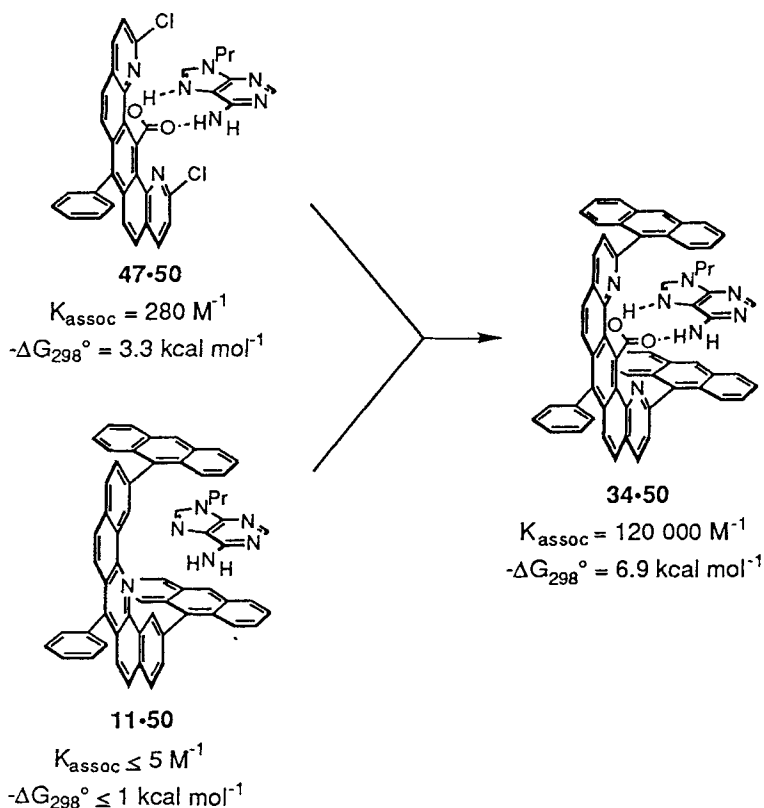


Fig. 15. Complex additivity of binding energies seen by comparing the stabilities of the complex formed between **50** and hosts **11**, **47**, and **34**

the pKa of the carboxylic acid by ca. 1.5 units. For calibration, the pKa of four simple benzoic acids (**61**–**64**) were determined in 4:1 dioxane-water and their association constants with **50** were measured in chloroform (Table 7). The data for **61**–**64** indicate that a lower pKa results in a higher affinity toward **50**, although the effect is not large ($\rho = 0.36$). Strikingly, the opposite trend is seen with **47**, **56**, **34** (Table 7, Fig. 16). In this case, a higher pKa correlates with a higher affinity toward **50** and the effect is dramatic. It is not inconceivable that the ordering of pKa values may change from 4:1 dioxane-water to chloroform, but the results with benzoic acids **61**–**64** suggest that changes in pKa of the tweezer carboxylic acid will have at most a small effect on its affinity toward adenine.

The large increase that each anthracene induces in the pKa of the carboxylic acid in **47** can be explained by steric desolvation of the carboxylate (carboxylic acid) group and by a destabilizing interaction between the carboxylate anion and the anthracene rings [65]. Is the acid group desolvated in chloroform, and is this in part the origin of the complex additivity in binding energies? Jorgensen has

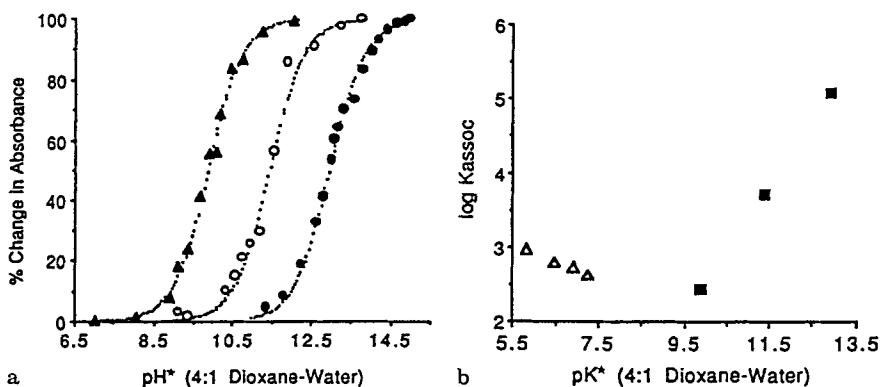


Fig. 16a. Titration curves in 4:1 dioxane-water: ▲: 47 ($\lambda = 413 \text{ nm}$), ○: 60 ($\lambda = 413 \text{ nm}$), ●: 34 ($\lambda = 410 \text{ nm}$). Dotted lines (.....) are the calculated curves. b) Relationship between carboxylic acid acidity and binding affinity for 50 in chloroform. △: 61–64, ■: 34, 47, 60. Data from Table 7

addressed this question in a particularly interesting computational study [66]. Monte Carlo simulations were carried out in boxes (ca. 33 \AA per side) containing 250 chloroform molecules and either a molecular tweezer-adenine complex or a molecular tweezer alone. In a study of the latter type, an analogue of 34 lacking the phenyl substituent was found to contain one chloroform molecule well inside the aromatic cleft and two additional chloroform molecules solvating the oxygen

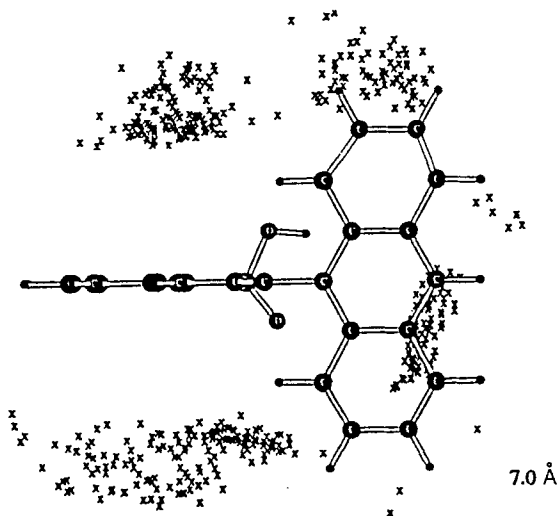


Fig. 17. Graphical analysis showing the solvation of tweezer acid in chloroform. Location of chloroform carbon atoms found within 7 \AA of tweezer carbonyl group from 80 configurations are labelled by X. From Ref. [66]

atoms of the acid on either side of the spacer (Fig. 17). Gas phase calculations further suggested that molecular tweezers like **34** are actually good hosts for chloroform [66]. It can be concluded from these studies that molecular tweezers, such as **34**, do not have naked clefts and guest binding must occur with some degree of competition with solvent.

4 Summary and Outlook

The broadest conclusion that can be drawn from these studies is that non-macrocyclic hosts can bind neutral guests with affinities and selectivities that are as high as their macrocyclic counterparts. Because guests of any size can be complexed without having to be fully included in the host, this strategy significantly extends the scope, and also the potential applications, of host-guest chemistry. For example, the simplest molecular tweezers described in this review bind nitrated polycyclic aromatic hydrocarbons (nitro-PAH) with very high affinities and selectivities (e.g. for **11**, $K_{\text{assoc}} = 20000$ for TENF vs $K_{\text{assoc}} < 5$ for anthracene). These particular guests represent a significant health and environmental concern because nitro-PAH are potent mutagens and potential carcinogens that are found in gasoline exhaust, cigarette smoke, and coal-burning power plants [67]. As such, immobilized molecular tweezers such as **11** have potential uses in the detection and separation of these compounds.

On a more fundamental note, several aspects of the complexation chemistry shown by these molecular tweezers need to be more extensively studied. The simple molecular tweezers that bind guests by π -stacking alone, and those that additionally use hydrogen bonding, form host-guest complexes that are more stable than expected from the binding efficiencies of their constituent parts. The origin of this complex additivity of binding energies needs to be determined. While a number of approaches to this problem have been envisaged, a particularly useful one will involve a careful measurement of enthalpies and entropies of binding in a range of solvents.

The role of computational chemistry in addressing these and related issues cannot be underestimated. Studies by Jorgensen have provided remarkable insights into several host-guest systems [66, 68, 69]. As described above, computational studies of molecular tweezers have elucidated the contribution that solvation makes to binding affinities [66]. These same studies have allowed the absolute binding constant of the **34**·**50** complex to be calculated with impressive precision, and allowed the relative importance of hydrogen bonding and π -stacking to be determined. These successes also underscore the important role that computational approaches will play in the design of new host-guest systems.

One goal of future studies is to optimize the complexation power of molecular tweezers. A particularly interesting possibility is that the affinity that molecular tweezer **34** shows for 9-propyladenine can be improved by introducing additional hydrogen bonding contacts. This is possible because: 1) complex **51** uses only two out of five possible hydrogen bonding sites of adenine, and 2) the syntheses that have been developed are flexible enough to allow attachment of chromophores holding additional groups. A second carboxylic acid appears to be a superb

candidate for added hydrogen bonding interactions given the recent results of Adrian and Wilcox [70]. These workers have shown that a host containing two benzoic acid groups attached to a Tröger's base unit binds 9-ethyladenine with remarkable efficiency ($K_{\text{assoc}} = 44000 \text{ M}^{-1}$) in chloroform. Since the entropic price has largely been paid for in the **34·50** complex, there is the possibility that the full enthalpic worth of each additional hydrogen bond will be seen in the free energy of complexation (ΔG°). Thus, the stability of such complexes may rise dramatically.

The fact that biological systems operate in water makes the development of water soluble molecular tweezers a special challenge. The complexation power of molecular tweezers that use EDA forces alone in organic solvents is expected to rise considerably in aqueous solution because the association of aromatic systems is usually much stronger when driven by the hydrophobic force. The situation is potentially quite different for the molecular tweezers that also use hydrogen bonding. In water, hydrogen bonds between water and the host and guest will have to be broken prior to complexation [71]. Whether these hosts remain effective may depend upon the strength of the stacking interactions. In many senses this situation is similar to that of natural binding sites where dispersion forces are believed to contribute heavily to overall binding affinities while hydrogen bonding is important in specificity [72].

Acknowledgements: The work described from this laboratory was carried out by Monica Baloga, Scott Davis, Greg Hamilton, Milan Mrksich, Dave Reichert, Kurt Saionz, Craig VanZyl, Weiming Wu, and Zijian Zeng. I thank this dedicated group of coworkers for their efforts in molecular tweezers chemistry. Professors W. L. Jorgensen and S. D. Kahn are thanked for their interest in this work, and for insightful discussions. This work was supported by the University of Illinois, the National Institutes of Health (GM 38010), and the National Science Foundation (CHE 58202).

References

1. Rigby M, Smith EB, Wakeman WA, Maitland GC (1986) The forces between molecules, Oxford University Press New York
2. Maitland GC, Rigby M, Smith EB, Wakeham WA (1987) Intermolecular forces, Oxford New York
3. Israelachvili JN (1985) Intermolecular and surface forces, Academic, New York
4. Fischer, E (1894) Chem Ber 27: 2985
5. Bender ML, Komiyama M (1978) Cyclodextrin chemistry, Springer, Berlin Heidelberg New York, p 23
6. Cram DJ (1988) Angew Chem, Int Ed Engl 27: 1009
7. Lehn JM (1988) Angew Chem, Int Ed Engl 27: 89
8. Pedersen CJ (1988) Angew Chem, Int Ed Engl 27: 1021
9. Cram DJ (1986) Angew Chem, Int Ed Engl 25: 1039
10. Ebmeyer F, Vögtle F (1990) In: Dugas H (ed) Bioorganic chemistry frontiers, Springer, Berlin Heidelberg New York, p 143
11. Caranague DR, Diederich, F (1990) Angew Chem, Int Ed Engl 29: 769
12. Cram DJ (1985) In: Vögtle F, Weber, E (eds) Host guest complex chemistry, Macrocycles, Springer, Berlin Heidelberg New York, p 125

13. Chen C-W, Whitlock HW (1978) *J Am Chem Soc* 100: 4921
14. Rebek J Jr (1990) *Angew Chem, Int Ed Engl* 29: 245
15. Foster R (1969) *Organic charge-transfer complexes*, Academic, New York
16. Hunter CA, Saunders JKM (1990) *J Am Chem Soc* 112: 5525
17. Foster R, Payne HAS (1971) *Recueil* 90: 630
18. Adams SP, Whitlock HW Jr (1981) *J Org Chem* 46: 3474
19. Stoddart JF (1988) *Pure Appl Chem* 60: 467
20. Colquhoun HM, Goodings EP, Maud JM, Stoddart JF, Wolstenholme JB, Williams DJ (1985) *J Chem Soc, Perkin Trans* 2 607
21. Stoddart JF, et al (1987) *J Chem Soc, Chem Commun* 1054, 1058, 1061, 1064, 1066
22. Herbststein FH (1971) In: Dunitz JD, Ibers JA (eds) *Perspectives in structural chemistry*, vol 4, Wiley, New York, p 166
23. Mason R (1960) *Proc R Soc London A* 258: 302
24. Zimmerman SC (unpublished results)
25. Zimmerman SC, VanZyl CM (1987) *J Am Chem Soc* 109: 7894
26. Zimmerman SC, VanZyl CM, Hamilton GS (1989) *J Am Chem Soc* 111: 1373
27. Newman MS, Seshardi S (1962) *J Org Chem* 27: 76
28. Fieser LF, Seligman AM (1938) *J Am Chem Soc* 60: 170
29. Zeng Z (unpublished results)
30. Adams SP, Whitlock HW Jr (1982) *J Am Chem Soc* 104: 1602
31. Rabideau PW (1989) *The conformational analysis of cyclohexenes, cyclohexadienes, and related hydroaromatic compounds*, VCH, New York
32. Davis DS (unpublished results)
33. Zimmerman SC, Mrksich M, Baloga M (1989) *J Am Chem Soc* 111: 8528
34. Saionz KW (unpublished results)
35. Wells A (1990) *Biochemistry* 37: 8509
36. Jencks WP (1981) *Proc Natl Acad Sci USA* 78: 4046
37. Chudek JA, Foster R, Mackay RL, Page FM, Twiselton DR (1988) *J Chem Soc, Faraday Trans* 1 84: 1145
38. Jayadevappa ES, Budni ML (1988) *Z Phys Chem (Leipzig)* 269: 145
39. Page MI, Jencks WP (1971) *Proc Natl Acad Sci (USA)* 68: 1678
40. See footnote 22 in Ref. 33
41. Chapman KT, Still WC (1989) *J Am Chem Soc* 111: 3075
42. Chetkina LA, Semidetko OV, Belsky VK, Sobolev AN, Andrievsky AM (1987) *Acta Cryst Sect C* 43: 931
43. Baughman RG (1987) *Acta Cryst Sect C* 43: 933
44. Ferguson SB, Diederich F (1986) *Angew Chem Int, Ed Engl* 25: 1127
45. Wakelin LPG (1986) *Medicinal Research Reviews* 6: 275
46. Saenger W (1984) *Principles of nucleic acid structure*, Springer, Berlin Heidelberg New York, chap 18
47. Bruskov VI (1975) *Mol Biol (Moscow)* 9: 245
48. Pabo CO, Jordan SR, Frankel AD (1983) *J Biomol Struct Dyn* 1: 1039
49. Matthews BW (1988) *Nature (London)* 335: 294
50. Jordan SR, Pabo CO (1988) *Science (Washington, DC)* 242: 893
51. Otwinowski Z, Schevitz RW, Zhang R-G, Lawson CL, Joachimiak A, Marmorstein RQ, Luisi BF, Sigler PB (1988) *Nature (London)* 335: 321
52. Lancelot G (1977) *J Am Chem Soc* 99: 7037
53. Zimmerman SC (1988) *Tetrahedron Lett* 983
54. Katritzky AR (1982) *Pyrylium salts*, Academic Press, New York
55. Griffin DA, Staunton J (1975) *J Chem Soc, Chem Commun* 675
56. Zimmerman SC, Zeng Z, Wu W, Reichert DE (1991) *J Am Chem Soc* 113: 183
57. Zimmerman SC, Zeng Z (1990) *J Org Chem* 55: 4789
58. Zimmerman SC, Wu W (1989) *J Am Chem Soc* 111: 8054
59. Zimmerman SC, Wu W, Zeng Z (1991) *J Am Chem Soc* 113: 196
60. Wilcox CS, Cowart MD (1986) *Tetrahedron Lett* 5563

61. Engel JD, von Hippel PH (1974) *Biochemistry* 13: 4143
62. Adrian JC Jr, Wilcox CS (1991) *J Am Chem Soc* 113: 678
63. Jorgensen WL Severance DL (1990) *J Am Chem Soc* 112: 4768
64. Miller KJ, Savchik JA (1979) *J Am Chem Soc* 101: 7206
65. Royer J, Beugelmans-Verrier M (1979) *Tetrahedron* 35: 2369
66. Blake JF, Jorgensen WL (1990) *J Am Chem Soc* 112: 7269
67. Robbat A Jr, Corso NP, Doherty PJ, Wolf MH (1986) *Anal Chem* 58: 2078
68. Jorgensen WL, Pranata J (1990) *J Am Chem Soc* 112: 2008
69. Jorgensen WL, Boudon S, Nguyen TB (1989) *J Am Chem Soc* 112: 755
70. Adrian JC Jr, Wilcox CS (1989) *J Am Chem Soc* 111: 8055
71. Fersht AR, Shi J-P, Knill-Jones J, Lowe DM, Wilkinson AJ, Blow DM, Brick P, Carter P, Waye MMY, Winter G (1985) *Nature (London)* 314: 235
72. Jencks WP (1969) *Catalysis in chemistry and enzymology*, McGraw-Hill, New York

Cyclotrimeratrylenes and Cryptophanes: Their Synthesis and Applications to Host-Guest Chemistry and to the Design of New Materials

André Collet,¹ Jean-Pierre Dutasta,¹ Bénédicte Lozach,¹ and Josette Canceill²

¹ Stéréochimie et Interactions moléculaires, Unité mixte de recherche No 117 du C.N.R.S., Ecole normale supérieure de Lyon, 69364 Lyon cedex 07, France

² Chimie des Interactions moléculaires, Unité de recherche No 285 du C.N.R.S., Collège de France, 75231 Paris cedex 05, France

Table of Contents

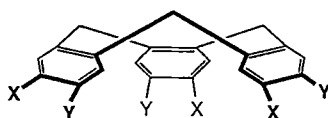
1 Introduction	104
2 Synthesis of Cyclotrimeratrylenes and Cryptophanes	105
2.1 Cyclotrimeratrylenes	105
2.2 Cryptophanes	106
3 Applications to Host-Guest Chemistry	114
3.1 Hosts Containing One Cyclotrimeratrylene Unit	114
3.2 Cryptophanes as Hosts	116
4 Applications to the Design of New Materials	125
4.1 Ferroelectric Liquid Crystals	125
4.2 Three-dimensional Charge Transfer Salts	127
5 References	129

A review is given of the recent developments of the chemistry of cyclotrimeratrylenes and cryptophanes, and of their use in the study of host-guest interactions. Experiments dealing with the complexation of tetrahedral species including neutral molecules (halogenomethanes and alkanes) and organic soft cations (tri- and tetramethyl ammonium cations, acetylcholine) are discussed. Prospective applications of cyclotrimeratrylenes and cryptophanes to the design of ferroelectric liquid crystals and of three-dimensional charge transfer materials are presented.

1 Introduction

In a report dated 1915, Mrs Gertrude Maud Robinson (the first wife of Sir Robert Robinson) showed that the acid catalyzed condensation of veratryl alcohol produced, in excellent yield, a solid, m.p. 227 °C, which she considered to be 2,3,6,7-tetramethoxy-9,10-dihydroanthracene [1]. In making this proposal (which, however, was not entirely accepted by her husband [1]), she was perhaps influenced by an earlier, hardly justified claim by Ewins (1909) that piperonyl alcohol, under acidic conditions, furnished a high-melting compound similar in many respects to hers described as being “with considerable probability” 2,3,6,7-dimethylenetetraoxy-9,10-dihydroanthracene [2].

That Robinson's and Ewins' compounds did in fact have the trimer structures **1** and **2**, respectively, was only established 50 years later by the works of Lindsey [3], Erdtman et al. [4], and Goldup et al. [5]. The name cyclotrimeratrylene (CTV) was given by Lindsey to **1**, which was shown by NMR to adopt the locked crown conformation shown on the stereoformula and later evidenced by X-ray crystallography (Fig. 1) [6, 7]. More recently [8], the inversion barrier of the crown in **1** was found to be ca. 26.5 kcal · mol⁻¹ from the racemization rate of the isotopically chiral C3-cyclotrimeratrylene-d₉ (**3**); relatively uniform values (ΔG^* 26.5 to 27.2 kcal/mol) were found [9] for a variety of chiral cyclotrimeratrylenes, including the parent compound **4**, C3-cyclotribenzylene-d₃. Thus, in these compounds, the half-life of a crown conformer in solution is around one month at 20 °C, a few minutes at 100 °C and less than 0.1 second at 200 °C.



- 1 X = Y = OCH₃
- 2 X, Y = OCH₂O
- 3 X = OCH₃, Y = OCD₃
- 4 X = H, Y = D

For a long time, Robinson's compound has attracted attention in view of its ability to form crystalline inclusion compounds with certain small molecules. This property was initially mentioned in 1931 by Bhagwat et al. [10], and some of these inclusion complexes were investigated in detail some 25 years later by Caglioti et al. [11] (at the time Robinson's compound was believed to be a hexamer—see Ref. [9]).

Since the end of the seventies, interest in cyclotrimeratrylene has moved towards the use of its cone shaped structure for applications in various fields, including investigations of the electronic transitions of the benzene chromophore via UV and CD spectroscopy, studies in the area of host-guest chemistry, synthesis of new types of liquid crystals, and searches for new three-dimensional organic charge-transfer materials. These works have been made possible because efficient synthetic

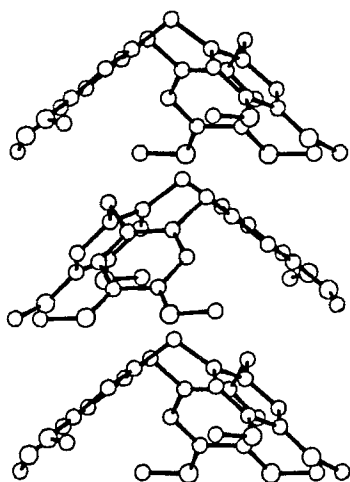


Fig. 1. X-ray crystal structure of cyclotrimeratrylene (ref. 7)

routes have been set up during the last two decades, allowing the preparation of functionalized cyclotrimeratrylenes. The basic aspects of the chemistry of **1** and of the preparation of its analogues have been reviewed in 1987 [9], and the present article will therefore be restricted to the more recent developments in this area. Special emphasis will be given to the synthesis and properties of the “cryptophanes”, hollow molecules of the cavitand type, made of two CTV units linked in front to one another. These compounds form inclusion complexes in solution with guests of tetrahedral geometry, and present interesting redox properties.

The paper is organized as follows. Sect. 2 describes the general principles and recent results for the synthesis of cyclotrimeratrylenes; Sect. 3 describes some applications of these compounds to host-guest chemistry. This latter section is devoted principally to the cryptophanes, and to host molecules containing one CTV unit that have recently been described. Sec. 4 presents some prospective work in the field of material sciences, i.e., ferroelectric liquid crystals and organic three-dimensional charge transfer salts.

2 Synthesis of Cyclotrimeratrylenes, Cryptophanes, and Related Compounds

For a detailed discussion of the synthetic methods, reaction mechanisms, and chemical aspects see the previous review [9].

2.1 Cyclotrimeratrylenes

We focus here on the preparation of functionalized C3-cyclotrimeratrylenes bearing two different substituents X and Y on the peripheral positions of the three benzene rings. The synthesis of such compounds is based on the reaction shown in Fig. 2,

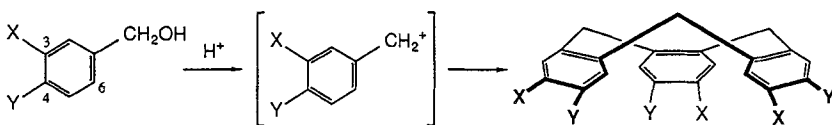


Fig. 2. Synthesis of cyclotrimeratrylene by trimerization of 3,4-disubstituted benzyl cations

in which a 3,4-disubstituted benzyl alcohol is converted under acidic conditions to the corresponding C3-trimer.

Experimental data for the trimerization of 3,4-disubstituted benzyl alcohols are assembled in Table 1. In this reaction, position 6 on the aromatic ring must be activated towards electrophilic attack, which requires that a strongly electron releasing substituent X is present at position 3. The effect of this substituent on the trimerization yield is not always entirely predictable, however. For instance vanillyl alcohol (Y=OH) affords tars under the conditions where its allyl ether is converted to the trimer **9** in 55% yield. Nevertheless, the importance of having a strongly electron releasing X group is evidenced by comparing the behaviour of 4-bromo-3-methoxybenzyl alcohol (X=OCH₃, Y=Br) with that of its regio-isomer (X=Br, Y=OCH₃); only the former can be converted to the cyclic trimer **11**.

It is likely that the role of substituent Y at position 4 is mostly to prevent side reaction at this position. This idea is based on the observation that 3-methoxybenzyl alcohol (X=OMe, Y=H) affords a small yield of trimer **12**, besides polymeric by products. In all examples reported thus far, Y is also an electron releasing group; however, a weak electron withdrawing group might perhaps be acceptable, providing that it does not deactivate the aromatic ring too much.

It is interesting that C3-cyclotrimeratrylenes bearing heteroatoms different from oxygen at the periphery of the ring system can now be synthesised by this strategy in fair to excellent yield (bromine, nitrogen, sulfur, **11–15**). Functional group transformations of the C3-cyclotrimeratrylenes obtained by trimerization and listed in Table 1 give access to a "second generation" of compounds, the most important of which, for synthetic applications, are assembled in Table 2. Some of these compounds have been obtained in optically active form. Their optical rotations are indicated in the Table together with their absolute configurations *M* or *P*, established by X-ray crystallography and chemical correlations.

Several host molecules containing a single cyclotrimeratrylene unit will be described in Sect. 3.1.

2.2 Cryptophanes

The name cryptophane [23], which designates molecules made of two cyclotrimeratrylene units assembled by three bridges in the way shown in Fig. 3, recalls the [1.1.1]orthocyclophane structure of CTV and underlines the presence of an enforced cavity in these compounds allowing the inclusion of suitable guest species (Sect. 3).

Only two types of cryptophanes have hitherto been synthesized in which the three bridges are identical and the R and R' substituent display an *anti* or *syn*

Table 1. C3-cyclotrimeratrylenes obtained by trimerization of 3,4-disubstituted benzyl alcohols (see Fig. 2)

X	Y	No	Yield	Refs
OCH ₃	OCH ₃	1	70	9
OCH ₃	OH	5	0	12
OCH ₃	OC ₂ H ₅	6	51	13
OCH ₃	OCH ₂ CO ₂ H	7	45	14
OCH ₂ CO ₂ H	OCH ₃	7	42	9
OCH ₃	OCH ₂ CH ₂ OCH ₂ CO ₂ H	8	40	15
OCH ₃	OCH ₂ CH=CH ₂	9	55	12, 16
OC ₂ H ₅	OCH ₂ CH=CH ₂	10	15	13
OCH ₃	Br	11	25–40	17–19
Br	OCH ₃	11	0	17
OCH ₃	H	12	6.5	18
OCH ₃	NHCOCH ₃	13	90	20
OCH ₃	NHCOCH ₂ Cl	14	95	20
OCH ₃	SCH ₃	15	93	20

Table 2. Functionalized cyclotrimeratrylenes of the second generation (see Fig. 2 and for the stereochemistry Fig. 1)

X	Y	No	[α] _D	Conf	Refs
OH	OH	16			3
OCH ₃	OH	5	–272	<i>P</i>	12, 16, 21
OC ₂ H ₅	OH	17	–293	<i>P</i>	21
Br	OH	18	–174	<i>P</i>	21
OCH ₃	CH ₂ OH	19	–221	<i>P</i>	21
OH	H	20	–199	<i>P</i>	21
OCH ₃	OCH ₂ CO ₂ CH ₃	21			14, 22
OCH ₃	OCH ₂ CO ₂ H	22			14, 22
OCH ₃	OCH ₂ CH ₂ OH	23			14, 22
OCH ₃	OCH ₂ CH ₂ I	24			14, 22
OCH ₃	Li	25			18, 19
OCH ₃	CO ₂ C ₂ H ₅	26			18, 19
OCH ₃	CO ₂ C ₆ H ₅	27			18, 19
OCH ₃	CO ₂ H	28			18, 19
OCH ₃	CH ₂ Cl	29			18, 19
OCH ₃	CH ₂ SH	30			18, 19
SCH ₃	OH	31			20
OCH ₃	NH ₂	32			20
OCH ₃	OCH ₂ CONHCH ₃	33			20

relationship as shown in Fig. 3. In general, the bridges are of structure O(Z)O (where Z equals (CH₂)_n, CH₂–CH=CH–CH₂, or CH₂–C≡C–CH₂). In most cases R=R' and the D3-*anti* and C3_h-*syn* isomers have been identified. Also a pair of C3-*anti* and C3-*syn* isomers exist, with R=OCH₃ and R'=H, and a pair with unsymmetrical bridges of structure O(CH₂)₃S (see formulae 40–43, below).

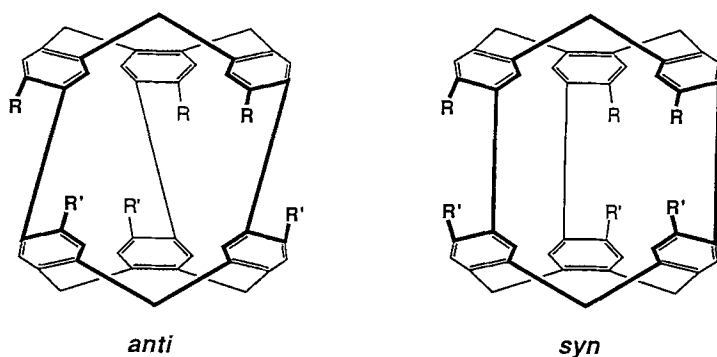


Fig. 3. *anti* and *syn* cryptophanes

For the designation of these compounds, we have adopted a system based principally on the chronology of their description; the first member of the family (*anti* stereochemistry) was thus named cryptophane-A, and its *syn* isomer cryptophane-B. This was followed by the *anti/syn* pair C/D, respectively, then E/F, and so forth.

For the construction of the cryptophanes depicted in Fig. 3, two different synthetic routes have been employed (Fig. 4). With reference to method (a), a suitably substituted benzyl alcohol is first converted to a C3-cyclotrimeratrylene, to which three chains ending with benzyl alcoholic groups are attached and eventually cyclized intramolecularly; in this reaction, the first cap serves as a template to direct the trimerization [14]. In a second, shorter route (b), a benzyl alcohol is first transformed into a 'dimer', which under suitable conditions trimerizes to a cryptophane; in this reaction, six carbon-carbon bonds have to be created in a single sequence [24].

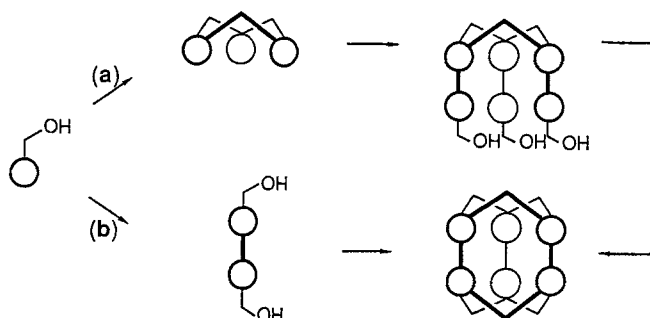
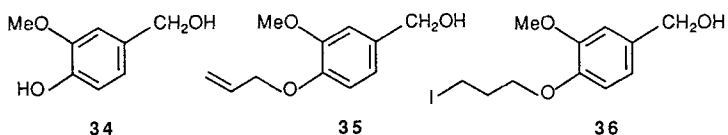


Fig. 4. Strategies for cryptophane synthesis

Both routes actually use vanillyl alcohol **34** (3-methoxy-4-hydroxybenzyl alcohol) as the starting material. Application of method (a) requires that **34** could be trimerized to C3-cyclotriguaiacylene, **5** (Table 1). However, as was said above, this reaction does not work, presumably because the phenolic group makes the molecule too reactive under the strong acidic conditions employed; the allyl protected derivative **35** was thus used instead of **34** itself, and, on reaction with perchloric acid in methanol, gave the tris-allyl protected derivative **9** in 55% yield. Palladium catalysed cleavage of the allyl groups then led to the desired racemic triphenol **5**. The latter could eventually be resolved by separation of its diastereoisomeric esters with ω -camphanic acid [13].



An example of cryptophane synthesis using **5** as a template is depicted in Fig. 5. The cyclization precursor **37** was obtained by alkylation of **5** with iodide **36**; in warm formic acid solution (high dilution: 10^{-4} M), it was smoothly converted to a mixture of two cryptophane isomers in 77% overall yield [25]. The minor (27%)

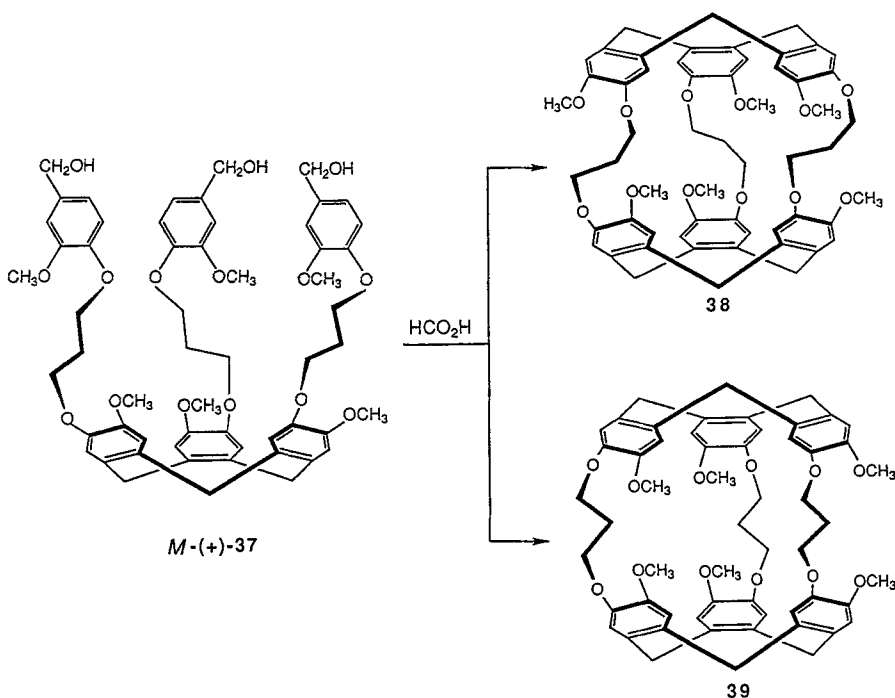
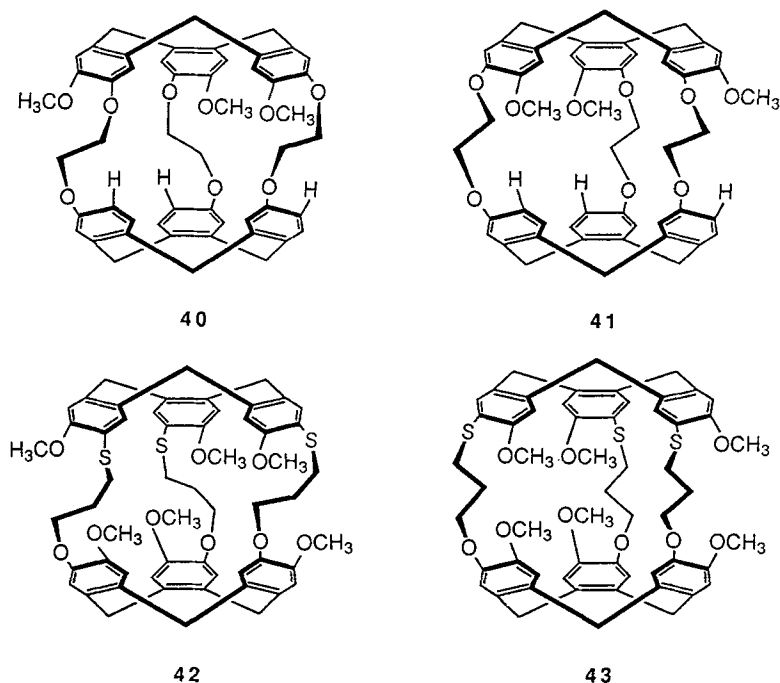


Fig. 5. Template directed synthesis of cryptophanes **38** and **39**

and major (50%) isomers were assigned as the *anti* and *syn* structures **38** and **39**, respectively, because the same reaction carried out from optically active *M*-(+)-**37** afforded optically active (–)-**38**, showing $[\alpha]_D -49^\circ$ in CHCl_3 , and optically inactive **39**. Thus **38** must be the chiral D3 isomer (named cryptophane-E) and **39** the C3h *meso* isomer (cryptophane-F).

The template directed cryptophane synthesis works reasonably well for cryptophanes having bridges of structure $\text{O}(\text{CH}_2)_n\text{O}$, at least up to $n = 8$, or unsaturated bridges such as $\text{OCH}_2\text{CH}=\text{CHCH}_2\text{O}$ (*Z* or *E*) and $\text{OCH}_2\text{C}\equiv\text{CCH}_2\text{O}$ (see Table 3) [26]. The template ring may also have a structure different from that of the newly created ring as, for instance, in cryptophanes **40–43**. For the synthesis of **40** and **41**, the triphenol **20** (Table 2) was used as the template [23], whereas thiovanillyl alcohol was employed instead of vanillyl alcohol for **42** and **43** [20].



Another advantage of this template procedure is that it allows access to optically active cryptophanes of known absolute configuration, from suitable optically active C3-cyclotrimeratrylene templates. The cyclization step, however, requires high dilution conditions, which certainly represents a limitation, if the preparation of large quantities of these substances is contemplated.

New perspectives in cryptophane chemistry have been opened by the discovery [24] that these compounds could be synthesized in two steps from vanillyl alcohol **34**. Following this method [(b) in Fig. 4], a bis(vanillyl alcohol) derivative such as **44** (Fig. 6) is converted directly, under mildly acidic conditions (formic acid) to a mixture of cryptophane-E (**38**, 15–17%) and –F (**39**, 0–3%). In addition to its

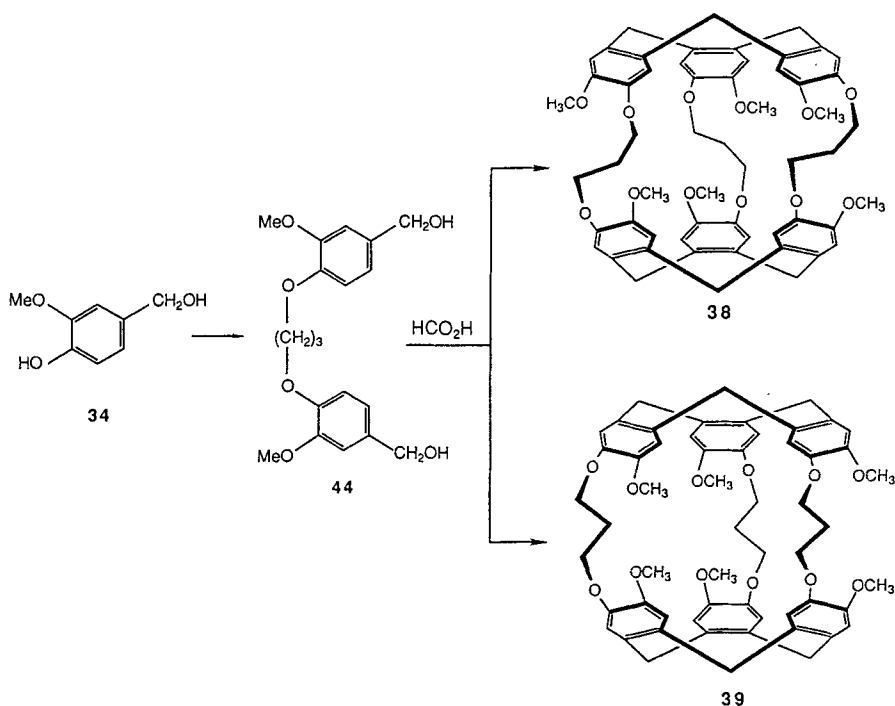


Fig. 6. Two-step cryptophane synthesis

simplicity and shortness, this direct method has the advantage that high-dilution conditions are not necessary, and therefore much larger quantities of cryptophanes can be prepared than by using the template procedure [cf. (a) in Fig. 4].

Data on the yields for the cyclization reactions concerning the two methods are given in Table 3. The direct method is suitable for preparing cryptophanes

Table 3. Yields (%) of *anti* and *syn* isomers by using the template procedure or the direct method [20]

Bridges O—(Z)—O	Template procedure		Direct method	
	<i>anti</i>	<i>syn</i>	<i>anti</i>	<i>syn</i>
$(\text{CH}_2)_2$	80	0	5	0
$(\text{CH}_2)_3$	27	50	17	3
$(\text{CH}_2)_4$	—	—	8	2
$(\text{CH}_2)_5$	21	43	12	6
$(\text{CH}_2)_6$	18	9	8	2
$(\text{CH}_2)_7$	—	—	5	1
$(\text{CH}_2)_8$	60	20	0	0
$\text{CH}_2\text{CH}=\text{CHCH}_2$ (<i>E</i>)	34	5	5	1
$\text{CH}_2\text{CH}=\text{CHCH}_2$ (<i>Z</i>)	25	50	10	8
$\text{CH}_2\text{C}\equiv\text{CCH}_2$	43	20	0	0

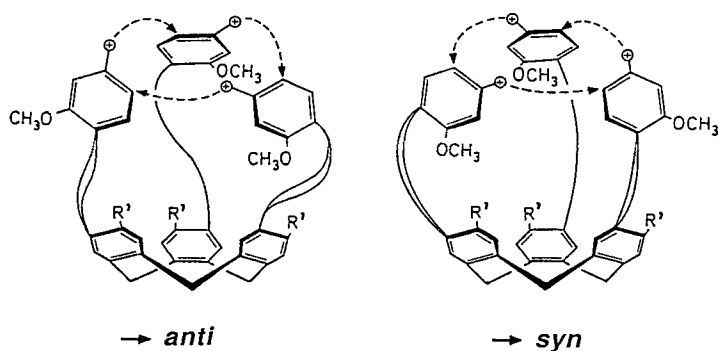


Fig. 7. Proposed cyclization mechanism in the template method

having $\text{O}(\text{CH}_2)_n\text{O}$ bridges with n in the range of 3 to 6. In all cases, the *anti* isomer is obtained preferentially. Although the yields may seem low, as compared with the template procedure, the desired compounds are easy to isolate from the side products, which are mostly polymeric in nature. It is interesting that the stereochemical outcome of the two methods are different. In the template method, the *syn/anti* ratio shows an odd/even dependence on the number of methylene units in the bridges. Precursors with an odd number (such as **37** in Fig. 5)

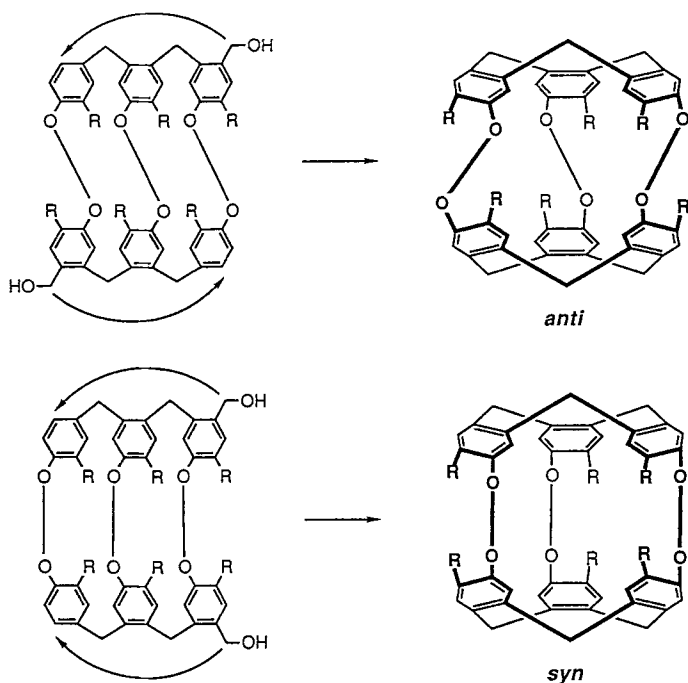


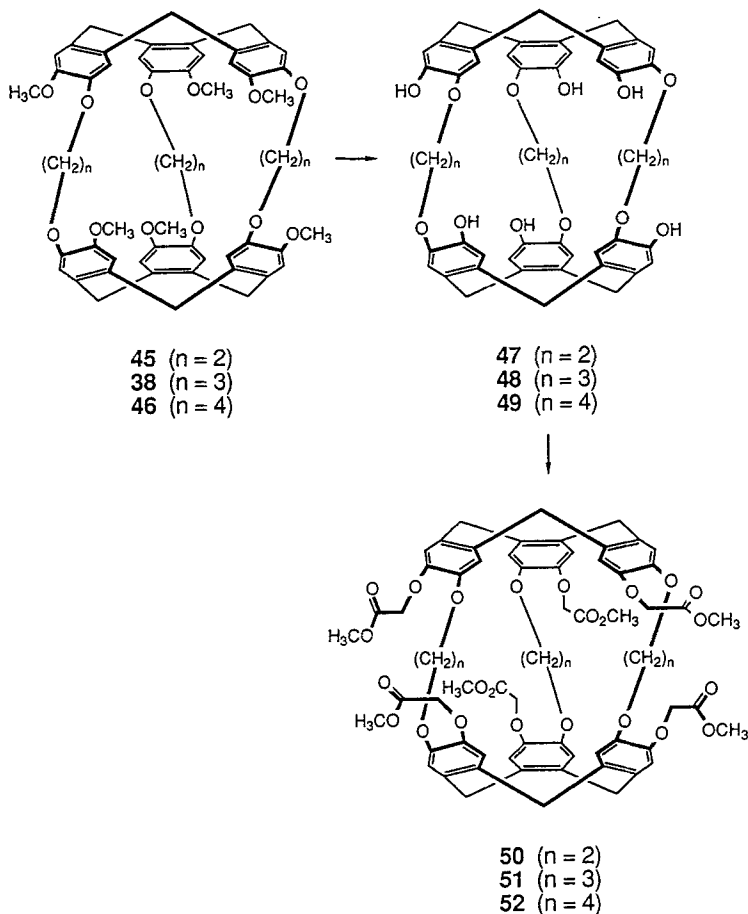
Fig. 8. Probable intermediates leading to *anti* and *syn* cryptophanes in the two-step method

preferentially cyclize to *syn* cryptophanes whereas those with an even number of methylene units cyclize to the *anti* isomers. Changing a double bond from *cis* to *trans* has a similar effect.

These observations are not surprising since the presence in the bridges of an even or odd number of atoms, or of a *cis* or *trans* double bond, determines the orientation of the reactive benzyl alcohol ends, and, in turn, the clockwise or counter-clockwise sense of the cyclization, as illustrated in Fig. 7.

The fact that the direct method does not exhibit the same odd/even dependence as does the template procedure obviously means the reaction does not proceed via the intermediate of Fig. 7 but suggests that the two cyclotrimeratrylene caps are formed simultaneously. Possible intermediates leading to *anti* and *syn* cryptophanes are shown in Fig. 8.

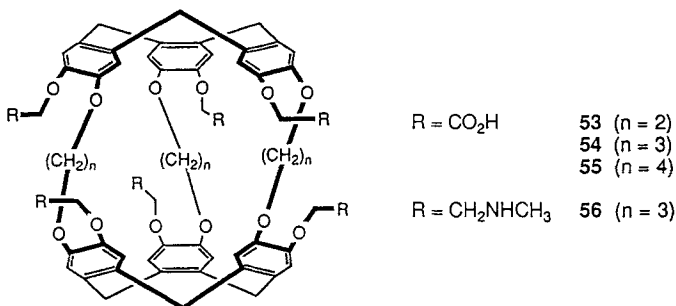
The above methods furnish cryptophanes provided with methoxy substituent at the periphery of the cyclotrimeratrylene caps. These hosts are soluble in organic solvents such as halogenated hydrocarbons but are insoluble in water or in alcoholic solvents. A way to make them water-soluble would be to incorporate



ionizable substituents to their structure. This goal can be achieved by selective demethylation of the methoxy substituents to give the corresponding phenols. However, this reaction is not trivial here, as the cleavage of the methyl ethers must be effected without affecting the $\text{OCH}_2(\text{X})\text{CH}_2\text{O}$ bridges.

This transformation was satisfactorily achieved [27, 28] in the *anti* cryptophanes **38**, **45**, and **46** by means of lithium diphenylphosphide to give the corresponding hexaphenols **47–49** in good yields.

Hexaphenols **47–49** are water-soluble at $\text{pH} > 12$. On alkylation with methyl bromacetate they were converted to hexaesters **50–52**, followed by hydrolysis to yield hexaacids **53–55**. These hexaacids are soluble in water at $\text{pH} > 5$ (less than 6 equivalent amounts of base added). Alternatively [20], on reaction with methylamine, followed by reduction of the intermediate hexaamide, hexaester **51** was converted to the corresponding hexaamine **56**. The latter is soluble in mildly acidic water.



3 Applications to Host-Guest Chemistry

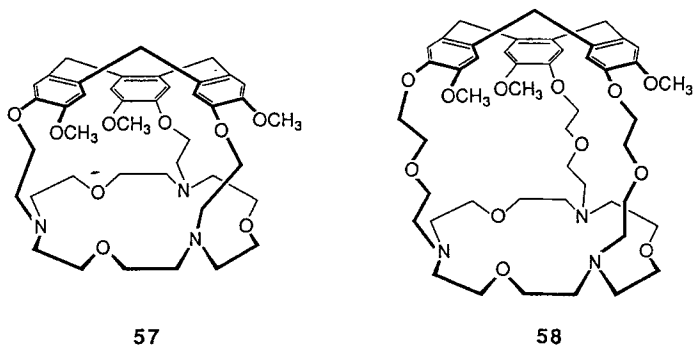
Cyclotrimeratrylene (**1**) and its hexademethylated derivative cyclotricatechylene (**16**) (Table 2) form crystalline inclusion compounds with a great variety of small to medium-sized molecules. These inclusion compounds have been described in a previous review [9] and will not be further considered here.

3.1 Hosts Containing One Cyclotrimeratrylene Unit

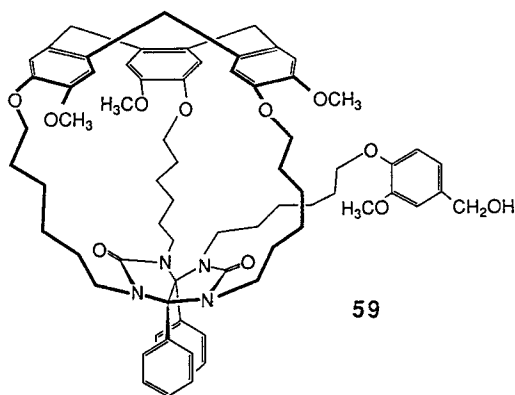
Simple cyclotrimeratrylenes such as those listed in Tables 1 and 2 do not complex guest species in solution, at least to a measurable extent. To reach this goal, various structural modifications have been proposed by several groups including: i) replacement of the methoxy substituents of **1** by six polyoxyethylene [29] or fatty acid [30] chains (octopus molecules); ii) incorporation of crown ethers to each benzene ring using the phenolic oxygens of **1**, so as to provide specific binding sites for alkali metal ions [31]. In these compounds, the complexing properties are due to the chains, not to the CTV unit itself.

Other groups have used the cyclotrimeratrylene cone both as a shaping unit and as a lipophilic cavity for designing and constructing hollow molecules of various types.

Some of these combine a cyclotrimeratrylene moiety with a specific binding site for cations (speleands). In the first speleands **57** and **58**, the specific binding site is a 18-[N₃O₃] crown ether linked to the cyclotrimeratrylene by three bridges [15].



Recently, speleand **59** containing a diphenylglycoluril unit as the binding site has been described by the Nolte group [32]. This compound was synthesized by a process similar to the method described in Fig. 4a, using a diphenylglycoluril unit instead of a cyclotrimeratrylene as the template. It bears an additional pendant arm intended to perform catalytic functions.



In order to increase the extension of the concave surface of cyclotrimeratrylene, and to obtain potentially useful host structures, Cram and coworkers have synthesised cavitands **60–65** [33]. In these compounds the additional walls (e.g., the *o*-xylylene units in **60**) are conformationally very mobile in solution. On crystallization from CH₂Cl₂-cyclohexane, **60** afforded a complex with one CH₂Cl₂ molecule inside the host cavity. The stereoview in Fig. 9 shows that two of the *o*-xylylene walls are turned upward from the cavity bottom and the third outward.

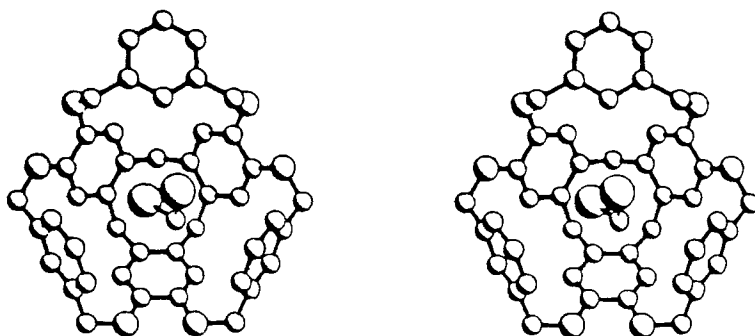
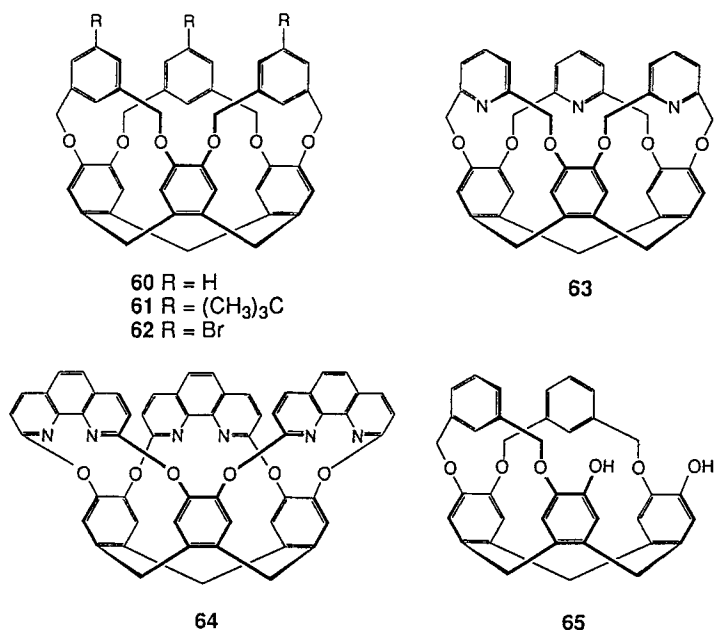


Fig. 9. Crystal structure of **60** · CH₂Cl₂ (ref. 33)

A similar conformation is found by molecular mechanics, and the calculations suggest that this host with CH₂Cl₂ inside the cavity in the position shown in Fig. 9 would be 13.7 kcal · mol⁻¹ more stable (ΔH) than the free host, a surprisingly large value which should probably be taken with a grain of salt. The binding constant of CH₂Cl₂ to **60** in solution is not known.



3.2 Cryptophanes as Hosts

The extraordinary ability of certain cryptophanes to bind neutral molecules of complementary size in lipophilic solvents is illustrated in Fig. 10, showing the

NMR spectrum of cryptophane-E (**38**) in $(\text{CDCl}_3)_2$, in the presence of two equivalents of CHCl_3 at 300 K. The peaks at δ_0 7.28 and δ_c 2.84 ppm correspond to the free and complexed chloroform molecules, respectively, which slowly exchange at this temperature on the NMR spectrometer time scale [25]. On heating, the guest signals broaden, as the exchange rate increases, but even at 340 K the fast exchange limit is not yet reached. The binding constant K_a is unusually strong, 470 M^{-1} at 300 K, which means that **38** can withdraw CHCl_3 from $(\text{CDCl}_3)_2$ at this temperature (at lower temperature, the binding constants are still higher).

This type of complexation is by no means limited to halogenomethanes, and the same behaviour is observed with aliphatic hydrocarbons such as isobutane [34], which shows a comparatively strong binding (K_a ca. 100 M^{-1}) with host **38** under the same conditions as above (Fig. 11). It is interesting to note that in the isobutane complex, the upfield shift of the CH group ($\delta_0 - \delta_c$ 4.25 ppm) is close to that of CHCl_3 (4.44 ppm); the structures of the two complexes are thus probably similar [35].

For host **38**, the complexation processes are slow, on the NMR time scale; the barrier for guest inclusion, calculated by line-shape analysis of the exchanging guest signals, is found between 13 and 15 $\text{kcal} \cdot \text{mol}^{-1}$ at 300–330 K, for guests ranging from CH_3I to CHBr_3 . Other cryptophanes show much faster exchange rates. For instance, the NMR spectrum of **40** (cryptophane-C) in the presence of CH_2Cl_2 (Fig. 12) at 293 K does not show any signal for this guest; the fast exchange averaged resonance is probably between 3 and 5 ppm where it is obscured by the host signals. However, at 233 K, the free and complexed CH_2Cl_2 peaks become visible. In this case, the inclusion barrier is around 11–12 $\text{kcal} \cdot \text{mol}^{-1}$. The magnitude of the binding constant K_a is not affected by the exchange rate, however: 325 M^{-1} for **40** and CH_2Cl_2 at 300 K [36].

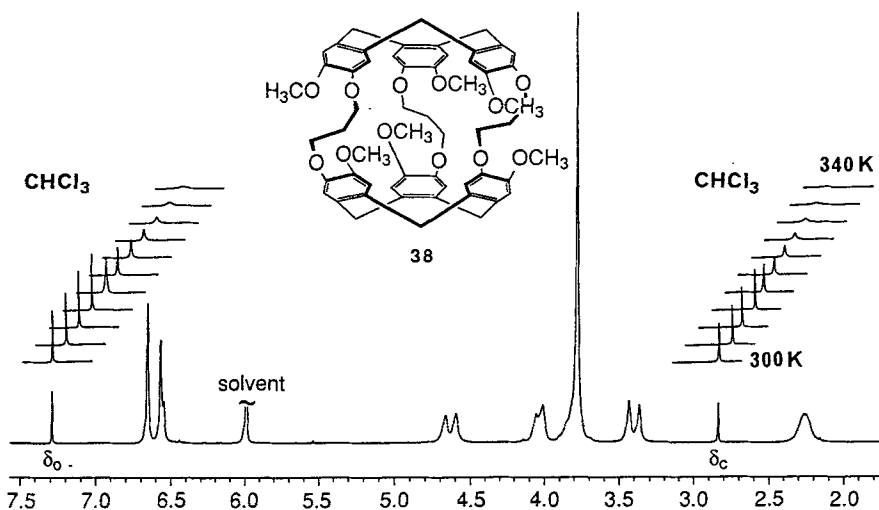


Fig. 10. ^1H NMR spectrum of cryptophane **38** in $(\text{CDCl}_3)_2$ in the presence of CHCl_3

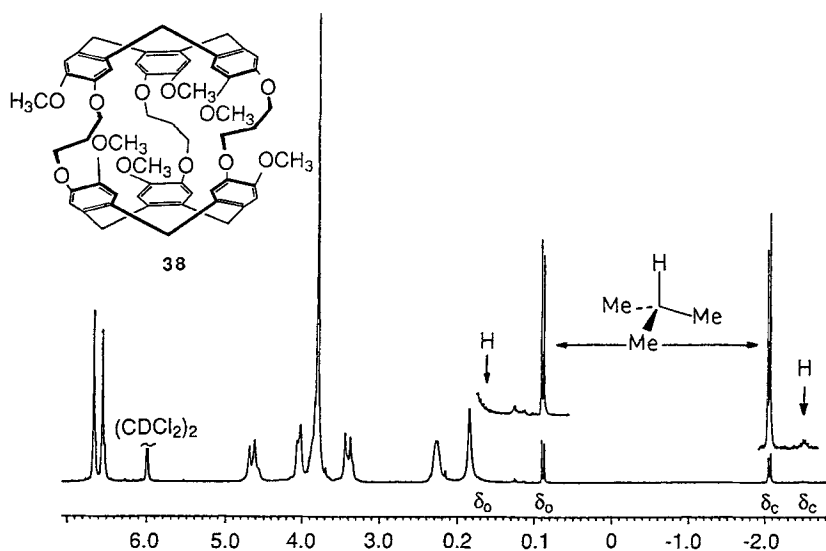


Fig. 11. ^1H NMR spectrum of cryptophane **38** in the presence of isobutane, in $(\text{CDCl}_2)_2$

A summary of the complexing properties of hosts **38** and **40** in $(\text{CDCl}_2)_2$ towards neutral guest species is given in Fig. 13, where the experimental free energy of association $\Delta G_a^\circ (= -RT \ln K_a)$ at 300 K has been plotted as a function of the guest van der Waals volumes [35].

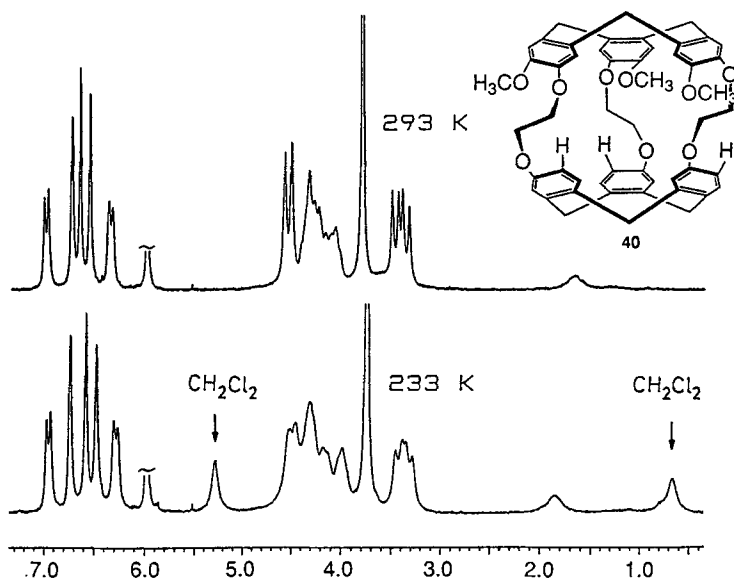


Fig. 12. ^1H NMR spectra of cryptophane **40** and CH_2Cl_2 , in $(\text{CDCl}_2)_2$

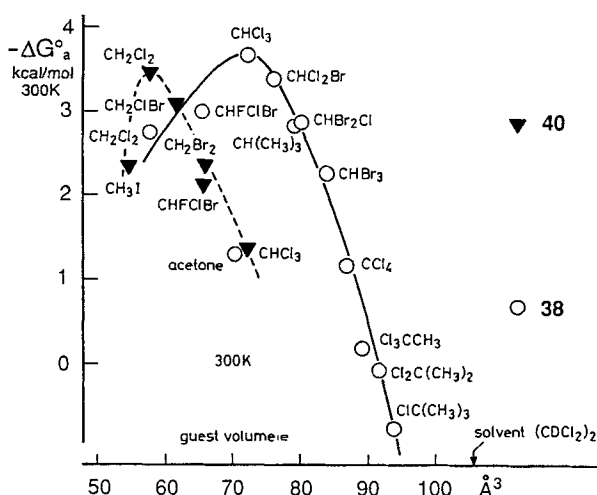


Fig. 13. Free energy of association ΔG°_a for complexes of **38** and **40** with neutral guests at 300 K, in $(\text{CDCl}_2)_2$

Both cryptophanes exhibit a smooth and steep size recognition. The smallest one, **40**, prefers to bind guests of size around 60 \AA^3 , whereas the preference of the largest, **38**, is shifted to ca. 75 \AA^3 . In the two cases, the selectivity is quite distinct. For instance, **38** discriminates between CHCl_3 and CHBrCl_2 by $0.3 \text{ kcal} \cdot \text{mol}^{-1}$, an energy difference which is best appreciated by considering that the difference in volume of these two molecules is only 5%. However, **38** does not discriminate between isobutane and CHBr_2Cl which have the same van der Waals volume.

On the other hand, acetone is much more weakly bound than chloroform, although they have about the same size. Host **38** therefore efficiently recognizes tetrahedral (sp^3) versus flat (sp^2) molecules.

At this point, it is interesting to think about the meaning of these experimental binding constants K_a . They correspond to an equilibrium state in which guest and solvent compete to occupy the host cavity, as sketched in Fig. 14a. The actual binding constant of the guest, K , can be determined only if that of the solvent, K_s , is known, by using the following relationship where $[S]$ represents the molar concentration (or the activity) of the solvent:

$$K = K_a(1 + K_s[S]).$$

Accordingly, K will be close to K_a if $K_s[S] \ll 1$. Since $[S]$ is usually around 10 M, the above condition will be fulfilled only if $K_s < 10^{-2} \text{ M}^{-1}$. The following example is illustrative: host **40** binds CH_2Cl_2 in CDCl_3 , with an *apparently* very weak binding constant $K_a = 2.6 \text{ M}^{-1}$. In fact, the solvent ($[S] = 12.4 \text{ M}$) is also bound, with $K_s = 10 \text{ M}^{-1}$. Application of the above equation indicates that the actual binding constant K of CH_2Cl_2 should be around 325 M^{-1} .

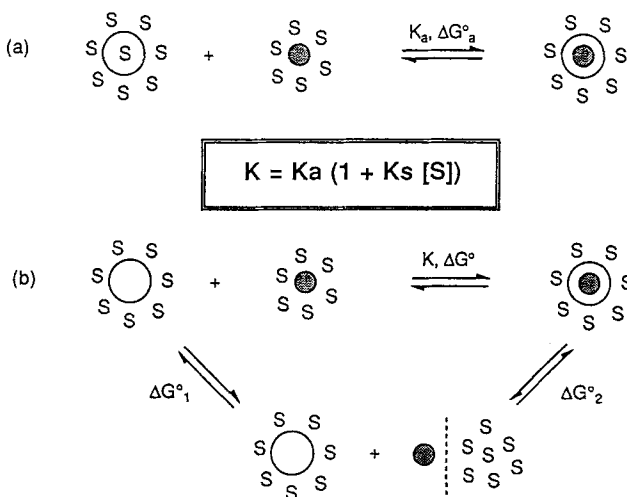


Fig. 14. Dissection of the complexation equilibria

This is the reason why 1,1,2,2-tetrachloroethane- d_2 was employed as the solvent in the experiments described in Figs. 11–13. This solvent seems to be too big (108 \AA^3) to occupy the cavity of hosts **38** and **40**, hence its K_s must be very small and therefore the measured K_a should be close to their actual value K .

The physical meaning of K can be analyzed in more details. It formally corresponds to the horizontal equilibrium displayed in Fig. 14b, to which the free energy change ΔG° is associated. This equilibrium can in turn be dissected into (at least) two sub-equilibria: the first one can be related to guest desolvation (ΔG°_1). It may be connected with the opposite of the energy of mixing of the guest in solvent S at infinite dilution, or more generally with “solvophobic forces”. The second equilibrium (ΔG°_2) represents the interaction between the desolvated guest and the empty host in solvent S . Thus ΔG° is the sum of ΔG°_1 and ΔG°_2 . In our relatively simple experimental model system, guest and solvent are very similar in nature, both being lipophilic. Hence the contribution of ΔG°_1 should be negligible and the observed ΔG° is thus expected to be reasonably close to ΔG°_2 , the term representing the interaction energy of the host and guest partners.

It is interesting to split ΔG° into its enthalpic and entropic components, which can be done by means of the usual van t'Hoff plots ($\ln K$ vs. $1/T$). Relevant data for cryptophane-A (**45**), C (**40**), and E (**38**) are assembled in Table 4. Cryptophane-A is similar in structure to cryptophane-E, and has shorter bridges ($\text{O}(\text{CH}_2)_2\text{O}$ in **45** instead of $\text{O}(\text{CH}_2)_3\text{O}$ in **38**). Thus cryptophane-A and C should have cavities of the same size, slightly smaller than that of cryptophane-E.

The data assembled in Table 4 indicate that the apparently simple size dependence of the recognition is no longer valid when the enthalpies and entropies of complexation are considered. For the smallest hosts **40** and **45**, enthalpy strongly favors chloroform over methylene chloride, although the latter is the preferred

Table 4. Complexation thermodynamics for cryptophane-A (**45**), -C (**40**), and -E (**38**) in (CDCl₂)₂ at 300 K [20]

Host	Guest	ΔG° kcal · mol ⁻¹	ΔH kcal · mol ⁻¹	ΔS cal · mol ⁻¹ · K ⁻¹
(45)	CH ₂ Cl ₂	-3.7	-3.3	+1
	CH ₂ Br ₂	-3.5	-1.3	-7
	CHCl ₃	-3.3	-8.2	-16
(40)	CH ₂ Cl ₂	-3.5	-3.9	-1
	CHCl ₃	-1.4	-6.4	-16
(38)	CH ₂ Cl ₂	-2.8	+1.0	+6
	CHCl ₃	-3.7	-6.0	-7
	CHBrCl ₂	-3.4	-5.2	-6
	CH(CH ₃) ₃	-2.8	-3.8	-3
	CHBr ₂ Cl	-2.9	-1.5	+4
	CHBr ₃	-2.3	-1.4	+4

guest at 300 K. This paradox can be explained by considering the large negative entropy of formation of the chloroform complexes, corresponding to a TΔS term of +4.8 kcal · mol⁻¹ at 300 K. In other words, a good fit between host and guest leads to a favorable ΔH, but has to be paid by a large negative entropy of formation, which in turn destabilizes the complex at room temperature.

The fit between host **38** and chloroform is still good (ΔH -6 kcal · mol⁻¹), however, the entropy of complexation is less negative than it is with **40** and **45**, possibly because the host cavity of **38** is, in fact, slightly too large for this guest. On the other hand, methylene chloride displays a small, positive ΔH which means that it does not interact with the host cavity very efficiently (it is too small). Here, one can draw a relatively simple picture of the phenomenon; for tetrahedral guests of type CHXYZ with sizes between 70 and 80 Å³, the enthalpic stabilization of the complexes overcomes their entropic destabilization at 300 K. Since as stated above, this stabilization cannot come from solvophobic forces (ΔG°₁ in Fig. 14), it should be ascribed to attractive host-guest interactions provided by dispersion forces operating in the interior of the cavity. The observed magnitude of these forces implies that the complexes are geometrically well defined; the crystal structure of the chloroform complex of **38** is consistent with this view (Fig. 15), and shows that the guest aligns its threefold axis with that of the host [35].

The study [26, 37] of the complexation of polymethylammonium cations by **38** in (CDCl₂)₂ gave unexpected results (Fig. 16). One observes a very strong complexation of Me₄N⁺ (K_a of the order 250000 M⁻¹), although the size of this substrate is nearly the same as that of Me₃CCl, which is only very weakly bound. The size of a molecule, or of a molecular cavity, is thus a somewhat fuzzy notion!

Moreover, the strong binding displayed by the tetramethyl ammonium cation led to consider that cryptophanes of the size of **38** might be suitable receptors for substrates of structure Me₃N⁺ - R in which R would be an aliphatic chain or a functionalized chain such as that of choline and acetylcholine. In fact, it is found that, in (CDCl₂)₂, the binding constant drops rapidly as the length of an aliphatic

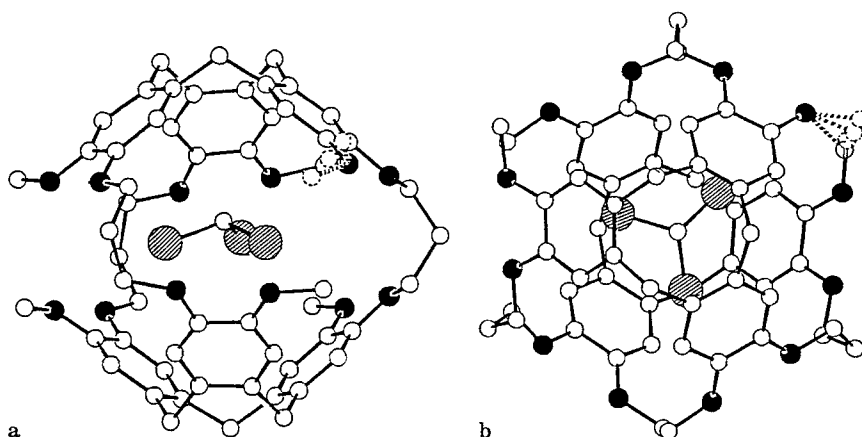


Fig. 15. X-ray crystal structure of complex **38** · CHCl₃; **a**) side view; **b**) top view (ref. 35)

chain increases ($R = \text{Me, Et, Pr}$). However, the presence in the chain of a well positioned OH group leads again to a strong complexation: choline ($R = \text{CH}_2\text{CH}_2\text{OH}$) is thus better bound than its hydrocarbon analogue ($R = \text{Pr}$). In fact the OH group of choline can form an hydrogen bond to one of the oxygens of the methoxy groups of the host (see Fig. 16). Acetylcholine, in which such H-bonding is no longer possible, is only weakly complexed by **38** under these conditions.

The reasons why Me_4N^+ is so strongly bound are not yet well understood. In this case, the ΔG°_1 term of Fig. 14 may be important, as this cation is probably more hydrophilic than lipophilic. Moreover, the high electron density of the six alkoxy substituted benzene rings of **38** may certainly favor the binding of soft cations of suitable size and shape. It is noteworthy that anions of comparable size, such as BF_4^- or PF_6^- do not show any evidence of complexation under the same conditions.

The dramatic effect of the 'tail' (R) of the ammonium substrates on the binding strength is difficult to explain. This tail, which points outside the windows if the length of R is at least that of a propyl group, might restrict the rotational freedom of the guest in the cavity; this phenomenon would be expected to generate a defavorable entropy term. A more precise discussion of this point must await the determination of the enthalpies and entropies of complexation for these charged substrates.

In water or hydrophilic solvents, the contribution of hydrophobic forces (ΔG°_1 in Fig. 14) is expected to enhance the stability of the complexes between cryptophanes and neutral, lipophilic substrates. The following experiment [27] furnishes a good illustration of this effect. The NMR spectrum of the empty water-soluble host **53** in $\text{D}_2\text{O}/\text{NaOD}$ (pH ca. 6) is shown in Fig. 17a. On addition of less than one equivalent of CHCl_3 , a new set of sharp resonances appears for the host (Fig. 17b), while no signal is detected for CHCl_3 at the expected position. Instead, a peak at 3.15 ppm is present, assigned to complexed CHCl_3 . Thus this cryptophane virtually scavenges CHCl_3 from water. Only when slightly more than

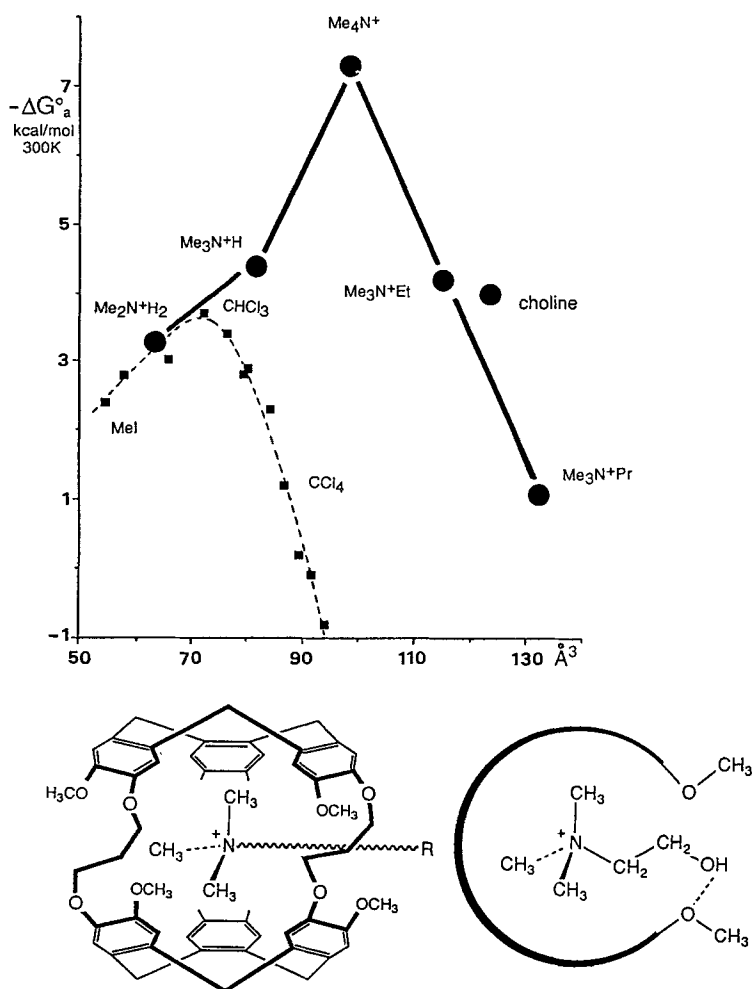


Fig. 16. ΔG°_a of complexation of ammonium guests by cryptophane 38 in $(\text{CDCl}_3)_2$

one equivalent of the guest is added does the free CHCl_3 become observable at 7.69 ppm, and then all the resonances of the host simplify to a single set of sharp peaks ascribed to the CHCl_3 complex (Fig. 17c).

The complexation of CH_2Cl_2 by **53** follows the same trend. However, CHCl_3 (K_a 7700 M^{-1}) is better complexed than CH_2Cl_2 (5000 M^{-1}), although the corresponding host **45** displays in $(\text{CDCl}_3)_2$ an inverse preference (see Table 5). The hydrophobic contribution (ΔG°_1) is expected to be larger for CHCl_3 , which is ca. 30% bulkier in volume than CH_2Cl_2 , and therefore might account for the inversion of the selectivity of **45** and **53** on going from a lipophilic to a hydrophilic solvent. A rough estimate of the magnitude of this contribution may be given by the difference of the ΔG°_a values for the same guest in $(\text{CDCl}_3)_2$ and in water: $-2.0 \text{ kcal} \cdot \text{mol}^{-1}$ for CHCl_3 , instead of -1.4 for CH_2Cl_2 .

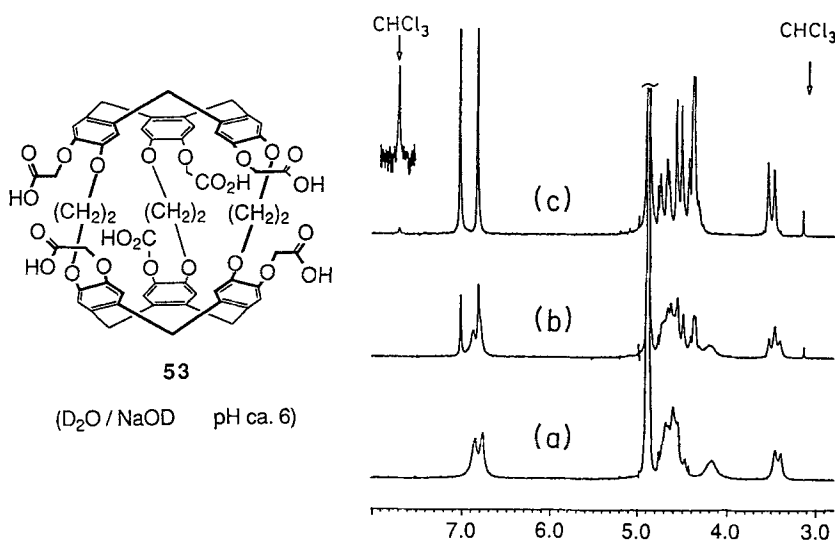


Fig. 17. ^1H NMR spectra of cryptophane **53** and CHCl_3 in $\text{D}_2\text{O}/\text{NaOD}$ solution

Relevant complexation data for C_4 -aliphatic hydrocarbons and host **54** in water, and **38**, in $(\text{CDCl}_2)_2$, are given in Table 5. Isobutane appears to be more than five hundred times better bound by **54** in water than by **38** in the organic solvent. The hydrophobic contribution in this case ($-3.8 \text{ kcal} \cdot \text{mol}^{-1}$) is larger than that reported above for CHCl_3 (isobutane is more polar and about 10% bulkier in volume than CHCl_3) [37].

In water, isobutane is fifty times better bound than isobutene, and ten times better than *n*-butane. These results confirm the preference of the cryptophane cavity for tetrahedral structures, and show that branched hydrocarbons are much better substrates than linear ones. Separation processes based on such molecular

Table 5. Complexation data for neutral guests in water and in $(\text{CDCl}_2)_2$ at 300 K [20]

Host	Solvent	Guest	K_a M^{-1}	ΔG°_a $\text{kcal} \cdot \text{mol}^{-1}$	ΔG°_1 $\text{kcal} \cdot \text{mol}^{-1}$
Cryptophane-A (45)	$(\text{CDCl}_2)_2$	CH_2Cl_2	475	-3.7	
		CHCl_3	230	-3.3	
Cryptophane-A (COOH) ₆ (53)	D_2O	CH_2Cl_2	5000	-5.1	-1.4
		CHCl_3	7700	-5.3	-2.0
Cryptophane-E (38)	$(\text{CDCl}_2)_2$	isobutane	115	-2.8	
Cryptophane-E (COOH) ₆ (54)	D_2O	<i>n</i> -butane	6000	-5.2	
		isobutane	60000	-6.6	-3.8
		isobutene	1200	-4.2	

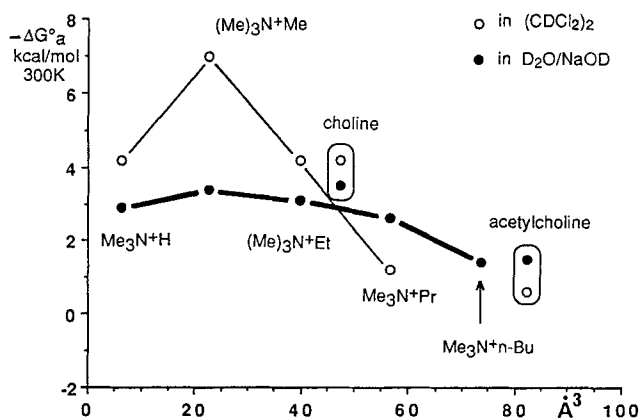


Fig. 18. Free energy of association ΔG°_a for complexes of **38** with ammonium guests in $(\text{CDCl}_2)_2$ and in $\text{D}_2\text{O}/\text{NaOD}$ solutions

recognition phenomena rather than on distillation or diffusion can thus be envisioned [28].

Finally, the complexing properties of the water-soluble host **54** in water (pH 5–8) towards polymethyl ammonium cations are summarized in Fig. 18. For comparison, the complexing properties of host **38** in $(\text{CDCl}_2)_2$ are displayed on the same graph [37].

On going from the organic solvent to water, one observes a decrease of the binding constants for the smallest substrates (up to choline), and an increase for the largest ones, $\text{Me}_3\text{N}^+ - \text{Pr}$, $\text{Me}_3\text{N}^+ - \text{Bu}$, and acetylcholine. This behaviour again emphasizes the role of hydrophobic forces, which favor the complexation of the substrates having the longest side chains. Moreover, it is noteworthy that acetylcholine is now bound, albeit not very strongly, in water at neutral pH. We now expect that suitable modifications of the cryptophane structure will lead to a stronger binding of this guest.

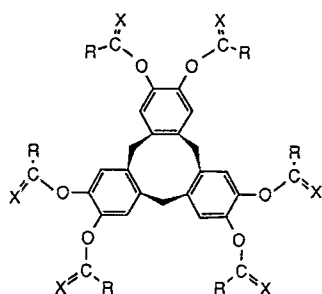
4 Applications to the Design of New Materials

Applications of cyclotrimeratrylenes and cryptophanes to the design of materials for optoelectronics are still in the area of prospective research. We only mention here works dealing with ferroelectric liquid crystals and three-dimensional charge transfer salts.

4.1 Ferroelectric Liquid Crystals

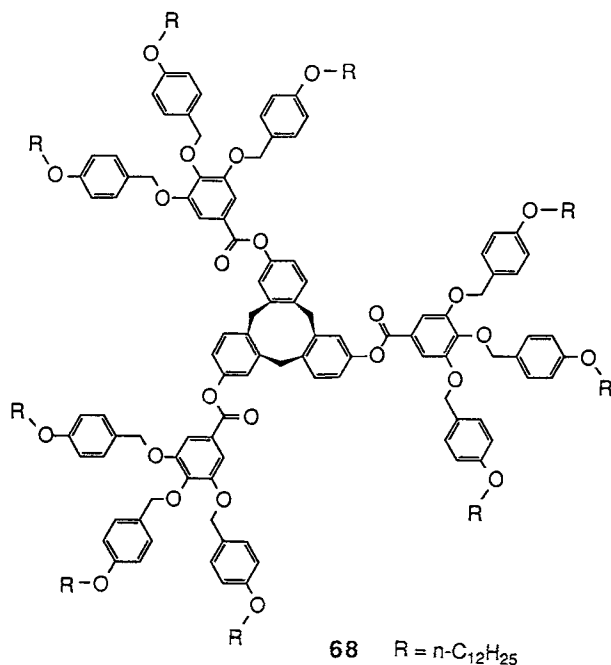
Certain hexaesters **66** and hexaethers **67** [38–41], as well as triester **68** [42], form thermotropic columnar mesophases. In these mesophases, which generally exist in a wide temperature domain (e.g. from r.t. to 200 °C), the cone-shaped cores

stack in columns, at a distance of 4.8 Å, identical to that observed in the crystals of cyclotrimeratrylene [6, 7, 39]. In a column, the cones are embedded in one another, making the column axis polar. The conical shape of the cores certainly contributes to the stability of these mesophases, in making the displacements perpendicular to the column axis more difficult.



66 C=X : C=O

67 C=X : CH₂



Such mesophases might be ferroelectric, if all the columns adopt the same polarization direction within a macroscopic domain, e.g. in an electric field, as sketched in Fig. 19 (the cones may have a strong dipole moment along their axis).



Fig. 19. Antiferroelectric to ferroelectric transition in a columnar mesophase made of molecules with a cone-shaped core

However, the high viscosity of these mesophases severely restricts the freedom of the molecules to turn upside down, and hence this mechanism would not easily allow orientation of the cones. Alternatively, one can think about using the possibility of conformational inversion of the cyclotrimeratrylene core, which takes place in solution over a barrier of ca. $27 \text{ kcal} \cdot \text{mol}^{-1}$ (see Sect. 1). If the inversion process could still occur at a sufficient rate in a mesophase such as those of **66**–**68**, one would expect to achieve the process depicted in Fig. 19 without need for any upside-down rotation of the molecules; only an umbrella-like inversion of their core is required.

It has been found [42] that the barrier for the CTV ring inversion in **68** in isotropic solution at 100°C is $\Delta G^\ddagger 26.9 \text{ kcal} \cdot \text{mol}^{-1}$, a figure which does not differ from that of other cyclotrimeratrylenes. In the mesophase at 100°C , the inversion rate is slower by two orders of magnitude, with $\Delta G^\ddagger 30.3 \text{ kcal} \cdot \text{mol}^{-1}$. Thus the tight embedding of the CTV units in the mesophase columns increases the inversion barrier by $3.4 \text{ kcal} \cdot \text{mol}^{-1}$.

The estimated half-life of a cone in the mesophase of **68** at 3°C below the clearing temperature (150°C) is 3 minutes, which seems fast enough to allow the mesophase columns to be oriented under the influence of an electric field with more than 50% of the cones eventually pointing in one direction. Quenching the oriented mesophase to room temperature would then give a ferroelectric material in which the polarization of the columns might last several decades, since at 20°C the estimated half-life of the cones is 80 years. The next step of this approach is to synthesise cyclotrimeratrylene mesogens with a strong dipole moment along the C3 axis, in order to facilitate their orientation.

4.2 Three-dimensional Charge-Transfer Salts

Most organic electron donor or acceptor are flat molecules and form charge transfer salts of low dimensionality (e.g. TTF/TCNQ). In contrast, it may be anticipated that the electron rich spherical cryptophane molecules (10 \AA in diameter), when associated with suitable electron acceptors, would form three-dimensional charge transfer salts. In fact, oxidation of cryptophane **38** in acetonitrile solution shows two reversible oxidations at 0.69 V ($38/38^+$) and 0.85 V ($38^+/38^{2+}$) versus Ag/Ag^+ . Another oxidation ($38^{2+}/38^{3+}$) approaching chemical reversibility is observed at 1.11 V (Fig. 20). Charge transfer salts of formula $[(38^+)(X^-)(\text{CHCl}_3)]$ are actually formed by electrolysis of **38** in a $\text{CH}_2\text{Cl}_2/\text{CHCl}_3$ mixture containing ammonium salts of BF_4^- , ClO_4^- , PF_6^- and ReO_4^- as supporting electrolytes (43).

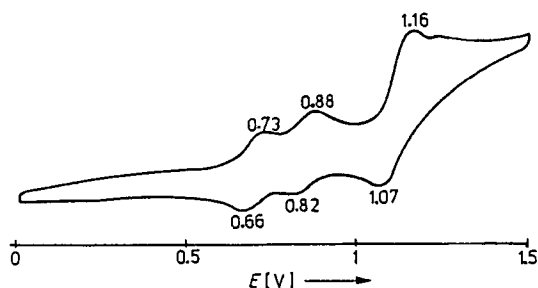


Fig. 20. Cyclic voltammogram of **38** in acetonitrile; 0.1 M $n\text{-Bu}_4\text{NPF}_6$ as electrolyte; Ag/AgNO_3 reference electrode (ref 43)

The crystal structure of $[(\mathbf{38}^+) (\text{PF}_6^-) (\text{CHCl}_3)]$ depicted in Fig. 21 shows the 1 : 1 complex formed between the oxidized cryptophane $\mathbf{38}^+$, including a chloroform molecule in its cavity, and one PF_6^- anion. EPR spectra of the crystals are consistent with the existence of quasi free delocalized π electrons. The persistence of the paramagnetic signal in solution indicates that $\mathbf{38}^+$ is a stable species. The crystal packing is a closed packed three-dimensional fcc array of the giant radical cations, with the small anions located in the octahedral sites.

The cryptophanes and their complexes may thus be considered as a new family of organic donors; in contrast with the flat donors, their spherical shape and large size drive the crystallization towards three-dimensional rather than unidimensional arrays. This feature may aid in the design of new materials with isotropic physical properties (e.g. electric conductivity).

We gratefully acknowledge additional support of this work by Société LIPHA (Lyon), Institut Français du Pétrole, A.D.R. (Grenoble), and Région Rhône-Alpes.

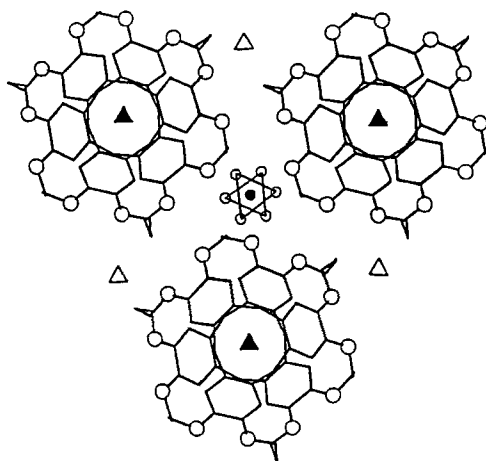


Fig. 21. X-ray structure of complex $[(\mathbf{38}^+) (\text{PF}_6^-) (\text{CHCl}_3)]$; ▲ and △ centers of **38**, ● center of PF_6^- (ref 43)

5 References

1. Robinson GM (1915) *J Chem Soc* 102: 266; Robinson R (1976) In: *Memoirs of a minor prophet*, vol 1 p 51, Elsevier, Amsterdam
2. Ewins AJ (1909) *J Chem Soc* 95: 1482
3. Lindsey AS: *J Chem Soc* 1965: 1685
4. Erdtman H, Haglid F, Ryhage R (1964) *Acta Chem Scand* 18: 1249
5. Goldup A, Morrison AB, Smith GW: *J Chem Soc* 1965: 3864
6. Cerrini S, Giglio E, Mazza F, Pavel NV (1979) *Acta Cryst B35*: 2605
7. Cesario M, Guilhem J, Pascard C (1979) Unpublished work
8. Collet A, Gabard J (1980) *J Org Chem* 45: 5400
9. Collet A (1987) *Tetrahedron* 43: 5725
10. Bhagwat VK, Moore DK, Pyman FL: *J Chem Soc* 1931: 443
11. Caglioti V, Liquori AM, Gallo N, Giglio E, Scrocco M (1958) *J Inorg Nucl Chem* 8: 572
12. Canceill J, Gabard J, Collet A: *J Chem Soc, Chem Commun* 1983: 122
13. Canceill J, Collet A, Gabard J, Gottarelli G, Spada P (1985) *J Am Chem Soc* 107: 1299
14. Gabard J, Collet A: *J Chem Soc, Chem Commun* 1981: 1137
15. Canceill J, Collet A, Gabard J, Kotzyba-Hibert F, Lehn JM (1982) *Helv Chim Acta* 65: 1894
16. Canceill J, Collet A, Gottarelli G (1984) *J Am Chem Soc* 106: 5997
17. Canceill J, Collet A (1986) *Nouv J Chim* 10: 17
18. Keipert SJ (1985) Ph. D. Thesis, University of California, Los Angeles; *Diss Abstr* 46: 4246B
19. Cram DJ (1983) *Science (Washington D C)* 219: 1177 (see Ref 18)
20. Garcia C, Andraud C, Malthête J, Canceill J, Collet A, Vériot G (1990) to be published
21. Collet A, Gottarelli G (1989) *Croat Chem Acta* 62: 279
22. Canceill J, Collet A: *J Chem Soc, Chem Commun* 1983: 1145
23. Canceill J, Lacombe L, Collet A (1985) *J Am Chem Soc* 107: 6993; Canceill J, Cesario M, Collet A, Guilhem J, Riche C, Pascard C: *J Chem Soc, Chem Commun* 1985: 361; Canceill J, Cesario M, Collet A, Guilhem J, Pascard C: *J Chem Soc, Chem Commun* 1986: 339
24. Canceill J, Collet A: *J Chem Soc, Chem Commun* 1988: 582
25. Canceill J, Lacombe L, Collet A (1986) *J Am Chem Soc* 108: 4230
26. Collet A, Dutasta JP, Lozach B (1990) *Bull Soc Chim Belg* 99: 617
27. Canceill J, Lacombe L, Collet A: *J Chem Soc, Chem Commun* 1987: 219
28. Collet A, Dutasta JP, Lozach B, Canceill J, Weill J (1990) *Demande de Brevet Français (to Institut Français du Pétrole) No 90 10614 (22 August)*
29. Hyatt JA (1978) *J Org Chem* 43: 1808
30. Menger F, Takeshita M, Chow JF (1981) *J Am Chem Soc* 103: 5938
31. Frensch K, Vögtle F (1979) *Liebigs Ann Chem* 733: 37
32. Smeets JWH, Coolen HKAC, Zwikker JW, Nolte RMJ (1989) *Recl Trav Chim Pays-Bas* 108: 215
33. Cram DJ, Weiss J, Helgeson RC, Knobler CB, Dorigo AE, Houk KN: *J Chem Soc, Chem Commun* 1988: 407
34. Canceill J, Lacombe L, Collet A (1987) *C R Acad Sci Paris Sér I/304*: 815
35. Canceill J, Cesario M, Collet A, Guilhem J, Lacombe L, Lozach B, Pascard C (1989) *Angew Chem Intern Ed Engl* 28: 1246
36. Canceill J, Lacombe L, Collet A (1989) Unpublished work
37. Lozach B, Dutasta JP, Collet A (1990) Unpublished work
38. Malthête J, Collet A (1985) *Nouv J Chim* 9: 151
39. Levelut AM, Malthête J, Collet A (1986) *J Physique* 47: 351
40. Zimmermann H, Poupko R, Luz Z, Billard J (1985) *Z Naturforsch* 40A: 149
41. Zimmermann H, Poupko R, Luz Z, Billard J (1986) *Z Naturforsch* 41A: 1137
42. Malthête J, Collet A (1987) *J Am Chem Soc* 109: 7544
43. Renault A, Talham D, Canceill J, Batail P, Collet A, Lajzerowicz J (1989) *Angew Chem Int Ed Engl* 28: 1249

From Classical Chirality to Topologically Chiral Catenands and Knots

Jean-Claude Chambron, Christiane Dietrich-Buchecker and Jean-Pierre Sauvage

Laboratoire de Chimie Organo-Minérale, U.R.A. au CNRS n° 422, Institut de Chimie,
1, rue Blaise Pascal, 67000 Strasbourg, France

Table of Contents

1 Introduction	132
2 Euclidean Chirality	132
3 Molecular Topology	136
3.1 Topological Properties of Molecules	136
3.2 Topological Stereoisomerism	137
3.3 Topological Chirality	141
4 A Review of Some Topologically Chiral Molecules	141
4.1 Molecules with a Non-Planar Graph K_5	141
4.2 Molecules with a Non-Planar Graph $K_{3,3}$	144
4.3 Interlocked Rings	148
4.4 The Molecular Trefoil Knot	152
5 Conclusion	158
6 References and Notes	159

1 Introduction

Intuitively, there is a fundamental difference between molecules that can be racemized by pathways in which bonds are bent, compressed or stretched, or chemical groups compressed, and molecules which cannot be racemized except by breaking and reforming chemical bonds. In practice, the first type of molecules may be almost as difficult to racemize as the second group of compounds, but the conceptual difference is essential. One of the best examples and certainly the first one is that of Le Bel and van't Hoff's asymmetric carbon [1]. Two mirror-image tetrasubstituted carbon centres cannot be interconverted, because of prohibited inversion, the energy barrier to the formation of a hypothetical planar intermediate being too high. In this case, however, no bond breaking would be required.

In the present article, we will try to go beyond the above intuitive view and treat in a more rigorous fashion the concept of chirality, starting with the classical definitions and going further by discussing in detail the more recent notion of topological chirality.

2 Euclidean Chirality

Chirality [2] has different meanings depending on whether a single rigid molecule or sets of conformationally mobile molecules are considered [3, 4]. We will first focus on the former case. *Euclidean* or *geometrical* chirality is the property of rigid molecular objects that cannot be superimposed upon their mirror images by translation or rotation. The only symmetry elements that they may possess are proper rotational axes C_n , $n \geq 1$. (Those molecules which possess only such symmetry elements are called dissymmetric. In particular, asymmetric molecules are those devoid of any symmetry element). In other words, the symmetry criterion for chirality is that a molecule is chiral if and only if it does not possess any improper axis of symmetry. Thus the chirality of a molecule may be deduced from an analysis of its symmetry elements and its symmetry point groups. The groups which chiral molecules must belong to are: C_1 , C_n ($n > 1$), D_n , T , O and I . C_1 is asymmetric, C_n and D_n are dihedral symmetric and T , O , I are polyhedral symmetric groups. A classification of chiral molecular structures according to symmetry has been used in a review of highly symmetrical chiral molecules [5].

In numerous cases, however, molecules cannot be represented by a single rigid model: in this second case, sets of conformationally mobile molecules (that is, real chemical compounds) must be considered. Now we are concerned with geometrical *chemical* chirality. A molecule is then said to be chemically chiral if any of its transient conformations cannot be brought into congruence with its mirror image by a translation or a rotation, and by those intramolecular motions (conformational changes) that can occur under the observation conditions (which are determined by temperature, time-scale of experiment, instrument sensitivity, etc. . . . [3, 4, 6]). This more general definition is necessary to understand the achirality of a meso compound such as *cis*-1,2-difluorocyclohexane (1) [3] or Mislow's L-menthyl-D-menthyl-2,6,2',6'-tetranitro-4,4'-diphenate (2) [7] (Fig. 1). In the

former case, at least one conformation with a plane of symmetry is accessible, while in the latter all possible conformations are chiral. Nevertheless compound **2** is achiral because rotation about the unhindered phenyl-ester bonds allows interconversion between mirror-image conformations. Thus **2** is an example of a compound which is chiral in all of its conformations, but does not exist in stable enantiomeric forms. According to the more general definition of chirality given above, the problem of chirality becomes the resolution of a chemical compound into enantiomers, the ultimate criterion being optical activity. The necessary and sufficient condition for a chemical compound (set of molecules) to be optically active [8] is that each molecule does not have any improper element of symmetry and that there is no conformationally allowed deformation taking any conformation to its mirror image by a chiral pathway.

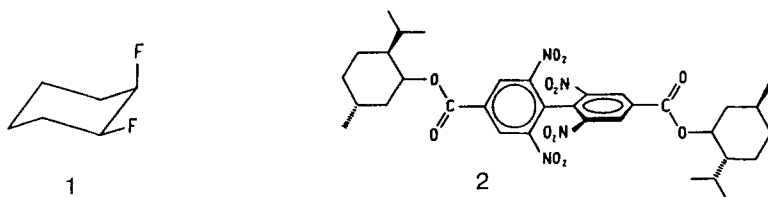
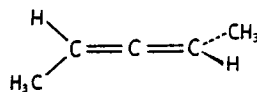
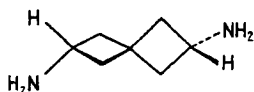
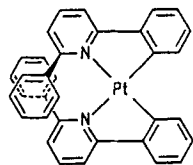
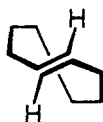
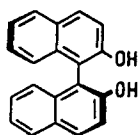
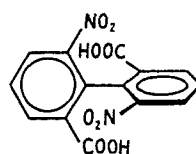
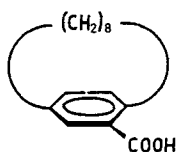
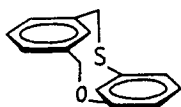
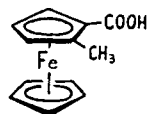
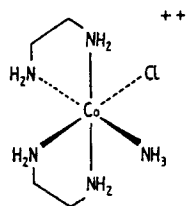
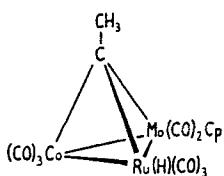
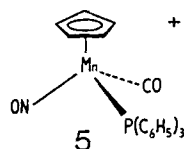
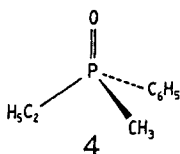
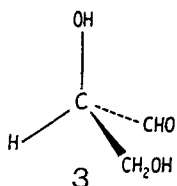


Fig. 1. *cis*-1,2-Difluorocyclohexane (**1**) and L-menthyl-D-menthyl-2,6,2',6'-tetranitro-4,4'-diphenate (**2**)

At this point, we are concerned only with chirality as a property of molecular objects with a certain rigidity, that is a rigidity which is controlled by chemically allowed conformational changes. Molecular rigidity in ambient conditions is achieved in different ways, all of which differing in energy. Several examples are shown in Fig. 2. All these compounds have been resolved. The first recognized class of chiral compounds is that of molecules containing a chiral carbon atom (i.e. bound to four different substituents in a tetrahedral fashion [1]), such as glyceraldehyde **3**. Phosphorous [9] in phosphine oxide **4** [9b] for example and many other heteroelements [10] (N [11], S [12], B [13], Si [14], Ge [15], As [16], ...) or even metal atoms [17] such as Ti [18], Cr [19], Mn in organometallic complex **5** [20] and Fe [21] can play a similar role. Cluster compound **6** [22] owes also its chirality to the substitution of its tetrahedral skeleton with four different atoms. Other molecules lacking any symmetry element are Werner's complex **7** [23], ferrocene derivatives such as **8** [24] and related Cr or Mn cyclopentadienyl complexes [25] and cyclophanes **9** [26] and **10** [27]. The rigidity of the latter is due to restricted rotation about C—C single bonds. Inhibited rotation is also responsible for the chirality of many molecules with C_2 symmetry like biphenyl **11** [28], binaphthyl **12** [29], and *trans*-cyclooctene **13** [30]. Steric hindrance may also play a role: this is the case for hexahelicene **14** [31] and the related platinum complex **15** [32]. Classical examples of molecules with C_2 symmetry are spirane **16** and allene **17** [33]. Molecules belonging to point group C_3 are scarce: examples

are trishomobullvalene **18** [34], cyclotrimeratrilene **19** [35], and perchlorotriphenylamine **20** [36] for which chirality is due to hindered rotation. Betweenanene **21** [37] and bridged biphenyl **22** [38] also owe their chirality to some restricted motions; they belong to the D_2 symmetry group, as well as hexaphenylene **23** [39], twistane **24** [40], vespirene **25** [41] and bilayered *p*-cyclophanes (**26**, [42], **27** [43]).



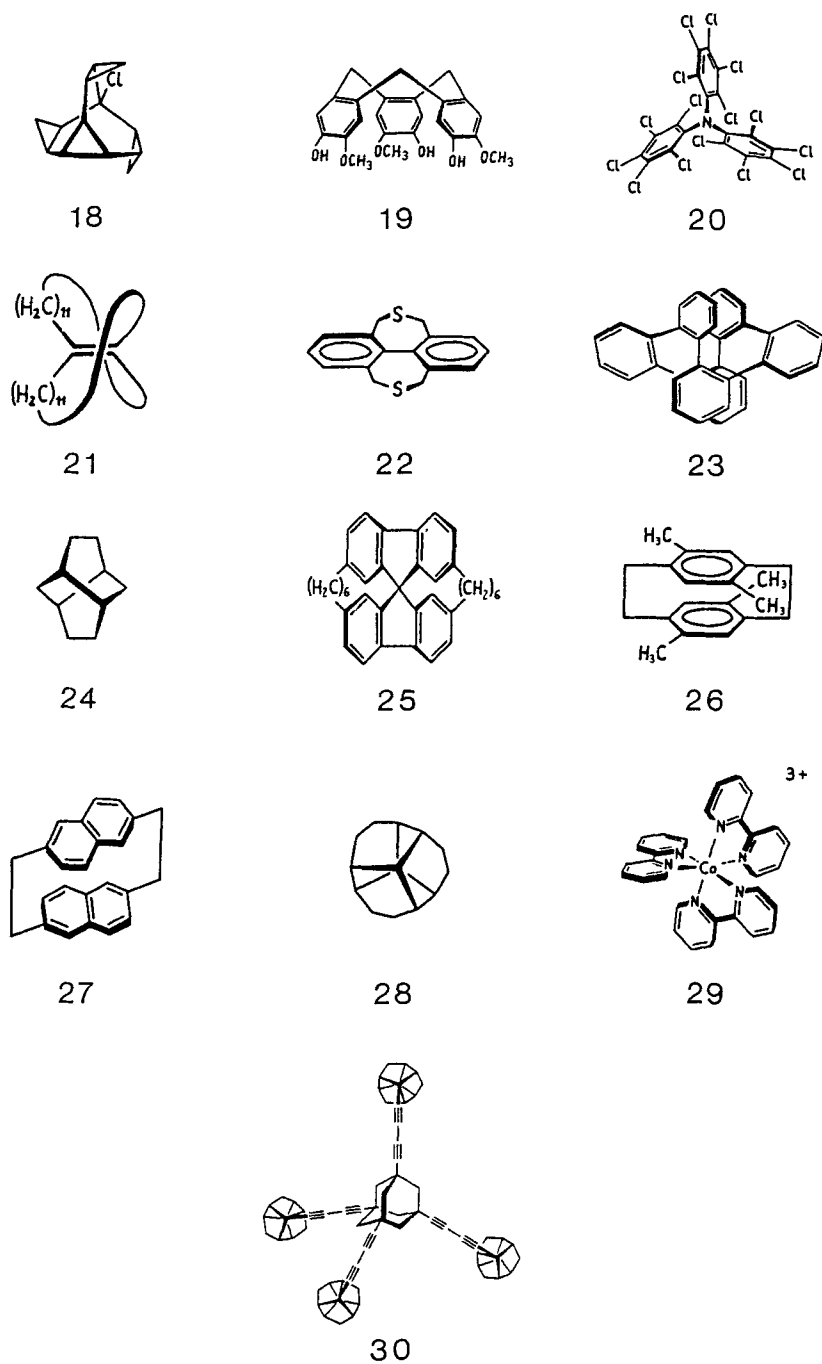


Fig. 2. Several examples of molecules with Euclidean chirality, displayed in the order of increasing symmetry: C_1 (3–10), C_2 (11–17), C_3 (18–20), D_2 (21–27), D_3 (28, 29), T (30)

Trishomocubane [44a, b] (see below), tritwistane **28** [44c] and another Werner's complex **29** [45] are chiral molecules with D_3 symmetry. But the most symmetrical chiral molecule (point group T) is the adamantane **30** [46] substituted with four chiral trishomocubane groups.

In numerous cases, it may be useful to realize that all these chiral structures may be described in terms of helicity [47], that is the arrangement of atoms can be described as a combined rotation and translation. If all the compounds presented above require a certain rigidity to be chiral, there are however molecules which do not require any rigidity at all to remain chiral. This seems at first paradoxical, but it is the case of the so-called topologically chiral molecules (as opposed to Euclidean chiral molecules). Before examining these objects, it is necessary to briefly review the bases of molecular topology.

3 Molecular Topology

Molecules are three-dimensional objects: thus they have Euclidean geometrical and topological properties [48–53]. Euclidean geometrical properties are those which chemists usually refer to when describing the stereochemistry of a molecule, that is bond lengths and bond angles. Unlike Euclidean properties of rigid structures, topological properties are invariant given that the molecule is subjected to conceptual continuous deformation in 3D-space. They may be intrinsic or extrinsic in nature; intrinsic topological properties are not related to the embedding of the molecule in 3D-space, whereas extrinsic topological properties are. In this section we will define the topology of a molecule and what may be called topological stereoisomerism, finally emphasizing on topological chirality.

3.1 Topological Properties of Molecules

When examining topological properties of molecules, it is convenient to describe them by their *molecular graph* [51]. In general, a simple graph is an ordered pair $G = (V(G), E(G))$ where $V(G)$ is a non empty finite set of elements called vertices and $E(G)$ a finite set of unordered pairs of distinct elements of $V(G)$ called edges [54]. The molecular graph of a molecule is simply defined as the graph whose vertices are atoms and whose edges are bonds. Bonds which are considered as edges are purely covalent bonds, metal-ligand and metal-metal bonds; bonds which cannot be taken into account are H-bonds, ion-ion, ion-dipole and dipole-dipole bonds [51]. As defined above, the molecular graph describes only bond connectivity. This is the *intrinsic* topology of a molecule [51]. Indeed, bond connectivity, or molecular constitution, is what chemists usually refer to when talking about topology of a molecule. Generally speaking, when pairwise relationships between isomeric molecules are considered, the intrinsic topological property of molecules is associated with a mathematical transformation called *homeomorphism* [51]: a pair of isomers with identical connectivity have homeomorphic graphs, whereas constitutional isomers have non-homeomorphic graphs [55].

So far, we have considered molecular graphs as mathematical entities, describing bond connectivity only. However, they have the property that they can be embedded in the three-dimensional space [54a]. This means that they can be constructed in 3D-space without crossings [56]. When additionally they are assigned specific geometrical Euclidean properties, they stand for the spatial geometric structure of molecules with their chemically allowed conformational changes. The *extrinsic* topology of a molecule appears when its graph in 3D-space is endowed with complete, even non-chemically significant flexibility [51]. The only requirement in the use of such graphs is that no bonds (edges) are passed through each other (in other words, the intrinsic topology must remain invariant). The topology of a molecule is thus conserved when its molecular graph is subjected to conceptual continuous deformation. When stereoisomeric molecules are compared, their extrinsic topological property is the mathematical transformation called isotopy [51, 57]: a pair of stereoisomers which are interconvertible conceptually by continuous deformation have isotopic molecular graphs. The only isomers possessing isotopic molecular graphs are Euclidean stereoisomers. Additionally, graphs of these molecules share a common property: they are all planar graphs [58a], i.e., they have presentations in 3D-space which can be projected in a plane without crossings; in other words, they can be embedded in 2D-space. It is useful to realize that a molecule such as dodecahedrane **31** [59] (Fig. 3) has a planar graph; **32** is a plane presentation of this graph [58a]. In fact it nicely illustrates the theorem according to which a graph is planar, namely if and only if it can be embedded on the surface of a sphere [54] (dodecahedrane is a spherically annelated polyquinane; we will see later that centrally annelated polyquinanes derivatives have non-planar graphs).

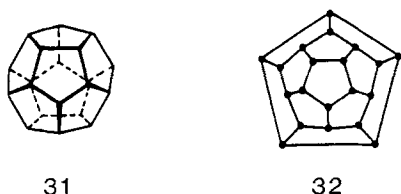


Fig. 3. Two presentations of dodecahedrane: a familiar chemical one (**31**) and a plane one (**32**)

3.2 Topological Stereoisomerism

Topological stereoisomers have identical bond connectivity, but they cannot be interconverted one into another by continuous deformation [51]. They are homeomorphic, not isotopic. Their molecular graphs are non-planar, either intrinsically or extrinsically.

Intrinsically non-planar graphs are non-planar by virtue of their connectivity only. It has been shown [51] that they all contain one of the two basic non-planar graphs as a subgraph [60]: the first and the second Kuratowski graphs K_5 and

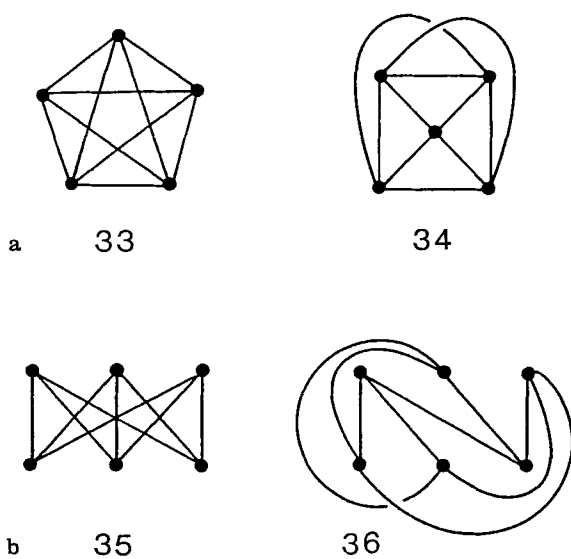
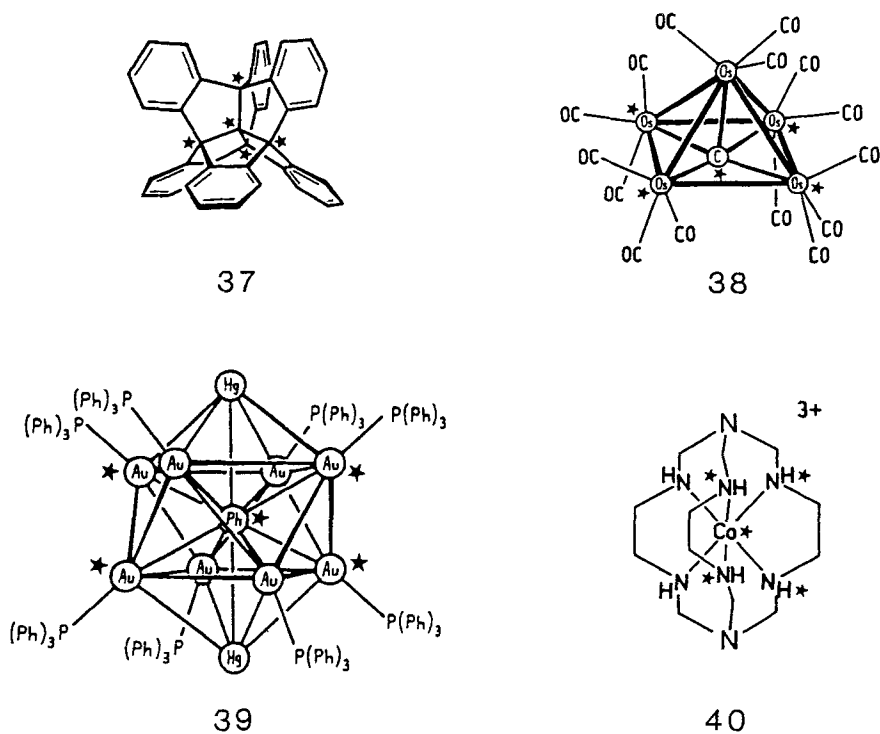


Fig. 4. a) The first Kuratowski K_5 graph: 33 is the maximal symmetry presentation, whereas 34 is a presentation with the minimum number of crossings (1); b) The second Kuratowski $K_{3,3}$ graph: 35 is the well-known, crown-shaped presentation and 36 is a presentation with the minimum number of crossings (1)



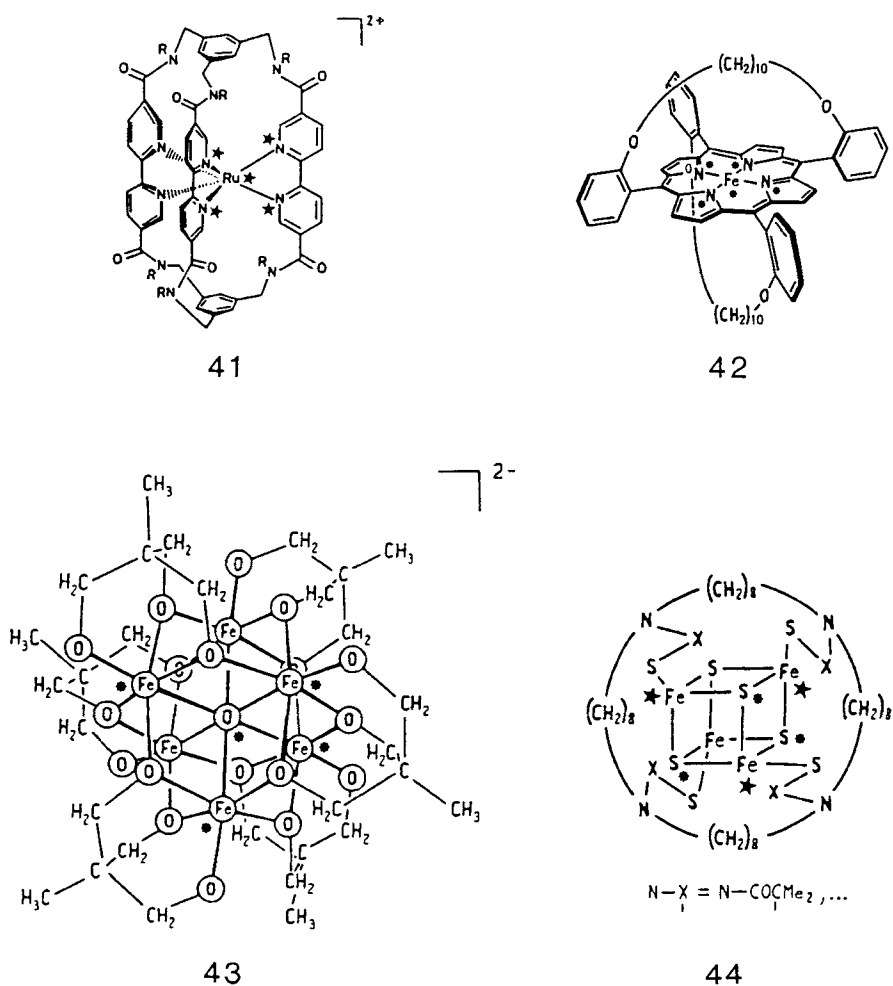


Fig. 5. Examples of molecules whose graphs contain non-planar K_5 (37–43) or $K_{3,3}$ (44) graphs as a subgraph. In each case, a possible subgraph is shown by the means of starred atoms

$K_{3,3}$ respectively. In other words, all non-planar graphs can be contracted [61] either to K_5 or $K_{3,3}$. K_5 is the complete [62] graph on five vertices, different presentations of which (33, 34) are shown in figure 4a. $K_{3,3}$ is the complete bi-partite graph on two sets of three vertices each (35, 36) (Fig. 4b). Both K_5 and $K_{3,3}$ are said to be minimally non-planar graphs, since they have presentations with only one crossing (for example 34 in the case of K_5 , 36 in the case of $K_{3,3}$). Since the only topological stereoisomer of K_5 is K_5 itself (the same is true for $K_{3,3}$), topological enantiomerism is the only topological stereoisomerism displayed by molecules with intrinsically non-planar graphs (provided that these can be contracted to a *single* basic non-planar graph). Examples of molecules with non-planar molecular graphs are shown in Fig. 5.

In organic chemistry molecules with non-planar graphs are very scarce. An example is the centrally annelated polyquinane derivative **37** [63]. In inorganic chemistry it is much easier to find examples since coordination numbers of metals are high, e.g., carbide clusters [64] with a carbon atom in the center of a metallic polyhedron (**38**) [64b], some high nuclearity metal clusters (**39**) [65], sepulchrates (**40**) [66] and related cage coordination compounds (**41**), [67], basket-handle porphyrins (**42**) [68] and some metal-heteroatom aggregates (**43**, **44**) [69, 70]. Except for the last example whose graph can be contracted to $K_{3,3}$, the graphs of most compounds contain K_5 as a subgraph.

Extrinsically non-planar graphs are non-planar by virtue of their embedding in the 3D-space. They may be intrinsically planar at the same time (Fig. 6): this is the case of links (**45**) which are homeomorphic to disjoint sets of circuit graphs [71, 72] (**46**) and knots (**47a** and **b**) which are homeomorphic to a circuit graph (**48**).

In their extrinsically non-planar presentations, the minimum number of crossings in links and knots are respectively 2 and 3, thus higher than that of the intrinsically non-planar graphs K_5 and $K_{3,3}$. In addition to topological enantiomerism, which will be developed below, molecules possessing an extrinsically non-planar graph can exhibit *topological diastereomerism*. The most typical example is the recently synthesized molecular trefoil knot **86** [73] which exists in two topologically enantiomeric forms and whose topological diastereomer is the unraveled macrocycle **87** (see Fig. 33).

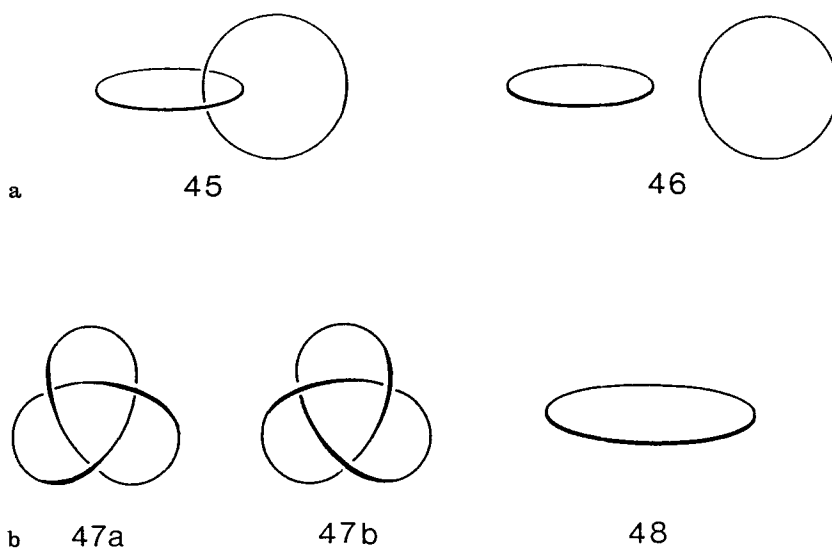


Fig. 6. Extrinsically non-planar homeomorphic figures: **a**) a link (**45**) and the pair of disconnected circuit graphs (**46**); **b**) the trefoil knot shown as its mirror-images **47a** and **47b** and its corresponding plane circuit graph (**48**)

3.3 Topological Chirality

Topological chirality of a molecule is realized when any presentation of its graph is topologically distinct from its mirror image, that is, cannot be converted into its mirror image by continuous deformation in 3D-space [51]. No molecular rigidity at all is required for topological enantiomers to remain distinct. This is the point which distinguishes Euclidean from topological chirality. Let's take the example of helicene [31]: deformations of the benzene rings which are forbidden at room temperature are energetically allowed at higher temperatures, thus racemization becomes possible; on the contrary, in the case of a molecular trefoil knotted macrocycle, no continuous deformation, however easy it is, will never allow interconversion of its enantiomers. Since chiral molecules, even those with a non-planar topology are generally more or less rigid objects, the above property remains formal in many cases, but in a few instances (see below), especially for large, flexible molecules, it can be applied fruitfully.

Topological chirality of a molecule is ruled out if its graph may achieve an achiral presentation. Therefore, molecules having a planar graph cannot be topologically chiral. Thus it has been conjectured [51] that topological chirality may be achieved only by molecules with a non-planar graph, either intrinsically (chiral K_5 or $K_{3,3}$ graphs) or extrinsically (oriented links, chiral links, and chiral knotted rings). Chiral links and knots are conventional elements of topological dissymmetry: their chirality has been demonstrated mathematically. Recently, the topological nature of the chirality of molecules having a non-planar K_5 or $K_{3,3}$ graph has also been demonstrated by mathematical methods [74]. These molecules will be examined in the next section along with other molecules for which topological chirality is only conjectured. The latter have graphs which can be contracted to K_5 or $K_{3,3}$ subgraphs containing either suitably coloured vertices and edges, or oriented edges [75]. None of the few today known topologically chiral compounds has been resolved. In most cases, chirality was tested by NMR spectroscopy of the sample in a chemically chiral environment [76] (chiral lanthanide shift reagents [77a], 2,2,2-trifluoro-1-(9-anthryl) ethanol (Pirkle's reagent; [77b])).

4 A Review of Some Topologically Chiral Molecules

This review is not comprehensive. Only the most relevant topologically chiral molecules are presented here.

4.1 Molecules with a Non-Planar Graph K_5

One of the first topologically chiral molecule whose graph contains K_5 as a subgraph is probably the completely asymmetric cluster **49** $\text{Rh}_8(\text{CO})_{19}\text{C}$ (Fig. 7) synthesized in 1974 by P. Chini et al. [78]. (Note that the C—Rh bonds are not

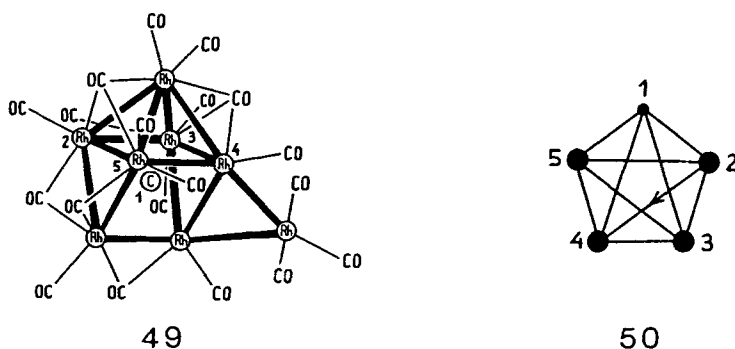


Fig. 7. A chiral rhodium carbide cluster (49) and its K_5 subgraph (50). The atoms chosen as the vertices of 50 have been numbered in 49 (the Rh—C bonds have been neglected for clarity)

represented). The topological nature of its chirality is only conjectured. Its molecular graph may be contracted to the graph 50 which contains a coloured vertex (C atom) and an oriented edge (path Rh(2) to Rh(4) via the appended Rh atom).

Another topologically chiral K_5 molecule is the chiral ferrocenophane ketone derivative 51 (Fig. 8), which is an intermediate in the synthesis of tetrabridged ferrocenophanes [79]. It is important to notice that in order to obtain a non-planar molecular graph, at least four of the ten Fe—C bonds must be taken into account. The K_5 subgraph (52) also contains an oriented edge (—CH₂CH₂CH₂CO-fragment) and a coloured vertex (Fe atom).

At the time they were synthesized, these molecules were not recognized as having a non-planar graph, and actually the first topologically chiral K_5 molecule recognized as such, is the centered polyquinane derivative 53, independently synthesized by H. E. Simmons and J. E. Maggio [80] on the one hand, and by L. A. Paquette and M. Vazeux [81] on the other hand (Fig. 9). That it is topologi-

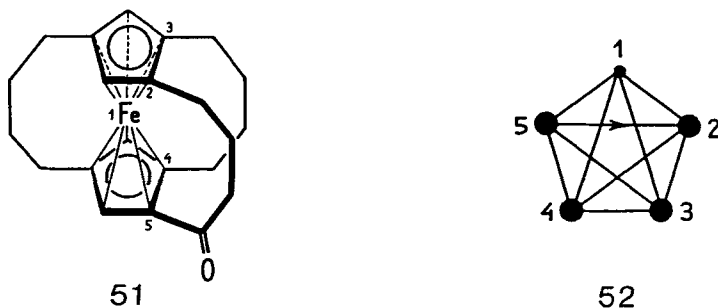


Fig. 8. A chiral tribridged ferrocenophane (51) and its K_5 subgraph (52). Again, the atoms involved as vertices in 52 have been numbered in 51

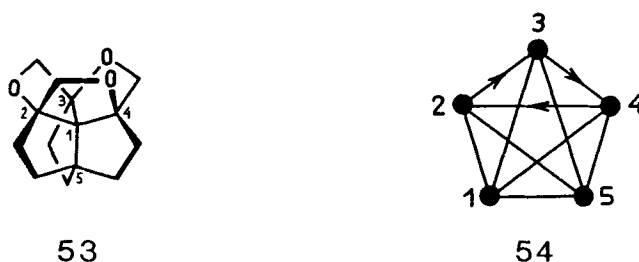


Fig. 9. The first topologically chiral K_5 molecule: the centrally annelated polyquinane **53** and its K_5 subgraph (**54**)

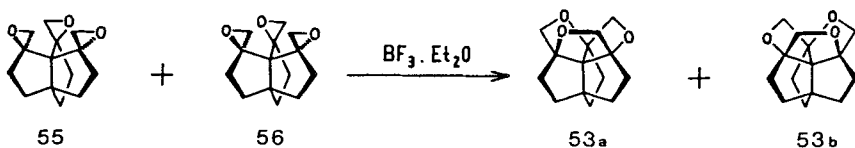


Fig. 10. The topologically relevant step in the synthesis of the propellane **53**; **53a** and **53b** are topological enantiomers

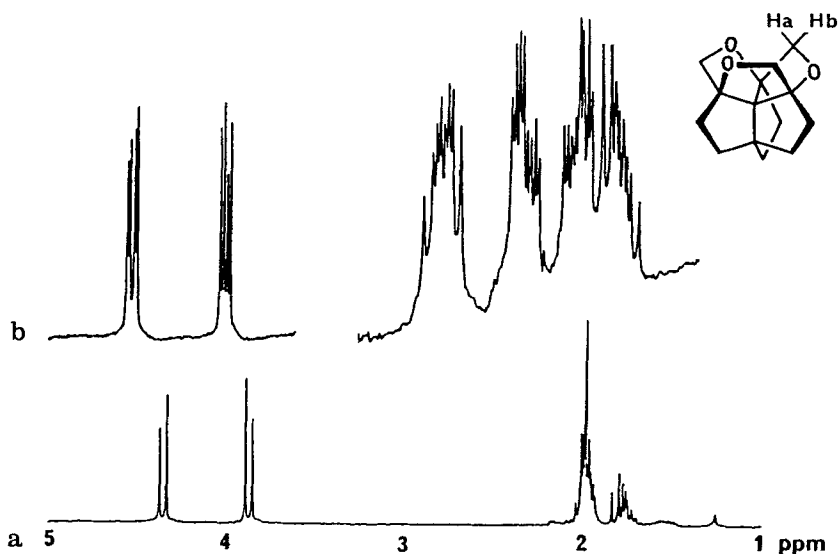


Fig. 11 a, b. ^1H -NMR spectrum of **53** in CDCl_3 : **a**) Normal spectrum showing the AB pattern of the methylene protons H_a and H_b . **b**) Spectrum after addition of tris-[3-(trifluoromethyl hydroxymethylene)-D-camphorato]-europium(III) showing (*left*) the splitting of the signals of H_a and H_b , and (*right*) the intricate pattern arising from the other diastereotopic cyclopentyl protons

cally chiral was demonstrated later by J. Simons [74]. Its K_5 molecular graph contains an oriented circuit graph as a subgraph (54). The molecule was synthesized in one step from a 50/50 mixture of two diastereomeric epoxides 55 and 56 (Fig. 10). Chemical chirality of 53 was evidenced by $^1\text{H-NMR}$ in the presence of the chiral lanthanide shift reagent: tris-(3-(trifluoromethylhydroxymethylene)-d-camphorato)-europium(III), (+)-Eu(fod)₃. In the absence of the reagent, the diastereotopic tetrahydrofuran methylene protons H_a and H_b give rise to an AB system. In the presence of the chiral reagent, the two doublets are split as shown on Fig. 11.

4.2 Molecules with a Non-Planar Graph $K_{3,3}$

The triple-decker naphthalene cyclophane 57 (Fig. 12) was synthesized by T. Otsubo et al. in 1983 [82a]. The chirality of this molecule has been shown experimentally by a crystal structure analysis: the unit cell contains four molecules which form two distinct enantiomeric pairs [82b]. The fact that this molecule has a topological non-planar $K_{3,3}$ graph was not explicitly recognized by the authors. The two different sets of vertices are indicated. Two different presentations of the graph are also shown (58, 59): we conjecture that the graph is topologically chiral because of different colouring of the edges. Molecule 57 can be compared to the triple decker *p*-cyclophane 60 (Fig. 13) [83]. Both are chiral molecules but the first is topologically non-planar, whereas the latter has a planar graph (61), and thus displays only Euclidean chirality.

A hypothetical example of a topologically chiral $K_{3,3}$ cyclophane would be the [m][n][p] *paracyclophane* 62 (Fig. 14) as suggested by M. Nakazaki in his review of highly symmetrical chiral molecules [84].

The first flexible, topologically chiral $K_{3,3}$ molecule is the so-called three-rung Möbius ladder 63 (Fig. 15). It was synthesized by D. M. Walba et al. in 1982 [85] and is represented on Fig. 15, together with several presentations of its graph (64–66). It is important to notice that the rungs of the ladder are different from

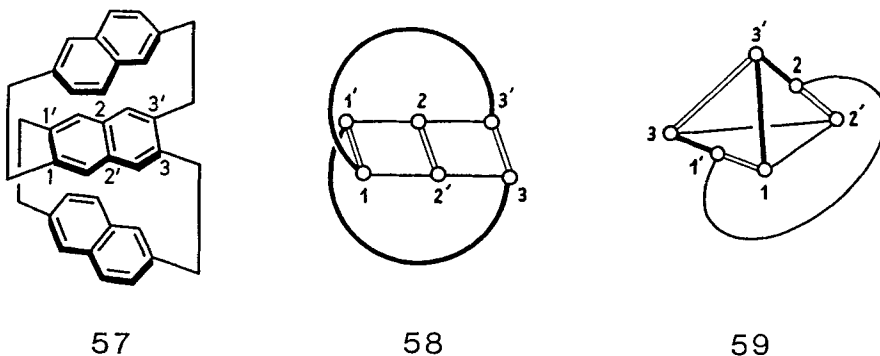
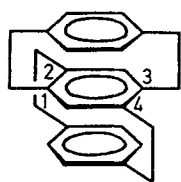
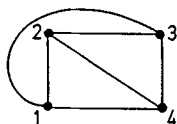


Fig. 12. A topologically chiral triple-decker naphthalene cyclophane (57) and different presentations of its $K_{3,3}$ graph (58, 59). The two sets of vertices are indicated in structure 57

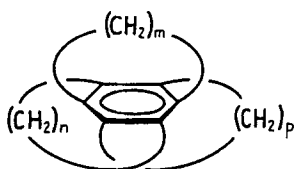


60



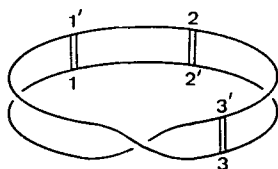
61

Fig. 13. An Euclidean chiral triple-decker benzene cyclophane (60) and a plane presentation of its graph (61)

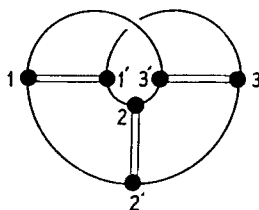


62

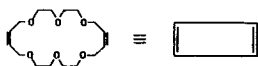
Fig. 14. A hypothetical topologically chiral $K_{3,3}$ cyclophane: $[m][n][p]$ paracyclophane 62



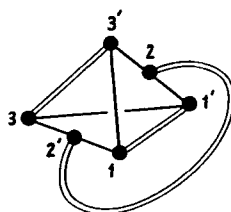
63



64



65



66

Fig. 15. The topologically chiral three-rung Möbius ladder (63) and several presentations of its graph (64–66). 64 and 66 are presentations with the minimum number of crossings (1). Note that the edges $(1,1')$, $(2,2')$ and $(3,3')$ are differently coloured than the others (i.e. $(1',2)$, $(2,3')$, etc. . . .)

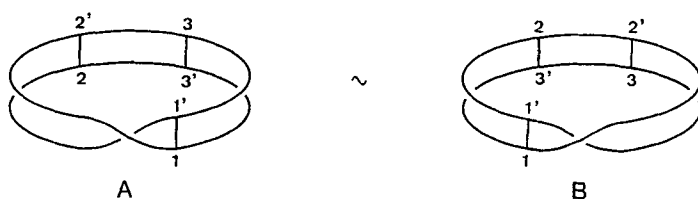


Fig. 16. Homotopicity of edges in an uncoloured three-rung Möbius ladder. For example, the vertical edge (rung) (2,2') in A is equivalent to the rung (3',2) in B

the other edges. **63** has thus a coloured graph; this is the reason why the molecule is chiral. If edges (1,1'), (2,2') and (3,3') were of the same colour as the others, then **63** would not be chiral, since in the $K_{3,3}$ graph, all the edges are topologically equivalent (Fig. 16).

The topological nature of the chirality of **63** has been demonstrated mathematically by J. Simons [74]. It is interesting to compare compound **63** with the hypothetical four-rung Möbius ladder **67** (Fig. 17). Molecule **67** has not yet been synthesized, but the cylindrical constitutional isomer **68** has been [86]. **67** is unconditionally topologically chiral, without graph colouring: the rungs are heterotopic [87] to the other edges [88].

The molecule **63** was synthesized from the diol precursor **69** (molecular ladder) in a high dilution experiment, which produced in nearly equal amounts the untwisted cylinder molecule **70** (constitutional isomer of **63**), as shown in Fig. 18. Note that both chirality and non-planar topology are achieved in the last cyclization step. This is very different from other topologically non planar molecules for which Euclidean chirality is preexistent to the topologically relevant reaction step. The three-rung Möbius ladder **63** is the first topologically chiral molecule for which it was demonstrated that rigidity is not required for a dissymmetric molecule to achieve chirality. It was shown that ^1H - and ^{13}C -NMR spectra could be understood only if a dynamic structure in which the twist of the Möbius ladder was rapidly propagating along a path normal to the ladder's axes, was involved, as indicated in Fig. 19. Only a single peak, corresponding to the six olefinic carbon atoms, is observed in the ^{13}C -NMR spectrum. This implies that these carbons are all magnetically equivalent and homotopic on the time scale of the experiment. The consequence is that the Möbius molecule **63** could not be

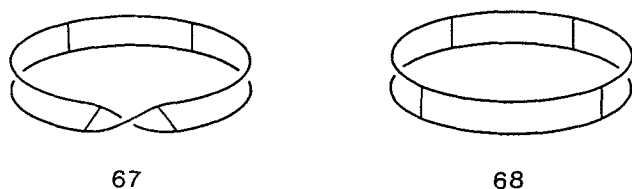


Fig. 17. The four-rung Möbius ladder (**67**) and its cylindrical constitutional isomer (**68**)

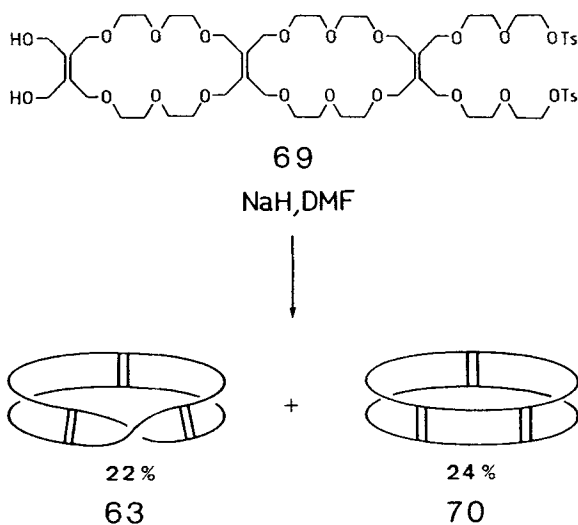


Fig. 18. The topologically-relevant step in the synthesis of the chiral three-rung Möbius ladder **63**, starting from the linear molecular ladder **69**

distinguished from its cylindrical isomer **70** by a simple ^{13}C -NMR or ^1H -NMR experiment. Actually they were differentiated using a chemically chiral medium (solution saturated with *S*(+)-2,2,2-trifluoro-1-(9-anthryl)ethanol) [76]. Splitting of their signal is only observed for compound **63** ($\Delta\delta = 1.9$ Hz at 67.9 MHz).

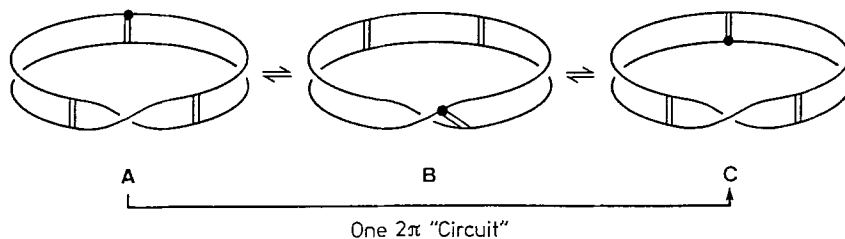


Fig. 19. Homotopy of an olefinic carbon atom (●) in the chiral three-rung Möbius ladder **63**

4.3 Interlocked Rings

The chemical name for interlocked rings or molecules whose graph is a link (in fact two disconnected [71] circular graphs) is *catenane*. The simplest catenanes have extrinsically non-planar graphs. Despite this fact they are achiral, as are molecules with uncoloured graph K_5 or $K_{3,3}$. As discussed by Schill [89], an achiral catenane can be dissymmetrized by a suitable substitution of its constitutive rings. The resulting chiral catenanes **71** and **72** are represented in Fig. 20. In fact, this approach is equivalent to one making use of oriented macrocycles. In other words, the graph of the resulting catenane is the union of two disconnected digraphs [90]: one macrocyclic ring is used to give an orientation to space and the other defines the configuration of the chiral catenane, as illustrated in Fig. 21. Indeed, oriented macrocycles have been used fruitfully in the design of molecules showing Euclidean chirality. Examples are cycloenantiomeric molecules [91] and the *N*-alkylated zinc etioporphyrin **73** [92] (Fig. 22).

There are however links which are unconditionally chiral: these are for example links with a minimum number of four crossings **74** (Fig. 23).

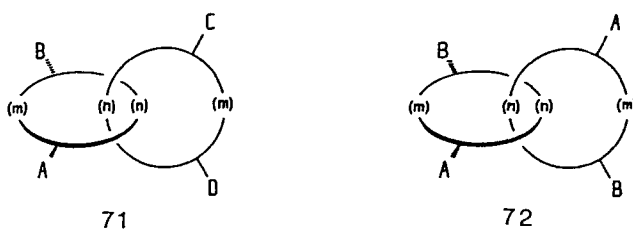


Fig. 20. Two topologically chiral catenanes **71** and **72** with oriented rings; *m* and *n* are the numbers of atoms in-between the substituents of the constitutive macrocycles. Note that these catenanes lose their chirality when $m = n$

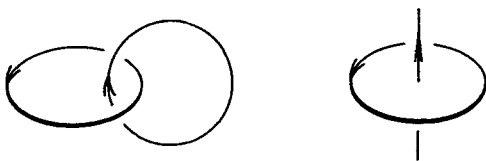


Fig. 21. Left: an oriented link. Right: an oriented ring divides the space into two mirror-image half-spaces which can be distinguished one from the other by a direction normal to the plane of the ring

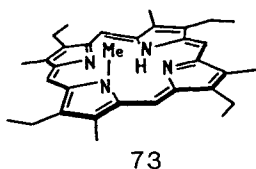


Fig. 22. Left: a chiral *N*-alkylated etioporphyrin (**73**). Right: a schematic representation. The porphyrin ring is oriented by the sequence of the substituents on the β -positions and the space is given a direction by the *N*-methyl group

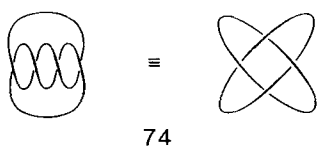


Fig. 23. An unconditionally topologically chiral catenane (**74**) and its two topologically equivalent presentations. The minimum number of crossings is 4

The template synthesis of the first isolable chiral catenane **78⁺** (Fig. 24) in which the constitutive oriented rings **75** were built up from an asymmetrically substituted 1,10-phenanthroline (Fig. 25) was realized [93]. Starting compounds and synthetic pathway are depicted on Fig. 26. The synthetic strategy uses the three-dimensional template effect (Fig. 27) already described for the synthesis of catenates [94]. Diphenol **76** was prepared by reacting *p*-lithioanisole with 4-Phenyl-1,10-phenanthroline followed by demethylation as previously described [94c]. In the presence of $\text{Cu}(\text{CH}_3\text{CN})_4\text{BF}_4$, the diphenol led quantitatively to the entwined complex **77⁺** which was submitted to final cyclization in high-dilution conditions, using the di-iodo derivative of pentaethylene glycol. Racemic Cu^+ catenane **78⁺** was obtained

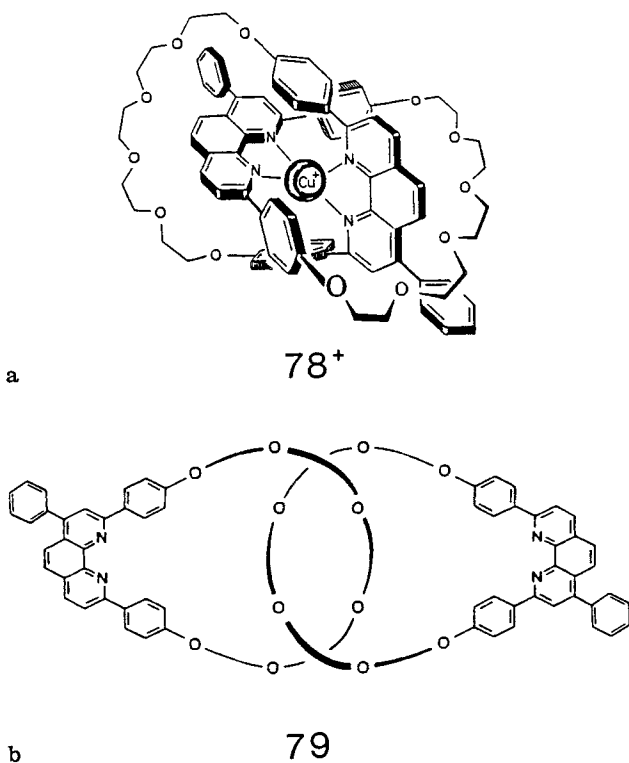


Fig. 24. a) A topologically chiral copper(I) catenane (**78⁺**) b) A topologically chiral catenand (**79**)

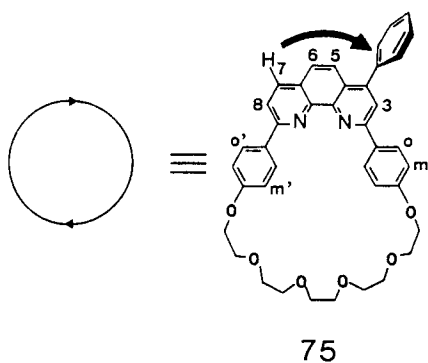


Fig. 25. An oriented ring in a topologically chiral catenane

in 12% yield. Demetallation with KCN afforded the free catenand **79** [94d] (Fig. 24). The chirality of **78⁺** was evidenced by ¹H-NMR spectroscopy as shown in Fig. 28. In the presence of a slight excess of Pirkle's chiral reagent, most of the signals corresponding to the aromatic protons were split. Additionally, diastereotopic

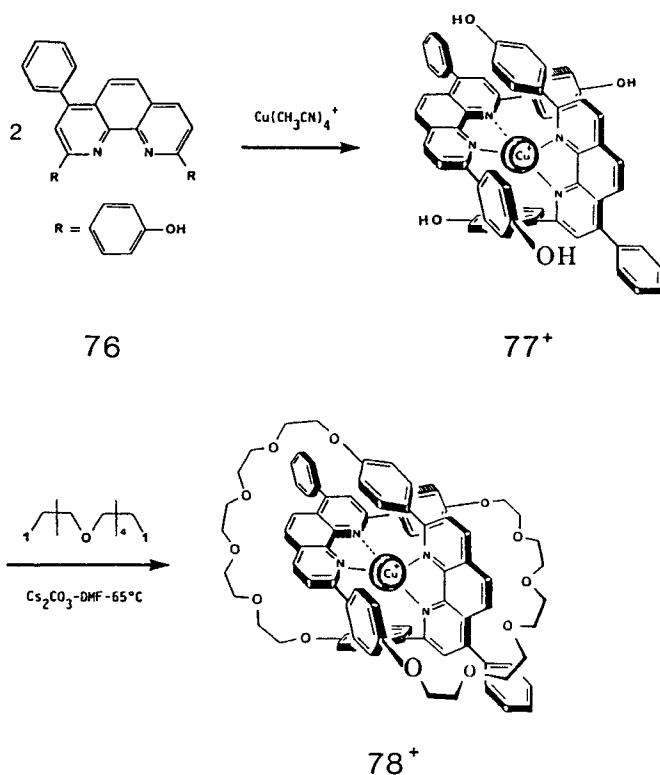


Fig. 26. Precursors and synthetic pathway towards the topologically chiral catenane **78⁺**

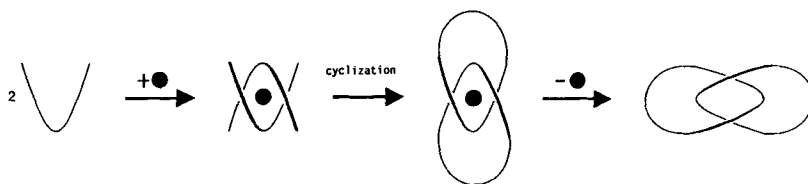


Fig. 27. Principle of the template synthesis of a catenane. The U fragment is a metal-chelating ligand and the *black dot* is a transition-metal ion with a pseudo-tetrahedral coordination geometry

protons of the polyoxyethylenic chains give rise to complicated patterns in the 2–4 ppm region. An analogous resolution of the topological enantiomers **79** could not be observed. However if the chiral reagent is unable to recognize the two enantiomers of this highly flexible ligand at the NMR time scale, topological chirality of the latter is obvious from the synthetic pathway followed. Unlike the Möbius ladder molecule **63**, topological chirality is achieved in the last synthetic

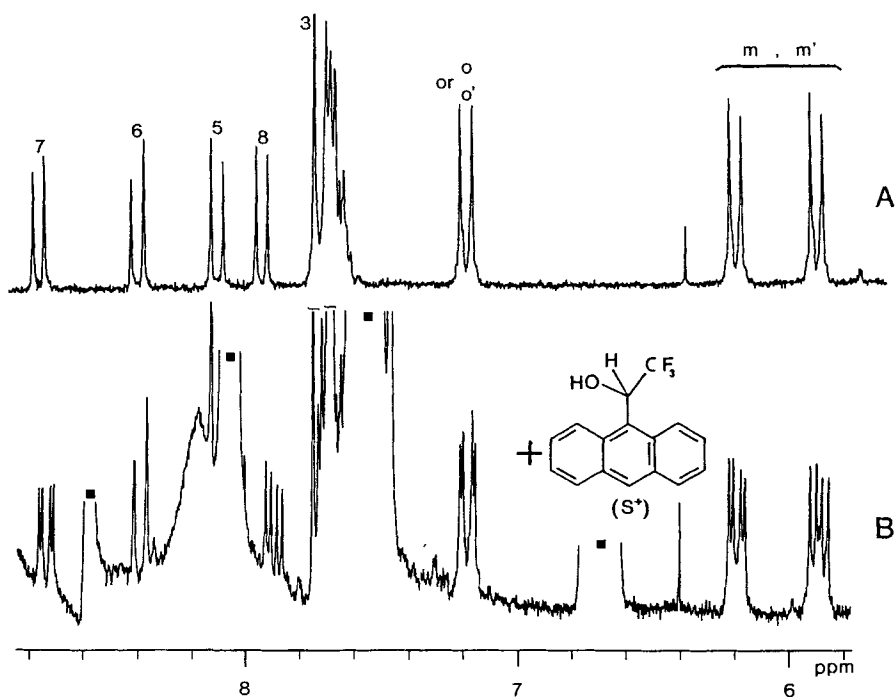


Fig. 28a, b. Part of the ^1H -NMR spectra (200 MHz, CD_2Cl_2) of **a**) **78**⁺ and **b**) **78**⁺ plus ten equivalents of Pirkle's reagent. The signals corresponding to the chiral reagent are marked by a *black square* (see Fig. 25 for atom numbering). Clear splitting is observed for most of the aromatic protons ($\text{H}_{\text{o},\text{o}'}$, $\text{H}_{\text{m},\text{m}'}$, H_7 and H_8)

step, the starting complex 77^+ being geometrically chiral. More interestingly, **79** is a molecule which does not need to be rigid in order to remain chiral, as is the Möbius ladder molecule **63** (see above): mutual gliding of the two rings has been demonstrated experimentally by NMR: the proton NMR spectrum of **79** is nearly superimposable to that of the single macrocyclic ring **75**.

4.4 The Molecular Trefoil Knot

The simplest knot is the trefoil knot **47** (Fig. 6b). Unlike all the above described topologically chiral molecules, the molecular trefoil knot requires no condition (such as bond colouring, ring orientation) to be chiral: it is unconditionally topologically chiral. The strategy of its synthesis is given in Fig. 29. It takes advantage of the fact that the trefoil knot with D_3 symmetry has a presentation **80** with lower symmetry (D_2) (Fig. 30). The key step is thus the double helix formation: Euclidean chirality is introduced at this stage, as in the case of catenate 78^+ (cf. Fig. 26). After many attempts with various linkers, we found that arylated 1,10-phenanthroline units connected via their 2-positions by a $-(CH_2)_4$ -bridging unit indeed formed a double helix when complexed to two Cu(I) centres. Introduction of appropriate reactive functions at the 9-positions allowed the strategy of Fig. 29 to be followed. The precursors used and the reactions carried out are represented on Fig. 31. Compound **81** was prepared in 86% yield from $Li(CH_2)_4Li$ and 1,10-phenanthroline. Addition of *p*-lithioanisole to **81**, followed

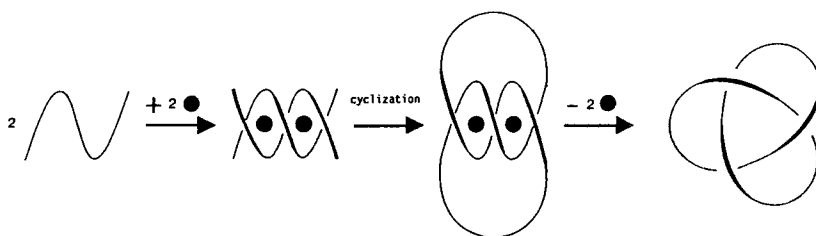


Fig. 29. Template synthesis of the trefoil knot. The molecular thread is a metal-ligand that contains two chelating sites and the *black dot* represents a transition-metal ion in a pseudo-tetrahedral environment

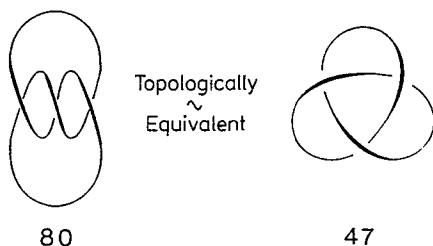


Fig. 30. The topological equivalence between two presentations of a trefoil knot. Note that the minimum number of crossings is 3

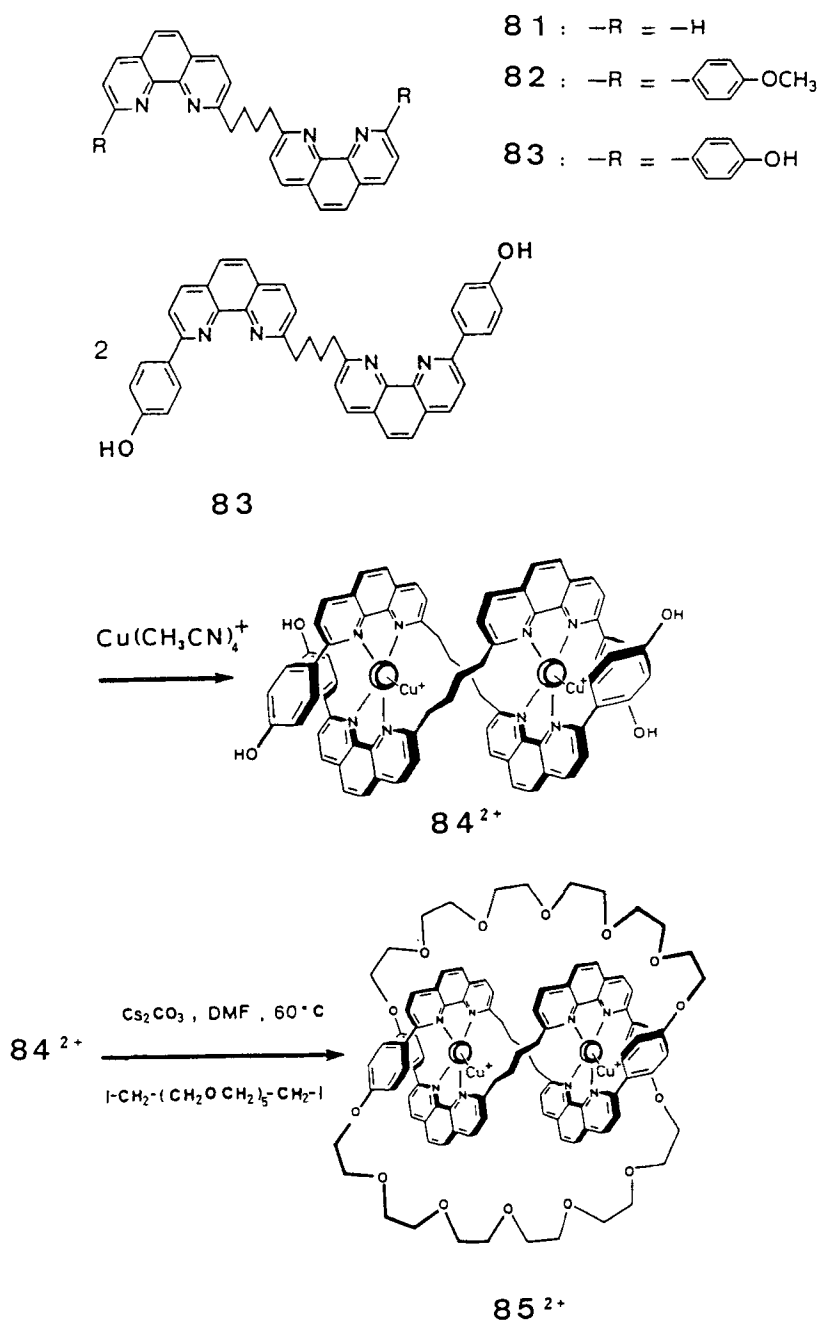


Fig. 31. Precursors and reaction scheme leading to the dicopper(I) trefoil knot **85²⁺**

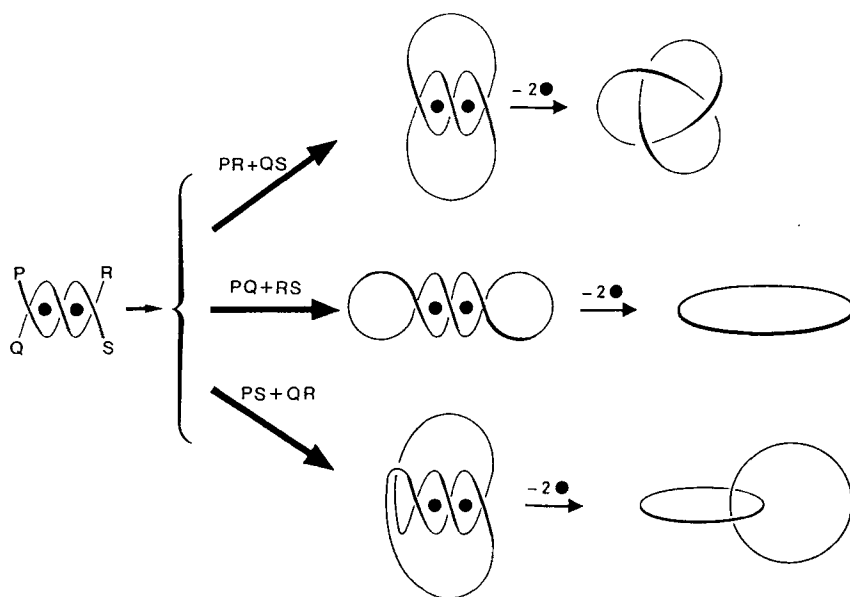


Fig. 32. Most probable $[2 + 2]$ connections between the four ends of a double-stranded dimetallic helix

by hydrolysis and MnO_2 oxidation gave **82** in 83% yield. Demethylation of **82** to **83** was carried out quantitatively under drastic conditions: pyridinium hydrochloride at 210°C . The double helix **84**²⁺ was prepared by addition of a stoichiometric amount of $\text{Cu}(\text{CH}_3\text{CN})_4\text{BF}_4$ to **83**. ^1H -NMR studies showed that the double helical complex is formed together with an important proportion of other Cu(I) complexes. The mixture was reacted under high-dilution conditions with two equivalents of the di-iodo derivative of hexaethyleneglycol in the presence of Cs_2CO_3 in DMF at 60°C . A small amount of the knotted system **85**²⁺ containing two copper centres could be isolated and purified with great difficulties.

This bis-copper complex **85**²⁺ (BF_4^-)₂ is a dark red crystalline solid. Its high resolution mass spectrum (FAB) shows a molecular peak at 1816.74 (calcd. for **85**²⁺: 1817.10). The ^1H -NMR spectrum of **85**²⁺ is in complete agreement with its structure. Its chirality was demonstrated by ^1H -NMR in the presence of Pirkle's reagent. Splitting of some characteristic aromatic protons was observed after a small amount of the chiral reagent was added. In order to prove the knotted topology of **85**²⁺, we had to consider the various possible compounds obtained in the cyclization reaction. From a tetrafunctional double helical precursor, several $[2 + 2]$ connections are possible, with the most probable ones being depicted in Fig. 32. If the three bimetallic complexes of Fig. 32 all display Euclidean chirality, because of the presence of a double helix as core of the system, this is no longer true for the products obtained after demetallation. As expected, the trefoil knot is the only chiral demetallation product. Quantitative demetallation of the various

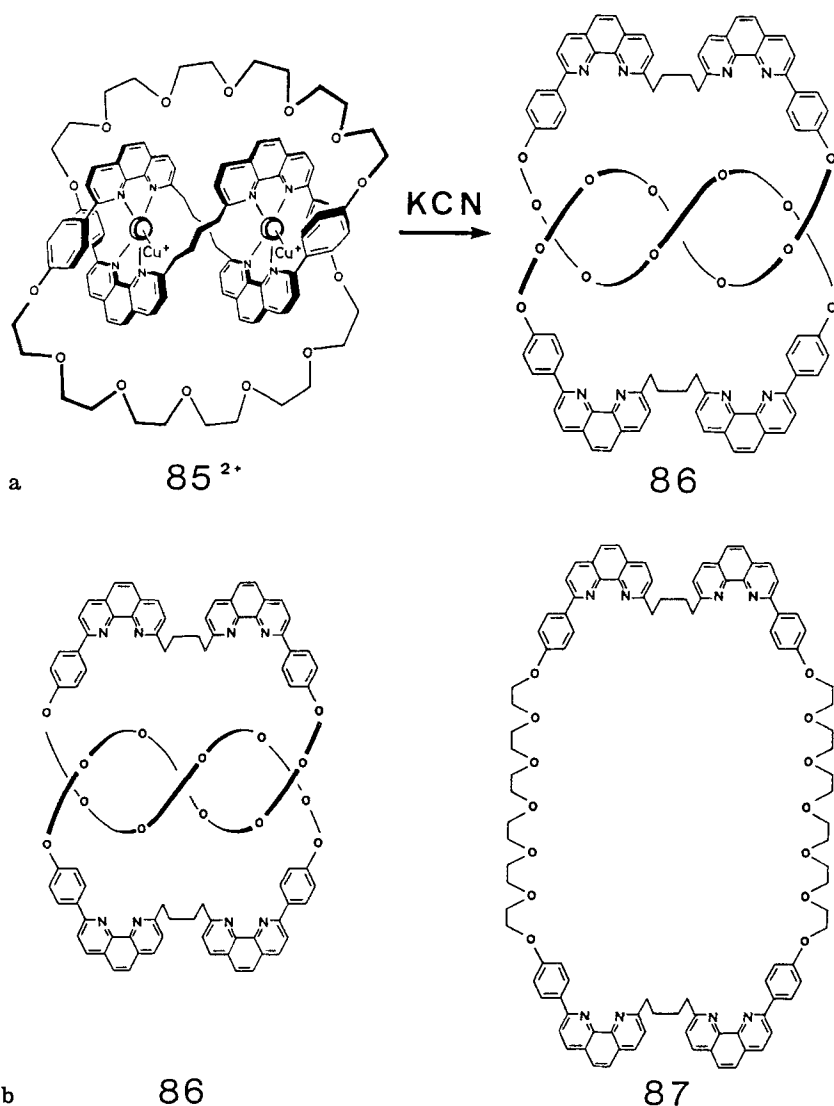
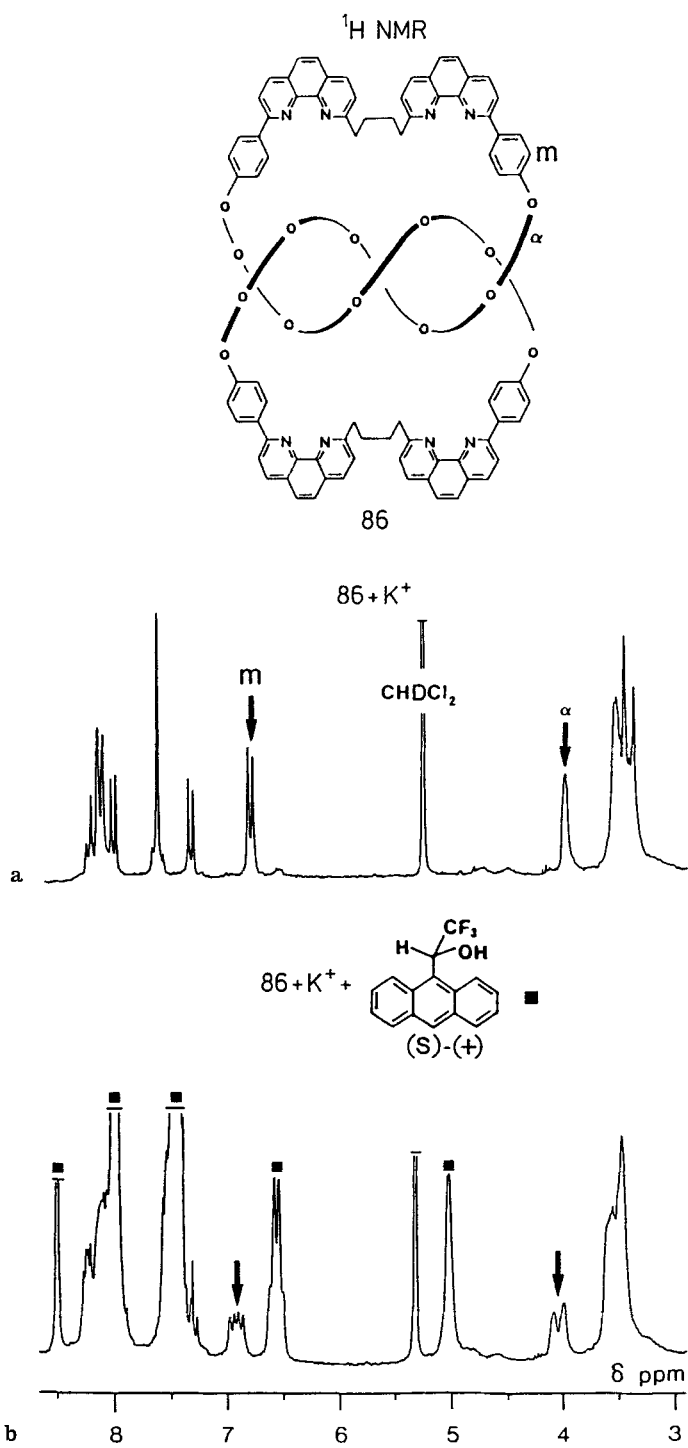


Fig. 33. a) Demetallation of the dicopper(I) trefoil knot **85**²⁺ leading to the trefoil knot **86**.
 b) Two topological stereoisomers; trefoil knot **86** and unraveled macrocycle **87**

Cu(I) complexes by KCN led to the corresponding free ligands represented in Fig. 33. Demetallation of **85**²⁺ afforded the free trefoil knot **86** as a colourless glass. Very small amounts (0.5%) of **87**, the unraveled *topological diastereomer* of **86** could also be isolated and characterized.

A comparison between the two isomers **86** and **87** produced strong evidence for the knotted topology of **86**. Both compounds have identical mass spectra (FAB): molecular peaks appear at the same value. In addition, the general pattern



◀ **Fig. 34a, b.** $^1\text{H-NMR}$ spectrum of **86**: **a)** after addition of an excess of KPF_6 ; **b)** in the presence of Pirkle's reagent (signals indicated by *black squares*). Note that important splitting can be observed for the signals of H_m and H_x (*black arrows*)

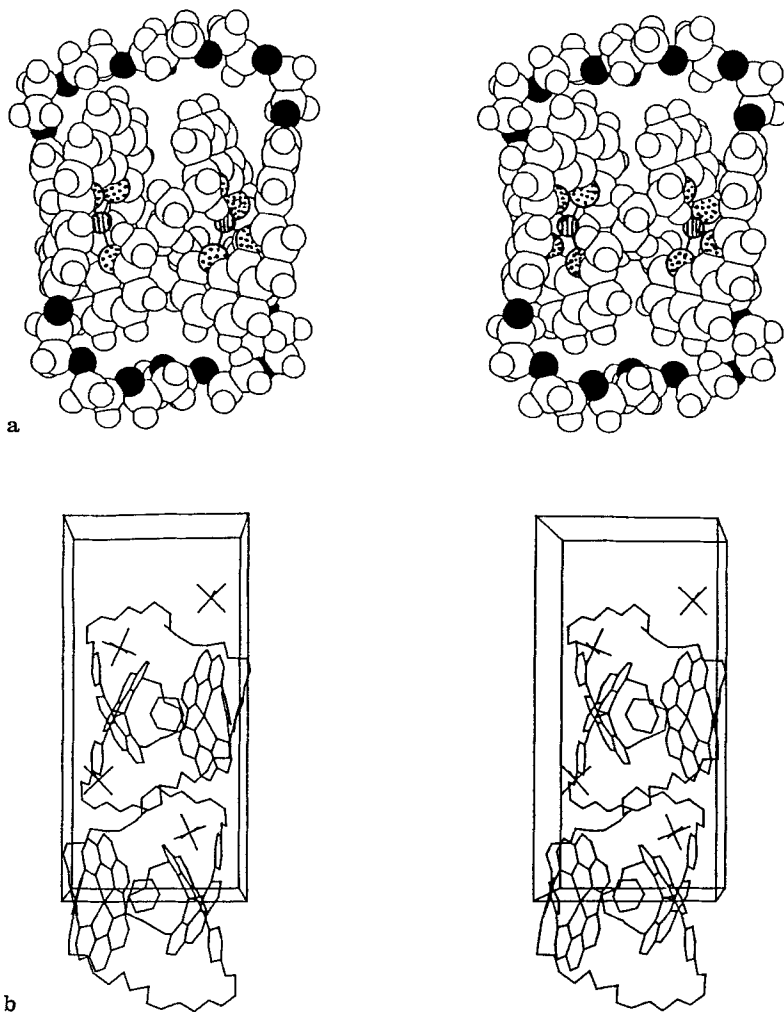


Fig. 35a, b. Crystal structure of the dicopper trefoil knot **85**²⁺: **a)** stereoview of a single molecule (the *circles* representing the atoms are given *in black* for oxygen, *dotted* for nitrogen and *crosshatched* for copper); **b)** stereoview of the unit cell. It contains two homochiral molecules, four PF_6^- anions and two benzene molecules

and the various fragmentations of both compounds are strikingly similar. By contrast, the ^1H -NMR spectra of **86** and **87** are dramatically different. Whereas the spectrum of the latter large macrocycle is well resolved, that of **86** shows broad peaks; this probably reflects the raveled nature of its organic skeleton undergoing slow conformational changes: once again, molecular rigidity is not required at all for the molecule to remain chiral. Addition of KPF_6 to **86** led to a drastic change in its ^1H -NMR spectrum, that is, evidence for an interaction between K^+ and the polyether oxygen atoms of **86**. In this sharp, well resolved spectrum, large splittings of peaks were observed upon addition of Pirkle's chiral reagent (Fig. 34). This was a convincing demonstration that the molecular system **86** was chiral, in agreement with the known topological chirality of a trefoil knot.

These results were very recently confirmed by the X-ray crystal structure analysis of 85^{2+} (Fig. 35a) [95]. Interestingly, this dicopper(I) knot crystallizes as a conglomerate of enantiomers. This spontaneous resolution is easily recognized by noticing that the unit cell contains only a single enantiomer (Fig. 35b).

5 Conclusion

Topologically chiral molecules are not numerous in the chemical literature. Much work remains to be done in this field. Thus challenging new molecules are for example the doubly interlocked [2]-catenane **74** (Fig. 23) whose chirality does not depend on any ring orientation and the figure-eight knot **88** (Fig. 36), which however is not chiral; indeed it contains an S_4 axis and thus is a topological analogue of the achiral spiro molecule **89** [96] (Fig. 37). Of course, the synthesis of other topologically chiral, oriented and more complex knots remains of utmost interest.

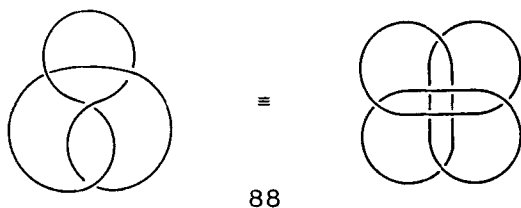


Fig. 36. The achiral figure-eight knot (**88**) with S_4 axis easily seen in right presentation. Its minimum number of crossings is 4

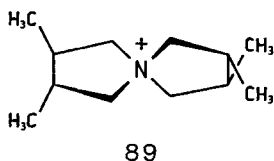


Fig. 37. An achiral stereoisomer of 3,4,3',4'-tetramethylspiro-(1,1')-bipyrrolidinium (*p*-toluenesulfonate salt) **89** possessing an S_4 axis

To our knowledge, topologically chiral molecules have not yet been resolved into enantiomers. However, we may anticipate that their energy barrier to racemization will be extremely high, compared to Euclidean chiral molecules. Therefore they are expected to be useful in enantioselective interactions or reactions. For example, it has been shown that tetrahedral copper(I) bis-2,9-diphenyl-1,10-phenanthroline complexes (which form the catenate subunits) are good reductants in the excited state [97]; therefore the chiral Cu(I) catenates could be used for enantioselective electron-transfer reactions. Alternatively, the resolution of topologically chiral molecules would allow to answer fundamental questions, such as: what are the chiroptical properties of molecular trefoil knots?

Acknowledgements: Prof. T. W. Bell is gratefully acknowledged for fruitful discussions. The C.N.R.S. is thanked for its constant financial support.

6 References and Notes

1. a) Le Bel JA (1874) *Bull Soc Chim Fr* 22: 337
b) van't Hoff JH (1874) *Arch Neer* 9: 445
c) van't Hoff JH (1875) *Bull Soc Chim Fr* 23: 295
2. Prelog V (1976) *Science* 193: 17
3. Mislow K, Bickart P (1976/77) *Isr J Chem* 15: 1
4. Dugundji J, Kopp R, Marquarding D, Ugi I (1978) *Top Curr Chem* 75: 165
5. Farina M, Morandi C (1974) *Tetrahedron* 30: 1819
6. Eliel EL (1976/77) *Isr J Chem* 15: 7
7. Mislow K, Bolstad R (1955) *J Am Chem Soc* 77: 6712
8. O'Loane JK (1980) *Chem Rev* 80: 41
9. a) Naumann K, Zon G, Mislow K (1969) *J Am Chem Soc* 91: 7012
b) Meisenheimer J, Lichtenstadt L (1911) *Ber Dtsch Chem Ges* 44: 356
c) Korpium O, Mislow K (1967) *J Am Chem Soc* 89: 4784
10. Sokolov VI, Reutov OA (1965) *Russ Chem Rev* 34: 1
11. Pope WJ, Peachey SJ (1899) *J Chem Soc* 1899: 1127
12. Pope WJ, Peachey SJ (1900) *J Chem Soc* 1900: 1072
13. Böeseken J, Mijs JA (1925) *Recl Trav Chim P Bas* 44: 758
14. Sommer LH, Frye CL, Parker GA, Michael KW (1964) *J Am Chem Soc* 86: 3271
15. Brook AG, Peddle GJD (1963) *J Am Chem Soc* 85: 1869
16. Horner L, Ernst M (1970) *Chem Ber* 103: 318
17. Brunner H (1975) *Top Curr Chem* 56: 67
18. Moise C, Leblanc JC, Tirouflet J (1975) *J Am Chem Soc* 97: 6272
19. Simonneaux G, Meyer A, Jaouen G (1975) *J Chem Soc, Chem Commun* 1975: 69
20. a) Brunner H (1969) *Angew Chem* 81: 395; *Angew Chem Int Ed Engl* 8: 382
b) Brunner H (1969) *Z Anorg Allg Chem* 368: 120
21. Flood TC, DiSanti FJ, Miles DL (1975) *J Chem Soc, Chem Commun* 1975: 336
22. Mani M, Vahrenkamp H (1986) *Chem Ber* 119: 3639
23. a) Werner A (1911) *Ber Dtsch Chem Ges* 44: 1887
b) Kauffman GB (1974) *Coord Chem Rev* 12: 105
24. Haller G, Schlögl K (1967) *Monatsh Chem* 98: 2044
25. Schlögl K (1967) *Top Stereochem* 1: 39
26. Meurer K, Vögtle F, Mannschreck A, Stühler G, Puff H, Roloff A (1984) *J Org Chem* 49: 3484
27. Nakazaki M, Yamamoto K, Ito M, Tanaka S (1977) *J Org Chem* 42: 3468
28. Oki M (1983) *Top Stereochem* 14: 1

29. a) Pummerer R, Rieche A (1926) *Chem Ber* 59: 2159
b) Akimoto H, Shioiri T, Iitaka Y, Yamada S (1968) *Tetrahedron Lett* 1968: 97
30. Cope AC, Ganellin CR, Johnson Jr HW (1962) *J Am Chem Soc* 84: 3191
31. a) Martin RH (1974) *Angew Chem* 86: 727; *Angew Chem Int Ed Engl* 13: 649
b) Laarhoven WH, Prinsen WJC (1984) *Top Curr Chem* 125: 63
32. Deuschel-Cornioley C, Stoeckli-Evans H, von Zelewsky A (1990) *J Chem Soc, Chem Commun* 1990: 121
33. March J (1985) In: *Advanced Organic Chemistry Third Edition*. Wiley-Interscience p 91
34. Spielmann W, de Meijere A (1976) *Angew Chem* 88: 446; *Angew Chem Int Ed Engl* 15: 429
35. Collet A, Gottarelli G (1981) *J Am Chem Soc* 103: 204
36. Hayes KS, Nagumo M, Blount JF, Mislow K (1980) *J Am Chem Soc* 102: 2773
37. a) Marshall JA (1980) *Acc Chem Res* 13: 213
b) Nakazaki M, Yamamoto K, Naemura K (1984) *Top Curr Chem* 125: 1
38. Mislow K, Glass MAW, Hopps HB, Simon E, Wahl Jr GH (1964) *J Am Chem Soc* 86: 1710
39. Wittig G, Rümpler KD (1971) *Liebigs Ann Chem* 751: 1
40. Adachi K, Naemura K, Nakazaki M (1968) *Tetrahedron Lett* 1968: 5467
41. a) Haas G, Hulbert PB, Klyne W, Prelog V, Snatzke G (1971) *Helv Chim Acta* 54: 491
b) Haas G, Prelog V (1969) *Helv Chim Acta* 52: 1202
42. Longone DT, Reetz MT (1967) *J Chem Soc, Chem Commun* 1967: 46
43. Haenel M, Staab HA (1973) *Chem Ber* 106: 2203
44. a) Underwood GR, Ramamoorthy B (1970) *Tetrahedron Lett* 1970: 4125
b) Nakazaki M, Naemura K, Arashiba N (1978) *J Org Chem* 43: 689
c) Nakazaki M, Naemura K, Chikamatsu H, Iwasaki M, Hashimoto M (1980) *Chem Lett* 1980: 1571
45. Werner A (1912) *Chem Ber* 45: 433
46. Nakazaki M, Naemura K, Hokura Y (1982) *J Chem Soc, Chem Commun* 1982: 1245
47. a) Meurer KP, Vögtle F (1985) *Top Curr Chem* 127: 1
b) Garst JF (1990) *J Chem Soc, Chem Commun* 1990: 211
48. Frisch HL, Wasserman E (1961) *J Am Chem Soc* 83: 3789
49. Sokolov VI (1973) *Russ Chem Rev (Engl Transl)* 42: 452
50. Walba DM (1983) In: King RB (ed) *Chemical Applications of Topology and Graph Theory*. Vol 28. Elsevier Science Publishers BV, Amsterdam, p 17
51. Walba DM (1985) *Tetrahedron* 41: 3161
52. Walba DM (1987) In: King RB, Rouvray DH (eds) *Graph Theory and Topology in Chemistry*. Vol 51. Elsevier Science Publishers BV, Amsterdam, p 23
53. Simon J (1987) In: King RB, Rouvray DH (eds) *Graph Theory and Topology in Chemistry*. Vol 51. Elsevier Science Publishers BV, Amsterdam, p 43
54. a) Wilson RJ (1972) *Introduction to graph theory*. Oliver and Boyd, Edinburgh
b) Gutman I, Trinajstić N (1973) *Top Curr Chem* 42: 49
55. We believe it important to stress out that the expression "topological isomers" should never be used instead of "constitutional isomers", since, as we will see later, the expression "topological stereoisomers" is used only for stereoisomers differing by extrinsic topology
56. A presentation of a graph G is any construction of the graph in a two- or three-dimensional space [54a]
57. Walba suggested that "isotopy" be replaced by the term "homeotopy"
58. a) A planar graph is one which is isomorphic [58b] to a plane graph. A plane graph is a graph drawn in the plane in such a way that two edges do not intersect geometrically except to a vertex at which they are both incident [54a]
b) Two graphs G_1 and G_2 are isomorphic if there is a one-one correspondence between the vertices of G_1 and those of G_2 with the property that the number of edges joining any two vertices of G_1 is equal to the number of edges joining vertices of G_2 [54a]
59. Ternansky RJ, Balogh DW, Paquette LA (1982) *J Am Chem Soc* 104: 4503
60. A subgraph of a graph G is a graph, all of whose vertices belong to $V(G)$ and all of whose edges belong to $E(G)$ [54a]

61. A contraction of a graph G is a graph which results from G after a succession of edge-contractions. An edge-contraction is obtained by removing an edge e (with incident vertices v and w [62]) and identifying v and w in such a way that the resulting vertex is incident to those edges which were originally incident to v or w [54a]
62. A complete graph is a simple graph in which every pair of distinct vertices are adjacent. (Two vertices v and w of a graph G are said to be adjacent if there is an edge joining them; the vertices v and w are then said to be incident to such an edge) [54a]
63. Kuck D, Schuster A (1988) *Angew Chem* 100: 1222; *Angew Chem Int Ed Engl* 27: 1192
64. a) Lewis J, Johnson BFG (1982) *Pure Appl Chem* 54: 97
b) Jackson PF, Johnson BFG, Lewis J, Nicholls JN, McPartlin M, Nelson WJH (1980) *J Chem Soc, Chem Commun* 1980: 564
65. Bour JJ, v. d. Berg W, Schlebos PPJ, Kanters RPF, Schoondergang MFJ, Bosman WP, Smits JMM, Beurskens PT, Steggerda JJ, van der Sluis P (1990) *Inorg Chem* 29: 2971
66. Creaser II, Geue RJ, Harrowfield J MacB, Herlt AJ, Sargeson AM, Snow MR, Springborg J (1982) *J Am Chem Soc* 104: 6016
67. Barigelletti F, de Cola L, Balzani V, Belser P, von Zelewsky A, Vögtle F, Ebmeyer F, Grammenudi S (1989) *J Am Chem Soc* 111: 4662
68. Momenteau M, Mispelter J, Looock B, Bisagni E (1983) *J Chem Soc, Perkin Trans I* 1983: 189
69. Hegetschweiler K, Schmalte H, Streit HM, Schneider W (1990) *Inorg Chem* 29: 3625
70. Okuno H (Y), Uoto K, Sasaki Y, Yonemitsu O, Tomohiro T (1987) *J Chem Soc, Chem Commun* 1987: 874
71. The union $G_1 \cup G_2$ is defined as the graph which vertex set is $V_1 \cup V_2$ and edge set is $E_1 \cup E_2$. A disconnected graph is a graph which can be expressed as the union of two graphs [54a]
72. A circuit graph is a connected graph which is regular of degree 2. (A graph in which every vertex set has the same degree is called a regular graph, the degree of a vertex being the number of edges incident to this vertex) [54a]
73. Dietrich-Buchecker CO, Sauvage JP (1989) *Angew Chem* 101: 192; *Angew Chem Int Ed Engl* 28: 189
74. Simons J (1986) *Topology* 25: 229
75. A graph can be coloured: vertices or edges can be drawn in different colours in order to be distinguished one from each other
76. In a chiral medium, enantiotopic protons become diastereotopic and thus their $^1\text{H-NMR}$ signals are split (see ref. [87]). Therefore, a positive test with the Pirkle's reagent is the necessary but not sufficient condition for chirality
77. a) McCreary MD, Lewis DW, Wernick DL, Whitesides GM (1973) *J Am Chem Soc* 96: 1038
b) Pirkle WH, Sikkenga DL, Pavlin MS (1977) *J Org Chem* 42: 384
78. Albano VG, Chini P, Martinengo S, Sansoni M, Strumolo D (1974) *J Chem Soc, Chem Commun* 1974: 299
79. Hisatome M, Kawaziri Y, Yamakawa K, Iitaka Y (1979) *Tetrahedron Lett* 20: 1777
80. Simmons III HE, Maggio JE (1981) *Tetrahedron Lett* 22: 287
81. Paquette LA, Vazeux M (1981) *Tetrahedron Lett* 22: 291
82. a) Otsubo T, Ogura F, Misumi S (1983) *Tetrahedron Lett* 24: 4851
b) Otsubo T, Aso Y, Ogura F, Misumi S, Kawamoto A, Tanaka J (1989) *Bull Chem Soc Jpn* 62: 164
83. Nakazaki M, Yamamoto K, Tanaka S, Kametani H (1977) *J Org Chem* 42: 287
84. Nakazaki M (1984) *Top Stereochem* 15: 199
85. Walba DM, Richards RM, Haltiwanger RC (1982) *J Am Chem Soc* 104: 3219
86. Walba DM, Armstrong III JD, Perry AE, Richards RM, Homan TC, Haltiwanger RC (1986) *Tetrahedron* 42: 1883
87. a) Mislow K, Raban M (1967) *Top Stereochem* 1: 1
b) Eliel EL (1982) *Top Curr Chem* 105: 1
88. Walba DM, Simon J, Harary F (1988) *Tetrahedron Lett* 29: 731

89. Schill G (1971) In: Catenanes, Rotaxanes and Knots. Academic Press, New York, pp 11–14
90. A digraph is a graph G where $E(G)$ is a set of ordered pairs of edges [54a].
91. a) Prelog V, Gerlach H (1964) *Helv Chim Acta* 47: 2288
 b) Gerlach H, Owtschinnikow JA, Prelog V (1964) *Helv Chim Acta* 47: 2294
92. Kubo H, Aida T, Inoue S, Okamoto Y (1988) *J Chem Soc, Chem Commun* 1988: 1015
93. Mitchell DK, Sauvage JP (1988) *Angew Chem* 100:985; *Angew Chem Int Ed Engl* 27:930
94. a) Dietrich-Buchecker CO, Sauvage JP, Kintzinger JP (1983) *Tetrahedron Lett* 24: 5094
 b) Dietrich-Buchecker CO, Sauvage JP (1983) *Tetrahedron Lett* 24: 5091
 c) Dietrich-Buchecker CO, Sauvage JP (1990) *Tetrahedron* 46: 503
 d) Dietrich-Buchecker CO, Sauvage JP, Kern JM (1984) *J Am Chem Soc* 106: 3043
 e) Dietrich-Buchecker CO, Sauvage JP (1987) *Chem Rev* 87: 795
 f) Sauvage JP (1990) *Acc Chem Res* 23: 319
95. Dietrich-Buchecker CO, Guilhem J, Pascard C, Sauvage JP (1990) *Angew Chem* 102: 1202; *Angew Chem Int Ed Engl* 29: 1154
96. McCasland GE, Proskow S (1955) *J Am Chem Soc* 77: 4688
97. a) Dietrich-Buchecker CO, Marnot PA, Sauvage JP, Kirchhoff JR, McMillin DR (1983) *J Chem Soc, Chem Commun* 1983: 513
 b) Edel A, Marnot PA, Sauvage JP (1984) *Nouv J Chim* 8: 495

Recognitory Coloration of Cations with Chromoacerands

Soichi Misumi

Department of Applied Physics and Chemistry, Fukui Institute of Technology, Gakuen
3-6-1, Fukui 910, Japan

Table of Contents

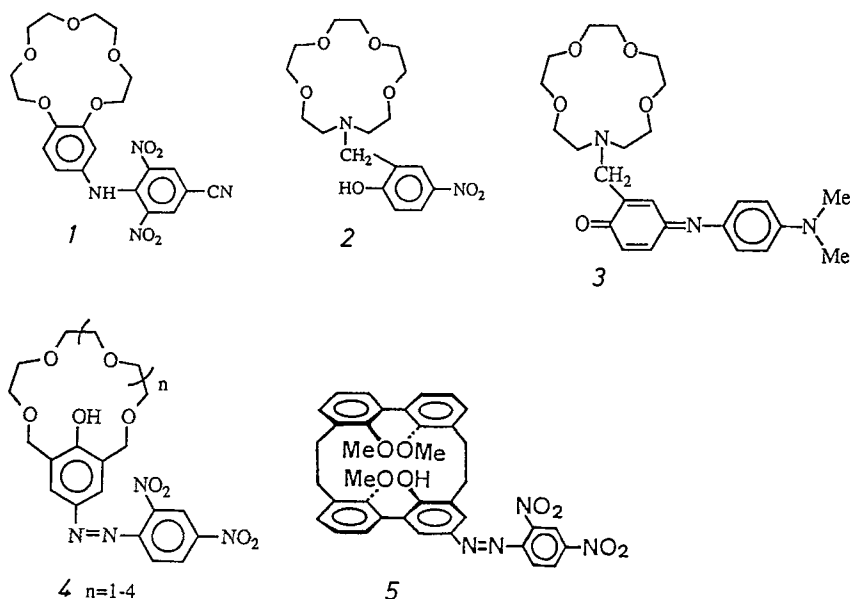
1 Introduction	165
2 Selective Complexation of Metal Salts and Chromoacerands with Coloration or Fluorescent Emission	166
2.1 Selective Coloration of Metal Salts with Azophenol Acerands	166
2.1.1 Synthesis and Dissociation of Acerands	166
2.1.2 Selective Coloration of Metal Salts	167
2.2 Specific Fluorescent Emission with Benzothiazolyphenol Acerands	169
2.2.1 Synthesis of Acerands	169
2.2.2 Spectral Properties of Acerands	171
2.3 Specific Coloration with Azophenol Biphenylophane	172
2.3.1 Synthesis of Acerand 5	172
2.3.2 Specific Coloration with Lithium Salts	174
2.4 Analytical Applications of Chromoacerands for Li ⁺ -Determination	176
3 Selective Coloration of Amines with Azophenol Acerands	177
3.1 Azophenol Acerand-Amine Systems	177
3.2 Dibasic Azophenol Acerand-Amine Systems	181
3.2.1 Synthesis of Acerand	181
3.2.2 Selective Binding for Amines	183
3.2.3 Molecular Structure of Saltex	185
3.3 Enantiomer Selective Coloration of Chiral Amines with Chiral Acerands	186
3.4 Discriminative Coloration for Substitution Pattern of Amines	188
4 References	191

A series of azophenol-dyed macrocycles, which accommodate selectively a given metal or ammonium ion in their cavity and undergo a concurrent color change, were designed and synthesized in order to study molecular recognition in biological systems. Selective coloration of some azophenol hosts and selective fluorescent emission of benzothiazolyl crowns for metal cations are observed to be useful for lithium analysis. Amine selective coloration with some azophenol hosts including enantiomeric discrimination are reported and X-ray crystal structures of sec.-amine inclusion complexes are illustrated. Selective coloration with two acerands is capable of discriminating the substitution pattern of alkylamines.

1 Introduction

A variety of inclusion compounds [1] and complexes between neutral hosts, e.g. crowns, cryptands, cyclodextrins, antibiotics, and cationic or neutral guests have been studied so far to develop the phase transfer catalysis and to elucidate the biological molecular recognition of enzyme/substrate and naturally occurring ionophore/metal cation interactions. On the other hand, studies on complementary complexation involving the coulombic attractive force between oppositely charged host and guest species have been expected to initiate a new trend in the molecular recognition, since this additional binding force will support the stability and selectivity of complex formation and bring into play efficient hydrogen bonding.

During the last decade, design and synthesis of host molecules which accommodate selectively a given metal ion in their cavity and undergo a concurrent color change have been considered as a worthwhile subject in host-guest chemistry. Various chromoionophores, named so by Vögtle [2], have been made available for this purpose to date [3]. A remarkable color change was shown on the complexation of (2,5-dinitro-4-cyano-anilino)benzo-15-crown-5 (**1**) [4] with alkaline metal ions (ca. 130 nm red shift of absorption maximum of the host), compared to that of the corresponding picrylamino compound (50 nm red shift) [5]; selective complexation of nitrophenol crown **2** [6] with lithium ions causes a 86 nm red shift and phenolblue crown **3** [3] with metal ions such as nickel perchlorate a 102 nm red shift.



Structures 1

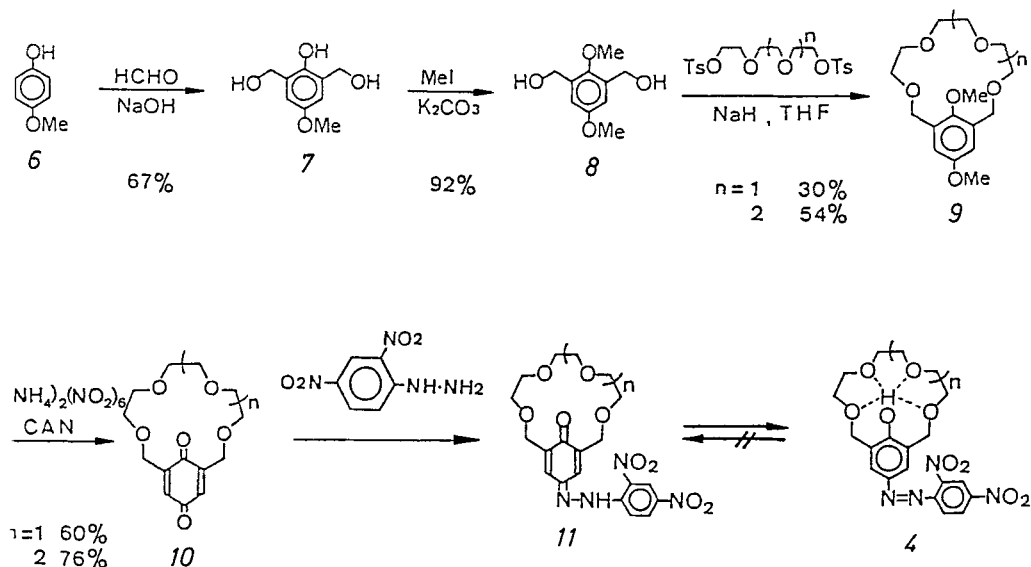
Chromoionophores of crown **4** and spherand cyclophane-type **5** with 2,4-dinitrophenylazophenol groups as a chromophore were also designed [7a]. They show marked color changes from yellow into blue on complexation with cations in ethanol and chloroform solutions. This chapter describes selective complexation and coloration of azophenol hosts or fluorescent emission of benzothiazolyl crowns with alkaline metal ions and alkyl amines.

2 Selective Complexation of Metal Salts and Chromoacerands with Coloration or Fluorescent Emission

2.1 Selective Coloration of Metal Salts with Azophenol Acerands

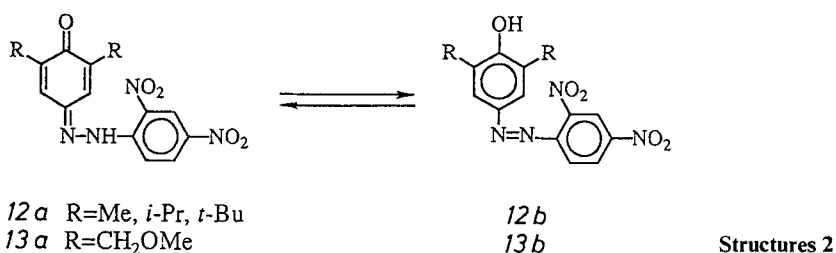
2.1.1 Synthesis and Dissociation of Acerands

A series of azophenol acerands **4** was prepared by condensation of crowned benzoquinones **10** with 2,4-dinitrophenylhydrazine in ethanol [7b]. The quinone was derived from *p*-methoxyphenol (**6**) as shown in Scheme 1 [8]. By bis(hydroxymethylation) (67% yield of **7**, followed by methylation (92%) of the phenol group and Williamson-type reaction with ditosylates of oligoethyleneglycol in the presence of sodium hydride, crowned 1,4-dimethoxybenzene **9** was obtained in reasonable yields. Oxidative demethylation of **9** with ceric ammonium nitrate (CAN) in aqueous acetonitrile at 50 °C gave the desired crowned benzoquinones **10** in good yields.



Scheme 1. Synthesis of azophenol acerands **4**

As compounds of comparison, the uncrowned azophenols **12b** and **13b** were similarly prepared from the corresponding quinones **12a** and **13a** (**13b**: 94% yield). An NMR study reveals that uncrowned azophenol **13** consists of an azophenolhydrazone equilibrium mixture (**13a**:**13b** = 2:3 in CDCl₃) and that crowned azophenols **4** exist only as the preferable azophenol isomer due to the stabilization of the phenol form by hydrogen bonding with the ether oxygens of the macroring. The equilibrium ratios of **13** and **4** are in marked contrast to **12** (dialkyl-substituted derivatives) with more than 95% content of the hydrazone form (**12a**).



Before the study of complexation, pK_a values of acerands **4** and of the reference azophenol **13** were determined by spectrophotometry in 10% dioxane-water (Table 1). The table shows the increase of pK_a values with decreasing crown ring size. This fact is explained by destabilization of the phenolate anion due to both the electrostatic repulsion between the phenoxide anion and the lone pair electrons of ethereal oxygen atoms and the blocking of the crown ring against solvation of the anion.

Table 1. Dissociation constants of azophenol dyes

Dye	4 (n = 1)	4 (n = 2)	4 (n = 3)	4 (n = 4)	13b
pK _a	7.30	6.98	6.88	6.83	6.50
Ring Size	15	18	21	24	—

25 °C in 10% Dioxane-water

2.1.2 Selective Coloration with Metal Salts

In ethanol: acerands **4** and the reference compound **13** dissociate partially in ethanol to give pale blue solutions of phenolate anions (λ_{max} 586 nm for **13**). Addition of triethylamine to the solution allows nearly complete dissociation. This blue solution was changed to violet-yellow by addition of crystalline alkali or alkaline earth metal salts. For example, a marked hypsochromic shift (λ_{max} 586–536 nm) of the longest wavelength absorption band was observed with lithium salts, LiCl and LiClO₄ [7]. The phenolate anion **4** (n = 2) is less susceptible than that of **4** (n = 1) for color change with metal salts. The uncrowned azophenol

13 also shows a small hypsochromic shift. In other words, they are less sensitive for a metal-ion dependent blue shift.

On the other hand, all of the alkaline earth metal salts brought about larger hypsochromic shifts than the alkali metal salts. A system magnesium perchlorate/triethylamine and **4** ($n = 1$) shows the largest hypsochromic shift in all the systems examined.

In chloroform: No phenolate anion in chloroform solution of azophenol acerands **4** is detected even in the presence of pyridine as a base, in contrast to the case in ethanol. On addition of crystalline metal salts to this yellow solution, color change to orange-purple is observed as shown in the salt-dependent visible spectra of **4** in chloroform (Figs. 1 and 2). Especially, azophenol crown-4, **4** ($n = 1$)

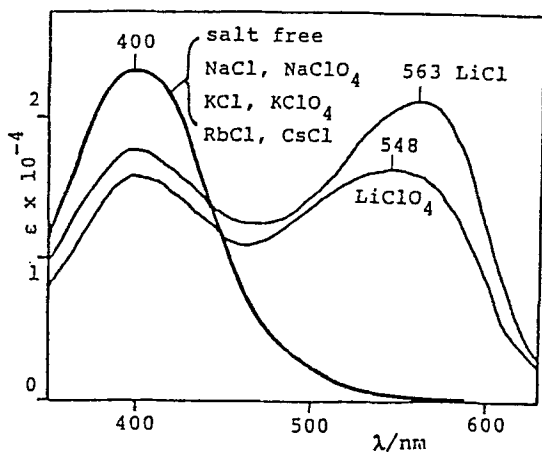


Fig. 1. Visible spectra of **4** ($n = 1$) alkali metal salt-pyridine systems in CHCl_3 .

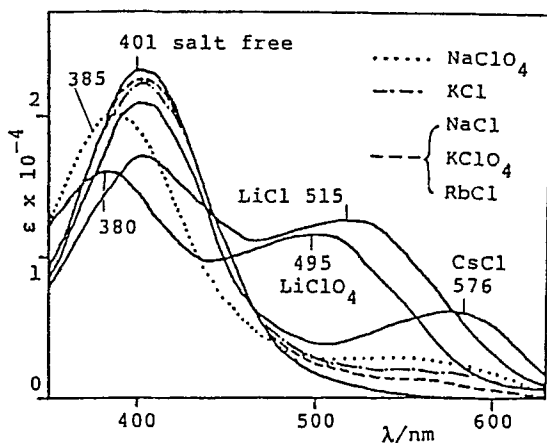
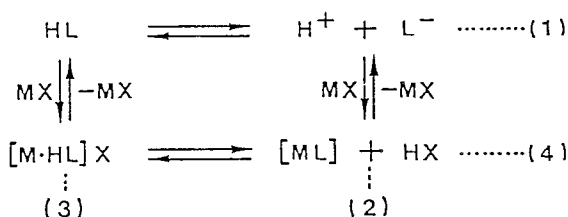


Fig. 2. Visible spectra of **4** ($n = 2$) alkali metal salt-pyridine systems in CHCl_3 .

clearly shows selective coloration only with lithium salts among a series of alkali metal salts. A dramatic color change from yellow to purplish red took place rapidly on addition of lithium chloride or perchlorate to a **4** ($n = 1$) pyridine system in chloroform. On the other hand, this lithium ion selectivity on coloration decreases in the case of larger ring acerands **4** ($n = 2-4$), but the coloration with cesium salt increases; all the acerands **4** show no selective coloration for alkaline earth metal salts. It is noteworthy that uncrowned azophenol **13** is inactive to alkali and alkaline earth metal salts except for the formation of an orange precipitate with magnesium chloride.

The hypsochromic shift of the longest absorption band on complexation in ethanol solution and the bathochromic shift in chloroform solution are explained as follows. The hypsochromic shift in ethanol is affected by the phenol dissociation equilibrium (Eq. (1) in Scheme 2), the ion-exchange equilibrium, and the interaction of phenolate anion-metal cation [Eq. (2)]. In facts, the observed shifts depend upon the cation species, the amount of added salts, the reaction time, and, in some case, the counter anion species.



Scheme 2. Equilibrium in azophenol (HL)-metal salt (MX) systems

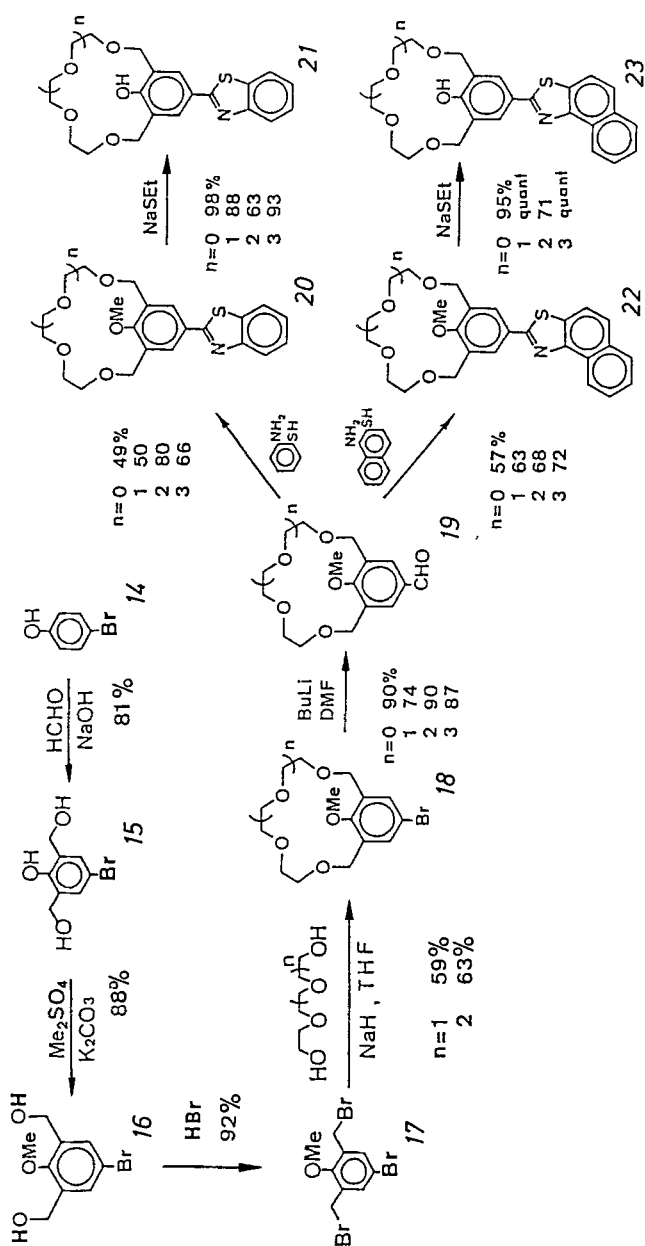
On the other hand, since no dissociation of the phenol **4** occurs in a pyridine-chloroform system, the observed salt-dependent coloration or bathochromic shift seems to be based on an equilibrium (Eq. (4)) between colored intramolecular salt [ML] and postulated intermediate complex $[\text{M} \cdot \text{HL}] \text{X}$ which may be stable without the presence of a base and dissociates easily on addition of a relatively weak base, e.g. pyridine, to yield the salt [ML].

2.2 Selective Fluorescent Emission of Benzothiazolylphenol Acerands

The incorporation of a fluorescent group in the place of the azophenol group stated above should provide a reaction much more sensitive than coloration to the formation of a host-guest complex. From this view point, we designed new fluorescent acerands containing a benzothiazolylphenol group which fluoresces strongly in alkaline solution [9].

2.2.1 Synthesis of Acerands [10]

As shown in Scheme 3, 4-bromo-2,6-bis(hydroxymethyl)anisole (**16**) [11], derived from *p*-bromophenol (**14**) by treatment with 37% aq. formaldehyde at room temperature for 12 days, followed by methylation with dimethyl sulfate and



Scheme 3. Synthesis of thiazolylphenol acerands, 21 and 23

bromination with conc HBr gave the corresponding bis(bromomethyl) compound **17** in 92% yield. Crowned anisaldehyde **19** was prepared by cyclization of **17** with oligoethylene glycol, followed by treatment with butyllithium and DMF in good yield. Reaction of aldehyde **19** with *o*-aminothiophenol or 2,2'-dithio-bis(1-aminonaphthalene) [12] and tributylphosphine gave crowned benzo- or naphthothiazolylianisoles **20** and **22**, respectively, in 49–80% yields. Demethylation of **20** and **22** was carried out with sodium ethanethiolate [13] in DMF to give the desired thiazolyphenols, **21** and **23**, in excellent yields. This method of ether cleavage was used in place of the usual demethylation with LiAlH_4 –THF which gave relatively low yields of **21** and **23** besides decomposed substance.

2.2.2 Spectral Properties of Thiazolyphenol Acerands

Though acerand **21** in chloroform does not dissociate even in the presence of excess triethylamine, addition of crystalline metal salts immediately gives rise to a remarkable change in the absorption spectra, indicating the formation of the phenolate anion (Figs. 3 and 4). On irradiation of the heterogeneous specimen containing the predominant phenolate complex, strong blue-violet fluorescence of the solution was observed. According to screening for the fluorescent emission, the thiazolyphenol acerands with small ring size, **21** ($n = 0$) and **21** ($n = 1$), shows selective emission for the lithium ion among alkali metal salts, while the acerands with a larger cavity, **21** ($n = 2$) and **21** ($n = 3$) tend to bind larger alkali metal ions other than lithium salts without emission. This lithium selective fluorescent emission was confirmed to provide a quantitative way to detect a small amount of lithium from a bulk of the other alkali and alkaline earth metal ions. The application for lithium analysis will be described together with colorimetric analysis in Sect. 2.4.

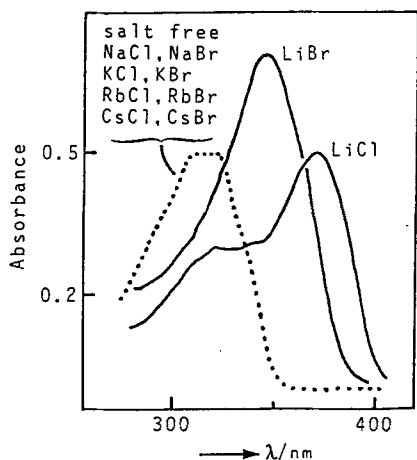


Fig. 3. Absorption spectra of **21** ($n = 1$)-alkali metal halide- Et_3N systems in chloroform

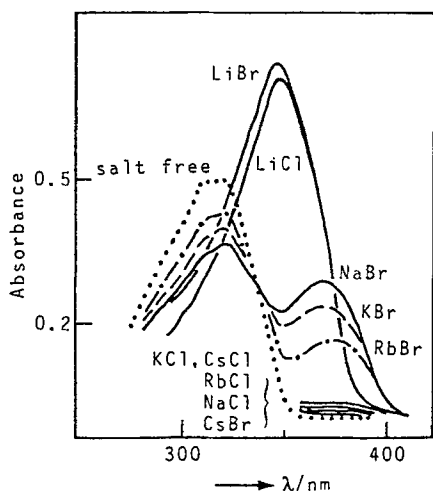
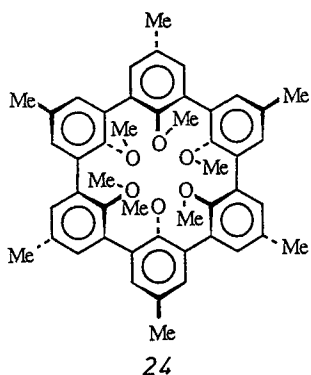


Fig. 4. Absorption spectra of 21 ($n = 2$)-alkali metal halide- Et_3N systems in chloroform

2.3 Specific Coloration with Azophenol Biphenylophane

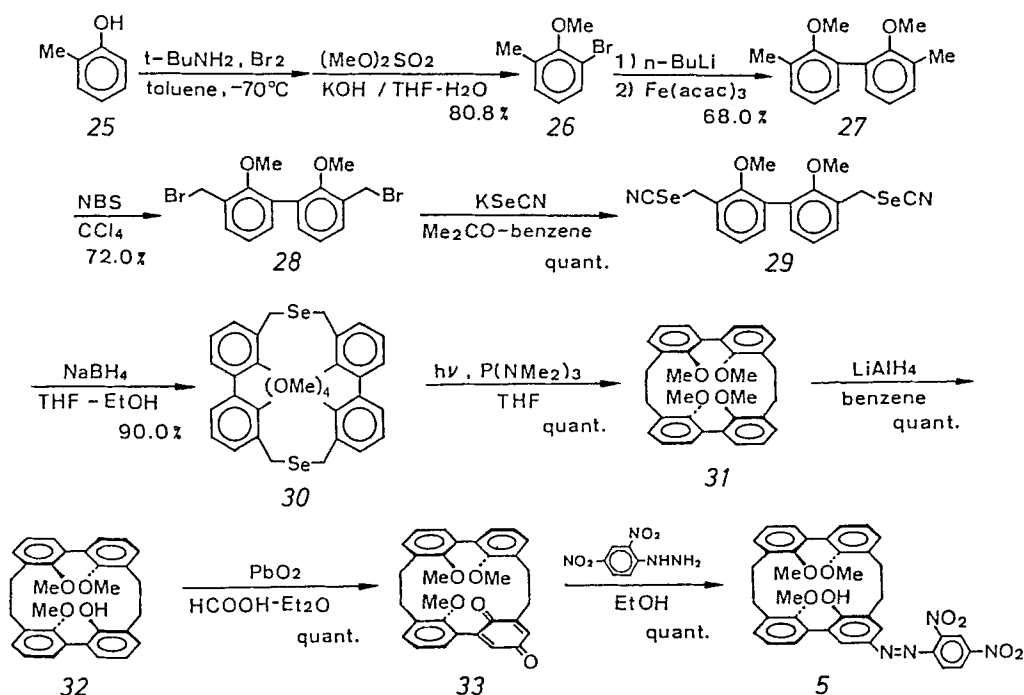
In order to develop hosts with a much higher level of lithium selectivity, we planned a macrocyclic ligand which is of a capsular type, has a rigid structure as well as the function of concomitant coloration on complexation. An azophenol biphenylophane 5, which has a rigid cavity to accommodate only the lithium ion in the center, was designed by considering the fact that Cram's spherand 24 [14] can reject multivalent metal ions perfectly.



Structure 3

2.3.1. Synthesis of Acerand 5 [15]

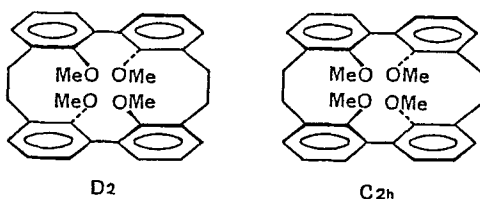
As shown in Scheme 4, using as the key step a photodeselenation which was developed by us for preparing [2.2]cyclophanes [16], tetramethoxy[2.2]biphenylophane 31 was synthesized via a sevenstep reaction sequence in 30% overall yield from *o*-cresol (25). By comparison of ^1H -NMR data, this cyclophane was assigned



Scheme 4. Synthesis of azophenol biphenylophane 5

to D_2 structure **31** having the same geometry as that of crystallographically defined tetramethyl derivative **36** which was previously synthesized via another cyclization step of dibromide **35**. Demethylation of **31** was carried out by reflux with LiAlH_4 in benzene to give exclusively the monodemethylated product **32** in quantitative yield. After oxidation of **32** using PbO_2 , treatment of the obtained quinone **33** with 2,4-dinitrophenylhydrazine gave the desired azophenol cyclophane **5** as orange crystals in quantitative yield, which was derived by isomerization of the first-formed hydrazone.

Two possible structures, D_2 and C_{2h} symmetry as shown in Fig. 5, are assumed for the cyclophanes **31** and **36**. The molecular structure of **36** was determined by X-ray analysis (Figure 6) to be of D_2 symmetry [15]. The four methoxyl oxygens are at the corners of a tetrahedron and the size of the cavity (0.68 \AA) is compatible with the ionic radius of Li^+ (0.60 or 0.73 \AA).


 Fig. 5. Two possible structures of **31**

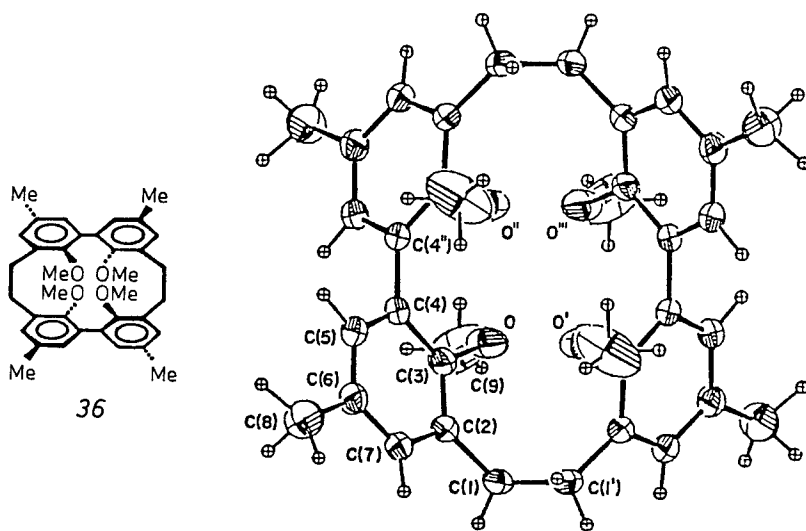


Fig. 6. ORTEP drawing of cyclophane 36

2.3.2 Specific Coloration with Lithium Salts

On neutralization with a series of alkali metal hydroxides or tetramethylammonium hydroxide in ethanol, weak acid **5** gave a colored solution with an absorption maximum at 615 nm independent of the cation species. This fact suggests that the phenolate anion from **5** interacts with the solvated cations or form solvent-separated ion pairs in the protic solvent, in marked contrast to those of azophenol crowns **4** with alkali metal salts.

In chloroform, no phenolate anion of **5** was detected even in the presence of excess piperidine as a base. Addition of crystalline lithium salts to this mixture gives rise to changes in absorption spectra, indicating the formation of the phenolate salt (Fig. 7). A dramatic color change from yellow to violet took place rapidly on addition of lithium salts, except for that with nitrate, fluoride, and sulfate counter anions. No tendency for the interaction was observed with any of the other 58 inorganic salts listed in Fig. 7.

In the hydrophobic solvent (CHCl_3), the lithium ion in the colored species is believed to be encapsulated in the hydrophilic cavity of the counter anion on the basis of the following facts: (1) the cavity is expected to be small but able to accommodate the guest.

The extraordinarily large pK_a for **5** (13.5 in 10% water-dioxane at 25 °C) is compatible with this small cavity because of the instability of the resulting anion due to a large electronic repulsive force; (2) the coloration takes place only when the specimen is in contact with lithium salts; (3) the monodemethylation of tetramethoxycyclophanes **31** and **36** occurs exclusively in an aprotic solvent such as benzene even in the presence of excess LiAlH_4 (no evidence for complexing lithium with **36** was obtained by both picrate salt extraction and NMR spec-

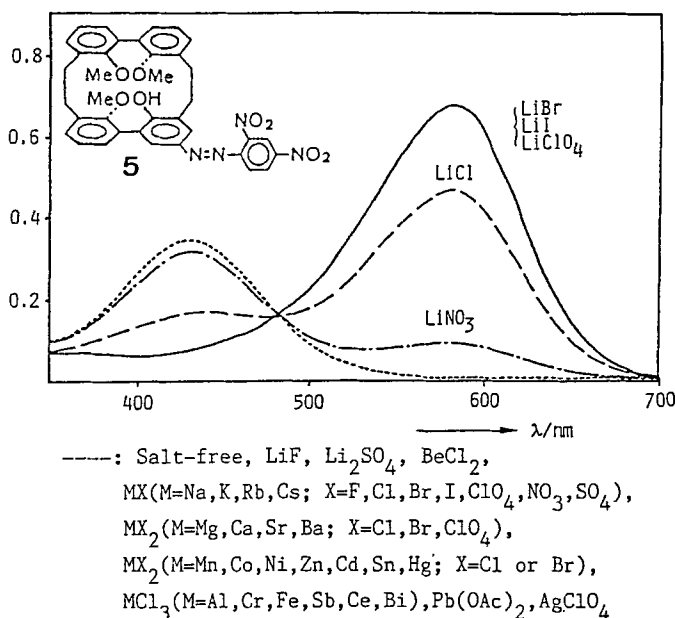
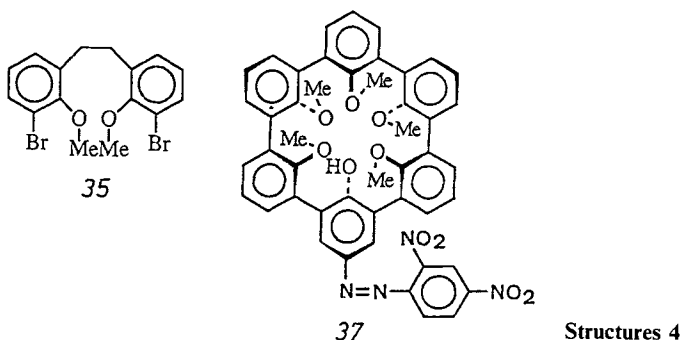


Fig. 7. Visible spectra of the azophenol biphenylophane **5**-salt-piperidine system in chloroform

troscopic techniques); (4) no cation exchange between Li^+ and Ca^+ or Ba^{2+} was observed.

The perfect lithium selectivity observed under the given conditions is described in terms of binding the guest cation by both the coulombic attractive force and ion-dipole interactions, and rejecting larger or multivalent cations by the narrow entrances to the small cavity in the cyclophane dye **5**.

Recently, Cram and his group reported the synthesis and chromogenic properties of the azophenol spherand **37** which is a chromogenic ion-selective indicating system capable of detecting Li^+ and Na^+ at concentrations as low as 10^{-8} M in the presence of other common ions [17].



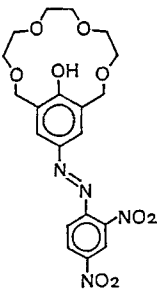
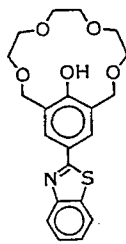
2.4 Analytical Applications of Chromoacerands for Li⁺-Determination

As described in the previous section, azophenol crown **4** ($n = 1$) shows a characteristic coloration only for Li⁺ ion among alkali metal ions. After extensive examinations in a number of solvent systems, lithium analytical conditions were determined as shown in Table 2 [18a]. The resulting reddish purple color is very stable and its absorbance is maintained for 10–90 min after developing color. The calibration curve for Li⁺, in other words, sensitivity is linear from 25–250 ppb. Na⁺ does not interfere, but K⁺, Rb⁺, Ca²⁺, Sr²⁺, Ba²⁺, and Mg²⁺ interfered in the determination with a similar coloration. This method was applied to the analysis of a commercial pharmaceutical preparation, a lithium carbonate tablet, since the Li₂CO₃ tablet has been used for medical treatment of manic depressive illness [18b]. On the other hand, the azophenol crown **4** ($n = 1$) is also useful as a reagent for colorimetric determination of Rb⁺ and Cs⁺ [19].

As expected, benzothiazolylphenol crown **21** ($n = 1$) proved to be superior to the azophenol crown **4** ($n = 1$) in sensitivity toward Li⁺ determination. Excitation and emission spectra of this reagent and its complex of Li⁺ show that the reagent is useful for determination of Li⁺ (Fig. 8).

On addition of lithium chloride in methanol to **21** ($n = 1$) in benzene, the curves c(excit.) and d(emiss.) change to the curves a(excit.) and b(emiss.) with marked increase of their fluorescent intensity. The emission intensity of the reagent

Table 2. Determination of lithium ion

	Colorimetry	Fluorometry
Solvent	CHCl ₃ /DMSO (99:5 v/v%)	Benzene-MeOH (99:0.5 v/v%)
Base	NEt ₃ (0.5 v/v%)	NEt ₃ (0.5 v/v%)
λ_{\max}	565 nm	$\lambda_{\max}^{\text{ex}}$ 375 nm $\lambda_{\max}^{\text{em}}$ 410 nm
Sensitivity	25–250 ppb	0.39–39 ppb
Interfering cations	K ⁺ , Rb ⁺ , Mg ²⁺ , Ca ²⁺ , Sr ²⁺ , Ba ²⁺	—
	 <p>4 ($n=1$)</p>	 <p>21 ($n=1$)</p>

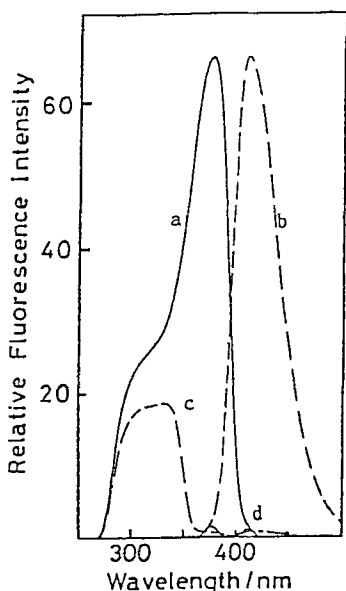


Fig. 8. Fluorescence and excitation spectra of **21** ($n = 1$) and the **21** ($n = 1$) Li complex

blank (curve d) is negligible compared with that of the complex when an excitation at 375 nm is used for analysis. Consequently, this fluorometric method is also applied satisfactorily for Li^+ determination with both excellent sensitivity (0.39–39 ppb) and fairly good selectivity as well as the marked advantage of there being no interfering cation (see Table 2).

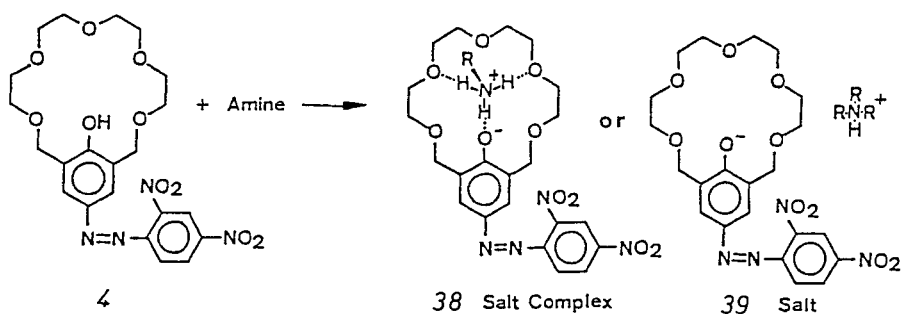
3 Selective Coloration of Amines with Azophenol Acerands

An alternative type of complex with crown ethers is concerned with a tripod arrangement of protonated primary amines by three ethereal oxygens of the crown ring. Such a nesting type complexation was observed, for example, by X-ray crystallography of the *t*-butylamine complex of pyrido[18]crown-6 [20], and its representative application is the enantiomeric separation of protonated amino acid derivatives through chiral recognition of host crowns incorporating an optically active binaphthyl group [21].

3.1 Azophenol Crown-Amine Systems

We examined molecular recognition of protonated amines with a series of azophenol crowns. When an ammonium cation is accommodated in the crown cavity, the complexes produced should be differentiated from ion-dipole complexes of neutral crowns by an additional binding force, i.e. coulombic interaction.

If the substituent R of guest amines is a bulky group, a solvent-separated ion pair such as structure **39**, which is generated by neutralization or proton-transfer reaction, will be produced with concurrent color change from yellow to blue



Scheme 5. Formation of acerand amine complexes

(Scheme 5). On the other hand, when the substituent R is of a suitable size, an intramolecular ion pair such as structure **38** will be formed and stabilized by interionic hydrogen bond $N^+ - H - O^-$ in addition to hydrogen bond $N^+ - H - O$ and ion-dipole interaction $N^+ - O$. At the same time, the solution will be turned to violet because of short interionic distance between N^+ and O^- , which is strongly affected on the electronic state of the dinitrophenylazophenol chromophore. Accordingly, the absorption maximum wavelengths of the amine complexes in visible spectra will possibly be indicative of the type of complex, i.e. salt complex (abbreviated as saltex) **38** or simple salt **39**.

To the pale blue solution of azophenol crown **4** in ethanol, addition of a series of amines causes the high degree dissociation of the phenol to yield the phenoxide anion with an accompanying color change into reddish to bluish violet. The values of absorption maxima of the resulting ammonium phenolates (**38** or **39**) are summarized as an example in Fig. 9 [22]. The figure shows as follows: 1) acyclic azophenols, **12b** and **13b**, reveal constant values of the maxima regardless of the

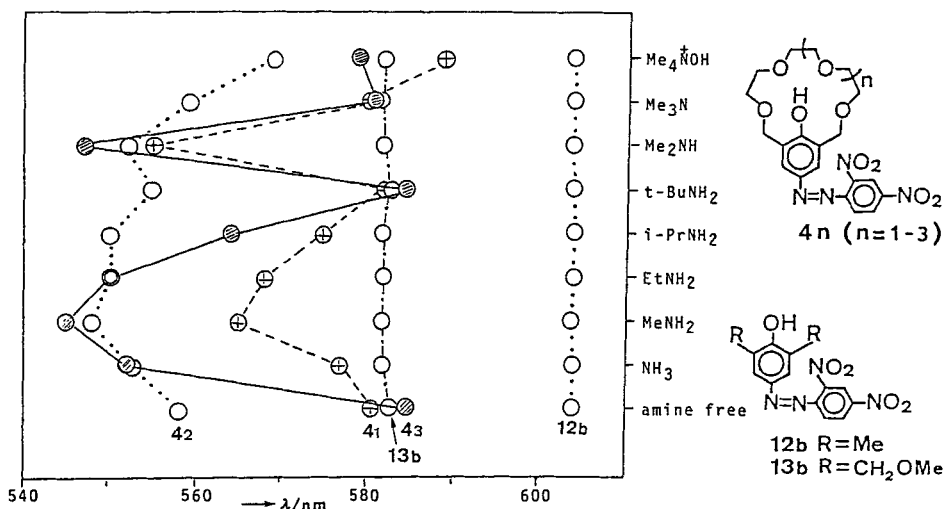
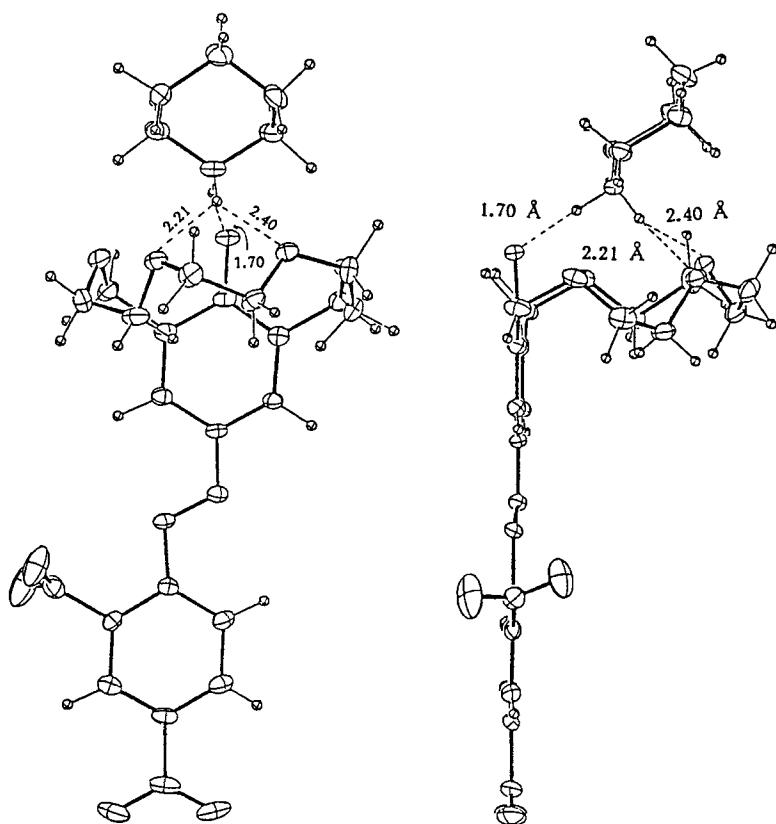


Fig. 9. Absorption maxima of azophenol dye-amine systems in EtOH

Table 3. Absorption maxima of azophenol crown 4-sec. amine systems in EtOH (nm)

	4 (n = 1)	4 (n = 2)	4 (n = 3)	4 (n = 4)
BuMeNH	572	560	557	574
Et ₂ NH	582	575	576	580
Pyrrolidine	561	558	568	583
Piperidine	559	559	580	586
2-Me-piperidine	583	575	584	587
2,2,6,6-Tetra-Me piperidine	586	579	587	588

amine species, indicating no formation of inclusion complexes; 2) the shifts of maxima are dependent strongly upon the molecular structure of amine as well as the size of the crown cavity rather than either the acidity of azophenols and the basicity of the amines, since less bulky amines show more blue shifts of the complex maxima. It is of especial interest that dimethylamine shows a marked blue shift


Fig. 10. ORTEP drawing of the molecular structure of azophenol crown 4 (n = 1) · piperidine salt

comparable to that of monomethylamine, in spite of the larger molecular size and smaller number of hydrogen bonds of the former sec. amine compared to the latter prim. amine.

In order to study the exceptional blue shift of absorption maximum for dimethylamine, the inclusion with azophenol crown **4** was carried out for a series of sec. amines in ethanol. Table 3 shows maxima of some sec. amine-**4** systems. There, marked blue shifts are observed for **4** ($n = 1$) and **4** ($n = 2$) with pyrrolidine and piperidine. Such a blue shift for both cyclic amines disappears with the increase of crown size.

To confirm the inclusion mode for a sec. amine, the 1:1 piperidine · **4** ($n = 1$) complex was isolated and its molecular structure was determined by X-ray analysis (Fig. 10) [22]. The chromophore is planar (except the *o*-nitro group) within 0.1 Å, to which the cyclic polyether ring extends perpendicularly. The protonated piperidine having a chair form structure is placed on the crown ring and stabilized by very short $N^+ - H \cdots O^-$ (2.65 Å) and $N^+ - H \cdots O$ (2.93 Å) hydrogen bonds, and two $N^+ \cdots O$ ion-dipole interactions (3.17 and 3.16 Å). The remaining ether oxygen, O(2), seems to be ineffective on the complexation.

Moreover, the contribution of the *o*-nitro group on the spectral behavior was confirmed to be clearly effective in solution by comparison with amine complexes of *p*-nitrophenylazophenol crown **40** (λ_{\max} ca. 40–50 nm in EtOH). Figure 11

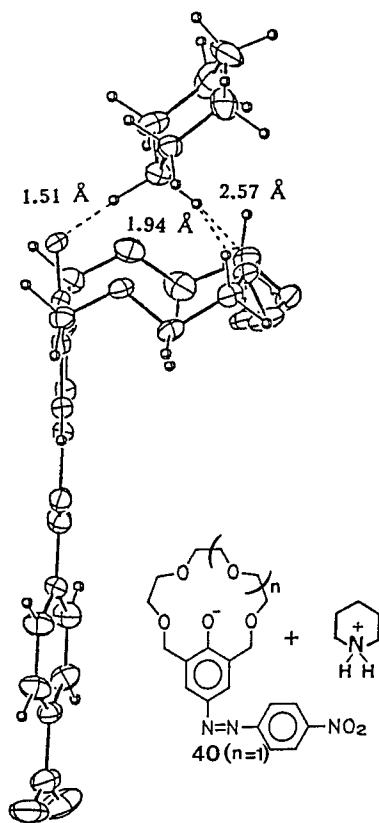


Fig. 11. ORTEP drawing of the molecular structure of *p*-nitrophenylazophenol **40** · piperidine.

shows the similar type of molecular structure for piperidine **40** ($n = 1$) and much shorter length of the $N^+ - H - O^-$ bond than the corresponding bond in Fig. 10, reflecting the electron density on the phenolate oxygen atom.

In addition, the stability constants of amine complexes were determined with the dyed-host **40** using the Benesi-Hildebrand method in acetonitrile and chloroform at 25 °C [23]. The data show the following order of complex stability;

log K of amine **40** ($n = 2$): prim. > sec. > tert.

log K of amine **40** ($n = 1$): sec. > prim. > tert.

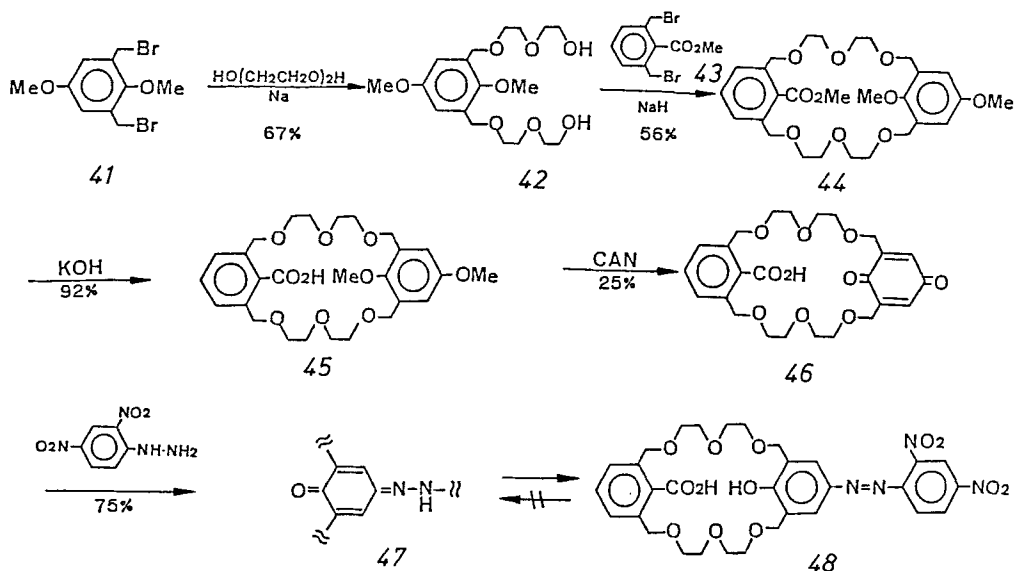
It is noteworthy that the stability for amine **40** ($n = 1$) complexes is ordered to be dominant for sec. amines. This fact indicates that the stability is caused by various factors, i.e. steric complementarity between host and guest, acidity of the azophenol, basicity of the amine, number of hydrogen bonds, ion-dipole interaction, and solvent polarity.

3.2 Dibasic Azophenol Acerand-Amine Systems

In connection with azophenol crown complexes in the preceding section, a dibasic azophenol crown incorporating a benzoic acid unit in the ring was studied for inclusion of amines.

3.2.1 Synthesis of the Acerand **48** [24]

The podand-type compound **42** was prepared by coupling of diethyleneglycol with 2,6-bis(bromomethyl)-1,4-dimethoxybenzene (**41**) which was derived via a three-step sequence from *p*-methoxyphenol (**6**) as usual (Scheme 6). Coupling of **42** with



Scheme 6. Synthesis of acerand **48**

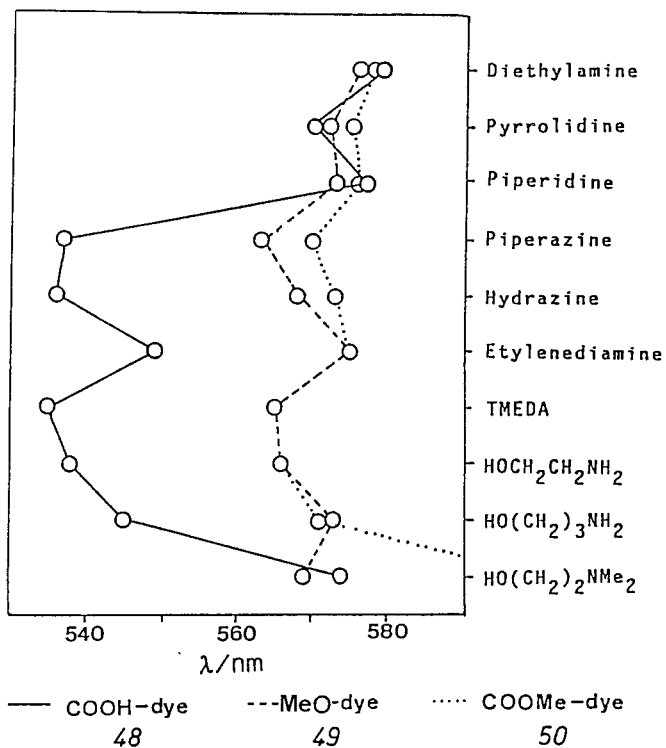
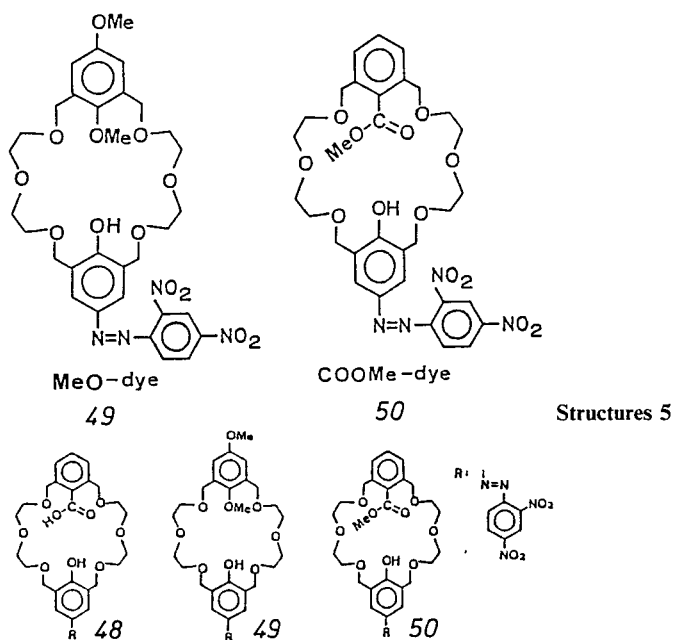


Fig. 12. Absorption maxima (in nm) of visible spectra for dye-amine systems in CHCl_3

dibromoester **43** gave a cyclic oligoether **44** in 56% yield. Alkaline hydrolysis of **44**, followed by oxidation with CAN gave a crowned quinone benzoic acid **46**. On the other hand, the corresponding quinone methyl benzoate was obtained in a low yield by direct oxidation of **44** with CAN. The COOH-dye **48** was obtained via the intermediate hydrazone **47** by treatment of **46** with 2,4-dinitrophenylhydrazine and was assigned to pure azophenol form **48** on the basis of NMR spectra. A reference azophenol, MeO-dye **49**, which was synthesized in a similar manner, consists of an equilibrium mixture of the hydrazone form and the azophenol form **49** in a 1:4 ratio.

3.2.2 Selective Binding with Amines

Three acerands **48**–**50** show absorption maxima at ca. 400 nm in chloroform and turn blue on addition of amines. After many examinations of the complexation of the three acerands with large excess of various amines in alcohol and chloroform, it was found that COOH-dye **48** shows a marked blue shift (ca. 40 nm) of the absorption maximum by the addition of several diamines (piperazine, hydrazine, TMEDA = tetramethylethylenediamine), and two aminoalcohols in chloroform, in contrast to slight fluctuation of the maxima for amine complexes of the two references (Fig. 12). In other words, the yellow solution of **48** turns to blue with monoamine whereas to pink color with diamine, indicating very different coloration based on the two binding sites in the crown cavity.

To study the relationship between the absorption maxima of **48** diamine saltexes and concentration of the diamines, titration experiments were carried out in ethanol and chloroform. Variable concentration spectra for **48** piperazine in chloroform are shown in Fig. 13 as an example. With the increase of piperazine concentration,

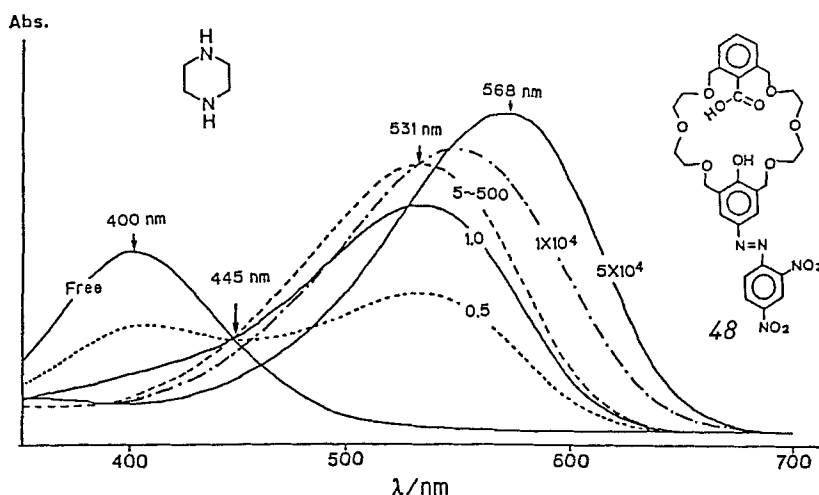


Fig. 13. Visible spectra of acerand **48** · piperazine systems in chloroform

the spectra show the lowering of the maximum at 400 nm and the raising of the maximum at 531 nm, accompanying color change to deep violet. However, the maximum at 531 nm shifts gradually to a longer wavelength region with the addition of more than 500 equivalents of piperazine and the solution turns blue gradually.

This spectral behavior dependent on amine concentration is interpreted by the formation of a 1:1 ratio saltex for the case of less than 500 eq. amine and of a 1:2 (=48:piperazine) salt for the case of more than 500 eq. amine. The 1:1 saltex was prepared in quantitative yield in chloroform and characterized by $^1\text{H-NMR}$ and X-ray analysis (Fig. 14) [24]. The 1:2 salt is presumed to be a structure bearing

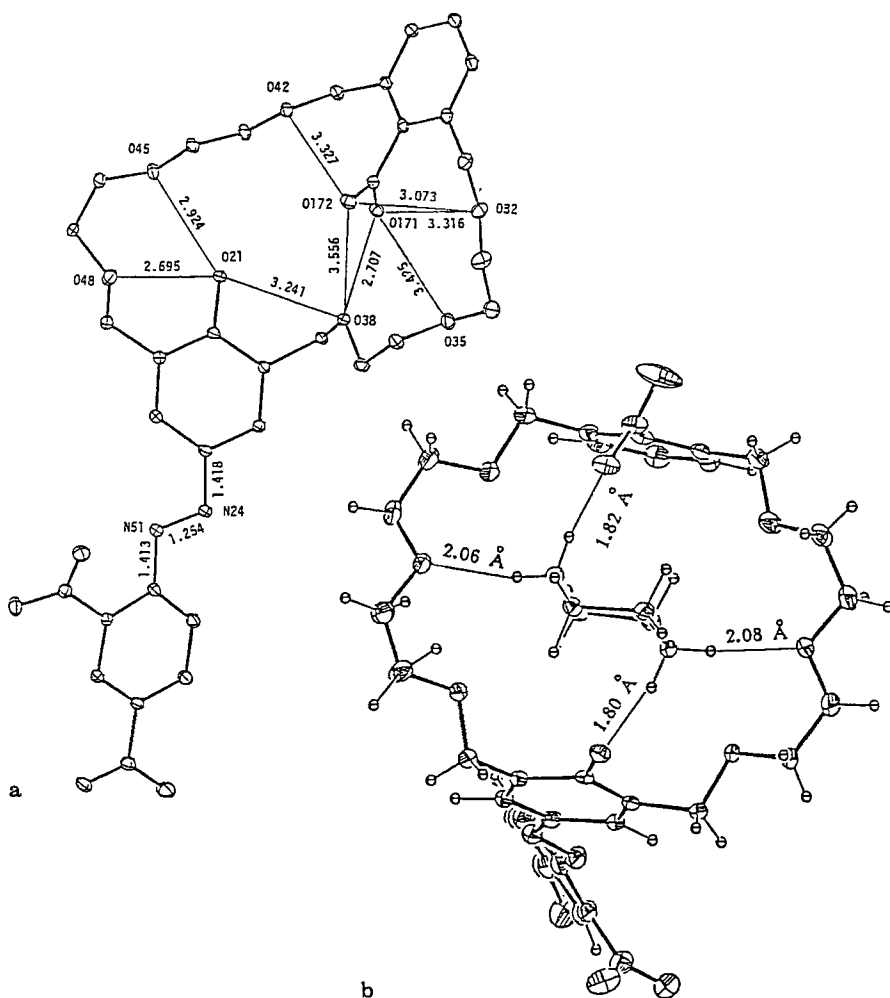


Fig. 14. ORTEP drawings of the molecular structures of (a) acerand 48 and (b) its piperazine saltex

an amine to each binding site of **48** on the basis of the spectral behavior of some reference dye amine complexes.

On the other hand, TMEDA and Dabco (1,4-diaza-bicyclo[2.2.2]octane), both of which have an ethylenediamine unit and sterically bulky geometry, show time dependency of the spectral curves of intermediate saltex, indicating the instability of kinetically formed 1:1 ratio saltex and the thermodynamic transformation of the saltex to the 1:2 salt (Fig. 15).

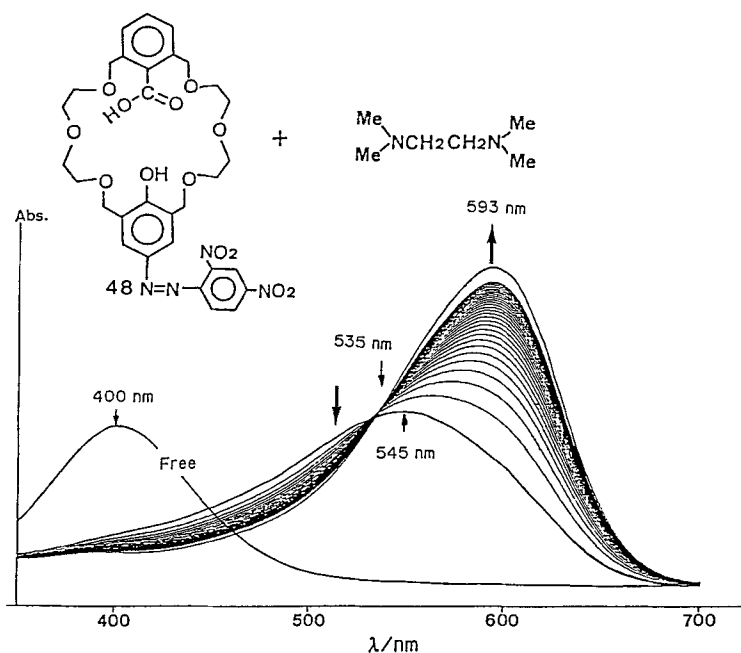


Fig. 15. Visible spectra of acerand **48** · TMEDA systems in chloroform

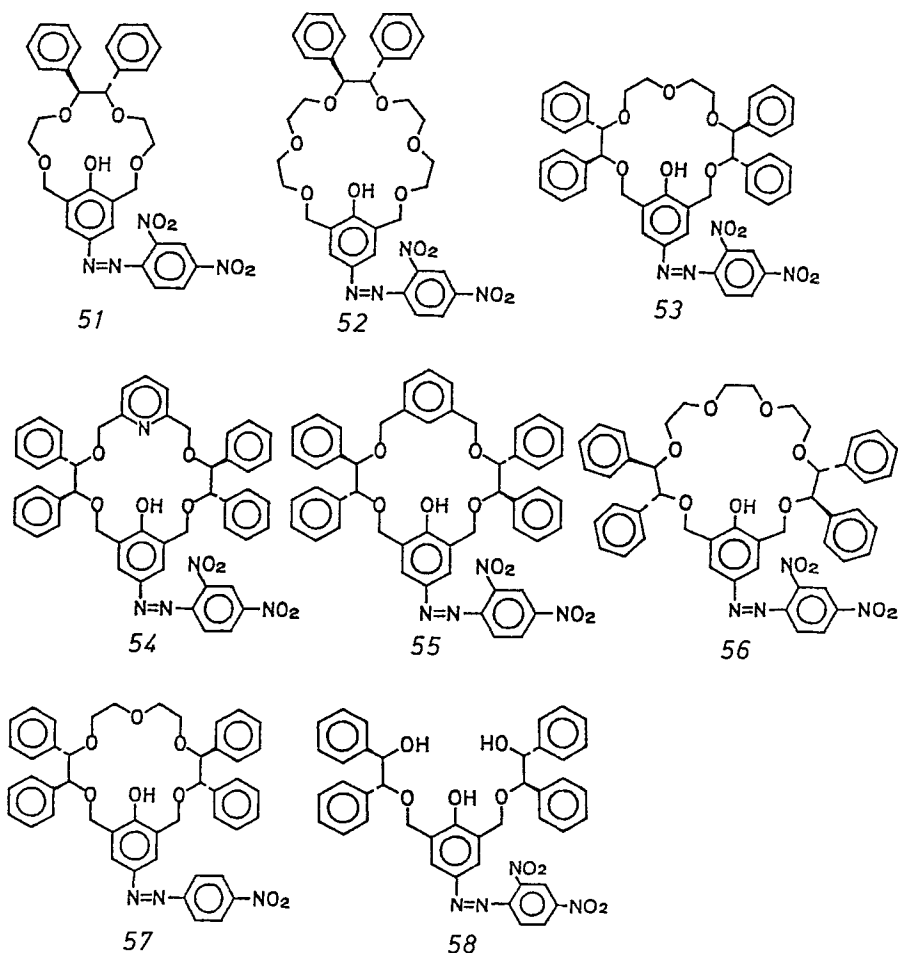
3.2.3 Molecular Structure of a Dibasic Acerand Saltex

The molecular structures of host acerand **48** and its piperazine 1:1 saltex were determined by X-ray crystallography as shown in Fig. 14 [24]. The hydroxyl and carboxyl groups are separate from each other and are bound by hydrogen bonds and ion-dipole interactions. Both benzene rings in the crown cycle are situated in an *anti*-form, probably due to dipole repulsion between the carboxyl and the phenol groups. On the other hand, the piperazinium dication is well accommodated with a chair form in the cavity of the host **48** dianion. The axial NH protons of the guest make strong $N^+ - H - O^-$ hydrogen bonds with the two anions, judging from marked short bond lengths, 2.694 and 2.655 Å. The great shortening of the former one compared to the standard $N^+ - H - O^-$ hydrogen bond, 2.83 Å,

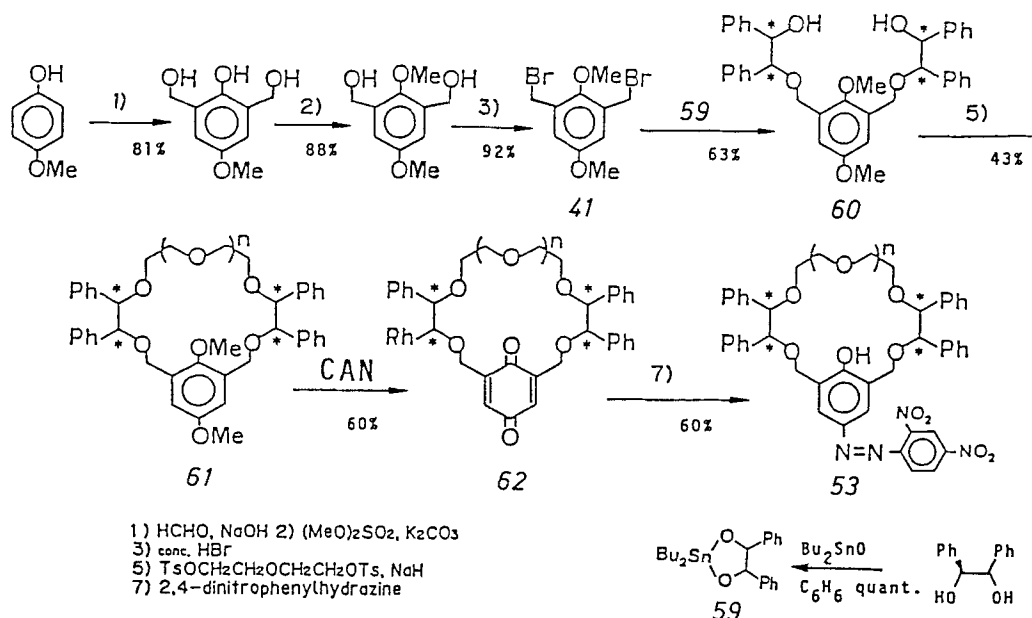
stresses the importance of coulombic attraction [25]. It is noteworthy that both benzene rings in the saltex are placed in a *syn*-form to sandwich the guest dication.

3.3 Enantiomer Selective Coloration with Chiral Acerands

To recognize a chiral ammonium guest, binaphthyl hinge crowns were designed and proved the enantiomeric separation of protonated amino acid ester racemates [21]. A series of chiral azophenol acerands incorporating one or two optically active hydrobenzoin unit, **51–58**, has been synthesized to study the title theme, enantiomer selective coloration with chiral amines.



Structures 6



Scheme 7. Synthesis of chiral acerand 53

The synthesis of a typical compound containing two units of dihydrobenzoin is shown as an example in Scheme 7 [26]. Reaction of 2,6-bis(bromomethyl)-1,4-dimethoxybenzene **41** with the dibutyltin derivative of optically active dihydrobenzoin **59** yields a chiral podand **60** in 63%. Cyclization of **60** with the ditosylates of oligoethylene glycols, followed by oxidation with CAN and treatment with dinitrophenylhydrazine, affords the desired chiral dyed acerand **53**. Some chiral azophenol acerands **51**–**58** are synthesized in a similar manner.

Of examinations with commercially available chiral monoalkylamines and ethanolamines, complexation of chiral acerand **53** (*RRRR* and *SSSS* having four chiral carbons of *R* and *S* configurations, respectively) and norpseudoephedrine **63** (having two chiral carbons of *R,R*-configuration) in chloroform is shown as a representative example in Fig. 16. The (*SSSS*)-**53** · **63** complex reveals a higher intensity of the absorption maximum near 550 nm compared to that of (*RRRR*)-**53** · **63**. This means that norpseudoephedrine is more easily accommodated in the cavity of (*SSSS*)-**53** than that of (*RRRR*)-**53**, in accord with CPK molecular model examinations.

From the study with variable concentration of the amine, the yellow solution of (*RRRR*)-**53** in chloroform remains unaltered by addition of the amine in a range of concentrations, 4.8×10^{-7} to 1.2×10^{-6} M, whereas the solution of (*SSSS*)-**53** reveals a color change from yellow to reddish violet with the same concentration of the amine. In other words, enantiomer selective complexation and enantiomer specific coloration were realized by this finding.

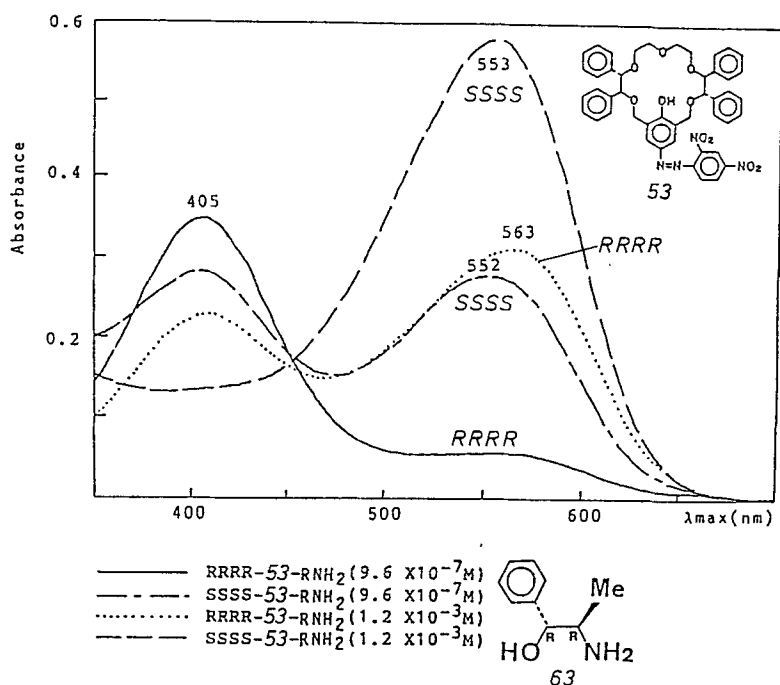


Fig. 16. Absorption spectra of 53-norpseudoephedrine (63) systems in chloroform

3.4 Discriminative Coloration for Substitution Pattern of Amines

A series of acyclic azophenol-dyed oligoethers **64** (azophenol podand, PoOn: n = number of oxygen atoms in the two side arms; Fig. 17) also show the complexation-coloration with amines in similar manner as described for the azophenol crowns. For example, PoO₆ (**64**, $n = 2$) makes a saltex (λ_{\max} 568 nm) with bulky primary amine, *t*-BuNH₂ in chloroform, whereas it does not with tertiary amine, tri-*n*-butylamine (Fig. 17).

As seen in Fig. 18, podand dye PoO₆ (**64**, $n = 2$) shows generally hard complexation-coloration with bulky sec. amines, i.e. diisopropylamine (G in Fig. 18) and 2,2,6,6-tetramethylpiperidine (J in Fig. 18), as well as with all tert. amines. On the other hand, PoO₄ (**64**, $n = 1$) is able to form a saltex with all prim. and sec. amines including the bulky ones but not with tert. amines. The two end hydroxyl groups in the two side arms of both podand dyes, PoO₄ and PoO₆, are required for such coloration of amines, because no coloration is observed on addition of various amines when the hydroxyl groups are substituted with methoxyl groups.

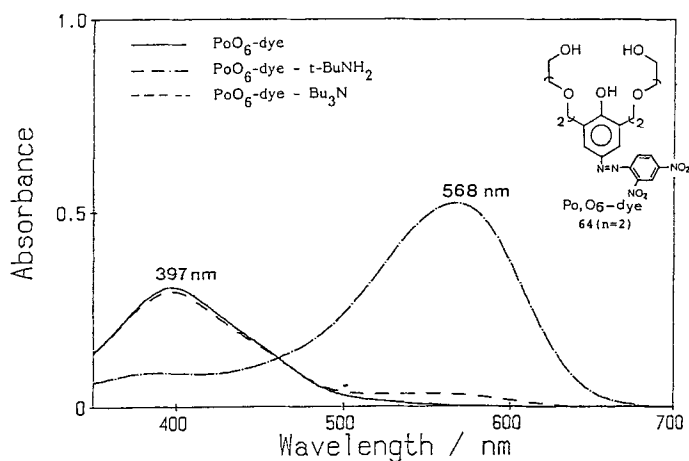
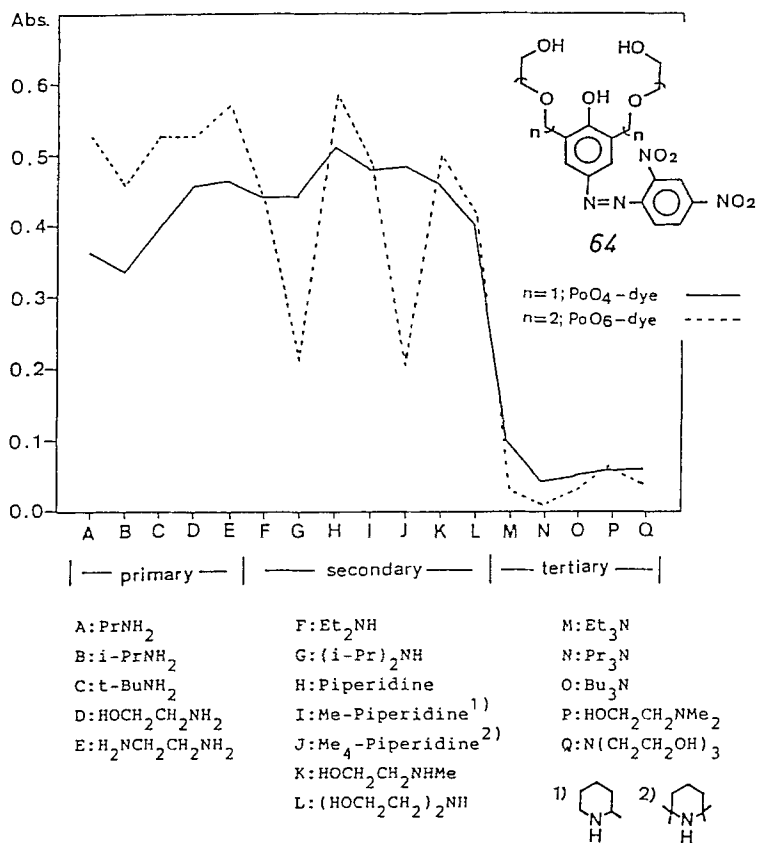

 Fig. 17. Visible spectra of PoO_6 (**64**, $n = 2$)-amine system in chloroform


Fig. 18. Absorbance at absorption maxima of podand dye-amine systems in chloroform

An azophenol crown including a pyridine unit, **66**, (Fig. 19) reacts with all of amines in acetonitrile to form ammonium phenolates. The absorption maxima of **66**-prim. amine systems appear in a region of 574–586 nm, which is definitely distinct from those of sec. and tert. amine systems (λ_{\max} 602–606 nm except for the dimethylamine system which gave 592 nm) as shown in Fig. 19. On the other hand, a dyed crown including an additional benzene unit, **65** (Fig. 19), reacts with various amines to make ammonium phenolates which show absorption maxima of nearly constant wavelength.

As a result of these findings, the combined use of the two azophenol hosts, PoO_4 (**64**, $n = 1$) and pyridine dye **66**, is able to discriminate the substitution pattern of amines, i.e. prim., sec. and tert. amines. In other words, when an unknown alkylamine is treated with PoO_4 in chloroform and the yellow solution remains unchanged, the amine should be a tert. amine (Fig. 20). On addition of pyridine dye **66** in chloroform to the unknown amine which shows color change with PoO_4 ,

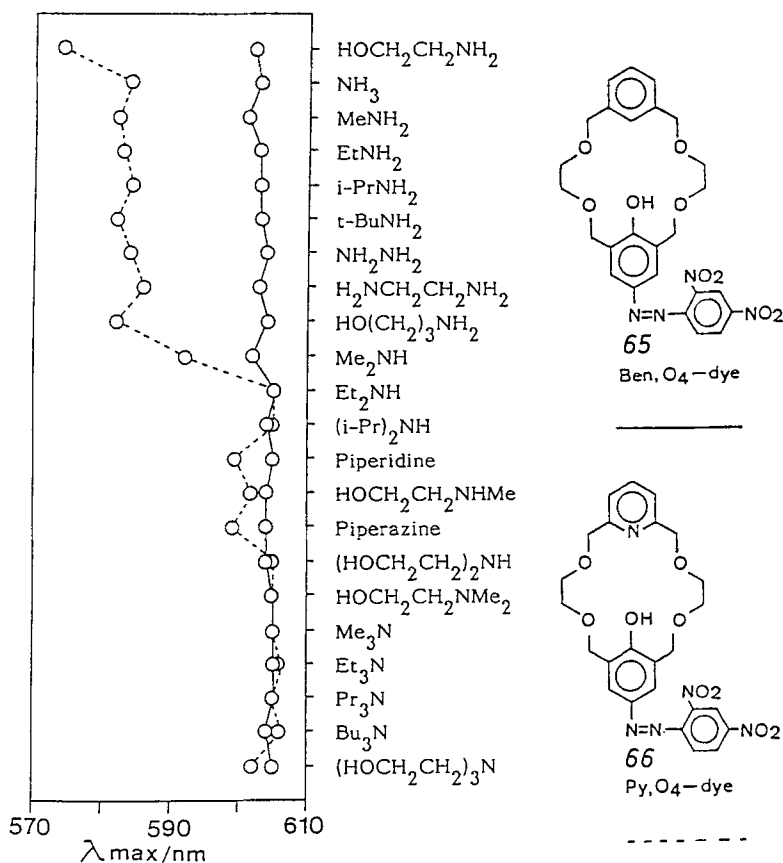


Fig. 19. Absorption maxima (in nm) of azophenol crown-amine systems in ethanol

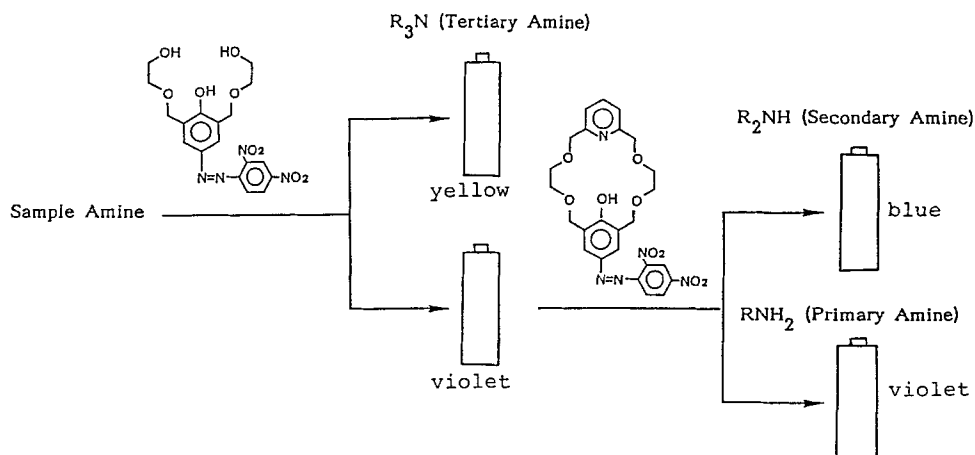


Fig. 20. Discrimination of the substitution pattern of amines by coloration with acerands

it should be demonstrated that the violet color of ammonium phenolate appears with prim. amine whereas the blue color demonstrates that a sec. amine is present in spite of bulky alkyl groups.

Acknowledgement. The authors wish to express their deep thanks to Profs. N. Kasai and Y. Kai, Osaka University, Prof. S. Akiyama and Dr. K. Nakashima, Nagasaki University, Dr. I. Tanigawa, Mr. K. Sugihara, Mr. S. Umeda, Dr. K. Hirose, Dr. Y. Ishizaki, and the other coworkers for their valuable contributions to this research. They are also indebted to the Ministry of Education, Science and Culture of Japan for a support by Grant-in-Aid for Scientific Research and to the Material Analytical Center of ISIR, Osaka University for spectral measurements and microanalysis.

4 References

1. For nomenclature, see Weber E (1987) *Top Curr Chem* 140: 1
2. Dix JP, Vögtle F (1987) *Chem Ber* 114: 638
3. Takagi M, Ueno K (1984) *Top Curr Chem* 121: 39
4. Pacey CE, Bubnis BP (1980) *Anal Lett* 13: 1085
5. Takagi M, Nakamura H, Ueno K (1977) *Anal Lett* 10: 1115
6. Nakamura H, Sakka H, Takagi M, Ueno K (1981) *Chem Lett* 1305
7. (a) Reviews: Misumi S, Kaneda T (1989) *J Incl Phenom* 7: 83; (1990) *Pure Appl Chem* 62: 493; (1990) *Mem Inst Sci Ind Res, Osaka University* 47: 29. (b) Kaneda T, Sugihara K, Kamiya H, Misumi S (1981) *Tetrahedron Lett* 22: 4407; Sugihara K, Kaneda T, Misumi S (1982) *Heterocycles* 18: 57
8. Sugihara K, Kamiya H, Yamaguchi M, Kaneda T, Misumi S (1981) *Tetrahedron Lett* 22: 1619
9. Uno T, Taniguchi H (1976) *Japan Analyst* 21: 76; Nakano S, Taniguchi H, Mikoshiba K (1973) *Yakugaku Zasshi* 93: 344
10. Tanigawa I, Tsuamoto K, Kaneda T, Misumi S (1984) *Tetrahedron Lett* 25: 5327
11. Knorr L, Harlein L (1909) *Chem Ber* 42: 3499; Bender HL, Farnham AG, Guyer JW, Apel FN, Gibb, Jr TB (1952) *Ind Eng Chem* 44: 1619

12. Jacobson P (1887) Chem Ber 20: 1895; Ohtsubo K, Okada Y, Zaitzu K, Kohashi K (1979) Anal Chem Acta 110: 335
13. Feutrill GL, Mirrington RN (1970) Tetrahedron Lett 1327
14. Cram DJ, Kaneda T, Helgeson RC, Lein GM (1979) J Am Chem Soc 101: 6752
15. Kaneda T, Umeda S, Tanigawa H, Misumi S, Kai Y, Mori H, Miki K, Kasai N (1985) J Am Chem Soc 107: 4802
16. Higuchi H, Kugimiya M, Otsubo T, Sakata Y, Misumi S (1983) Tetrahedron Lett 24: 2593
17. Cram DJ, Carmack RA, Helgeson RC (1988) J Am Chem Soc 110: 571
18. a) Nakashima K, Nakatsuji S, Akiyama S, Kaneda T, Misumi S (1982) Chem Lett 1781; b) Idem (1986) Chem Pharm Bull 34: 168
19. Nakashima K, Yamawaki Y, Nakatsuji S, Akiyama S, Kaneda T, Misumi S (1983) Chem Lett 1415
20. Marverick E, Grossenbacher L, Trueblood KN (1979) Acta Cryst B35: 2233
21. Cram DJ et al (1973) J Am Chem Soc 95: 3021; (1974) 96: 6762, 7100, 7367; (1976) 98: 3038
22. Kaneda T, Umeda S, Ishizaki Y, Kuo HS, Misumi S, Kai Y, Kanehisa N, Kasai N (1989) J Am Chem Soc 111: 1881
23. Kaneda T, Ishizaki Y, Misumi S, unpublished result
24. Kaneda T, Ishizaki Y, Misumi S (1988) J Am Chem Soc 110: 2970
25. The corresponding $N^+ - H - O^-$ hydrogen bond has been reported in ammonium saltexes of phenolic (2.690 Å) and benzoic (2.676 Å) crowns. The present saltex is the first example including both types of hydrogen bonding
26. Kaneda T, Hirose K, Misumi S (1989) J Am Chem Soc 111: 742

Genealogically Directed Synthesis: Starburst*/Cascade Dendrimers and Hyperbranched Structures

Donald A. Tomalia¹ and H. Dupont Durst²

¹ Department of Chemistry, Michigan Molecular Institute, 1910 West St. Andrews Road, Midland, Michigan 48640, USA

² Inhalation Toxicology Branch, Toxicology Division, Research Directorate, U.S. Army Chemical Research, Development and Engineering Center, ATTN: SMCCR-RST-I, Aberdeen Proving Ground, Maryland, 21010-5423, USA

Table of Contents

1 Introduction	197
2 Dimensional Hierarchy in Organic Matter	202
2.1 Critical Molecular Design Parameters (CMDPs)	202
2.1.1 Level of Organization: Picoscopic → Nanoscopic → Microscopic → Macroscopic Dimensions	204
2.1.2 Comparison of Synthetic with Evolutionary Strategies for Controlling Critical Molecular Design Parameters (CMDP's)	206
2.2 Why are Abiotic, Nanoscopic Structures Important?	208
2.3 Exoskeleton Structural Strategy: Buckminsterfullerenes/Carcerands/Metallo-Carbohedrenes	209
2.4 Endoskeleton Structural Strategy: Starburst/Cascade Dendrimers	211
2.5 "Magic Numbers" — Number Patterns Associated with the Hierarchy of Matter	212
2.6 Mimicking Macroscopic Branching Assemblies at the Molecular Level	215
3 Three Dimensional Molecular Level Branching Concepts — Historical Overview	217
4 Starburst/Cascade Topology and Branching Concept	220
4.1 Mathematical and Geometrical Precedence	220

* Trademark of Michigan Molecular Institute

4.2	Molecular-Level Perspective of Cubic Space	221
4.3	Structural Aspects	221
4.3.1	Dendrimer Branch-Cell Hierarchy	221
4.3.2	Dendrimer Branch-Cell Symmetry Properties	223
5	Dendron and Dendrimer Syntheses	224
5.1	Dendron Construction	227
5.1.1	Divergent Controlled Method	227
5.1.1.1	Poly(alkyleneimine)-Monodendrons (Vögtle Dendrons)	227
5.1.1.2	Poly(amidoamine)-(PAMAM-Starburst) Monodendrons	228
5.1.1.3	Poly(amide)-Monodendrons (Denkewalter Dendrons)	230
5.1.1.4	Poly(amidoalcohol)-Monodendrons (Arborols)	231
5.1.2	Divergent Uncontrolled Method	231
5.1.2.1	Poly(germanium perfluoroaryl)-Monodendrons	233
5.1.2.2	Poly(arylene)-Monodendrons	234
5.1.2.3	Poly(arylester)-Monodendrons	235
5.1.2.4	Poly(siloxysilane)-Monodendrons	237
5.1.2.5	Poly(imidazo[1,2-a][1,3,5]triazine)-Monodendrons	238
5.1.2.6	Poly(arylamide)-Monodendrons	238
5.1.2.7	Poly(haloalkylaryl ether)-Monodendrons	238
5.1.3	Convergent Controlled Method	238
5.1.3.1	Poly(arylalkylether)-Monodendrons	239
5.1.3.2	Poly(arylester)-Monodendrons	243
5.1.3.3	Poly(arylene)-Monodendrons	244
5.1.3.4	Poly(arylacetylenic)-Monodendrons	245
5.1.3.5	Poly(nucleotide: DNA/RNA)-Dendrons/Dendrimers	247
5.1.3.6	Poly(aryl/azacrown ether)-Monodendrons	249
5.2	Dendrimer Construction	249
5.2.1	Divergent Dendron/Divergent Anchor Core Method	249
5.2.1.1	Poly(amidoamine)-PAMAM-Dendrimers (Ester, Ether, Amide and Urethane Core Coupling)	249
5.2.2	Convergent Dendron/Divergent Anchor Core Method	249
5.2.2.1	Poly(arylester)-Dendrimers	250
5.2.2.2	Poly(arylene)-Dendrimers	251
5.2.2.3	Poly(arylalkyl ether)-Dendrimers	251
5.2.2.4	Poly(aryl/azacrown ether)-Dendrimers	254
5.2.3	Divergent Initiator Core Method	254
5.2.3.1	In Situ Construction of Branch Cells	254
5.2.3.2	Coupling of Pre-formed Branch Cell Reagents	261
6	Characterization of Dendrimers	272
6.1	Branching Ideality	274
6.2	Monodispersity vs Polydispersity	278
6.3	Dendrimer Topology, Branch-Cell Differentiation and Surfaces	279

6.3.1 Initiator Core and Core Cell Effects	279
6.3.2 Interior Development	280
6.3.3 Starburst (de Gennes) Dense Packing — A Critical Branched State?	280
7 Dendrimer Surface Reactions	285
7.1 Sterically Induced Stoichiometry (SIS) and Reaction Rates	286
7.2 Surface Chemistry	287
7.2.1 Protonation	287
7.2.2 Chelation to Endo- and Exo-Receptor Sites	288
7.2.3 Reactions with Electrophilic and Nucleophilic Reagents . .	290
8 Genealogical Aspects of Dendrimer Synthesis and Structure	292
9 Related Hyperbranched Systems — Comb-burst Dendrimers	298
10 Nanotechnology — Synthesis, Engineering and Applications of Nanoscopic Structures	301
11 Conclusions	307
12 References	307

"Molecular complexity can be used as an indicator of the frontiers of synthesis since it often causes failures which expose gaps in existing methodology. The realization of such limitations can stimulate the discovery of new chemistry and new ways of thinking about synthesis".

E. J. Corey

A paradigm shift is in progress which is directed at the mimicry of complex, highly sophisticated biomolecular architecture and phenomena. Mimicry of these targeted phenomena and structures is driven by the realization that these prototypes have been derived and perfected over billions of years in a dazzling molecular level effort to introduce and sustain life. In the past, natural product synthesis or *de novo* protein/polynucleic acid syntheses have been targeted to produce direct equivalency to various prototypes in biomolecular schemes. Unlike this objective, synthetic structures and strategies in this account will focus on the mimicry of architecture and phenomena found in life processes, utilizing less complex reagents and protocol to give novel products not found in Nature.

With this in mind we introduce a new organic synthesis strategy which we refer to as "*genealogically directed synthesis*" (GDS). Simply stated the central theme of this strategy utilizes mimicry of seven key phenomena/architectural criteria invoked by Nature to initiate and sustain life. These criteria deal with the flow and transfer of molecular level information through a chemical hierarchy, be it abiotic or biological.

A comparison of such GDS mimicry with certain targeted biomolecular phenomena/-structures is listed below:

<i>Targeted Biomolecular Phenomena/Structures</i>	<i>Genealogically Directed Synthetic Mimicry</i>
1. <i>Primary/stem genes</i>	: <i>Synthetic initiation/construction from an initiator core (i.e., a seed)</i>
2. <i>Genetic transcription/translation</i>	: <i>Templated dendrimer structural information (generation to generation)</i>
3. <i>Chronological polynucleotide/protein sequencing</i>	: <i>Time sequenced, step growth of "branch cells" and dendrimer structure</i>
4. <i>Self replication of DNA, cells, etc.</i>	: <i>Self replication of "branch cells" throughout dendrimer construction</i>
5. <i>Geometric growth of DNA, cells, etc. according to 2^G (G = generation)</i>	: <i>Structural proliferation of dendrimers with exponential amplification of "branch cells" and "surface functionality" as a function of generation</i>
6. <i>Iteration — structural building phases (i.e. generations)</i>	: <i>Iterated — dendrimer growth stages (generation to generation)</i>
7. <i>Malthusian-like packing behavior; Exponential proliferation in a limited space.</i>	: <i>Starburst/cascade dendrimer dense-packing; critical branching state, nanoscopic steric effects.</i>

These seven italicized criteria are integrated into a variety of (GDS) schemes thus allowing construction of hyperbranched macromolecular structures referred to as "dendrons" or "dendrimers". A direct consequence of this strategy is a systematic "molecular morphogenesis" [1] with an opportunity to control "*critical molecular design parameters*" (CMDP's); (i.e., size, shape, surface chemistry, topology and flexibility) as one advances with covalent connectivity from molecular reference points (seeds) of picoscopic/sub-nanoscope size (i.e., 0.01–1.0 nm) to precise macromolecular structures of nanoscopic dimensions (i.e., 1.0–100 nm) [2]. Genealogically directed synthesis offers a broad and versatile approach to the construction of precise, abiotic nanostructures with predictable sizes, shapes and surface chemistries.

1 Introduction

The descriptors “Starburst, dendrimers, arborols, cascade molecules, and hyper-branched” all describe specific geometric forms of structure. Recent progress in understanding the synthesis of these structures, allows us to introduce phenomenological terms which more accurately describe both the necessary sequential synthetic operations and the resulting molecular level information controlled during the course of these constructions. Hence we refer generically to synthetic strategies directed toward these structures as “*genealogically directed synthesis*” (GDS).

The term “genealogy” carries with its definition the very essence of life, origin, genes, lineage, ancestry, transfer of characteristics, pedigree, progeny; the science and study of family descent. All of these terms are usually associated with the biological world and are often used to describe the succession of biological products that may result in a proliferation from a source/origin or genesis (cf. Ref. 199).

Stoddart, in 1989 [3a–e], introduced the concept of *structure-directed synthesis* as a synthetic organic paradigm. As defined, structure-directed synthesis states that:

“There are inherently simple ways of making apparently complex unnatural products from appropriate substrates without the need for reagent control or catalysis. It implies that the required stereoelectronic information is pre-programmed into the substrates of a chemical reaction; this allows the efficient and precise spontaneous self-assembly of these ‘intelligent’ substrates, thus yielding either large molecules with completely defined superstructures and/or organized molecular assemblies composed of unique molecular components.”

Examples of *structure directed synthesis* abound in Stoddart’s extensive work [3a–e] on catenanes and rotaxanes, where “they are obtained as pretemplated products in the final step of the syntheses without the need for reagent control or external catalysis.” Nonenzymatic, “template-directed synthesis” on hairpin oligonucleotides (see Ref. 202) represent an analogous approach involving regiospecific sequencing on oligonucleotides (see Ref. 203)

It is in this spirit that we introduce the term *genealogical-directed synthesis* which is involved in the construction of dendrons and dendrimers. Genealogically directed strategies impose additional requirements to that of structural-directed synthesis. It incorporates into the concept, features which are remarkably similar to generational transfer of information in biological systems, yet these features all directly influence and determine the final synthetic structures that result from these strategies. The GDS strategies usually include the following features; which are illustrated in Fig. 1.

- A. Molecular Reference Point or Genesis in Dendron/Dendrimer Structure
- B. Chronological Sequencing of Dendron/Dendrimer Structure
- C. Radial Template Effect in Deriving Dendron/Dendrimer Structure
- D. Dendron/Dendrimer Structure Based on Geometric Progressions
- E. Self Replication of Branch Cells in Dendron/Dendrimer Structure
- F. Dense Packing of Dendron/Dendrimer Structure Caused by Tethering of Extended Covalent Connectivity
- G. Iterated-Dendron/Dendrimer Growth Stages

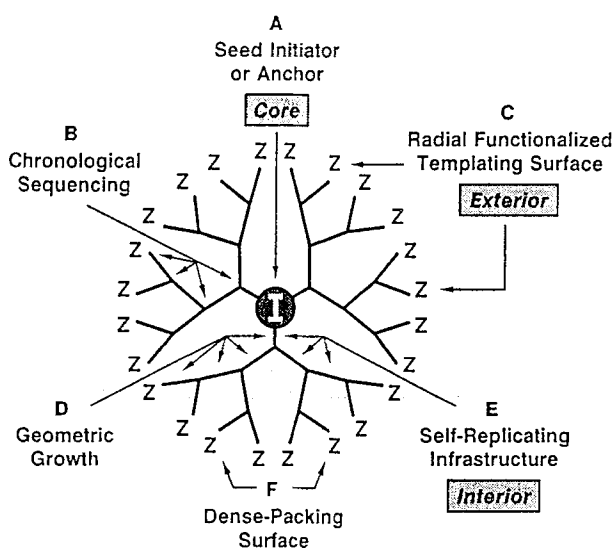


Fig. 1. Genealogical components involved in dendrimer synthesis

Genealogically directed synthesis (GDS) is therefore defined as those synthetic strategies which involve a sequence of chronological steps wherein critical intermediates involved in the sequence function as radial templates upon which subsequent structural components are introduced in some chronological order. As a consequence, structural errors and/or ideality are recorded as a function of chronological sequencing (i.e. generation). On the other hand, important molecular information can be chronologically designed into the final structure.

This paradigm recognizes that a "structure-directed" form of self assembly may be necessary, but not an exclusive component of a "genealogically directed" process. The essence of GDS implies inclusion of at least 7–8 characteristics. The inclusion of criteria such as A, B, D, E, F and G clearly differentiate GDS from the familiar "structure directed" model of Stoddart. These features, superimposed on templating effects in a synthesis protocol provides a combination of criteria which embodies the essence of genealogy in biological systems. However, we confine our usage of the term "genealogically directed synthesis" to abiotic systems.

Biological examples of this "information flow" strategy are ubiquitous throughout Nature. Some of the most fundamental examples in Nature involve DNA replication as well as DNA transcription to RNA followed by translation to produce proteins. More specifically, the biotic synthesis of DNA involves the following steps:

1. A germ line acting as a one-dimensional template and consisting of a double strand helix of nucleic acids (i.e. a "seed").
2. A time sequenced, homogeneous transfer of molecular information to new nucleic acid components giving rise to self replication in the form of two new daughter strands. This leads to *extramolecular* proliferation (transfer of information to successive generations).

3. Reiteration of this process produces progeny DNA strands that multiply according to the geometric progression: 2^G , where G = generation or number of reiterations (synthetic proliferation).

Recently, the discovery of “polymerase chain reactions” (PCR) by K. B. Mullis [4] in 1985 clearly demonstrates that “in vitro”, abiotic construction of DNA in a flask by these “genealogical directed synthesis” strategies is presently a routine and significant commercial process. These “genealogically directed syntheses” lead to an extramolecular proliferation of molecular level progeny.

Similarly, the successful “*in vitro*” synthesis and assembly of an active, virulent polio virus with empirical formula; $C_{332.682}H_{492.238}N_{98.245}O_{131.196}P_{7501}S_{2340}$ has recently been reported [5]. This synthesis was completed without the use of biological organisms, cells or membranes. Such an accomplishment suggests that the possibility of synthesizing extremely complex organic structures by completely abiotic methods is no longer idle speculation. Just as certain GDS criteria were involved in this experiment, so may it be expected that these criteria will be required and used in the eventual, abiotic synthesis of other complex molecules.

Using more simple reagents and protocols, the GDS strategy has been used to successfully produce over twenty different families of dendrons/dendrimers based on classical repeat (monomer) units and branch cell reagents. Interestingly, these GDS strategies have been used recently by Damha (see Refs. 121–123) to produce dendritic DNA and RNA type structures.

In this account we extend the definition to include the concept of systematic, synthetic proliferation within an abiotic molecular structure starting from an origin “core initiator” and continuing through a succession of well-defined, stoichiometric compounds and structures. In general, this synthetic strategy involves the following criteria:

1. The genesis of these constructions involves a reactive “seed” (initiator core) which may be an atom, simple molecule or polymeric core.
2. Homogeneous transfer of molecular information from the “seed” to successive concentric generations within the molecular structure via covalent connectivity and according to specified branching rules. This gives intramolecular proliferation according to a defined geometric progression.
3. Synthetic proliferations which involve sequential, radial templating to give concentric/radially assembled molecular organization with an infrastructure upon which functionalized surfaces may be displayed for subsequent radial templating and proliferation.

This article describes recent efforts to develop, characterize, and predict three-dimensional organizations of ordered, covalent connectivity around various picoscopic and sub-nanosopic reference points (i.e., initiator cores: sub-nanosopic (point-like) reactive organic molecules). The resulting covalent architecture can be systematically controlled by stepwise reiterative reaction sequences (generations) as described below:

1. Start with an initiator core (Ⓢ) possessing N_c reactive sites (e.g., $N_c = 3$ for ammonia).

2. Choose a reaction sequence so that each of the N_c reactive sites adds a reactant B_1 possessing new N_b ($N_b > 1$) reactive sites (thereby introducing multiplicity) to obtain dendrimer D_0 of generation 0. With ammonia as initiator core, a β -alanine derivative ($N_b = 2$) might be chosen as reactant.
3. Use protection/deprotection strategies to ensure that B_1 reacts with all reactive sites of (\odot), but that no reactions occur at the new reactive sites on B_1 of dendrimer D_0 .
4. Define an iterative sequence involving addition of new reactants B_{i+2} to the molecule D_i of generation i to form a new dendrimer D_{i+1} of generation $i + 1$.

In this fashion, it is possible to control the critical molecular design parameters (CMDPs, i.e., size, shape, topology, flexibility, and surface chemistry) and grow predictable, stoichiometric structures up to a self-limited dimension (generation) which is determined by N_c and N_b as well as by the dimensions of the structural components. Such space-filling, terminally functionalized molecular organizations have been coined *Starburst dendrimers* [2]. Two dimensional projections of such "molecular morphogenesis" [1] are as illustrated in Fig. 2.

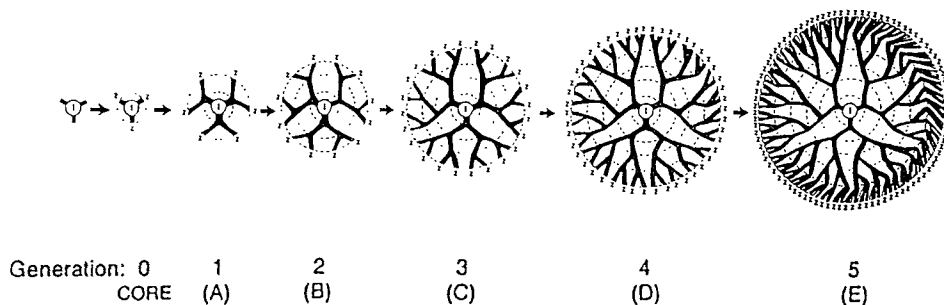


Fig. 2. Two dimensional projections of tridendron dendrimers with $N_c = 3$ and $N_b = 2$ as a function of generation: 0-5

The branching implicit in $N_b > 1$ leads to geometric growth in the number of atoms, repeat units and branch cells for each generation. For example, the number of monomers assembled in a dendrimer series with $N_c = 3$ and $N_b = 2$ is 3, 9, 21, 45, 93, 189, 381, 765, and 1533 for generations 0-8, respectively. Since the overall size can only grow linearly within the constraints of the covalent bonds and surface groups add on in an exponential fashion, these systems eventually become congested and change from an open, starfish-shaped molecule to a ball-shaped structure.

Starburst dendrimers, such as above, possess three major architectural components.

- I. an initiator core/core cell
- II. an interior
- III. an exterior (surface)

By definition or construction, these three components are interdependent and reflect a unique molecular genealogy. In the progression from the initiator-core

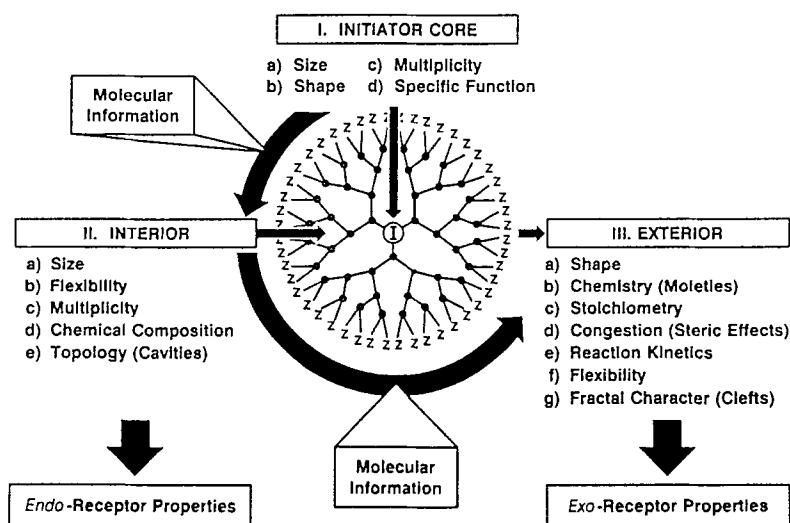


Fig. 3. Dendrimer architectural components as a function of molecular genealogy associated with CMDPs that contribute to *endo*- and *exo*-receptor properties

stage to an advanced dendrimer stage (e.g., generation 4.0 in Fig. 3), this molecular genealogy manifests itself in a variety of ways.

Just as ancestry and lineage can be traced in higher organisms, a molecular-level parallel is observed when these transformations are considered in the context of (1) stored molecular information at each dendrimer stage and (2) molecular information transferred (transcribed) to the progeny dendrimer surface at each transformation. For example, if the initiator core is thought of as a primitive abiotic gene [6–8] molecular details are sequentially transcribed and stored to produce interior and ultimately exterior (surface) features which are characteristic of that dendrimer family (phenotype).

It is in this fashion that such interior features as size, chemical composition, flexibility, and topology (cavities) are developed and manifested as stored molecular information, which may exhibit convergent, endo-recognition [1, 2, 9–11] or divergent exo-receptor properties [1]. Important biological analogies to these microenvironments may be found in the active binding sites of enzymes. The interior of a dendrimer consists of a scaffolding upon which surface properties such as shape, reactivity (functionality), stoichiometry, congestion, special kinetic features, flexibility, and “fractal” character (clefts) can be generated and controlled. This conjecture of fractal characteristic of the dendrimer surface has recently been confirmed. Direct evidence that these surfaces are highly clefted and indeed fractal has been described by Avnir et al. [12] who report a surface fractal dimension of $D = 2.41$. This fractal dimension is very similar to that of proteins. These surface features govern divergent recognition and as such may be expected to exhibit exo-receptor properties [1]. Interestingly, Lewis and Rees [13], using the same analysis, obtained a general value of $D = 2.4$ for the surfaces of various enzymes. Significant biological analogies include antibody-antigen inter-

faces involved in immunological recognition processes [14–16] as well as most protein-protein interactions and exo-recognition at membranes [17] or cell walls [13, 18].

2 Dimensional Hierarchy in Organic Matter

In order to comprehend the complex architectures obtainable from control of a few critical molecular design parameters, consider the following aspects of natural processes from the perspective of these parameters.

2.1 Critical Molecular Design Parameters (CMDPs)

The most plausible current models for the origin and evolution of life revolve around self-assembling molecular systems: “Order begot order from chaos” [19, 20]. These models have the following features:

1. Small picoscopic or sub-nanosopic molecules were assembled into more complex, “intelligent”, nanoscopic biomacromolecules and assemblies possessing ordered, retrievable molecular information for specialized functions.
2. Successful molecular evolution required very faithful transfer of molecular information possible only by exquisite molecular-level control of size, shape, *topology*, *flexibility*, and *surface chemistry* (CMDPs).

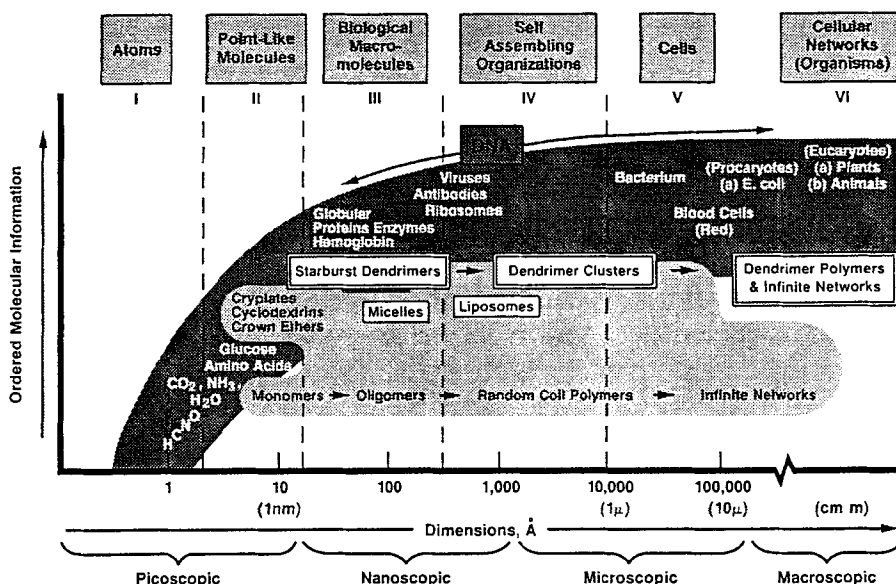


Fig. 4. Dimensional hierarchy of organic matter, assemblies, and cells involved in life processes

3. Control of CMDPs allowed the development of features and functions inherent in all living systems; namely, their ability to reproduce, to pass on genetic information (i.e., a prototype blueprint) to their progeny, to perform various specialized functions, and finally to grow to prespecified limited dimensions, usually with some characteristic morphology.

These very simple principles, together with Darwin's natural selection processes, have led to an incredibly rich array of life forms. Figure 4 illustrates a hierarchy which describes the advancement of atomic- and molecular-level entities (I, II) along various biological pathways to biomacromolecules (III) and higher-ordered molecules and assemblies such as IV–VI. Advancement from atoms (I) to picoscopic/sub-nanoscope molecules and finally to biocellular networks (VI) can generally be related to the amount of ordered molecular information possessed by the entities II–VI as well as to their relative dimensions. Superseding and in fact directing the assembly and function of many members of categories III–VI is the fundamental template of life, deoxyribonucleic acid (DNA). Because of its relatively high aspect ratio, DNA may be thought of as a one-dimensional template which transmits molecular information through a cascade of intermediates (e.g. *m*-, *t*-, and *r*RNAs, ribosomes, etc.). Ultimately, this genetic (molecular) information becomes translated into one-dimensional protein sequences whose size is determined by the length of the polypeptide chain, and whose shape, interior topology, and surfaces result from foldings and convolutions determined by the sequence and the side chains of the amino acids [21]. By this process the initial one-dimensional molecular information is ultimately translated into a three-dimensional message. Precise control of the CMDPs is the foundation upon which evolution chemistry has advanced and reached its present state of development. This information transfer can be visualized as illustrated in Fig. 5.

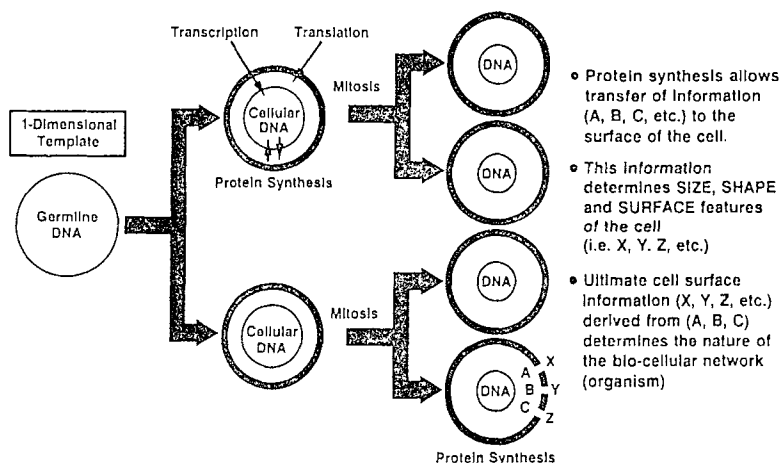


Fig. 5. Molecular information transfer from DNA to cellular protein during bio-cellular network development

2.1.1 Level of Organization: Picoscopic → Nanoscopic → Microscopic
→ Macroscopic Dimensions

In order to better appreciate the source and control of space in the following dimensional sequence (i.e., Picoscopic → Nanoscopic → Microscopic → Macroscopic) it is necessary to reflect back to fundamental atomic level aufbau (build-up). Figure 6 illustrates a hierarchy of elements that are critical to the repertoire of the organic chemist as well as the picoscopic/sub-nanoscopic building blocks and functional groups that can be derived from them.

The electrons are assembled around nuclei by simple charge neutralization to give energy minimized atomic particles. These discrete, quantized organizations of electrons require only seven radial shells or levels around the nuclei to define the entire periodic table. They are so precise, dependable and indestructible in chemical reactions that they are accepted as the fundamental building blocks of the universe. With these particles, Nature has successfully organized nuclei and electrons to control “atomic space” at the sub-picoscopic level (i.e., $< 10^{-12}$ m) as a function of size (atomic number), shape (bonding directionality), surface stickiness (valency) and flexibility (polarizability). These variables may, thus, be considered “critical atomic design parameters” — CADPs. These parameters may be visualized by the various shapes, valencies, and polarizabilities associated with carbon in its well-known sp , sp^2 , or sp^3 hybridized states. A wide variety of CADPs are recognizable for the other elements of the periodic table. Inherent properties of atoms dictated by the CADPs literally assure substantial control of critical molecular design parameters (CMDPs) as synthetic organic chemists assembled them into picoscopic/subnanoscopic molecular building blocks or functional group connectors as illustrated in Fig. 6. The endless combinations, arrangements and organizations which result as these atomic building blocks follow the rules imposed by their “critical atomic design parameters,” trace and define the growth and development of this “first chemistry set”, offered to us by Nature.

The 19th century was a rich period for the discovery of picoscopic/sub-nanoscopic building blocks and functional groups. Understanding of organic chemistry was markedly advanced by such leading chemists of the time such as August Kékulé (1829–1896), Emil Erlenmeyer (1825–1909) and Alexander Crum Brown (1838–1922) who defined sub-nanoscopic building blocks such as benzene (1865 — aromatics), acetylene (1862 — triple bonds) and ethylene (1864 — double bonds), respectively. Familiar functional groups (e.g., $-\text{CO}_2\text{H}$, $-\text{NO}_2$, $-\text{SO}_3\text{H}$, $-\text{OH}$, $-\text{NH}_2$, etc.), referred to as ‘derived radicals’, provided the stickiness (valency) for developing covalent connectivity between these hydrocarbon building blocks. Such concepts and ideas were earlier advanced by a variety of notable European scientists such as Jöns Jacob Berzelius (1779 to 1848), Justus von Liebig (1803–1873), Jean B. A. Dumas (1800–1884), Auguste Laurent (1807–1853) and others. The millions of combinations and permutations provided by these assemblies since the days of Wöhler (1828) have given humanity a wealth of beneficial medicinal, agricultural, and pesticide products as well as monomers for synthetic fibers, rubbers, composites and other structural materials.

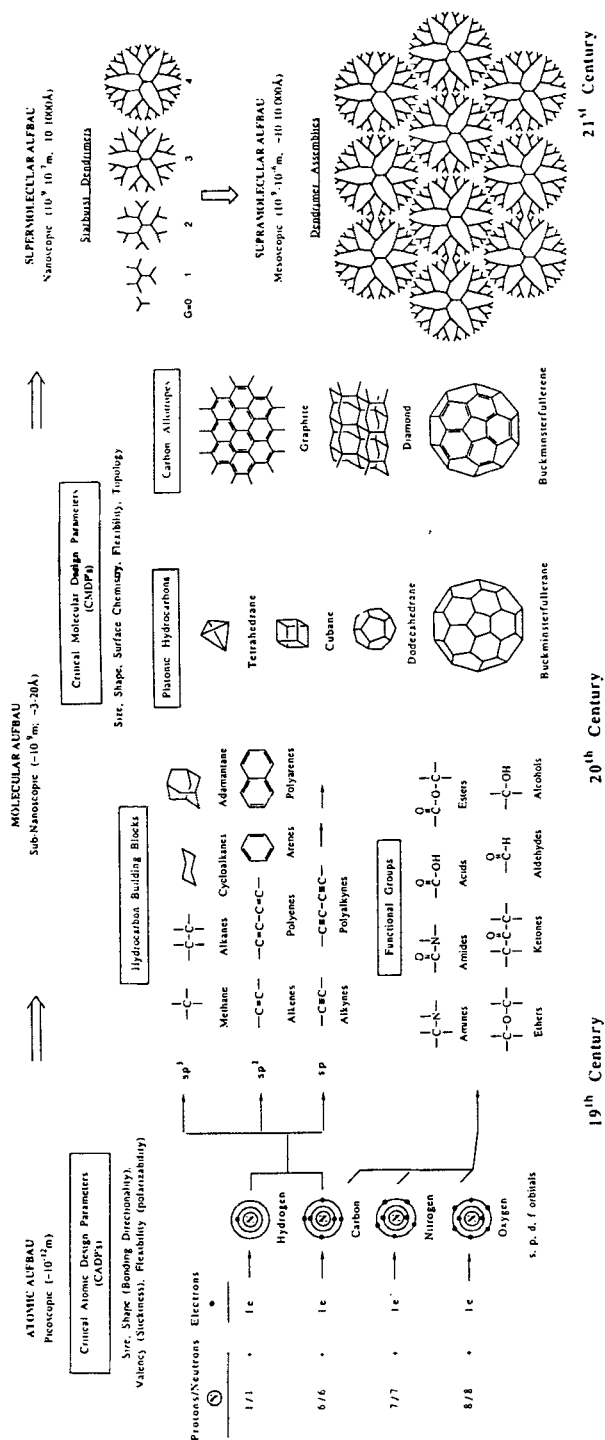


Fig. 6. Critical atomic design parameters (CADPs) and critical molecular design parameters (CMDPs) involved in atomic, molecular, supramolecular and supramolecular aufbau leading to natural and un-natural products

2.1.2 Comparison of Synthetic with Evolutionary Strategies for Controlling Critical Molecular Design Parameters (CMDPs)

Over the last 150 years, organic chemists have learned to synthesize highly complex compounds by exploring options for precisely controlling the CMDPs of point-like organic molecules (category II, Fig. 4). Recent attention has been directed toward the synthesis of larger, yet structurally well defined macromolecules. For example, such molecules have been the subject of intense interest over the past 20 years as “endo-receptors” for the examination of guest-host relationships. Their design has been derived largely from macrocyclic [1, 9–11, 22, 23] or macropolycyclic [23] structures as well as from acyclic architecture (podands) [9]. The selectivity achieved by such endo-supramolecular chemistry [1, 9–11, 24] has been compared with that of binding substrates in the cavities (active sites) of larger proteins (enzymes) [25]. A very extensive overview of this field has been published by Vögtle [26] and Gokel [27]. Currently, these synthetic constructions depend largely on low-aspect-ratio, three-dimensional architecture for their endo-receptor design. Most notable are the cavitands and carcerands, whose interiors are large enough to enclose covalent guest molecules. They have been referred to recently by Cram in his Nobel lecture [11] as “synthetic molecular cells”.

In contrast, biological protein synthesis involving one-dimensional sequences of amino acids is the fundamental theme of evolution chemistry in the construction of biomacromolecules (category III, Fig. 4). This one-dimensional polymerization strategy, which involves specific sequences of just 20 naturally occurring amino acids, leads to proteins with an enormous variety of possible shapes and sizes. Control of their chemical reactivity, provided by the juxtaposition of electrostatic and hydrogen-bonding “scenarios” at their surfaces, governs the CMDPs of living systems. By this means, very “intelligent”, information-laden protein structures (i.e. bio-morphic/receptor molecules) have evolved to fulfill intricate molecule-recognition roles in biological membranes. In other instances, these CMDPs have been used to create microdomains (cavities) suitable for the amazingly selective substrate binding and catalytic chemical transformation carried out by enzymes. The cavity and cleft dimensions required for these important life processes generally seem to necessitate globular proteins with around 300 amino-acid units and molecular dimensions of the order of 25–200 Å in order to provide adequate scaffolding and tertiary-structure development [28].

On the other hand, a completely different strategy is used for constructing biological compartments and assemblies such as micelles, liposomes, viruses, protein coats, and biological cells. Here the game plan is organization and aggregation of either point-like molecules or biomacromolecules, which involve *self-assembly* processes. The primary function and role of these entities is the very precise control of size, shape, topology, flexibility, and surface chemistry (CMDPs) in various life processes. These self-assembling systems produce precise three-dimensional structures by use of such weaker interactions as van der Waals forces and hydrophobic associations.

Since the days of Staudinger [29] and the birth of polymer science early in this century, vast arrays of oligomers and high-molar-mass synthetic polymers have been produced with coil dimensions well over 10 Å [30]. Although many advances

have been made in defining classical polymerizations as a function of types, mechanisms, and processes, substantial progress will be necessary to approach the control of CMDPs that Mother Nature has mastered in the production of biomacromolecules and assemblies (categories III and IV, Fig. 4). Considering only size, for example, most globular proteins are obtained as monodisperse products with $M_w/M_n = 1.00$, whereas, classical random coil polymers, are usually polydisperse with $M_w/M_n \gg 1.00$. It is only recently that significant progress has been made in the production of such monodisperse synthetic polymer systems [31, 32] without the use of protection/deprotection strategies. This progress has been accomplished primarily by the use of “living polymerization techniques” [33]. At best, these methods offer reproducible control of one-dimensional lengths but not necessarily control over such ultimate three-dimensional features as shape, surface chemistry, or topology.

Without doubt, the solid-phase peptide synthesis (Merrifield method) remains a preferred method for controlling all five critical molecular design parameters (size, shape, topology, flexibility, and surface chemistry) by precisely producing amino-acid sequences in a stepwise fashion. The scope and limitations of this approach have been reviewed [34] and widely recognized [35]. These solid-phase syntheses with protection/deprotection procedures are used routinely to produce numerous, previously unattainable [36], polypeptides and polynucleotides. One of the ultimate synthetic efforts in the control of CMDPs was the total synthesis by Khorana et al. [37] of a DNA molecule in the 1960s.

Despite these accomplishments, no synthetic strategy has yet approached the diversity and precise molecular morphogenesis that Nature has mastered in the successful evolutionary development from simple picoscopic organic molecules to more complex biomacromolecules and assemblies. It is in this quest that we sought not necessarily total solutions, but at least new synthetic strategies to produce nanoscopic abiotic structural mimics of category III and IV type architecture. The development of GDS strategies has led to new insights into the molecular-level control of size, shape, topology, flexibility, and surface chemistry, and has demonstrated some remarkable parallels between biological systems and information transfer in dendrimers.

As synthetic organic chemists seek new challenges and objectives, the targeted structures become more complex and larger in dimension. Multi-stem, convergent synthesis, with multi-site chiral control were pioneered by such chemists as Woodward, Corey, Eschenmoser, Prelog and others during the last half of this century [38]. In fact, synthesis of the complex, precise macromolecular, sub-nanosopic structure (i.e., palytoxin, see Figure 7) by Kishi [39a–c] may be viewed as “the Mount Everest” for synthetic chemists.

“Synthetic organic chemists fall into two groups: those who prepare old naturally occurring compounds and those who prepare new compounds. The synthetic targets of the former group are provided by the evolutionary chemistry of Nature. The synthetic targets of the latter group are designed by the investigator”.

D. J. Cram in *Cyclophanes*; P. M. Keehn and S. M. Rosenfield, eds.; Academic Press, New York, (1983) Vol. I, p 14.

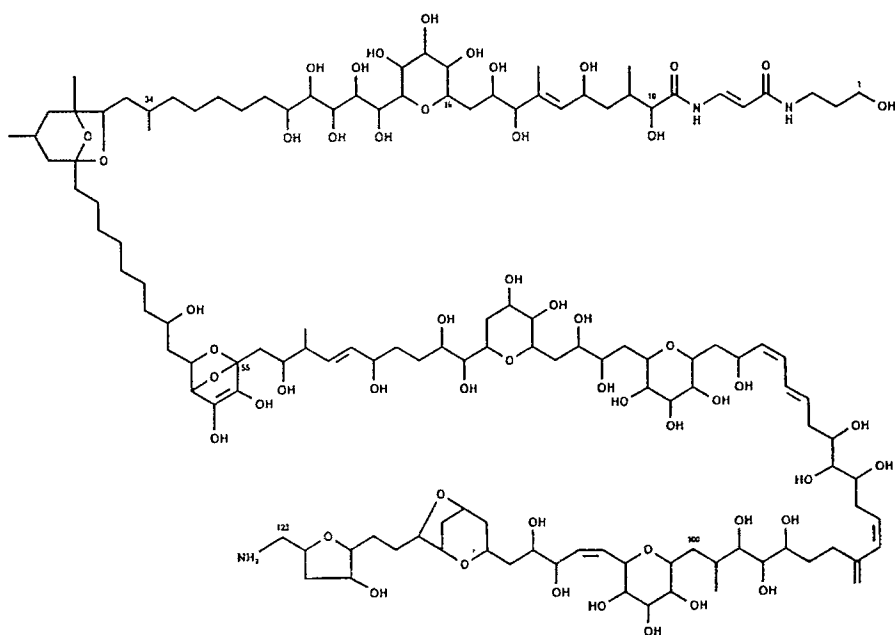


Fig. 7. Gross structure of palytoxin

Recently attention has turned to concepts and strategies leading to new organizations of matter, both supramolecular and supermolecular, based on “directed synthesis”, “molecular self assembly”, “molecular recognition”, “supramolecular chemistry”, “higher dimensional (nanoscopic) building blocks” (e.g., Buckminsterfullerene — a new form of carbon, $\approx 8\text{--}9\text{ \AA}$ in diameter). Where are we today relative to the development of our “first chemistry set” derived from picoscopic building blocks? Questions and comments are numerous concerning this issue. Is it time to consider new possibilities? How can this be done? Why not mimic the “aufbau” principles of our first chemistry set — but at the molecular level! Can we mimic these so-called “critical atomic design parameters (CADPs)” with molecular level aufbau components? Can we synthesize new unimolecular nanoscopic entities over which we can control “critical molecular design parameters” (CMDPs)?

2.2 Why are Abiotic, Nanoscopic Structures Important?

First, essentially all the important biological macromolecules and self-assembling organizations illustrated in categories II and III (Fig. 4) are nanoscopic in dimension. The ability to synthesize robust mimics of these prototypes, either by supermolecular construction or supramolecular assembly, will allow deeper insights into the molecular level roles of these entities in various biological processes. Mimicry of gross properties, such as dimensionality, surface area, morphology and topology are just a few parameters which may be examined.

Secondly, the geometric closure of nanoscopic space, either by endo-skeletal or exo-skeletal constructions, creates new surfaces and enclosures upon and where in reactions may be examined. Turro, Barton and Tomalia [40] refer to these domains, whether evolving from micelles, dendrimers or DNA, as “*nano-reactors*”. Cram has described such contained space in his carcerands as “new phases of matter” [41]. Miller et al. [42] have used related linear nanostructures as “molecular rulers” which are observable as single molecular species by transmission electron microscope. On the other hand, Amit et al. [16]; have shown that important biological events, such as the formation of antigen-antibody complexes involve nanoscopic areas of $600\text{--}1000\text{ \AA}^2$ ($6\text{--}10\text{ nm}^2$).

It is apparent that these new structured clefts, struts, surfaces and enclosures in the 1–100 nm size range will have important roles as quantum confinement domains, receptors, containers, carriers, catalytic surfaces or scaffolding for molecular recognition in the emerging area of nanotechnology (see Ref. 183).

2.3 Exoskeleton Structural Strategy: Buckminsterfullerenes/Carcerands/Metallo-Carbohedrenes

In the mid-1980s, virtually simultaneous reports on two new precise molecular level constructions of sub-nanoscopic/nanoscopic size appeared in the literature. In 1984 we (DAT) reported the synthesis, isolation and characterization of the first iterated series of “Starburst/cascade” dendrimers based on genealogical synthesis [2, 77–83]. The following year Smalley, Curl and Kroto described the first observation of a 60-carbon fullerene by mass spectroscopy [43a]. More recently the synthesis of buckminsterfullerene has been achieved by physicists at the Max Planck Institute in Heidelberg [44] to give macroscopic quantities of the third allotropic and first molecular form of carbon, named after Buckminster Fuller. Similarities between these two constructions were not initially apparent, but in retrospect they deserve comment in so far as they each involve molecular level synthesis leading to “*closed geometrical architecture*”.

Work by Diederich and others [46] has shown that larger, all carbon members of this series such as C_{70} , $C_{76/78}$, C_{84} and C_{94} are possible and open up vast new visions for organic and organometallic chemistry. It would seem that as benzene is the parent compound in the aromatic field, the C_{60} buckminsterfullerene will be the parent of this “fulleride” family. As in the benzenoid family, a set of rules are needed to predict where to look for the other members of this family. Recent work from Great Britain [47] proposed a simple set of rules for predicting the most stable, and hence the most likely, structures for any number of carbon atoms “fullerenes”. The resulting number patterns associated with these structures have been referred to as “magic numbers”. They are discussed in Sect. 2.5 and compared with analogous “magic numbers” (geometric progressions) associated with the endo-skeleton dendrimer structures.

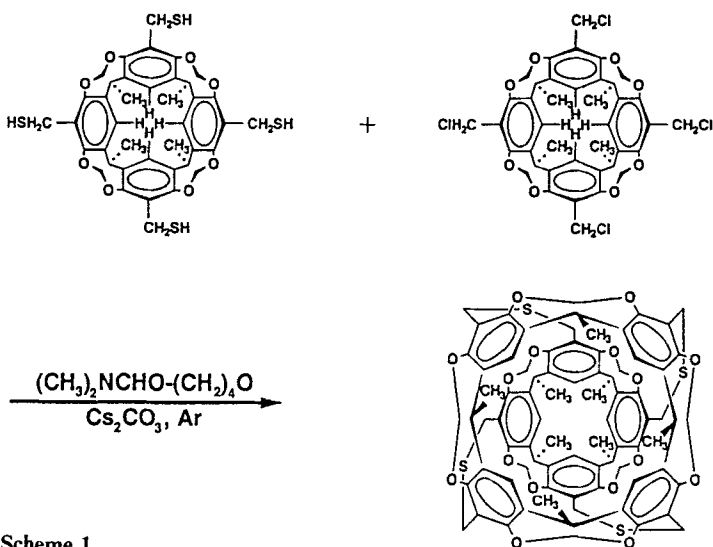
In the case of “buckminsterfullerene”, a “magic number” of sixty carbons (i.e., 12-pentagons and 20 hexagons) become organized to form the outside surface of a hollow sphere (i.e., the exoskeleton) with sub-nanoscopic dimensions that

approach 10 Å. These hollow spheres are self-supporting and require no infrastructure to support their surfaces. Since the discovery of the fullerenes, H. W. Kroto co-discoverer, has predicted the advent of a so-called “round chemistry” in which fullerenes become established as fundamental, new building blocks in organic chemistry [43b]. Recent efforts by Wudl, Diederich, Whetten, Hawkins and others directed toward this objective are extensively reviewed in an important series of papers [45].

Incarceration of metals varying from potassium to heavy atoms such as lanthanum or uranium within the fullerenes have given new classes of metallofullerenes. These materials clearly demonstrate the exoskeleton required for these encapsulations [48a, b]. Conversely metals may also be attached to the exterior of the fullerene cage [48c] to give a distinctly different class of metal complexes.

Examination of the vertical column entitled Platonic hydrocarbon in Fig. 6 illustrates a dimensional progression of exoskeleton structures beginning with tetrahedrane \rightarrow cubane \rightarrow dodecahedrane \rightarrow buckminsterfullerene. This progression shows how space may be incarcerated from the sub-nanoscopic to the nanoscopic level by geometric closure with exoskeleton structures.

Cram [49a] elaborated further on this concept by enclosing space in his carcerands and hemicarcerands (See Scheme 1) to form a “new inner phase” which he has referred to as “a new phase of matter”. In contrast to the hollow space found inside clathrates and zeolites for instance, the cages of these molecules are independent of the form and physical state. For example, hemicarcerands and related supramolecular systems (i.e. hemicarceplexes) prevail in the solid, liquid, or gas phase. This characteristic-hollow space, the inside surface — is maintained across all phase transitions. The inner surfaces and spaces of these systems are not manifested as bulk properties. An extensive review on the synthesis of these materials has been published recently [205].



Scheme 1

Very recently, exoskeletal organometallic clusters referred to as *metallo-carbohedrenes* have been reported by A. Welford Castleman, Jr. and coworkers at Penn State University [49b–e]. The new compositions correspond to the empirical formula, M_8C_{12} , where M is Ti, V, Zr or Hf. Mono-cage like pentagonal dodecahedron structures are proposed to account for the extraordinary stability of the most simple member in each series. Metal-carbon clusters are produced through plasma reactions between the respective metals and various small hydrocarbons [49b–d]. The neutral clusters are formed into a molecular beam which are then ionized by a laser and analyzed by a reflectron, time of flight (TOF) mass spectrometer.

These *exoskeleton structures* should now be compared with the *endoskeleton structures* offered by the Starburst/cascade dendrimer constructions.

2.4 Endoskeleton Structural Strategy: Starburst/Cascade Dendrimers

In contrast, Starburst dendrimer structures appear more like biological cells [50] in that they possess cytoskeleton-like infrastructure upon which the surface groups reside. Iteration of these endoskeletal infrastructures and surfaces proceed according to prescribed branching rules. They are consistent with “magic numbers” related to the multiplicity of the initiator core (N_c), the multiplicity of the branch cells (N_b) and the number of reiterations (generations, G). Ultimately these reiterations lead to a so-call “Starburst dense-packed generation” as described by de Gennes [85]. At this point ideal branching can no longer occur due to steric congestion. This steric congestion ultimately produces a closed geometric structure with surface functionality that can no longer follow prescribed branching rules. Two-dimensional projections of dendrimer families, as a function of N_c and N_b , are illustrated in Fig. 8.

Just as “magic numbers” have been evolved for the prediction of new fullerene families [47] and metallo-carbohedrenes [49b–d], so can similar predictions be

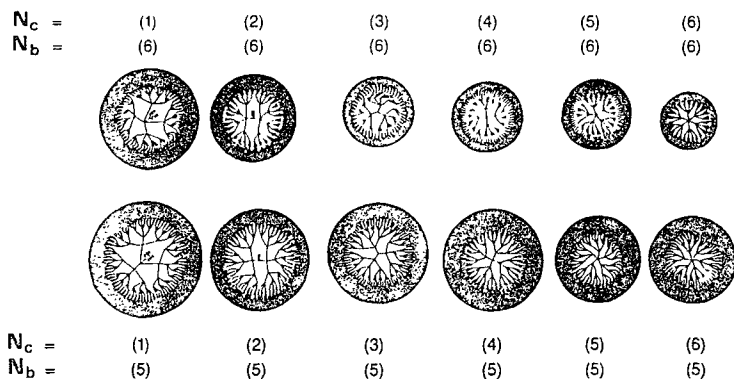


Fig. 8. Two-dimensional projections of dendrimer families as a function of core multiplicity (N_c) and branch cell multiplicity (N_b)

made about new dendrimer families. Both the initiator-core multiplicity N_c and the branch-juncture multiplicity N_b directly affect the number of terminal groups, the number of repeating units (branch segments), and the molar mass of the dendrimers as a function of generation. These values can be predicted mathematically for ideal systems according to the following expressions: where; M_c , M_{RU} or M_{BC} , and M_t are the molar masses of the initiator core, repeat units or branch cells, and terminal units, respectively. A general structural notation for a homogeneous dendrimer with core multiplicity N_c and branch-juncture multiplicity N_b may be represented in empirical form as follows:

$$\text{Number of dendrimer terminal groups } z = N_c N_b^G$$

$$\begin{array}{l} \text{Number of dendrimer} \\ \text{repeat units} \\ \text{(degree of polymerization)} \end{array} \quad N_{RU} = N_c \left(\frac{N_b^{G+1} - 1}{N_b - 1} \right)$$

$$\begin{array}{l} \text{Number of} \\ \text{dendrimer} \\ \text{branch cells} \end{array} \quad N_{BC} = N_c \left(\frac{N_b^G - 1}{N_b - 1} \right)$$

$$\begin{array}{l} \text{Theoretical molar mass} \\ \text{of dendrimer} \end{array} \quad M = M_c + N_c \left[M_{RU} \left(\frac{N_b^{G+1} - 1}{N_b - 1} \right) + M_t N_b^{G+1} \right]$$

$$M = M_c + N_c \left[M_{BC} \left(\frac{N_b^G - 1}{N_b - 1} \right) + M_t N_b^G \right]$$

From a molecular perspective, dendrimers are simply assemblies of dendrons attached to a common initiator core, (①), or a variety of initiator cores in the same molecule. Beginning with, (①), these branched assemblies are developed by growing dendrons in a stepwise, radial manner according to multiplicity rules. Figure 8 shows an example of dendrimer growth for various N_c , N_b multiplicities. A wide range of multiplicities N_c are possible, varying from mono- to polydendron assemblies. Both the initiator core multiplicity (N_c) and the branch cell multiplicity (N_b) dramatically influence the CMDP's as well as determine the (de Gennes) dense packed stage [85] of the dendrimer.

2.5 “Magic Numbers” — Number Patterns Associated with the Hierarchy of Matter

In systems that are constructed from discrete components under well defined rules, geometric or arithmetic patterns usually develop. These may involve various symmetries or repetitive structures, with or without scaling, or regular sequences of numbers describing quantities of the components. In addition to being aesthetically pleasing, these patterns serve both as memory aids and predictive tools for the understanding of ordered systems.

For example, the rules involved in the pairing of electrons and the symmetry of molecular orbitals lead to patterns of what were initially recognized as unusually

stable materials, namely aromatic compounds. The inertness of these materials appears to depend on their having the right number of valence electrons for all the valence electrons to move freely around the circles of atoms. Of course, Hückel did not derive his well known $4n + 2$ p-electron rule for aromaticity via molecular orbital theory. He studied the patterns of molecular formulae of known aromatics to infer the relationship. Application of the relationship led to the discovery of more aromatic materials with larger or smaller rings than the common benzenoid aromatics, such as [18]-annulene, or with charges that complete the aromaticity, such as cyclopentadienyl anion and cycloheptatrienyl cation.

This type of thought process has been extended into the realm of supermolecular chemistry with the term "magic number", which has been used to describe the patterns of abundant fullerene species. The carbon clusters formed in soot from combustion or electric arc processes have weights corresponding to even multiples of 12, the atomic weight of carbon. Under appropriate conditions, the formation of certain molecular weight species are favored, most notably those corresponding to C_{60} and C_{70} , indicating an enhanced stability relative to other molecular weights. Spherical and ellipsoidal structures were proposed for these materials, since these would maximize orbital overlap as in the aromatic compounds and confirmation of the proposed structures soon followed. Examination of potential extensions of these structures has led to the derivation of three series of magic numbers, corresponding to larger spheres and cylinders with $60 + 6k$, $70 + 30k$, or $84 + 36k$ (k is a integer) carbon atoms. A species consisting of 84 carbon atoms has since been identified. Thus, the predictive powers of these magic numbers have been demonstrated.

Magic clusters, those with magic numbers of atoms or molecules, derive their enchantment from the fact that they are chemically more stable or inert than their immediate neighbors. The cause of the stability – and the magic number itself – is unique to each cluster genre [49e].

Extraordinary structural growth patterns have been found for metallo-carbohedrenes in the series of Zr_mC_n , in which multicage structures are formed [49d]. Experimental evidence shows that the first cage closes at Zr_8C_{12} . Unexpectedly, further cluster growth does not lead to the enlargement of the cage size as is the case for pure carbon clusters or water clusters. Instead, multicage structures are developed to give a double cage at $Zr_{13}C_{22}$ and $Zr_{14}C_{21/23}$, a triple cage at $Zr_{18}C_{29}$ and a quadruple cage at $Zr_{22}C_{35}$. This feature distinguishes the general class of metallo-carbohedrenes from the well known metal doped fullerenes. In the mass spectra of these metallo-carbohedrenes, "magic number" type intensity groups are observed which display a truncation of intensity levels, as a function of the "magic number" associated with the mono-, di-, triple- and quadruple-cage structures. These truncated intensity patterns ("magic numbers") are completely analogous to those observed in the mass spectra of Starburst PAMAM dendrimers ($G = 0-4$) (Ref. 169), (see Sect. 6.1).

The sequences of electron orbital filling of the elements is another example of patterns resulting from the application of well-defined rules, namely, the principles of quantum mechanics. It is well recognized that organization patterns for electrons in the elements of the periodic table are defined with such "magic numbers" as

principal quantum numbers (i.e., $n = 1, 2, 3, 4$) associated with saturated electron shells leading to the stable inert gas configuration (i.e. 2, 8, 18, 32, etc). As an operational definition, it is unnecessary to know precisely why these magic numbers exist. Chemists of the 19th and early 20th centuries recognized these patterns and used them to predict reaction processes and elemental properties. Theoretical explanation of the precise nature of these "atomic magic numbers" had to wait the development of quantum theory in the 1920–1930s.

Noting the similarities of the shell construction and the mathematical predictability of occupancy in shell filling in the preparation of dendrimers and the Aufbau in atoms has led to the recognition of parallels between the two systems and the development of the parallel concepts of "critical atomic design parameters" (CADPs) and "critical molecular design parameters" (CMDPs). Just as the mathematical formalisms of quantum mechanics set the maximum number of electrons that may reside in a given shell by defining the number of orthogonal orbitals for a given shell, the geometric progressions that result from the application of core and branch multiplicities in dendrimers set the maximum number of repeat units and branch cells that may reside in a given dendrimer shell. Thus, atomic orbitals fill with electrons in the sequence, 2, 8, 18, 32, etc., and the shells of dendrimers (with core multiplicity = 3 and branch multiplicity = 2) fill with repeat units in the sequence, 3, 6, 12, 24, etc.

It should be emphasized that, in each case, the mathematics determine maximum occupancy of respective shells. In atoms, partially filled shells have unfilled orbitals that will readily accept electrons, which become the basis for chemical reactions, such as ionization or bonding. A filled shell is seen as a satisfied valency which requires more extreme conditions to elicit further chemical reactivity. Similarly, unfilled shells in dendrimers possess reactive sites that may be further modified under conditions similar to those used to construct the dendrimer. Filled shells in dendrimers require more vigorous conditions for further modifications.

In some cases, a further parallel can be drawn between the order of filling of electron orbitals and the order of filling a dendrimer shell. In atomic Aufbau, electrons are placed in each *p* or *d* orbital until each orbital contains one electron before any pairing of electrons within the orbitals takes place. In the preparation of poly(amidoamine) dendrimers, there is a significant difference in the rates of the first and second alkylation of a given amine such that most of the primary amines are converted to secondary amines before the conversion to tertiary amines becomes the predominant process. This can be viewed as analogous to the orbital filling and can, within the limits of the selectivity of the alkylation, be used in the control of dendrimer "valence".

One limitation of this analogy lies in the energetics of shell filling. The relative energies of electrons in their orbitals vary greatly from the interior shells to exterior shells of an atom so that a vacant interior orbital will be filled by transfer of an electron from a higher shell. In dendrimers, however, the energy differences between the shells are small enough that there is little driving force to cause an analogous rearrangement. The result is that an unfilled shell has a permanent effect on the further elaboration of the dendrimer. The only means for filling the vacant interior sites is by addition of new, free monomer during the building of a subsequent

shell. While this does fill the original vacancy, these new monomers may not be immediately available for addition of the next layer and, therefore, the subsequent shell may not be completed to the full, theoretical capacity. These defects may result in a distribution of molecular weights that reflect the history, (the *genealogy*), of the synthesis. High efficiency at every step gives a distribution that approaches the “magic number” limit. A low efficiency at any step will move the distribution away from the theoretical limit to some lower molecular weight “mutant (defect laden) population”.

Experimental evidence for the efficiency of shell filling in dendrimer synthesis has been found in the mass spectra of these materials. For example, the mass spectrum of a fourth generation poly(amidoamine) dendrimer has shown a narrow spread of masses, starting at the theoretical maximum, 10.632 daltons, and decreasing through a series of masses corresponding to structures lacking integral multiples of repeat units. Comparison of the relative abundances of the various species with a statistical model of dendrimer growth, including the filling of the vacancies described above, implies that each cycle of the dendrimer synthesis incorporates between 97 and 98 percent of the maximum possible number of repeat units (Ref. 169) (see Sect. 6.1).

2.6 Mimicking Macroscopic Branching Assemblies at the Molecular Level

The belief that molecular-level prototypes can be constructed to imitate familiar macroscopic objects has been the inspiration for many intensive and successful synthetic efforts [51–57]. Molecular-level construction of Platonic solids such as the tetrahedron [54], the cube [55], and the dodecahedron [56], as well as non-Euclidian objects such as molecular knots [57a], Möbius strips [57b], and even molecular machinery [57d] exemplifies such efforts (cf. Chapter 5 of this book). Synthetic organic chemists have developed a rich legacy in this area as described in more detail by Nickon and Silversmith [57c].

Inspired by the beauty and efficiency with which Nature “controls” macroscopic three-dimensional space as seen in the branching networks of trees [58], coral [59], and physiological structures [60, 61], one of us (D.A.T.) sought to mimic such branched assemblies at the molecular level. Analysis of parameters involved in synthetically mimicking such branching included the following hypothetical steps (see Fig. 9):

1. Construction and control of branch cell segment lengths l .
2. Control and development of branch cell multiplicities (N_b) and core multiplicities (N_c).
3. Development of a reiterative growth process which would allow concentric, radial construction of branches upon branches around an initiator core ($\textcircled{1}$), which specifies the direction of growth.

The branching angles $\angle a$ are determined by the chemical nature (geometry) of the branch juncture, whereas the rotational angles $\angle b$ are influenced by secondary-structure parameters such as steric effects and hydrogen bonding.

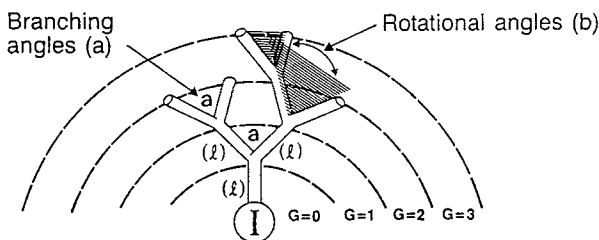


Fig. 9. Construction parameters involved in controlling nanoscopic space in a dendron

These parameters contribute significantly to the development of excluded volume around the branch juncture. Reiteration of these branching patterns in an ideal, tiered manner ($G = 0, 1, 2, 3 \dots$) should lead to highly ordered macromolecular domains ("nanodomains"). The ultimate interplay of all the above parameters would be expected to produce near total control of size, shape, and disposition of chemical moieties, both in the interior and on the exterior surface of these nanodomains.

This hypothesis for producing a low-aspect-ratio, three-dimensional molecular prototype can be contrasted with Nature's one-dimensional protein synthesis strategy for "molecular morphogenesis". Beginning with a reference carbon (Fig. 6), one can use its tetravalency to construct a wide variety of sub-nanoscale molecules. In this molecular category, one can find molecules which may function as initiators as well as monomers. Nature elected to use α -amino acids with various side chains (R) for this function. In this case, polymerization involves unidirectional accumulation of α -amino-acid units in a one-dimensional mode. The ultimate size of this one-dimensional protein is controlled by the degree of polymerization n . Its shape, however, is determined by the sequence of the R groups, which, of course, produces a variety of secondary shapes connected by random sequences; these secondary structures include α -helices, β -sheets, and ω -loops. These domains then self-assemble into three-dimensional shapes; the tertiary protein structures. In contrast, the conceptual three dimensional construction offered by "cascade synthesis" is illustrated in Fig. 10. In this case it involves, first, the assembly of three picoscopic sized repeat units (RU) possessing a monovalent terminus (\bullet) which is reactive with a divalent terminus ($*$) to produce a branch cell (Be) containing a branch juncture (\sim). Attaching this first branch cell to the reference point (\textcircled{I}) yields a labelled branch cell with a valency of four which is referred to as generation = 0. Stepwise attachment of RUs according to their valency, produces, next, a generation = one with valency of eight. Reiteration gives a generation = three, cascade assembly consisting of 5 BC's, 15 RU's, and 8 terminal surface atoms. This single trunked two dimensional projection which resembles a tree is referred to as a *dendron* (Greek word for tree). These dendrons are fundamental components that may be assembled in multiples around cores, (\textcircled{I}), to produce *dendrimers* (see Sect. 5).

Should this genealogically driven concept be viable experimentally, this morphogenesis strategy differentiates itself from that used by Nature to control

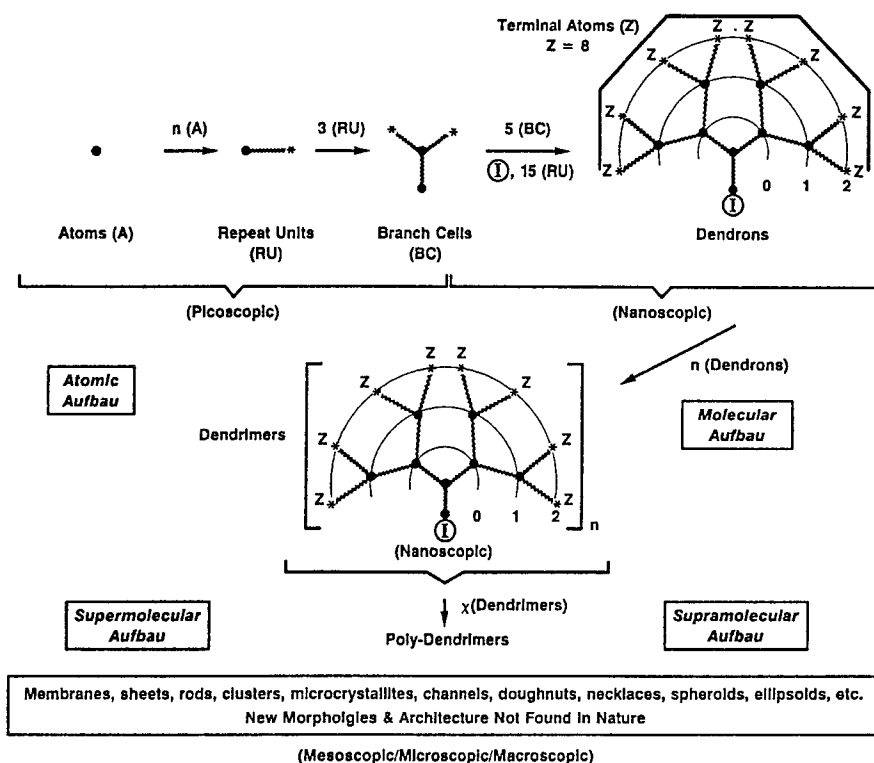


Fig. 10. Assembly strategy involved in genealogically directed synthesis (GDS) leading to dendrimer building blocks and subsequent construction of supramolecular and supermolecular assemblies

CMDPs. Although clearly different molecular arrangements are involved, the CMDPs of these highly branched synthetic macromolecules might be controlled and designed to mimic the CMDPs of naturally occurring biomacromolecules and assemblies. Success in this quest would give rise to a new molecular realm of nanoscopic building blocks.

3 Three-Dimensional Molecular Level Branching Concepts — Historical Overview

The origins of the present three-dimensional molecular-level branching concepts can be traced back to the initial introduction of infinite network theory by Flory [62–65] and Stockmayer [66, 67]. In 1943, Flory introduced the term *network cell*, which he defined as the most fundamental unit in a molecular network structure [68]. To paraphrase the original definition, it is the recurring branch juncture in a network system as well as the excluded volume associated with this branch juncture. Graessley [69, 70] took the notion one step further by describing

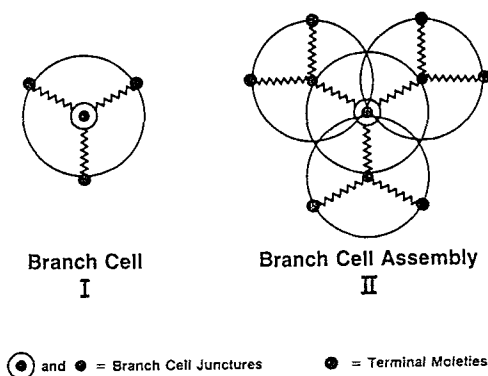


Fig. 11. Branch cell and branch cell assemblies leading to dendrons and dendrimers

ensembles of these network cells as micronetworks. Taken from the context of Flory's and Graessley's statistical treatment of Gaussian-coil networks, analogous species that are part of an open, branched organization are respectively known as *branch cells* and *branch-cell assemblies*. (Fig. 11).

Subsequent statistical modeling by Gordon et al. [71] and others [71d, e] reduced such branched species to graph theory designed to mimic the morphological branching of trees (Fig. 12). These dendritic models were combined with "cascade theory" [72] mathematics to give a reasonable statistical treatment for network-forming events at that time.

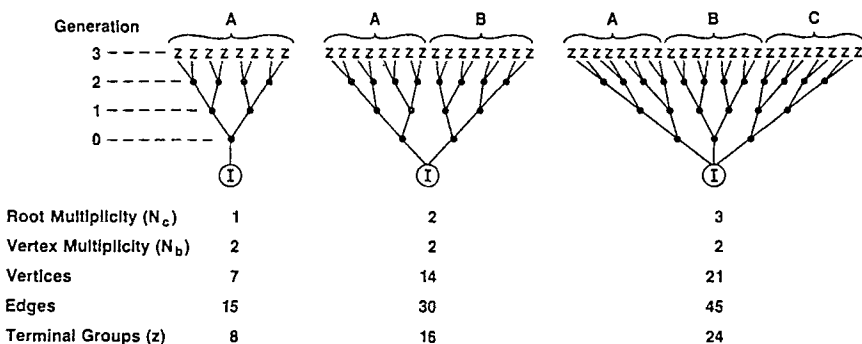


Fig. 12. Chemical graphs for a monodendron (A), a didendron (A-B) and a tridendron (A-B-C)

Since these species were conceptual, there were no well-characterized synthetic examples of such regular architecture. Meyer [73] proposed such a symmetrically, ordered architecture for amylopectin, but subsequent work by Erlander and French [74] and Burchard et al. [75], showed that neither amylopectin nor glycogen is so regular, but are instead, random *f*-functional polycondensates possessing a large, hyperbranched dextrin core (in Fig. 13).

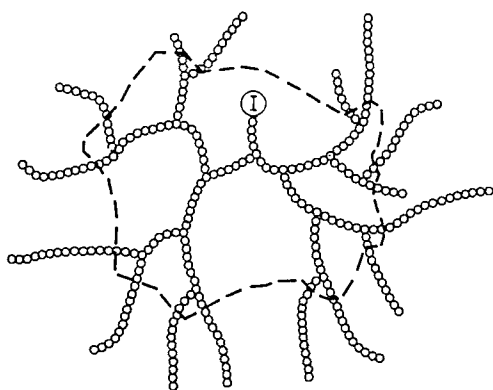


Fig. 13 Dendritic branching topology of amylopectin

It was not until 1978 that Vögtle et al. [76] reported a single, isolated example of a protection/deprotection scheme which assembled branches upon branches. Consisting of a sequence of reactions, the scheme involved Michael addition of an amine to acrylonitrile, followed by reduction of the nitrile group to an amino group. Possibly because of the difficulties and disappointing yields in the reduction step, no subsequent reports on this work could be found. Nonetheless, this was the first introduction to the literature of “cascade synthesis”. Virtually concurrent with these activities, we began our work at the Dow Laboratories in Midland, Michigan (USA), on the synthesis of Starburst/cascade dendrimers [77]. In 1979, we discovered that a variety of amines could be added to methyl acrylate and the products subsequently amidated with α , ω -diaminoalkanes to give “cascade products” (Sect. 5). With this chemistry, controlled concentric “Starburst growth” could be produced around various initiator cores. This growth could be dramatically influenced by both the geometry and multiplicity of the initiator core, as well as by the reiterative chemistry. Subsequent synthetic effort at Dow (1981–1984) showed that, much as anticipated from the macroscopic tree and coral branching analogies, these Starburst systems offered a wide range of synthetic options for controlling size, shape, interior topology, flexibility, and surface chemistry at the molecular level [77–84].

In 1983, mathematical predictions by de Gennes et al. [85] showed that a Starburst dendrimer series should reach a so-called limited generation beyond which branching can no longer occur in an ideal fashion. More recent studies have shown that advancement to higher-generation dendrimers ultimately leads to this new critical branching state which is referred to as Starburst (de Gennes) dense-packing [2, 82, 84–86]. At this critically branched generation, an apparent surface association occurs to yield solvent-filled spheroids [86, 87] which are reminiscent of “unimolecular cells” [11b, 86, 88]. Such morphologies were suggested in a theoretical paper by Maciejewski [89] in 1982, where he referred to them as “shell topologies”.

At that time, an isolated, yet related, dendrimer example appeared in the patent literature. Denkewalter et al. [90] reported that highly monodisperse macromolecular products were produced by a stepwise linking of α , ω -protected diamino acids

(e.g., lysine). Using protection/deprotection methods of polypeptide chemistry, these workers synthesized a series of dendrimers possessing unsymmetrical branch cell segments (lengths). Although the precise nature of these branch cells and these chemical structures have not been established, subsequent work by Aharoni et al. [91] and ourselves [84] showed that they differed dramatically from the present symmetrical Starburst dendrimers in certain important physical properties. Unlike Starburst dendrimers, they were found to be constant density, nonhollow macromolecules with “nondraining” character and may constitute a subclass to the present dendritic series.

Since 1985, Newkome and co-workers [92–94] have reported the synthesis of related symmetrically branched macromolecules which they refer to as “arborols”. These macromolecules are highly branched dendrimers which are not amenable to size control as a function of generation in that reiterative chemistry for advancing concentric growth has not been reported. These prototypes have been used successfully for controlling molecular shape and, in some cases, surface moieties. To date, examples of uni-, di- and tri-dendron arborols have been reported [92–94] (see Sect. 5).

4 Starburst/Cascade Topology and Branching Concept

4.1 Mathematical and Geometrical Precedence

Mathematicians such as Cantor and Koch [95, 96] and, more recently, Mandelbrot [97] have partitioned dimensionality in a variety of ways. Cantor started with a simple line, removed the middle third of the line segment, repeated this process on the two remaining segments, and so on to produce increasingly more segments

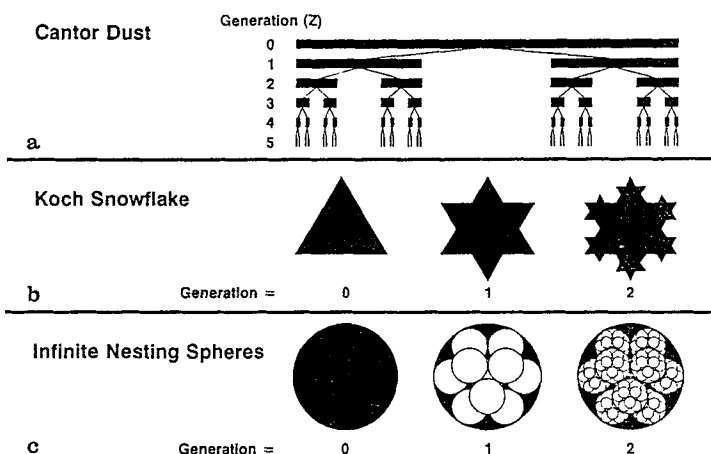


Fig. 14a–c. Mathematical models of dendritic/fractal systems **a)** Bifurcation of a line segment with connectivity paths to define Cantor dust. **b)** Bifurcation of a triangle (two-dimensions) to define Koch snowflakes. **c)** Fitting of a sphere (three-dimensional) to define a series of infinite nesting spheres

(Fig. 14a). Connecting the midpoints of the segments produces a branching pattern which remains confined in width to the original length of the line. Hence, the connectivity pattern becomes more congested as a function of generation. Subsequently, the Swedish mathematician Helge von Koch (1904) partitioned two-dimensional triangles in an analogous fashion to produce the well-known Koch snowflakes [98] (Fig. 14b). This reiterative process produces triangular-edged Koch curves, whose shapes depend on the generation. These curves enclose areas which are less than — but approach — the limiting area of the circumscribed circle around the curve [99]. In a similar manner, one may envision the partitioning of three-dimensional space by conceptualizing a “spherical universe within a universe” as a series of nesting spheres [60] (Fig. 14c).

These three cases are classical examples of fractal curves and dimensions as pioneered by Mandelbrot [96, 97] for macroscopic objects. They suggested to us possible extensions for the creation and analysis of unique spatial organizations of atoms within monomer repeat units, within branch cells, within dendrons, within a dendrimer, to give molecular-level surfaces in three dimensions of nanoscopic properties.

4.2 Molecular-Level Perspective of Cubic Space

The present dendritic branching concept uses these mathematical/geometrical notions in the context of partitioning or occupying three-dimensional molecular-level space around a reference point, with atoms, chemical bonds, repeating chemical units, and branch cells as the construction parameters. The dendritic branching of coral [61], Bryozoan colonies [59], trees [58, 60], and physiological networks [60] provided prototypes to mimic at the molecular level. The resulting branch-cell assemblies were referred to as possessing Starburst/cascade topology, and the molecular entities, constructed by reiterative synthetic steps, were coined Starburst dendrimers [100]. Two-dimensional projections of these dendrimers (A–E, Fig. 2) illustrate the concentric assembly of branches upon branches to produce radial arrays of branch junctures and terminal functionality (Z) around a reference point or initiator core, (⊙) [100]. In a geometrical context, the treelike structures A–E are recognized by physicists and mathematicians as Bethe lattices or Cayley trees. According to graph theory [101], dendrimers in this series may be viewed as triads of symmetrical trees rooted to a common initiator core (⊙). Each of these trees is referred to as an ideal dendron which consists of a root, (⊙), with connectivity to vertices (branch cell junctures) through edges (branch cell segments) which expand symmetrically according to a geometric progression to produce generations containing predictable numbers of vertices and edges (see Fig. 12).

4.3 Structural Aspects

4.3.1 Dendrimer Branch-Cell Hierarchy

Dendrimers possess three distinguishing architectural features: (1) an initiator-core region, (2) interior zones containing cascading tiers of branch cells with radial

connectivity to the initiator core, and (3) an exterior or surface region of terminal moieties attached to the outermost generation. Even in an ideal, homologous dendrimer series there exists a hierarchy of branch cells that are differentiated not only by their topological positions but also by structural features. This is illustrated in Figure 15, where a fully developed dendrimer is grown in four stages from an initiator core, (①), with $N_c = 3$.

The initiator core (①) may be as small as an atom or as large as a molecule. It may be homogeneous with the other dendrimer components or it may contain special design features (e.g., metal atoms, chromophores, etc.) that differentiate it from the dendrimer interior thus making it heterogeneous.

Synthetic elaboration to create the first tier of terminal functionality or branch junctures defines a microdomain referred to as the *core cell* (in Fig. 15). In situ construction of branch junctures or coupling partially masked, branch-cell reagents ($N_b \geq 2$) gives the first three surface cells, each of which possesses two reactive surface groups (Z). Upon progressing from dendrimer A to B, the three surface cells become initiator cells and six new surface cells are added. Advancement from B to dendrimer C leads to complete development of the cell hierarchy, which consists of one initiator core cell, three initiator cells, six interior cells, and twelve surface cells with a total surface stoichiometry of twenty-four Z groups. Owing to these surface groups, the dendrimer should function as an exo-receptor [23c].

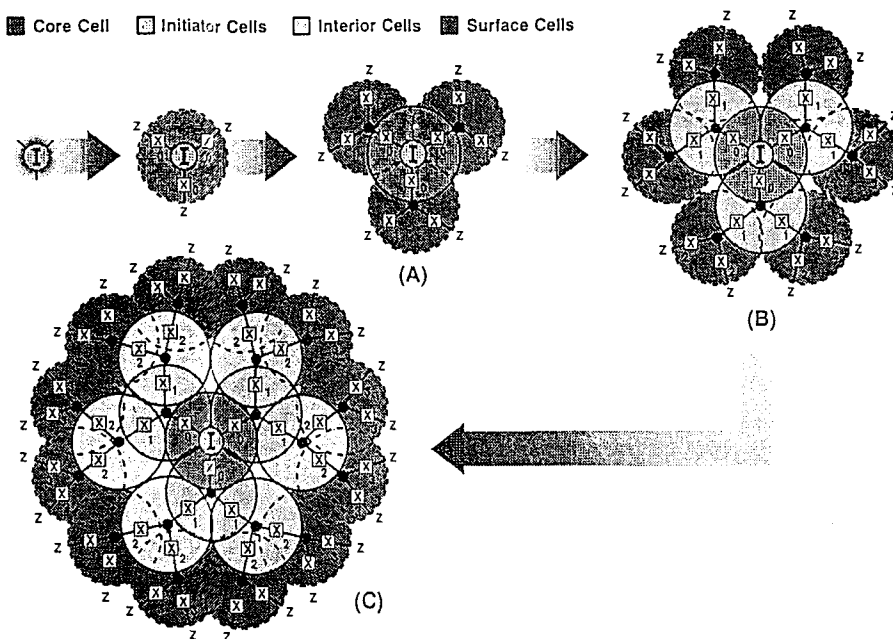


Fig. 15. Divergent assembly of branch cells into a generation = 3 dendrimer. Branch cell hierarchy is noted in (A), (B) and (C)

If the branch junctures or the coupling junctures are heteroatoms or contain designed moieties amenable to reaction or chelation, the dendrimer should exhibit endo-receptor characteristics [23c]. Each of these bonding features has been observed experimentally (for examples, see Sect. 7).

4.3.2 Dendrimer Branch-Cell Symmetry Properties

The symmetry properties of the interior branch cells can dramatically affect the physical and perhaps chemical properties of a dendrimer. For example, symmetrical interior and surface branch cells, such as those in Figs. 11 and 15, exhibit identical connectivity paths from the initiator core to the termini. The equal radii place the terminal groups on a sphere or a segment of a sphere, thus making these dendrimers ideal models of functionalized nanoscopic spheres.

In contrast, the polylysine dendrimers described by Denkwalter et al. [90] have unsymmetrical branch cells with either three or seven bonds between branch points. If one considers the paths of connectivity from initiator core to termini of a single dendron (see Fig. 16), it can be seen that no two paths are identical. In fact, every possible permutation of the sequences of the two given linear segments is present in the branch. If the two segment lengths are given values of s and l , and the number of tiers in the dendron is N , the number of different paths, X , is given by the relation $X = 2^N$. Since the paths are constructed from all possible combinations of the two given segment lengths, the number of paths of a given length follows a binomial distribution. Thus, the number of paths composed of a short segments s and l long segments (in a molecule consisting of $s + l$ tiers) is given by the following relation:

$$X_{s+l} = (s + l)! / (s! l!).$$

For example, a molecule with three tiers of branching has eight terminal groups. One path consists of three short segments, three paths consists of two short and

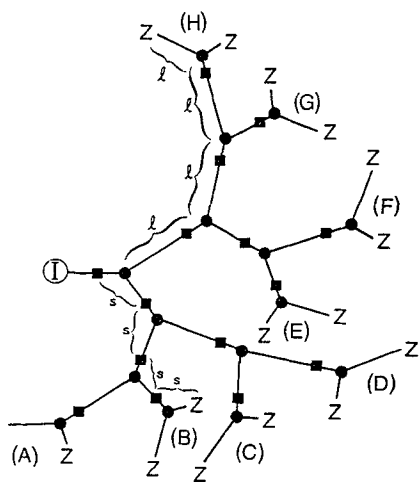


Fig. 16. Two-dimensional projection of a monodendron with unsymmetrical branch junctures (Denkwalter topology) and surface branch cells (A–H). s and l are the lengths of the short and long segments, respectively

one long segment, three paths consist of one short and two long segments, and one path consists of three long segments (see Fig. 16).

The different lengths of these paths mandate that some terminal groups will be tethered closer to the center of the branched assembly than others and be subject to more steric interactions. This suggests that this dendrimer class has surfaces with higher fractal dimensions [13, 97–99] and interior branching zones which are less ordered than those of the symmetrical Starburst dendrimers (Fig. 17).

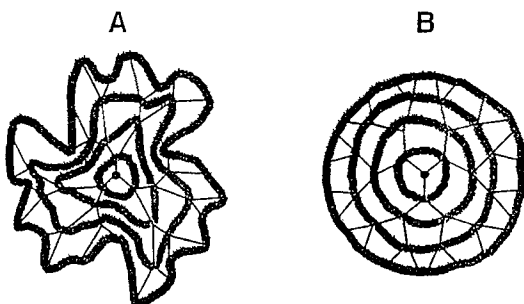


Fig. 17. Two-dimensional projection of a tridendron dendrimer ($N_c = 3$; $N_b = 2$) with unsymmetrical branch junctures (A) compared with one possessing symmetrical branch junctures (B)

These two classes differ substantially in certain physical properties [2, 84]. Although it has not been demonstrated, one might expect the various terminal groups in the Denkewalter dendrimers to show a range of chemical reactivities based on different steric environments. These clefted, highly fractal surfaces are similar to microenvironments usually associated with enzymes. This issue as well as other topological questions will, no doubt, provide ample reason for wanting to characterize and gain a deeper understanding of dendrimer infrastructure and surfaces.

5 Dendron and Dendrimer Syntheses

It should be re-stated and emphasized that dendrimers are large collections of atoms that are systematically organized around a reference point (core) by means of branched connectivity (usually covalent). As such, the synthetic strategies leading to the construction (*Aufbau*) of these molecular assemblies can be examined and experimentally manipulated. We described earlier the *Aufbau* steps leading to dendrimer synthesis which include the following stages:

(picoscopic) \Rightarrow (sub-nanoscopic) \Rightarrow (nanoscopic)

[Atoms] \rightarrow [Repeat Units] \rightarrow [Branch cells] \rightarrow [Dendrons] \rightarrow [Dendrimers]

In this account, we would like to focus on synthetic activities relating to the last two stages of this *Aufbau* scheme which dimensionally advance these covalent structures into the nanoscopic regime. An overview of synthetic operations that have been used is described in Fig. 18. As illustrated in Fig. 18, the general area

of “Cascade/Starburst synthesis” can presently be visualized as consisting of methods for; I *Dendron construction* and II *Dendrimer construction*. Since dendrons are vital architectural components involved in dendrimer construction, this area will be examined first.

Presently, there are two broad strategies known for dendron construction. They include I (A) *Divergent Methods*, which may involve either (i) controlled sequencing techniques or (ii) uncontrolled propagation methods based on the original hypothesis of Flory [64, 65], wherein AB_2 type monomers are polymerized in an uncontrolled manner. In either case, if suitable functional groups are introduced at the focal point of the dendron, these moieties may be used to subsequently anchor multiples of dendrons to a core substrate in a divergent manner to produce dendrimers. Early in our work, we demonstrated this approach [83] and refer to it as the two stage “Divergent Dendron/Divergent Anchoring” method to dendrimer construction.

More recently an interesting dendron construction method was reported independently by Fréchet et al. [102] as well as by Neenan and Miller [103] which has been referred to as the I(B) *Convergent Method*. This method differs from the divergent dendron approach in that exponential proliferation of surface groups is accomplished by use of a limited number of growth reactions per sequence. Its advantages and limitation will be discussed later. With this method a variety of dendron families have been successfully synthesized and subsequently coupled to various point-like as well as hyper-branched cores, to produce dendrimers. This

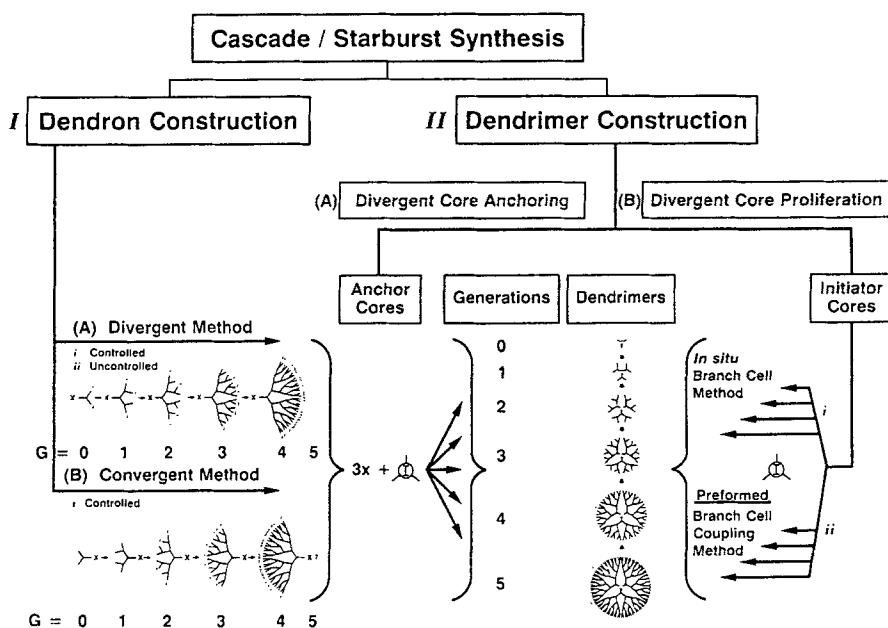


Fig. 18. Various genealogically directed synthesis (GDS) strategies for the construction of dendrons and dendrimers

approach to dendrimer synthesis has been referred to as the two stage Convergent Dendron/Divergent Anchoring method for dendrimer construction.

Alternatively, dendrimers may be synthesized directly by our original II Divergent Core Proliferation method. This method may involve the exponential covalent assembly of monomer units around a multi-valent core to produce branch cells in situ or it may involve the direct use of pre-formed branch cell reagents. In either case the resulting covalent structure consists of precise numbers of dendrons organized around the initiator core.

It can be seen that dendron synthesis may be categorized into three general approaches; namely, I(A) (a) Divergent controlled, I(A) (b) Divergent uncontrolled and I(B) (a) Convergent controlled methods. On the other hand dendrimer synthesis may be broadly divided into two general approaches involving either; I. Divergent core anchoring or II. Divergent core proliferation techniques. In the first strategy for dendrimer construction, dendrons are functionalized at their focal points by either divergent or convergent methods and then used as reagents to react with appropriate multifunctional core substrates to produce the desired dendrimers. Using the second approach, dendrimers are produced directly by proliferating divergently from an initiator core. This may be accomplished by either constructing branch cells in situ or by coupling pre-formed branch cell reagents according to geometrical progression branching rules.

Using any of the above methods, the genealogical aspects of these synthetic approaches become obvious in that these synthetic operations involve/manifest all or a portion of the genealogical components listed below:

- (a) Anchoring/Initiator Core reference points
- (b) Chronological Sequencing
- (c) Functionalized Radial Templating Surfaces
- (d) Geometric growth and proliferation
- (e) Self-replication of infrastructure
- (f) Ultimate dense packing surfaces
- (g) Iterated growth stages

Dendrons and dendrimers have been synthesized with a variety of cores, interiors, and surface functionalities. Presently, over twenty different chemical families of dendrons/dendrimers have been reported.

Classical, random coil, functional macromolecules are substrates upon which it is often difficult to perform high-yield, efficient reactions. Their coiled configurations frequently lead to inaccessible buried functionality frustrating even the most patient synthetic chemist. In contrast, the radial orientation of Starburst topology presents the terminal functionality in a very favorable fashion, accessible to incoming reagents and media. For this reason, essentially any reaction that proceeds well on a point-like organic molecule can be expected to occur equally well on a dendrimer surface, at least in the earlier generations. As surface congestion develops, however, reaction kinetics and stoichiometry change dramatically.

In general, it should be obvious that one can design and articulate the total construction of a dendrimer based on the choice of strategies used. Use of the

pre-formed dendron assembly approach followed by stepwise dendron coupling via the divergent core anchoring strategy allows one to differentiate sectors or hemispheres on the final dendrimer structure. On the other hand, the divergent core proliferation technique is more appropriate and facile for the construction of dendrimers with homogeneous interiors and surfaces. This approach is also very amenable, for the synthesis of dendrimers containing differentiated radial infrastructures. The respective strategies offer synthetic advantages, or limitations, depending on the perspectives and objectives of the synthetic chemist. These aspects are reviewed below:

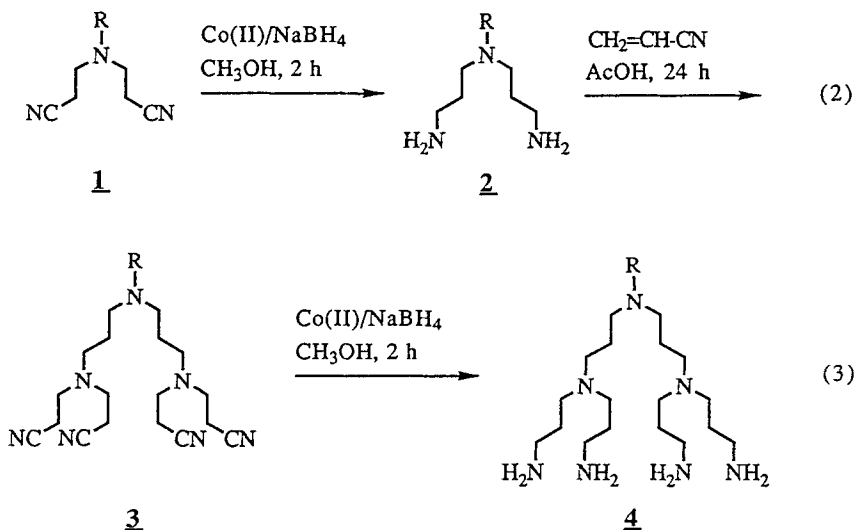
5.1 Dendron Construction

5.1.1 Divergent Controlled Method

5.1.1.1 Poly(alkyleneimine)-Monodendrons (*Vögtle Dendrons*)

Vögtle et al. [76] reported some of the first examples of dendrons synthesis by the divergent method. Using a protect/deprotect scheme based on cyanoethylation of alkyl amines with acrylonitrile followed by reduction to amine moieties with sodium borohydride/ Co^{+2} reagents, several low molecular weight dendrons were produced in 35–76% yields possessing hydrocarbon cores and either amine or cyano-functionalized surfaces. Since the initiator cores used were alkyl or arylalkyl amines, these dendrons were not (Scheme 2) suitable for divergent anchoring to other multiple cores to produce dendrimers.

These structures were supported by both NMR and mass spectral analyses, however, they were not carried beyond the generation = 1.0 level, giving dendrons with molecular weights under 1,000.



Scheme 2

5.1.1.2 Poly(amidoamine)-(PAMAM-Starburst)-Monodendrons

Among the first Starburst (Cascade) syntheses we performed in the early 1980s [83] involved partially masked (differentiated) initiator cores. For example dodecylamine, hydroxyalkyl amines or partially protected alkylene diamines were used as initiator cores and submitted to sequential (a) Michael addition with methyl acrylate followed by (b) reaction with an excess of ethylene diamine to give in situ branch cell construction in a divergent manner. The resulting products were core functionalized monodendrons as shown below:

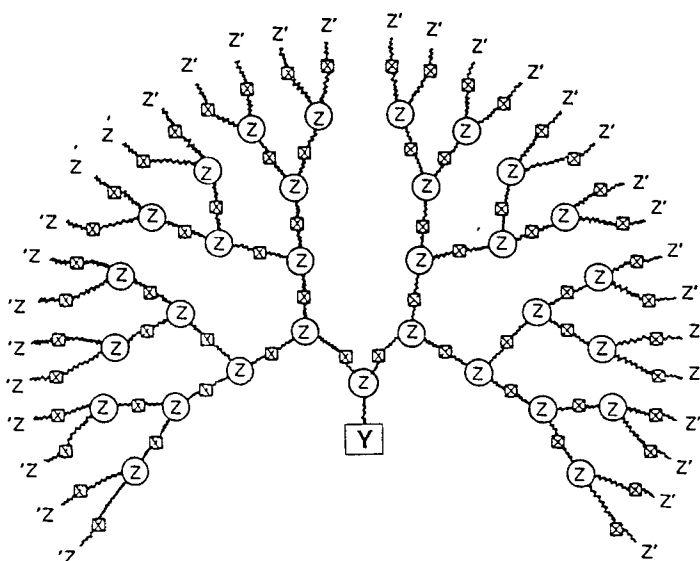


Fig. 19. Core functionalized monodendron, where Y may be either a masked/protected nucleophilic or electrophilic moiety, X = branch cell coupling, Z = branch cell juncture and Z' = surface groups

Alternatively, the synthesis was initiated with an electrophilic initiator core such as *p*-(methoxy)benzoic acid. This reagent was allowed to react with ethylene diamine, followed by sequencing to give a mono-dendron where $Y = p\text{-MeO}-\text{C}_6\text{H}_4-\text{CONH}-\text{CH}_2\text{CH}_2-$ (see Fig. 19).

These differentiated, core functionalized monodendrons were very useful as reactive intermediates for the construction of higher multiple dendron-dendrimers. In the case of the hydrophobically substituted dendrons, these products were used directly as amphiphilic reagents that readily organized into novel, Starburst type micelles. Among the many interesting properties these micelles displayed was the ability to sequester hardness ions (i.e. Mg^{+2} , Ca^{+2} , etc.) to produce "in situ" self building surfactant properties.

Within this poly(amidoamine) series it was generally noted that beyond generation = 3 or 4 the functionalized core became so sterically congested that coupling with various anchoring cores was substantially more difficult. Likewise

when the core was a twelve carbon chain the first two generation dendrons were hydrocarbon soluble (THF), however, beyond that generation they became very water soluble. This suggests that the exponential accumulation of hydrophilic surface groups beyond generation = 2, literally engulfs the hydrocarbon core.

As mentioned earlier by us [2], subsequent tethering of these core functionalized mono-dendrons around various divergent anchoring cores allows one to synthesize high multiple dendron dendrimers to give quadrant or hemispherically differentiated dendrimers as shown below: (see Fig. 20)

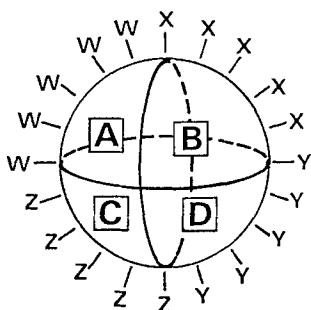
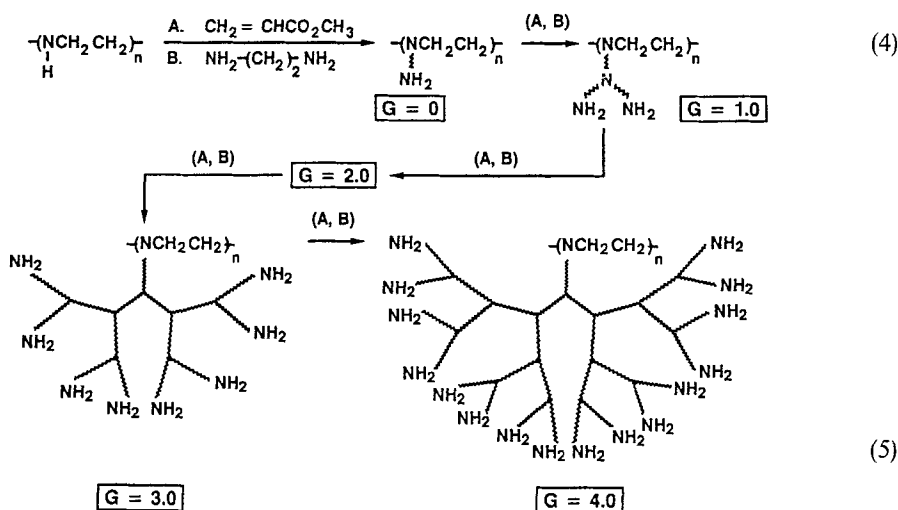


Fig. 20. a) Differentiation of dendrimer quadrants with various dendron surface moieties (W, X, Y, Z). b) Differentiated initiator or anchoring cores (A, B, C, D)

Alternatively, we synthesized several series of PAMAM dendrimers which were found to have rod-like characteristics by simply sequencing in the usual fashion with the reagents methyl acrylate and ethylene diamine upon linear poly-ethylenimines with core multiplicities, N_c of 300–400. The resulting high aspect ratio, rod-like dendrimers were proliferated out to generation = 4. Their length is determined by the degree of polymerization (n) of the initiator core and their diameter is derived from the number of generations as shown in Scheme 3.



Scheme 3

These rod-like PAMAM dendrimers [83] are formally derived from the core functionalized aziridinyl macromonomer (dendron) A, just as Fréchet et al. [104] have produced similar rod-like dendrimers by polymerization of the styrene functionalized monodendron (B) which was prepared via the convergent approach (see Fig. 21).

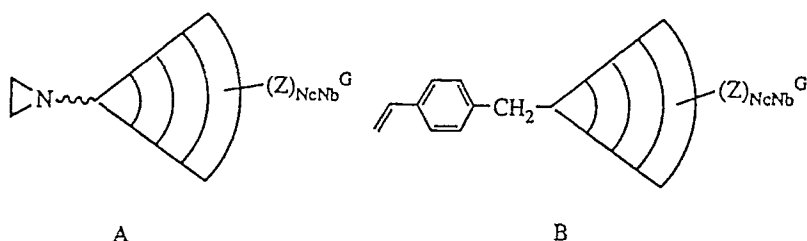
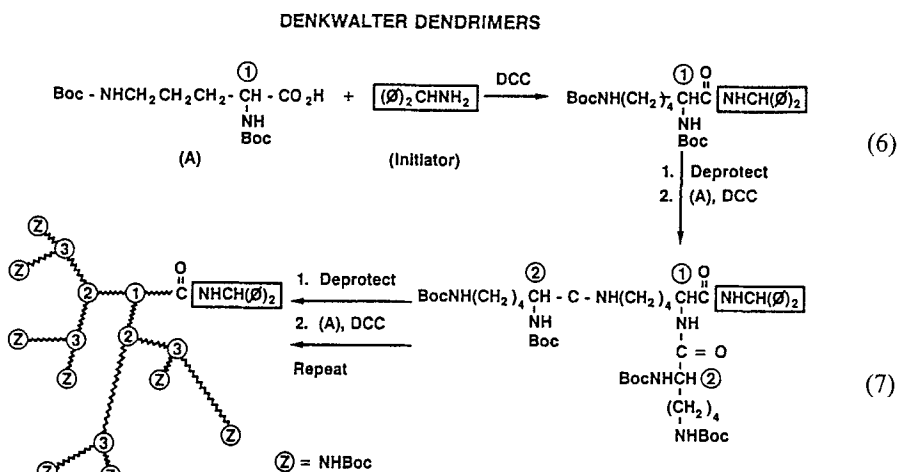


Fig. 21. Dendron macromers for preparation of rod dendrimers

5.1.1.3 Poly(amide)-Monodendrons (Denkewalter Dendrons)

Denkewalter et al. [90] reported the synthesis of monodendron polyamides through generation 10. The scheme involved protection/deprotection methods commonly used by polypeptide chemists. Dendron construction started with benzhydrylamine as the initiator core and an activated ester of amino-protected L-lysine as the branching reagent (Scheme 4).

N,N'-Bis(tert-butoxycarbonyl)-L-lysine nitrophenyl ester was the branching monomer used in the stepwise propagation. The dendron surfaces initially possessed hydrophobic Boc units and then, after deblocking, hydrophilic amine moieties. Although the dendron structures were not rigorously verified, subsequent



Scheme 4

work by Aharoni et al. [91] showed that they were quite monodispersed and behaved as “nondraining” spheres.

Tam and co-workers [105–107] produced related dendrons on a Merrifield resin followed by surface functionalization with various antigenic polypeptide sequences. A comparison of molar mass, number of terminal groups, and dimensions as a function of generation for the Denkewalter dendrons is shown in Table 1. Unlike all the other dendron examples reported, the branch cells in this system are unsymmetrical since they are constructed from unequal branchcell-segments as described in Sect. 4.3.2.

Table 1. Starburst Polyamides $N_c = 1$; $N_b = 2$ (asymmetric)

Generation	Molecular Weight	Monomer Units (Lysine)	Number of Terminal Groups, $Z(-NH_2)$	Hydrodynamic Diameter (Å)*	Diameter from SAX (Å)
Core Cell	511	1	2	11.8	—
1	967	3	4	14.6	—
2	1900	7	8	18.2	16.0
3	3700	15	16	22.8	20.0
4	7300	31	32	28.6	25.8
5	14600	63	64	36.0	—
6	29200	127	128	45.2	39.8
7	58400	255	256	57.0	59.2
8	116800	511	512	71.8	—
9	233600	1023	1024	90.6	86.8

* From intrinsic viscosity measurements (Ref: 91a, b)

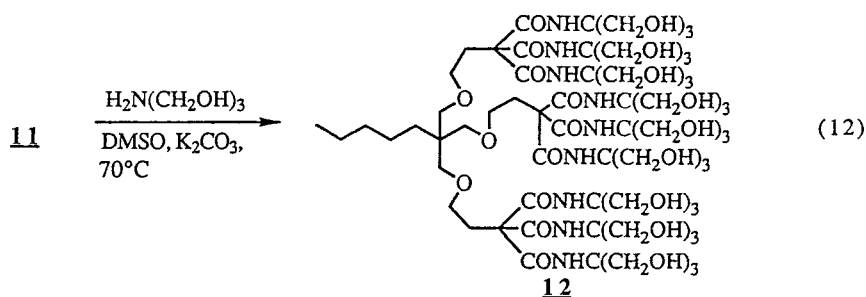
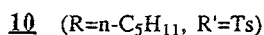
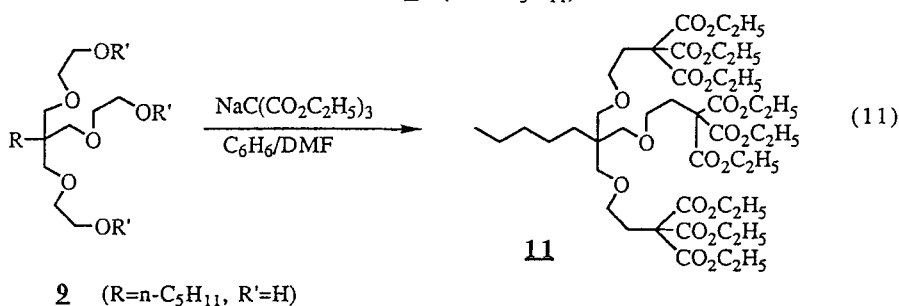
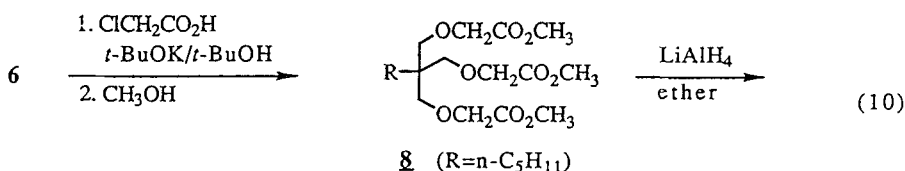
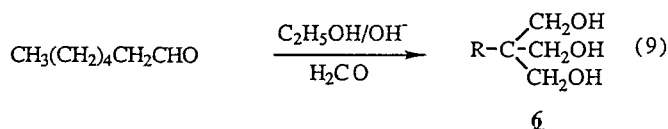
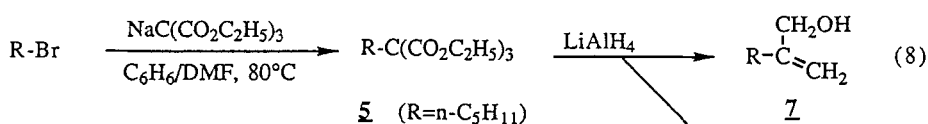
5.1.1.4 Poly(amido alcohol)-Monodendrons (Arborols)

This dendron class is a special example of a dendron series possessing radially oriented heterogeneous generations. The dendrons possess branch cells derived from three different branch cell reagents, namely an alkyltriol, triethyl methanetricarboxylate and aminotris-(hydroxymethyl)methane. Newkome [92] refers to this series as uni-directional arborols (Scheme 5, see next page). A maximum of three branch cell layers were grown from the hydrocarbon core.

Reiterative chemistry which would allow further advancement was not reported until very recently. Other examples of multi-(directional) dendron series have been reported by this group (See Sect. 5.2.3.2). Certain di-dendron prototypes that possess hydrocarbon interiors and “barbell-like” architecture are reported to self-assemble into rod-like nanostructures [94].

5.1.2 Divergent Uncontrolled Method

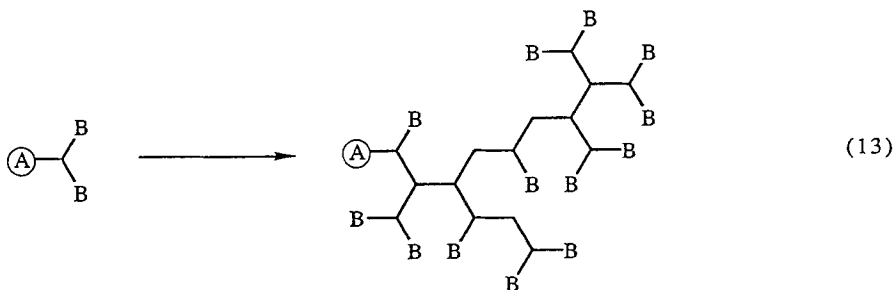
Flory [64, 65] first suggested the possibility of forming highly branched, treelike networks by polymerization of a differentiated monomer such as $A-R-B_n$, where n is greater than one and functional group A can react with B (see Scheme 6).



Scheme 5

Very early reports on these systems described them as polycondensates, consisting of broad molar-mass distributions with randomly branched topologies. The methods of synthesis included Friedel-Crafts coupling of benzyl alcohols [108] and the polymerization of 2,5,6-tribromophenol involving aryl ether formation [109]. In addition, hyperbranched natural carbohydrate polymers, such as amylopectin, dextrin, and glycogen have been extensively studied [73–75].

More recent examples of this type of polymerization have involved AB_2 type monomers leading to completely aromatic, polyester, organo-metallic and silicone containing "hyperbranched" systems. In general the final products are substantially more polydispersed than products from the controlled divergent method with branching idealities ranging from 50–75%.



The number of unreacted A groups = one.

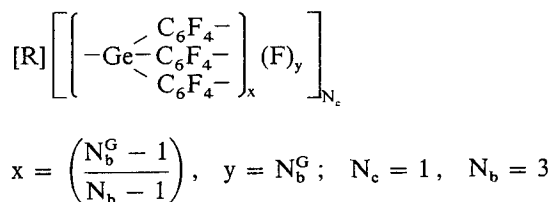
The number of unreacted B groups = (functionality - 2) DP + 1

DP = degree of polymerization.

Scheme 6

5.1.2.1 Poly(germanium perfluoroaryl)-Monodendrons

Bochkarev et al. [110] have recently described the anionic polymerization of $HM(C_6F_5)_3$, $M = Ge, Si, \text{ or } Sn$ ($N_c = 1$, $N_b = 3$). Most noteworthy is the germanium system, where they have obtained self-limiting molecular-mass ranges of approximately 100000–170000, in spite of the mode of preparation. These workers hypothesize that deprotonation at germanium produces anions that nucleophilically displace fluorine atoms in *para* positions to produce a dendrimer structure of the following general formula:

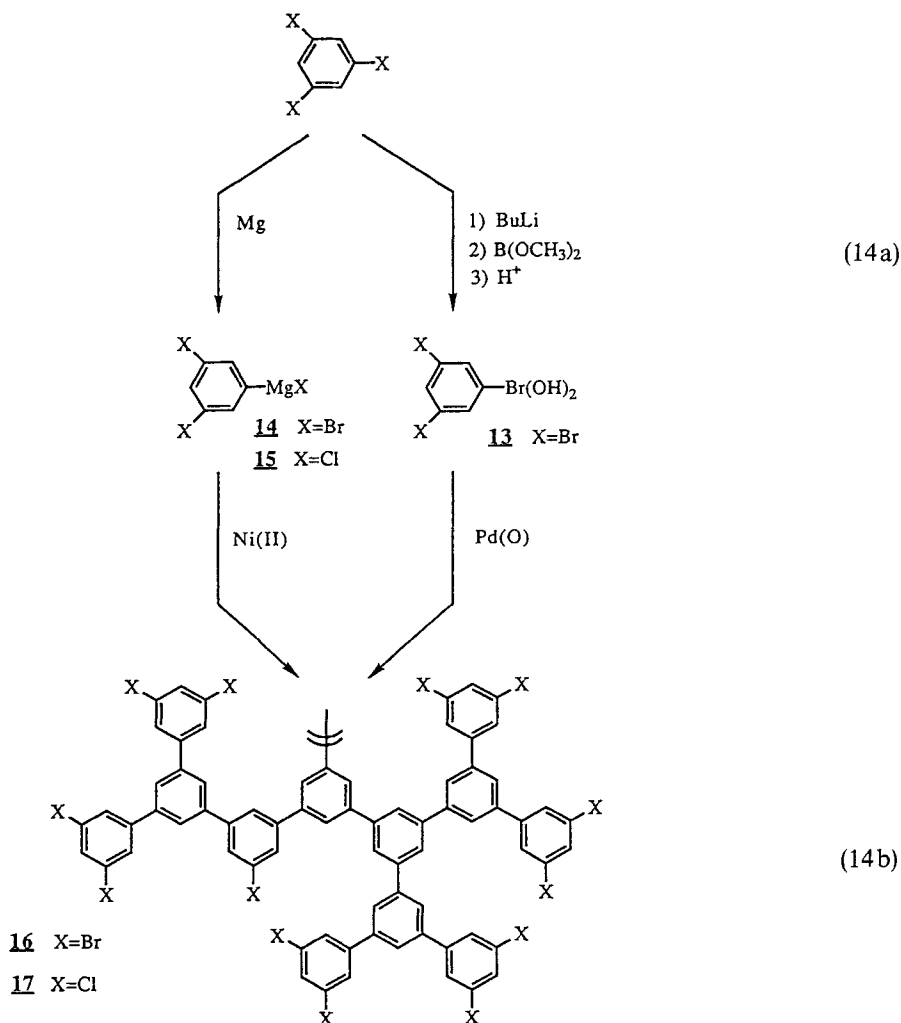


Structural verification is based on viscosity data (indicating Einstein spheroid characteristics), elemental analyses, light-scattering experiments, and direct observation of individual dendrimers by electron microscopy. The self-limiting molar-mass ranges correspond to approximately 38 branch-cell propagations (three tiers) around a germanium initiator core. Furthermore, analysis of molecular

models indicates that further propagation is precluded due to "steric screening". This appears to be the first example of a self-limiting polymerization to form a (de Gennes) dense packed starburst dendron by the "divergent uncontrolled method".

5.1.2.2 Poly(arylene)-Monodendrons

Completely aromatic, hyperbranched polyphenylenes were synthesized as monodendrons from AB₂ type monomers by Kim and Webster [111, 112]. These dendrimers were prepared either by the homocoupling of 3,5-dibromophenyl boronic acid under modified Suzuki conditions, or by aryl-aryl coupling reactions involving 3,5-dihalo-phenyl Grignard reagents in the presence of Ni(II) catalysts as shown in Scheme 7.



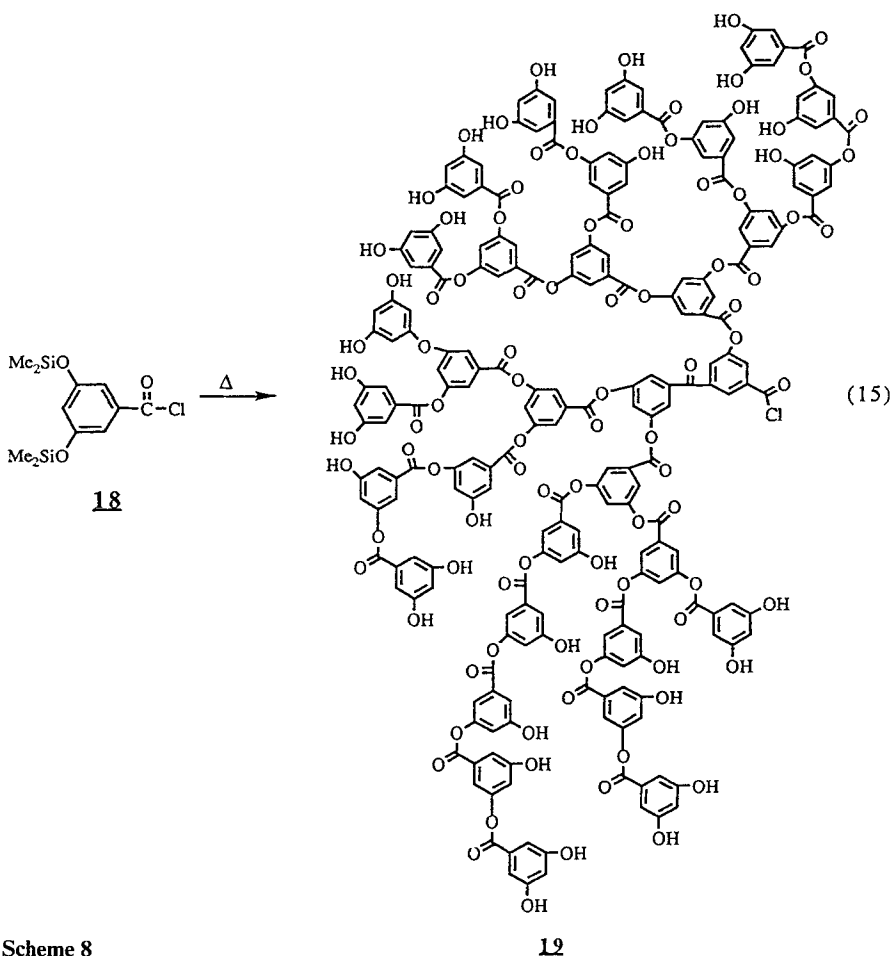
Scheme 7

The macromolecules were obtained as brittle, non-film forming materials with molecular weight ranges of 5000–35000 and $M_w/M_n < 1.5$. They were soluble in many organic solvents and thermally stable up to 550 °C. Branching efficiencies were estimated to be approximately 70% by ^{13}C -NMR analyses. For this reason, no evidence for Malthusian-like, dendrimer dense-packing was observed as a function of molecular weight enhancement.

The halo-surface groups were readily converted to lithiated derivatives which allowed their use as macromolecular templates from which to initiate anionic polymerizations. A wide variety of surface functionalities were introduced by combining the lithiated monodendron with various electrophiles.

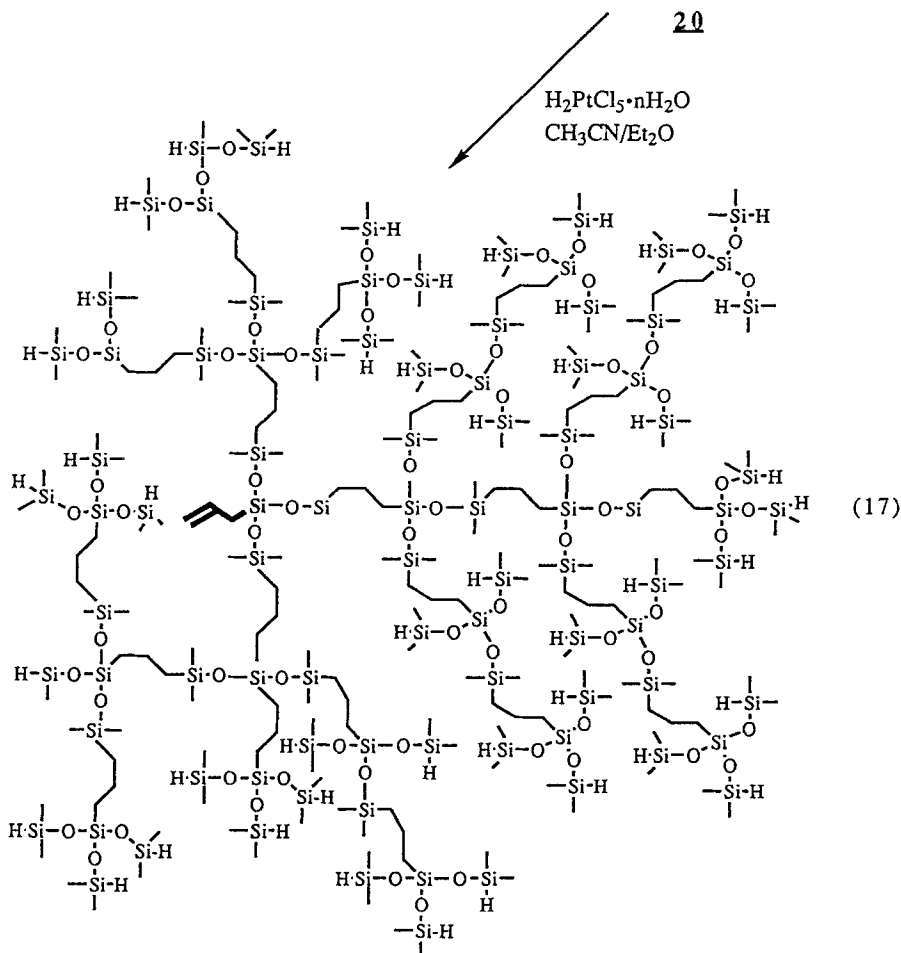
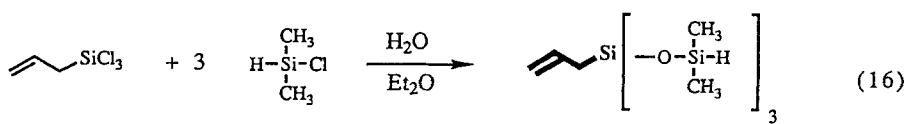
5.1.2.3 Poly(arylester)-Monodendrons

Recently, Fréchet et al. [113] have reported a so called one-step synthesis of hyperbranched polyarylesters by the thermal self-condensation of 3,5-bis(trimethylsiloxy)benzoyl chloride



Scheme 8

thylsiloxy)benzoyl chloride. This uncontrolled divergent propagation produced products in 80% yield with weight average molecular weights of 30000–200000 as illustrated in Scheme 8. These hyperbranched systems were determined to have a degree of branching between 55–60% by NMR examination, with poly-

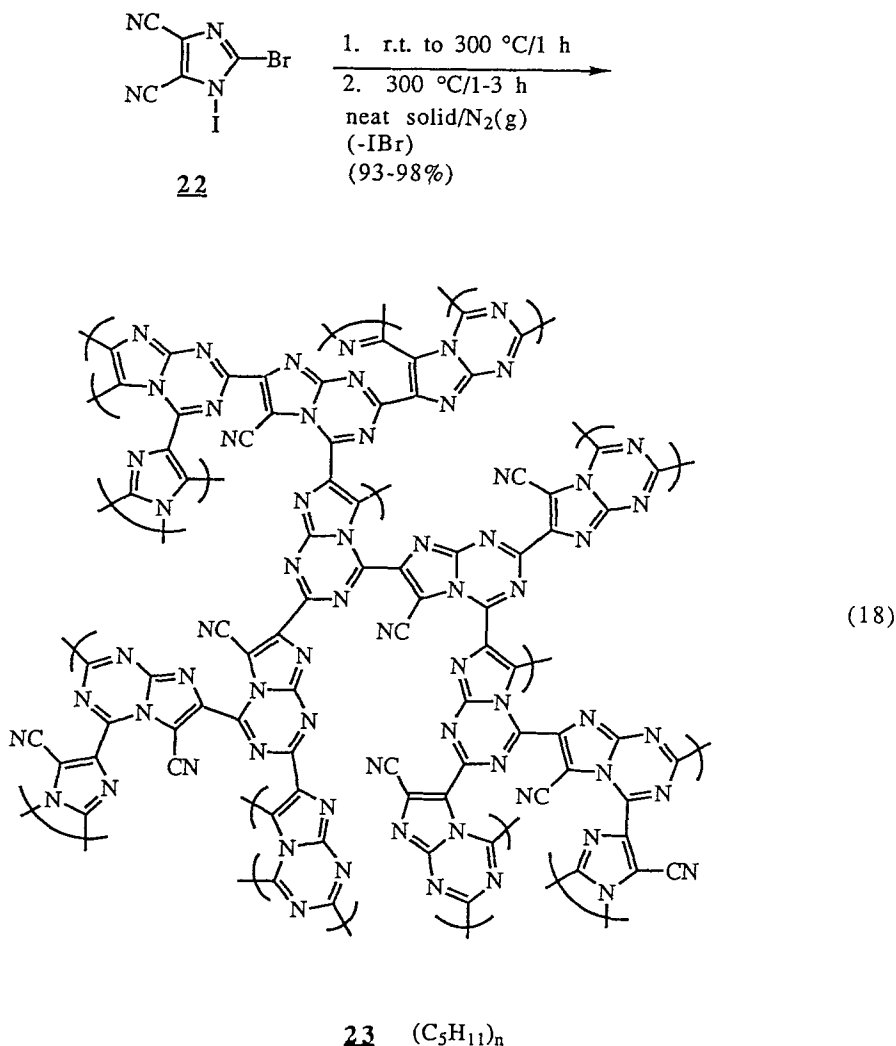


Scheme 9

dispersities M_w/M_n varying between 1.9 and 2.9 depending on reaction temperature. The hyperbranched polyesters are glassy materials containing reactive functional groups at all chain extremities.

5.1.2.4 Poly(siloxysilane)-Monodendrons

Hyperbranched poly(siloxysilanes) possessing an allyl group as a core functionality were prepared by the self-hydrosilation of the AB_3 monomer illustrated in Scheme 9. The products were obtained in a molecular weight range of 11000–35000, thus indicating they had advanced to the third or fourth generation. Mathias et al.



Scheme 10

[114] speculate that further chain extension may be sterically inhibited since the addition of more catalyst did not increase the molecular weight any further.

5.1.2.5 Poly(imidazo[1,2-*a*][1,3,5]triazine)-Monodendrons

Work reported recently by Rasmussen et al. [115] suggests that dihalodicyanoimidazoles undergo thermal self condensation to the hyperbranched heterocycle illustrated in Scheme 10. These cyanoazacarbons with empirical formula $(C_5N_4)_n$ contain no hydrogen and are viewed as heterocyclic analogs of aramides.

5.1.2.6 Poly(arylamide)-Monodendrons

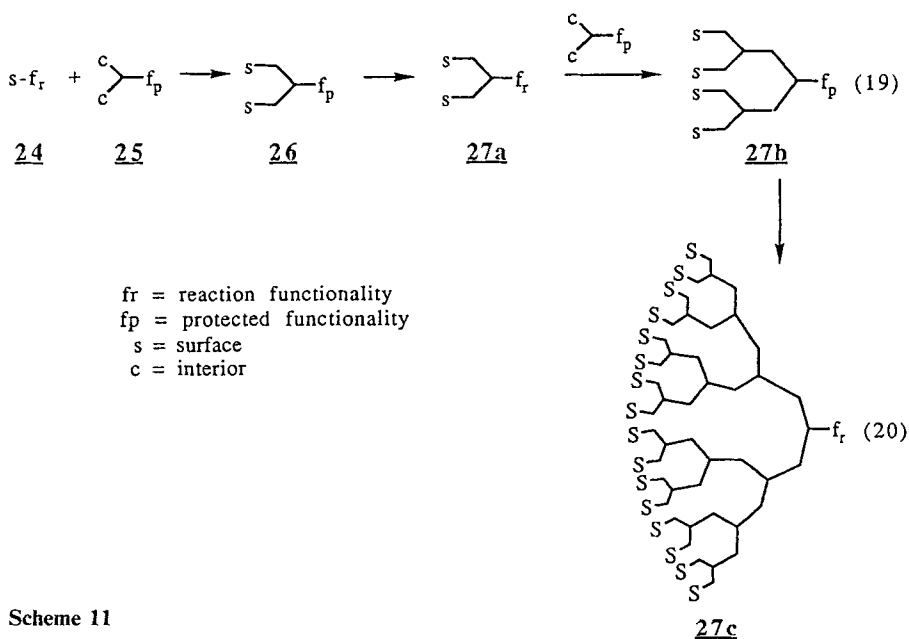
Lyotropic liquid crystalline properties were observed for poly(arylamide) monodendrons derived from 1,3,5-substituted amino acid chloride hydrochlorides according to Kim [168]. These systems aggregate readily to form high molecular weight species in the absence of complexing ions. Amide solvents containing more than 40 wt.% of the dendrons exhibit nematic phase liquid crystalline texture under a polarizing microscope, whereas, 60 wt.% solutions produce a hard gel under static conditions.

5.1.2.7 Poly(haloalkylaryl ether)-Monodendrons

Percec and Kawasumi [201] have recently reported homopolymerization of the AB₂ branch cell reagent; 10-bromo-1-(4-hydroxy-4'-biphenyl)-2-(4-hydroxyphenyl)decane, under phase transfer catalyzed polyetherification conditions. The resulting dendrimeric macromolecules possessing phenolic terminal groups were alkylated in situ with various hydrophobic reagents. These products are the first dendrimeric materials to exhibit a thermotropic enantiotropic nematic mesophase, although dendrimers have been used as solvents to generate a nonaqueous lamellar liquid crystal with octanoic acid [156]. See also [168] for related work by Kim.

5.1.3 Convergent Controlled Method

Nearly simultaneously, two groups namely; Fréchet et al. [102] at Cornell University and Neenan and Miller [103] at A.T. & T. Bell Labs introduced a new method for constructing dendrons which they refer to as the "convergent method". The synthesis begins at what will become the periphery of the final dendron and proceeds inwardly. Dendron growth is designed to occur via a limited number of reaction sites. For example, one starts first with a monomer unit **24** possessing what will eventually constitute the dendron surface functionality (s) and a reactive functionality (fr). This is then coupled to a branch cell reagent **25** containing at least two coupling sites and a protected functionality (fp) to give **26** as illustrated in Scheme 11. After coupling, (fp) is activated to (fr) to give the reactive branch cell reagent **27a** which is then allowed to react with **25** to produce the new cascade fragment **27b**. This process is reiterated until the dendron **27c** is obtained. This dendron has a single reactive group (fr) which may be used to couple to a multi-valent anchoring core to produce dendrimers (see Fig. 18).



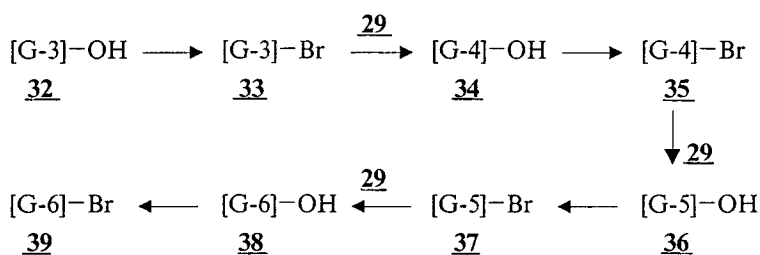
Scheme 11

Advantages offered by this convergent approach include the involvement of a very limited number of reactive sites (usually three) for each generation growth, thereby giving more monodispersed products with commensurate ease of purification and characterization. Conversely, a serious limitation of the convergent growth method is that, as the size of the dendron increases, the focal point functional group becomes increasingly more sterically encumbered. Of course, as we described in the earlier section, these dendrons which are functionalized at their focal points are suitable for coupling to various anchoring cores. This allows one to produce final dendrimer structures with surfaces that can be specifically differentiated as a function of sector, quadrant or hemisphere. This capability offers interesting possibilities for constructing new directionalized building blocks leading to new supramolecular assemblies and nano-devices [2, 116, 183].

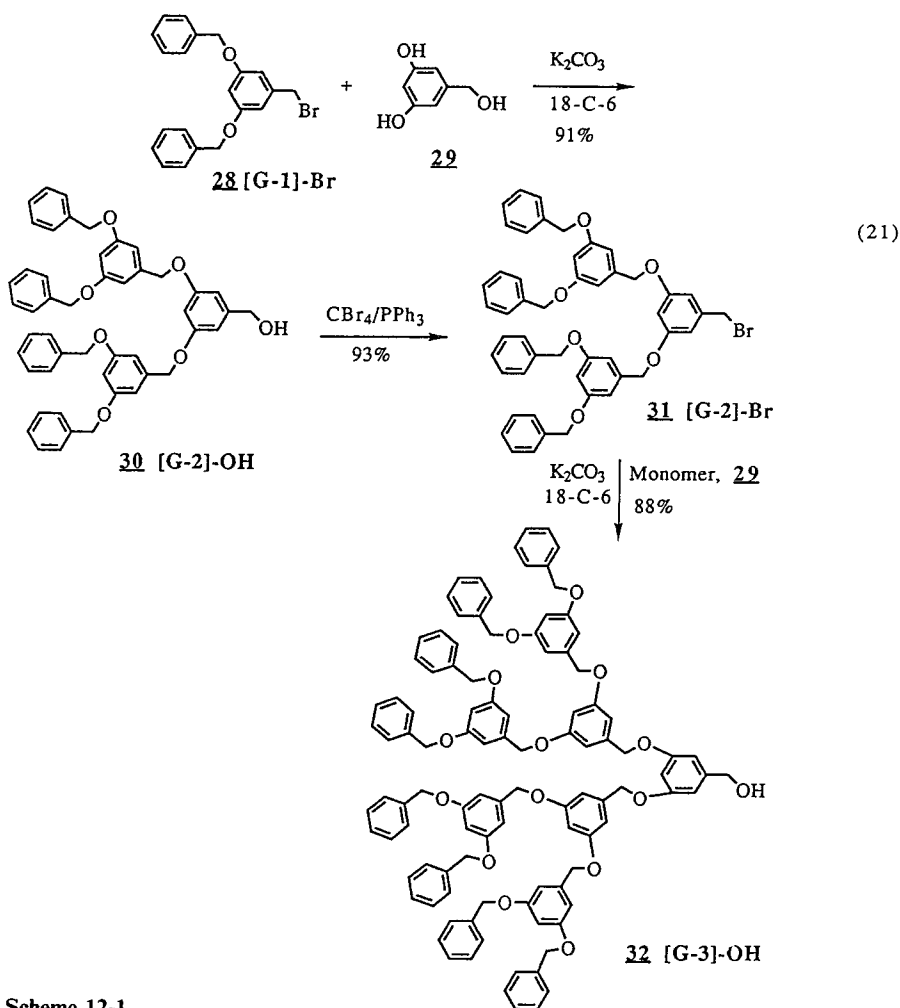
5.1.3.1 Poly(arylalkyl ether)-Monodendrons

Using the convergent strategy described earlier, Fréchet et al. [102] completed the synthesis of a series of polyether monodendrons based on the use of 3,5-dihydroxybenzyl alcohol **29** as the branch cell reagent unit. The synthesis is illustrated in Scheme 12 and involves first reaction of benzylic bromide, [G-1]-Br, **28**, with monomer, **29**, to produce [G-2]-OH, **30**.

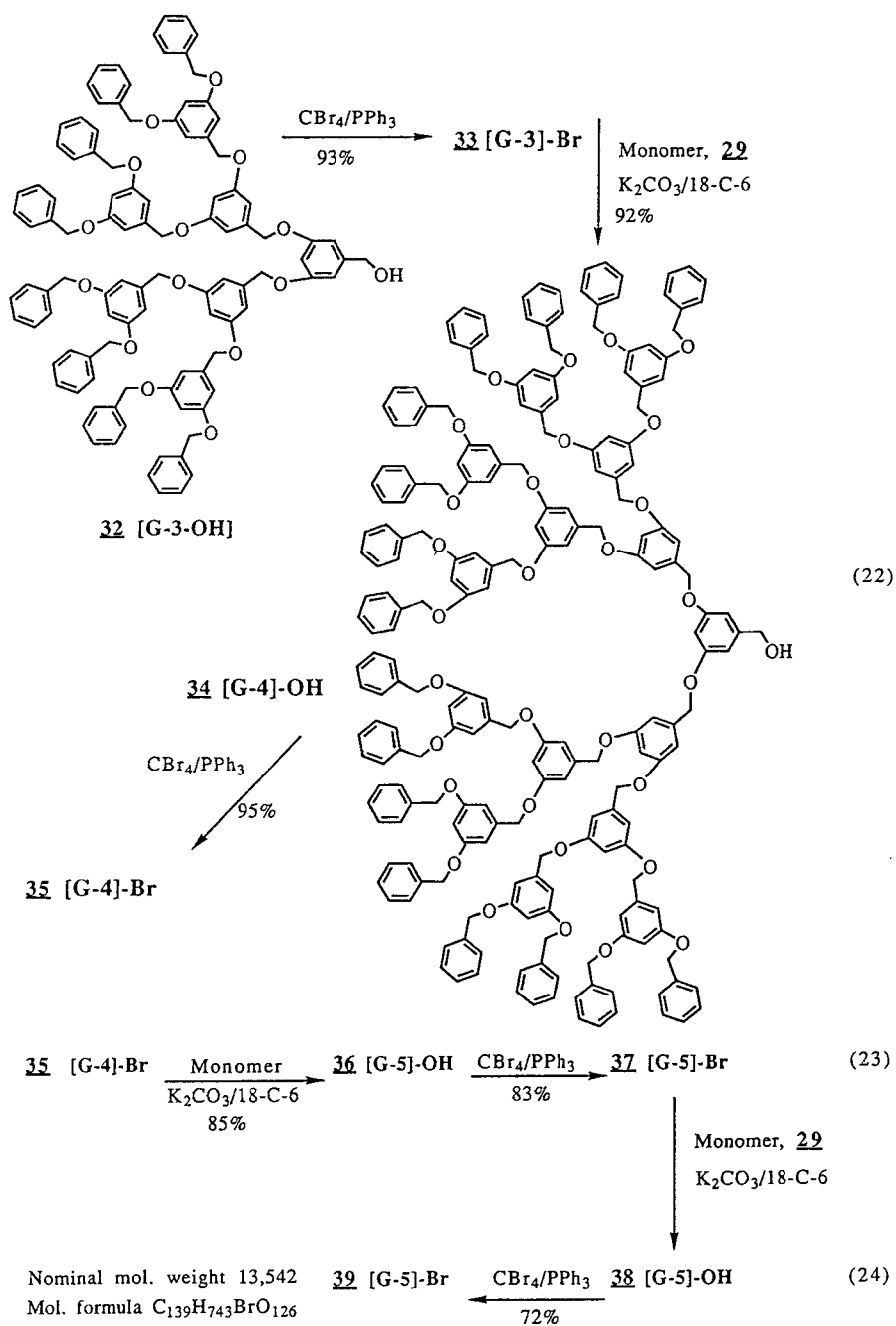
[The various generation dendrons are designated by use of the following notation [G-X]-f, in which [G-X] refers to generation number (X = 0, 1, 2, ...) and f refers to the functional group located at the focal point of the dendron.] Conversion of [G-2]-OH to the corresponding benzylic bromide, [G-2]-Br, **31**, occurs in 93% yield in the presence of CBr₄/PPh₃. Reiteration of this reaction sequence with monomer, **29**, produces the following monodendron series:



It was noted by Fréchet that the yields of monodendrons were very good (i.e. 84–91%) for [G-0] → [G-4], however, for [G-6]-OH and [G-6]-Br they declined to 78% and 72%, respectively, even in the presence of excess reagents. The authors attribute this yield decline and progressive difficulty in purification to increased



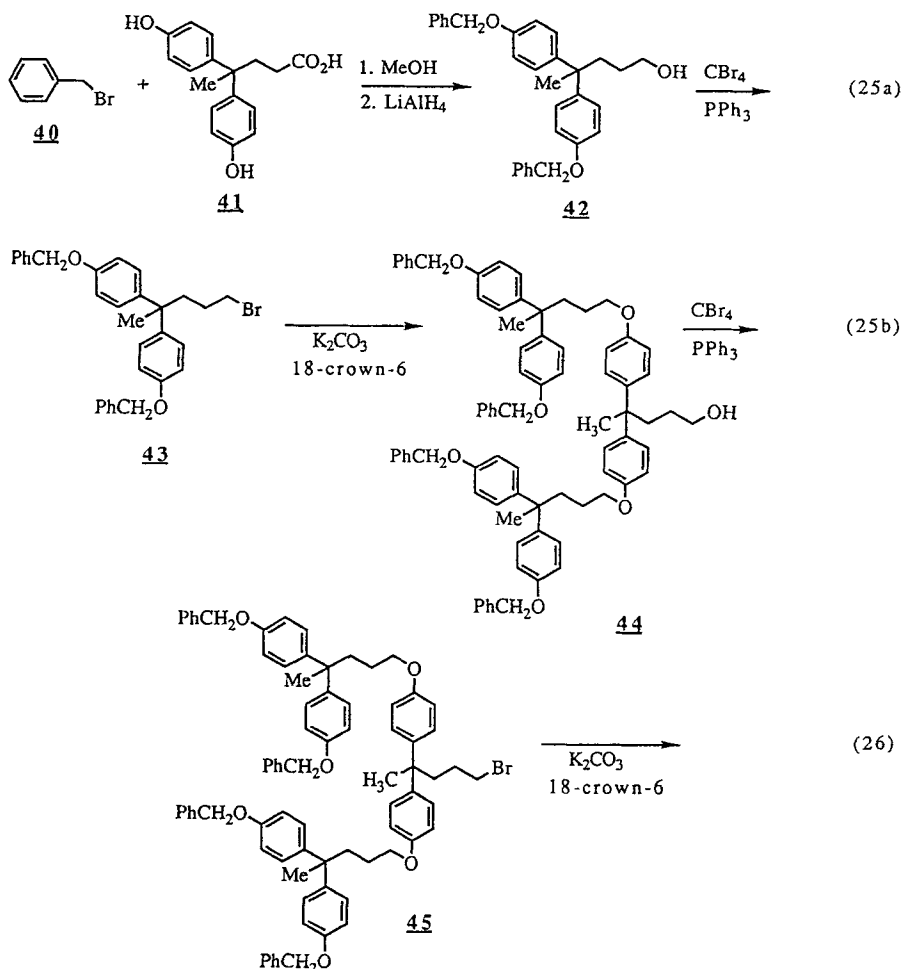
Scheme 12-1



Scheme 12-2

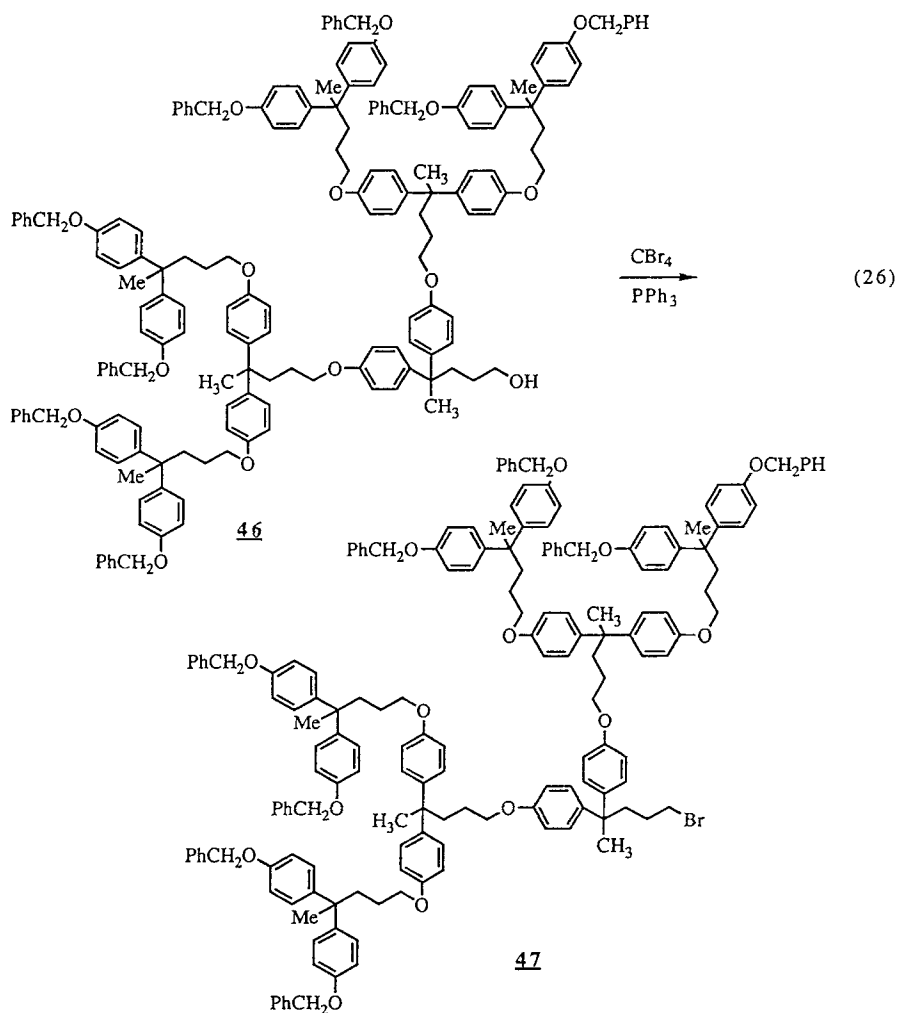
steric congestion around the functional group located at the focal point of the dendron, thus reducing its reactivity. These reactive dendrons were converted to dendrimers by allowing them to react with poly-functional cores and will be discussed in the next section.

In a second dendritic series, Fréchet et al. [117] selected 4,4-bis (4'-hydroxy-phenyl)pentanol **42** as the branch cell reagent unit for construction of a more flexible dendron. This synthetic sequence is illustrated in Scheme 13-1, 2.



Scheme 13-1

Protection of the peripheral phenolic groups as benzyl ethers was selected so that regioselective cleavage of these ethers in the presence of interior aliphatic ether linkages could be effected to liberate phenolic groups at some later stage. These functionalized dendrons were coupled to various anchor cores to produce

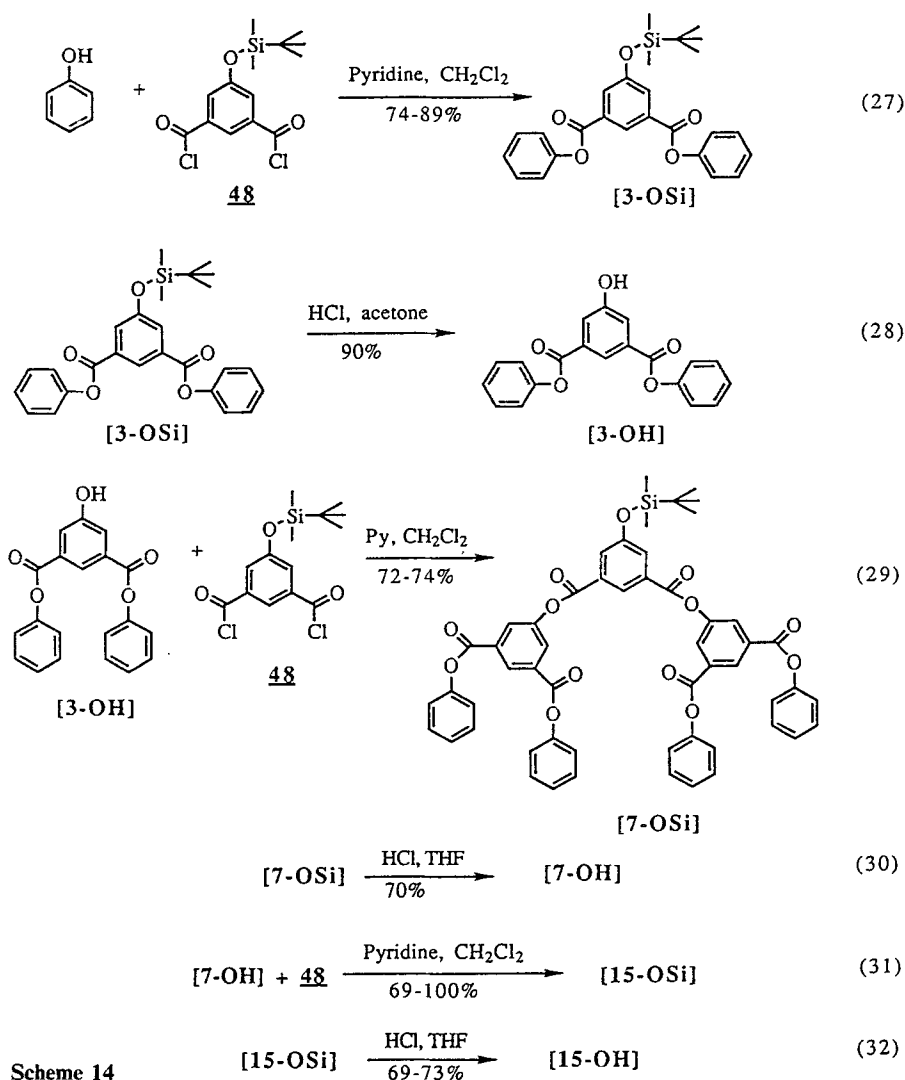


Scheme 13-2

more flexible dendrimers that Fréchet referred to as “hypercores” in his so called “double-convergent” growth strategy. These aspects will be discussed in the next section (see Sect. 5.2.2).

5.1.3.2 Poly(arylester)-Monodendrons

Neenan and Miller [118] reported the preparation of poly(arylester) dendrons using a convergent iterative sequence consisting of esterification and hydrolysis reactions as illustrated in Scheme 14. The key intermediate in the synthesis of these dendrons is 5-(*tert*-butyldimethylsiloxy)isophthaloyl dichloride, **48**, which is first converted to the diester with phenol, followed by hydrolysis to the diester phenol. This dendron is designated [3-OH] indicating it contains three phenyl

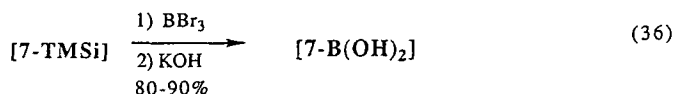
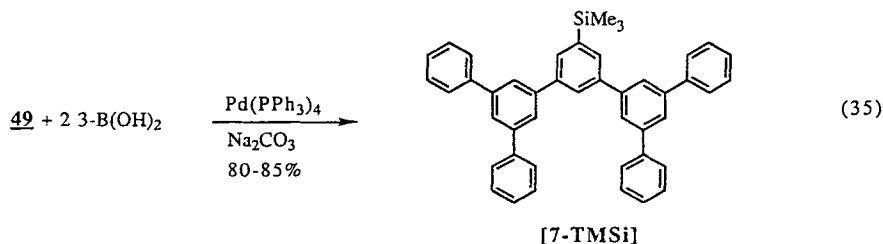
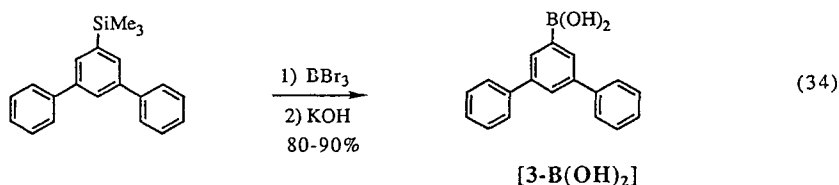
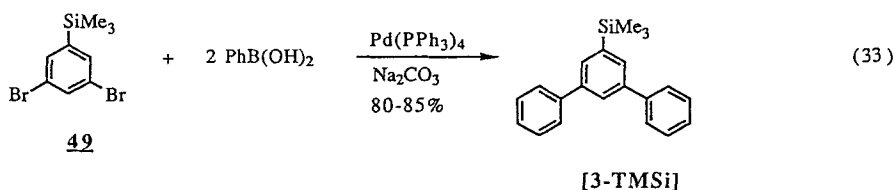


rings and possesses a phenolic group at its focal point. Reiteration of this reaction sequence ultimately produced a dendron [15-OH], containing fifteen phenyl rings with sequencing yields ranging between 69–90%. These monofunctionalized dendrons were then anchored to 1,3,5-benzenetricarbonyl trichloride to produce tridendron-dendrimers containing from 4–46 phenyl rings (see Sect. 5.2.2).

5.1.3.3 Poly(arylene)-Monodendrons

A unique series of monodendrons possessing extraordinary symmetry (i.e., D_{3h}) and no flexible methylene linkages has been recently reported by Neenan and Miller [119]. These dendrons consist of geometric tiers of aryl groups linked at

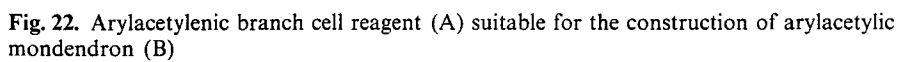
the 1,3,5-positions, yet with a reactive boronic acid group at its focal point. The key intermediate in these dendron syntheses is 3,5-dibromo-1-(trimethylsilyl)benzene, **49**. This intermediate was allowed to react with two moles of phenylboronic acid under Suzuki coupling conditions to give the masked 3,5-diphenyl-1-(trimethylsilyl)benzene [3-TMS] as illustrated in Scheme 15. Hydrolysis of this intermediate, followed by subsequent coupling with **49** allowed convergent growth to produce a boronic acid functionalized dendron containing seven phenyl rings, designated as 7-B(OH)₂.



Scheme 15

5.1.3.4 Poly(arylacetylenic)-Monodendrons

Recently Moore and Xu [120] reported the successful synthesis of rigid poly(arylacetylenic) dendrons through generation = 2, using a convergent strategy and the masked 1-ethynyl-3,5-dibromobenzene branch cell reagent, **50**, as shown in



Scheme 16. Attempts to continue proliferation to generation = 3 were unsuccessful, giving only half of the desired dendron at this synthesis stage. Efforts to correct this failure by introducing peripheral solubilizing groups were unsuccessful, whereas molecular modeling suggested that a sterically induced stoichiometry effect (SIS) may be involved. This hypothesis was supported by the fact that simply enlarging the arylacetylenic branch cell reagent to the structure (A) (in Fig. 22) rather than using, **50**, (Scheme 16), produced the desired, non-defective dendron (B) (Fig. 22). These observations have prompted these workers to propose that dendrimer growth could continue indefinitely, even in two dimensions, if one were to modulate the “branch cell” size as a function of generation as illustrated in Fig. 23.

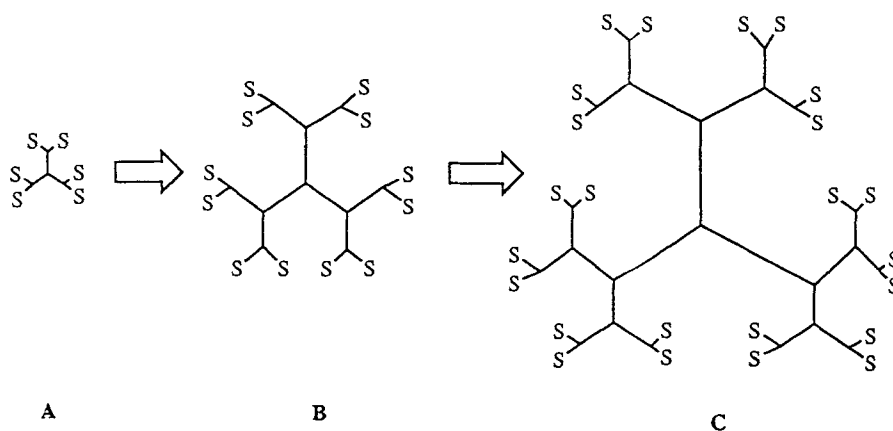


Fig. 23. Changing the branch cell reagent size as a function of generation which could allow rigid dendrimers to be grown indefinitely even in a plane

5.1.3.5 Poly(nucleotide: DNA/RNA)-Dendrons/Dendrimers

Damha and co-workers [121–123] have reported the use of a fully protected adenosine 2',3'-*O*-bis-*N,N*-diisopropylcyanoethylphosphoramidite reagent to join together neighboring polymer-bound oligomers to form a variety of unique “oligonucleotide branch cells”. Several such “branch cell reagents” are illustrated in Fig. 24.

These adenine containing branch cell reagents were subsequently used in a “convergent type” synthesis to produce RNA or DNA derived dendrons and dendrimers. Two adenylylthymidylic acid dendrimers were assembled by the addition of adenine branch cells to polymer bound thymine oligomers to give a generation = 1.0 reactive dendron containing 33 bases. Further extension of this polymer branch dendron with ten more thymine units, followed by coupling with the adenine branch cell reagent produced a second generation, di-dendron, oligonucleotide dendrimer containing seven adenine and eighty thymine units as shown in Scheme 17.

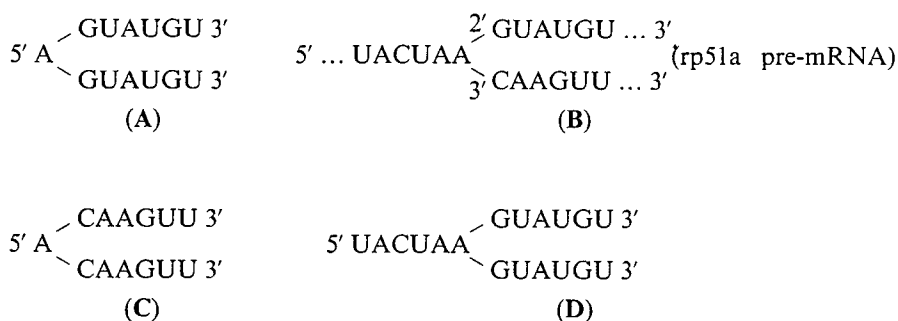
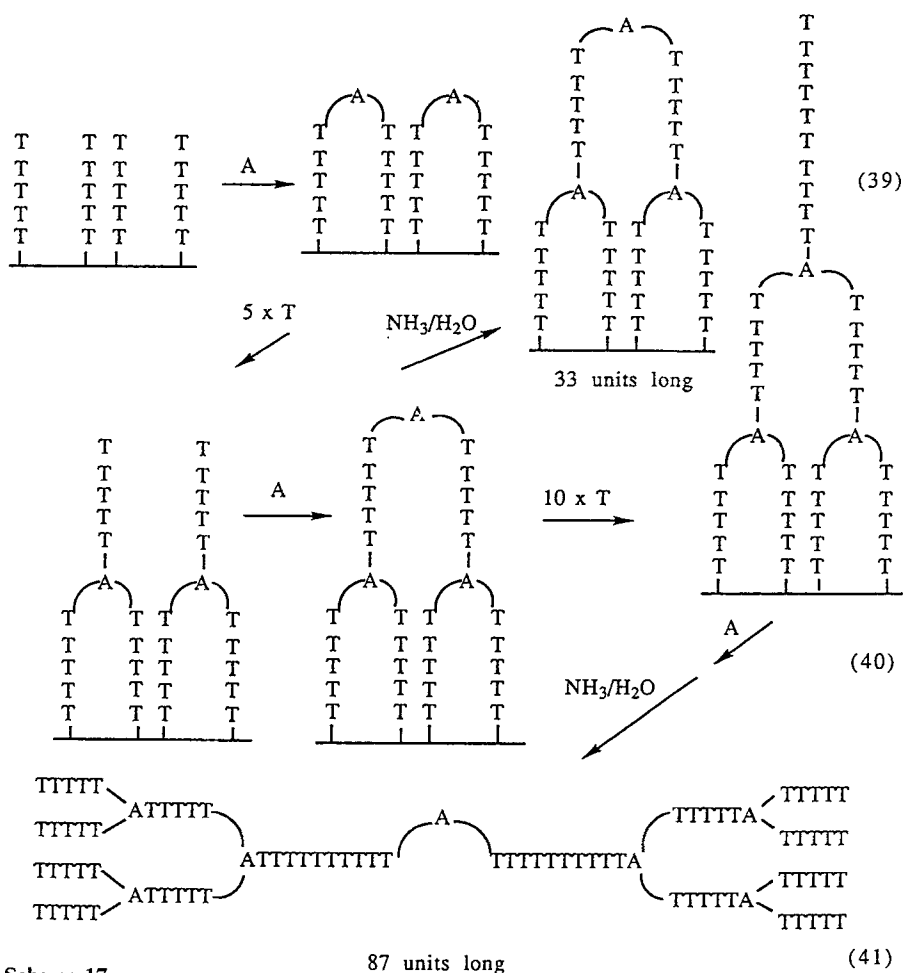


Fig. 24. Various oligonucleotide branch cell reagents [(A), (B), (C), (D)] suitable for constructing DNA/RNA dendrons and dendrimers



Scheme 17

5.1.3.6 Poly(aryl/azacrown ether)-Monodendrons

Shinkai and coworkers (see Ref. 200) recently synthesized very fascinating azacrown ether linked dendrons by utilizing a branch cell reagent derived from 1,4,10,13-tetraoxa-7,16-diazacyclooctadecane. These dendrons were constructed *via* the controlled convergent strategy and advanced to generation = 2. Tri-dendrons were constructed as described in Sect. 5.2.2.4.

5.2 Dendrimer Construction

5.2.1 Divergent Dendron/Divergent Anchor Core Method

5.2.1.1 Poly(amidoamine)-PAMAM-Dendrimers

(Ester, Ether, Amide and Urethane Core Coupling)

A variety of di-, tri- and poly-(dendron) type PAMAM-dendrimers were synthesized by first preparing dendrons functionalized at their focal points with hydroxyl or blocked primary amine moieties [83]. By suitably modifying the surface groups to alkyl selected passive moieties (i.e. ester, hydroxyl or *t*-Boc), these divergently derived dendrons were coupled to electrophilic anchoring cores such as 1,3,5-benzene tricarboxyl chloride, hexamethylene diisocyanate or poly(vinylbenzyl chloride). Generally, functionalized dendrons proliferated beyond generation = 4 or 5 exhibited sluggish reactivity and complex products, presumably due to the steric congestion surrounding the dendron focal point functional group.

The convergent growth approach offers a number of features less readily accessed by the “divergent-growth” approach such as control over surface functionality and involvement of a very limited number of reactive sites (typically three) for generation growth. One limitation of the convergent growth approach is that, as the size of the dendrimers increase, they are increasingly more susceptible to steric inhibition at the focal point group. This effectively limits the size of the macromolecules that may be prepared by the convergent method. This limitation is not as significant with the divergent or Starburst approach, although a somewhat similar steric inhibition is known to manifest itself as “dense packing” usually at very advanced generations.

Coincidentally, rather than using point like (sub-nanosopic) anchoring cores, we also used divergently synthesized dendrimers as anchoring cores. To these substrates we successfully coupled either dendrons or appropriate surface functionalized dendrimers to these “hyperbranched cores” to produce discrete dimers, trimers or covalently linked assemblies of dendrimers possessing uniquely differentiated surfaces (see Ref. 167). Similar dendrimer structures have also been reported recently by Fréchet et al. [117] and are described below as products resulting from the convergent dendron/divergent anchoring method.

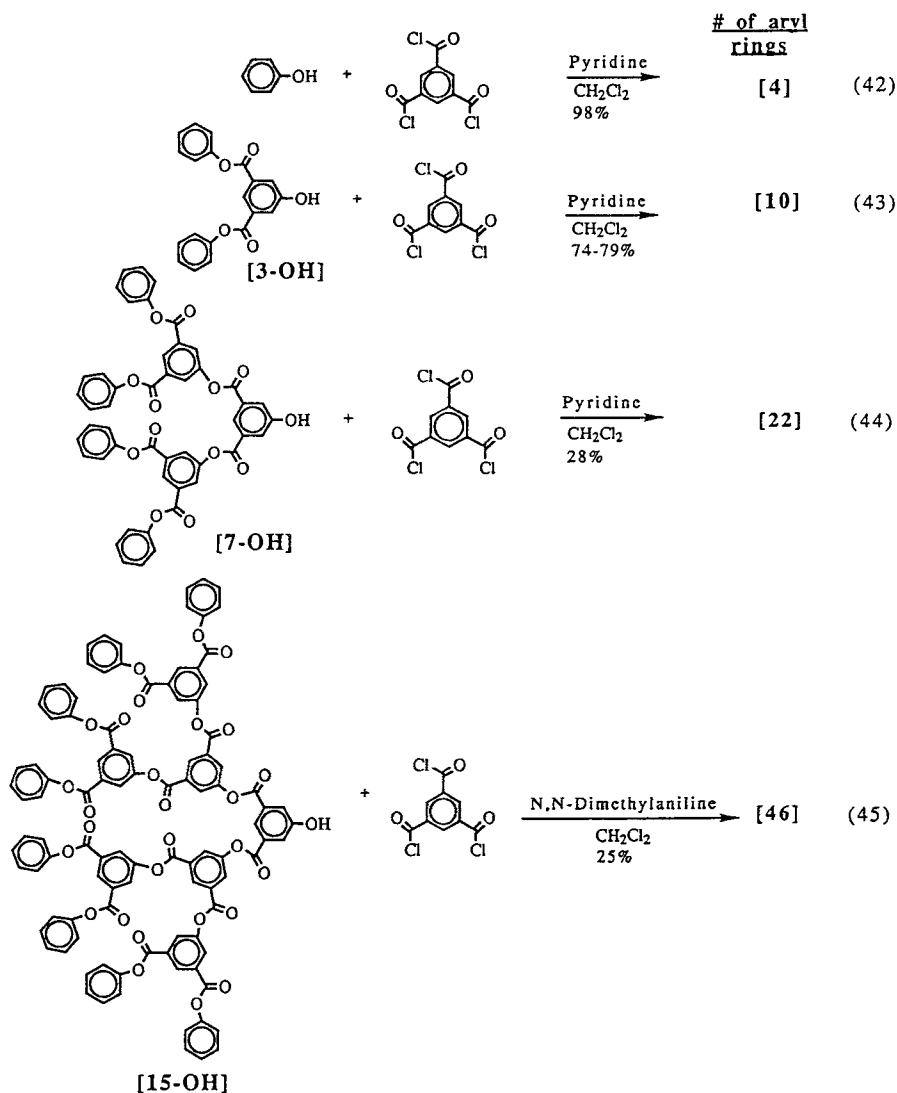
5.2.2 Convergent Dendron/Divergent Anchor Core Method

Dendrimers synthesized by this approach have been reported almost exclusively by both the Fréchet group [102] and the Neenan/Miller [103, 118, 119] group.

This approach has been used successfully to produce at least four different types of dendrimer families which include poly(arylester), poly(arylene), poly(arylalkyl) ether, and poly(aryl/azacrown ether) type dendrimers.

5.2.2.1 Poly(arylester)-Dendrimers

An example of the convergent approach to synthesize the corresponding dendrons followed by the divergent anchor core method to produce tri-dendrons containing

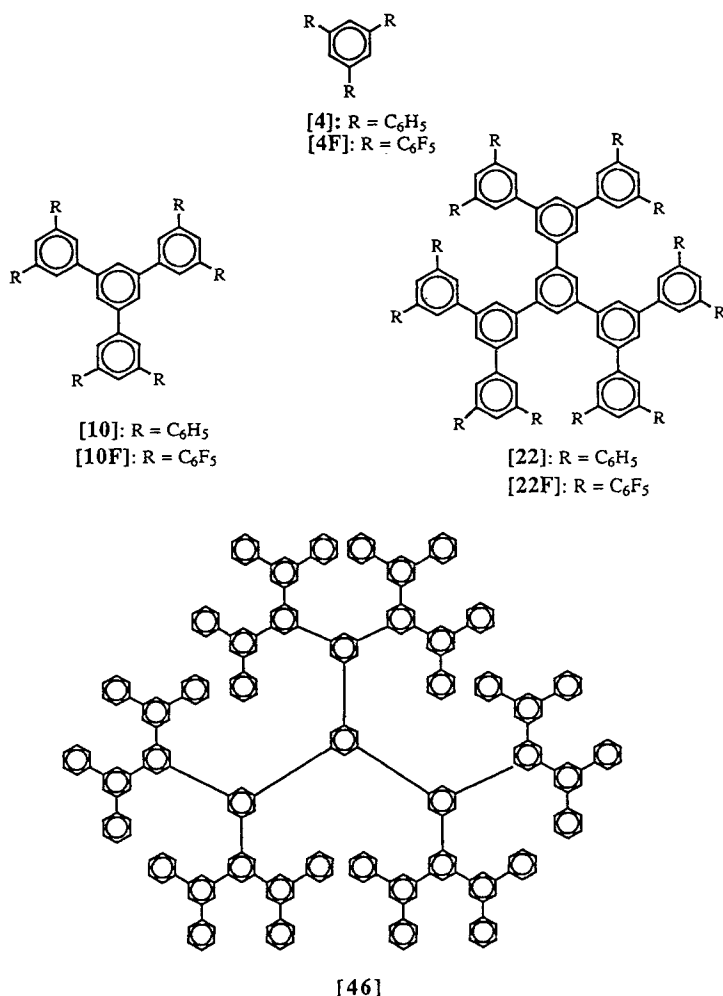


Scheme 18a

4, 10, 22 and 46 aromatic rings in a poly(arylester) dendrimer series is as illustrated in Scheme 18(a).

5.2.2.2 Poly(arylene)-Dendrimers

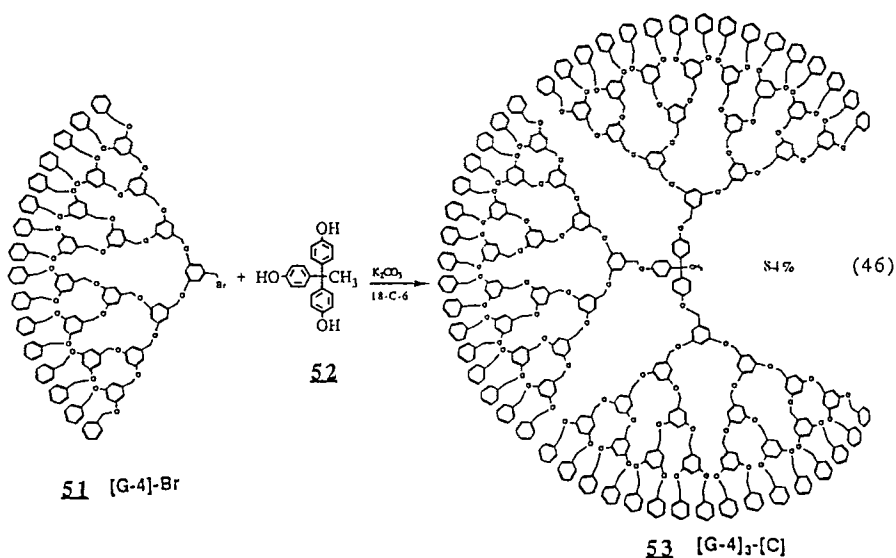
In a similar fashion, all arylene dendrimers possessing 4, 10, 22 or 46 aromatic rings were also reported by Neenan and Miller [119]. As illustrated in Scheme 18(b), surface aryl rings could be perfluorinated.



Scheme 18b

5.2.2.3 Poly(arylalkyl ether)-Dendrimers

Similarly, Fréchet et al. [102a] utilized a benzyl bromide functionalized dendron, **51**, (generation = 3) as a reagent which was then divergently coupled to the tri-valent phenolic, anchoring core, **52**, to give the tri-dendron, **53**, shown in Scheme 19.



Scheme 19

Advancing this strategy to an even higher level of sophistication, this group selectively introduced differentiated surface groups during the convergent dendron synthesis. Using differentiated dendrons A or B, illustrated below in Fig. 25, it was possible to control dendrimer surface functionality by introduction of only

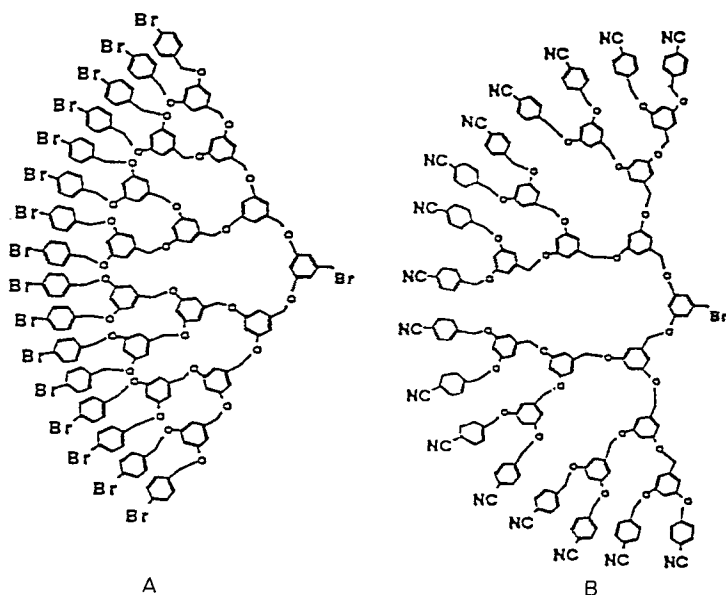
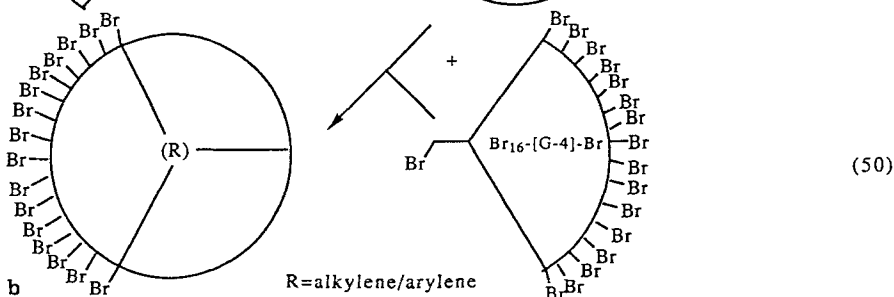
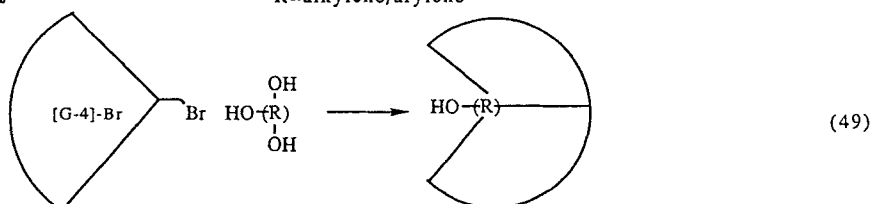
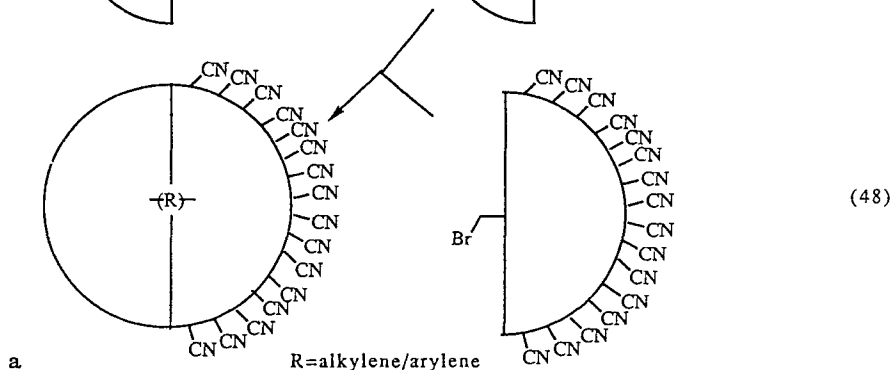
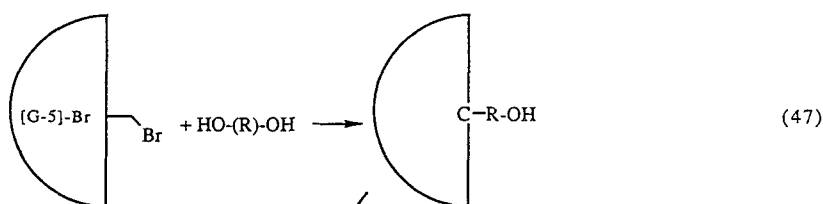


Fig. 25. Differentiated dendrons with (A) aryl bromide surface; benzyl bromide core and (B) aryl nitrile surface; benzyl bromide core



Scheme 20a, b

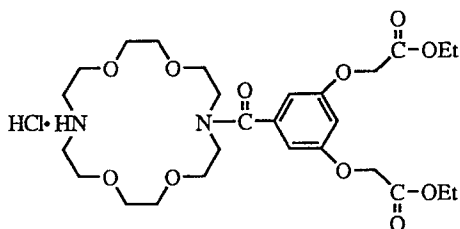
one differentiated hemisphere or dendron sector per dendrimer as shown (see Scheme 20a, b, Eqs. 47–50). Alternatively Fréchet's group demonstrated that mono-functionalization of one sector or total functional of one sector of the dendrimer surface could be performed to produce either cyano or bromine functionalized surfaces.

Finally, a two stage dendrimer synthesis [117] was demonstrated by pre-constructing a lower generation dendrimer using the convergent dendron/divergent anchor method as shown in Scheme 13. Secondly, coupling pre-formed dendrons to this multi-valent "hyperbranched/dendrimer" core produced a

double-staged dendrimer, wherein the inner core could be designated to be chemically differentiated from the outer dendrimer domain composed of coupled dendron units.

5.2.2.4 Poly(aryl/azacrown ether)-Dendrimers

Very recently, Shinkai et al. (see Ref. 200) synthesized tri-dendron type dendrimers (generation = 1 and 2). The branch cell reagent shown below was utilized in a convergent approach to synthesize the dendrons. These dendrons were then anchored in each case around a 1,3,5-benzene tricarbonyl chloride core. This



dendrimer series is under investigation to determine allosteric effects during metal-binding and to determine binding selectivity toward various alkali metal ions.

5.2.3 Divergent Initiator Core Method

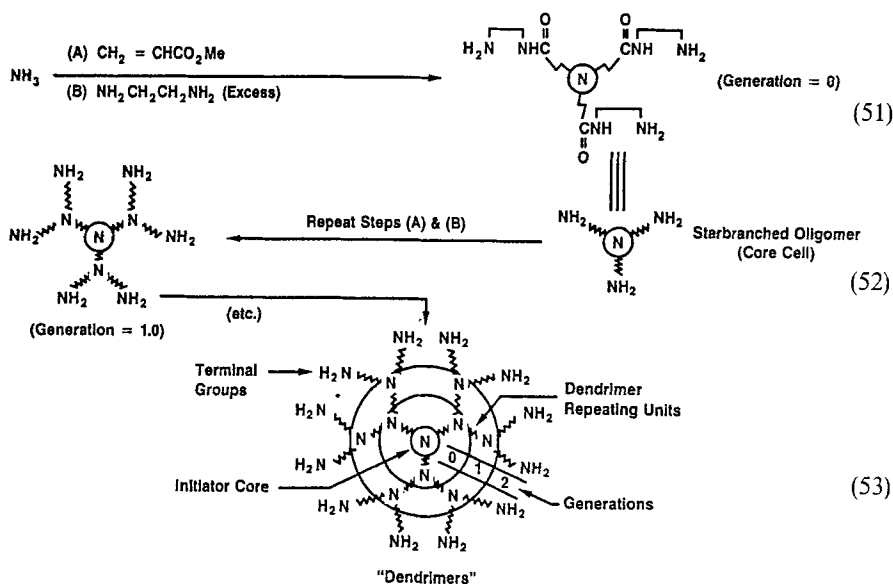
5.2.3.1 In Situ Construction of Branch Cells

Dendrimer construction with this synthetic strategy requires very high yield/conversion syntheses as well as efficient workup procedures for separation of the dendrimers from the reagents. A variety of polypeptide synthesis methods were used successfully for this approach. They included (1) protection/deprotection methods, (2) solid-phase synthesis and (3) excess reagent methods. Either ultrafiltration or preparative HPLC techniques were used for workup and purification. A major advantage offered by this approach is that the steric bulk of the reagents is usually much lower than that of branch cell reagent coupling synthons. This allows one to advance to higher generations by iterative reaction sequences before the cascade (de Gennes) dense-packing occurs.

Poly(amidoamine)-(PAMAM-Starburst)-Dendrimers

Starburst polyamidoamine (PAMAM) synthesis [2, 77–81, 83] may begin with either a nucleophilic or an electrophilic core. In the case of nucleophilic cores such as ammonia or amine, step A in Scheme 21 involves exhaustive Michael addition to methyl acrylate. This addition occurs very rapidly and in high yield with essentially complete selectivity and no amidation at room temperature. Step B requires addition of this triester intermediate to a large excess of ethylenediamine at room temperature to produce the terminal triamine core cell shown in Fig. 2 and Scheme 21. Repeating the sequence of steps A and B leads, via a hexaester

(generation = 0.5), to a hexamine (generation = 1.0). Continuing the sequence of steps A and B (Scheme 21) produces increasingly higher generations. Dendrimer growth beyond generation 3 simply introduces more concentric tiers of interior branch cells which provide scaffolding for surface branch cells whose number follows a geometric progression. Ideal branching growth will produce dimensionally precise surfaces with a defined number of surface groups (see Table 2).



Scheme 21

Table 2. Starburst Polyamidoamines $N_c = 3$; $N_b = 2$

Generation	Molecular Weight	Monomer Units	Number of Terminal Groups, Z(-NH ₂)	Diameters (Å)		
				Predicted* (A) \longleftrightarrow (B)		Actual SEC
(Core Cell)	359	3	3	9.6 \longleftrightarrow 19.2		10.8
1	1043	9	6	12.8 \longleftrightarrow 28.8		15.8
2	2411	21	12	17.6 \longleftrightarrow 41.6		22.0
3	5147	45	24	24.1 \longleftrightarrow 51.2		31.0
4	10632	93	48	30.6 \longleftrightarrow 65.6		40.0
5	21563	189	96	38.5 \longleftrightarrow 81.6		53.0
6	43451	381	192	47.5 \longleftrightarrow 91.2		80.0
7	87227	765	384	61.8 \longleftrightarrow 104.0		10.8
8	174779	1533	768	78.0 \longleftrightarrow 117.0		92.0
9	349883	3069	1536	98.0 \longleftrightarrow 130.0		105.0
10	700091	6141	3072	123.0 \longleftrightarrow 143.0		124.0

* Measured from CPK models

(A) = 3-dimensional contracted

(B) = 3-dimensional extended

The present tridendron PAMAM dendrimer series increases its diameter by approximately 10 Å per generation, evolving from a disk-like shape (generations 0–2) to an oblate spheroid (generations 3, 4), to a nearly symmetrical spheroid at generations 5 and higher [147] (see Fig. 36). Successful syntheses of ideal highly branched PAMAM dendrimers through generation 10 have been completed.

Alternatively, initiator cores have been tethered to solid support (Merrifield resins [83]). Using protein synthesis procedures that avoid the workup difficulties involved in handling large excesses of reagents, one can readily control dendrimer growth. Unfortunately, only noncleavable linkers have been examined to date with these PAMAM dendrimers. The use of initiator cores possessing cleavable linkers should make dendrimer synthesis and isolation very facile. This was demonstrated for mono-dendrons derived from poly(lysines) as reported by Tam et al. [105–107] (Fig. 26).

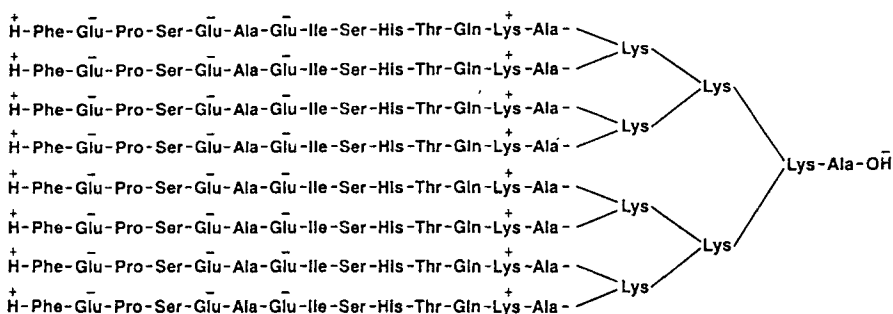


Fig. 26. An octameric multiple antigen peptide grafted to the surface of a poly(lysine) monodendron

A variety of mono-, di-, tetra-, and polydendron PAMAMs have been synthesized from simple amines as well as linear polyamine cores [2, 83, 124]. Linear poly(ethylenimines) with core multiplicities (N_c of ca. 300–400) have been shown to produce high-aspect ratio, rod-like dendrimers at generation 3 or 4 [2]. Their length is determined by the degree of polymerization (n) of the initiator core and their diameter is derived from the number of generations (see Scheme 3).

Poly(ethyleneimine)-(PEI)-Dendrimers

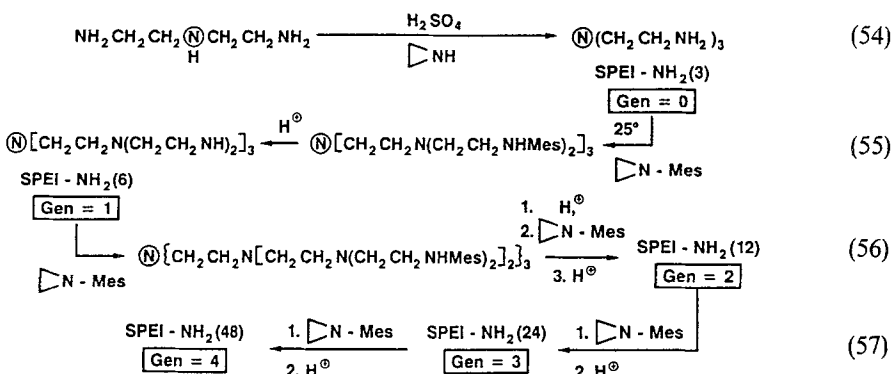
Poly(ethyleneimine) (PEI) has been examined extensively both in its classical, random branched topology [125] and in its linear form [126]. The various architectural and topological forms of PEI have been reviewed recently [127]. Here we describe the first example of this polymer system as an ideal, hyper-branched molecular assembly. Synthesis of a tri-dendron poly(ethyleneimine) dendrimer derived from an ammonia core involved, first the selective alkylation of diethylenetriamine (DETA) with aziridine to produce a symmetrical core cell, namely tris-(2-aminoethyl)amine. Subsequent exhaustive alkylations of the terminal amino moieties with activated aziridines [2, 127, 128], such as *N*-tosyl- or *N*-mesylaziridine gave very good conversions to the first-generation protected

Starburst PEI (SPEI) dendrimer (see Scheme 22). Deprotection by acid hydrolysis yielded the demasked first-generation dendrimer. The higher generations were obtained by simply repeating these sequences. These SPEIs are described by the following general notation:

$$N[(CH_2CH_2N^<)_x (H)_y]_{N_a}$$

$$x = \left(\frac{N_b^{G+1} - 1}{N_b - 1} \right), \quad y = N_b^{G+1}, \quad N_c = 3, \quad N_b = 2$$

STARBURST POLYETHYLENEIMINE CHEMISTRY



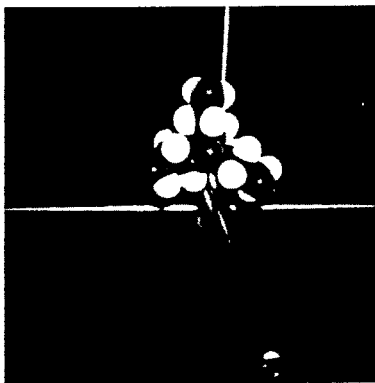
Scheme 22

Table 3. Starburst Polyethyleneimines $N_c = 3$; $N_b = 2$

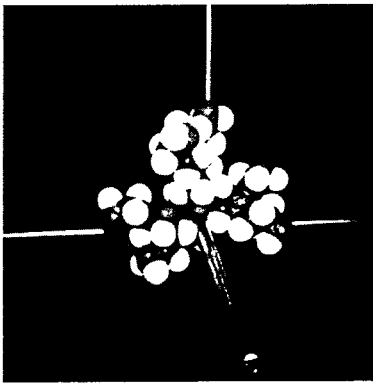
Generation	Molecular Weight	Number of Terminal Groups, Z(-NH ₂)	Diameters (Å)		Actual SEC
			Predicted* (A) \longleftrightarrow (B)		
(Core Cell)	146	3	7.2 \longleftrightarrow 8.8		7.9
1	398	6	11.2 \longleftrightarrow 15.6		15.1
2	917	12	13.6 \longleftrightarrow 19.2		20.0
3	1949	24	18.2 \longleftrightarrow 24.8		—
4	3968	48	23.0 \longleftrightarrow 29.0		—
5	Forbidden Molecular Structure				

* Measured from CPK models
 (A) = 3-dimensional contracted
 (B) = 3-dimensional extended

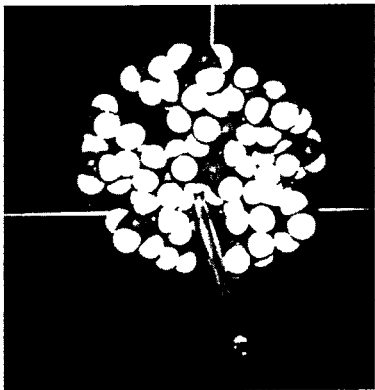
Fig. 27. Corey-Pauling-Koltun (CPK) models of Starburst poly(ethyleneimine) dendrimers of generations 0–5



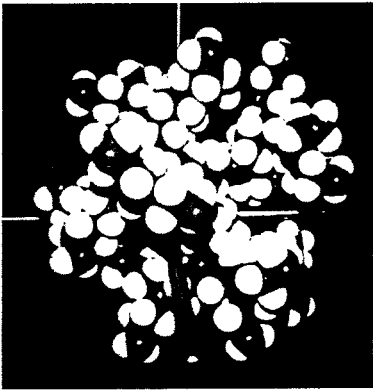
27-1 $G = 0$



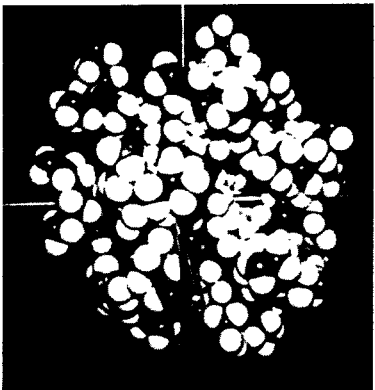
$G = 1$



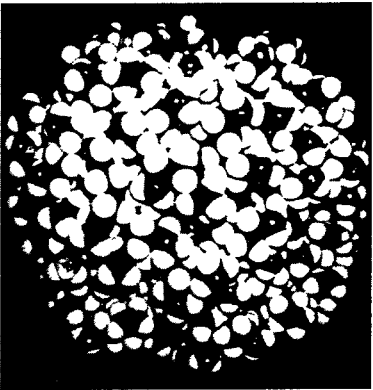
27-2 $G = 2$



$G = 3$



27-3 $G = 4$



$G = 5$

The defect levels become progressively higher and divergence from branch ideality becomes substantial as one approaches generations 3 and 4 and especially generation 5 [2].

These dendrimers have branch cell segments which are approximately one-half the dimensions of the PAMAM series (5 Å versus 10 Å) and possess chemical linkages which have much greater chemical and physical stability. A comparison of theoretical molar masses, number of terminal groups, CPK predicted diameters, and measured diameters (size exclusion chromatography, SEC) as a function of generation is shown in Table 3.

CPK models of generations 0–5 (Fig. 27) show that these SPEIs are much more congested and compact than the Starburst PAMAMs. These models indicate that ideally branched generation 5 is forbidden due to dense packing as described and predicted by be Gennes and others [81, 82, 85, 86].

Hydrocarbon-Dendrimers

(a) Iptycenes

A unique class of structures referred to as iptycenes has recently been reported by Hart et al. [129–131]. These architectures represent the first examples of all-hydrocarbon dendrimer prototypes. Starting with either benzene or triptycene as the initiator core, branch junctures were constructed in situ by Diels-Alder adduct formation to give the heptaipitycene (A) and the nonaipitycene (tri-

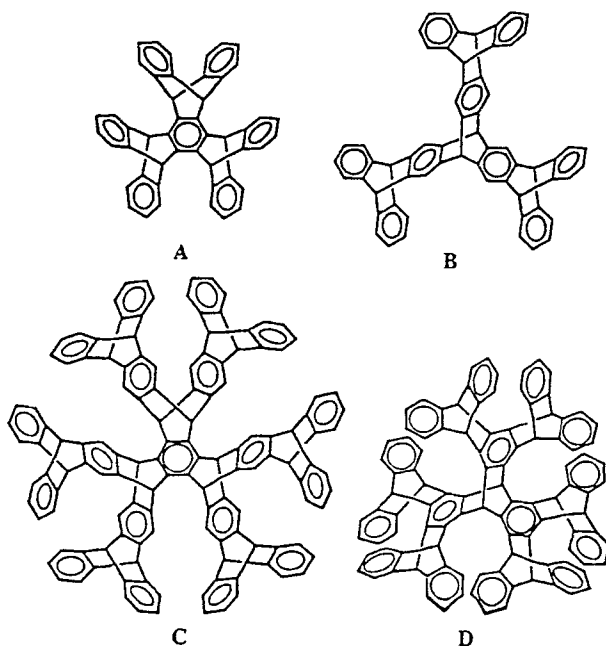
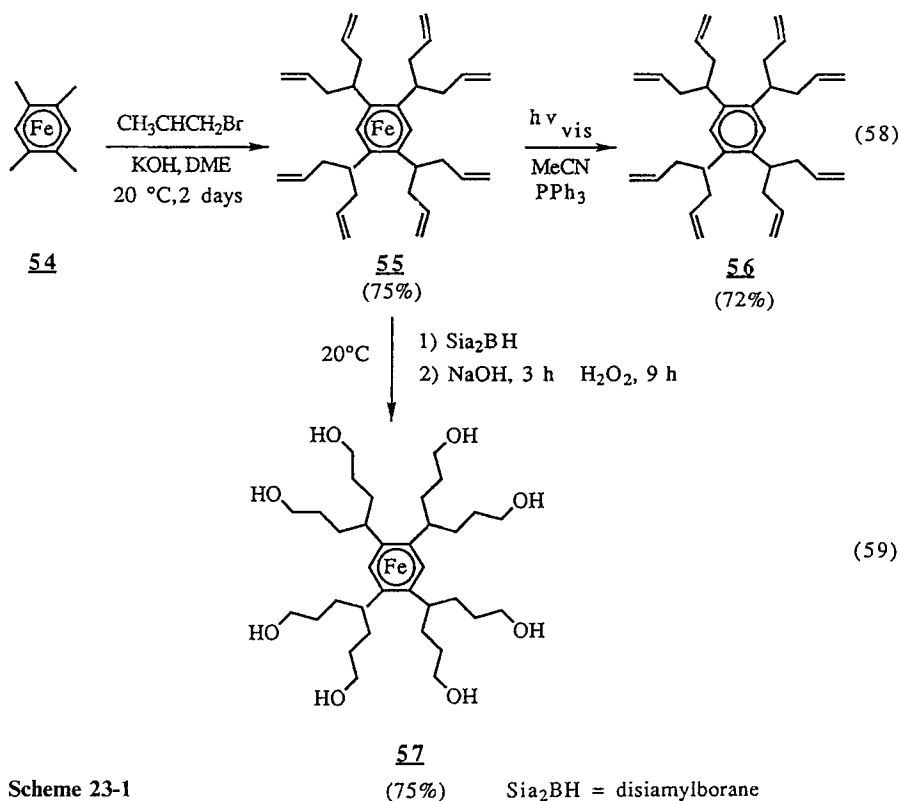


Fig. 28. Hydrocarbon dendrimers (iptycenes): (A) heptaipitycene, (B) nonaipitycene, (C) nonadecaipitycene, (D) supertriptycene

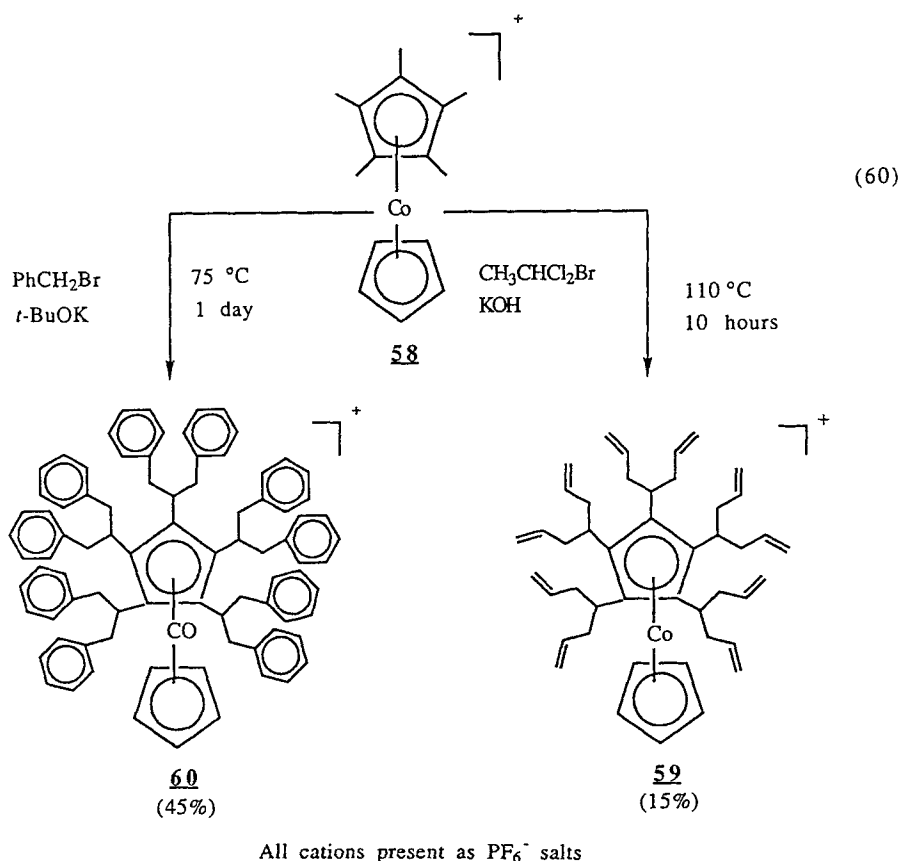
trityptcene) (**B**), respectively (Fig. 28). The tritriptycene derivative possesses molecular clefts defined by parallel benzene moieties ca. 9 Å apart. These U-shaped cavities defined by the arene planes accommodate acetone to form a 1 : 1 crystalline complex which was verified by X-ray structure studies. More recently, Hart et al. [131] have successfully added six more 9,10-dihydroanthracene moieties to (**A**) giving the $C_{132}H_{78}$ hydrocarbon (**C**) (nonadecaityptcene). Similar reactions led to the $C_{104}H_{62}$ hydrocarbon designated supertrityptcene (**D**). These all-hydrocarbon dendrimers clearly illustrate an endo-skeleton strategy for defining three dimensional space at the molecular level.

(b) Organometallic Initiator Cores

Astruc and co-workers [132] have recently described hydrocarbon dendrimers possessing organometallic cores (i.e., Fe or Co). Alkylation or benzylation reactions on polymethyl hydrocarbon ligands complexed with cationic organo-transition metal fragments gave either all-hydrocarbon examples by photolysis or surface functionalization as illustrated in Scheme 23. Substantial evidence was presented for de Gennes type dense packing [85] and sterically induced stoichiometries (SIS) [2, 167] as a function of the size and number of branch cells that were introduced around these organo-metallic cores.



Scheme 23-1



Scheme 23-2

5.2.3.2 Coupling of Pre-formed Branch Cell Reagents

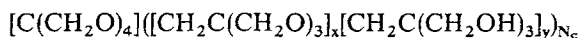
The use of protection/deprotection methods or highly differentiated, branch cell reagents allows selective coupling without bridging or looping side reactions. Table 4 summarizes just a few of the branch reagents used successfully so far.

Poly(ether)-Dendrimers

This dendritic series includes examples of the most highly branched, as well as the shortest-branch, segmented dendrimers produced to date [82, 133]. The high initiator core multiplicity ($N_c = 4$), combined with high branch multiplicity ($N_b = 3$), produces very compact, highly congested microdomains which possess, at most, only very small internal voids. This homologous series has the following general notation:

Table 4. Branch cell Reagents

$N_b = 2$	References	$N_b = 3$	References
$\text{NH}_2 \diagup \text{N} \begin{cases} \text{CH}_2\text{CH}_2\text{NH}_2 \\ \text{CH}_2\text{CH}_2\text{NH}_2 \end{cases}$	(83)	$\text{HO} - \text{C} \begin{cases} \diagup \text{OH} \\ \text{---} \text{OH} \\ \diagdown \text{OH} \end{cases}$	[133]
$\text{NH}_2 - (\text{CH}_2)_5 - \text{CH} \begin{cases} \text{CO}_2\text{H} \\ \text{NH}_2 \end{cases}$ $-(\text{CH}_2)_{1-3}$	(90)	$\text{HS} - \text{C} \begin{cases} \diagup \text{OH} \\ \text{---} \text{OH} \\ \diagdown \text{OH} \end{cases}$	[133]
$\text{H} - \text{N} \begin{cases} \text{CH}_2 - \text{CH}_2\text{OH} \\ \text{CH}_2 - \text{CH}_2\text{OH} \end{cases}$	(83)	$\text{NH}_2 - \text{C} \begin{cases} \diagup \text{OH} \\ \text{---} \text{OH} \\ \diagdown \text{OH} \end{cases}$	[92-94]
$\begin{array}{c} \text{Me} \\ \\ \text{C} \begin{cases} \diagup \text{OH} \\ \text{---} \text{OH} \\ \diagdown \text{OH} \end{cases} \end{array}$	(133)	$\text{HC} \begin{cases} \diagup \text{CO}_2\text{Et} \\ \text{---} \text{CO}_2\text{Et} \\ \diagdown \text{CO}_2\text{Et} \end{cases}$	[92-94]
		$\text{HGe} \begin{cases} \diagup \text{C}_6\text{F}_5 \\ \text{---} \text{C}_6\text{F}_5 \\ \diagdown \text{C}_6\text{F}_5 \end{cases}$	[110]
		$\text{Cl} - \text{C} \begin{cases} \diagup \text{C}_6\text{H}_5 \\ \text{---} \text{C}_6\text{H}_5 \\ \diagdown \text{C}_6\text{H}_5 \end{cases}$	[83]

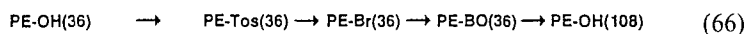
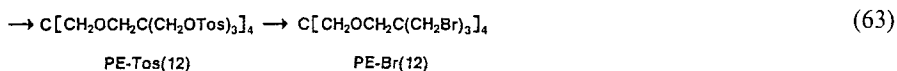
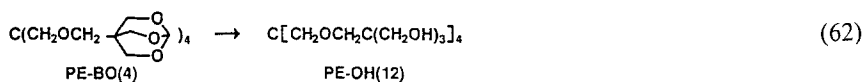
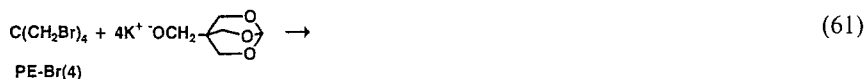


$$x = \left(\frac{N_b^G - 1}{N_b - 1} \right), \quad y = N_b^G, \quad N_c = 4, \quad N_b = 3$$

Standard synthetic methods are used to couple partially protected pentaerythritol to the core cell and subsequent dendrimer surfaces [82, 133]. Synthesis of the first generation involves displacement of bromide from $\text{C}(\text{CH}_2\text{Br})_4$ with a masked pentaerythritol (bicyclic orthoester). One obtains three hydroxyl groups per terminal group after deprotection (Scheme 24). Therefore, a series that triples both its surface hydroxyl groups and its molar mass is obtained (see Table 5).

Molecular dynamics simulations described by Goddard et al. [2], clearly demonstrate that these tetra-dendron prototypes assume spheroidal shapes early in their development. Synthetic efforts revealed that branching defects became progressively higher [82] as one advanced from generation 2 to generation 3. The simulations indicate that the fourth-generation dendrimer, possessing 324 hydroxyl surface groups, is a highly constrained, rigid system with essentially no internal voids or channels (see Fig. 29). Starburst dense packing appears to occur between generations 3 and 4.

STARBURST POLYETHER CHEMISTRY



Scheme 24

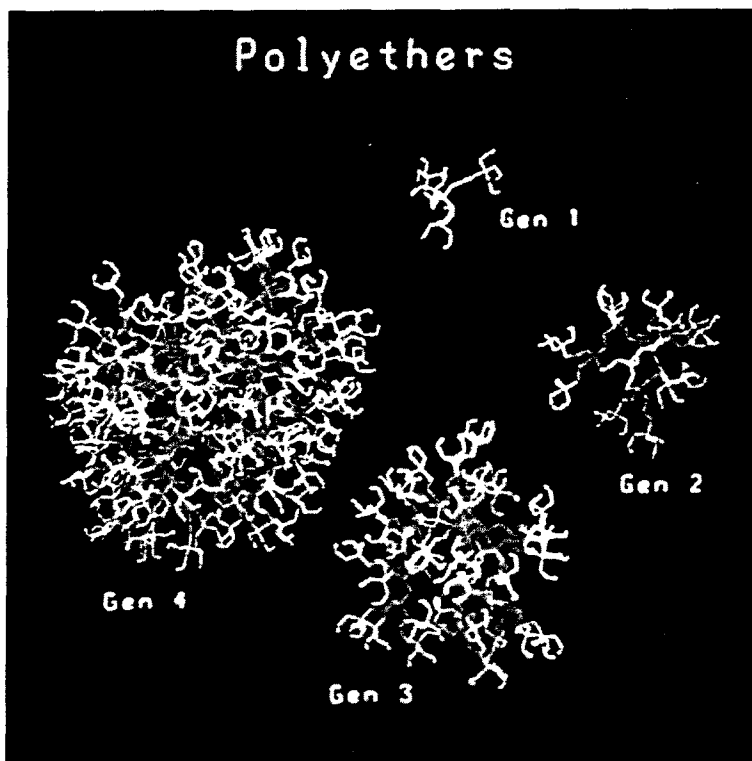


Fig. 29. Computer simulated molecular graphics (wireframe) using POLYGRAF for STARBURST (polyether) dendrimers of generations 1–4

Table 5. Starburst Polyethers $N_c = 4$; $N_b = 3$

Generation	Molecular Weight	Number of Terminal Groups, Z(-NH ₂)	Diameters (Å)		
			Predicted* (A) \longleftrightarrow (B)	Actual SEC	
(Core Cell)	136	4	—	—	—
1	606	12	10.4 \longleftrightarrow 12.0	9.8	
2	2024	36	16.2 \longleftrightarrow 18.4	18.6	
3	—	108	22.4 \longleftrightarrow 24.0	25.0	
<div>4</div>	Forbidden Molecular Structure				

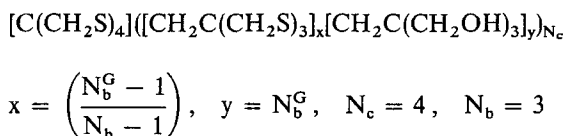
* Measured from CPK models

(A) = 3-dimensional contracted

(B) = 3-dimensional extended

Poly(thioether)-Dendrimers

This series was synthesized according to Scheme 24 as described for the polyethers, with the exception that a mercapto-functionalized, bicyclic orthoester (4-mercapto-methyl-2,6,7-trioxabicyclo-[2.2.2]octane), was used as the branch cell reagent for the coupling step [2, 133]. This produced a dendrimer series containing thioether linkages in the interior with hydroxyl surface groups as described by the following general notation:

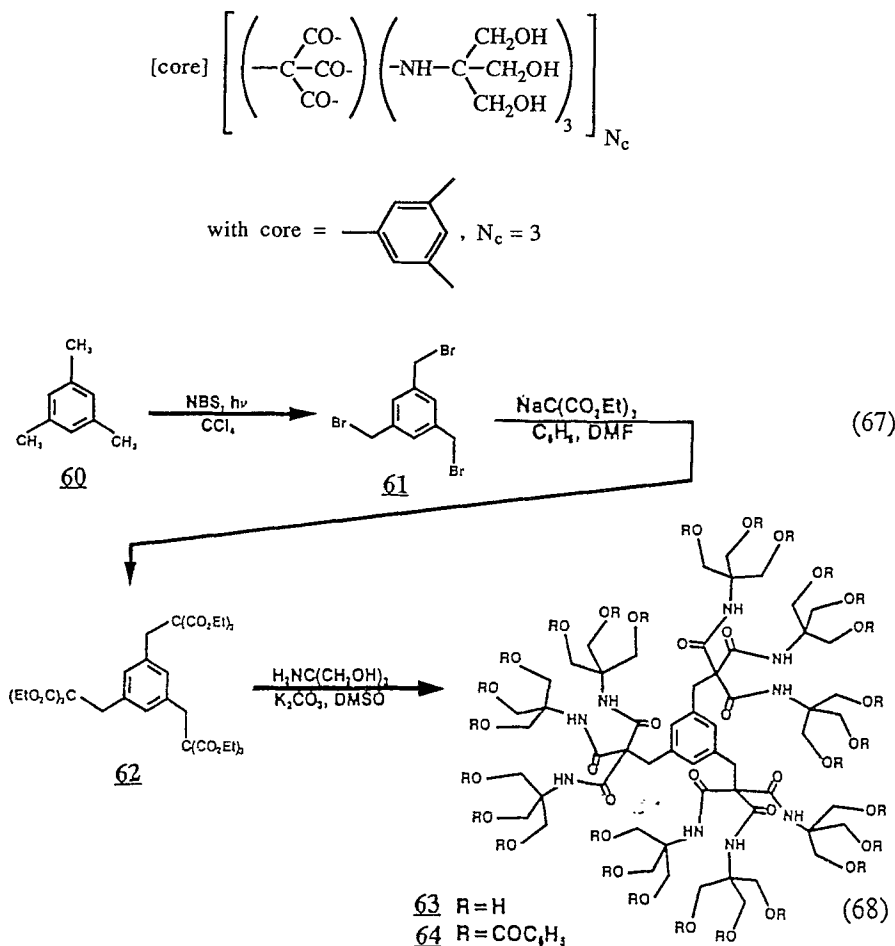


This dendrimer family was successfully proliferated through the second generation to give the poly(thioether) dendrimer with 36 surface hydroxyl groups. This product was confirmed by mass spectroscopy, ¹³C-NMR spectroscopy and size exclusion chromatography. Attempts to advance to generation = 3, by displacement of the 36 terminal bromide groups, gave a product which lost only twelve bromide moieties. Although computer assisted, molecular simulation suggests that this dendrimer family should not “dense pack” until the fourth generation, steric requirements of the bulky mercapto anion in an S_N2 displacement reaction may be leading to this “sterically induced stoichiometry” (SIS) product. In this poly(thioether) series, sterically-induced stoichiometry (SIS) effects are occurring one generation earlier than in the poly(ether) series [2, 167].

Poly(amidoalcohol)-Dendrimers

This dendrimer class is a special example of a heterogeneous series. It possesses branch cells derived from the branch cell reagents; triethyl methanetricarboxylate and aminotris(hydroxymethyl)methane. In the present case, a tri-dendron dendrimer with $N_b = 3$ is obtained by advancement through an alkylation stage and

an amidation step (Scheme 25). The resulting hydroxyl-functionalized dendrimers from these “cascade” syntheses have been coined “arborols” by Newkome and co-workers [92–94]. They described the synthesis of mono-, di-, and tri-dendron prototypes, with the following general structural notation ($N_b = 3$);

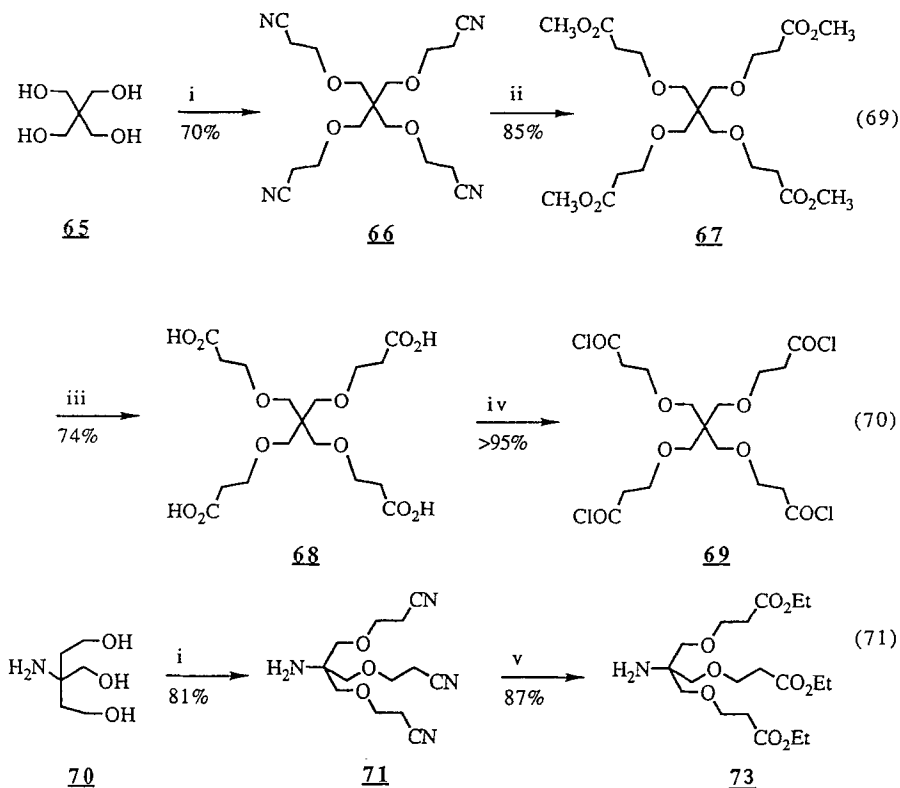


Scheme 25

This method leads to very compact, highly branched dendrimers possessing as many as 27 surface groups. Reiterative chemistry, which would allow advancement to higher generations, was not reported on this series, presumably due to the “neopentyl” terminal branch cells which inhibited further dendrimer proliferation. In order to circumvent this problem, homologation by introduction of a separate spacer was reported, but added additional synthetic steps [92]. Certain di-dendron prototypes possessing a hydrocarbon interior and a “barbell-like” architecture, self-assemble into an orthogonal array to give rod-type nanostructures [134].

Poly(amidoether)-Dendrimers

More recently, however, an iteration sequence has been developed by these workers which involves elongation of the arms on tris-(hydroxymethyl)aminoethane as shown in Scheme 26. Using such a differentiated branch cell reagent ($-\text{CO}_2\text{H}$ form), successive coupling in the presence of dicyclohexylcarbodiimide and



Reaction Conditions:

- (i) $\text{CH}_2=\text{CHCN}$, KOH, *p*-dioxane, 25 °C, 24 h
- (ii) MeOH, dry HCl, reflux, 2 h
- (iii) 3 N NaOH, 70 °C, 24 h
- (iv) SOCl_2 , CH_2Cl_2 , reflux, 1 h
- (v) EtOH, dry HCl, reflux 3 h

Scheme 26

1-hydroxybenzotriazole gave dendrimer families with several combinations of initiator cores and branch cell reagents. For example Fig. 30 illustrates dendrimers derived from a pentaerythritol core and tris-[(carboxyethoxy)methyl]aminomethane branch cells [135], whereas in the other case an adamantane core and 4-amino-4-(3-acetoxypentyl)-1,7-diacetoxy-heptane branch cell reagent was used

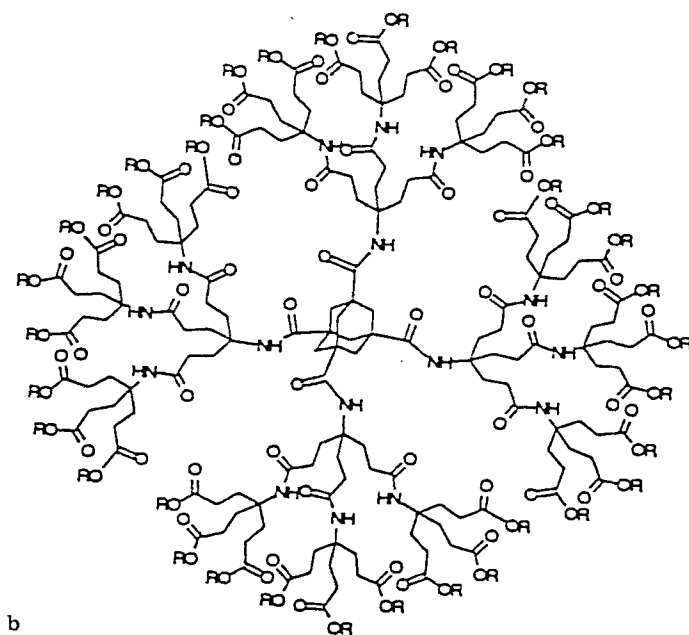
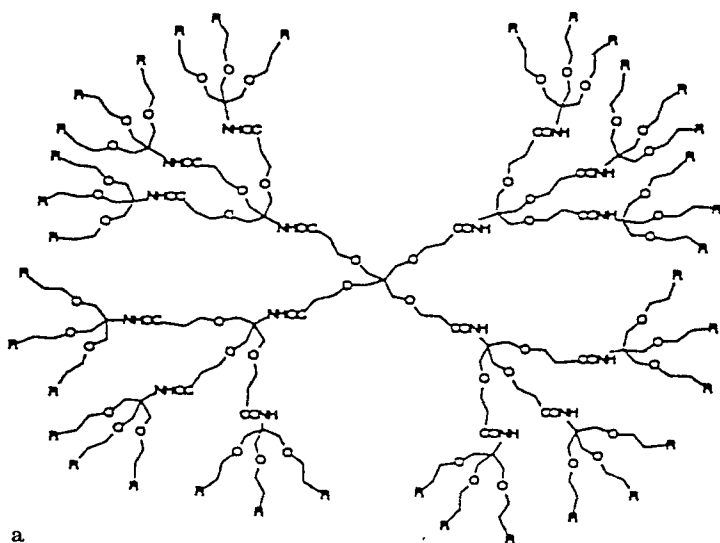
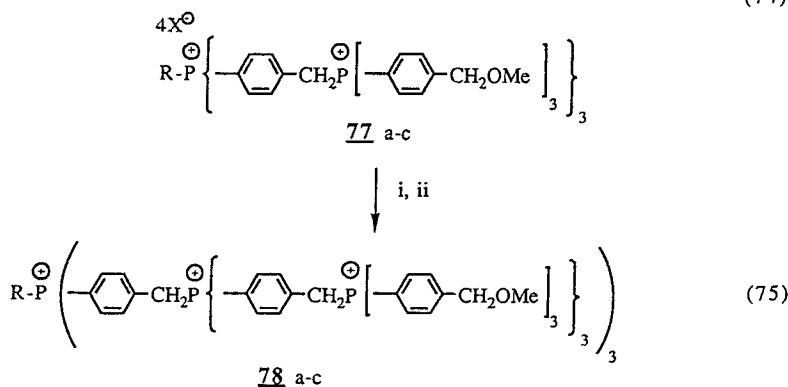
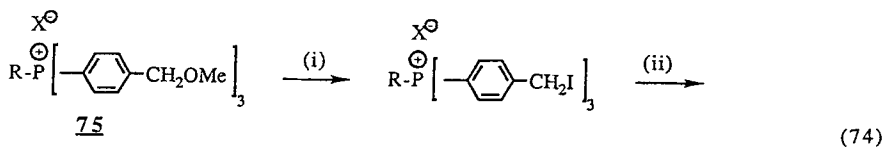
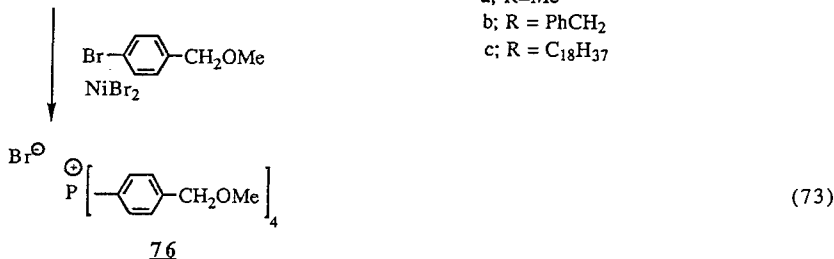
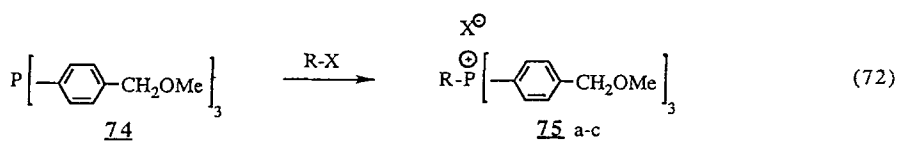


Fig. 30. a) Tetra-dendron dendrimers derived from tris-[(carboxyethoxy)methyl]aminomethane branch cell reagents and a pentaerythritol core. b) Tetra-dendron dendrimer derived from 4-amino-4-(3-acetoxypentyl)-1,7-diacetoxypentane branch cell reagents and an adamantane core

[136]. A unique dendrimer series possessing an all-hydrocarbon interior and up to 36 surface carboxylic acid groups has exhibited very interesting unimolecular micelle properties. These products have been shown to form host-guest complexes with various hydrophobic guest molecules. Newkome refers to these products as "micellanes" [137, 138].

Poly(arylamine)-Dendrimers

Hall et al. [139] produced a low-molar-mass series of polyarylamine dendrimers by using a protection/deprotection scheme involving the protected, branch cell reagent; 2,4-dinitrofluorobenzene. Using various anilines as initiator cores, the



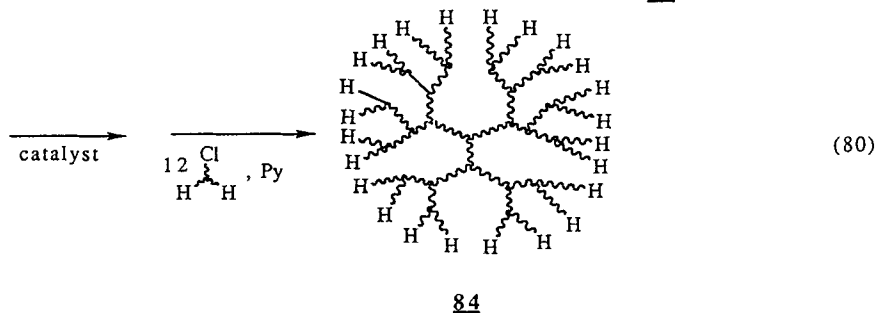
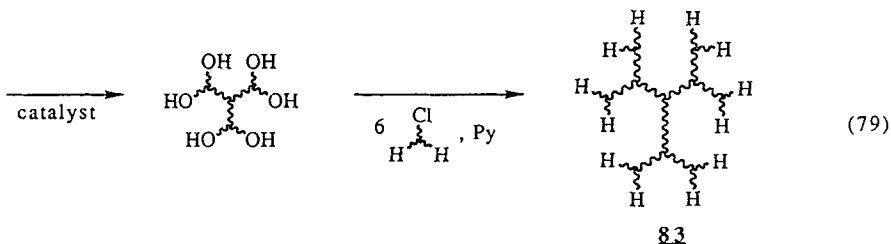
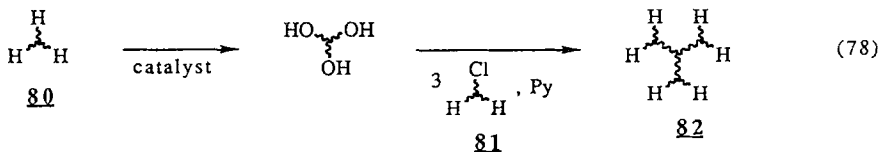
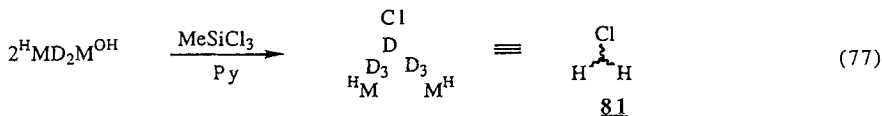
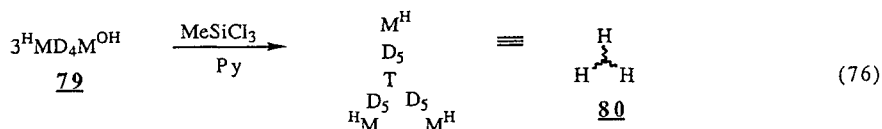
Reagents: (i), $\text{ISi}(\text{Me})_3$; (ii), Compound **74**

Scheme 27

reiteration scheme involved fluoride displacement by the anilines, reduction of nitro groups to amino groups, and subsequent reaction with 2,4-dinitrofluorobenzene.

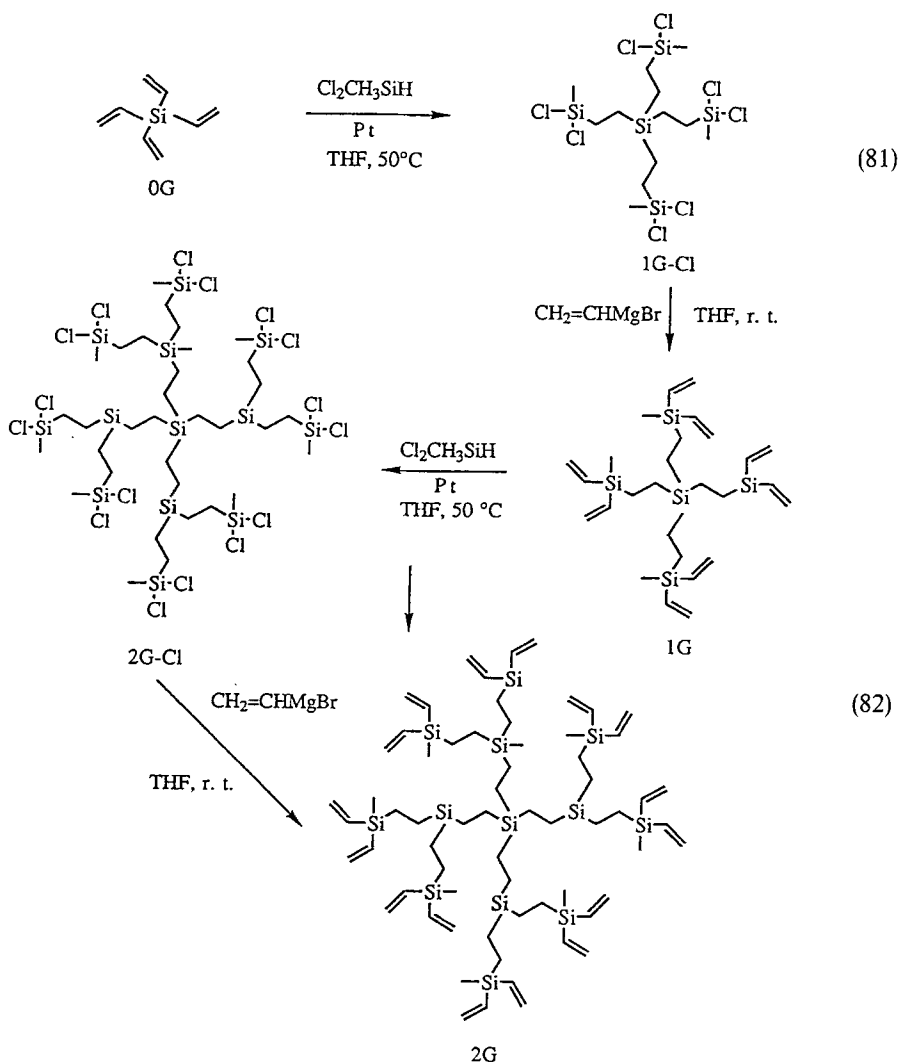
Poly(phosphonium)-Dendrimers

Several dendrimer series in which ionic sites were incorporated at both the initiator core as well as the branch cell juncture have been reported by Engel et al. [140–142]. Dendrimers derived from the initiator cores **74**, **75a–c** and **76** have been synthesized by the reiterative sequence described in Scheme 27. These polycations possess some of the highest N_c and N_b multiples reported for any dendrimer series.



Scheme 28

The reactive branch cell reagent tris(4-methoxymethylphenyl)phosphine (74) was used to construct dendrimers with up to 40 cationic sites within the infrastructure of the molecule. Simply advancing the valency of the central core phosphorous atom, produced tri-, and tetradendron dendrimers. In most of these poly(phosphonium) dendrimers, separate ^{31}P -NMR signals for the core and peripheral phosphonium ion sites could be observed thus illustrating the hierarchial nature of the branch cells within these molecules.

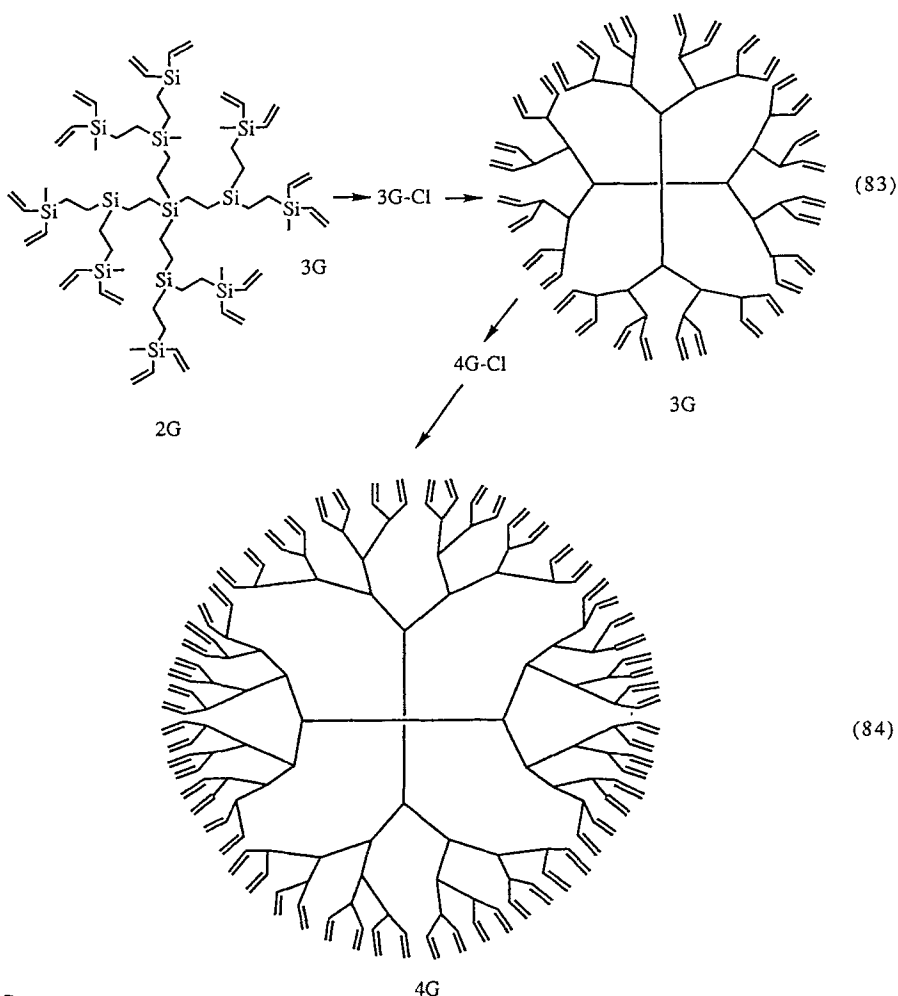


Scheme 29-1

Poly(siloxane)-Dendrimers

Masamune et al. [143] were the first to report the synthesis of silicone dendrimers. They used a divergent strategy similar to that used by Tomalia et al. for the construction of PAMAM dendrimers [2, 79]. The synthesis of these dendrimers involved first the use of a trifunctional core unit possessing ($-\text{Si}-\text{H}$) surface groups. Catalytic conversion of these surface groups to ($-\text{Si}-\text{OH}$), followed by treatment with a silicone branch cell reagent with the general structure ($\text{Cl}-\text{Si}(\text{Me})_2-\text{Si}(\text{Me})_2-\text{Si}(\text{Me})_2-\text{Cl}$) introduced the geometric branching characteristics of dendrimers. The general iterative sequencing required for these dendrimer constructions is illustrated in Scheme 28.

This group was successful in proliferating the dendrimeric structures out to generation = 3 to give molecular weights of greater than 14000. All dendrimer



Scheme 29-2

structures were confirmed by ^1H , ^{13}C , ^{29}Si , NMR, size-exclusion chromatography and mass spectroscopy. It should be noted that the surfaces of these silicone dendrimers are coated with $-\text{Si}-\text{H}$ groups, thus rendering them amenable to further chemical modifications.

Kakimoto and coworkers [144] and independently, shall researchen [209] synthesized a series of Starburst poly(siloxanes) using [(phenyldimethyl-siloxy)dimethylsiloxy] methylsilane as an initiator core and divergently proliferating with bis[(phenyldimethylsiloxy)methylsiloxy]dimethylsilanol as the branch cell reagent. Using protection/deprotection schemes, a poly(siloxane) dendrimer (generation = 3) possessing 24 phenylsilyl groups was synthesized and characterized by ^1H , ^{13}C , ^{29}Si , NMR and gel permeation chromatography.

Poly(carbosilane)-Dendrimers

Roovers et al. [145] have reported a high yield iteration sequence leading to the synthesis of poly(carbosilane) dendrimers. The sequences involve (a) hydrosilylation of the initiator core, tetravinylsilane, with four moles of dichlorosilane, followed by (b) treatment with vinyl magnesium bromide to generate a dendrimer with eight vinyl groups attached to four silicon atoms (generation = 1.0) as illustrated in Scheme 29.

Reiteration ultimately leads to a generation = 4 stage dendrimer possessing as many as 64 silicon chloride or vinyl surface groups. These dendrimers have been utilized as macromolecular termination templates for quenching polybutadienyl lithium to give 64 armed star polymers.

6 Characterization of Dendrimers

The structural subtleties represented in these dendrimer topologies require a variety of analytical methods for unequivocal characterization. The following dendrimer features were studied by these methods:

1. *Elemental composition*: C, H, N analyses; mass spectrometric fragmentation patterns.
2. *Molar mass versus generation*: low-angle laser light scattering (LALLS); chemical ionization, fast atom bombardment, laser desorption and electrospray mass spectroscopy; vapor phase osmometry; electrophoresis.
3. *Homogeneity*: size exclusion chromatography (SEC) coupled with low-angle laser light scattering (SEC-LALLS); electron microscopy, atomic force microscopy, scanning tunnel microscopy; capillary electrophoresis.
4. *Interior and end groups*: IR spectroscopy; ^{15}N , ^{13}C , ^{31}P , ^{29}Si , ^2H and ^1H NMR spectroscopy; titration.
5. *Structures*: ^{13}C , ^1H and ^2H NMR spectroscopy (T_1 relaxation times, signal intensity ratio versus generation); rheology studies; electron microscopy; computer-assisted molecular simulations, comparison to CPK models; electrospray mass spectroscopy; fluorescence probe analysis.
6. *Dimensions*: Electron microscopy; intrinsic viscosity measurements; size exclusion chromatography; computer-assisted molecular simulations, comparison with CPK models; atomic force microscopy; electrophoresis; neutron scattering.

These methods were used extensively for structure verification of dendrimers prepared by the divergent initiator core method such as Starburst PAMAM [124] poly(ether) [82], and poly(ethylenimine) dendrimers [2], as well as poly(siloxane), poly(phosphonium), poly(arylalkyl)ether, poly(arylene) and poly(arylester) dendrimers. In many cases, small-molecule model systems were used for process optimization, defect identification, and stoichiometry studies.

In the case of PAMAMs, dendrimer bridging, looping and branching defects were identified and minimized by process optimization and/or special purification techniques. Initial work indicated that it would be difficult to prepare dendrimers beyond generations 4 and 5 without bridging [124]. More recent work [167, 169] has shown that generations 0–10 can be obtained in very monodispersed form with branching “idealities” of 95 mole% or greater per generation.

A repertoire of possible defects that might be encountered in the synthesis of many of these dendrimer families is as illustrated in Fig. 31.

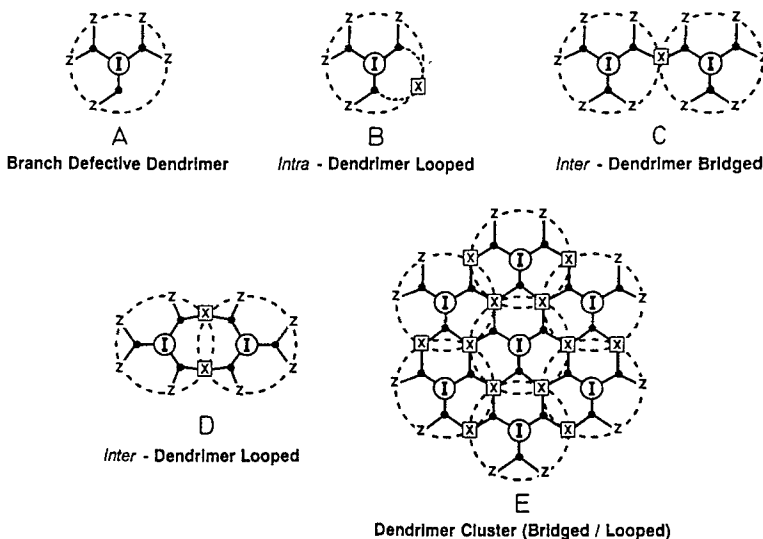


Fig. 31. Two-dimensional projections of various branch-cell defects which may lead to divergence from ideal dendrimer development. Branch defective dendrimer, A; intra-dendrimer looping, B; inter-dendrimer bridging, C; inter-dendrimer looping, D; dendrimer cluster (bridged/looped), E

Presently, defects of the type A and B are the only serious side-reactions encountered in the synthesis of Starburst PAMAM dendrimers (generation = 0–10) by the “divergent initiator core method”. Defects of the types C, D and E have been minimized to under 3–5 mole% per generation. Polydispersities (M_w/M_n) of 1.0007 have been routinely observed for Starburst PAMAM dendrimers (generation = 4; NH_3 core) which has an empirical formula of $\text{C}_{465}\text{H}_{933}\text{N}_{187}\text{O}_{93}$ and a calculated molecular weight of 10632, as verified by electrospray mass spectroscopy [169].

6.1 Branching Ideality

^{13}C -NMR spectroscopy and electrospray mass spectroscopy have served as the best methods for appraising branch defects. With ^{13}C -NMR, the symmetry of ideally branched dendrimers produces discrete resonances which are well separated from branch-defect signals (Fig. 32). The branch defects occur when acrylate alkylations are incomplete. The result of such a defect is to give lower molar-mass and surface-group values than theoretically expected. Secondary amine groups resulting from branch defects may become alkylated during advancement to the next generation. The consequence of such an event is that the progeny of such defects are one generation retarded in branch-cell development compared to the rest of the molecule.

The structure of a molecule that results from a sequential, reiterative process must reflect its unique history of preparation. If an individual dendrimer is incompletely reacted at a given generational stage of the synthesis, the molecule will have less than the ideal molecular weight, and further iterations will also give correspondingly low molecular weights at the higher generations. For any

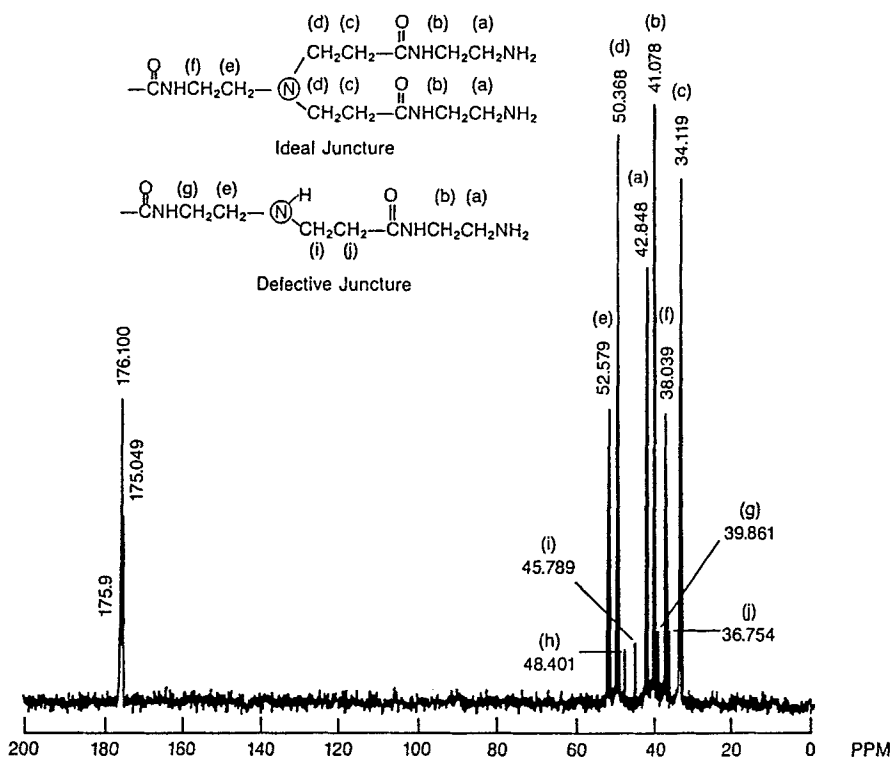


Fig. 32. ^{13}C -NMR spectrum of Starburst PAMAM dendrimers of generation = 7 with assignments for ideal and defective branches (defective branch level ca. 5 mol%)

molecular weight, there will be a finite number of isomers and the isomeric form must reflect the stage at which the incomplete conversion took place. Thus, a selected isomer may only be formed from a subset consisting of the precursor generation masses/isomer distributions and may be converted only into a subset of the successor generation masses and isomer distributions. The partitioning of the isomers derived from a given structure will be the product of the statistics for the conversion into those isomers.

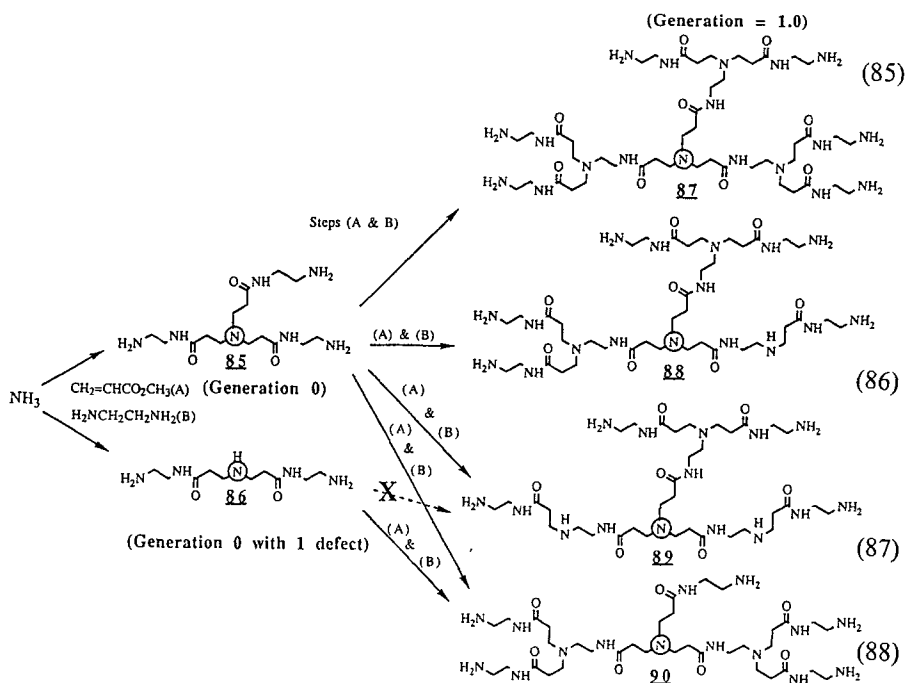
Examination of the product distribution of a given sample should, therefore, provide an insight into the history of the sample preparation, with the average molecular weight giving an overall efficiency of the conversions and the shape of the mass/isomer distribution indicating whether the efficiency was higher earlier or later in the sequence of reactions. This can be accomplished by comparison of a statistical model for branching defects with measured distributions. As a first approximation, all of the reactive sites of the dendrimer may be treated as equivalent, allowing the use of a simple binomial model which requires only an extent of reaction parameter to calculate theoretical molecular weight distributions. For example, the proportions of each component for generation 0 is given by:

$$\begin{aligned} & \text{[mole fraction of D.P. (degree of polymerization) = } n \text{]} \\ &= \frac{3!}{n!(3-n)!} p^n (1-p)^{3-n} \end{aligned}$$

where p is the probability that an individual site is substituted.

For generation 1, the distributions derived from each of the four components of generation 0 are similarly computed, giving 7 terms from the ideal, D.P. = 3 component and 6, 5, and 4 terms from the D.P. = 2, 1, and 0, respectively. Each term is weighted by the mole fraction of its precursor, the terms for each given D.P. are combined to give a total distribution from D.P. = 0 to 9. Reiteration of this procedure to the fourth generation gives a distribution from D.P. = 0 to 93.

Substitution of different values of p at each generation allows the modelling of variations of reaction efficiency from generation to generation. An example of this is presented in Scheme 30 for generation = 1; Starburst poly(amidoamine). Reaction of ammonia with methyl acrylate, following by treatment with ethylenediamine, gives predominantly the ideal generation 0 dendrimer, **85**, with traces of dendrimer lacking one or more branches. The one missing branch species is the major non-ideal component. Reiteration of the process converts **85** predominantly to ideal generation 1 dendrimer **87** and lesser amounts of one branch missing **88** and isomeric two branch missing **89** and **90** components. Simultaneously, the non-ideal components are converted to corresponding higher mass components as illustrated by the complete substitution of **86** to give **90**. Note that **86** is not converted to **89** the isomer of **90** or any of the more ideal species **87** and **88**. *Thus, the isomeric composition of a sample could be used to infer the synthesis history of a sample.*



Schema 30

If, for example, two samples were prepared such that $p = 1.00$ for the first iteration (sample 1) and $p = 0.95$ for the second iteration (sample 2), the distribution of masses would be as follows:

<i>Dendrimer</i>	87	88	89 & 90
Sample 1	73%	23%	3%
Sample 2	86%	0%	13%

The portion unaccounted for includes all of the lower mass components. For each of these samples, the number average molecular weight would be $M_n = 1009.8$, but the weight average molecular weights would be $M_w = 1013.5$ and 1017.1 , respectively. A sample prepared with $p = .0975$ for both iterations would have a distribution of 80%:12%:7%, $M_n = 1009.8$, and $M_w = 1015.4$.

Data for comparison to the model were obtained via the electrospray ionization mass spectrum of a Starburst PAMAM; dendrimer (core = NH_3); generation = 4 between m/z 600 and 1600. The ESI mass spectrum consisted predominantly of multiple charged ions at +7, +8, +9, +10, and +11 charge states. The deconvoluted mass spectrum between 9600 and 10747 daltons suggest the presence of at least 16 components in the sample. The last significant peak at 10632 daltons corresponds with the theoretical mass 10632.96, “magic number” which is within one mass unit for the ideal generation = 4 structure (see Fig. 33).

Generation = 4.0

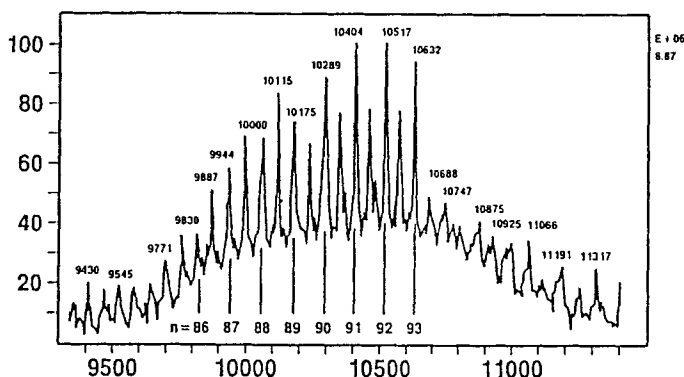
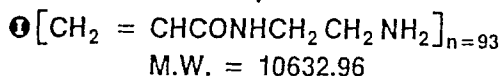
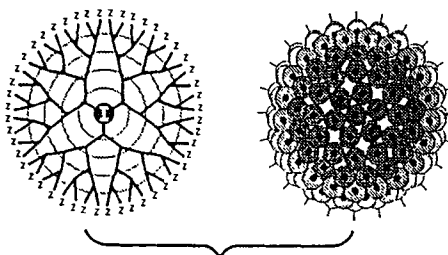
 $N_c = 3; N_b = 2$ $\textcircled{1} = \text{NH}_3$ 

Fig. 33. Electrospray ionization mass spectrum of a Starburst PAMAM (generation = 4). Note the last significant peak; $M = 10632$ daltons (degree of polymerization = 93), corresponding to the “magic number” for ideal structure. The remaining labeled species correspond to $M - x(114)$; (defects due to missing monomer units) and the unlabeled species which correspond to $M - x(60)$; (defects due to macrocycle formation)

All components differing by 114 mass units correspond to incomplete reaction leading to molecules lacking various numbers of poly(amidoamine) repeat units ($\text{CH}_2 = \text{CHCONHCH}_2\text{CH}_2\text{NH}_2$; MW 114).

A summary of the measured data from the deconvoluted spectrum in Fig. 33 is presented in Table 6. Based on these data the polydispersity is calculated to be 1.0007, which is a significant step toward producing a monodisperse macromolecular system.

Fitting the experimental distribution to distributions calculated as described above leads to the conclusion that the efficiency of reactions for the synthesis of the sample must be between 97 and 98% for each step [169]. Polydispersity indices derived from the calculated distributions include the trace low molecular weight species that would be present but undetectable at the experimental signal to noise ratio, giving a more realistic measure of polydispersity. Thus, this statistical treatment would place the polydispersity of the sample between 1.005 and 1.003.

In addition to the ideal dendrimer and the molecules lacking whole repeat units ($M = 9600\text{--}10632$), the mass spectrum shows $M-60$ masses for each of the M peaks. These peaks correspond to an additional missing ethylenediamine unit,

Table 6. Number Average Molecular Weight

$$\overline{M}_n = \frac{\sum N_i M_i}{\sum N_i}$$

Weight Average Molecular Weight

$$\overline{M}_w = \frac{\sum N_i M_i^2}{\sum N_i M_i}$$

Intensity (N)	M	N × M	N × M ²
35	9828	343980	3380635440
48	9885	474480	4690234800
44	9950	437800	4356110000
50	10000	500000	5000000000
52	10059	523068	5261541012
58	10115	586670	5934167050
51	10174	518874	5279024076
55	10229	562595	5754784255
82	10288	843616	8679121408
70	10344	724080	7489883520
100	10404	1040400	1.0824E + 10
65	10458	679770	7109034660
77	10518	809886	8518380948
70	10627	743890	7905319030
88	10631	935528	9945598168
945		9714637	1.0013E + 11

$$\overline{M}_n \quad 10290.6212$$
$$\overline{M}_w \quad 10296.3387$$
$$\overline{M}_w/\overline{M}_n \quad 1.0005556$$

which corresponds to cyclic structures, formed during synthesis, which have also been identified by ¹³C-NMR (see Fig. 32). A single cyclization per molecule would account for the M-60 species which, at this generation, would involve two of forty eight terminal groups or 4%. Since the M-60 peaks are less than one half of the intensity of M peaks, less than 2% of the total terminal groups have cyclized. This is also consistent with the observed levels near the detection limit of the NMR spectrometer.

6.2 Monodispersity vs Polydispersity

Very precise appraisals of polydispersities due to branch defects can be made by HPLC fractionation, electrophoresis and mass-spectral analyses of the components. The molecular-mass and polydispersity values thus obtained, corroborate branch-defect ranges determined by high-field ¹³C-NMR spectroscopy.

Although branch defects may contribute in a minor way to dendrimer polydispersities, inter-dendrimer bridging/looping and extraneous Starburst dendrimer growth derived from unremoved propagating reagents are the major contributors. PAMAM dendrimers may be obtained as very monodispersed samples, if

propagating reagents and bridged forms can be removed at each stage. This is accomplished by ultrafiltration with appropriate pore-size membranes. With this technique, polydispersities of 1.01–1.08 were obtained for generations 0–10. Molecular masses, polydispersities, and hydrodynamic diameters are routinely determined by use of size exclusion chromatography (SEC), low-angle laser light scattering (LALLS), electrophoresis and intrinsic viscosity measurements ($[\eta]$). Figure 34 illustrates typical size exclusion chromatograms that may be obtained for a Starburst PAMAM (NH_3 core) series; generations = 0–8.

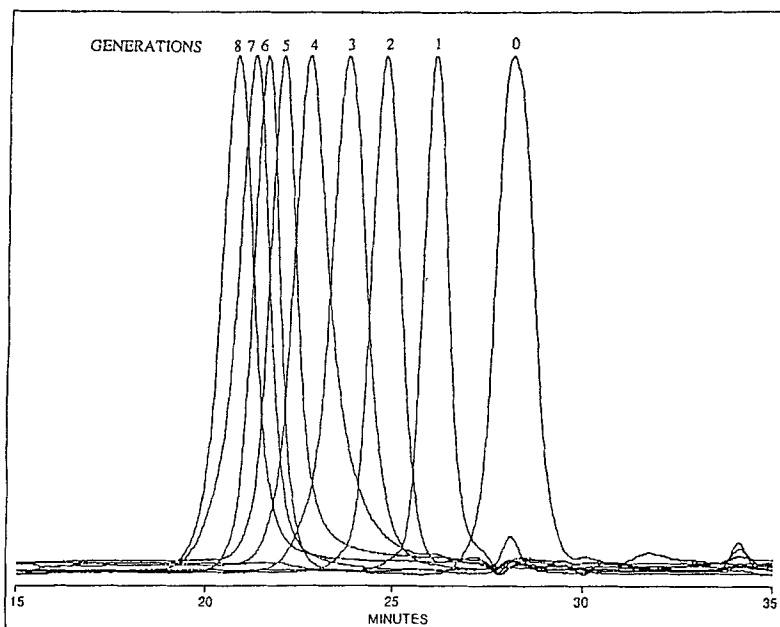


Fig. 34. Size exclusion chromatograms (SEC) for Starburst PAMAM dendrimers (generations = 0–8) as a function of elution times (minutes)

Using half-generation dendrimers possessing ($-\text{CO}_2^{\ominus}\text{Na}^{\oplus}$) surfaces, Dubin and Tomalia [155] have shown that a single universal (SEC) calibration curve for spheres can be derived which has important implications for protein chromatography.

6.3 Dendrimer Topology, Branch-Cell Differentiation and Surfaces

6.3.1 Initiator-Core and Core-Cell Effects

As previously mentioned (see also Fig. 3), the initiator core/core cell acts as the primary template which permits the introduction of very important molecular information (size, shape, multiplicity $[\text{N}_c]$) and specific function. For example, introduction of a specific function such as a chromophore [2] or metal chelator [132] in the initiator core represents stored information which will become buried

by subsequent generations. In contrast, parameters such as size, shape, and multiplicity will be transcribed and displayed (translated) throughout the dendrimer development. These variables frequently have dramatic effects on the ultimate shape, the interior topology, and the exterior surface properties (congestion) of the developing dendrimer.

6.3.2 Interior Development

The interior of a dendrimer may be characterized by branch-cell differentiation, topology, and the evolution of a branch-cell hierarchy as well as by size, chemical composition, multiplicity, and flexibility. Branch-cell differentiation, in particular, can dramatically change not only the interior topology but also the gross exterior surface of a dendrimer. Symmetrical branch junctures appear to favor "shell topology" formation if they have adequate branch-segment lengths l and the N_c and N_b values are not too high. Asymmetrical branch junctures, as represented by Denkwalter dendrimers (Figs. 16 and 17) exhibit a more classical relationship between density and molecular mass [84] (Fig. 35). Presumably, this is due to more effective interior packing of the asymmetrical branch cells.

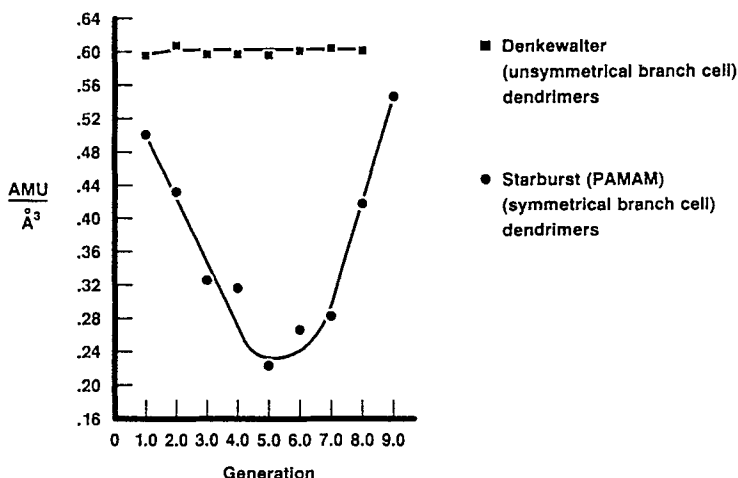


Fig. 35. Dependence of density on generation for symmetrically branched and asymmetrically branched dendrimers. amu = atomic mass unit. ■, Denkwalter dendrimers (unsymmetrical branch cells); ●, Starburst PAMAM dendrimers (symmetrical branch cells)

6.3.3 Starburst (de Gennes) Dense Packing — A Critical Branched State?

Dendrimer surface congestion can be mathematically appraised as a function of generation, from the following relation:

$$A_z = \frac{A_D}{N_z} \propto \frac{r^2}{N_c N_b^G}$$

where A_z is the surface area per terminal group Z, A_D the dendrimer surface area, and N_z the number of surface groups Z per generation. This relationship predicts that at higher generations G, the surface area per Z group becomes increasingly smaller and experimentally approaches the cross-sectional area or van der Waals dimension of the surface groups Z. The generation G thus reached is referred to as the Starburst (de Gennes) dense-packed generation. As predicted by de Gennes and Hervet [85], an ideal cascade growth without branch defects is possible only for those generations preceding this dense-packed state. This critical dendrimer property gives rise to self-limiting dendrimer dimensions, which are a function of the branch cell segment length l , the core multiplicity N_c , the branch cell juncture multiplicity N_b , and the steric dimensions of the terminal group Z. Whereas the dendrimer radius r in the above expression is dependent on the branch cell segment lengths l , larger l values delay this congestion, whereas, larger N_c , N_b values and larger Z dimensions dramatically hasten it.

As early as 1983, de Gennes and Hervet [85] proposed a simple equation derived from fundamental principles, to predict the Starburst limited or dense-packed generation m_1 for PAMAM dendrimers. Based on ideal dendrimer growth, with tertiary amine branch junctures connected by linear, flexible branch cell segments P, this equation relates m_1 to the branch cell segment length l or P:

$$m_1 \approx 2.88(\ln P + 1.5)$$

This equation, together with branch cell segment lengths described for PAMAMs (see Sect. 5.2.3.1), predicts occurrence of the dense-packed generation m_1 between generations 10 and 11. This appears to have been experimentally verified.

Clearly, this proposed congestion at the critical branched state M_1 should exhibit (1) *sterically-inhibited reaction rates*, (2) *sterically-induced stoichiometry*, and, quite possibly, (3) *a critical phase change due to surface cooperativity (association)*. These phenomena have been observed experimentally for the Starburst PAMAM dendrimers and may prove to be diagnostic probes for this critical branched state in other dendrimer families.

Computer-assisted molecular modeling has shown that Starburst PAMAM dendrimers progress through a continuum of morphologies ranging from open hemispherical domes to closed spheroids (see Fig. 36) [147]. The simulations indicate that the closed spheroids possess well-developed internal hollows and channels beyond generations 4 and 5. These morphological changes are paralleled by monotonic decreases in the spin lattice relaxation times T_1 when various guest molecules (e.g. acetylsalicylic acid or 2,4-dichlorophenoxyacetic acid) are present. Presumably, this finding indicates a multiple guest-host relationship. Guest: host stoichiometries as high as 4:1 (by weight) and 3:1 (based on molar comparison of the interior tertiary amino groups of the dendrimer to the carboxylic acid moieties of the guest) were observed for generations 1.5 to 4.5.

Calculation of dendrimer exterior surface areas, assuming spherical geometry, allows the determination of surface area per Z group, A_z as a function of generation (Fig. 37). The curves show that A_z values remain relatively constant (ca. 100–120 Å² per Z group) for generations 0–3 and then decline to a minimum value of ca.

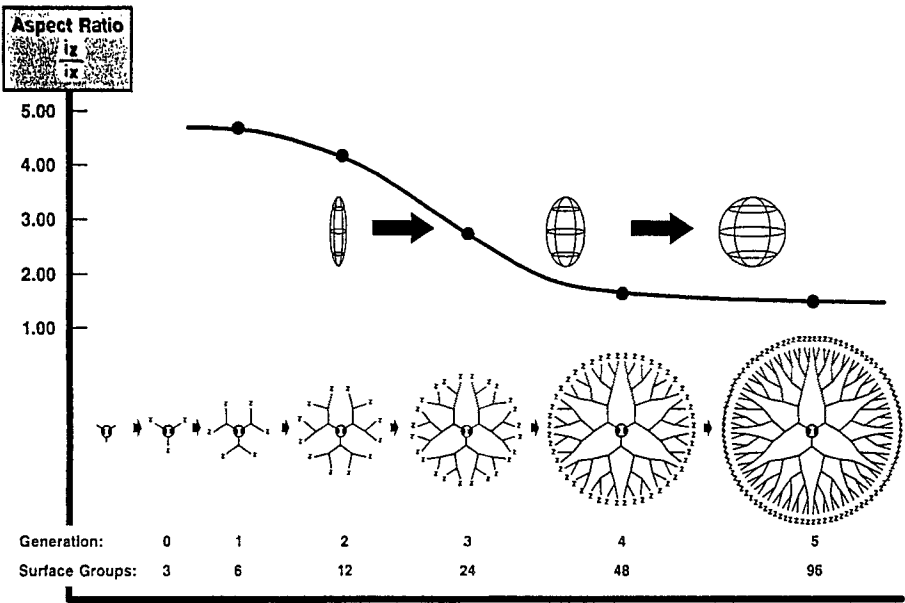


Fig. 36. Comparison of change in Starburst PAMAM dendrimer morphology (aspect ratios, I_z/I_y) as a function of generation

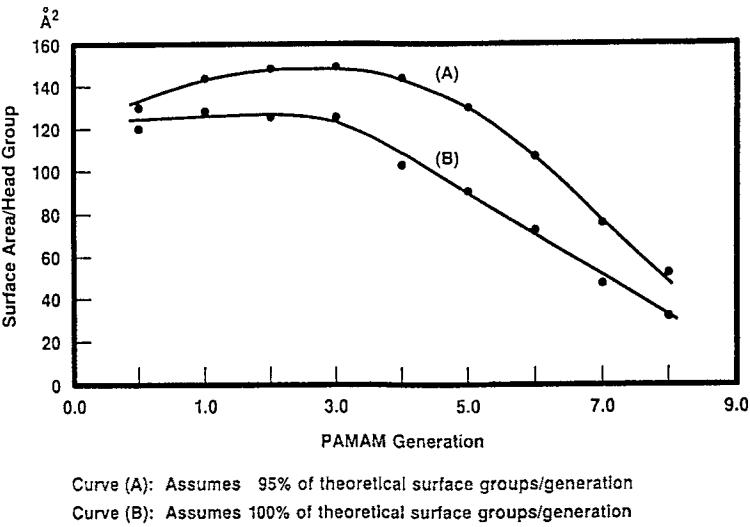


Fig. 37. Plot of surface area per terminal Z group, A_z , as a function of generation for Starburst PAMAM dendrimers. Curves A and B assume 95% and 100%, respectively, of the theoretical number of surface groups

33 \AA^2 per Z group at generation 8. These experimental data are supported by computer-assisted simulations and surface areas derived from these calculations.

These effects all contribute to the differentiation of dendrimer branch cells during the advancement to higher generations (Fig. 38). A comparison of T_1 values for dendrimer interior carbons and surface carbons shows that although the T_1 values for interior carbons remain relatively constant with increasing generation, the T_1 values for the surface carbons decrease dramatically [148].

STARBURST T_1 RELAXATION vs. GENERATION

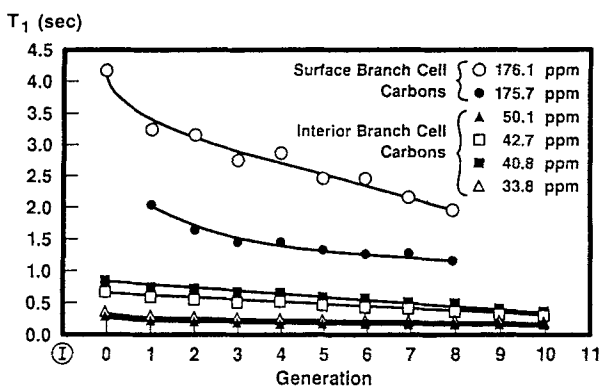


Fig. 38. Plot of spin-lattice relaxation times T_1 for interior and surface carbons versus generation

The sequential, reiterative process by which dendrimers are prepared allows the introduction of structural variations at any stage of the synthesis. The timing of these variations can be used to control the spacing between two sites within a molecule or the distance from a site to the surface of the molecule. This type of control opens the door to positioning functional groups in ways reminiscent of protein active sites or creating layered structures similar to micelles and bilayers. In either of these structures, functionality varies radially with the distance from the origin or synthetic center of the molecule. Such radial variations might be expected to lead to gradients in the properties of the molecule as distance from the center increases.

Systematic studies of selectively labelled dendrimers were carried out in order to evaluate these radial gradients. Deuterium was incorporated into poly-(amidoamine) dendrimers by substitution of β - d_2 -methyl acrylate for the unlabelled acrylate at various stages of the synthesis. Thus, it was possible to prepare the various generations from 1–8 with any selected layer deuterium labelled as shown in Fig. 39. The choice of isotopic labelling allows comparisons with unlabelled material without concern for perturbations caused by changes in solubility, solvation, sterics, geometry, or chain flexibility.

The method employed for the evaluation was determination of deuterium NMR relaxation times as a measure of molecular motion. If radial differences in concentration, or solvation were present such that the segmental mobility of the structure varied significantly between layers, measurable changes in T_1 and T_2

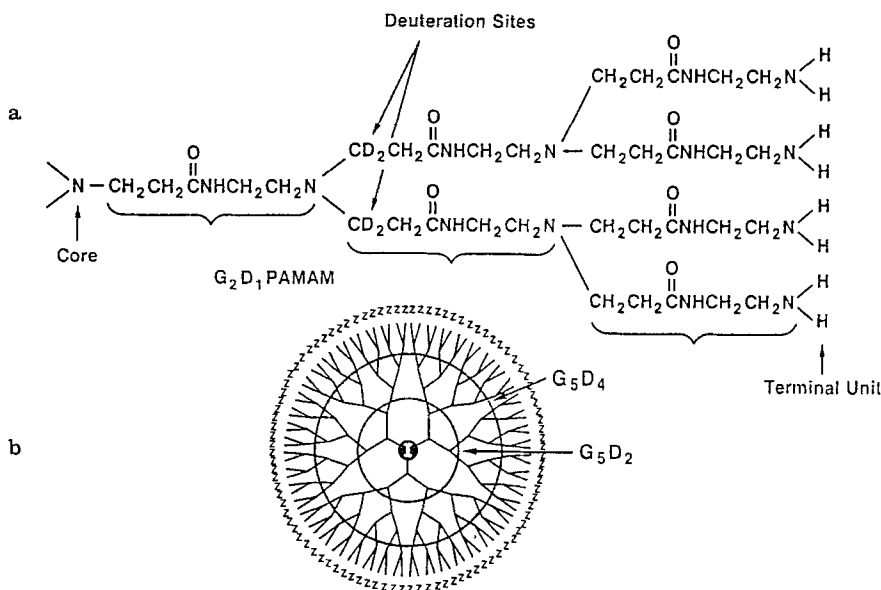


Fig. 39. Genealogical directed deuterium labelling of PAMAM dendrimers as a function of generation. (A) structural formula illustrates deuterium labelling at the β -position in the generation = 1 tier of a generation = 2, dendrimer; designated G_2D_1 -PAMAM dendrimer. (B) genealogical labelling at generation = 2 and 4 tiers in a generation = 5, dendrimer; designated G_5D_2 and G_5D_4 , respectively

would be expected. While the studies showed the expected differences in mobility of chain ends vs. interior segments and the restriction of the motion of chain ends due to steric crowding, the differences between the relaxation times of the deuterium in the interior layers were not great enough to confirm the existence of gradients within the dendrimer (see Fig. 40). This may be due to a uniformly immobilized interior [148].

Additional physical evidence which supports the anticipated development of congestion as a function of generation is shown in the composite comparison in Fig. 41. The plots of intrinsic viscosity $[\eta]$, density z , surface area per Z group (A_z), and refractive index n as a function of generation clearly show maxima or minima at generations = 3–5, paralleling computer-assisted molecular-simulation predictions [2, 147]. The intrinsic viscosities $[\eta]$ increase in a very classical fashion as a function of molar mass (generation) but decline beyond generation 4, presumably because of surface congestion which would reduce optimum surface solvent interactions. In effect, the dendrimer begins to act more like an Einstein spheroid beyond generation 4. The dendrimer density z (atomic mass units per unit volume) clearly minimizes between generations 4 and 5, then begins to increase due to the increasingly larger exponential accumulation of surface groups as a function of generation. Since refractive indices are directly related to density parameters [149], their values should minimize and parallel the above density relationship.

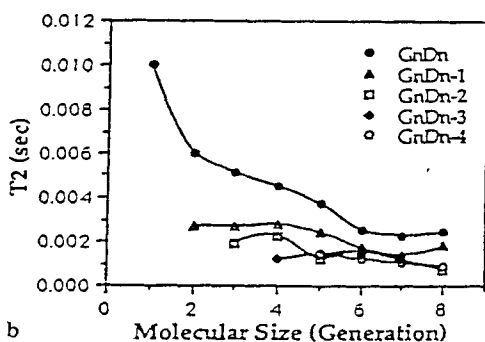
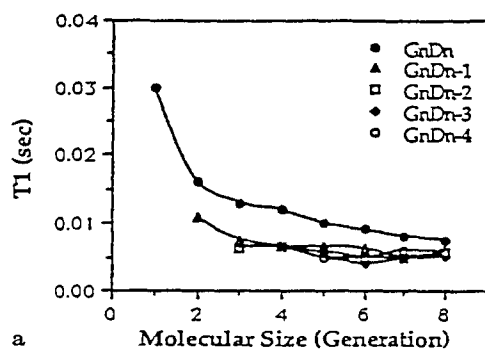


Fig. 40a, b. The dependencies of (a) ^2H T_1 and (b) ^2H T_2 on molecular size for primary amine terminated PAMAM dendrimers (25 °C, 46 MHz, D_2O)

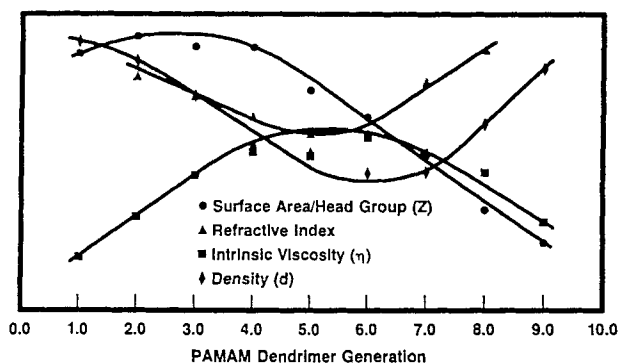


Fig. 41. Variation of surface area per terminal group, refractive index, intrinsic viscosity and density as a function of generation. The units along the ordinate are arbitrary

7 Dendrimer Surface Reactions

In biological systems, the size and shape of smaller components is often controlled (morphogenesis) to produce self-assemblies (e.g., cellular vesicles, viruses, and phages). As noted by Stryer [150] and others [151], many of these biological

assemblies are spheres, rods, or a combination of these shapes. Analogous molecular-level morphogenesis [1] from point-like organic molecules to well-defined covalent macromolecular entities were rarely observed until the present. The ability to construct Starburst dendrimers with similar shapes, sizes, and well-defined surfaces is no doubt of considerable importance in the effort to mimic the CMDPs and biomorphic features of these fundamental biological entities.

It is well known that small viruses possess many identical protein subunits symmetrically arranged around their RNA, which provide both protection and fulfill targeting functions. Topologically, dendrimers may be viewed as analogues of the surfaces of these biological particles. The dendrimer surface cells would be expected not only to provide steric protection to its interior, but also would function in primary molecular recognition of external reagents and solvents. This has indeed been observed in dendrimer protonation modes [77, 79] as well as in the solubility characteristics of well-developed dendrimers. Solubilities are determined by the hydrophilic/hydrophobic characteristics of the surface branch cells (groups) of dendrimers. For example, dendrimers with very hydrophobic interiors and hydrophilic surfaces are water-soluble (e.g., Starburst polyethers); dendrimers with hydrophilic interiors and hydrophobic surfaces are hydrocarbon-soluble (e.g., Starburst PAMAMs).

Starburst dendrimers may be functionalized with either reactive or passive surface branch cells. It is implicit that all dendrimers involved in reiterative Starburst growth schemes possess reactive surface groups. On some occasions, however, reactivity needs to be reduced or suppressed altogether.

In either case, the homogeneity of symmetrical, branch-junctured dendrimer surfaces provides unique opportunities to study the effect of congestion on surface stoichiometry, reaction kinetics, surface cooperativity [40, 152–154], and surface charge repulsion [155]. Physical evidence for surface congestion was noted in Sect. 6. A constriction in the surface area per Z group due to the dendrimer tethering effect does not occur until approximately generation 4.0. This congestion is manifested in the higher generations by dramatically decreased surface reactivity as the (de Gennes) dense-packed generation is approached.

7.1 Sterically Induced Stoichiometry and Reaction Rates

Examination of Fig. 37 shows that, at generation 8, the surface area per Z group in PAMAM dendrimers approaches the cross-sectional area of the amine-terminated branch segment (ca. 33 \AA^2) of the surface cell. Curve B assumes quantitative reactions and 100% branching ideality at each stage. Since our present analytical methods assure branching ideality detection limits of no more than 95%, curve A may more nearly approximate experimental congestion levels.

Sterically induced stoichiometry (SIS) is manifested whenever the summation of dendrimer surface-group volumes \mathbb{R} and incoming reagent volumes \mathbb{R}' approach available exterior volume surrounding the reactive dendrimer surface groups Z as illustrated in Figure 42. So long as the summation of the volumes \mathbb{R} and \mathbb{R}' involved in bond formation with Z remains much less than $4/3 \pi (r_a^3 - r_b^3)$, ideal

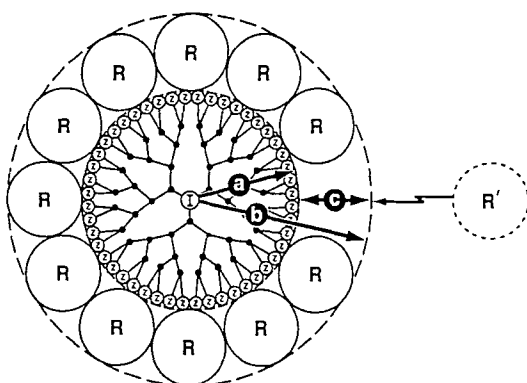


Fig. 42. Sterically induced stoichiometry (SIS); wherein Z = available dendrimer surface groups, R = chemically bound groups derived from a reagent (R')

starburst surface stoichiometry can be expected. Large increases in the volume R' relative to the surface groups Z can be used as a means for controlling or, in fact, dramatically reducing surface stoichiometry at a particular generation. Preliminary evidence for this phenomenon was observed when advanced-generation Starburst PAMAM dendrimers (where $Z = -CO_2CH_3$) were combined with a large excess of a dendrimer with volume R' and NH_2 surface functionality. As much as 70% of the CO_2CH_3 groups remained unreacted (vide infrared spectroscopy) in the bridged dendrimer adducts, although less sterically hindered model systems (i.e. ethylenediamine) indicated the amidation was nearly quantitative under the same conditions.

7.2 Surface Chemistry

Dendrimer surface chemistry used to introduce both reactive and passive chemical moieties for a wide variety of interior or exterior design functions include:

1. chelation
2. dendrimer stratification (heterogeneous generations)
3. optically active groups
4. molecular-level templating (antigenic surfaces)
5. modification of dendrimer stoichiometry
6. modification of dendrimer solubility

7.2.1 Protonation

Analyses of NH_2 -terminated PAMAM dendrimers by titration and concurrent ^{13}C -NMR monitoring of carbons attached to primary and tertiary amino groups were very interesting. Usually, tertiary amines are assumed to be more basic than primary amines. With the present prototypes, the opposite was true. Titrations with hydrochloric acid showed that neutralizations occurred to give rather sharp breaks at $pH = 6.85$ and $pH = 3.86$ (Fig. 43), which were in very close agreement with theoretical values for terminal primary amino groups and interior tertiary amino groups, respectively [2, 79]. The distinctive endpoints exhibited by these

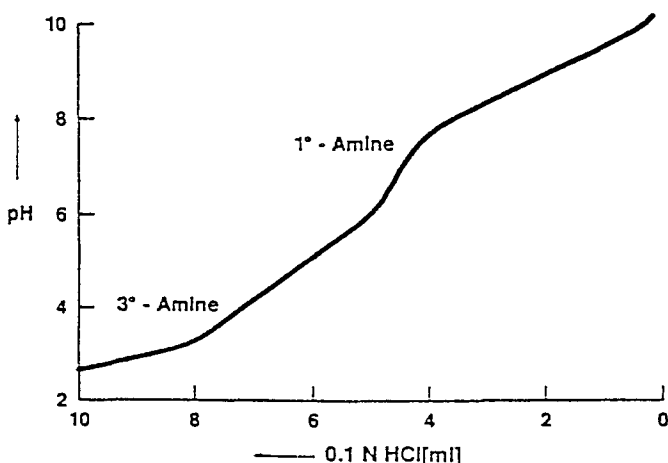


Fig. 43. Titration curve for Starburst PAMAM dendrimers of generation = 1 with endpoints observed for tertiary and primary amino groups

dendrimers are quite different from those observed for classical amino macromolecules, such as poly(ethylenimine) [125–127].

Reaction of various primary amine-terminated dendrimers with either inorganic or organic acids allows the preparation of a wide variety of crystalline derivatives. One such intermediate was implicated in the development of lyotropic phases [156] when octanoic acid was combined with Starburst poly(ethylenimine) (generation-3).

7.2.2 Chelation to Endo- and Exo-Receptor Sites

Construction of Starburst dendrimers can be controlled by appropriate choices of N_c , N_b , and branch cell segment lengths l , as well as by the flexibilities and shapes of the branch cell segments. A qualitative overview of how N_c and N_b may affect interior topology is provided by the two-dimensional projections shown in Fig. 8. Because of the variety of possible heteroatoms or functional groups, it is easy to conceptualize many new endo-receptor microenvironments, which would resemble multiarmed entities described by Vögtle and Weber [157], Suckling [158] and Menger [159] or pseudo-macrocyclic (cryptate-like) prototypes [1, 23, 24, 26, 160–162].

Very little is known about these dendrimer properties, although it has been noted that ester-terminated PAMAM dendrimers form deep blue complexes with CuSO_4 solutions, and that NH_2 -terminated homologues produce deep purple solutions [2, 79]. The well-known coordination properties of the amide bond, which lead to the formation of metal-ion complexes [163], should make this a very rich area for further investigation.

PAMAM dendrimers develop molecular clefts [10] on their surfaces which may be visualized from de Gennes' Starburst dendrimer model (Fig. 44) [85]. De Gennes hypothesizes that the Starburst structures should be quite flexible in the early generations, whereas the surface branch cells should become substantially more

de Gennes Model

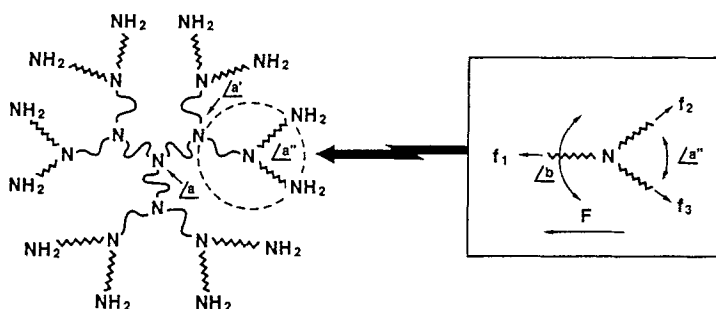
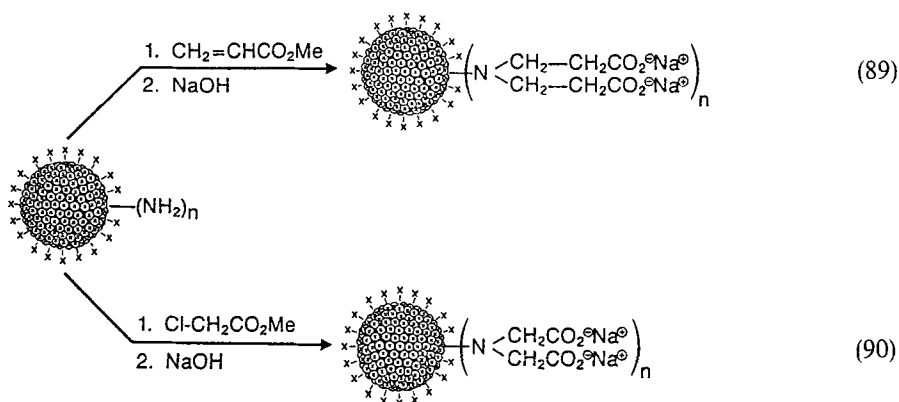


Fig. 44. The de Gennes model for self-consistent force field operating on a dendrimer branch cell

rigid and constrained as the Starburst dense-packed limit is approached. This would be expected to affect the branching angles $\angle a$ of the branch cells or dendrons as well as their rotational angles $\angle b$. Suppressed spin lattice relaxation times for dendrimer surface cells in advanced generations appear to support this notion, as do apparent enhanced complexation constants for advanced generations.

The most facile entry into surface complexation involved hydrolysis of ester-terminated dendrimers (derived from Michael additions of surface NH_2 groups to methyl acrylate) with stoichiometric amounts of alkali-metal hydroxides. In this manner, salts of Na^+ , K^+ , Cs^+ , or Rb^+ were readily obtained (Scheme 31) as white hygroscopic powders. Dilute solutions of the sodium salts allowed direct observation of the individual dendrimer molecules by scanning transmission electron microscopy without the use of staining techniques [79–81]. Elemental analyses showed that essentially stoichiometric exchanges with divalent cations such as Ca^{2+} could be performed [164].

Alternatively, $\text{N}(\text{CH}_2\text{CO}_2^-)_2$ salts were prepared by the reaction of Starburst PAMAM or PEI primary amine-terminated dendrimers with methyl bromoacetate, followed by hydrolysis. Each of the above dendrimer carboxylate families readily formed complexes with such metals as Fe^{3+} , Gd^{3+} , Mn^{2+} , Pr^{3+} , and Y^{3+} . In general, the $\text{N}(\text{CH}_2\text{CO}_2^-)_2$ complexes were more stable than the $\text{N}(\text{CH}_2\text{CH}_2\text{CO}_2^-)_2$ complexes. Within the latter series, it was found that the complexes were considerably more stable (e.g., toward OH^- attack) for the higher generations (6, 7) than for the lower generations (2, 3). For example, a multimetal chelate with the empirical formula $[\text{Na}_5\text{H}_{127}\text{Fe}_{20}][\text{C}_{1521}\text{H}_{2469}\text{N}_{379}\text{O}_{573}]$ was readily formed from FeCl_3 and a Starburst PAMAM dendrimer {96 $\text{N}(\text{CH}_2\text{CH}_2\text{CO}_2^-)_2$ groups} [165, 166]. An orange complex containing approximately 60 iron atoms was obtained from the next-generation dendrimer possessing 192 $\sim \text{N}(\text{CH}_2\text{CH}_2\text{CO}_2^-)_2$ groups. These two complexes were stable up to pH 9–10, whereas ferric hydroxide precipitated from lower-generation homologues at pH 5.



Schema 31

Sub-stoichiometric yttrium complexes of Starburst PAMAMs with $\sim \text{N}(\text{CH}_2\text{CH}_2\text{CO}_2^-)_2$ surface groups displayed intramolecular exchange reactions as determined by ^{13}C -NMR spectroscopy and ^{90}Y tracer experiments [166]. These and other complexation properties may serve as useful probes for the systematic characterization of dendrimer surfaces.

7.2.3 Reactions with Electrophilic and Nucleophilic Reagents

Table 7 lists a small sampling of surface reactions which have been successfully carried out. Well over one hundred types of dendrimer surface modifications have been reported and are too numerous to articulate completely in this account. Reactions 1–3, 8, 9, 13–17, and 19–22 have been used in reiterative Starburst propagation schemes. They are generally very high yield, quantitative processes, except when close enough to the Starburst (de Gennes) limited generation. Reactions 1–3 and 14–17 were used in various combinations to create stratified dendrimers with differentiated generations possessing different branch cell segment lengths, different branch cell juncture multiplicities, and varied hydrophobicity. Reaction 17 is of special interest in combination with reactions 1–3 in that it can be used to produce linear nonbranched dendrimer segments which possess interior OH groups. Since the OH groups do not participate in their Michael addition reactions, these hydroxylated segments can be subsequently functionalized.

Reactions 1–3 produce intermediates which can be hydrolyzed to give dendrimers with anionic surfaces. Intermediates derived from reaction 11 yield cationic surfaces after quaternization. Dendrimers possessing chiral surfaces were readily prepared from optically active epoxides, as in reaction 4. Hydrophobic surfaces result from reactions 4–10, 11, and 20–22. The resulting dendrimers are soluble in organic solvents, although their interiors might be quite hydrophilic. Conversely, water-soluble dendrimers are obtained from reactions 1–3 (after hydrolysis), 4 (R = H), 14, and 16–19.

Table 7. Dendrimer surface reactions with various electrophiles and nucleophiles

DENDRIMER TYPE	DENDRIMER SURFACE, (X)	GENERATIONS	REAGENT	DENDRIMER SURFACE, (Y)	REFERENCE
ELECTROPHILIC REAGENTS					
1. S.B. -PAMAM	-NH ₂	0 - 10	CH ₂ =CHCO ₂ Me	-N-(CH ₂ CH ₂ CO ₂ Me) ₂	13, 84, 94, 124
2. S.B. -PAMAM	-NH ₂	0 - 4	BrCH ₂ CO ₂ Me	-N-(CH ₂ CO ₂ Me) ₂	83, 165, 166
3. S.B. -PEI	-NH ₂	0 - 3	CH ₂ =CHCO ₂ Me	-N(CH ₂ CH ₂ CO ₂ Me) ₂	83
4. S.B. -PAMAM	-NH ₂	0 - 10	 (R=H, alkyl, aryl)	-N(CH ₂ CHOHR) ₂	83
5. S.B. -PEI	-NH ₂	0 - 3	 (R=H, alkyl, aryl)	-N(CH ₂ CHOHR) ₂	83
6. S.B. -PAMAM	-NH ₂	0 - 6	 (R=C ₆ -C ₁₈)	-NHCOR	164
7. S.B. -PAMAM	-NH ₂	0 - 4	Aryl-CH ₂ -Cl	-NH-CH ₂ -Aryl	164
8. S.B. -PEI	-NH ₂	0 - 4	 (R=Mesyl, Tosyl)	-N-(CH ₂ CH ₂ NHSO ₂ R) ₂	83
9. S.B. -PE	-OH	0 - 3	Tosyl-Cl	-Tosyl	82
10. Arborol	-OH	2	ArylCOCl	-OCOArlyl	92-94
11. S.B. -PEI	-NH ₂	0 - 2	HCHO	-N(Me) ₂	83
12. S.B. -PA	-NH ₂	0 - 9	di(t-butyl) dicarbonate	-NHBoc	90
13. S.B. -PA	-NH ₂	0 - 9	p-Nitrophenyl ester of lysine di-Boc	 -NH-C(=O)-CH(CH ₂) ₂ -NHBoc	90
NUCLEOPHILIC REAGENTS					
14. S.B. -PAMAM	-CO ₂ Me	0 - 10	-NH ₂ (CH ₂) _n -NH ₂ (n=2) (n=6)	-CONH(CH ₂) _n -NH ₂	77-84, 124
15. S.B. -PAMAM	-CO ₂ Me	0 - 3	-NH ₂ (CH ₂) _n -NH ₂ (n=2) (n=6)	-CONH(CH ₂) _n -NH ₂	83, 87
16. S.B. -PAMAM	-CO ₂ Me	0 - 3	N-(CH ₂ CH ₂ NH ₂) ₂	-CONH-(CH ₂) ₂ -N[(CH ₂) ₂ -NH ₂] ₂	83
17. S.B. -PAMAM	-CO ₂ Me	0 - 4	NH ₂ -(CH ₂) ₂ -NH-(CH ₂) ₂ -OH	-CONH-(CH ₂) ₂ -NH-(CH ₂) ₂ -OH	83
18. Arborol	-CO ₂ Me	1	NH ₂ -C-(CH ₂ OH) ₃	-CONH-C-(CH ₂ OH) ₃	92-94
19. S.B. -PAMAM	-CO ₂ Me	0 - 9	NH ₂ CH ₂ CH ₂ OH	-CONHCH ₂ CH ₂ OH	83, 148
20. S.B. -PE	-Tosyl	0 - 3	NaBr	-Br	82
21. S.B. -PE	-Br	0 - 3	 O Na	 -O	82
22. S.B. -PTE	-Br	0 - 2	 S Na	 -S	133

*Chiral center

8 Genealogical Aspects of Dendrimer Synthesis and Structure

Examination of the genealogical mimicry involved in the construction and synthesis of Starburst/cascade dendrimers places this activity at the interface between chemistry and biology. Essentially all genealogical phenomena in biological systems involve and evolve around two generic classes of compositions, namely; (a) nucleic acids and (b) proteins. The nucleic acids, DNA and RNA are estimated to be over three billion years old by radioactive carbon dating (see Ref. 206) (see Fig. 45).

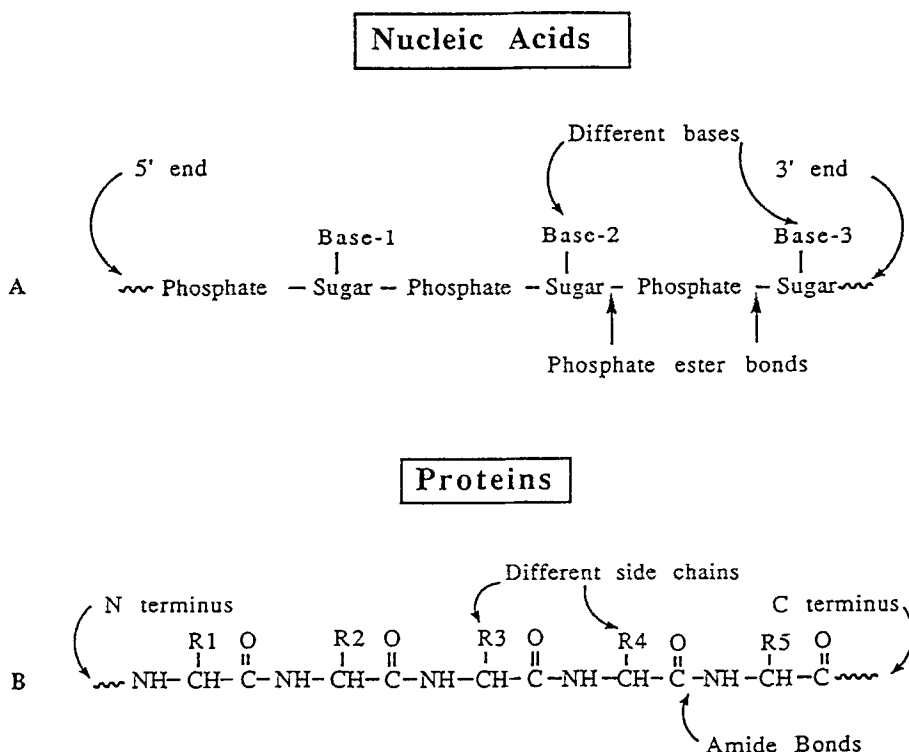


Fig. 45. One dimensional genealogically derived molecules involved in the transfer of molecular level information in biological systems: (A) nucleic acids, (B) proteins

During that time the involvement of nucleic acids as well as proteins in biological systems has evolved to very heightened levels of sophistication. The object of this account is not to examine and mimic these extraordinary, complex phenomena and structures in fine detail, but to present and compare alternate, abiotic chemistries that offer more simple, minimal mimicry of these biological targets in the context of new synthetic strategies. Exploration of this perspective offers both the promise of developing new synthetic approaches/techniques as well as a

deeper understanding of fundamental principles underlying prebiotic chemistry (see Ref. 206).

The *central dogma of molecular genetics* according to Crick [188] states that the function of DNA is to store molecular information and pass it on to RNA at the appropriate time, whereas the function of RNA is to read, decode, and utilize the information received from DNA to make proteins at various ribosome sites in the organism. Each of the many individual genes constituting the chromosomes or genome of the organism contains the necessary instructions to synthesize the specific protein required for a specific biological purpose. By decoding the appropriate genes at the right time and in the right molecular locations, an organism can use this genetic (molecular) information to synthesize the many thousands of proteins necessary for carrying out the biochemical reactions required to initiate and sustain life. The flow of molecular information from DNA through the various hierarchy levels to cells and organisms may be envisioned as follows: (see Fig. 46).

Various phenomena and structural distinctions that can be associated with this information flow and hierarchy are noted in the vertical columns. At least seven distinct criteria can be listed for the DNA molecular level behavior of this hierarchy. Adherence by DNA to certain of these criteria allows nearly complete control of critical molecular design parameters (CMDPs) such as size, shape, surface chemistry, flexibility and topology. Control of this information flow places DNA in its present role as the supreme orchestrator of life and higher organism structure. *Collectively, these criteria may be used to define and describe the genealogy of DNA at the molecular level and the influence it has on the genealogy of cells/organisms at the macroscopic level.* The ideal performance or dysfunction of these criteria defines the ultimate genealogical result or fate of a prototype whether it is of molecular level or macroscopic dimensions.

Synthesis with concurrent control of CMDPs to produce ordered, abiotic dendrimer structures manifests all of the criteria illustrated in Fig. 46, which are associated with biological systems. These observations taken with recent efforts to mimic more complex biological phenomena such as self-replication [170–174], base-pairing by the use of minimal experimental models [175] and cooperativity on abiotic polymers [176] prompted us to compare dendrimer synthesis/structure with the genealogical aspects of biological systems. These analogies were especially striking if one compared the flow of information in dendrimer construction by the *divergent/core/in situ branch cell method* to that described in Fig. 46. In order to visualize dendrimer syntheses and structure as minimalist models mimicking biological genealogy, one has to reconcile a “complexity and scaling problem”. An illustration such as Fig. 5 (Sect. 1) is required to describe this information flow and genealogical components involving DNA → RNA → Protein → Cells. These genealogical events are substantially more complex, involving enzymes, base-pairing, DNA replication forks, codon-anti-codon, sequencing, ribosomes, etc. More importantly, this biological genealogy involves structural entities (i.e., DNA, RNA, proteins, cells, etc.) that vary in size from nanoscopic dimensions (i.e., 1 nm–1000 nm) to microscopic proportions (i.e., > 50 nm). In the case of dendrimer constructions *these same genealogy*

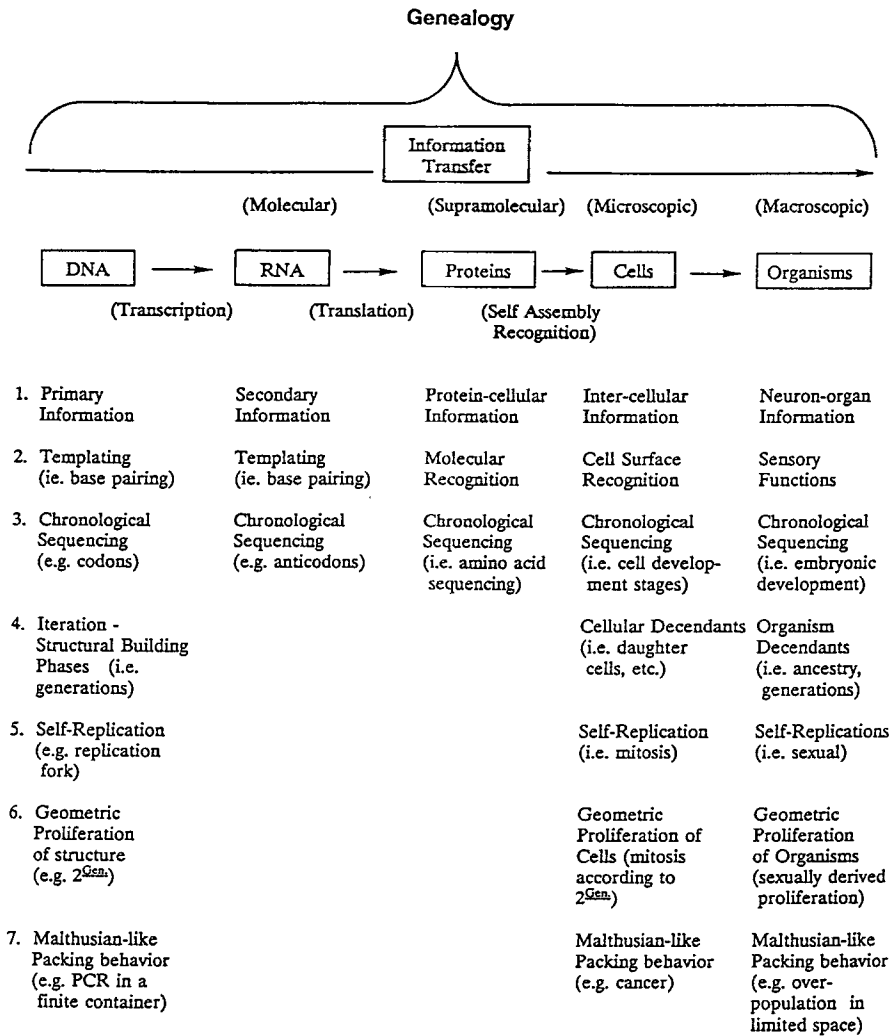


Fig. 46. Genealogy (information transfer) defined as a function of molecular supra-molecular, microscopic and macroscopic level entities found in biological systems. Vertical columns list various genealogical components involved throughout this hierarchy

criteria can be observed within individual molecules that are less than 10 nm in diameter.

As early as 1926, the American geneticist, H. J. Muller and others proposed that the first organisms were simply naked genes. Nearly 25 years before the role of DNA was defined, Muller described genetic material as any substance which, in given surroundings, protoplasmic or otherwise, is capable of causing the reproduction of its own specific composition, but which can nevertheless change repeatedly – “mutate” and yet retain the property of reproducing itself in its various forms [6]. Subsequently, Cairns-Smith [7] proposed inorganic

genes based on clays as the earliest templates, predating nucleic acids and proteins.

Within this context and by using Figs. 5 and 46 as conceptual references, let us examine the degree of mimicry offered by the more simplistic dendrimers in the transfer of genealogical information. First, as one assembles poly(amidoamine) (PAMAM) dendrimer (see Sect. 5.2.3.1) around an ammonia initiator core, it becomes readily apparent that important molecular ("genetic") information about the dimensions, shape and multiplicity of NH_3 are being transferred from the initiator core to the surface of the PAMAM dendrimers as a function of generation. This may be visualized as shown in Fig. 47. In this context, the dendrimer initiator

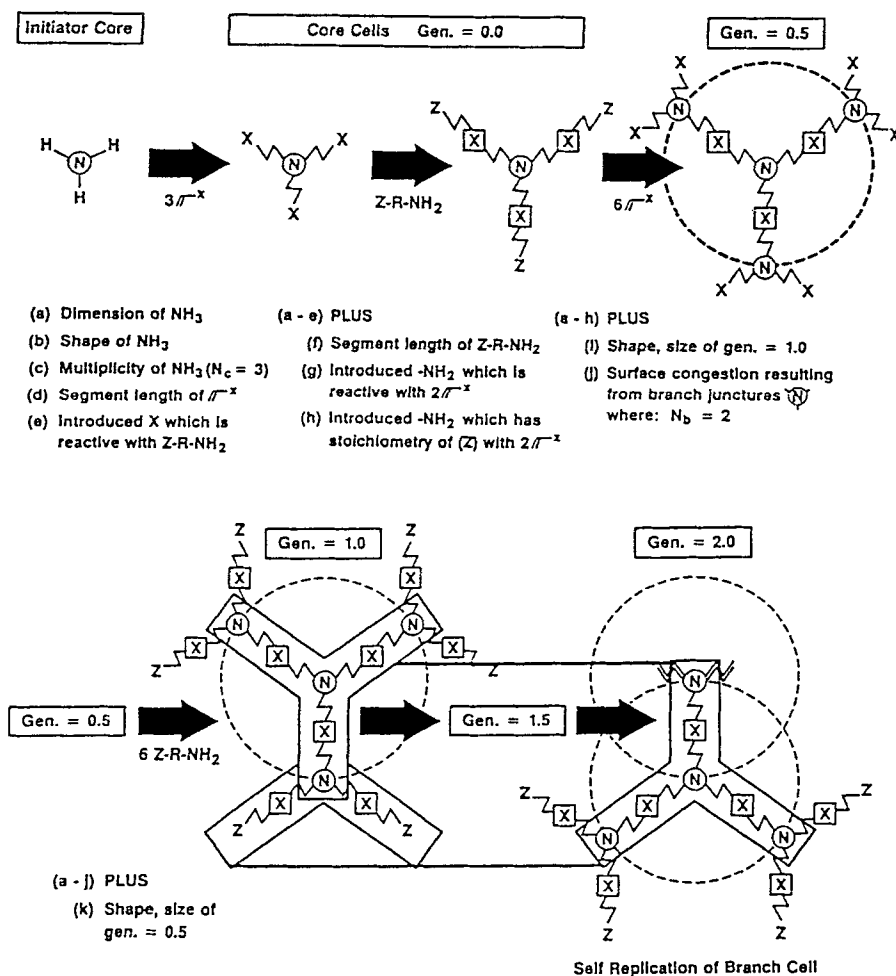


Fig. 47. Molecular information (genealogy) transferred from the initiator core (NH_3) to the surface of Starburst dendrimers as a function of generation, using a divergent synthesis protocol

core (i.e., NH_3) may be regarded as an abiotic (minimal) analogue of the germ-line gene illustrated in Fig. 5. The sequence of transcription, translation and ultimately, somatic cell self-replication noted in Fig. 5, can be readily identified in the construction protocol of a PAMAM dendrimer as shown in Fig. 47.

The first step in this minimalistic transcription/translation process that mimic genealogical criteria in Fig. 46 involves Michael addition of methyl acrylate to the nucleophilic ammonia surface to produce an electrophilic, carbomethoxy functionalized surface, followed by reaction with ethylenediamine to translate the functionalized dendrimer surface back to a nucleophilic primary amine functionalized surface. This iterative sequence is the key in providing alternating nucleophilic – electrophilic dendrimer surfaces that in turn may be used to develop uninterrupted, covalent connectivity from the initiator core to the surface throughout the dendrimer construction. This covalent connectivity provides the conduit for transferring important genetic information (see Fig. 47) from the interior (initiator core) to the exterior (dendrimer surface) as a function of generational growth. It should be noted that in this synthesis protocol there is (1) a primary information source (i.e., NH_3), (2) a templating effect (i.e., exo-presentation of functional groups in a radial orientation around NH_3), (3) a chronological sequencing of reagents (i.e., methyl acrylate/ethylenediamine), (4) iteration of structure growth (i.e., generation), (5) self-replication of branch cells after three iterations (i.e., generation = 2.0) and (6) a geometric proliferation of these self-replicating branch cells (i.e., $2^{\text{Gen.}}$). The seventh criterion (Fig. 46) is a phenomenon first predicted by de Gennes [85] in 1983 describing the “critical branching state” observed for dendrimer growth (see Sect. 7.3.3) if this Malthusian-fixed system is allowed to proliferate exponentially in a limited space. This effect can also be visualized for the expected $2^{\text{Gen.}}$ proliferation of DNA by use of “polymerase chain reaction” (PCR) protocol [4] in a reaction vessel of limited and fixed size. As a matter of comparison, this same effect is observed within individual dendrimer molecules, when using (GDS) dendrimer synthesis protocol.

A complete list of genealogical criteria should include at least two more entries. First, the capacity for a system to “mutate” (i.e., the ability of a system to change repeatedly, yet retain the property of replicating itself in various forms) [19, 20]. Secondly, the ability to participate in molecular level Darwinian evolution schemes. These schemes usually involve a population of self-replicating entities that give a continuous flow of mutant species, wherein those with advantageous properties (i.e., appropriate geometry, kinetically or thermodynamically favored) force an evolutionary reevaluation of “most fit species” at each generation. If dendrimer structural growth may be thought of as a “molecular level organism”, then the defects and digression from this ideal structure, as recorded in the electrospray mass spectra [169], (see Fig. 33), represent documentation of mutations. These mutations include defects arising from missing repeat units [ideal structure, $\text{MWt} - n$ (114 amu)] and those resulting from macrocycle formation [ideal structure/ $\text{MWt} - m$ (60 amu)] derived from intra-molecular cyclization of end groups (see Fig. 31). Monitoring these mutations by electrospray or laser desorption mass spectroscopy, within a genealogical series, shows that there are enhancements and diminutions of mutant species as a function of (a) temperature (b) solvent system

(c) amount of reagents used, (d) reaction times and (e) generation level. These parameters play a direct role in determining relative amounts of mutants that may be labeled as kinetically or thermodynamically derived products. Recent experimental mass spectroscopy analyses of a genealogically continuous dendrimer series [180] have shown that familiar transformations such as *retro*-Michael additions, macrocycle formation, ester hydrolysis and trans-amidation reactions have been implicated as minimalistic reactions in the production of mutant dendrimer species. Figure 48 illustrates a mass spectrum for a PAMAM (NH_3 core) dendrimer (Gen. = 3.0), wherein perfect structure is noted at 5154 daltons.

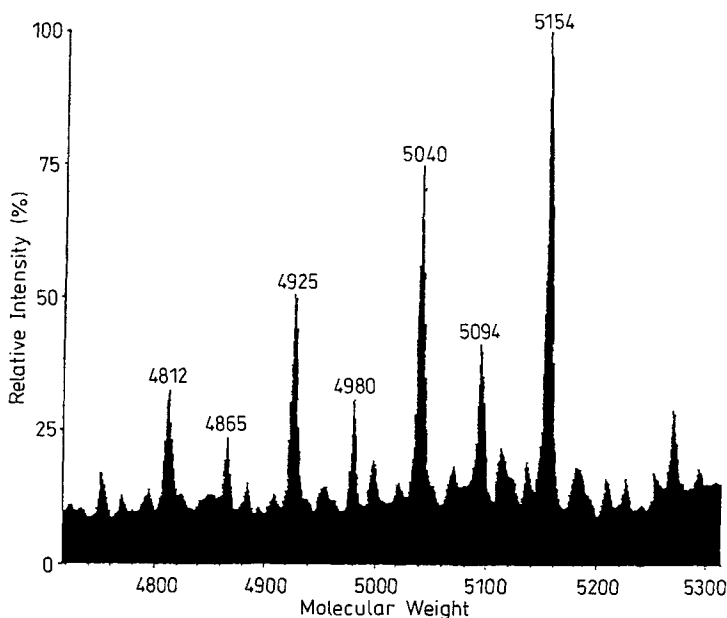


Fig. 48. Electrospray ionization mass spectrum of a Starburst PAMAM (generation = 3). Note the last significant peak; $M = 5154$ daltons (degree of polymerization = 45), corresponding to the “magic number” for ideal structure. The remaining peaks at 5040, 4925 and 4812 correspond to $M - x$ (114) species; defects due to missing monomer units. The peaks at 5094, 4980 and 4865 correspond to $M - x$ (60) species and have been assigned to defects arising from macrocycle formation

Retro-Michael reactions produce mutant species at $[5154 - n(114)]$ (e.g., 5040, 4925 and 4812 daltons), whereas macrocycle formation gives mutant products at $[5154 - n(60)]$ (e.g., 5094, 4980 and 4865 daltons). Note the perfect structure at 5154 daltons is the predicted “magic number” for generation = 3. In some cases a mutant defect (i.e., a *retro*-Michael reaction site) may be repaired in subsequent iteration sequence to give a regressed branch cell. Many of these errors (mutations) are found to be generation dependent. In any case, these errors may be routinely appraised as a function of generation by mass spectroscopy, electrophoresis and

high field ^{13}C -NMR. Using these analytical methods one can quantify relative amounts of ideal dendrimer structure and mutant species as a function of generation. This documentation provides important genealogy information about a dendrimer series. In fact these dendrimer genealogy profiles are very useful diagnostic tools that allow one to determine at which generation an error was introduced, the nature of the error and in general the skill of the individual who synthesized the series.

Genealogically directed synthesis (GDS) not only involves strategies and chemistry that document ideal and mutant structure as a function of generation, but also provide insights into generation dependent molecular shape changes. As early as 1988 [147] we predicted dendrimer shape changes as a function of generation, based on computer assisted molecular simulations. These predictions, illustrated in Sect. 6.3.3, Fig. 36 have been confirmed by fluorescence probe experiments [40] and more recently by dendrimer surface probe reactions [40, 167]. This molecular level morphogenesis [1] can be expected to be a characteristic feature in future genealogically directed syntheses, if the branch cells and repeat units are non-rigid and flexible enough to exhibit shape changes.

9 Related Hyperbranched Systems — Comb-burst Dendrimers

Genealogically directed synthesis (GDS) is a well established synthetic strategy leading to an entirely new class of macromolecules. Since the pioneering work of Vögtle [76] and the first extensively reiterated PAMAM dendrimer series was reported in 1984 [77–79], over 20 different dendrimer families exhibiting more than 100 varied surface functional groups and reactions have been described. In all cases the central theme has involved the organization of low molecular weight monomer units or branch cell reagents around a reference core, utilizing either the divergent or convergent synthesis approach (see Sect. 5). These molecular organizations follow systematic branching rules (geometric progressions) that allow prediction of the number of repeat units assembled (degree of polymerization) and calculation of dendrimer theoretical molecular weights (“*magic numbers*”) as a function of initiator core multiplicity (N_c), branch cell multiplicity (N_b), and generations (G). (See Sect. 2.4.) Although this GDS approach produces very precise macromolecular structures with stoichiometric surfaces, it can be seen from the geometric progression expressions that the increase in molecular weight as a function of generation is not dramatic since molecular weights of the repeat units, as well as N_c and N_b are usually small values.

Early in 1991 we (DAT) reported a new GDS approach wherein N_c and N_b may be very large values, thereby leading to *dramatic molecular weight enhancements* in relatively few generations [179]. This synthesis strategy involves reiterative grafting of “reactive end groups” (telechelic) [187] polymer chains to form dendritic graft polymers. These “graft upon graft” comb-branched entities are referred to as Comb-burst dendrimers. Conceptually, the scheme first involves grafting appropriate reactive chains onto an “initiator core” chain to produce a “comb-branched” macromolecular precursor (see Scheme 32).

The first demonstration of this GDS method employed polyoxazoline methodology to produce Comb-burst poly(ethyleneimine) – poly(2-ethyl-2-oxazoline) copolymers and poly(ethyleneimine) homopolymers.

Deprotection or introduction of suitable functionality onto the four “teeth” of the comb-branched polymer provides grafting sites for attachment of a second tier of branches to give the first generation in this Comb-burst series. Further reiteration produces “grafts upon grafts”, theoretically leading to dramatic increases in molecular weight in relatively few iterations. The number of monomer units assembled as a function of generation is determined by (a) the degree of polymerization of the graft chains and (b) the graft density upon the precursor chains. It can be seen in Fig. 49 that substantial design and control of these macromolecular structures is possible. Use of appropriate nucleophilic or electrophilic moieties (B) pendant to the chains or in the backbone permits grafting with either electrophilic or nucleophilic telechelic groups. Non-grafting co-monomers may be introduced into the grafted chains and the branch densities (graft sites) can be controlled as a function of generation. Furthermore, various R groups derived from graft chain initiator reagents may be inserted at specified generations. Most importantly, the degree of polymerization ($n_0 \rightarrow n_i$) can be controlled and introduced at desired generation levels.

In order to maintain good monodispersity, generation to generation, it is very desirable to use “living end group” polymers (anionic and cationic) [33, 187] for

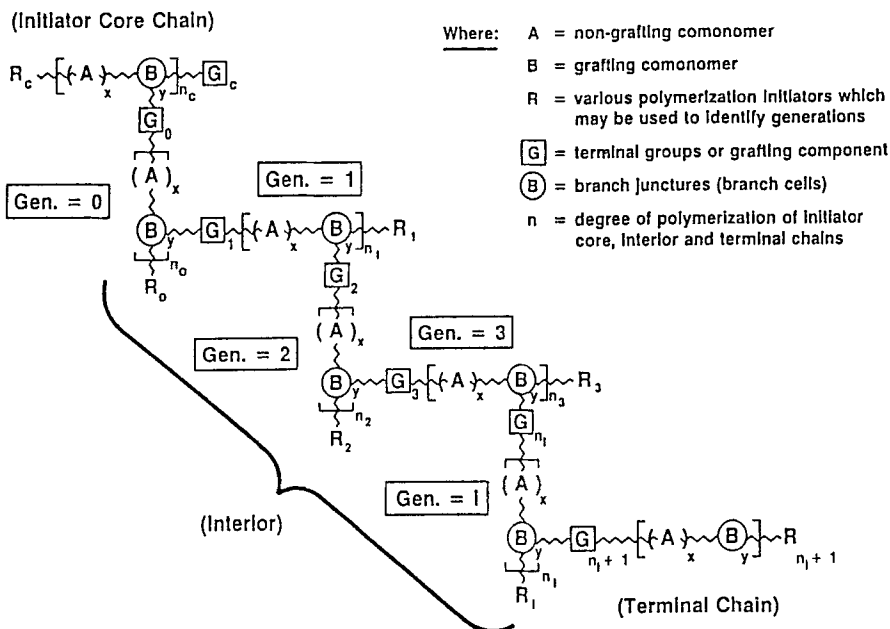


Fig. 49. Empirical structure for a Comb-burst dendrimer series (Generation = 0 – i), wherein the key architectural components (a) initiator core chain, (b) interior and (c) terminal chains are designated

the grafting stages, which exhibit efficient grafting characteristics. If that is not possible, effective methods for separating ungrafted chains from the Comb-burst dendrimer are important to maintain monodispersity.

Architecturally, Comb-burst dendrimers are similar to Starburst dendrimers in that they possess three distinguishable components: (a) an initiator core, (b) an interior (consisting of ensembles of graft sites to produce branch cells) and (c) terminal graft chains (i.e., analogous to terminal functionality/moieties in Starburst systems). Topologically the two systems may differ dramatically [180]. Whereas the Starburst system builds by branch cell development at the termini, the Comb-burst system involves branch cell construction by developing graft sites along the entire terminal graft chains.

Comb-burst branching strategies allow considerable versatility for controlling “critical molecular design parameters” (CMDPs). For example, dimensions of the Comb-burst dendrimer may be controlled by the size of the initiator core (N_c) as well as by the subsequent ($n_0 \rightarrow n_i$) values introduced throughout the dendrimer construction. Comb-burst morphology (aspect ratios) can be designed or modulated by adjusting N_c values relative to the ($n_0 \rightarrow n_i$) values, (e.g., large N_c vs. small $n_0 \rightarrow n_i$ values would lead to rod type morphologies, whereas, spheroids would be expected from low N_c values). Surface chemistry will be determined by the selection of moieties for A, B, and R at the $n_i + 1$ generation. Introduction of $R_c R_i$ type moieties can make interior design very specific. More generally, various interior properties arise (i.e., hydrophobic/hydrophilic or flexibility/rigidity, upon introduction of A and B co-monomers. Other interior design may involve selection of appropriate graft (branching) moieties to assure thermal/hydrolytic stability. Topological control to develop hollow interiors can be envisioned by adjusting graft densities during the construction of the dendrimers (i.e., low graft densities for the early generations and higher graft densities for the later iterations).

More recent work has shown that this GDS strategy may be used to produce all hydrocarbon, poly(styrene) type dendrimers that the authors refer to as being derived from “arborescent grafting” [181]. Hybridization of Starburst/Cascade architecture with Comb-burst dendrimer structure, has been reported by our group very recently [182], thus clearly establishing the vast breadth and scope of GDS techniques for the construction and design of nanoscopically sized macromolecules (i.e., 1–100 nm in diameter).

10 Nanotechnology-Synthesis, Engineering and Application of Nanoscopic Structures

Key conceptual influence on nanotechnology can be traced back over 30 years ago to physicist and Nobel laureate R. Feynman [183]. Like many contemporary nanotechnologists such as Drexler [207] and others, Feynman credited his inspiration to the molecular-scale devices and information systems observed in the biological world.

The importance of nanostructures, their definition and their applications to engineering principles have been reviewed eloquently by Whitesides et al. [184].

Nanostructures are defined as assemblies of bonded atoms with dimensions in the range of 1–100 nm (10^3 – 10^9 Å), possessing as many as 10^3 – 10^9 atoms and having molecular weights of 10^4 – 10^{10} daltons. Thus the total synthesis of palytoxin by Kishi [39b] and the buckminsterfullerenes [43a] which are less than 10 Å in diameter, represent structures at the lower boundary of this dimensional range. A comparison of the relative structural sizes generated in biology, synthetic chemistry and microfabrication (see Fig. 50) illustrates the unfilled void for precise nanostructures and the spectacular challenge now facing synthetic chemists. In the middle of this nanostructure region (i.e., 50–500 Å) are such protein structures as insulin, albumin and hemoglobin (55 Å). Thus, essentially all of the GDS derived dendrimers described in this article may be thought of as ideal, well defined functional building blocks suitable for the development of more complex nanostructures required for this emerging technology. In fact generation = 5 (NH_3 core) PAMAM dendrimers have been shown to have a dimension and spheroidal shape essentially identical to hemoglobin [2]. A similar role has been envisioned for the use of buckminsterfullerenes as fundamental building blocks in the construction of nanostructures. Kroto [185] has predicted “the advent of a round chemistry in which fullerenes become established as new building blocks in organic chemistry”.

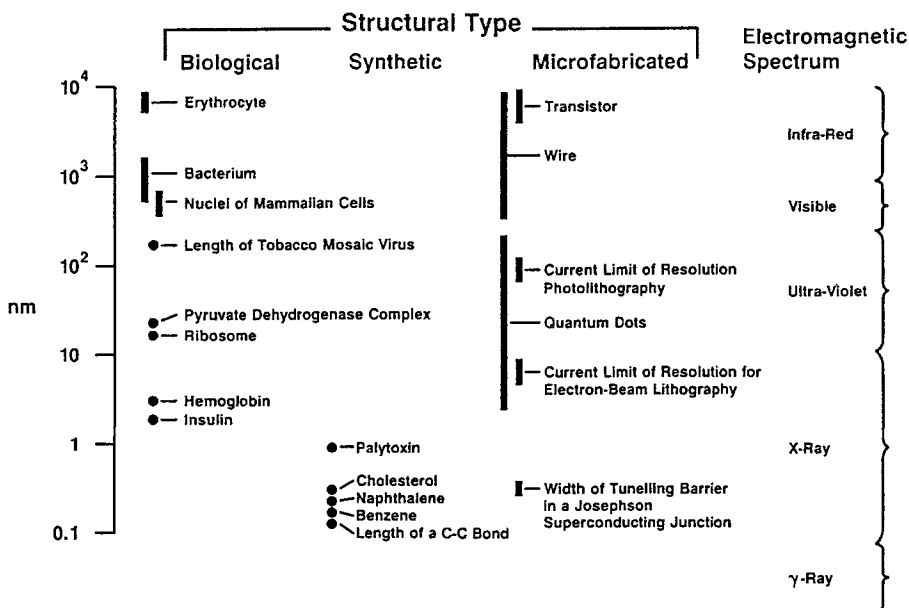
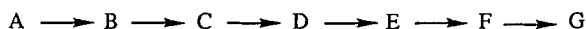


Fig. 50. A comparison of the relative sizes of structures generated in biology, synthetic chemistry, and microfabrication. The scale (*left*) is logarithmic and the electromagnetic spectrum (*right*) is included as a reference. Both biology and microfabrication provide examples of structures with dimensions ranging from 1 to 10^4 nm. Structures prepared by chemical synthesis are concentrated in the 0.1- to 2-nm range. The application of self-assembly in chemical synthesis may make it possible to obtain structures that have sizes of 10 to 10^3 nm. (G. Whitesides, et. al. [184] with permission from *Science*)

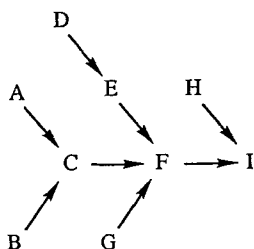
At least four classical synthesis strategies have been used successfully to prepare subnanoscopic or nanoscopic structures. These approaches have been reviewed [2, 184] and involve covalent bond formation or non-covalent bond assembly.

I. Classical Linear/Convergent Covalent Synthesis

Individual sequential covalent bond formation in a series of reaction-isolation steps. Bond formation usually involves only one or several connections per step. The method can be used to construct one-dimensional linear structures (e.g., polypeptides/polynucleic acids) where chronological sequencing can be used to introduce desired side groups or chirality by this linear covalent method.



More sophisticated methods have been developed for the assembly of very complex two dimensional molecules (i.e., palytoxin, Mwt. 2680 or vitamin B₁₂) or three dimensional architecture (i.e., cryptates/carcerands) involving a convergent covalent approach. The resulting assemblies of covalently linked atoms are precise



compositions which allow excellent control of critical molecular design parameters (CMDPs). This approach can be used to synthesize monomers, branch cell reagents, surfactants or molecular components suitable for synthetic strategies II – IV (see below). However, in practice it does not offer a practical route to true macro-molecules of nanoscopic dimensions.

II. Classical Covalent Polymerization

Staudinger first introduced this approach in the 1930s [29, 30] which involves the covalent linking of a monomer AB to itself to produce a statistical distribution of one dimensional molecules with relatively high molecular weights (i.e., > 10⁶ daltons).



Conversion of styrene to polystyrene is an example of such molecular structure, which is repetitive and simple. Relatively little opportunity is offered to precisely control critical molecular design parameters. Although nanostructure dimensions can be attained, virtually no control over atom positions, covalent connectivity or shapes is possible.

III. Self Organizing Synthesis of Nanoassemblies

Usually this synthetic strategy involves smaller, covalently assembled components that organize into extended layers or generalized architecture wherein the molecules or ions adjust their positions in order to reach a thermodynamic minimum. Examples include organization of surfactants into micelles [17], liquid crystals [189], Langmuir-Blodgett films [190], molecular crystals [191], bilayer membranes [208], and other assemblies that depend on weaker, non-directional connectivity such as hydrogen bonds, ionic bonds, van der Waals interactions or hydrophobic bonding to develop these nanoscopic assemblies. A certain amount of control over CMDPs is possible with this approach if properly designed into the self-organizing components to give true nanoscopic structures. However, in many instances the resulting assemblies are not robust and are disturbed by even minor external perturbations.

IV. Abiotic Molecular Self Assembly

This approach mimics familiar biological self-assembly phenomena such as protein folding [192], protein aggregation [192] and nucleotide pairing [188]. It incorporates features described in each of the above strategies (i.e., I–III) to give specialized nanoscopic structures, that can be precisely designed, usually with excellent control over CMDPs. Recent examples include so called “structure directed synthesis” by Stoddart [3a] (see Chapter 1 of this book) to produce toroidal bis-bipyridinium cyclophanes that are reminiscent of a “molecular abacus”, melamine-cyanuric acid lattices by Whitesides [193] and unique helical structures based on coordination of bipyridyl units to copper (II) ions by Lehn [194].

How does the genealogically directed synthesis (GDS) approach compare to these above strategies for the construction of nanoscopic structures? The following features differentiate this method:

- (a) GDS derived dendrimers possess three essential architectural components including (i) an initiator/anchor core, (ii) an interior (endoskeletal, infra-structure) and (iii) an exterior or surface (usually functional groups).
- (b) Monomers and branch cell reagents required for GDS are usually synthesized by approach (I). Assembly of these components involves features of both method (I) and (II). Standard covalent bonding techniques (i.e., protect/de-protect schemes) are utilized. However, large multiples of monomers or branch cell reagents may be assembled at each iteration stage which is reminiscent of method II.
- (c) GDS assembly of monomer or branch cell reagents occur according to a geometric progression to give “magic numbers” of atoms, monomer units or branch cells organized around a reference core. These “magic numbers” can be predicted by reference to Sect. 2.4 and use of certain geometric progression expressions.
- (d) Precise, covalently linked assemblies may be produced which mimic self-organization products derived by method (III) (e.g., micelles, etc. [40]).
- (e) GDS display “molecular level morphogenesis” [1]. Both the size and shape of the dendrimers change in a predictable manner as one advances through

- various generation levels with GDS. Molecular shape changes are usually observed due to tethering congestion around the core as one proceeds through several iteration stages [147].
- (f) Structures can be generated by the GDS method that are far from the thermodynamic minimum for that collection of atoms, unlike methods III and IV.
 - (g) GDS produces robust covalently linked nanostructures with complete control of CMDPs (i.e., size, shape, surface chemistry, topology and flexibility) [2].
 - (h) GDS derived dendrimers possess surface groups that behave collectively, exhibiting cooperativity [40].
 - (i) GDS structure can be designed to exhibit shape dependent “self assembly” behavior [195].
 - (j) GDS produces three dimensional nanoscopic structures with precise molecular masses and stoichiometric surfaces (valency). In view of these features they may be thought of as molecular level analogs of atoms [196] suitable for the construction of more complex nanostructures and assemblies, either by covalent bond formation, self-organization or molecular self-assembly.

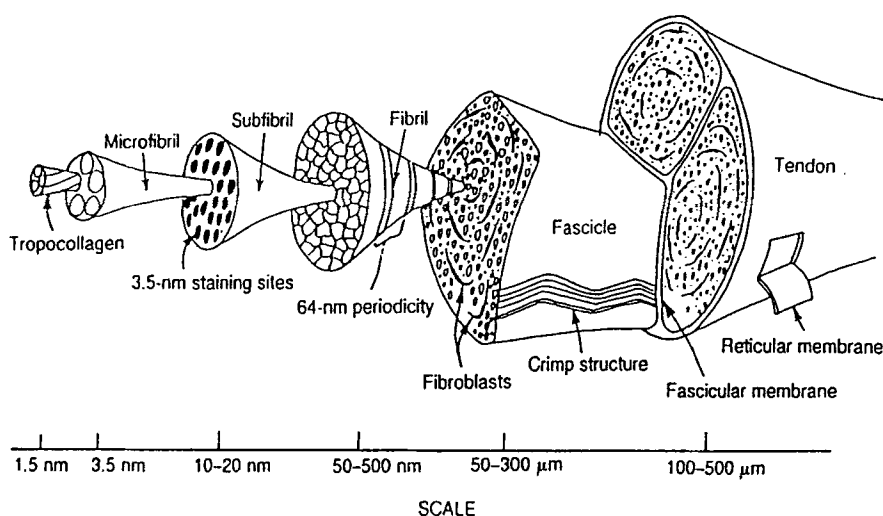


Fig. 51. Hierarchical structure of the tendon. The hierarchical organization of connective tissues is illustrated in the tendon. Beginning at the molecular level with tropocollagen, progressively larger and more complex structures are built up on the nano- and microscopic scales. At the most fundamental level is the tropocollagen helix. These molecules aggregate to form microfibrils which, in turn, are packed into a lattice structure forming a subfibril. The subfibrils are then joined to form fibrils in which the characteristic 64 nm banding pattern is evident. It is these basic building blocks that, in the tendon, form a unit called a fascicle. At the fascicular level the wavy nature of the collagen fibrils is evident. Two or three fascicles together form the structure referred to as a tendon. It is this multi-level organization that imparts toughness to the tendon. (E. Baer, et al. [197] with permission from *Science*)

The assembly of dimers, trimers and other well defined dendrimer clusters have recently been described by us [167, 186], thus demonstrating the viability of GDS derived dendrimers as fundamental, nanoscopic building blocks for covalent constructions. The ability to differentiate sectors of a dendrimer as described by Fréchet et al. [102a] and others [2] should allow directionalized assembly of more complex nanostructures.

As noted by Baer et al. [197, 198] important lessons concerning nanoscopic engineering may be learned from biology. Just as the hierarchical structures in bio-composite systems exhibit (a) various scaling levels (dimensions) (b) possess very specific connectivities (interactions) between these levels and (c) have appropriate architectures to manifest a desired spectrum of functional properties (see Fig. 51), so can one envision a hierarchy of abiotic, nanoscopic complexity.

Mimicry of this biological hierarchy can readily be seen in the abiotic hierarchy defined by GDS to reach molecules of nanoscopic proportion (see Fig. 52).

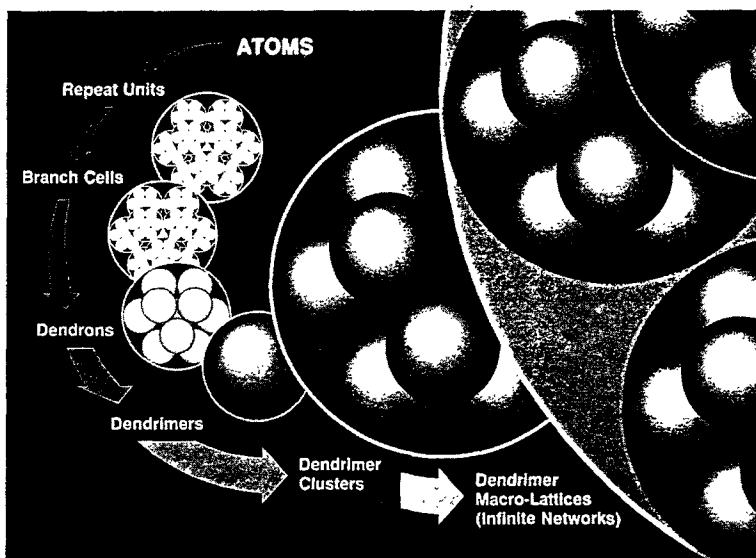


Fig. 52. Finite series of nesting spheres representing atoms, repeat units, branch cells, dendrons, dendrimers, dendrimer clusters, and dendrimer macro-lattices (ordered infinite networks) illustrating an abiotic hierarchy analogous to that found in biological system

The future use of dendrimers as fundamental building blocks will allow construction of an infinite variety of nanoscopic, microscopic, macroscopic assemblies and devices. These systems are expected to be of significant importance in the areas of advanced materials, biophysics, microelectronics, as well as medical diagnostics and therapy.

11 Conclusions

Adding a perspective of genealogy to a general synthetic strategy has most certainly added a heightened sense of satisfaction and a keen anticipation of new possibilities.

"To a synthetic chemist, the complex molecules of Nature are as beautiful as any of her other creations . . . The chemist who designs and completes an original and aesthetically pleasing multistep synthesis is like a composer, artist or poet who, with great individuality fashions new forms of beauty from the interplay of mind and spirit."

E. J. Corey [204]

Genealogy is by definition: *an account or history of the descent of a group or form from an ancestor or older form; an enumeration of ancestors and their descendants in the natural order of succession; regular descent of a group of organisms from a progenitor or older form; pedigrees, lineage generation to generation* [199]. These definitional terms very appropriately describe key fundamental features and characteristics of our molecular level approach to dendrimer construction, whether it involves divergent or convergent protocol. The term *genealogically directed synthesis* (GDS) represents a general strategy for constructing endoskeletal, cascade-like compositions referred to as Starburst macromolecules, arborols, dendrons, dendrimers and other hyperbranched covalent assemblies. Over twenty different chemical families of dendrimers with over one hundred varieties of surface modifications have been reported to date and appear to be limited only by the imagination of the synthetic chemist.

Genealogy in a molecular biology sense, describes information flow, generation to generation, at the molecular level. Similar statements can be made about biology and organisms at the macroscopic level. Throughout this article we have attempted to illustrate parallelisms between our abiotic, minimalistic synthesis strategy and biological strategies. Understanding key issues at this interface should provide a very rich frontier for exploration by molecular biologists and synthetic organic chemists alike.

Acknowledgement. We wish to sincerely thank Dr. D. M. Hedstrand for valuable discussions and contributions of graphics as well as Ms. L. S. Nixon for manuscript preparation. This work has been supported by the New Energy and Technology Development organization (NEDO) of the Ministry of International Trade and Industry of Japan (MITI), the U.S. Army Chemical Research Development and Engineering Center (CRDEC), and the U.S. Air Force Office of Scientific Research (AFOSR).

12 References

1. Lehn JM (1988) *Angew Chem* 100: 91; (1988) *Angew Chem Int (ed) Engl* 27: 89
2. Tomalia DA, Naylor AM, Goddard III WA (1990) *Angew Chem* 102: 119; (1990) *Angew Chem Int (ed) Engl* 29: 138
3. a) Philip D, Stoddart JF, (1991) *Synlett* 7: 445; b) Ashton PR, Isaacs NS, Kohnke FH, Mathias JP, Stoddart JF (1989) *Angew Chem* 101, 126; (1989) *Angew Chem Int (ed) Engl* 28: 1258; c) Ashton PR, Isaacs NS, Kohnke FH, D'Alcontres GS, Stoddart JF (1989) *Angew Chem*; (1989) *Angew Chem Int (ed) Engl* 28: 1261; d) Kohnke FH,

- Mathias JP, Stoddart JF (1989) *Angew Chem Adv Mater* 101: 1129; e) Kohnke FH, Mathias JP, Stoddart JF (1989) In: Roberts SM (ed) *Molecular recognition: Chemical and biochemical problems*, The Royal Society of Chemistry, Cambridge, UK p 233
4. Mullis KB, Faloona FA (1987) *Methods Enzymol* 155: 335
5. Wimmer W, Molla A, Paul AV (1991) *Science (Washington D.C.)* 254: 1647
6. Cairns-Smith AG (1985) *Sci am* (No. 6) 253: 90; (1985) *Spektrum Wiss* (No. 8): 82
7. Cairns-Smith AG (1982) *Genetic takeover and the mineral origins of life*, Cambridge University Press, Cambridge, UK
8. Dawkins R (1986) *New Scientist* 25: 24
9. Vögtle F, Weber E (1970) *Angew Chem* 91: 813; (1979) *Angew Chem Int (ed) Engl* 18: 753
10. Rebek Jr, J (1984) *Acc Chem Res* 17: 258; (1987) *Science (Washington D.C.)* 235: 1478; (1990) *Angew Chem* 102: 261; (1990) *Angew Chem Int (ed) Engl* 29: 245
11. a) Cram DJ, Cram JM (1978) *Acc Chem Res* 11: 8; b) Cram DJ (1986) *Angew Chem* 98: 1041; (1986) *Angew Chem Int (ed) Engl* 25: 1039; c) *ibid.* (1988) 100, 104, 27, 109; (1988) *Science (Washington D.C.)* 240: 760
12. Farin D, Avnir D (1991) *Angew Chem* 103: 1409; (1991) *Angew Chem Int (ed) Engl* 30: 1379
13. Lewis M, Rees DC (1985) *Science (Washington D.C.)* 230: 1163
14. Milstein C, (1985) *Angew Chem* 97: 819; (1985) *Angew Chem Int (ed) Engl* 24: 816
15. Nurnen A, Demotz S, Corradin G, Binz H, Bosshard HR (1987) *Science (Washington D.C.)* 235: 780
16. Amit AG, Mariuzza RA, Phillips SEV, Poljak RJ (1986) *Science (Washington D.C.)* 233: 747
17. Fendler JH (1982): *Membrane Mimetic Chemistry*, J. Wiley, New York
18. Leszczynski JF, Rose GD (1986) *Science (Washington D.C.)* 234: 849
19. a) Kuhn H, Waser J (1981) *Angew Chem* 93: 435; (1981) *Angew Chem Int (ed) Engl* 20: 500; b) Haken H (1986): *Erfolgsgeheimnisse der Natur – Synergetik: Die Lehre vom Zusammenwirken*, Deutsche Verlagsanstalt, Stuttgart; c) Küppers BO (ed) (1987): *Ordnung aus dem Chaos, Prinzipien der Selbstorganisation und Evolution des Lebens*, Piper, München; d) Cramer F (1988) *Chaos und Ordnung. Die komplexe Struktur des Lebendigen*, Deutsche Verlagsanstalt, Stuttgart
20. a) Eigen M (1971) *Naturwissenschaften* 10: 465; b) Eigen M, Gardiner W, Schuster P, Winkler-Oswatitsch R (1982) In: Smith JM (ed) *Evolution now*, Freeman, New York, p 11; c) Prigogine I (1972) *Phys. Today* 25 No. 12, p 38
21. Anfinsen CB (1973) (Washington D.C.) 181: 223; Jaenicke R (1984) *Angew Chem* 96: 285; (1984) *Angew Chem Int (ed) Engl* 96: 395
22. Pedersen CJ (1967) *J Am Chem Soc* 89: 7017; Pedersen CJ, Frensdorff HK (1972) *Angew Chem* 84: 16; (1972) *Angew Chem Int (ed) Engl* 11: 16; Pedersen CJ, (1989) *ibid* 100: 1053 and 27 (1988) 1029
23. a) Lehn JM (1973) *Struct Bonding (Berlin)* 16; (1978) *Acc Chem Res* 11: 49; b) Potvin PG, Lehn JM (1987) In: Izatt RM, Christensen JJ (eds) *Synthesis of macrocycles: The Design of selective complexing agents (Prog. Macrocyclic Chem. 3, Wiley, New York, p 167* c) Lehn JM (1988) *Angew Chem* 100: 91; (1988) *Angew Chem Int (ed) Engl* 27: 89
24. a) Tabushi I (1982) *Acc Chem Res* 15: 66; b) Gutsche CD (1983) *ibid* 16: 161; c) Diederich F (1988) *Angew Chem* 100: 372; (1988) *Angew Chem Int (ed) Engl* 27: 362
25. a) Jurnak FA, McPherson A (eds) (1987): *Biological Macromolecules and Assemblies*, Wiley, New York; b) Kraut J (1988) *Science (Washington D.C.)* 242: 533; c) Whitesides GM, Wong C-H (1985) *Angew Chem* 97: 617; (1985) *Angew Chem Int (ed) Engl* 24: 617
26. Vögtle F (1991) *Supramolecular chemistry – An introduction*, J. Wiley, New York
27. Gokel GW (1991) *Crown ethers and cryptand* In: Stoddart JF (ed) *Monographs in supramolecular chemistry*, The Royal Society of Chemistry, Cambridge, UK
28. Doolittle RF (1985) *Sci Am* 253 No. 10, p 74; (1985) *Spektrum Wiss*, No. 12, p 78

29. a) Jostkleigrewe E (ed) (1967) *Macromolekulare Chemie – Das Werk Hermann Staudingers in seiner heutigen Bedeutung*, Schnell und Steiner, München; b) Morawetz H (1987) *Angew Chem* 99: 95; (1987) *Angew Chem Int (ed) Engl* 26: 93
30. Morawetz H (1985) *Polymers. The Origin and Growth of a Science*, Wiley, Chichester, UK
31. a) Webster OW, Hertler WR, Sogah DY, Farnham WB, Rajan Baba TV (1983) *J Am Chem Soc* 105: 5706; b) Reetz MT (1988) *Angew Chem* 100: 1026; (1988) *Angew Chem Int (ed) Engl* 27: 994
32. a) Higashimura T, Aoshima S, Sawamoto M (1988) *Macromol Chem Macromol Symp* 13/14 457; b) (1988) *ibid* 13/14 513; c) Zsuga M, Faust R, Kennedy JP (1989) *Polym Bull* 21: 273
33. Webster OW (1991) *Science* 251: 887
34. a) Merrifield RB, Barany G (1980) In: Gross, E, Meienhofer J (eds) *The peptides*, vol 2, Academic Press, New York
35. Merrifield RB (1985) *Angew Chem* 97: 801; (1985) *Angew Chem Int (ed) Engl* 24: 799
36. a) Bodanzky M (1984) *Principles of peptide synthesis*, Springer, Berlin Heidelberg New York; d) Bodanzky M, Bodanzky A (1984) *The practice of Peptide Synthesis*, Springer, Berlin Heidelberg New York
37. Khorana HG (1973) In: *Nobel Lectures: Physiology or Medicine 1963–1970*, Elsevier, New York, p 341; (1969) *Angew Chem* 81: 1027
38. Corey EJ, Cheng X-M (1989) *The logic of chemical synthesis*, Wiley, New York, p 2
39. a) Moore RE, Bartolini G (1981) *J Am Chem Soc* 103: 2491; b) Armstrong RW, Beau J-M, Cheon SH, Christ WJ, Fujioka H, Ham W-H, Hawkins LD, Jin H, Kang SH, Kishi Y, Martinelli MJ, McWhorter Jr. WW, Mizuno M, Nakata M, Stutz AE, Talamas FX, Taniguchi M, Tino JA, Ueda K, Uenishi J-I, White JB, Yonaga M (1989) *J Am Chem Soc* 111: 7525; c) *ibid* (1989) 111: 7530
40. Turro NJ, Barton JK, Tomalia DA (1991) *Acc Chem Res* 24: 332
41. Cram DJ (1983) (*Washington D.C.*) 213: 1177
42. Miller LL, Kenny PW (1988) *J Chem Soc, Chem Commun*; Miller LL et al (1988) *J Am Chem Soc* 110: 641
43. a) Kroto HW, Heath JR, O'Brien SC, Curl RF, Smalley RE (1985) *Nature* 318: 162; b) Baum RM (June 1, 1992) *Chem & Eng News*, p 25–33
44. Krätschmer W, Lamb LD, Fostiropoulos K, Huffman DR (1990) *Nature* 347: 354
45. Special Issue On Buckminsterfullerenes (1992) *Acc Chem Res* 25: 98
46. Diederich F, Ettl R, Rubin Y, Whetten RL, Beck R, Alvarez M, Anz, Sensharma D, Wudl F, Khemani KC, Koch A (1991) *Science (Washington D.C.)* 252: 548
47. Fowler P, Manolopoulos D (October 26, 1991) *New Scientist* 24
48. a) Curl RF, Smalley RE (October 1991) *Scientific Am* 54; b) Haddon RC (1992) *Acc Chem Res* 25: 127; c) Fagan PJ, Calabrese JC, Malone B (1992) *Acc Chem Res* 25: 134
49. a) Cram DJ, Tanner ME, Thomas R (1991) *Angew Chem* 103: 1048; (1991) *Angew Chem Int (ed) Engl* 30: 1024; b) Guo BC, Kerns KP, Castleman, Jr. AW (1992) *Science (Washington D.C.)* 255: 1411; c) Guo BC, Wei S, Purnell J, Buzza S, Castleman, Jr. AW (1992) *Science (Washington D.C.)* 256: 515; d) Wei S, Guo BC, Purnell J, Buzza S, Castleman, Jr. AW (1992) *Science (Washington D.C.)* 256: 818; e) LaBrecque M (1991) *Mosaic* 22: 40
50. Marx JL (1983) *Science (Washington D.C.)* 222: 1109
51. Turro N (1986) *Angew Chem* 98: 872; (1986) *Angew Chem Int (ed) Engl* 25: 882
52. Fendler JH (1980) *Acc Chem Res* 13: 7
53. Kohnke FH, Slawin AMZ, Stoddart JF, Williams DJ (1987) *Angew Chem* 99: 941; (1987) *Angew Chem Int (ed) Engl* 26: 892; see also Kohnke FH, Mathias JP, Stoddart JF (1989) *Angew Chem, Int Ed Engl Adv Mater* 28: 1103; (1989) *Adv Mater* 1: 275
54. Maier G, Pfriem S, Schäfer U, Matusch R (1978) *Angew Chem* 90: 552; (1978) *Angew Chem Int (ed) Engl* 17: 520
55. Eaton PE, Cole TW (1964) *J Am Chem Soc* 89: 3157
56. a) Paquette LA (1989) *Chem Res* 89: 1051; b) Melder JP, Pinkos R, Fritz H, Prinzbach H (1989) *Angew Chem* 101: 314; (1989) *Angew Chem Int (ed) Engl* 28: 305

57. a) Dietrich-Buchecker FO, Sauvage J-P (1989) *Angew Chem* 101: 192; (1989) *Angew Chem Int (ed) Engl* 28: 189; b) Walba DM (1985) *Tetrahedron* 41: 3161; c) Nickon A, Silversmith EF (1987) *Organic chemistry: The name game*, Pergamon, New York; d) Mislow K (1989) *Chemtracts-Org Chem* 2: 151
58. Niklas KJ (1986) *Sci Am* 254 No. 3, p 78
59. Cheetham AH et al (1983) *Paleobiol* 9: 240
60. a) West BJ, Goldberger AL (1987) *Am Sci* 75: 354; b) MacDonald N (1983) *Trees and networks in biological models*, Wiley, New York
61. Thompson D'Arcy W (1961) *On growth and form*, Cambridge University Press, Cambridge, UK
62. Flory PJ (1941) *J Am Chem Soc* 63: 3083, 3091, 3096
63. Flory PJ (1953) *Ann NY Acad Sci* 57 No. 4, p 327
64. Flory PJ (1952) *J Am Chem Soc* 74: 2718
65. Flory PJ (1953) *Principles of polymer chemistry*, Cornell University Press, Ithaca, NY, USA
66. Stockmayer WH (1943) *J Chem Phys* 11: 45; (1944) 12: 125
67. Zimm B, Stockmayer WH (1949) *J Chem Phys* 17: 1301
68. Flory PJ, Rehner J (1943) *J Chem Phys* 11: 512
69. Graessley WW (1975) *Macromolecules* 8: 185
70. Graessley WW, *Macromolecules* 8: 865
71. a) Gordon M, Malcolm GN (1966) *Proc R Soc (London)* A295 29; b) Gordon M, Ross-Murphy SB (1975) *Pure Appl Chem* 43: 35; d) Dusak K (1979) *Makromol Chem Suppl* 2: 35; e) Burchard W (1988) *Adv Polym Sci* 48: 1
72. a) Good IJ (1948) *Proc Cambridge Phil Soc* 45: 360; b) (1963) *Proc R Soc (London)* A263 54
73. Beckman CO (1953) *Ann NY Acad Sci* 57: 384
74. Erlander S, French D (1956) *J Polym Sci* 20: 7
75. a) Burchard W (1972) *Macromolecules* 5: 604; b) Burchard W, Kranztz I, Pfannenmüller B (1971) *Makromol Chem* 150: 63
76. Buhleier E, Wehner W, Vögtle F (1978) *Synthesis* 155
77. Tomalia DA (August, 1984) 1st Society Polymer Science, Japan, Int Polym Conf, Kyoto, Japan; (see also Ref. 85)
78. Tomalia DA (19 March 1985) 6th Biennial Carl S. Marvel Symp, Tucson, AZ, USA
79. Tomalia DA, Baker H, Dewald JR, Hall M, Kallos G, Martin S, Roeck J, Ryder J, Smith P (1985) *Polymer J (Tokyo)* 17: 117
80. Tomalia DA, Baker H, Dewald JR, Hall M, Kallos G, Martin S, Roeck J, Ryder J, Smith P (1986) *Macromolecules* 19: 2466
81. Tomalia DA, Berry V, Hall M, Hedstrand DM (1987) *Macromolecules* 20: 1164
82. Hall H, Padias A, McConnell R, Tomalia DA (1987) *J Org Chem* 52: 5305
83. Tomalia DA, Dewald JR, US Pat. 4507466 (1985); US Pat. 4558120 (1985); US Pat. 4568737 (1986); US Pat. 4587329 (1986); US Pat. 4631337 (1986); US Pat. 4694064 (1987); US Pat 4713975 (1987); US Pat. 4737550 (1988); US Pat. 4871779 (1989); US Pat. 4857599 (1989)
84. Tomalia DA, Hall M, Hedstrand DM (1987) *J Am Chem Soc* 109: 1601
85. de Gennes PG, Hervet HJ (1983) *Phys Lett (Paris)* 44: 351
86. Tomalia DA, Bürgenstock Conf, May 3, 1987; Bürgenstock, Switzerland. See (1987) *Nachr Chem Tech, Lab* 35: 693
87. Wilson LR, Tomalia DA (1989) (*Polym Prepr Am Chem Soc Div Polym Chem*) 30: 115
88. Cram D (1987) *Science (Washington D.C.)* 238: 612
89. Maciejewski M (1982) *J Macromol Sci Chem* A17 689
90. Denkwalter RG, Kolc JF, Lukasavage WJ, US Pat. 4410688 (1983); (1984) *Chem Abstr* 100: 103907
91. a) Aharoni SM, Crosby III CR, Walsh EK (1982) *Macromolecules* 15: 1093; b) Aharoni SM, Murthym NS (1983) *Polym Commun* 24: 132
92. Newkome GR, Yao Z-Q, Baker GR, Gupta VK (1985) *J Org Chem* 50: 2003

93. Newkome GR, Yao Z-Q, Baker GR, Gupta VK, Russo PS, Saunders MJ (1986) *J Am Chem Soc* 108: 849
94. Newkome GR, Baker GR, Saunders MJ, Russo PS, Gupta VK, Yao Z-Q, Miller JE, Bouillion K (1986) *J Chem Soc, Chem Comm* 752
95. Cantor G (1915) *Contributions to Transfinite Numbers*, Dover Press, London
96. Gleick J (1987) *Chaos: Making a new science*, Viking Penguin, New York, pp 99
97. Mandelbrot BB (1977) *Fractals: Form, chance and dimensions*, Freeman WH, New York; (1982) *The fractal Geometry of Nature*, Freeman WH, New York
98. Kaye BH (1989) *A random walk through fractal dimensions*, VCH Verlagsgesellschaft/VCH Publishers, Weinheim, FRG
99. See also the following communication in this issue: Blumen AB, Schnörer H (1990) *Angew Chem* 102: 158; (1990) *Angew Chem Int (ed) Engl* 29: 113
100. The single trunked branched assemblies were coined *dendrons*. (Greek word for tree); Multiples of dendrons organized around a reference point or core are referred to as *dendrimers*
101. Merrifield RE, Simmons HE (Eds) (1989) *Topological methods in chemistry*, Wiley, New York
102. a) Hawker CJ, Fréchet JMJ (1990) *J Am Chem Soc* 112: 7638; b) Hawker CJ, Fréchet JMJ (1990) *J Chem Soc, Chem Commun* 1010; c) Hawker CJ, Fréchet JMJ (1990) *Macromolecules* 23: 4726
103. Miller TM, Neenan TX (1990) *Chem Mater* 2: 346
104. Fréchet J et al. (1991) (Private communication)
105. Tam JP (1988) *Proc Natl Acad Sci USA* 85: 5409
106. Chang KJ, Pugh W, Blanchard SG, McDermed J, Tam JP (1988) *Proc Natl Acad Sci USA* 85: 4929
107. Posnett DN, McGrath H, Tam JP (1988) *J Biol Chem* 264: 1719
108. Jacobson RA (1932) *J Am Chem Soc* 54: 1513
109. Hunter WH, Woollett GH (1921) *J Am Chem Soc* 43: 135
110. Bochkarev MN (1988) *Organomet Chem (USSR)* 1: 115
111. Kim YH, Webster OW (1988) *Polym Prep Am Chem Soc Div Polym Chem* 29: 310
112. Kim YH, Webster OW (1990) *J Am Chem Soc* 112: 4592
113. Hawker CJ, Lee R, Fréchet JMJ (1991) *J Am Chem Soc* 113: 4583
114. Mathias LJ, Carothers TW (1991) *J Am Chem Soc* 113: 4043
115. Apen PG, Rasmussen PG (1991) (Private Communication)
116. a) Franks A (1987) *J Phys E Sci Instrum* 20: 1442; b) Drexler KE (1986) "Engines of Creation"; Anchor Press: New York
117. Wooley KL, Hawker CJ, Fréchet JMJ (1991) *J Am Chem Soc* 113: 4252
118. Kwock EW, Neenan TX, Miller TM (1991) *Chem Mater* 3: 775
119. Miller TM, Neenan TX, Zayas R, Bair HE (1992) *J Am Chem Soc* 114: 1018
120. Moore JS, Xu Z (1991) *Macromolecules* 24: 5893
121. Damha MJ, Zabarylo SV (1989) *Tetrahedron Lett* 30: 6295
122. Damha MJ, Oglivie KK (1988) *J Org Chem* 53: 3710
123. Damha MJ, Giannaris PA, Zabarylo SV (1990) *Nucleic Acid Research* 18: 3813
124. Smith PB, Martin SJ, Hall MS, Tomalia DA (1987) In: Mitchell Jr J (ed), *Applied polymer analysis and characterization*, Hauser, Munich, p 357
125. Dermer OC, Ham GE (1969) *Ethyleneimine and other aziridines*, Academic, New York
126. Tomalia DA, Killat G (1985) *Alkyleneimine polymers*. In: *Encyclopedia of polymer science and engineering*, 2nd ed, Wiley, New York, vol 1
127. Tomalia DA (1991) In: Kircheldorf H (ed) *Handbook of polymer synthesis*, Marcel Dekker, New York, Part A, p 43
128. Hedstrand DM, Meister P, Tomalia DA, unpublished results
129. Bashir-Hashemi A, Hart H, Wart DL (1986) *J Am Chem Soc* 108: 6675
130. Hart H, Bashir-Hashemi A, Luo J, Meador M (1986) *Tetrahedron* 42: 1641
131. Hart H, Shahlai K, *J Am Chem Soc* 112: 3687
132. Moulines F, Gloaguen B, Astruc D (1992) *Angew Chem* 104: 4523; *Angew Chem Int (ed) Engl* 31: 458

133. Tomalia DA, Padias A, Hall H (1989) *Polymer Prepr (Am Chem Soc Div Polym Chem)* 30: 119
134. Newkome GR, Baker GR, Arai S, Saunders MJ, Russo PS, Theriot KJ, Moorfield CN, Rogers LE, Miller JE, Lieux TR, Murray ME, Phillips B, Pascal L (1990) *J Am Chem Soc* 112: 8458
135. Newkome GR, Lin X (1991) *Macromolecules* 24: 1443
136. Newkome GP, Nayak A, Behera RK, Moorefield CN, Baker GR (1992) *J Org Chem* 57: 358
137. Newkome GP, Moorefield CN, Baker GR, Johnson AI, Behera RK (1991) *Angew Chem* 103: 1205; (1991) *Angew Chem Int (ed) Engl* 30: 1176
138. Newkome GR, Moorefield CN, Baker GR, Saunders MJ, Grossman SH (1991) *Angew Chem* 103: 1207; (1991) *Angew Chem Int (ed) Engl* 30: 1178
139. Hall Jr. HK, Polls DW (1987) *Polym Bull* 17: 409
140. Rengan K, Engel R (1990) *J Chem Soc, Chem Commun* 1084
141. Rengan K, Engel R (1991) *J Chem Soc Perkin Trans* 987
142. Engel R, Rengan K, Milne C, unpublished results
143. Uchida H, Kabe Y, Yoshino K, Kawamata A, Tsumuraya T, Masamune S (1990) *J Am Chem Soc* 112: 7077
144. Morikawa A, Kakimoto M, Imai Y (1991) *Macromolecules* 24: 3478
145. Roovers J, Toporowski PM, Zhou LL (April 1992) *Polym Prepr Am Chem Soc Div, Polym Chem* 33
146. Hester RD, Mitchell PH (1980) *J Polym Sci Chem Ed* 18: 1729
147. Naylor AM, Goddard III WA, Keifer G, Tomalia DA (1989) *J Am Chem Soc* 111: 2339
148. Smith P (unpublished results); Meltzer AD; Ph.D. Thesis entitled: Mobility of Poly-(amidoamine) Dendrimers: A Study of NMR relaxation times, University of Massachusetts, (Feb 1990); Meltzer AD, Tirrell DA, Jones AA, Inglefield PT, Hedstrand DM, Tomalia DA *Macromolecules*, in press
149. a) Kurtz, Jr SS, Ward AL (1936) *J Franklin Inst* 222: 563 *ibid* 224 (1937) 583, 697; b) Ward AL, Kurtz, Jr SS, Fuleveiler WH (1938) In: Dunstan AE, Nash, AW, Brooks BT, Tizard NT (eds) *Sci of petroleum*, Vol 2 Oxford Univ Press, London, p 1172; c) Kurtz, Jr SS, Sankin A (1953) In: Farkas A (ed) *Phys chem of hydrocarbons*, Vol 2, Academic Press, New York
150. Stryer L (1981): *Biochemistry*, 2nd ed, Freeman WH, New York, p 724
151. Erickson JW, Silva AM, Muthy MRN, Fita I, Rossman MG (1985) *Science (Washington)* 229: 625
152. Gopidas KR, Leheny AR, Caminati G, Turro NJ, Tomalia DA (1991) *J Am Chem Soc* 113: 7335; (August, 1991) *Polym Prepr (Am Chem Soc Div Polym Chem)* 32: 604
153. Caminati G, Turro NJ, Tomalia DA (1990) *J Am Chem Soc* 112: 8315
154. Moreno-Bondi MC, Orellana O, Turro NJ, Tomalia DA (1990) *Macromolecules* 23: 912
155. Dubin PL, Tomalia DA (1992) *Anal Chem* (in press)
156. Friberg SE, Podzimek M, Hedstrand DM, Tomalia DA (1988) *Mol Cryst Liq Cryst* 164: 157
157. Vögtle F, Weber E (1974) *Angew Chem* 86: 896; (1974) *Angew Chem Int (ed) Engl* 13: 814
158. Suckling CJ (1982) *J Chem Soc, Chem Commun* 661
159. Menger FM (1986) *Top Curr Chem* 136: 1
160. Vögtle F, Löhr H-G, Franke J, Worsch D (1985) *Angew Chem* 97: 721; (1985) *Angew Chem Int (ed) Engl* 24: 727
161. Vögtle F, Weber E (eds): *Host Guest Complex Chemistry I-III (Top Curr Chem* 98 (1981), 101 (1982), 121 (1984))
162. Vögtle F, Weber E (eds): *Biomimetic and Biorganic Chemistry I-III (Top Curr Chem* 128 (1985), 132 (1986), 136 (1986))
163. Sigel H, Martin RB (1982) *Chem Rev* 82: 385
164. Helmer B, Tomalia DA, unpublished results
165. Edwards DS, Jung CW, Tomalia DA, unpublished results

166. Tomlinson IA, Fazio MJ, unpublished results
167. Tomalia DA (June, 1992) presented at "24th Organic Reaction Mechanisms Conference" Orono, Maine (USA)
168. Kim YH (1992) *J Am Chem Soc* 114: 4974
169. Kallos GJ, Lewis S, Zhou J, Hedstrand DM, Tomalia DA (1991) *Rapid Comm Mass Spec* 5: 383
170. Tjivikua T, Ballester P, Rebek Jr, J (1990) *J Am Chem Soc* 11: 1249
171. Nowick JS, Feng Q, Tjivikua T, Ballester P, Rebek Jr, J (1991) *J Am Chem Soc* 113: 8831
172. Feng Q, Park TK, Rebek Jr., J (1992) *Science (Washington D.C.)* 256: 1179
173. Hong J, Feng Q, Rotello V, Rebek Jr, J (1992) *Science (D.C.)* 255: 848
174. Bachman PA, Walde P, Luisi PL, Lang J (1991) *J Am Chem Soc* 113: 8204
175. Murray TJ, Zimmerman SC (1992) *J Am Chem Soc* 114: 4010
176. Spaltenstein A, Whitesides GM (1992) *J Am Chem Soc* 113: 686
177. Eigen M, Gardiner W, Schuster, Winkler-Oswatitsch (April, 1981) *Sci Am*
178. Tomalia DA, Swanson D, Brothers III, H, Kallos G, Vinbod TK, to be published
179. Tomalia DA, Hedstrand DM, Ferritto MS (1991) *Macromolecules* 24: 1435
180. Lescance RL, Muthakumar M (1991) *Macromolecules* 24: 4892
181. Gauthier M, Möller M (1991) *Macromolecules* 24: 4548
182. Tomalia DA, Swanson D, Hedstrand DM (April, 1992), *Polymer Prepr (Am Chem Soc Div Polym Chem)* 33: 180
183. Appenzeller T (1991) *Science (Washington DC)* 254: 1300 and subsequent papers in this reference
184. Whitesides GM, Mathias JP, Seto CT (1991) *Science (Washington DC)* 254: 1312
185. Baum RM (June 1992) *Chem & Eng News* 25
186. Tomalia DA, Hedstrand DM, Wilson LR (1990) *Encycl of Polym Sci and Eng*, J Wiley, New York, 2: 46
187. Goethals EJ (ed) (1989) *Telechelic Polymers: Synthesis and Applications*, CRC Press, Boca Raton, FL, USA
188. Singer M, Berg P (1991) *Genes and Genomes*, University Science Books, Mill Valley, CA, USA
189. Pershan PS (1988) *Structure of liquid crystals phases*, World Scientific, Singapore
190. Ringsdorf H, Shlarb B, Venzmer J (1988) *Angew Chem* 100: 118; (1988) *Angew Chem Int (ed) Engl* 27: 113
191. Desiraju GR (1989) *Crystal engineering: The design of organic solids*, Elsevier, Amsterdam
192. Creighton TE (1983) *Proteins: Structure and molecular principles*, Freeman, New York
193. Seto CT, Whitesides GM (1990) *J Am Chem Soc* 112: 6409, *ibid* (1991) 113: 712
194. Koert U, Harding MM, Lehn J-M (1990) 346: 339
195. Newkome GR, Baker GR, Saunders MJ, Russo PS, Gupta VK, Yao Z-q, Miller JE, Bouillon K (1986) *J Chem Soc, Chem Commun* 752
196. Amato I (Nov 8, 1990) *Science News* 138: 298
197. Baer E, Hiltner A, Keith HD (1987) *Science (Washington DC)* 235: 1015
198. Baer E, Cassidy JJ, Hiltman A (1991) *Pure & Appl Chem*, No 7, 63: 961
199. Gove PB (1981) *Webster's Third New Int Dict of the Engl Language*, p 603
200. Nagasaki T, Ukon M, Arimore S, Shinkai S (1992) *J Chem Soc, Chem Commun* 608
201. Percec V, Kawasumi M (1992) *Macromolecules* 25: 3843
202. Wu T, Orgel LE (1992) *J Am Chem Soc* 114: 5496 and references therein
203. Wu T, Orgel LE (1992) *J Am Chem Soc* 114: 317
204. Corey EJ (1991) *Angew Chem* 103: 469; (1991) *Angew Chem Int(ed) Engl* 30: 455
205. An H, Bradshaw JS, Izatt RM (1992) *Chem Rev* 92: 543
206. Mason SE (1991) *Chemical evolution (Clarendon Press-Oxford)* Oxford University Press, New York
207. Amato I (1991) *Science (Washington D.C.)* 254: 1310
208. Kunitake T (1992) *Angew Chem* 104: 692; (1992) *Angew Chem Int (ed) Engl* 31: 709
209. van der Made RW, van Leeuwen PWNM (1992) *J Chem Soc, Chem Commun*

Author Index Volumes 151–165

Author Index Vols. 26–50 see Vol. 50

Author Index Vols. 50–100 see Vol. 100

Author Index Vols. 101–150 see Vol. 150

The volume numbers are printed in italics

Adam, W. and Hadjirapoglou, L.: Dioxiranes: Oxidation Chemistry Made Easy. *164*, 45–62 (1993).

Allamandola, L. J.: Benzenoid Hydrocarbons in Space: The Evidence and Implications *153*, 1–26 (1990).

Astruc, D.: The Use of π -Organoiron Sandwiches in Aromatic Chemistry. *160*, 47–96 (1991)

Balzani, V., Barigelletti, F., De Cola, L.: Metal Complexes as Light Absorption and Light Emission Sensitizers. *158*, 31–71 (1990).

Barigelletti, F., see Balzani, V.: *158*, 31–71 (1990).

Bignozzi, C. A., see Scandola, F.: *158*, 73–149 (1990).

Billing, R., Rehorek, D., Hennig, H.: Photoinduced Electron Transfer in Ion Pairs. *158*, 151–199 (1990).

Brunvoll, J., see Chen, R. S.: *153*, 227–254 (1990).

Brunvoll, J., Cyvin, B. N., and Cyvin, S. J.: Benzenoid Chemical Isomers and Their Enumeration. *162*, 181–221 (1992).

Brunvoll, J., see Cyvin, B. N.: *162*, 65–180 (1992).

Bundle, D. R.: Synthesis of Oligosaccharides Related to Bacterial O-Antigens. *154*, 1–37 (1990).

Burrell, A. K., see Sessler, J. L.: *161*, 177–274 (1991).

Caffrey, M.: Structural, Mesomorphic and Time-Resolved Studies of Biological Liquid Crystals and Lipid Membranes Using Synchrotron X-Radiation. *151*, 75–109 (1989).

Canceill, J., see Collet, A.: *165*, 103–129 (1993).

Chambron, J.-C., Dietrich-Buchecker, Ch., and Sauvage, J.-P.: From Classical Chirality to Topologically Chiral Catenands and Knots. *165*, 131–162 (1993).

Chen, R. S., Cyvin, S. J., Cyvin, B. N., Brunvoll, J., and Klein, D. J.: Methods of Enumerating Kekulé Structures, Exemplified by Application to Rectangle-Shaped Benzenoids. *153*, 227–254 (1990).

Chen, R. S., see Zhang, F. J.: *153*, 181–194 (1990).

Chiorboli, C., see Scandola, F.: *158*, 73–149 (1990).

Ciolkowski, J.: Scaling Properties of Topological Invariants. *153*, 85–100 (1990).

Collet, A., Dutasta, J.-P., Lozach, B., and Canceill, J.: Cyclotrimeratrylenes and Cryptophanes: Their Synthesis and Applications to Host-Guest Chemistry and to the Design of New Materials. *165*, 103–129 (1993).

Cooper, D. L., Gerratt, J., and Raimondi, M.: The Spin-Coupled Valence Bond Description of Benzenoid Aromatic Molecules. *153*, 41–56 (1990).

Cyvin, B. N., see Chen, R. S.: *153*, 227–254 (1990).

Cyvin, S. J., see Chen, R. S.: *153*, 227–254 (1990).

- Cyvin, B. N., Brunvoll, J. and Cyvin, S. J.: Enumeration of Benzenoid Systems and Other Polyhexes. *162*, 65–180 (1992).
- Cyvin, S. J., see Cyvin, B. N.: *162*, 65–180 (1992).
- Dartyge, E., see Fontaine, A.: *151*, 179–203 (1989).
- De Cola, L., see Balzani, V.: *158*, 31–71 (1990).
- Dear, K.: Cleaning-up Oxidations with Hydrogen Peroxide. *164*, 115–125 (1993).
- Descotes, G.: Synthetic Saccharide Photochemistry. *154*, 39–76 (1990).
- Dias, J. R.: A Periodic Table for Benzenoid Hydrocarbons. *153*, 123–144 (1990).
- Dietrich-Buchecker, Ch., see Chambron, J.-C.: *165*, 131–162 (1993).
- Dohm, J., Vögtle, F.: Synthesis of (Strained) Macrocycles by Sulfone Pyrolysis *161*, 69–106 (1991).
- Durst, H. D., see Tomalia, D. A.: *165*, 193–313 (1993).
- Dutasta, J.-P., see Collet, A.: *165*, 103–129 (1993).
- Eaton, D. F.: Electron Transfer Processes in Imaging. *156*, 199–226 (1990).
- El-Basil, S.: Caterpillar (Gutman) Trees in Chemical Graph Theory. *153*, 273–290 (1990).
- Fontaine, A., Dartyge, E., Itie, J. P., Juchs, A., Polian, A., Tolentino, H. and Tourillon, G.: Time-Resolved X-Ray Absorption Spectroscopy Using an Energy Dispersive Optics: Strengths and Limitations. *151*, 179–203 (1989).
- Fossey, J., Sorba, J., and Lefort, D.: Peracide and Free Radicals: A Theoretical and Experimental Approach. *164*, 99–113 (1993).
- Fox, M. A.: Photoinduced Electron Transfer in Arranged Media. *159*, 67–102 (1991).
- Fuller, W., see Greenall, R.: *151*, 31–59 (1989).
- Gehrke, R.: Research on Synthetic Polymers by Means of Experimental Techniques Employing Synchrotron Radiation. *151*, 111–159 (1989).
- Gerratt, J., see Cooper, D. L.: *153*, 41–56 (1990).
- Gigg, J., and Gigg, R.: Synthesis of Glycolipids. *154*, 77–139 (1990).
- Gislason, E. A.: see Guyon, P.-M.: *151*, 161–178 (1989).
- Greenall, R., Fuller, W.: High Angle Fibre Diffraction Studies on Conformational Transitions DNA Using Synchrotron Radiation. *151*, 31–59 (1989).
- Guo, X. F., see Zhang, F. J.: *153*, 181–194 (1990).
- Gust, D., and Moore, T. A.: Photosynthetic Model Systems. *159*, 103–152 (1991).
- Gutman, I.: Topological Properties of Benzenoid Systems. *162*, 1–28 (1992).
- Gutman, I.: Total π -Electron Energy of Benzenoid Hydrocarbons. *162*, 29–64 (1992).
- Guyon, P.-M., Gislason, E. A.: Use of Synchrotron Radiation to Study State-Selected Ion-Molecule Reactions. *151*, 161–178 (1989).
- Hadjarapoglou, L., see Adam, W.: *164*, 45–62 (1993).
- Harbottle, G.: Neutron Activation Analysis in Archaeological Chemistry. *157*, 57–92 (1990).
- He, W. C. and He, W. J.: Peak-Valley Path Method on Benzenoid and Coronoid Systems. *153*, 195–210 (1990).
- He, W. J., see He, W. C.: *153*, 195–210 (1990).
- Heaney, H.: Novel Organic Peroxygen Reagents for Use in Organic Synthesis. *164*, 1–19 (1993).
- Heinze, J.: Electronically Conducting Polymers. *152*, 1–19 (1989).
- Helliwell, J., see Moffat, J. K.: *151*, 61–74 (1989).
- Hennig, H., see Billing, R.: *158*, 151–199 (1990).
- Hesse, M., see Meng, Q.: *161*, 107–176 (1991).
- Hiberty, P. C.: The Distortive Tendencies of Delocalized π Electronic Systems. Benzene, Cyclobutadiene and Related Heteroannulenes. *153*, 27–40 (1990).
- Ho, T. L.: Trough-Bond Modulation of Reaction Centers by Remote Substituents. *155*, 81–158 (1990).
- Höft, E.: Enantioselective Epoxidation with Peroxidic Oxygen. *164*, 63–77 (1993).

- Holmes, K. C.: Synchrotron Radiation as a Source for X-Ray Diffraction — The Beginning. *151*, 1–7 (1989).
- Hopf, H., see Kostikov, R. R.: *155*, 41–80 (1990).
- Indelli, M. T., see Scandola, F.: *158*, 73–149 (1990).
- Itie, J. P., see Fontaine, A.: *151*, 179–203 (1989).
- Ito, Y.: Chemical Reactions Induced and Probed by Positive Muons. *157*, 93–128 (1990).
- John, P. and Sachs, H.: Calculating the Numbers of Perfect Matchings and of Spanning Tress, Pauling's Bond Orders, the Characteristic Polynomial, and the Eigenvectors of a Benzenoid System. *153*, 145–180 (1990).
- Jucha, A., see Fontaine, A.: *151*, 179–203 (1989).
- Kavarnos, G. J.: Fundamental Concepts of Photoinduced Electron Transfer. *156*, 21–58 (1990).
- Khairutdinov, R. F., see Zamaraev, K. I.: *163*, 1–94 (1992).
- Kim, J. I., Stumpe, R., and Klenze, R.: Laser-induced Photoacoustic Spectroscopy for the Speciation of Transuranic Elements in Natural Aquatic Systems. *157*, 129–180 (1990).
- Klaffke, W. see Thiem, J.: *154*, 285–332 (1990).
- Klein, D. J.: Semiempirical Valence Bond Views for Benzenoid Hydrocarbons. *153*, 57–84 (1990).
- Klein, D. J., see Chen, R. S.: *153*, 227–254 (1990).
- Klenze, R., see Kim, J. I.: *157*, 129–180 (1990).
- Knops, P., Sendhoff, N., Mekelburger, H.-B., Vögtle, F.: High Dilution Reactions — New Synthetic Applications *161*, 1–36 (1991).
- Koepp, E., see Ostrowicky, A.: *161*, 37–68 (1991).
- Kohnke, F. H., Mathias, J. P., and Stoddart, J. F.: Substrate-Directed Synthesis: The Rapid Assembly of Novel Macropolycyclic Structures *via* Stereoregular Diels-Alder Oligomerizations. *165*, 1–69 (1993).
- Kostikov, R. R., Molchanov, A. P., and Hopf, H.: Gem-Dihalocyclopropanos in Organic Synthesis. *155*, 41–80 (1990).
- Krogh, E., and Wan, P.: Photoinduced Electron Transfer of Carbanions and Carbocations. *156*, 93–116 (1990).
- Kunkeley, H., see Vogler, A.: *158*, 1–30 (1990).
- Kuwajima, I. and Nakamura, E.: Metal Homo-enolates from Siloxycyclopropanes. *155*, 1–39 (1990).
- Lange, F., see Mandelkow, E.: *151*, 9–29 (1989).
- Lefort, D., see Fossey, J.: *164*, 99–113 (1993).
- Lopez, L.: Photoinduced Electron Transfer Oxygenations. *156*, 117–166 (1990).
- Lozach, B., see Collet, A.: *165*, 103–129 (1993).
- Lymar, S. V., Parmon, V. N., and Zamarev, K. I.: Photoinduced Electron Transfer Across Membranes. *159*, 1–66 (1991).
- Mandelkow, E., Lange, G., Mandelkow, E.-M.: Applications of Synchrotron Radiation to the Study of Biopolymers in Solution: Time-Resolved X-Ray Scattering of Microtubule Self-Assembly and Oscillations. *151*, 9–29 (1989).
- Mandelkow, E.-M., see Mandelkow, E.: *151*, 9–29 (1989).
- Mathias, J. P., see Kohnke, F. H.: *165*, 1–69 (1993).
- Mattay, J., and Vondenhof, M.: Contact and Solvent-Separated Radical Ion Pairs in Organic Photochemistry. *159*, 219–255 (1991).
- Mekelburger, H.-B., see Knops, P.: *161*, 1–36 (1991).
- Meng, Q., Hesse, M.: Ring Closure Methods in the Synthesis of Macrocyclic Natural Products *161*, 107–176 (1991).
- Merz, A.: Chemically Modified Electrodes. *152*, 49–90 (1989).

- Meyer, B.: Conformational Aspects of Oligosaccharides. *154*, 141–208 (1990).
 Misumi, S.: Recognitory Coloration of Cations with Chromoacerands. *165*, 163–192 (1993).
 Moffat, J. K., Helliwell, J.: The Laue Method and its Use in Time-Resolved Crystallography. *151*, 61–74 (1989).
 Molchanov, A. P., see Kostikov, R. R.: *155*, 41–80 (1990).
 Moore, T. A., see Gust, D.: *159*, 103–152 (1991).
 Nakamura, E., see Kuwajima, I.: *155*, 1–39 (1990).
 Okuda, J.: Transition Metal Complexes of Sterically Demanding Cyclopentadienyl Ligands. *160*, 97–146 (1991).
 Ostrowsky, A., Koepp, E., Vögtle, F.: The “Vesium Effect”: Syntheses of Medio- and Macrocyclic Compounds *161*, 37–68 (1991).
 Parmon, V. N., see Lymar, S. V.: *159*, 1–66 (1991).
 Polian, A., see Fontaine, A.: *151*, 179–203 (1989).
 Raimondi, M., see Copper, D. L.: *153*, 41–56 (1990).
 Riekel, C.: Experimental Possibilities in Small Angle Scattering at the European Synchrotron Radiation Facility. *151*, 205–229 (1989).
 Roth, H. D.: A Brief History of Photoinduced Electron Transfer and Related Reactions. *156*, 1–20 (1990).
 Roth, H. D.: Structure and Reactivity of Organic Radical Cations. *163*, 131–245 (1992).
 Rüsck, M., see Warwel, S.: *164*, 79–98 (1993).
 Sachs, H., see John, P.: *153*, 145–180 (1990).
 Saeva, F. D.: Photoinduced Electron Transfer (PET) Bond Cleavage Reactions. *156*, 59–92 (1990).
 Sauvage, J.-P., see Chambron, J.-C.: *165*, 131–162 (1993).
 Sendhoff, N., see Knops, P.: *161*, 1–36 (1991).
 Sessler, J. L., Burrell, A. K.: Expanded Porphyrins *161*, 177–274 (1991).
 Sheldon, R.: Homogeneous and Heterogeneous Catalytic Oxidations with Peroxide Reagents. *164*, 21–43 (1993).
 Sheng, R.: Rapid Ways to Recognize Kekuléan Benzenoid Systems. *153*, 211–226 (1990).
 Schäfer, H.-J.: Recent Contributions of Kolbe Electrolysis to Organic Synthesis. *152*, 91–151 (1989).
 Sojka, M., see Warwel, S.: *164*, 79–98 (1993).
 Sorba, J., see Fossey, J.: *164*, 99–113 (1993).
 Stanek, Jr., J.: Preparation of Selectively Alkylated Saccharides as Synthetic Intermediates. *154*, 209–256 (1990).
 Stoddart, J. F., see Kohnke, F. H.: *165*, 1–69 (1993).
 Stumpe, R., see Kim, J. I.: *157*, 129–180 (1990).
 Suami, T.: Chemistry of Pseudo-sugars. *154*, 257–283 (1990).
 Suppan, P.: The Marcus Inverted Region. *163*, 95–130 (1992).
 Suzuki, N.: Radiometric Determination of Trace Elements. *157*, 35–56 (1990).
 Thiem, J., and Klaffke, W.: Syntheses of Deoxy Oligosaccharides. *154*, 285–332 (1990).
 Timpe, H.-J.: Photoinduced Electron Transfer Polymerization. *156*, 167–198 (1990).
 Tolentino, H., see Fontaine, A.: *151*, 179–203 (1989).
 Tomalia, D. A.: Genealogically Directed Synthesis: Starburst/Cascade Dendrimers and Hyperbranched Structures. *165*, 193–313 (1993).
 Tourillon, G., see Fontaine, A.: *151*, 179–203 (1989).
 Vögtle, F., see Dohm, J.: *161*, 69–106 (1991).
 Vögtle, F., see Knops, P.: *161*, 1–36 (1991).

- Vögtle, F., see Ostrowicky, A.: *161*, 37–68 (1991).
- Vogler, A., Kunkley, H.: Photochemistry of Transition Metal Complexes Induced by Outer-Sphere Charge Transfer Excitation. *158*, 1–30 (1990).
- Vondenhof, M., see Mattay, J.: *159*, 219–255 (1991).
- Wan, P., see Krogh, E.: *156*, 93–116 (1990).
- Warwel, S., Sojka, M. and Rüsche, M.: Synthesis of Dicarboxylic Acids by Transition-Metal Catalyzed Oxidative Cleavage of Terminal-Unsaturated Fatty Acids. *164*, 79–98 (1993).
- Willner, I., and Willner, B.: Artificial Photosynthetic Model Systems Using Light-Induced Electron Transfer Reactions in Catalytic and Biocatalytic Assemblies. *159*, 153–218 (1991).
- Yoshihara, K.: Chemical Nuclear Probes Using Photon Intensity Ratios. *157*, 1–34 (1990).
- Zamarev, K. I., see Lyman, S. V.: *159*, 1–66 (1991).
- Zamaraev, K. I., Khairutdinov, R. F.: Photoinduced Electron Tunneling Reactions in Chemistry and Biology. *163*, 1–94 (1992).
- Zander, M.: Molecular Topology and Chemical Reactivity of Polynuclear Benzenoid Hydrocarbons. *153*, 101–122 (1990).
- Zhang, F. J., Guo, X. F., and Chen, R. S.: The Existence of Kekulé Structures in a Benzenoid System. *153*, 181–194 (1990).
- Zimmermann, S. C.: Rigid Molecular Tweezers as Hosts for the Complexation of Neutral Guests. *165*, 71–102 (1993).
- Zybill, Ch.: The Coordination Chemistry of Low Valent Silicon. *160*, 1–46 (1991).